

Seismic vulnerability assessment
of traditional timber frame and
masonry wall buildings.
Application to the historical centre
of Valparaíso, Chile

Doctoral Thesis by:
Belén Jiménez Ramirez

Supervised by:
Luca Pelà

Barcelona, November 2020

Universitat Politècnica de Catalunya, UPC BarcelonaTech
Doctorat en Enginyeria de la Construcció
Departament d'Enginyeria Civil i Ambiental



Escola Tècnica Superior d'Enginyers
de Camins, Canals i Ports de Barcelona

UNIVERSITAT POLITÈCNICA DE CATALUNYA

PHD Dissertation

Seismic vulnerability assessment of traditional timber frame and masonry wall buildings. Application to the historical centre of Valparaíso, Chile

Doctoral Thesis submitted in fulfilment of the requirements for the
Degree of Doctor of Philosophy in Construction Engineering

by

BELÉN JIMÉNEZ RAMÍREZ

Barcelona, November 2020



Escola Tècnica Superior d'Enginyers
de Camins, Canals i Ports de Barcelona

UNIVERSITAT POLITÈCNICA DE CATALUNYA

Thesis Supervisor:

Luca Pelà – Technical University of Catalonia (UPC)

Board of Examiners:

Pere Roca Fabregat – Technical University of Catalonia (UPC)

Cristian Sandoval Mandujano – Pontifical Catholic University of Chile

Alessandra Aprile – Università degli Studi di Ferrara

External Reviewers:

Cristian Sandoval Mandujano – Pontifical Catholic University of Chile

Alessandra Aprile – Università degli Studi di Ferrara

Acknowledgments

This doctoral thesis has been developed within the ELARCH project (Euro LA partnership in natural Risk mitigation and protection of the Cultural Heritage) funded by the European Commission under the Erasmus Mundus Action 2 Partnership (EMA2). Reference number: 552129-EM-1-2014-1-IT-ERA MUNDUSEMA21. Website: <https://www.elarch.org>. The project, aimed at fostering scientific cooperation in the field of the protection of heritage between European and Latin American Higher Education Institutions, granted a scholarship to the PhD candidate. The research has received also the financial support from the Ministry of Science, Innovation and Universities (MCIU) of the Spanish Government, the State Agency of Research (AEI) and the European Regional Development Fund (ERDF) through the SEVERUS project (Multilevel evaluation of seismic vulnerability and risk mitigation of masonry buildings in resilient historical urban centres, ref. num. RTI2018-099589-B-I00). The financial support from the MINECO (Ministerio de Economía y Competitividad of the Spanish Government) and the ERDF (European Regional Development Fund) through the MULTIMAS project (Multiscale techniques for the experimental and numerical analysis of the reliability of masonry structures, ref. num. BIA2015-63882-P) is also gratefully acknowledged.

I would like to express my gratitude to the director of this thesis Prof. Luca Pelà, for sharing with me his invaluable knowledge on historical constructions, for accepting the challenge of investigating the timber frame construction, and for his continuous support and wise advice during all the research. I am very grateful for his perseverance and motivation even in difficult times.

I am very grateful to Savvas Saloustros for supervising the last stage of this work and giving very positive contributions to this thesis. His wisdom and vocation inspired me a lot.

I am also very grateful to Prof. Marcela Hurtado Saldías for encouraging my interest in the study of the heritage constructions of Valparaíso and for proposing me the big opportunity to apply to this international PhD.

I am thankful to all my friends and colleagues of the research group in UPC, who supported me countless times and were always able to have constructive engineering conversations that significantly contributed to the development of this thesis. I would say a special thank-you to my dear friend Nirvan Makoond for his amazing support and friendship, for sharing his knowledge on numerical methods with me and cheering me up always. To Larisa García-Ramonda, for her incredible support and friendship too.

No words to thank all my friends that shared this process with me in Barcelona for making me feel at home all these years. A particular thanks goes to Duda Bueno and Melisa Manoni, for supporting me in moments of weakness and motivated me with a lot of love, food and words of

encouragement. Thanks to my Chilean friends too, especially to Daniela Muñoz and Martin Rodriguez, for helping me with their amazing friendship, wisdom and love.

A very special thanks goes to Pablo Castellano, for his unconditional support, patience and love.

Finally, a huge thanks go to my parents, Griselda y José for their infinite love and unconditional support all these years. Thanks to my siblings Mary, Claudia, Nono and Pato, to my brothers-in-law and to my nephews and niece, for their love all these years far away from home and for giving me such a beautiful family.

To Valparaíso.

Belén Jiménez
Barcelona, November 2020

Abstract

The seismic vulnerability of urban assets exposed to earthquake hazard represents a growing concern in the engineering field due to the potential risk of collapse for the buildings, and the associated devastating consequences for the inhabitants. In the last decades, this concern has led to the development of novel strategies for the assessment of the seismic vulnerability of buildings located in urban centres. An accurate evaluation of the seismic vulnerability of the existing building stock constitutes the point of departure for the implementation of the necessary mitigation strategies aimed at increasing the seismic resilience of the cities.

Estimating the seismic vulnerability of the existing buildings at the urban scale represents a great challenge. This complex task requires the knowledge of the great variety of existing structural typologies, often biased by the intrinsic uncertainties related to local construction materials and techniques, especially in territories composed of historical and vernacular constructions. The results of this type of analysis are strongly influenced by several important factors, among which there are the amount and quality of the data collected during the analysis of the available documents, and the in-situ survey of the buildings.

A propaedeutic stage of the seismic vulnerability assessment of urban centres is the definition of building taxonomies to characterize the structural features of the buildings and their main sources of vulnerabilities. This difficult task requires the availability of consistent technical data, which are commonly scarce in cities with historical constructions. Such common problem is due to the fragmentary documentation available in local archives, as well as the inherent complexities related to the accessibility to the existing buildings for the necessary in-situ survey activities.

This doctoral thesis contributes to the development of suitable methodologies for the systematic surveying of urban buildings in historical urban centres, by proposing four complete survey forms for timber, masonry, reinforced concrete and steel/iron structural typologies. This tool aims to improve and optimize the complex process of collecting and gathering data about the structural characteristics of the existing building stock, that are necessary for further seismic vulnerability analyses.

Another contribution of this thesis is the calibration of simplified numerical models for the assessment of the seismic vulnerability of traditional buildings composed of timber frame and masonry wall structures. This peculiar structural typology of urban building has not been addressed exhaustively in the existing research literature, as available studies are focused mainly on more recurrent systems, such as reinforced concrete, masonry and steel structures. The nonlinear behaviour is simulated through the adoption of Lumped Plasticity Models (LPM) for timber frames, and continuum Finite Element (FE) models for masonry walls, respectively. The calibration of these models is pursued based on rigorous comparisons with numerous experimental

tests available in the scientific literature. The proposed numerical tools show to predict properly the seismic capacity and collapse mechanisms of this type of structures.

The developed simplified numerical models for hybrid timber frame and masonry wall structures are used to assess the seismic vulnerability of two existing buildings located in the historical centre of the city of Valparaíso, Chile. This case study, catalogued as UNESCO World Heritage Site, represents an emblematic urban built environment where traditional timber-masonry buildings represent the recurrent structural system.

The developed numerical models are employed afterwards to analyse the different structural configurations of timber-masonry buildings located in three historical neighbourhoods within the historical centre of Valparaíso. Although conserving similar and recurrent features, the different examined structural configurations differ in the organization of the resisting systems, number of storeys, and presence of structural irregularities. The different pushover analyses show the influence of the aforementioned parameters on the seismic behaviour of the buildings.

Based on the results of the sensitivity analysis of the different structural parameters to assess their influence on the seismic response of the buildings, the next stage of the research proposes a tentative set of scores and weights for the application of the Vulnerability Index Method (VIM) to traditional buildings composed of timber frame and masonry wall structures. The resulting VIM forms are calibrated by applying the N2 method to determine the seismic performance of the representative typologies within the study area. This additional contribution of the research is based on the results of a numerical study, unlike other available VIM forms available in the existing literature are based on past post-earthquake surveys of damaged buildings.

The thesis ends in a prospective study on the seismic vulnerability by VIM of the buildings located in three historical neighbourhoods of the historical centre of Valparaíso. Such neighbourhoods are of especial interest, as they include two of the main evacuation routes for the city in case of a tsunami, and have a central role in the case of a possible post-earthquake scenario. In addition, the investigated zone represents an exemplary area of study where different typologies of heritage buildings coexist, made of timber, masonry, and reinforced concrete. This heterogeneous urban system, comprised of 111 buildings, is analysed by using the proposed VIM forms for timber-masonry buildings, together with the VIM forms available for masonry and reinforced concrete structures. The obtained results are used to create seismic vulnerability maps in a GIS environment that may be used for future works aimed at the definition of proper policies for the implementation of mitigation strategies.

Keywords: Building Taxonomy – Building Survey – Seismic Vulnerability – Historical Centres – Timber Frame – Masonry Wall – Pushover Analysis – Lumped Plasticity Model – Continuum Finite Element Model – Vulnerability Index Method – N2 method - GIS.

Resumen

La vulnerabilidad sísmica de zonas urbanas expuestas a terremotos representa una creciente preocupación en el campo de la ingeniería debido al potencial riesgo de colapso de los edificios, y las consecuencias devastadoras que afectan a sus habitantes. En las últimas décadas, esta inquietud ha motivado el desarrollo de nuevas estrategias para la evaluación de la vulnerabilidad sísmica de los edificios existentes en centros urbanos. Un correcto estudio de la vulnerabilidad sísmica constituye el punto de partida para la correcta implementación de estrategias de mitigación enfocadas a aumentar la resiliencia sísmica de las ciudades.

El estudio de la vulnerabilidad sísmica de los edificios existentes a escala urbana supone un importante desafío. Esta compleja tarea requiere un alto nivel de conocimiento respecto a las tipologías constructivas existentes, información comúnmente sesgada por las incertidumbres intrínsecas de los edificios, asociadas a los materiales y técnicas de construcción locales, especialmente en territorios compuestos por construcciones históricas o de naturaleza vernácula. El alcance de los estudios de vulnerabilidad sísmica se ve comúnmente influenciados por varios factores, entre los que se encuentran la calidad y cantidad de información técnica obtenida desde el levantamiento de datos en archivos locales o en inspecciones in-situ de los edificios.

Una etapa propedéutica de los estudios de vulnerabilidad sísmica a escala urbana es la definición de taxonomías de los edificios, que permitan caracterizar los sistemas estructurales existentes y detectar sus principales fuentes de vulnerabilidad. Este tipo de tareas requiere la disponibilidad de información técnica, comúnmente escasa en ciudades con construcciones históricas. Esta escasez de datos se debe comúnmente a la fragmentariedad de la información, así como a las complejidades intrínsecas de los levantamientos in-situ relacionadas a la accesibilidad de los edificios existentes.

Esta tesis doctoral contribuye al desarrollo de una metodología para el levantamiento sistemático de edificios históricos en centros urbanos basada en la formulación de cuatro formularios de encuestas específicos para tipologías estructurales de entramado de madera, mampostería, hormigón armado y acero/hierro forjado, comúnmente existentes en centros históricos urbanos. La aplicación de estas herramientas permite a mejorar y optimizar los procesos de levantamiento de datos requeridos en los estudios de vulnerabilidad sísmica.

Otra importante contribución de esta tesis se centra en la calibración de modelos numéricos simplificados y orientados a la práctica para la evaluación de la vulnerabilidad sísmica de edificios tradicionales compuestos por muros de entramados de madera y mampostería. La investigación en torno a esta tipología constructiva no ha sido abordada exhaustivamente en la literatura, donde la mayoría de estudios se centra en la investigación de edificios con sistemas constructivos más recurrentes tales como mampostería, hormigón armado y acero. El comportamiento no lineal dichas estructuras es simulado mediante el uso de Modelos de Plasticidad Concentrada (MPC) para muros de entramado de madera, y modelos continuos de Elementos Finitos (FEM) para

muros de mampostería. La calibración de estos modelos se lleva a cabo en base a rigurosas comparaciones entre diferentes ensayos experimentales disponibles en la literatura científica. Los modelos propuestos demostraron predecir correctamente la capacidad sísmica y los mecanismos de colapso de este tipo de estructuras. Los modelos numéricos simplificados desarrollados para la evaluación de estructuras híbridas compuestas por muros de madera y mampostería se utilizan para la evaluar la vulnerabilidad sísmica de dos edificios existentes situados en el centro histórico de la ciudad de Valparaíso, Chile. Este caso de estudio, catalogado como Patrimonio de la Humanidad por la UNESCO, se caracteriza por su singular entorno urbano, donde predominan los sistemas estructurales compuestos por muros de entramados de madera y mampostería. Posteriormente, los modelos numéricos propuestos se utilizan para analizar diferentes configuraciones estructurales de los edificios de entramado de madera y mampostería localizados en tres barrios históricos del centro de la ciudad de Valparaíso. Si bien estas tipologías mantienen características y configuraciones similares, las diferentes configuraciones estructurales examinadas difieren en la organización de los sistemas resistentes, número de plantas y la presencia de irregularidades estructurales. Los resultados de la aplicación de diferentes análisis estáticos no lineales (*Pushover*) demuestran la influencia de dichos parámetros en el comportamiento sísmico de los edificios.

La siguiente etapa de esta investigación propone una calibración preliminar del Método del Índice de Vulnerabilidad (MIV) para edificios de entramado de madera y mampostería. Este estudio considera la asignación de puntajes y clases de algunos parámetros de evaluación sobre la base de análisis de sensibilidad de diferentes parámetros estructurales. La nueva ficha de vulnerabilidad se calibra aplicando Método N2 para determinar el rendimiento sísmico de los edificios dentro del área de estudio. Este estudio se basa en los resultados de un estudio numérico, a diferencia de otros formularios del MIV disponibles en la literatura existente, que se basan en datos de daños de los edificios después de un terremoto.

Esta tesis culmina con un estudio prospectivo de la vulnerabilidad sísmica aplicando el MIV a 111 edificios ubicados en tres barrios del centro histórico de Valparaíso. Esta zona es de especial interés, ya que incluye dos de las principales rutas de evacuación de la ciudad en caso de tsunami, cumpliendo un rol esencial en los planes de emergencia sísmica de la ciudad. Además, la zona investigada alberga diferentes tipologías de edificios patrimoniales, hechos de entramados de madera, mampostería y hormigón armado. Otros formularios del MIV disponibles para mampostería y estructuras de hormigón armado se aplican en conjunto con el nuevo formulario para edificios de entramado de madera y mampostería. Los resultados obtenidos se utilizan para crear mapas de vulnerabilidad sísmica en el entorno GIS que pueden utilizarse para llevar a cabo planes futuros para la implementación de estrategias de mitigación de la vulnerabilidad.

Palabras clave: Análisis del riesgo sísmico – Análisis de la vulnerabilidad sísmica – Centros históricos urbanos – Entramados de madera – Mampostería – Modelos numéricos – Modelos de Plasticidad Concentrada – Elementos Finitos continuos— Método del Índice de Vulnerabilidad – Método N2.

Contents

ACKNOWLEDGMENTS	5
ABSTRACT	7
RESUMEN.....	9
CONTENTS	11
CHAPTER 1. INTRODUCTION	15
1.1 BACKGROUND AND MOTIVATION	15
1.2 SCOPE AND OBJECTIVES	18
1.3 OUTLINE OF THE THESIS.....	20
1.4 RESEARCH DISSEMINATION	21
CHAPTER 2. LITERATURE REVIEW	23
2.1 INTRODUCTION.....	23
2.2 SEISMIC RISK ASSESSMENT MODELS FOR BUILT-UP AREAS	24
2.2.1 FUNDAMENTAL CONCEPTS	24
2.2.2 SEISMIC RISK ASSESSMENT MODELS	26
2.2.3 DATA MANAGEMENT AND GIS MAPPING STRATEGIES	30
2.3 SEISMIC VULNERABILITY ASSESSMENT METHODS	31
2.3.1 EMPIRICAL METHODS.....	31
2.3.2 ANALYTICAL METHODS.....	38
2.3.3 HYBRID METHODS	41
2.4 BUILDING SURVEY AND DATA-COLLECTION ACTIVITIES	41
2.5 NUMERICAL METHODS FOR SEISMIC VULNERABILITY ASSESSMENT OF TIMBER AND MASONRY BUILDINGS INCLUDING HYBRID TYPOLOGIES	45
2.5.1 MODELLING OF TIMBER FRAME STRUCTURES	45
2.5.2 MODELLING OF MASONRY STRUCTURES	46
2.5.3 MODELLING OF HYBRID TIMBER-MASONRY STRUCTURES.....	49
2.6 SUMMARY	50

CHAPTER 3. CERRO ALEGRE, CERRO CONCEPCIÓN AND THE PORT NEIGHBOURHOODS OF THE HISTORICAL CENTRE OF VALPARAÍSO, CHILE: AN OVERVIEW.....	53
3.1 INTRODUCTION.....	53
3.2 HISTORICAL OVERVIEW: URBAN CONFIGURATION AND MAJOR EARTHQUAKES	56
3.2.1 HISTORY OF THE URBAN DEVELOPMENT OF THE CITY	56
3.2.2 HISTORICAL EARTHQUAKES	58
3.2.3 UNESCO WORLD HERITAGE STATUS AND CURRENT CONDITION	61
3.3 SEISMIC HAZARD.....	62
3.4 EMERGENCY LIMIT CONDITION.....	66
3.4.1 CIVIL PROTECTION AND EMERGENCY PLANS.....	67
3.4.2 MAPPING OF THE EMERGENCY LIMIT CONDITION.....	70
3.5 BUILDING TYPOLOGIES.....	72
3.6 SUMMARY	78
CHAPTER 4. BUILDING SURVEY FORMS FOR HETEROGENEOUS URBAN AREAS IN SEISMICALLY HAZARDOUS ZONES.....	81
4.1 INTRODUCTION.....	81
4.2 BUILDING SURVEY METHODOLOGY	82
4.2.1 TYPOLOGICAL SURVEY FORMS	82
4.3 SURVEY IMPLEMENTATION PLAN	93
4.3.1 PRE-FIELD ACTIVITIES	93
4.3.2 ON-FIELD ACTIVITIES: USE OF THE SURVEY FORMS	95
4.3.3 POST-FIELD ACTIVITIES: DATA MANAGERMENTS AND OUTPUTS	95
4.3.4 CORRELATION AMONG PRE-FIELD, ON-FIELD, AND POST-FIELD SURVEY ACTIVITIES	96
4.4 APPLICATION TO TWO NEIGHBOURHOODS OF THE HISTORICAL CENTRE OF VALPARAÍSO, CHILE.....	99
4.4.1 PRE-FIELD SURVEY	99
4.4.2 ON-FIELD SURVEY	100
4.4.3 SURVEY RESULTS AND STATISTICAL ANALYSIS.....	113
4.5 SUMMARY	122
CHAPTER 5. CALIBRATION OF SIMPLIFIED NUMERICAL MODELS FOR TIMBER FRAMES AND MASONRY WALLS.....	123
5.1 INTRODUCTION.....	123
5.2 BENCHMARK EXPERIMENTAL PROGRAMS FOR CALIBRATION OF TIMBER FRAMES	124
5.2.1 EXPERIMENTAL TESTS ON PORTUGUESE “POMBALINO” TIMBER FRAMES	124

5.2.2	EXPERIMENTAL TESTS ON PERUVIAN “QUINCHA” TIMBER FRAMES	127
5.3	CALIBRATION OF LUMPED PLASTICITY MODELS FOR TIMBER FRAMES	132
5.3.1	LUMPED PLASTICITY FINITE ELEMENT MODEL FOR TIMBER FRAMES	132
5.3.2	NUMERICAL SIMULATION OF EXPERIMENTS ON BARE TIMBER FRAMES.....	134
5.3.3	NUMERICAL SIMULATION OF EXPERIMENTS ON INFILLED TIMBER FRAMES	144
5.4	BENCHMARK EXPERIMENTAL PROGRAMS FOR CALIBRATION OF MASONRY MODELS	157
5.4.1	EXPERIMENTAL TESTS ON IN-PLANE LOADED MASONRY WALLS	157
5.4.2	EXPERIMENTAL TESTS ON OUT-OF-PLANE LOADED MASONRY WALLS	160
5.5	CALIBRATION OF CONTINUUM MODELS FOR MASONRY WALLS.....	162
5.5.1	CONTINUUM FINITE ELEMENT MODEL FOR MASONRY STRUCTURES.....	162
5.5.2	NUMERICAL SIMULATION OF EXPERIMENTS ON AN IN-PLANE LOADED MASONRY FRAME.....	165
5.5.3	NUMERICAL SIMULATION OF EXPERIMENTS ON OUT-OF-PLANE LOADED MASONRY WALLS	171
5.6	SUMMARY	179
CHAPTER 6. NUMERICAL MODELLING OF HYBRID TIMBER-MASONRY BUILDING TYPOLOGIES OF VALPARAÍSO.....		181
6.1	INTRODUCTION	181
6.2	DESCRIPTION AND CHARACTERISATION OF THE BUILDINGS	182
6.3	NUMERICAL MODELS OF THE HYBRID TIMBER-MASONRY STRUCTURES	189
6.4	SEISMIC ANALYSIS OF TWO HYBRID TIMBER-MASONRY BUILDINGS OF VALPARAÍSO	192
6.5	SEISMIC PERFORMANCE OF THE BUILDINGS FOR THE SEISMIC HAZARD IN VALPARAÍSO	200
6.6	SUMMARY	206
CHAPTER 7. SEISMIC VULNERABILITY ASSESSMENT OF HETEROGENEOUS URBAN NEIGHBOURHOODS. APPLICATION TO VALPARAÍSO, CHILE.		209
7.1	INTRODUCTION	209
7.2	PROPOSAL OF A BUILDING FORM FOR THE APPLICATION OF THE VULNERABILITY INDEX METHOD TO HYBRID TIMBER-MASONRY STRUCTURES	210
7.2.1	CALIBRATION OF THE SEISMIC VULNERABILITY FORM	ERROR! BOOKMARK NOT DEFINED.
7.2.2	CALIBRATION OF THE NEW PARAMETERS FOR HYBRID TIMBER-MASONRY BUILDINGS BASED ON NUMERICAL SIMULATIONS	212
7.2.3	PROPOSED SEISMIC VULNERABILITY FORM.....	227
7.3	SEISMIC VULNERABILITY AT THE EMERGENCY LIMIT CONDITION OF THE NEIGHBOURHOODS OF CERRO ALEGRE, CERRO CONCEPCIÓN AND THE PORT IN VALPARAÍSO, CHILE.....	228
7.3.1	EVALUATION OF THE SEISMIC VULNERABILITY	228
7.3.2	FINAL REMARKS.....	234

7.4 SUMMARY	235
CHAPTER 8. CONCLUSIONS	237
8.1 SUMMARY	237
8.2 CONCLUSIONS	240
8.3 MAIN CONTRIBUTIONS	241
8.4 SUGGESTIONS FOR FUTURE WORK.....	243
REFERENCES.....	247

Chapter 1. Introduction

1.1 Background and motivation

The seismic hazard generates large concern due to its potential devastating consequences on urban areas. Human casualties and economic losses caused by the partial or total collapse of the structures represent an extremely concerning issue during major earthquakes. Many cities around the world have recently undergone the effects of major earthquakes in their urban territories, for instance Mamurras (Albania) in 2019, Ambon and Laiwui in Indonesia (2019), Manabí (Ecuador) in 2016, Bio-Bio (Chile) in 2010, Central Italy in 2016, Northern Italy in 2012 and L'Aquila in 2009. After many years, these urban centres have not yet recovered their original functionality due to their extremely low resilience to catastrophic events like earthquakes.

Research on seismic vulnerability of inhabited territories is very important today for two main reasons. First, predicting the impact of earthquakes provides the base knowledge for the development of mitigation strategies aimed to increase the resilience of the cities and reduce the amount of human casualties and critical damage on the vital networks of the city. Seismic risk management is essential to raise the awareness of communities of seismic hazards, and to support decision-making processes in the formulation of civil protection policies and investments. Second, the built cultural heritage concentrated in historical urban centres is critically exposed when located in seismic prone areas. Heritage buildings are especially vulnerable to earthquakes, particularly those built before the release of specific codes for seismic prone areas. Furthermore, cumulative damage on heritage constructions due to past seismic events, progressive ageing of the materials, environmental decay or lack of maintenance may increase their vulnerability against possible seismic events. Therefore, the studies aimed at the assessment of the seismic vulnerability of existing buildings in the historical urban centres constitute a valuable decision support tool for the initiatives of policy-makers and local communities in the preservation of the built heritage (Basaglia et al. 2020).

The seismic vulnerability of a structure is associated with its low performance in the case of the occurrence of an earthquake of certain intensity. The assessment of the vulnerability, together with the knowledge of the possible seismic hazard, permits the estimation of expected damage for potential future earthquakes. The seismic vulnerability assessment procedure of an individual building is based on the evaluation of different structural and non-structural parameters, e.g. distribution of the resisting elements, type and quality of the materials, ground conditions,

presence of structural irregularities, level of maintenance, existing damage, etc. This evaluation aims to determine the influence of each parameter on the global seismic behaviour of the buildings.

During the last decades, the research on seismic assessment methodologies has received significant attention in the academia. The advancements of the studies have promoted the use of several approaches to assess the vulnerability, ranging from individual buildings to large built-up areas. Several methods establish procedures more or less complex in function of the scale and specificity of the case study. The definition of criteria to develop seismic vulnerability studies intrinsically conditions the formulation of the methodology and the evaluation level, that can range from an expedite evaluation based on visual observations, until the most complex computational modelling of individual buildings. The methods for the assessment of the seismic vulnerability are classified into three major groups: empirical, analytical and hybrid methods. *Empirical* methods aim to evaluate a large number of buildings by establishing probabilistic relationships between the observed damage after a seismic event and the macro seismic scales. Different scales of damage categorize the buildings for different seismic intensities. *Analytical* approaches consider direct mechanical relationships between the construction attributes and the structural response by employing numerical simulations of the nonlinear seismic behaviour. The development of advanced numerical models for buildings has received a great attention from the scientific community in the last decades. *Hybrid* approaches combine the use of empirical databases of earthquake damage with analytical results of representative structural models. The pursuit of rigorous methodologies that can be used effectively for the analysis of built-up territories is still an on-going challenge.

Nowadays, different approaches for seismic vulnerability assessment at large-scale are available in the scientific literature (Kassem, Mohamed Nazri, and Noroozinejad Farsangi 2020; Pelà 2018). Among them, the Vulnerability Index Method (VIM) has received a wide acceptance within the empirical approaches, as it allows a simple evaluation of the most fundamental parameters influencing the structural vulnerability of the building. This method assesses the vulnerability of the buildings to seismic hazards by examining multiple quantitative parameters associated with critical structural and non-structural features, e.g. type of resisting system and horizontal diaphragms, presence of irregularities in plan and elevation, characteristics of non-structural elements, and current condition of conservation, among others. The simplicity of the VIM makes it suitable for the large-scale seismic assessment of urban buildings. The technique yields the calculation of a vulnerability index (I_V) for the building, defined as the weighted sum of different parameters, each of them appraising one specific aspect related to the building seismic response. Each parameter is catalogued into 4 classes of growing vulnerability (from A to D) which have a relative score. The weight of each parameter is assigned by judging its influence in the global behaviour of the building. This method, originally developed in Italy (Benedetti and Petrini 1984; GNDT 2007b) for masonry and reinforced concrete buildings, was calibrated based on post-earthquake damage observation and surveyed building data. The original format of the VIM has been later improved by different researchers to include more sophisticated criteria to

classify, score and weigh the parameters (Ferreira, Rodrigues, and Vicente 2020; Cara et al. 2018; Basaglia et al. 2018). New parameters accounting for the interaction between buildings have also been introduced (Formisano et al. 2015). Generally, the VIM is combined with macroseismic approaches to predict the damage grade of the buildings given by an earthquake of certain intensity. This combination correlates the mean damage grade of the buildings with macro seismic scale as a vulnerability function to measure the severity of an earthquake (Giovinazzi and Lagomarsino 2004).

One major problem in the applicability of the VIM consists in the calibration *ex novo* of the scores and weights, as well as the identification of specific parameters, for very peculiar building typologies, e.g. timber frame, steel or hybrid typologies existing in urban areas with heterogeneous building stock. The different available approaches based on VIM have been developed to date for the assessment mainly of masonry and reinforced concrete structures. The extension of the VIM to other structural typologies would require the evaluation of a large amount of data derived from post-earthquake surveys of damaged buildings. This type information is not available in many countries. In addition, the large-scale application of VIM to urban buildings would require the systematic collection of data about their structural characteristics, which are not always available in the local archives of the cities.

The development of advanced numerical analyses may constitute a possible source of information to build novel VIM forms for the cases in which there is a lack of organized information about the past post-earthquake surveys of damaged buildings. Unlike the Italian VIM approach based on the evidence of damage on existing building typologies after a seismic event, it emerges an alternative approach based on the numerical simulation of the seismic performance of urban buildings for different levels of seismic demand to calibrate VIM forms. For this reason, numerical analyses can be used to overcome this drawback by simulating the buildings' seismic behaviour through nonlinear dynamic and static (pushover) analyses. In the latter case, the Capacity Spectrum Method (Freeman, Nicoletti, and Tyrell 1975; Freeman 1998) and the N2 method (P. Fajfar and Eeri 2000) allow the evaluation of the seismic performance by means of the execution of nonlinear static analysis (NSA).

The systematic use of analytical approaches based on advanced numerical simulations is not feasible for the large-scale assessment of urban buildings, due to the complexities of the models preparation and the huge cost for executing all the analyses. A possible solution to overcome the aforementioned problems may be the adoption of a two-stage hybrid approach. The development of a rigorous building taxonomy of the recurrent structural typologies in an urban area can provide useful information for the identification of the most representative types of buildings within the area under study. This preliminary activity can lead to optimize the second stage of structural analysis by analytically modelling only specific benchmark structural systems. A sensitivity analyses performed with these benchmark models, by varying specific structural features (e.g. number of storeys, type of floors, presence of irregularities, etc.), can lead to the evaluation of the

influence of some specific parameters on the seismic response of the different building categories, providing useful information for the preparation of the VIM forms.

As this procedure implies the execution of a high number of structural analyses, the adoption of simplified structural models is of paramount importance. A good compromise between accuracy and acceptable computation effort seems the adoption of continuum Finite Element Models (FEM) for buildings composed of load-bearing walls, as well as the use of Lumped Plasticity Models (LPM) for the representation of framed structures.

After considering all the issues reported above, we can identify three different challenges associated with the seismic vulnerability assessment of urban centres with heterogeneous building stocks. The first one is the formulation of a rigorous strategy for the systematic acquisition of the buildings' data essential to feed the seismic vulnerability assessment, aimed to construct a complete building taxonomy of a large amount of buildings in urban areas. This task is essential especially for historical centres lacking of comprehensive building databases or with archives characterised by fragmentary information. The second challenge is the calibration of simplified but robust nonlinear structural models able to represent the seismic behaviour of different types of urban buildings. Although there are different possibilities available in the scientific literature for reinforced concrete, steel and masonry structures, the state of the art is still lacking of specific numerical modelling methods for the practice-oriented simulation of the seismic behaviour of timber frame and hybrid timber–masonry buildings, which often exist in historical centres worldwide. The third and last challenge consists in the calibration of the VIM for urban areas with heterogeneous structural typologies including timber frame and hybrid timber–masonry buildings, as these types of buildings have not been addressed exhaustively in the current research yet.

The three aforementioned tasks constitute the main motivation of this doctoral thesis. After addressing such topics, the research deals with the analysis of three neighbourhoods of the historical centre of the city of Valparaíso, Chile. This UNESCO World Heritage Site comprises different types of heritage buildings where timber–masonry traditional structure predominates.

1.2 Scope and objectives

The primary objective of this thesis is to develop and validate a seismic vulnerability assessment method for the analysis of traditional timber–masonry buildings located in urban historical centres, as those existing in the city of Valparaíso, Chile. The research contributes to the formulation of a novel hybrid seismic vulnerability assessment method, based on the development of nonlinear analyses of representative typologies of timber–masonry buildings and the subsequent definition of relevant VIM forms. The entire procedure is fed by information systematically organized through the adoption of ad-hoc building survey forms for heterogeneous urban areas including masonry, reinforced concrete, and hybrid timber frame–masonry wall structures.

A set of specific objectives are defined towards the accomplishment of the primary objective, which extends to all the aforementioned fields:

- Compile comprehensive state-of-the-art information concerning seismic vulnerability assessment methods developed for the large-scale evaluation of urban historical centres.
- Characterize the structural typologies located in the study area of the historical centre of the city of Valparaíso, Chile. This part includes two sub-objectives:
 - To identify the study zone by establishing an Emergency Limit Condition (ELC) system which includes emergency routes, strategic buildings for the emergency phase, and potential interfering buildings in case of partial or total collapse.
 - To develop a set of building survey forms to collect essential information for the seismic vulnerability assessment of urban buildings by creating a complete taxonomy which classifies relevant factors such as building morphology, structural configuration, damage, presence of irregularities, and current condition of the building.
- Develop practice-oriented numerical models capable of predicting the behaviour of masonry, timber frame and hybrid timber–masonry structures. This task involves the following three sub-objectives:
 - To gather information from the available scientific literature about numerical approaches suitable for the modelling of masonry and timber frame structures.
 - To calibrate and validate the models by comparing the predicted responses with benchmark experiments on different types of masonry and timber frame structures.
 - To apply the validated models to two representative cases-studies of real existing buildings located in the study-area of the city of Valparaíso (Chile).
- Calibrate a VIM form for hybrid timber–masonry buildings consistent with those available in the scientific literature for other structural typologies. The calibration procedure includes the following sub-objectives:
 - To re-examine the influence of the parameters usually included in the available VIM forms on this new building typology.
 - To develop a parametric analysis using the validated numerical models to study the influence of different geometric and physical parameters on the global seismic response of the buildings.
 - To assign consistent scores, classes and weights to the re-examined parameters in the proposed VIM form for timber–masonry buildings.
- Develop the seismic vulnerability analysis of the ELC system in the city of Valparaíso (Chile) by applying the calibrated VIM form.
- Create seismic vulnerability maps by using the Geographic Information System (GIS) to present a global picture of the results at the urban scale.

Even though special emphasis is set on timber frame and hybrid–timber masonry structures representatives of the city of Valparaíso, the proposed methodology and developed tools may be applied to other neighbourhoods of the city, as well as to similar urban centres in other countries.

1.3 Outline of the thesis

After this introductory chapter, the thesis is organized in seven chapters in the following way.

Chapter 2 provides a state of the art about the seismic risk assessment at large-scale, including a literature review focused on the seismic vulnerability assessment methodologies for buildings. An overview of the numerical simulation methods for the modelling of timber frame and masonry structures are also included in this chapter.

Chapter 3 includes a brief overview of the three neighbourhoods of the historical centre of the city of Valparaíso, Chile, which is examined in this thesis. Available data on the historical background and seismic hazard of the city are compiled. The Emergency Limit Condition (ELC) of the studied zone is established, followed by a preliminary description of the building typologies belonging to three selected neighbourhoods of the city.

Chapter 4 presents the formulation of a data-collection survey methodology to gather necessary information for the seismic vulnerability analysis of the buildings. An original methodology is presented, which includes the development of four different typological survey forms for masonry, reinforced concrete, timber frame and steel structural systems. A survey implementation plan that comprises pre-field, on-field, and post-field activities is included in the methodology. The results of the application of the proposed methodology to the ELC system of Valparaíso are presented, as well as the statistical analysis of 111 buildings with the comprehensive characterization of the most representative structural typologies within the building stock derived from the survey activity.

Chapter 5 focuses on the calibration of simplified numerical models for timber frame and masonry wall structures. The chapter is divided into two different parts. First, benchmark experimental programs on bare frame and infilled *Pombalino* and *Quincha* walls are described for the calibration of the timber frame models. The calibration of Lumped Plasticity Models (LPM) simulating the behaviour of the tested timber frame walls is detailed. Second, benchmark experimental programs, consisting in in-plane and out-of-plane loaded unreinforced masonry walls, are detailed for the definition of the models for masonry structures. The calibration of the continuum Finite Element Models (FEM) to simulate the response of the tested walls is detailed. Each section reports information about the material models, the constitutive laws, and discussion on the results in terms of capacity curves and failure mechanisms.

Chapter 6 presents the structural application of the calibrated numerical models to two representative real buildings existing in the historical centre of Valparaíso (Chile). The chapter includes the modelling of hybrid LPM and continuum FEM to represent the structural arrangement of the buildings under study. Seismic analyses of both the case studies provide the capacity curves along the two main directions of the building, as well as the failure mechanisms. The seismic performance of the buildings is analysed by applying the N2 Method by considering two response spectra: the one defined by the Chilean seismic standards (NCh433), and the one derived from the 2010 Earthquake in the city of Valparaíso.

Chapter 7 reports the seismic vulnerability assessment of the ELC system of the city of Valparaíso. A calibrated VIM form is developed for timber–masonry building typologies located in the analysed ELC system, and used together with the VIM forms available for other structural systems, such as reinforced concrete and masonry buildings. The calibration of the VIM form is based on a parametric numerical analysis, which allows the assignment of classes, scores and weights to the re-examined parameters. The vulnerability index results are graphically represented in seismic risk maps by using a GIS method.

Chapter 8 provides an extended summary, the main contributions, and the final conclusions derived from this doctoral thesis. Suggestions for future works are also pointed out.

1.4 Research dissemination

The work included in this thesis has resulted in the following scientific publication at the moment of the doctoral thesis submission:

- Jiménez B., Pelà L., and Hurtado M. (2018). “Building Survey Forms for Heterogeneous Urban Areas in Seismically Hazardous Zones. Application to the Historical Center of Valparaíso, Chile”. *International Journal of Architectural Heritage* 12:7-8, 1076-1111. <https://doi.org/10.1080/15583058.2018.1503370>.

Chapter 2. Literature Review

2.1 Introduction

This chapter presents a literature review of the seismic vulnerability assessment (SVA) approaches commonly included in seismic risk estimation models aiming at evaluating the potential consequence of major earthquakes in built-up areas. Due to the high importance of the seismic risk management of inhabited sites, the engineering community has shown an increasing interest in determining accurate models to predict the potential level of damage affecting the buildings in case of earthquakes. Seismic risk models (SRM) for large-scale assessment comprise different systematic phases of analysis aimed to determine the level of vulnerability of the exposed assets and to develop management strategies to increase the resilience of the cities. An accurate evaluation of the seismic vulnerability of the buildings constitutes an essential part of SRM, since it provides the base knowledge to develop multiple risk studies, such as quantifying the socio-economic impacts of an earthquake, estimate the repair cost, and develop localized strengthening solutions of the most vulnerable buildings to mitigate the risk.

Estimating the vulnerability of existing buildings at the urban scale is a complex task since it requires the knowledge of the great variety of construction typologies, especially in urban areas with heterogeneous building stock and historical constructions. Therefore, this type of analysis is strongly influenced by the nature and suitability of the selected vulnerability assessment method, as well as the amount and quality of the available building data.

This review attempts to explain the most renowned vulnerability methods for existing buildings in urban areas aiming at identifying an appropriate procedure for the assessment of urban areas with heterogeneous and historical buildings stock, including timber frame and masonry buildings. Besides, a review of the existing numerical methods for seismic vulnerability assessment of timber and masonry buildings including hybrid typologies is included in this chapter.

After a brief introduction (Section 2.1), the elemental concepts involved in seismic risk models are presented, followed by a general overview of the existing approaches developed to addressing the problem of risk estimation in large-scale applications. Subsequently, a comprehensive perspective of the concept of vulnerability assessment (Section 2.3) is introduced, including the early theoretical research and evolution of the methods existing to this aim. Among them, particular emphasis is given on the development of the Vulnerability Index Method (VIM) towards hybrid methodologies including numerical assessment. Section 2.4 focuses on building survey

strategies inherent to the SVA procedures. Lastly, Section 2.5 presents the existing numerical methods for the analysis of the seismic vulnerability of timber frame (Section 2.5.1), masonry (2.5.2) and hybrid timber-masonry structures (Section 2.5.3).

2.2 Seismic risk assessment models for built-up areas

2.2.1 Fundamental concepts

Seismic vulnerability studies are essential parts of seismic risk assessment (SRA) at large scale aiming to evaluate the potential consequences of major earthquakes on the vital function of the cities. On this basis, some relevant concepts are briefly explained in the present section.

Different authors have attempted to describe the main concepts involved in risk assessment analysis. According to the report of *Natural Disasters and Vulnerability Analysis* (UNDRO 1979) the term *risk* is strongly linked to the expected number of lives lost, person injured, damage to property *and* disruption of economic activity as consequences of a natural disaster. Coburn and Spence (2002) have conceptualized the seismic risk (R) as the convolution of hazard (H), vulnerability (V) and exposure (E) of the elements, as shown in Equation (2-1):

$$R = (H \times V) \times E \quad (2-1)$$

where R is the probability of exceedance of a certain level of loss of an exposed element as a consequence of the occurrence of a seismic event of intensity I, H is the probability of exceedance of a certain level of seismic activity of intensity I, V is the vulnerability, i.e. the intrinsic predisposition of a certain element to suffer damage resulting from a seismic event of intensity I, and E is the exposure of the elements at risk. The *seismic hazard* (H) depends on the characteristic of a seismic event and the geological characteristics of the area where the event is expected to occur.

The concept of *vulnerability* (V) can be defined as the characteristic of a community, system or asset that makes it susceptible to the damaging effects of a hazard, that means the “state of the reality” that underlies the concept of risk. According to Khazai et al. (2015), the measurement of the vulnerability is related to the degree of exposure, susceptibility, fragility and lack of resilience of a system that favours adverse effects. The exposure (E) is related to people, property, systems, activities, or other elements present in hazard zones that are thereby subjected to potential losses, e.g. buildings, infrastructure, and population density. From the civil engineering standpoint, this concept has been materialized in the developments performed in the field of the physical risk to management proposes.

According to UNISDR (2009), the term *natural hazard* describes a process or phenomenon that may cause loss of life, injury or other health impacts, property damage, loss livelihoods and services, social and economic disruption, or environmental damage. Different approaches are

available to evaluate the seismic hazard of specific territories, which are commonly classified into two groups: the deterministic (DSHA) and the probabilistic (PSHA) approaches. DSHA considers past earthquake scenarios that limits the study of important variables such as magnitude, distance, number of standard deviations of ground motions, etc. PSHA considers all possible seismic scenarios and ground motion levels of an area and compute rates of each scenario. The latter does not combine ground motions of different earthquakes but rank them combining the chance of getting specified scenarios, considering the effect of all the possible sources of seismic hazard in the territory. Another strategy to represent the hazard is the *seismic microzonation* defined as the process of subdividing a potential seismic prone area into zones with similar geological and geophysical characteristics. This tool aimed to contrast the seismic hazard at different locations of a territory, considering factors as ground shaking, liquefaction susceptibility, landslide and rock fall, and earthquake-related flooding. Generally, seismic microzonation is based on the dynamic characterization of the soil by recording or estimating the amplitudes of the ground accelerations. These features are commonly mapped into a closely spaced grid of the study area, and groups the sub-areas according to the predominant hazard (Gupta 2002). Such maps provide the basis for site-specific risk analysis and are very useful to characterize the seismic indicators involved in vulnerability assessments.

The concept of *risk management* comprises the definition of a methodology to determine the nature and extent of risk of inhabited areas, becoming population and government prepared for potential hazard and future disasters. In this framework, seismic risk models for urban assessment usually involve a systematic series of working stages, as shown in Figure 2-1, including the seismic hazard identification, the vulnerability assessment of the exposed buildings, the analysis of loss estimation, and the development of risk mitigation strategies. Each phase of the model comprises different evaluation strategies, which need to be carefully defined by the analysts or the stakeholders by taking into account important factors, such as the scale and scope of the assessment and the available information. The main objective of SRA is to increase the resilience of the cities by detecting previously possible situations of vulnerability that may harm exposed people, properties, services, livelihoods and the environment.

Cities are very complex systems, in terms of morphology and functionality, since they are composed of numerous elements or subsystems working together to guarantee the correct functioning of the whole network (Oliveira 2016). Therefore, in the seismic risk analysis of built-up areas, the different exposed elements have to be judiciously analysed. Staniscia, Spacone, and Fabietti (2017) proposed a performance-based methodology aimed to guarantee the vital and minimum essential functioning of cities after earthquakes. The study introduced the concept of Minimum Urban Structure (Fabietti 1999) as the minimum amount of elements that must remain functional after major earthquakes. This concept recognizes the needs to establish a certain hierarchy in the urban system components and to define acceptable risk (or performance) levels.

The main components of the urban network that define the minimum urban structure are strategic buildings, roads, and open spaces working together to connect the city. These relationships have to be deeply analysed to determine the Emergency Limit Condition (ELC) of a city. For instance, streets next to high-rise buildings constitute a primary concern, as they may potentially collapse and block vital routes (e.g. those of evacuation in case of tsunami) or important ways to strategic buildings (e.g. hospitals, fire stations, etc.). The identification of these vital sub-systems in the urban fabric contributes to optimize the seismic risk analysis in territories with a large number of buildings.

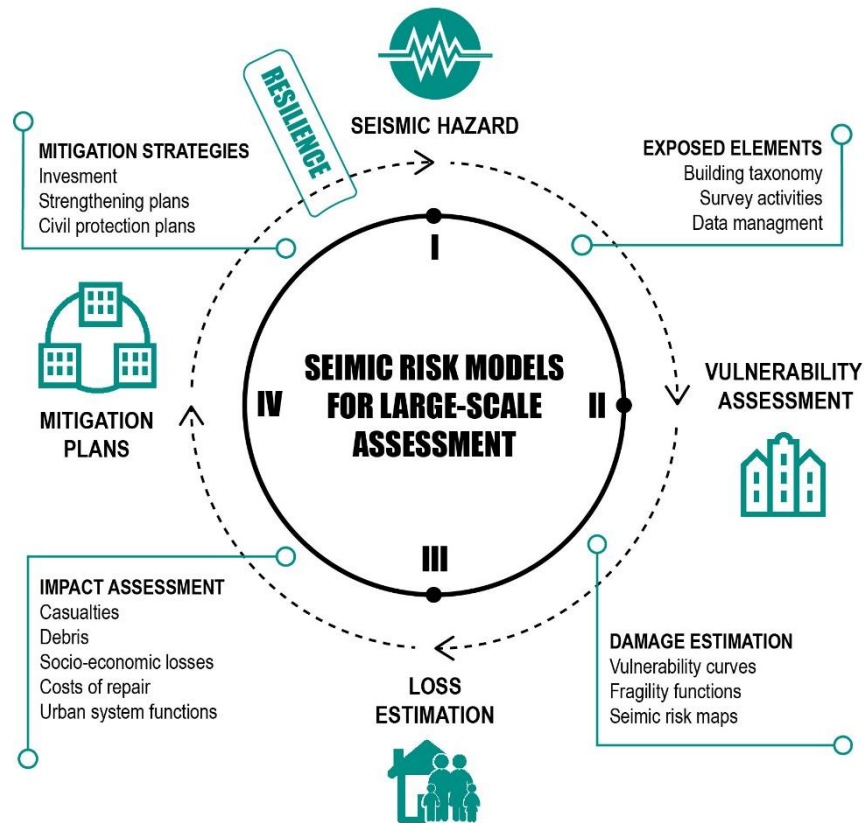


Figure 2-1. Main work stages and activities involved in models for large-scale assessment of the seismic risk.

2.2.2 Seismic risk assessment models

Different initiatives have proposed SRM frameworks to evaluate the seismic risk of urban centres from a holistic standpoint. These models are generally based on determining if the buildings and infrastructures are adequately designed and built to resist seismic forces (ASCE 2014) or, in other words, on estimating their seismic vulnerability.

For instance, a remarkable case is the European Risk-UE project (Mouroux et al. 2004) which proposed a standard guideline to perform an integrated assessment of the seismic risk in built-up areas. This model includes systematic work stages to evaluate the seismic hazard, urban systems configuration, vulnerability of the buildings and lifelines and seismic risk scenarios. For the

implementation of the method, the researchers responsible to apply them are free to deliberate their own way to analyse the vulnerability and damage grade of the buildings to obtain the expected results. The proposed model was implemented in seven eastern and western European cities named Barcelona, Catania, Bitola, Nice, Sofia and Thessaloniki. For the study of the city of Barcelona, carried out by M. N. Lantada (2007), different methods to estimate the vulnerability of the buildings were adopted. Firstly, the indirect Vulnerability Index Method (VIM) was implemented by analysing the available data of the Municipal Informatics Institute (MII) through the service of Civil protection of Barcelona Government. Afterwards, a most detailed analysis was employed based on the Capacity Spectrum Method (CSM) aiming at simulating the seismic response of some representative samples of the building stock. Geographic Information System (GIS) databases were implemented to manage and analyse the building information, and to create seismic risk maps that permitted an overall understanding of the vulnerability of the buildings and the expected losses in a territorial scale, as shown in Figure 2-2. The obtained results were in agreement with the historical evolution of the city, its current state and the characteristics of the soils. In general terms, a radial structure of damage was revealed from the centre of the city, where the oldest neighbourhoods are located, as shown in Figure 2-2a. In this case, the number of casualties (Figure 2-2b), debris and severe injured people were estimated by applying the Casualty Ratio Model developed by Coburn and Spence (2002). The above, considering a probabilistic scenario by taking into account the vulnerability of the building typologies and the population density (N. Lantada et al. 2010). The absolute cost scenario was also performed by considering the repair cost per unit area (Figure 2-2c). Similar approaches were derived for the remaining cities comprising the Risk-UE procedures, including the use of the EMS-98 scale, fragility curves and the Macroseismic Method (Giovinazzi and Lagomarsino 2004).

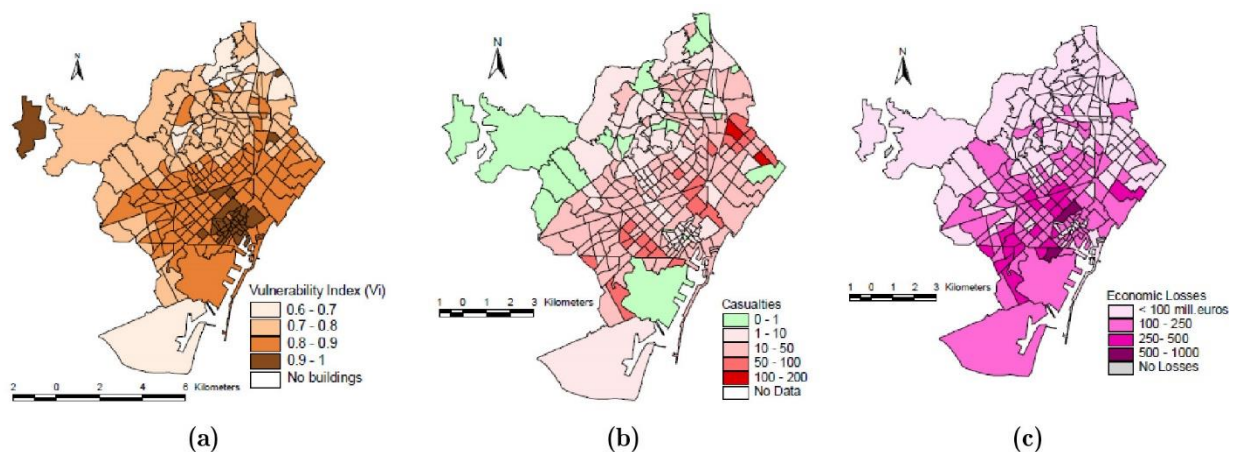


Figure 2-2. RISK-UE application in the city of Barcelona: (A) Vulnerability Index, (b) casualties and (c) costs and economic losses maps (Mouroux et al. 2004)

Another remarkable SRM was proposed in the framework of the HAZUS project (FEMA 2003) by the Federal Emergency Management Agency (FEMA) of the United State to estimate the potential losses from multi-hazard disasters in the cities. The proposed framework of the model

considers the development of comprehensive work stages which involves data-collection and classification strategies, seismic hazard models, direct physical damage of buildings, life-lines transportation systems, utility systems, and inundations studies. Furthermore, models for estimating debris and casualties' consequences due to hazard as well as loss of housing habitability, shelter need and economic loss models are integrated in the proposed guideline.

For the seismic vulnerability assessment and damage grade estimation of the buildings in built-up areas, the application of nonlinear analysis and the construction of fragility curves is recommended. These evaluations are preceded by the classification of the essential facilities of the urban area in order to define the scope of the analysis in case of large exposed elements populations. As in the previous SRA, this initiative also prompts the use of GIS technology to implement models for estimate loss and create seismic risk maps.

The SYNER-G project (Pitilakis et al. 2014) releases a guideline for the seismic risk management in urban areas. SYNER-G proposed a methodology starting from previous research on the seismic risk and vulnerability assessment of urban systems (buildings, lifeline networks and critical infrastructure) at international and European levels, which focused on the vulnerability of individual elements at risk. The goal of the project was to overcome the uncertainties associated with the use of fragility curves models proposed for their application in European countries. The proposed guideline aims to carry out systematic and holistic evaluations of the seismic risk towards the estimation of losses and socio-economic impacts at urban scale.

The proposed methodology consisted in the physical vulnerability assessment of the buildings through the use of statistical or probabilistic vulnerability functions, which represent the “typical” behaviour of a group of buildings characterized by a limited number of similar physical parameters (Pitilakis et al. 2014). Consequently, the definition of a preliminary description of the domain under study is proposed by establishing a detailed taxonomy of the systems, i.e. building typologies or infrastructure (Hancilar, Taucer, and Corbane 2013). The building taxonomies were the guidance for the following work stage packages, where typological fragility models and loss estimations are required.

The methodologies for the systemic vulnerability assessment of complex urban areas are not strictly defined in this model, and they can vary depending on the aim and scale of the analysis, as well as the available building data in the cities. In general terms, this assessment involves: (i) the definition of building taxonomies and census within the study area and (ii) the derivation of damage probability matrix or fragility curves that correspond to a certain typology. Different models are proposed to estimate the building damage, usability, habitability, as well as expected casualties and debris towards the development of socio-economic and loss estimation analysis. This model was integrally applied to the cities of Thessaloniki (Greece) (Figure 2-3) and Vienna (Austria) where most of the lifeline systems and buildings were assessed (Pitilakis et al. 2014).

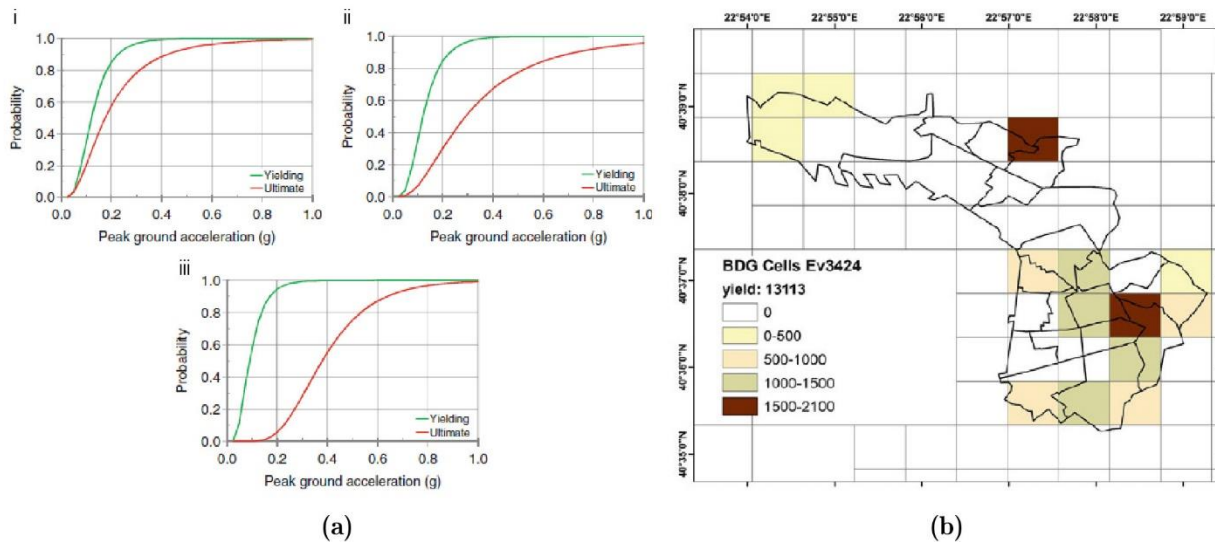


Figure 2-3. SYNER-G implementation in the city of Thessaloniki (Greece): (a) fragility curves for i) low-level, ii) medium-level and iii) high-level seismic code, and (b) distribution of estimated building damages into cells of the study area for a seismic event of $M=6.5$ (Pitilakis et al. 2014)

Most recently, other authors provide remarkable knowledge around seismic risk estimation models i.e. Khazai et al. 2015, Basaglia et al. 2020, and Fraume et al. 2020, among others. The latter considers the use of innovative strategies to analyse socioeconomic indicators and macroeconomic flows variables available in worldwide databases for more than 200 countries and territories by following the conceptual framework shown in Figure 2-4. This assessment aims to recognise risk drivers, which are associated not only to the physical vulnerability of countries' assets, but also to social, economic and financial issues that should be examined and tackled in a comprehensive way.

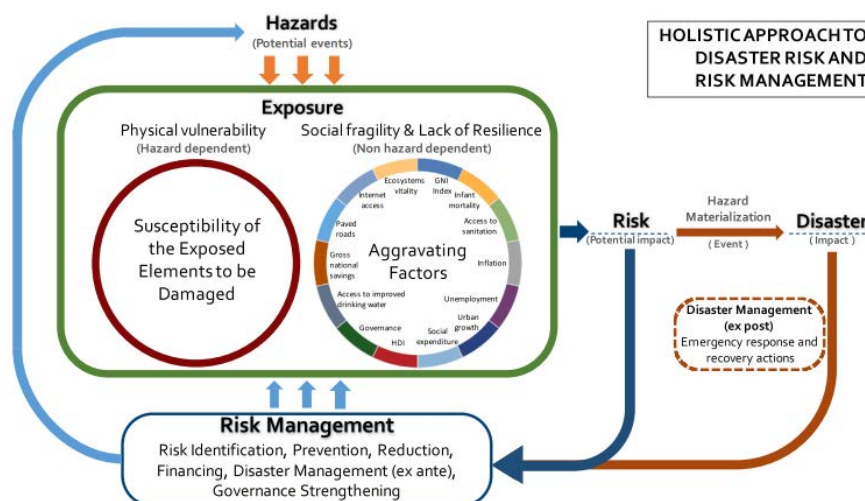


Figure 2-4. Conceptual framework of the holistic approach to disaster risk (Fraume et al. 2020).

2.2.3 Data management and GIS mapping strategies

Seismic risk assessments at the urban scale normally involve the analysis of detailed technical documentation that requests the management of a large amount of information. Geographic Information Systems (GIS) represent a very useful technology that permits to create georeferenced databases which facilitate the inventory, valuation and visualization of the output processes from seismic risk assessment at territorial scales. Besides, georeferenced maps can be easily produced in GIS environments, allowing the visualisation of the data in the territory. Mapping information is highly useful for decision-maker activities related to risk management and mitigation plans aimed to reduce the potential effects of earthquakes and to safeguard the vital network of the inhabited areas. Most of the seismic risk models presented in Section 2.2.2 applied GIS tools to organize the data and seismic risk maps (see Figure 2-2).

The implementation of GIS environments required the use of commercial software developed to manage georeferenced data and mapping activities. For instance, ArcGIS (ESRI) is a powerful mapping and spatial analytic technology usually implemented for seismic risk assessment. GIS maps related spatiotemporal locations of unequivocal elements (vectors or rasters) that represent territorial items, such as buildings or streets, linked to alphanumeric information gathered in databases' attributes. They are non-spatial characteristics that describe spatial entities of a group of features linked to the elements through an ID number in the database. That means that each attribute belonging to a certain group has a one-to-one relationship with the associated shape record, and all together represent a layer of data. Multiple layers can be used to characterize a territory in GIS environments (see Figure 2-5), interlocking in the sense that they are all georeferenced to true geographic space i.e. census data, socio-economic indicators, number of people, etc. The spatial data inherent contains geometric and topological properties, i.e. position and measurements (length, direction, area and volume), thus, spatial analysis can be developed based on these topological relationships such as connectivity inclusion and adjacency among the elements and data within the layers.

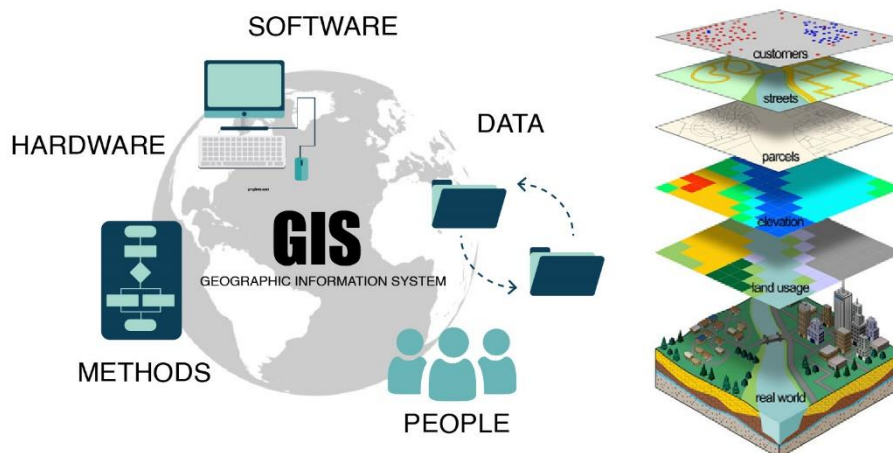


Figure 2-5. GIS environment and layer information concepts.

GIS implementation greatly improves the efficiency and coordination of seismic risk activities that include robust data analytic. Mapping the risk allows to localize the damage level distribution on inhabited areas and draw strategic and localized action lines to increase the resilience of the cities and also heighten community awareness. Nowadays, there is an increasing effort by cities to implement GIS databases and manage the existing information related to census, socio-economic indicators, and building stock within the territory. The availability of this data represents a huge advantage to start creating seismic risk management knowledge in the cities.

2.3 Seismic vulnerability assessment methods

Numerous methodologies have been developed in the last decades to determine the seismic vulnerability of the buildings both in single and large-scale assessments. Nowadays, there are no straightforward procedures to carry out such evaluations, especially in large-scale studies, since there are many factors involved and ways to set out the problem. Therefore, seismic vulnerability assessment methods must be carefully selected based on the scope and objectives of the investigation, as well as the available resources e.g. technical building databases, technology, examiners, etc.

Several methodologies are available for the seismic vulnerability assessment of existing buildings. Great effort has gone to classified these methods in the literature based on different criteria, such as the nature and objectives of the assessment, the availability and quality of the available building data, the scale of evaluation, the methodology criteria, and the reliability degree of the results and their use in practice (Herrera et al. 2013). For instance, Calvi et al. (2006), Herrera et al. (2013), Pitilakis et al. (2014) and Panagiotis and Vagelis (2015) agree in classifying them into *Empirical*, *Analytical* and *Hybrid* methods. The first two classes are also known as Indirect and Direct methods. The following sections present an overview of the most renowned methods belonging to each class with the aim of elucidating their feasibility to different case studies. The focus of this review is on the methods contained in the theoretical framework of this thesis.

2.3.1 Empirical Methods

Empirical or *indirect* seismic vulnerability methods are based on the establishment of probabilistic relationships between observed post-earthquake building damaged data and macro seismic scales. These methods are considered to be the most affordable for large-scale evaluations. According to Calvi et al. (2006), they are two main types of empirical methods that are based on damage after earthquakes, the damage probability matrices (DPM) and the vulnerability functions. The former express in a discrete form the conditional probability of obtaining a damage level due to a ground motion intensity. The second are continuous functions expressing the

probability of exceeding a given damage state, given a function of the earthquake intensity (Calvi et al. 2006).

The original concept of DPM, introduced by Whitman, Reed, and Hong (1974), is that a given structural typology will have the same probability of being in a given damage state in a given earthquake. Figure 2-6 shows the first DPM calibrated for Reinforced Concrete (RC) buildings by Whitman, Reed, and Hong (1974), using the damage surveyed data of 1600 buildings in the San Fernando earthquake (California USA, 1971). The classification of the building stock was based on a subjective description of physical damage and an objective ratio of repair cost to replacement cost of the buildings. The degree of damage of the buildings is expressed in probabilistic terms for each intensity (in Modified Mercalli scale) of the earthquake. Other initiatives, also considering the definition of DPMs based on expert judgment such as ATC-13 (ATC 1985). In this approach, more than fifty senior earthquake engineering experts were asked to define the damage factor for the MM Intensity from VI to XII for 36 building typologies, based on the ratio of loss to replacement cost expressed in percentage. Several applications of the ATC-13 DPM were successfully carried out in other cities such as Basel, Switzerland (Fah et al. 2001), Bogotá, Colombia (Cardona and Yamin 1997) and New Madrid, USA (Kunnumkal et al. 2002).

Damage State	Structural Damage	Non-structural Damage	Damage Ratio (%)	Intensity of Earthquake				
				V	VI	VII	VIII	IX
0	None	None	0-0.05	10.4	-	-	-	-
1	None	Minor	0.05-0.3	16.4	0.5	-	-	-
2	None	Localised	0.3-1.25	40.0	22.5	-	-	-
3	Not noticeable	Widespread	1.25-3.5	20.0	30.0	2.7	-	-
4	Minor	Substantial	3.5-4.5	13.2	47.1	92.3	58.8	14.7
5	Substantial	Extensive	7.5-20	-	0.2	5.0	41.2	83.0
6	Major	Nearly total	20-65	-	-	-	-	2.3
7	Building condemned		100	-	-	-	-	-
8	Collapse		100	-	-	-	-	-

Figure 2-6. Damage Probability Matrix proposed by (Whitman, Reed, and Hong (1974)).

The Vulnerability Index (VIM) method is another empirical approach originally introduced by Benedetti and Petrini (1984) to evaluate seismic vulnerability of the heritage masonry buildings at large-scale using vulnerability functions. This method is considered as “indirect” because a relationship between the seismic action and the response is established through an index (Calvi et al. 2006). The fundamentals of the methods grown after the devastating 1976 Friuli Earthquake (Italy) in the needed to have scientific support aimed to address seismic risk mitigation plans and building retrofiting interventions at territorial levels. Benedetti and Petrini (1984) evidenced that large-scale initiatives require a consistent level of knowledge regarding the vulnerability of the building stock as essential data to develop risk mitigation plans and retrofiting. Responding to this need, the VIM method proposes a vulnerability study by attributing a numerical value to each building representing the seismic quality of the building itself (Benedetti and Parisi 1988). A vulnerability index is obtained as a weight sum of the numerical values expressing the seismic

quality of those structural or non-structural elements which are determined to play a significant role in the seismic response of the building. The method formulated a typological survey form to evaluate the buildings, in a systematic and speedy way, considering ten structural and non-structural parameters which could potentially affect the seismic behaviour of the buildings.

The evaluation of the parameters are related to the configuration of the structural system, irregularities, interaction with the terrain, storeys and roof systems, state of conservation and secondary elements of the buildings as listed in Table 2-1. The multiple situations that can exist in the reality for each parameter are grouped into four classes of increasing vulnerability, from A to D. The Class A represents the cases that considerably comply with current seismic regulations, while class D contemplates the most unfavourable conditions, increasing the score from 0 to 45. A weight is assigned for each parameter reflecting their relevance within the global response of the building as: primary, important and secondary. The elements within the primary group have a weight of 1.5, the important elements are between 1 and 0.5, and the secondary ones lower than 0.5. Also variable weights are considered to be determined by the analyst. The VIM is calculated as the weighted sum of the relative score of each parameter, as defined in the equation in Table 2-1. The I_V can vary from 0 to 371.25, if the variable weights are defined as 1. This value is usually normalized from 0 to 1 considering the maximum vulnerability index equal to 1.

Table 2-1. Vulnerability Index survey form for masonry buildings defined by Benedetti and Petrini (1984).

	Parameter	Class $C_{v,i}$				Weight W_i	Vulnerability Index
		A	B	C	D		
1	Organization of vertical structures	0	5	20	45	1,0	$I_V = \sum_{i=1}^{11} C_i \cdot W_i$
2	Nature of vertical structures	0	5	25	45	0,25	
3	Building position and foundations	0	5	25	45	0,75	
4	Distribution of the resistant elements	0	5	25	45	1,5	
5	Plan regularity	0	5	25	45	0,5	
6	Elevation regularity	0	5	25	45	var	
7	Storey systems	0	5	15	45	var	
8	Roof system	0	15	25	45	var	
9	Non-structural elements	0	0	25	45	0.25	
10	Current state	0	5	25	45	1,0	

It is important to mention that vulnerability index is not a damage indicator by itself since its computation is not correlated to damage scales nor seismic indicators. Therefore, subsequent correlations between the relative vulnerability index and the seismic hazard of a particular site is required to estimate the damage grade of the buildings. This correlation was investigated by Baenedetti and Parisi (1988) as a measure of the health status of buildings based on regional application of the VIM versus the reported damage after different earthquakes in Italian areas, such as the Friuli (1976) and Gubbio (1983) earthquakes. Different earthquake intensities (MSK) were considered to proposed deterministic correlations between the seismic input and the expected

damage. Figure 2-7 displayed the obtained vulnerability functions derived from the correlation expressing the percentage of damage conditions for a given MSK intensity and the vulnerability index. Indicators for prior strengthening interventions were also suggested by the authors to identify those structural items which play a more significant role in the global damage of the buildings and their cost of repair.

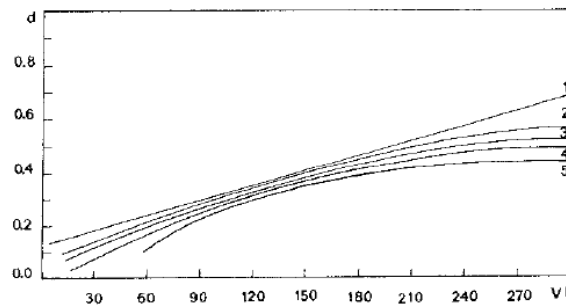


Figure 2-7. Vulnerability functions derived for different earthquake intensities (1 to 5) in terms of observed damage grade (0 to 1) and the Vulnerability Index (VI) from Gubbio and Friuli Earthquakes (Benedetti and Parisi 1988).

Different variations of the VIM method have been developed in the last years with the aim to include new parameters of evaluation or even calibrate new forms for other structural typologies (Indirli 2009; Formisano et al. 2015; Basaglia et al. 2018; Cara et al. 2018; R. Vicente et al. 2008; L. G. F. Salazar and Ferreira 2020).

The *Gruppo Nazionale per la Difesa dai Terremoti* (GNDT 2007a) contributed to improve the systematic application to the method by formulating practical survey forms and manuals to inspect and compute the vulnerability index of the buildings (GNDT-II level). These tools are aimed to facilitate the evaluation and data-collection procedures providing graphical guides to assess and classify the parameters of the buildings and compute the vulnerability index. GNDT-II also proposed a new vulnerability form for RC buildings belonging to the traditional building heritage of Italy. In this form, the definition criteria of the parameters and the classes were calibrated considering the expected behaviour of this particular resisting system. In this case, two new critical parameters influencing the seismic response of RC buildings were included: P8 “Connections and critical elements” and P9 “Elements with low ductility”. The parameters of the form are divided only into 3 classes from A to D.

Most recently, Formisano et al. (2015) upgraded the VIM method considering the assessment of masonry buildings in structural aggregates. This feature is very typical in cities, not only in Italy but worldwide. Buildings raised in continuity represent a challenge in the study of their vulnerability since distinguishing their structural independency is often a very difficult task, as well as identifying the global response of the whole compound. In this regard, Formisano et al. (2015) argue that the “aggregate effect” can influenced the seismic behaviour of the buildings in two ways: globally, since the force distribution obtained from the analysis of each building is

different from the one calculated in a whole compound, and locally, considering pounding damages due to change of building stiffness. The structural interaction among adjacent masonry buildings was defined by including the five parameters listed in Table 2-2 to the original form for masonry buildings proposed by Benedetti and Petrini (1984) (see Table 2-1). In order to achieve a form totally homogeneous to the original one, the scores and weights assigned to each new parameter were calibrated by developing a numerical investigation by employing a hybrid vulnerability assessment method named the N2 method (P. Fajfar and Eeri 2000). The methodology considers the sensitivity analysis of a reference physical masonry model defined through the Equivalent Frame Method (EFM) of a typical masonry aggregate of Sessa Arunca, a small city within the Campania region in Italy (Formisano et al. 2015). An isolated building unit (Figure 2-8a) was evaluated by inserting it in different aggregate scenarios to determine the boundary conditions of each parameter, as shown in the example of Figure 2-8b.

Table 2-2. New parameters to assess the masonry buildings in aggregate condition proposed by Formisano et al. (2015).

Parameter	Class				Weight
	A	B	C	D	
1 In elevation interaction	-20	0	15	45	1
2 In plan interaction	-45	-25	-15	0	1.5
3 Number of staggered floors	0	15	25	45	0.5
4 Structural or typological heterogeneity among adjacent structural units	-15	-10	0	45	1.2
5 Percentage difference of opening areas among adjacent facades	-20	0	25	45	1

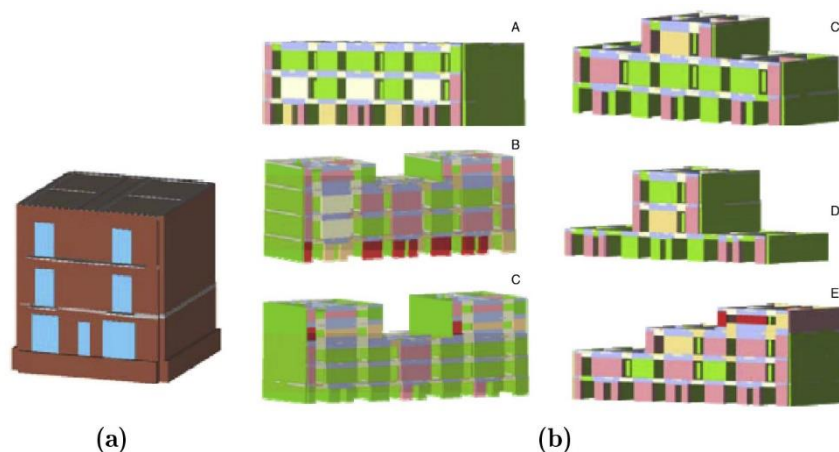


Figure 2-8. Mechanical models used to determine the boundary conditions of the parameter “In elevation interaction”: (a) base masonry model and (b) different possible elevation configurations (Formisano et al. 2015).

Nonlinear Static (Pushover) analyses were developed by applying horizontal accelerations proportional to the first vibration mode along the longitudinal (X) and transverse (Y) directions of the models. The results, expressed in terms of capacity curves, were evaluated in both cases by

defining a ductility indicator named mechanical vulnerability index I_M based on the N2 method theory as (Formisano et al. 2015):

$$I_M = \frac{D_{\max}}{D_u} \quad (2-2)$$

Where D_{\max} is the maximum horizontal displacement required by earthquake (displacement demand) and D_u is the building displacement in its ultimate capacity. For each parameter, the differences detected among the mechanical indexed ΔI_M were proportionally extrapolated to define the scores and classes of each parameter in the form. This formulation considers that the most basic configuration has to be scored with 0 assuming it as a reference point. For example, in Parameter 3, when no staggered conditions are present (Model A, in Figure 2-9a), the score is zero. Starting from this value, the differences among the mechanical vulnerability indexes ΔI_M are examined to calculate the remaining scores. The weights of each parameter were assigned in a proportional way to the maximum absolute difference of the mechanical vulnerability indexes ΔI_M , in the most vulnerable direction of each class.

To verify the calibration of the form, the mechanical and vulnerability index of an existing aggregate of four buildings was analysed in isolation and within the aggregate. The comparison of the results demonstrated that the simplified assessment provides the same vulnerability classification as respect to the mechanical method applied in the longitudinal direction. Furthermore, the original and the new form were applied to estimate the vulnerability indexes of a built-up pilot area of the Torre del Greco town in Italy, and GIS damage maps were plotted to visualize the mean damage of the buildings.

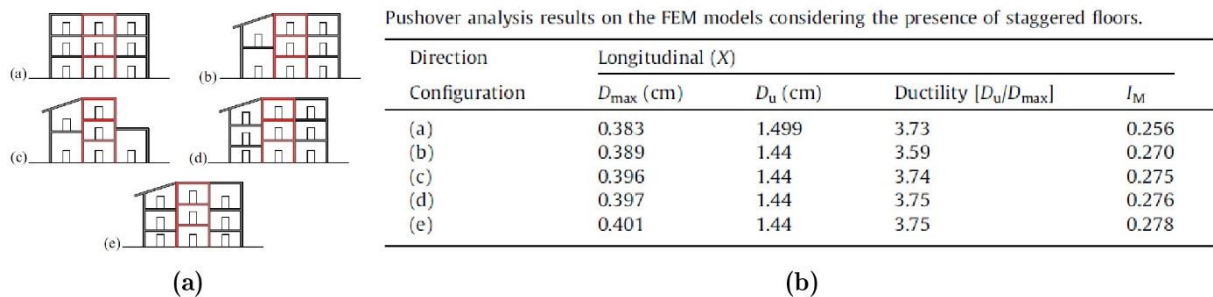


Figure 2-9. Parameter 3 analysis: boundary conditions and Mechanical index calculation (Formisano et al. 2015).

Classes				ΔI_m			
A	B	C	D	A-A	A-B	A-C	A-D
0	15	25	45	0	-0.014	-0.02	-0.022
Mechanical vulnerability Index (I_m)				Proportional correlation with scores			
0.256	0.27	0.276	0.278	0	28.64	40.9	45

(a) (b)

(c)

Figure 2-10 Parameter 3 analysis: definition of the classes (Formisano et al. 2015).

Vicente et al. (2008) and Salazar and Ferreira (2020) studied the application of the VIM to masonry and RC buildings of Portugal, respectively, by calibrating the scores, weight and classes of the vulnerability form for these specific structural systems. Other developments of the VIM are related to the correlation of the vulnerability index with seismic intensity indicators to estimate the damage grade of the buildings. The Macroseismic Method developed by Giovinazzi and Lagomarsino (2004) represents one of the most important contributions in this regard. This method aims to determine how likely is the belonging of a building to a determined damage grade level in certain earthquake intensity based on the EMS-98 using both DPM and vulnerability functions.

The MAR VASTO Project (Indirli 2009) addressed the application of the VIM method in an historical neighbourhood of the city of Valparaíso (Chile), named the *Cerro Cordillera*. This study proposed a calibrated vulnerability form based on the parameters including in GNDT-II for the specific building typologies existing in the neighbourhood, being timber frame and hybrid timber-masonry buildings. This form was calibrated from a qualitative standpoint for all the eleven parameters considering the singular characteristics of the building typologies under analysis. The vulnerability index was calculated for 70 buildings, where almost one half of them (42%) revealed a high vulnerability; $60 < I_v < 100$.

The evaluation of the buildings by using parametric indicators represents the major advantage of the VIM method allowing a comprehensive understanding of the elements influencing the vulnerability of the building. However, it is inherent in the essence of the problem the impossibility of setting a unique tool valid for any type of structural system. Therefore, the VIM should be properly calibrated to include the particular configurations of the buildings in different countries or made of different structural systems i.e. timber frame and steel. Numerous authors addressed the improvement of the VIM both including proper guidelines for the inspection of the

buildings, new parameters of evaluation and new vulnerability forms for different structural typologies.

2.3.2 Analytical Methods

Analytical seismic vulnerability assessment methods consider direct mechanical relationships between construction features, structural response and damage effects on the buildings. Nonlinear analyses are normally applied to simulate the seismic behaviour of the buildings asset and derive the seismic vulnerability pertaining to structural responses, damage or loss. These methods tend to feature more detailed vulnerability assessment algorithms that allow not only detailed sensitivity studies, but also provide straightforward calibration to various characteristics of building stock and hazards (Calvi et al. 2006). Numerical models need to be set involving explicit algorithms with direct physical meaning, starting by the definition 2D or 3D models to characterize the morphology of the structure, the behaviour of the materials and the boundary conditions of the buildings. For this aim, practice-oriented numerical modelling strategies and Multilinear Degree of Freedom (MDOF) models with appropriate nonlinear force-deformation relationships of its structural elements are required. Several modelling strategies are available to this aim, as explained below in Section 2.5, being the most common the Lumped Plasticity Models (LPM) and the Finite Element (FE) approaches.

Analytical methods can be also categorised into direct and indirect methods. The former is characterised by the use of nonlinear dynamic analysis which derive fragility curves as function of ground motion intensity measure types, e.g. PGA, PGV, $S_a(T)$, etc. These curves are derived subjecting the model to time-history analyses which evaluate its dynamic response under loads which may vary according to the specified time functions. Some authors such as Singhal and Kiremidjian (1996), Tiziana Rossetto and Elnashai (2005), Masi (2003) developed analytical fragility curves of different building typologies based on simulated damage data from dynamic nonlinear analysis. On the other hand, indirect methods involved nonlinear static analysis (NSA) to estimate the damage probability of the buildings concerning spectral response parameters. This group includes the application of capacity spectrum-based methods which compared the capacity of the structure with the demands of earthquake ground motion on the structure in the form of an elastic spectrum to define the capacity of the structure for a given scenario, as shown in Figure 2-11.

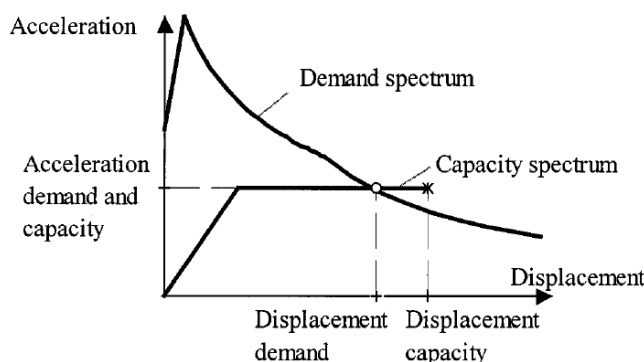


Figure 2-11. Capacity Spectrum Method (Peter Fajfar 1999).

The principle of the CSM is based on run NSA to generate a capacity curve of the structure in terms of acceleration-displacement which described its nonlinear global behaviour when subjected to gravity loads and lateral displacement, simulating statically the seismic action (Rossetto et al. 2014), as diagrammed in Figure 2-12. There is a robust level of knowledge concerning Pushover analysis in literature. Hence, the analyst should address the problem considering a proper methodology to accomplish each particular analysis based on its theoretical and computational requirements. The capacity curve is converted to the “capacity spectrum” by means of point-by-point conversion to the modal spectral coordinates (Najam 2018). This curve is generated by subjecting the detailed nonlinear structural model to the first mode inertia load vector. The seismic hazard is commonly represented by a 5%-damped acceleration response spectra, which is reduced based on the effective damping ratio of an equivalent linear system. This reduced response spectrum is also converted to the Acceleration-Displacement Response Spectrum (ADRS) format. The modified response spectrum in the ADRS format is referred to as the “demand spectrum”. This demand is overlaid with the capacity spectrum to find their intersection point which corresponds to a condition for which the seismic capacity is equal to the demand imposed on the structure. This point is named “target or performance point”, which represents an estimate of the actual maximum displacement expected during a certain seismic risk spectrum. The overall process is illustrated in Figure 2-12.

The original theory of the capacity based-spectrum method was proposed by (Freeman 1998) in the so-called Capacity Spectrum Method (CSM), and it appeared in the original version of the ATC-40 for the assessment of RC buildings (ATC 1996). A debatable part of this procedure was the used highly damped elastic spectra for determining the seismic demand since it significantly underestimated the deformation demands of systems for a wide range of period when used for hysteretic damping models (Lin, Chang, and Wang 2004). Shortly later, Reinhorn (1997) demonstrated that the use of inelastic demand spectra in the ADRS format can overcome this deficiency. The use of inelastic response spectra instead of reducing the elastic spectra by damping-dependent modifier factor. This resulted in better estimation of peak inelastic displacement ratio compared to the iterative procedures of the original model. Different models used elastic spectrum demand were proposed by the US initiative HAZUS-M (FEMA 2003) and by the so-called N2

Method (N2M) (P. Fajfar and Gaspersic 1996; Peter Fajfar 1999) by implementing the inelastic design response spectrum assumption as the demand diagram of the capacity spectrum method. The N2M is included in the Eurocode 8 (CEN 2004) and the Italian seismic standards NTC (Italian Ministry of Infrastructure and Transport 2018) for the seismic vulnerability assessment of the existing buildings.

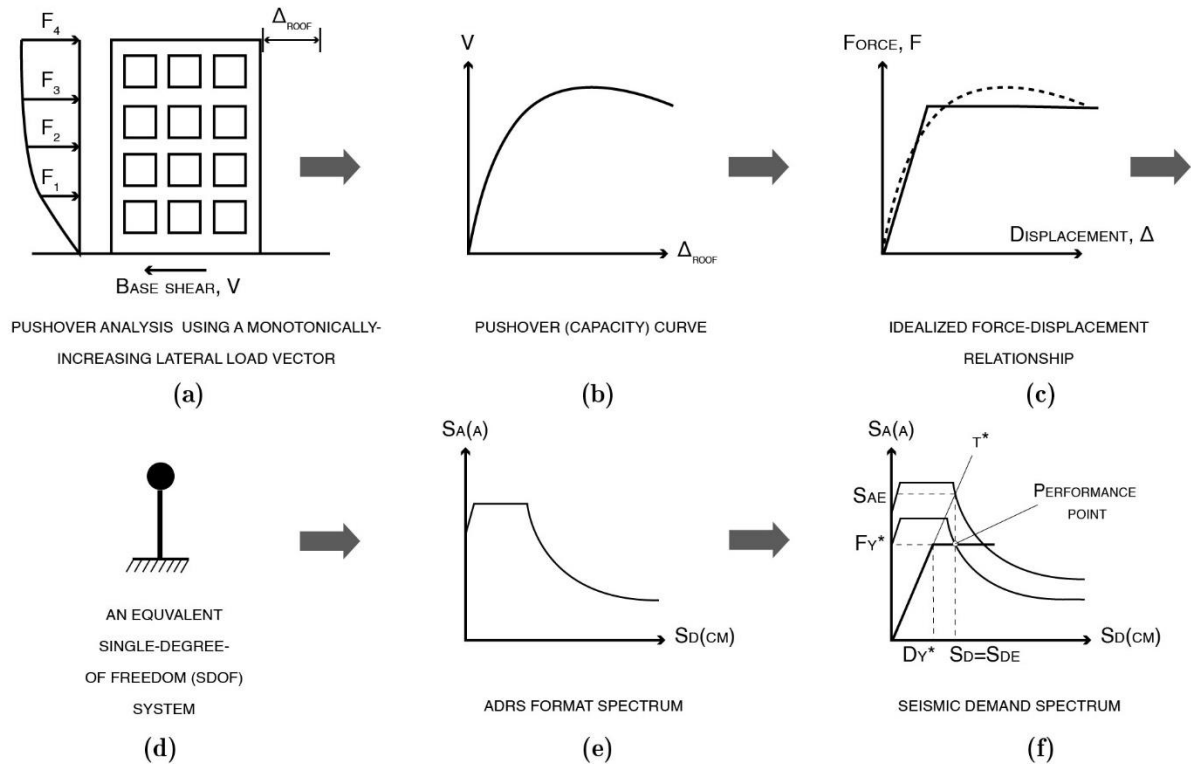


Figure 2-12. Capacity spectrum method stages (based on Najam 2018).

Substantial work has been developed within the framework of important European projects such as GEM (D'Ayala et al. 2013) (Tiziana Rossetto and Elnashai 2005) PERPETUATE and SYNER-G around the application of capacity spectrum-based approaches. For instance, Dumova-Jovanoska (2000) carried out the study of traditional RC building in Skopje, North Macedonia and Rossetto and Elnashai (2005) for several European building typologies.

Analytical vulnerability assessment methods required the development of detailed physical models to develop nonlinear static or dynamic analysis to estimate the seismic behaviour of the buildings. This approach usually involved high computational demanding and time-consuming procedures, hence, they are not affordable for large-scale applications. Nevertheless, they can be effectively employed to carry out typological or sensitivity studies considering a reduced sample of representative buildings of an urban area. This type of implementations can supply the need for post-earthquake damaged data of the buildings allowing the calibration of empirical vulnerability assessment methods for large-scale applications.

2.3.3 Hybrid Methods

Hybrid vulnerability approaches are based on the combination of different vulnerability assessment methods, using, for instance, both analytical and observational data, which can be completed by expert judgment (Pitilakis et al. 2014). A common combination is given by the use of statistical damaged data of the buildings (from empirical methods) and results from nonlinear static or dynamic analysis. In these cases, the analytical results contributed to compensate for the lack of observational damaged data or to calibrate empirical approaches using analytical simulations of certain building typologies as mentioned above. This strategy is particularly useful when there lacking building damaged data of a certain intensity level for a given geographical territory, or to calibrate empirical vulnerability approaches for cities without any post-earthquake register. The latter is very common in urban areas with historical constructions or buildings with vernacular nature.

The possibilities of hybrid methods are very extensive since they are set according to the specific requirement of the assessment. Several methods can be found in the literature using diverse material models, type of analysis and probabilistic models. For instance, Kappos et al. (2006) developed fragility curves for RC buildings of Thessaloniki (Greece) combining statistical data with appropriately processed results from nonlinear dynamic or static analysis. This strategy allowed the extrapolation of statistical data to PGA and/or spectral displacement scenarios to analyse the seismic vulnerabilities of cities where no data is available. Pushover analyses were derived for representative building typologies of the stock. Most recently, Kappos (2016) contributed with robust knowledge for the systematic application of hybrid methods to estimate the seismic vulnerability of the RC and masonry structures which combine the use of empirical databases of earthquake damage with results of nonlinear analysis of representative structural models.

2.4 Building survey and data–collection activities

As was explained in the previous sections, the building information constitutes an essential input to develop accurate seismic vulnerability assessments. The quality and completeness of the available information will determine the feasibility of the analysis application and the accuracy of the results. In this regard, one of the main challenges in large-scale seismic vulnerability assessments is the need for data-collection of a large number of buildings. However, access to such large amount of data is usually difficult and cities including historical architectural heritage usually have incomplete construction databases. For this reason, the construction of building taxonomy (Pitilakis et al. 2014, Brzev et al. 2013) is propaedeutic to the definition of classes of buildings. Building taxonomy describes and classifies the main features of different construction typologies, taking into account the structural attributes influencing the seismic performance of

the buildings, e.g. material properties, geometry, age, type of resistant system or foundation, etc. The goal of create taxonomies lies in create building catalogues classifying meaningful parameters and specific characteristics. The knowledge of existing buildings is fundamental to define reliable taxonomy and this activity shall be based on detailed survey activity.

Building survey strategies are inherent activities in seismic risk assessment procedures aimed to gather specific information required for each evaluation and create the taxonomies. The seismic vulnerability approaches can be also classified according to their level of complexity as for the quality and amount of the evaluated data. For instance, first level methods assess the seismic vulnerability through qualitative inputs such as the building typology and the age of construction. Second level approaches also consider specific parameters regarding the morphology conditions and structural configuration of the buildings. Lastly, third level approaches involve sophisticated analysis, such as numerical simulations, and consider detailed models of the buildings. First level approaches, usually consider more simple survey strategies to evaluate the vulnerability of the buildings such as the case of RADIUS (UNISDR 1999) and RISK-UE (Mouroux et al. 2004) projects which only required the age of construction and general information about the building typology. Most recently, the *Rapid Visual Screening of Buildings for Potential Seismic Hazards* method (FEMA 2015) proposed a simple survey form (Figure 2-13a) to collect information regarding the building documentation, its occupancy, the type of soil, the falling hazards and the building type. The vulnerability valuation of the building types is based on the previous studies of HAZUS and FEMA 155 report (ATC, 2002) which established vulnerability scores for fifteen structural typologies constructed with steel, reinforced concrete and masonry.

Second level strategies such as the VIM (GNDT 2007) requires a remarkable quality of the building knowledge to obtain reliable results, and provide practical survey forms and manuals to carry out survey activities on-field (see Figure 2-13b). The Italian National Seismic Survey (SSN) and the GNDT group continued developing this tools releasing the AeDES method (Baggio et al. 2007) which considering damage assessment as well as short-term countermeasures for damage limitation and evaluation of the post-earthquake usability of ordinary buildings. The AeDES form (Figure 2-13c) is composed of nine sections listed as: building identification, building description, building typology, damage to structural and non-structural components, external danger, soil and foundation, usability assessment, and notes. A noteworthy advantage of this tool is its user-friendly template for simple and fast on-field survey applications. AeDES forms were employed by Masi et al. (2014) for a vulnerability survey of 18 villages located in the Basilicata region (Sothern Italy).

Rapid Visual Screening of Buildings for Potential Seismic Hazards
FEMA-154 Data Collection Form **LOW Seismicity**

Address: _____ Zip: _____

Other Identifiers: _____

No. Stories: _____ Year Built: _____

Screened by: _____ Date: _____

Total Floor Area (sq. ft.): _____

Building Name: _____

Use: _____

PHOTOGRAPH

Scale: _____

OCCUPANCY		SOIL		TYPE		FALLING HAZARDS	
Assembly	Govt	Office	No. of Persons	A	B	C	D
Commercial	Industrial	School	100-1000	Rock	Rock	Soil	Soil

BASIC SCORE, MODIFIERS, AND FINAL SCORE, S															
Basic Score	7.4	5.0	4.5	4.8	4.5	4.8	5.3	4.4	4.8	4.4	4.4	4.6	4.5	4.6	4.5
Mid Rise (4 to 7 stories)	N/A	N/A	+0.2	-0.4	N/A	+0.2	-0.2	-0.4	-0.2	-0.4	N/A	-0.2	-0.4	-0.2	-0.6
High Rise (8 to 17 stories)	N/A	N/A	+1.0	-1.0	N/A	+1.0	+1.2	-1.0	-1.0	-0.4	N/A	-0.2	N/A	-2.0	N/A

FINAL SCORE, S

COMMENTS: _____

Detailed Evaluation Required: YES NO

(a)

G.N.D.T. - SCHEDA DI VULNERABILITÀ DI 2° LIVELLO (MURATURA)

Codice ISTAT Provincia _____ Comune _____ Scheda N° _____

PARAMETRI	Classi	Qual. Inf.	ELEMENTI DI VALUTAZIONE	SCHEMI - RICHIAMI	
1 TIPO ED ORGANIZZAZIONE DEL SISTEMA RESISTENTE (S.R.)	1	1	Nome nuove costruzioni (Clas. A) 1 Nome riparazioni (Clas. A) 2 Cordoli a catene tutti i livelli (Clas. B) 3 Busti ammorsati fra muri (Clas. C) 4 Senza sottile catini ammors. (Clas. D) 5	Parametro 3. Resistenza convenzionale Tipologia strutture verticali % (mm)	
2 QUALITÀ DEL S.R.	1	2	(vedi manuale)	Minimo tra A ₁ ed A ₂ A (mq) Massimo tra A ₁ ed A ₂ A (mq) Coeff. α ₁ =A ₁ /A ₂ Coeff. γ = D/A ₂ q ₁ = (A ₁ + A ₂) / h ₁ / A ₁ + A ₂ C _u = (q ₁ / 1.5) q ₁ (1+γ) α = C _u / 4	Parametro 5. Configurazione planimetrica
3 RESISTENZA CONVENZIONALE	1	2	Numero di piani N Area totale coperta A _t (mq) ¹⁾ Area A ₁ (mq) Area A ₂ (mq) h ₁ (mm) h ₂ (mm) Alt. media interpiano h (m) Peso specifico pareti p _w (t/mc) Carico permanente soletti p _s (t/mq)	Parametro 7. Configurazione in elevazione	
4 POSIZIONE ELEVATA E FONDAZIONE	1	2	Pendenza percentuale del terreno Rocce Fondazioni: SI 1) NO 2) Terr. sciolto non sping. Fond. SI 3) NO 4) Terr. sciolto spingente Fond. SI 5) NO 6) Differenz. max di quota Δh (m)	Parametro 9. Copertura	
5 ORIZZONTAMENTI	1	2	Piani sbalati: SI 1) NO 2) Orizzontam. rigidi e ben collegati 3) Orizzontam. deformabili e ben collegati 4) Orizzontam. deformabili e mal collegati 5) % Orizzontam. rigidi e ben collegati 6)	Parametro 10. ELEM. NON STRUTT.	
6 CONFIGURAZIONE PLANIMETRICA	1	2	Rapporto percentuale p ₁ = a ₁ / a ₂ Rapporto percentuale p ₂ = b ₁ / b ₂ % aumento (+) o diminuzione (-) di massa Rapporto percentuale T/H Percentuale superficie porticata Piano terra porticato SI 1) NO 2)	Parametro 11. STATO DI FATTO	
7 CONFIGURAZIONE IN ELEVAZIONE	1	2	Rapporto massimo tra Copert. non sp. 1) 2) 3) 4) 5) 6) 7) 8) 9) 10) 11) 12) Cordoli in copertura SI 1) NO 2) Catene in copertura SI 3) NO 4) Carico perman. copert. p _c (t/mq) Lungh. appoggio copert. l _a (m) Perimetro copertura l _p (m)		
8 MURATURE	1	2	Rapporto massimo tra Copert. non sp. 1) 2) 3) 4) 5) 6) 7) 8) 9) 10) 11) 12) Cordoli in copertura SI 1) NO 2) Catene in copertura SI 3) NO 4) Carico perman. copert. p _c (t/mq) Lungh. appoggio copert. l _a (m) Perimetro copertura l _p (m)		
9 COPERTURA	1	2	Rapporto massimo tra Copert. non sp. 1) 2) 3) 4) 5) 6) 7) 8) 9) 10) 11) 12) Cordoli in copertura SI 1) NO 2) Catene in copertura SI 3) NO 4) Carico perman. copert. p _c (t/mq) Lungh. appoggio copert. l _a (m) Perimetro copertura l _p (m)		
10 ELEM. NON STRUTT.	1	2	(vedi manuale)		
11 STATO DI FATTO	1	2	(vedi manuale)		

(b)

GENERAL FORM FOR THE BUILDING PRACTITIONERS

SERVIZIO PRESIDENZA DEL CONSIGLIO DEI MINISTRI
 DIFESA NAZIONALE
 TECNICI NAZIONALI

Presidenza del Consiglio dei Ministri
 DIPARTIMENTO NAZIONALE DELLA PROTEZIONE CIVILE

Consiglio Nazionale della Difesa
 GRUPPO NAZIONALE PER LA DIFESA DAI TERREMOTI

7.1.1.1 1° LEVEL FORM FOR POST-EARTHQUAKE DAMAGE AND USABILITY ASSESSMENT
7.1.1.1.1 AND EMERGENCY COUNTERMEASURES IN RESIDENTIAL BUILDINGS
 (AeDES 05/2008)

SECTION 1 Building identification

Province: _____ Terr. _____ Form. n. _____

Municipality: _____ Region Inst. _____ Province Inst. _____ Municipality Inst. _____ Aggregate No. _____ Building No. _____

Locality: _____

Address: _____

1 Street
 2 Road
 3 Alley
 4 Square
 5 Other

Building denomination or owner's name: _____ Determination Code: _____

Photocopy of the structural aggregate with building indication: _____

SECTION 2 Building description

Vertical data	Age	Use
Total number of stories	Construction and renovation [max 2]	Use
Average story height [m]	Else	No. of units in use
Average story surface [m ²]	Else	Exhibition
		No. of occupants

SECTION 3 Structural Data

Vertical Structure of the Building

If the building is in reinforced concrete:

B.1 The building has no walls at floors: B.2 The building has partially walls at floors:

B.3 The building is composed totally by walls B.4 The building has RC shear walls

(c)

Name of the complex _____
 Education level _____

1) Identification of the Building

Municipality _____
 Street name _____ Street number _____
 Name of the building _____ Building number _____

Geographical Coordinates (WGS 84 System - Decimal degrees) _____ Lat. _____ Long. _____

Position of Building:

1 Isolated Building 2 Internal Building 3 End Building 4 Corner Building

2) Description of the Building

N° Total floors with basement	Average of floor height [m]	Average of floor area [m ²]	Age	Use - Exposure	
				Type of Use	% of Use
0 1 2 3 4 5 6 7 8	1 2 3 4 5 6 7 8 9 10 11 12	A 100-150 B 150-200 C 200-250 D 250-300 E 300-350 F 350-400 G 400-450 H 450-500 I 500-550 J 550-600 K 600-650 L 650-700 M 700-750 N 750-800 O 800-850 P 850-900 Q 900-950 R 950-1000 S 1000-1050 T 1050-1100 U 1100-1150 V 1150-1200 W 1200-1250 X 1250-1300 Y 1300-1350 Z 1350-1400	1 ≤ 1919 2 19-45 3 46-61 4 62-71 5 72-81 6 82-91 7 91-02 8 ≥ 2002	<input type="checkbox"/> Housing <input type="checkbox"/> Production <input type="checkbox"/> Trade <input type="checkbox"/> Offices <input type="checkbox"/> Public Services <input type="checkbox"/> Deposit <input type="checkbox"/> Unfinished <input type="checkbox"/> Abandoned <input type="checkbox"/> Touristic Accommodation	A > 66% B 30-66% C < 30% D Under Construction E 7 7 7 F 8 8 8 G 9 9 9 H 9 9 9 I 9 9 9 J 9 9 9 K 9 9 9 L 9 9 9 M 9 9 9 N 9 9 9 O 9 9 9 P 9 9 9 Q 9 9 9 R 9 9 9 S 9 9 9 T 9 9 9 U 9 9 9 V 9 9 9 W 9 9 9 X 9 9 9 Y 9 9 9 Z 9 9 9

3) Structural Data

Vertical Structure of the Building

If the building is in reinforced concrete:

B.1 The building has no walls at floors: B.2 The building has partially walls at floors:

B.3 The building is composed totally by walls B.4 The building has RC shear walls

(d)

Figure 2-13. Available survey forms typologies: (a) FEMA-154 Rapid visual Screening of Buildings for Potential Seismic Hazards (ATC, 2002), (b) Gruppo Nazionale per la Difesa dai Terremoti (GNDT 2007), (c) AeDES (Baggio et al. 2007) and (d) SASPARM 2.0 project (Monteiro et al. 2016)

In this implementation, a “peacetime building-by-building survey methodology” was proposed aimed to develop a typological survey strategy for large-scale assessment in cities without post-earthquake databases. An upgraded form named Vulnerability Survey form in Peace-time (VSP) was calibrated and applied to obtain data from masonry and reinforced concrete buildings. The surveyed data was used to develop typological characterizations considering the information of representative buildings within the stock. The vulnerability of each building was evaluated referring to the most important structural characteristics, the age of construction or retrofitting, and the horizontal and vertical structural types of the most vulnerable story of the construction. Classes A, B, C and D established in EMS-98 (Grünthal 1998) were correlated to the evaluation of the surveyed buildings. The obtained results were statistically sorted and compared with the data of the 2001 census by the Italian Institute of Statistics (ISTAT), with significant differences associated with the different criteria of the considered methodologies. A similar typological survey was carried out by Taffarel et al. (2014, 2016) to evaluate the seismic vulnerability of the city centres of Safed (Israel), Acre (Israel) and Timisoara (Romania). The proposed methodology was based on a preliminary knowledge stage, consisting in the collection of data related to the historical evolution of the buildings, structural interventions, damage mechanisms and identification of the vulnerability elements. The knowledge stage considered on-site activities to recognize the building stock through a visual survey and a careful on-site inspection to identify the vertical and horizontal structural configuration. Next steps were the statistical and typological analysis, followed by the seismic vulnerability analysis based on the Vulnus methodology (Bernardini et al. 1988).

Another typological approach to building survey was proposed by Monteiro et al. (2016) in the framework of the SASPARM 2.0 project, where the main objective was the definition of fragility curves for the building structural typologies of the city of Nablus (Palestine). The first phase of this large-scale assessment was the definition of a catalogue of the building typologies of the city. Two forms were proposed, i.e. a more technical one for expert practitioners (Figure 2-13d) and a simpler one for the inexpert population. The expert forms have 6 sections, i.e. identification of the building, description of the building, structural data, regularity, geomorphological data, and notes. Nonlinear static analyses were carried out to estimate the structural seismic performance of the Palestinian building typologies and to plot eventually their fragility curves.

Building survey activities are essential in seismic vulnerability assessment, especially in cities lacking past-earthquake data or enough building knowledge. Survey strategies must be properly linked with the parameters analysing the vulnerability of the buildings which can vary depending on the structural typologies under assessment and the chosen methodology. Data-collection procedures often required on-field assessment, however, in-depth inspections of all the buildings are hardly feasible in large urban settlements with inhabited constructions. This problem is normally due to the lack of resources for comprehensive survey, inaccessibility to a large number

of buildings, and hidden conditions of the investigated structural systems. These obstacles are typical in historical centres with old and heterogeneous constructions characterized by a huge variety of conditions. To counteract such uncertainties, the definition of proper typological survey forms of the most representative structural schemes could help to determine the seismic vulnerability of each building. In parallel, the management of the collected data and the development of graphical outputs are central activities during and after surveys. Geographic Information System (GIS) applications are among the most suitable tools to generate databases, as well as to store, manipulate, analyse and manage a large amount of building information as explained in Section 2.2.3.

2.5 Numerical methods for seismic vulnerability assessment of timber and masonry buildings including hybrid typologies

The seismic vulnerability assessment of existing buildings making use of numerical simulation methods is an increasingly embraced strategy among civil engineering and seismic risk assessment fields. This type of analysis allows the global and local failure prediction of singular and complex structural units subjected to seismic loads. Analytical and hybrid seismic vulnerability assessment methods usually include numerical simulation to generate damage data and estimate the seismic capacity of the structures, as explained in the previous sections. Depending on different factors such as the structural typology and aim of the study, different modelling strategies need to be developed in order to derive reliable physical models and simulations. Such strategies are not straightforward for every case, and multiple solutions can be accepted to develop a proper model. In the present section, a brief overview of the most renowned modelling strategies used to simulate the seismic behaviour of masonry and timber frame walls are explained. Besides, the review presented different noteworthy studies around the simulation of complex timber-masonry structures.

2.5.1 Modelling of timber frame structures

The numerical simulation of timber frame structures represents an important challenge. The nature of this type of structural systems is characterized by the wide variability of framing design i.e. different size and disposition of the timber elements, type of connections, and presence of infill. This versatile nature explains the numerous existing timber frame typologies worldwide. Such differences need to be considered in numerical simulation, making modelling standardization a very difficult task. Several numerical methods can be used to model timber structures, commonly classified into micro and macro modelling strategies. Micro-modelling strategies are commonly based on FE methods which are employed to simulate the anisotropic behaviour of timber material as well as the interaction among the elements of the frame (Poletti 2013a; Kouris and Kappos 2012) as shown in Figure 2-14a. For these cases, sophisticated material models can be used to

represent the timber response, such as the anisotropic Rankine-Hill model, which captures the strength and softening responses in the orthogonal directions of the elements. Besides, friction models need to be used to simulate the interaction between the members at the connections (e.g. Coulomb Friction Model). Micro-models are suitable to simulate in detail the response of timber frame structures as they capture localized failures in the elements. However, they are usually very computationally demanding and thus unsuitable to model large structures or to be used in large-scale assessments.

Alternatively, macro-modelling strategies are commonly used to simulate the timber frame response by means of simplified structural assumptions. Lumped Plasticity Models (LPM) represent one of the most suitable strategies to represent simplified timber frame models. LPM uses linear elastic frame elements to represent the timber parts of the structure. The timber material is commonly modelled using isotropic materials, whereas nonlinear springs and hinges lumped at the end or the centre of the frames represent the behaviour of the connections, as shown in Figure 2-14b. The nonlinear constitutive laws controlling the springs and hinges response are usually calibrated based on experimental data or through analytical approaches. Several authors, i.e. Lukic et al. (2018) E. Poletti, Lourenco, and Ciocci (2016) and Quinn (2015), used LPM developing timber frame models and simulations. This approach is the most used in practice-oriented studies since it allows the modelling of entire buildings or complex structures given their low-computational demand.

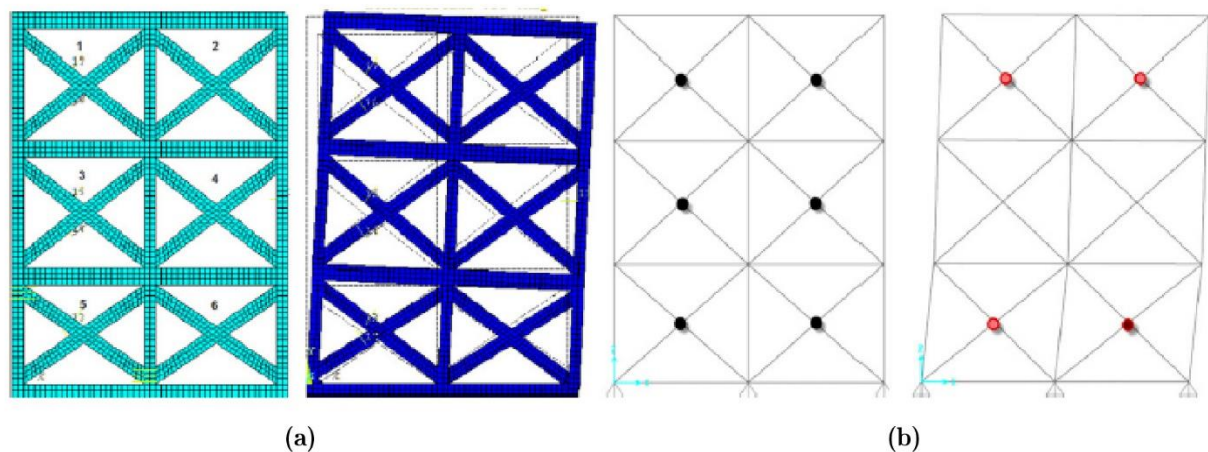


Figure 2-14. Modelling of a Pombalino wall using (a) Micro-modelling and (b) Lumped Plasticity Model (Kouris and Kappos 2012)

2.5.2 Modelling of masonry structures

The numerical simulation of unreinforced masonry structures (URM) has been extensively studied in the last decades. The diversity of modelling needs has driven the development of several approaches providing different levels of detail regarding the material modelling. Finite Elements methods are aimed to simulate the behaviour of masonry commonly categorized into: (i) micro-mechanical, (ii) multi-scale and, (iii) macro-mechanical approaches, as displayed in Figure 2-15.

Micro-modelling approaches are the most detailed methods, where all the masonry components are explicitly defined in the simulation, accounting for different mechanical properties and constitutive laws both for the units (bricks) and the mortar components.

Different discretization approaches are available for the development of masonry structures based on micro-modelling theories, as explained in Saloustros et al. (2017). Multi-scale approaches address the analysis of masonry considering two different Boundary Value Problems (BVP) in two different scales: micro and macro modelling (Petracca et al. 2017). Firstly, a Representative Volume Element (RVE) –existing in regular masonry types– must be modelled to obtain the nonlinear response of this representative sample, as shown in Figure 2-16a. Next, the whole structure is modelled considering masonry as a homogeneous material, incorporating the constitutive law obtained from the RVE at each integration point. Multi-scale models are considered more efficient than micro-models in terms of model setting, and computational costs, however, the RVE modelling can become a challenging task.

Lastly, macro-mechanical approaches consider masonry as a homogeneous material, making no distinction between masonry's components (Figure 2-16b). In macro models, the material behaviour is represented using proper constitutive laws simulating the nonlinear response of masonry under tensile and compressive loads. These approaches are the most appropriate for large-scale applications and practice-oriented simulations, where more importance is given to the global capacity, rather than to the representation of local damages. Several authors have adopted macro-modelling strategies to simulate the structural behaviour of masonry structures under lateral loads (Saloustros et al. 2019; Saloustros, Cervera, and Pelà 2019; Pantò et al. 2019; Kouris and Kappos 2012; D'Ambra, Lignola, and Prota 2016; Endo et al. 2015; Bilgin and Korini 2014; Spyrakos and Francioso 2012).

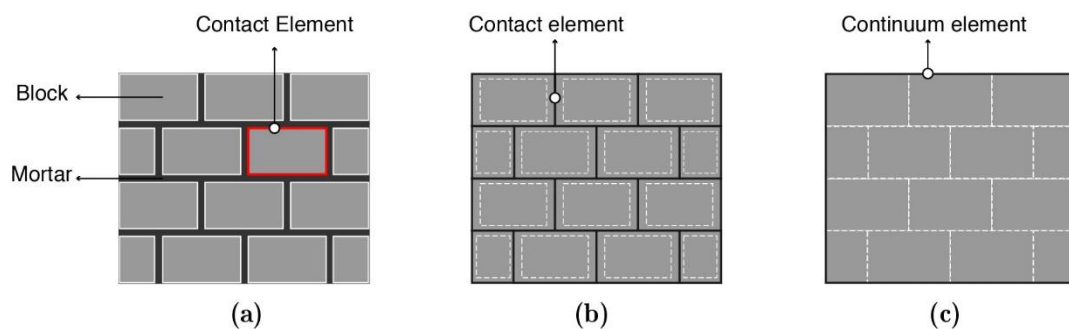


Figure 2-15. Level of masonry modelling: (a) micro-modelling, (b) multi-scale or simplified micro-modelling and (c) macro-modelling.

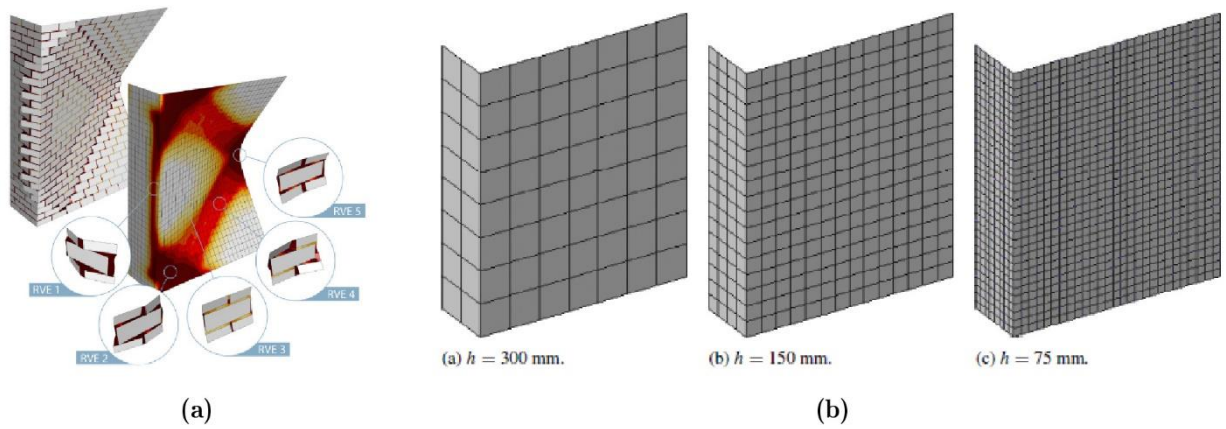


Figure 2-16. Masonry modelling: (a) RVE modelling and (b) macro-modelling using different element scales (Petracca et al. 2017).

Another simplified approach to simulate the behaviour of masonry walls is the Equivalent Frame Method, which is based on the frame idealization of the piers and spandrels of masonry buildings. This mathematical model considers walls decomposed into an assemblage of columns and beams, represented by linear elastic frame elements, where lumped nonlinear hinges determine the possible locations of the inelastic deformations and type of failures that might develop along the span of each element, as shown in the example of Figure 2-17. The nonlinear behaviour of the connections is commonly derived from experimental results of isolated tests on the connections or analytical estimations. EFM develops very simple and practice-oriented numerical models, which are characterized by a low computational expense, and suitable for large-scale applications. Several authors used EFM to determine numerical models both for masonry and RC structures i.e. Rossella Siano et al. 2017, 2018; Sonekar and Bakre 2015; Petrovčič and Kilar 2013; Belmouden and Lestuzzi 2009; Pasticier, Claudio, and Fragiaco 2007; Guido Magenes 2000.

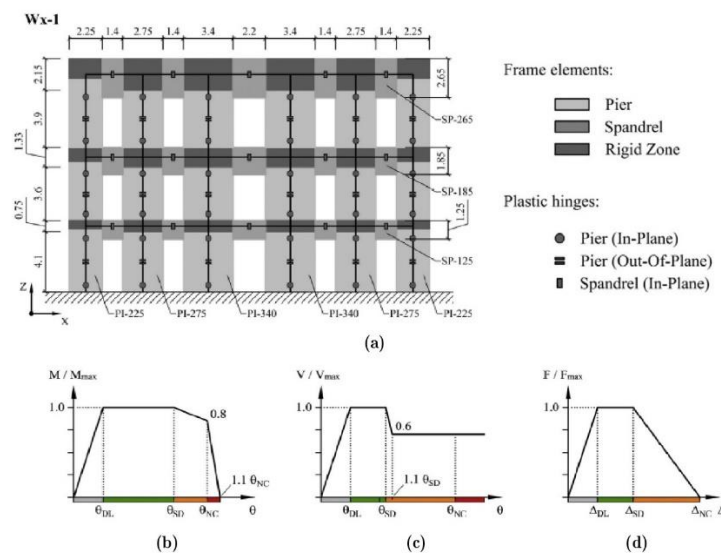


Figure 2-17. Equivalent Frame Model of a masonry building: (a) Hinges position, constitutive laws of the (b) pier in-plane, (c) spandrel and (d) pier out-of-plane elements (Petrovčič and Kilar 2013).

2.5.3 Modelling of hybrid timber–masonry structures

The modelling of masonry and timber frame structures have usually dealt with separately for homogeneous building typologies. Few researchers have addressed the modelling of hybrid timber–masonry structures until now. Ciocchi, Sharma, and Lourenço 2018 dealt with the modelling of the Ica the Cathedral of Peru, a super complex structure composed of masonry and quincha walls and timber roof structures as shown in Figure 2-18a. The modelling was addressed, in a first instance, using beam elements to model the timber and shell elements for the masonry by separating. Next, the complete structure was constructed by defining the connections between the two structural systems. These connections were modelled by merging the nodes of the frame and shell elements, where suitable restraints were applied to avoid compatibility issues. The model was subjected to seismic force by applying nonlinear static analysis NSA Figure 2-18b-c. The results were compared with the damage existent in the Ica Cathedral showing good agreement in terms of local mechanisms and crack patterns.

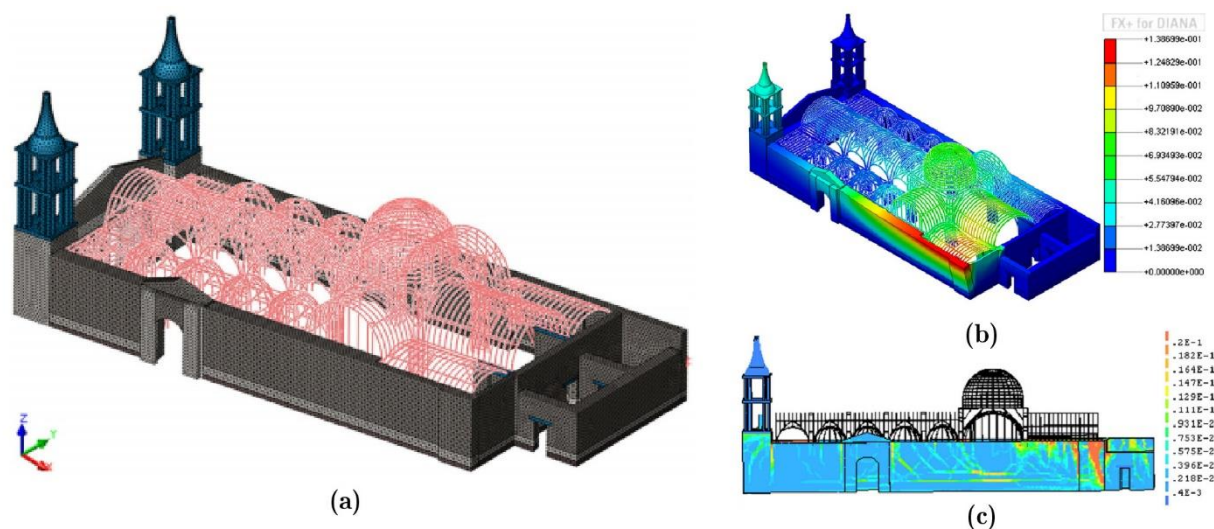


Figure 2-18. Ica Cathedral model: (a) geometry, (b) hybrid model under lateral loading in the direction Y, and (c) tensile strains from the nonlinear analysis in the direction Y (Ciocchi, Sharma, and Lourenço 2018)

Kouris and Kappos (2012) also developed a numerical model representing the behaviour of a hybrid timber and stone masonry building located in Lefkas, Greece (Figure 2-19). In this case, both timber and masonry structures were modelled using linear elastic beam elements by applying the LPM theory for timber and the EFM for masonry walls, as shown in Figure 2-19b. Nonlinear axial springs were placed where the nonlinearities were localized. For the determination of the nonlinear constitutive law of these points, a preliminary linear analysis was carried out to estimate the axial forces in the timber posts. Then, the results of a detailed micro-modelling of the timber panel were used to determine a reduced bilinear curve which was embodied in the diagonals' axial plastic springs. The simulation of the stone masonry at the ground story is implemented through an EFM based on literature studies.

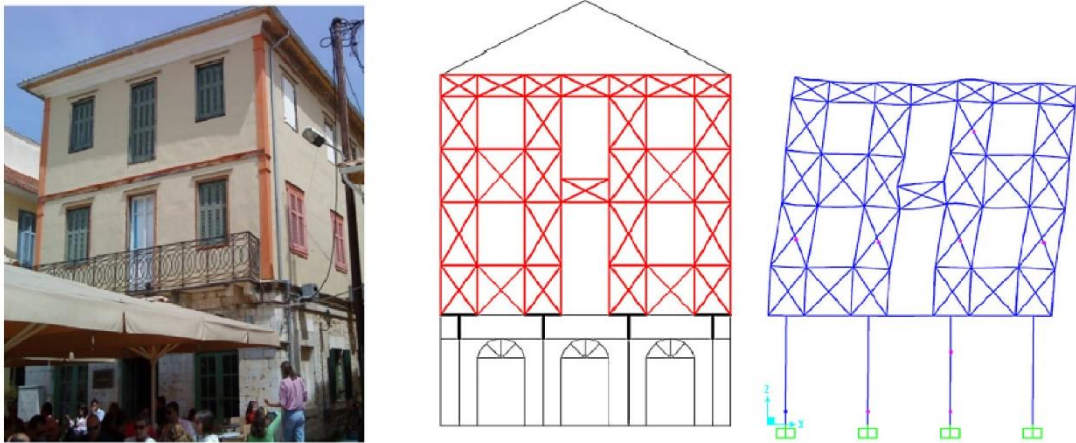


Figure 2-19. Modelling of a hybrid masonry-timber frame façade of a building in Lefkas, Greece (Kouris and Kappos 2012)

Numerical simulations are not straightforward procedures and they can be addressed using different strategies, particularly for hybrid structures which need to be defined following divergent structural assumptions and theoretical frameworks. Taking this into account, the best solution for each particular case has to be planned considering the goals of the study as well as the available resources. For seismic risk studies at large scale, simplified models need to be developed considering the macro-modelling and LPM approaches, which allow the application, for example, of analytic or hybrid seismic vulnerability assessment, or the numerical simulation of entire buildings.

2.6 Summary

This chapter has presented the theoretical framework and background of this thesis, aimed to develop a seismic vulnerability assessment method for the evaluation of historical centres with heterogeneous building stocks. The chapter has addressed four main topics. The first has considered a brief overview of seismic risk estimation models for large-scale, including the essential concepts of this activity. An overview of some remarkable initiatives developed to this aim has been presented. The second topic has referred to the existing seismic vulnerability methods, which represent the core of seismic risk studies. These methods can be grouped into three categories named empirical, analytical and hybrid. The third part of the chapter has focused on the survey building and data collection strategies since they are considered essential activities for seismic vulnerability applications. The last section of the chapter has introduced the state-of-the art about the numerical strategies for the seismic vulnerability study of existing buildings.

An important part of the chapter has focused on describing the existing vulnerability assessment methods for large-scale assessment since accurate analyses are needed to manage the risk and create mitigation plans increasing the resilience of the cities. This review has attempted to compare the methods in order to determine their suitability for evaluating different risk

scenarios, highlighting their main advantages, disadvantages and requirements. Special attention has been paid to the Vulnerability Index Method (VIM) for the indirect evaluation of the vulnerability of the buildings since representing the adopted methodology in this thesis. The method, originally developed by Benedetti and Petrini (1984) for the assessment of Italian masonry buildings, proposed a systematic analysis of different structural and non-structural parameters influencing the seismic behaviour of the buildings. This method received a great acceptance in the scientific community and several initiatives were attempted to enhance the method towards the analysis of different structural typologies (GNDT-SSN 1994; R. Vicente et al. 2008; Formisano, Landolfo, and Mazzolani 2015; Basaglia et al. 2018; Cara et al. 2018; L. G. F. Salazar and Ferreira 2020).

The extension of the VIM towards the analysis of different structural typologies requires proper calibration procedures, which commonly involve advanced numerical studies to simulate the seismic behaviour of the buildings and to predict their damage states. The vulnerability assessment of the buildings by using numerical analysis requires a comprehensive understanding of the physical characteristics of the structural system in order to determine robust models capable of simulating the seismic behaviour and collapse mechanisms. The final part of the chapter has presented some of the available modelling strategies for masonry, timber and hybrid timber-masonry buildings.

Chapter 3. Cerro Alegre, Cerro Concepción and the Port neighbourhoods of the historical centre of Valparaíso, Chile: an overview

3.1 Introduction

Between the mid-19th and early 20th century, the port of Valparaíso was one of the most important of the Pacific Ocean, being a major commercial attraction, especially for foreign investors and people looking for better economic opportunities. A large number of immigrants, especially from Europe and North America, settled in the city and brought with them new cultural trends and technological advances which positively impacted the social, cultural and urban environment of the city. New consolidated neighbourhoods emerged to house the growing population living in the city and the increased commercial activity. From an architectural standpoint, new constructive technologies emerged in the city including monumental iron-reinforced concrete (RC) and residential timber frame buildings. These new trends were combined with the local constructive culture configuring a singular urban fabric. Different from many other colonial settlements in Chile, Valparaíso faced several obstacles in its urban expansion because of its complex geographic physiognomies. The character of the city is strongly marked by the geography of its location. The bay, narrow coastal plains (largely artificial) and steep hills scored by multiple ravines together created the city's amphitheatre-like layout, as shown in Figure 3-1. Flat ground was scarce, which pushed taking over the hillsides without planning, bestowing an irregular and particular urban fabric. The staggered condition of the terrain in the hills determined innovative and singular settlement strategies such as the use of masonry retaining walls, columns and basements as mixed designs to configure hybrid building typologies.

Numerous major earthquakes have been recorded in the city of Valparaíso since ancient times. Some of them caused devastating consequences, such as the ones that occurred in 1906 and 1985. The evidence of these catastrophes demonstrated the initial low resilience of the city which was strongly damaged especially in the old downtown area of the city, where most of the buildings were made of unreinforced masonry (URM). However, they also showed evidence of the good anti-seismic behaviour of some traditional structural systems, such as the centennial timber frame

constructions located on the hills. The nature and quality of the structural systems have an unquestionable role in the anti-seismic behaviour of the buildings, but external factors can also influence their structural vulnerability.

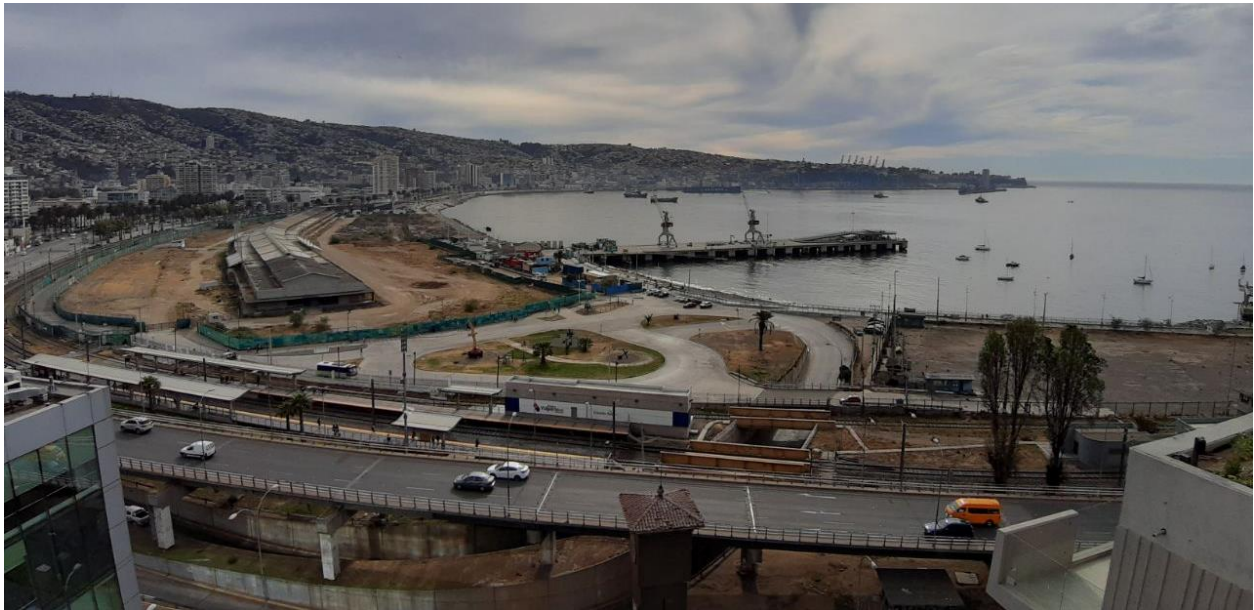


Figure 3-1. Panoramic view of the city of Valparaíso (Chile).

In this regard, the seismic hazard of the city must be evaluated considering that particular geological and geophysical characteristics of the territory could negatively affect their seismic response. Seismic microzonation studies of the city (Baquedano and Leyton (2012), Castañeda (2013) and SERNAGEOMIN (2018)) classified the hazard of the territory based on the fundamental vibration measurements of the soil and the superficial geology characteristics of the city, considering the assumption that the response of the soil in a high-intensity earthquake is not homogeneous. These results demonstrated that the plain zones within the study area present high levels of hazards compared with the hill zones, due to the artificial and poorly compacted nature of the soil. The plain areas of the city, including the Port downtown, have the highest Peak Ground Acceleration (PGA) values, as well as the lower fundamental frequencies and shear wave propagation values. The hills zones, including the Cerro Alegre and Cerro Concepción, present better conditions of the rocky soils. However, they still present high levels of hazard in terms of PGA, fundamental frequencies and shear wave propagation values of the soil. The microzonation maps derived by the seismic hazard studies are useful tools that help to evaluate the localized influence of site hazard on the vulnerability of the buildings. These investigations also contributed to the development of urban risk disaster assessment, as well as maker-sessions for the implementation of civil protection plans and infrastructure investments.

Seismic risk assessment at urban scale implies the vulnerability appraisal of the exposed infrastructure. An in-depth study of each building of the urban fabric is usually unaffordable due to the large amount of exposed elements, thus a delimitation strategy of the study area constitutes

a convenient approach. In this research, the Emergency Limit Condition (ELC) is considered to define the zone object of study. Such an approach, promoted by Italian Civil Protection (Commissione tecnica per la microzonazione sismica 2014), aims to determine integrated and coordinated mitigation strategies based on the emergency management systems of the cities. This can include the use of civil protection plans, identification of strategic buildings, emergency areas, routes and infrastructure of connection and accessibility. The purpose of this method is evaluate only the elements that can potentially interrupt the strategic functions of the city due to their collapse in an emergency scenario, such as the block of strategic areas (evacuation routes, security zones etc.). The study area within the historical centre of Valparaíso was delimited considering two of the main evacuation routes in the case of the occurrence of a tsunami, starting from the risky areas in the downtown part of the city towards the Cerro Alegre and Concepción hills: Arturo Prat, Urriola and Almirante Montt streets. The considered ELC system includes 111 buildings classified as interfering, meaning that their potential collapse may block the strategic evacuation routes. The seismic vulnerability of the strategic and interfering buildings is assessed in the following stages of the research.

The urban fabric within the ELC system is characterized by a heterogeneous character, where timber frame, unreinforced masonry, wrought iron and reinforced concrete structural systems define the building stock. Furthermore, many of these buildings have hybrid nature, e.g. mixing timber-masonry or wrought iron-RC systems. Most of the buildings of the stock have historical character, built between the late 18th and early 19th centuries, but there are some units built in compliance with the seismic codes, after 1960. Unfortunately, a large amount of buildings does not have any technical record in the local archives, thus an initial typological characterization was made based on published information of some representative examples and in-situ inspection. Further stages of this thesis present more accurate methodologies to obtain and manage the necessary information to evaluate the vulnerability of these buildings.

The outline of this chapter is divided into three parts. First, Section 3.2 presented an historical overview of the urban configuration and major earthquakes occurred in the city of Valparaíso. Section 3.2.1 includes the description of the development of the historical neighborhoods of the city and the traditional structural typologies raised in these areas. Section 3.2.2 relates the major earthquakes occurred in Valparaíso and their impacts within the urban tissue and society. Section 3.2.3 introduces the inclusion of the historical center of the city to the UNESCO World Heritage List. Next, Section 3.5 presents the definition of the ELC system within the pilot study zone. Section 3.4.1 includes the civil protection and emergency plans of Valparaíso which are the base of the ELC definition. Section 3.4.2 mapping the ELC system. Finally, Section 3.5 characterizes the representative typologies within the ELC system stock.

3.2 Historical overview: Urban configuration and major earthquakes

3.2.1 History of the urban development of the city

Between the mid-19th and early 20th centuries the city of Valparaíso became one of the leading ports on the South Pacific Ocean, considering as the principal entry and exit door of goods and people (Harris 1996). This prosperous time in the city had a major commercial impact from the 1880s until the opening of the Panama Canal in 1914. After this date, the harbour was no longer within the main shipping route, and the economic activity of the city decreased drastically. During the flourish period, immigrants of all social classes disembarked to the port of Valparaíso, most of them coming from Europe (English, Germans and Italians) and North America. The foreign population brought with them plenty of commercial goods, but also new social paradigms that induced a big transculturation process which was reflected not only in the society but also in the urban environment of the city. In the last two decades of the 19th century, Valparaíso experienced a big economic boom that left an indelible trace in the urban layout and the architectural heritage of the city. Valparaíso was divided into four main zones (see Figure 3-2): (1) the *Almendral* neighbourhood, (2) the Port downtown area, (3) the residential zone on the hills including the *Cerros Alegre* and *Concepción* (4). The Port downtown area was characterized to be the principal commercial and banking zone, where monumental buildings of high architectural value constituted the most important streets of the city. Most of these constructions belonged to the Neoclassical style and were designed by important architects of the time (Figure 3-3).

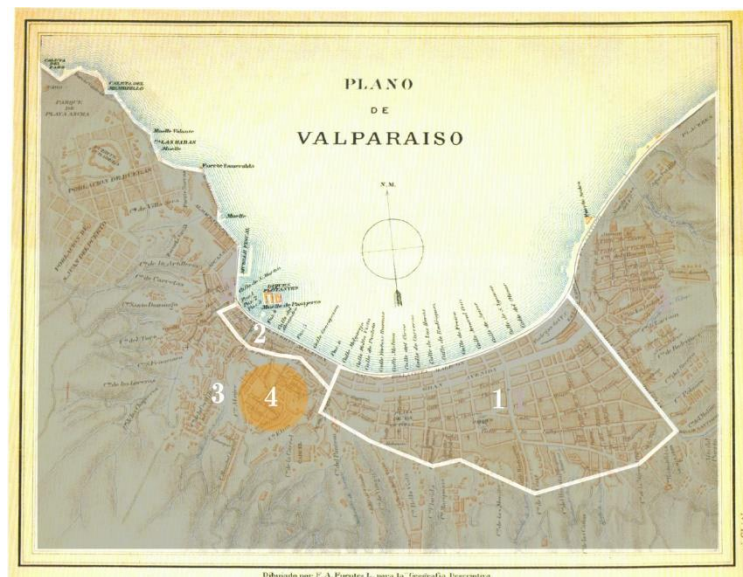


Figure 3-2. Plan of Valparaíso in 1879: (1) *Almendral* neighbourhood (2) Port and commercial downtown area, (3) residential zone on the hills and (4) *Cerro Alegre* and *Cerro Concepción* (Vásquez, Iglesias, and Molina 1999).



Figure 3-3. Buildings belonged to the Neoclassical style in the commercial downtown area of Valparaíso: (a) Valparaíso's Stock Exchange building and (b) Chile Bank (unknown author).

The residential areas of the city were mostly consolidated on the hills, where new neighbourhoods emerged to house the foreign population in the city. *Cerro Alegre* and *Cerro Concepción* (zone 4 in Figure 3-2) have the particularity of having grown based on European influences from their beginnings, since numerous English and German families made their communities there (Urbina 2002). The morphology of the hills is composed by a plateau between ravines. Contrary to other neighbourhoods of spontaneous growing, the *Cerro Alegre* and *Cerro Concepción* had clear urban planning in the plateau zones, constituted by an ordered grid similar to those of the Spanish foundation. Based on old chronicles of Valparaíso, Rivas (2000) describes the *Cerro Alegre* as the first hill with the best urban advances of the city: paved roads and sidewalks, beautified public spaces, and various other embellishment works, such as home gardens with green and flowery finishes, and houses with high architectural value. Urban equipment, such as schools, churches, as well as the houses, reflected the foreign influence in terms of both construction techniques and architectural styles. From an architectural standpoint, the buildings on these neighbourhoods showed a distinctive Victorian style, which was the trend in Europe and North America, as well as in many Latin American cities, from the mid-19th century on. In Valparaíso, this style is most recognizable in the houses' morphology and facade composition (e.g. bow-windows and sash windows) along with the ornamentation, door types, and finishes.

The houses were commonly built using timber frame techniques for the main structural system, but also mixed with unreinforced masonry load-bearing walls and foundations. Most of the houses used corrugated iron planks to cover the load-bearing structure, constituting a homogeneous appearance within the buildings of the neighbourhoods. This house typology reached big popularity in Valparaíso as testified in the newspaper's advertisements of the time offering prefabricated new housing models like those still extant on the *Cerro Alegre* and *Cerro Concepción* coming directly from Europe, as well as sales of construction material such as Oregon pinewood, national wood, zinc planks for house cladding, etc. Many of these advertisements were

also written in English to get the attention of foreign readers (see Figure 3-4), an evidence that demonstrated a clear transcendence and influence coming from the English and North American population in the city. Jiménez (2015) stated that traditional timber frame buildings existing in the *Cerro Alegre* and *Cerro Concepción* in Valparaíso have an evident foreign character, having several similarities with the well-known old English houses and evolved typologies, as the stud and platform frame systems. However, the buildings in the *Cerro Alegre* and *Cerro Concepción* are not mere copies of the English houses, but combined local techniques to solve the specific requirements of the city, such as the seismic hazard and the staggered conditions of the terrain.

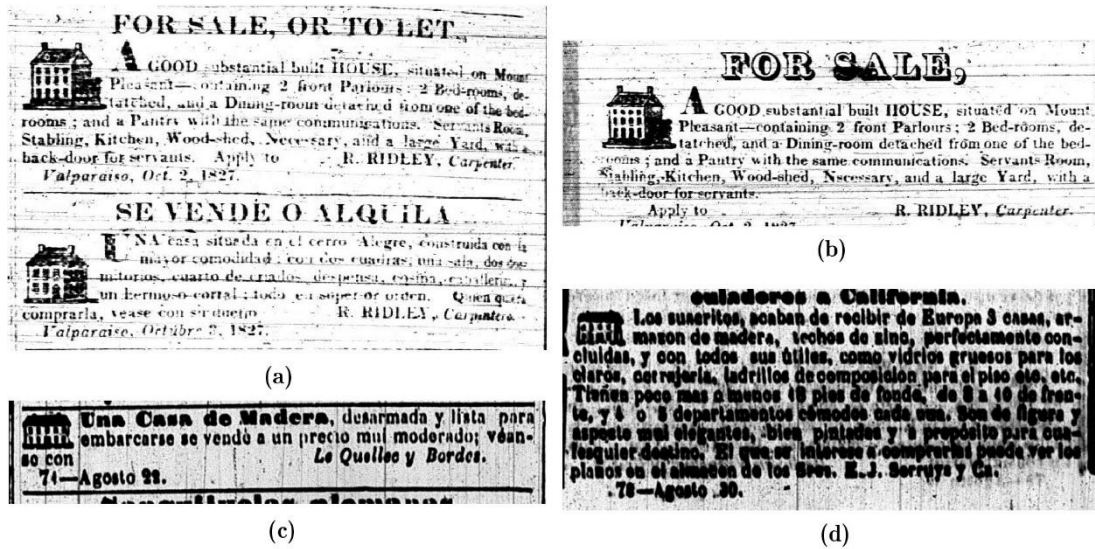


Figure 3-4. Old Newspapers advertisements (1827-1830) written in Spanish and English which offered (a-b) timber houses for rent and (b-c) prefabricated houses coming from Europe to sale in Valparaíso.

3.2.2 Historical earthquakes

Several major earthquakes struck the city of Valparaíso causing devastating effects on the urban tissue and a large number of fatalities. During the late 19th and early 20th centuries, two seismic events of very high intensity were recorded, in 1873 and 1906. The former had the epicentre at 173 km away from the city. According to the stories of chroniclers and travellers of the time, the city did not suffer important losses in the 1873 event. However, the 1906 earthquake was the most devastating seismic event recorded so far in the city, reaching an estimated magnitude of 8.2 Mw and IX degrees in the Mercalli scale. The 1906 catastrophe marked a turning point in the history of the city, which was almost completely destroyed and suffered a long period of recovery. According to Palacios (2015), there were more than 2000 fatalities and around 4000 people were injured, most of them due to the collapse of the buildings and the multiple fires. Palacios (2015) stated that after the earthquake, 39 fires were simultaneously triggered due to the overturning of stoves and gas pipes ruptures. The fire burned for three days and was very difficult to control due to the water pipes being broken and without any water supply in the city. Hence, the few buildings that resisted the earthquake were also destroyed by the flames. Figure 3-5 shows the affected zones after the 1906 earthquake where the *Almendral* neighbourhood (highlighted red zone at the

southeast of the city) was almost completely destroyed. Most of these buildings were made of URM. Conversely, the zones of the hills, including the *Cerro Alegre* and *Cerro Concepción* neighbourhoods, as well as the Port downtown area, did not suffer major damages in their constructions but only in the public spaces, as shown in Figure 3-6. The buildings of the hill zones were made of timber frame systems, while the buildings in the downtown area were made of concrete and wrought iron systems.

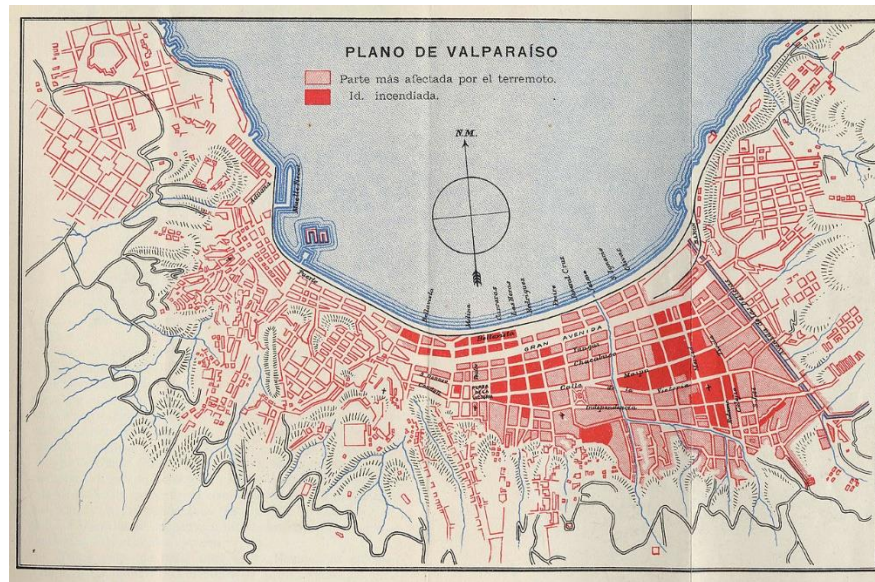


Figure 3-5. Plan of Valparaíso after the 1906 earthquake.



Figure 3-6. Paseo Atkinson in Cerro Concepción: (a) photography of 1870 and (c) after the 1906 Earthquake.

The consequences of the 1906 earthquake were desolating for the population of the city in terms of human and economic losses. The destruction was so thorough and widespread that the city completely lost its elemental functionality, revealing a very low seismic resilience. Eight months after the catastrophe, many people were still living in poor conditions, agglomerated either in small houses or in precarious shelters on the hills. The reconstruction of the city took more

than three years and required huge economic efforts. Nevertheless, the experience left important advances, such as the foundation of the Seismological Centre of Chile in 1908.

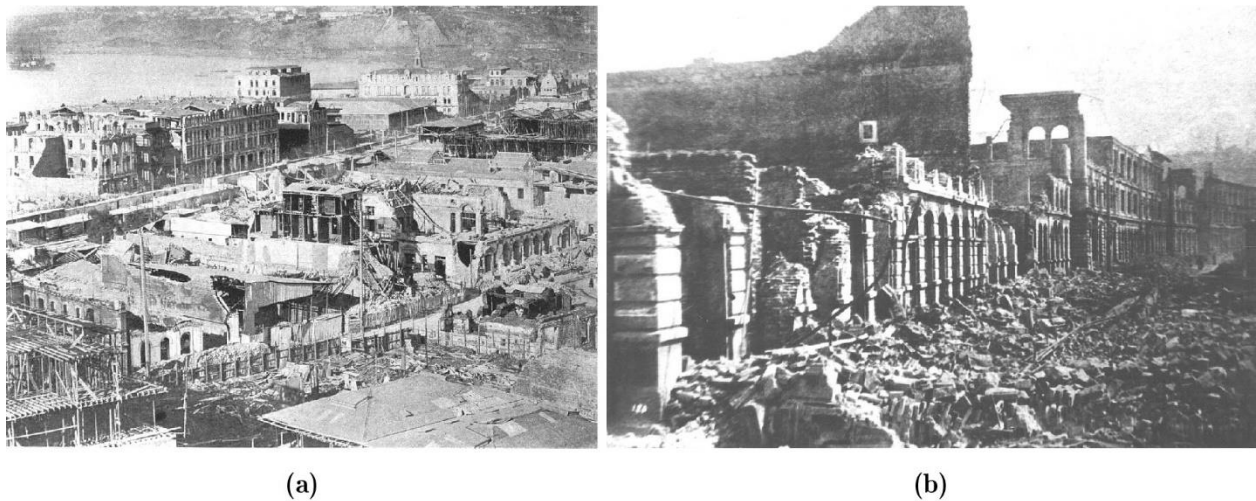


Figure 3-7. Panoramic views of the downtown area of city of Valparaíso after the 1906 earthquake.

Seventy-nine years later, another very destructive earthquake occurred in Valparaíso on March 3rd of 1985, which reached a magnitude of 8.0 Mw and VIII degrees in the Mercalli scale. The epicentre of the earthquake was located 20 km far of the coast of Valparaíso and 15 km of focal depth. According to the technical report by ONEMI - División de Protección Civil (2009), 68 lives were lost and 923 people were injured just in the city of Valparaíso, most of them as a consequence of the building' collapsing (see Figure 3-8). Furthermore, more than 17000 houses suffered total or severe damage, and more than 20000 were partially damaged, resulting in more than 3500 people being left homeless. Additionally, more than 30 health facilities and 30 educational establishments were completely destroyed in the city. As in the 1906 earthquake, the houses on the *Cerro Alegre* and *Cerro Concepción* demonstrated their anti-seismic character without suffering severe structural damages.

Two major earthquakes have hit the city of Valparaíso in the last ten years. The first occurred on January 27th of 2010 with epicentre 543 km south of Valparaíso (in Cobquecura city, Bio-bio region). Despite the remoteness of the epicentre, the event recorded a significant intensity of VII degrees in the Mercalli scale. There were 26 fatalities in Valparaíso, and more than 200 buildings, mostly located in the historical centre of the city, suffered critical structural damage. The public hospital of the city also suffered important structural damages. As in the 1906 and 1985 earthquakes, the timber frame buildings of *Cerro Alegre* and *Cerro Concepción* did not report either important structural damages or collapses. However, many timber frame buildings in the centre of Valparaíso were damaged, as shown in Figure 3-9. Unfortunately, there are no official detailed post-disaster survey data, thus the real levels of damage of the affected buildings were not catalogued. The last important seismic event was recorded in Valparaíso on April 24th of 2017 with epicenter in front of the coast. This event reached a magnitude of 6.9 Mw and VII degree in

the Mercalli scale, but it had a lower impact than the 2010 earthquake, with neither fatalities or collapses of buildings in the city. Despite the numerous earthquakes that affected the city of Valparaíso, an important part of the built heritage is still well conserved. This fact validates the anti-seismic nature of the historical buildings, many of them designed without any reference to seismic codes.

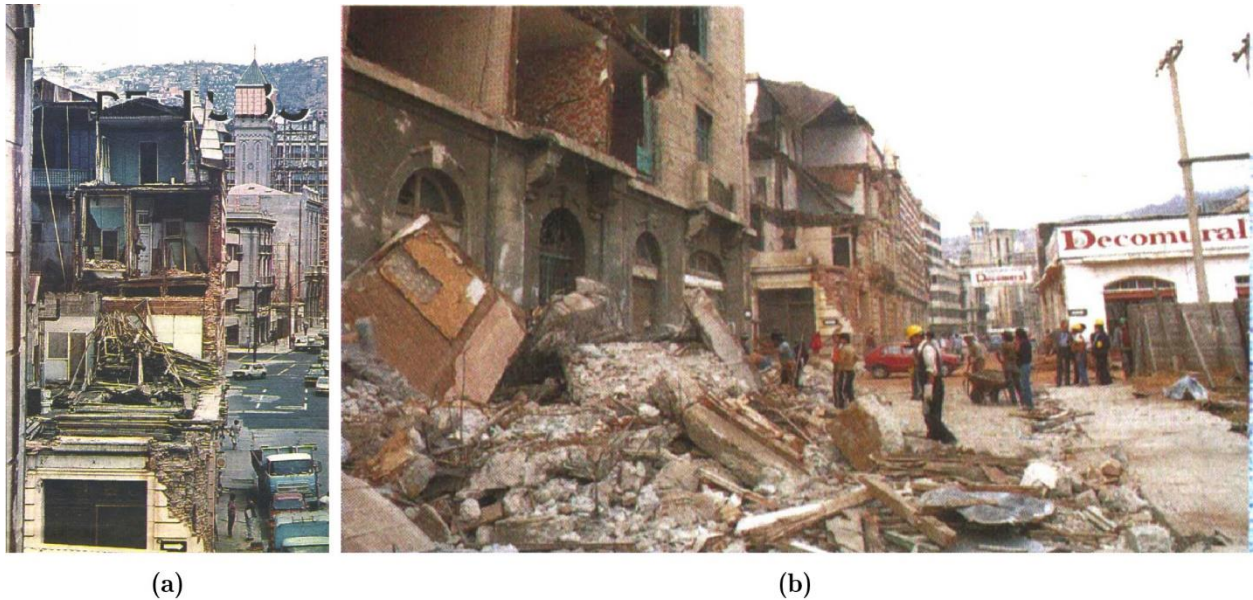


Figure 3-8. Collapsed buildings in the 1985 Earthquake located in the Blanco street at the Almendral neighbourhood.



Figure 3-9. Timber frame buildings damaged after the 2010 earthquake in the down town area of Valparaíso: (a-b) partial overturning of the façades. (Photos by Lautaro Triviño)

3.2.3 UNESCO world heritage status and current condition

The historic quarter seaport of the city was inscribed in the World Heritage Site list by UNESCO since 2003. The title was granted in recognition of the exceptional testimony to the early phase of globalization in the last 19th century, when the city was one of the principal

commercial routes of the Pacific coast of South America. This award remarked the integrity and authenticity of the historical centre of Valparaíso which includes a consolidated urban layout, valuable public spaces and buildings with a large variety of construction techniques, and different styles of adaptation strategies to the landscapes. UNESCO also highlighted the value of the port and naval heritage, as well as of the transportation infrastructure including funicular elevators and trolley electric systems.

Currently, the heritage buildings of Valparaíso are exposed to possible danger due to their poor condition of conservation, low investment in retrofitting, and the high seismic hazard levels on the city. The lack of technical information and detailed seismic studies increases the uncertainties regarding the seismic safety of the buildings. This lack of knowledge represents a high source of risk for the vital functions of the city since the potential collapse of the buildings could imply the partial or total loss of the vital networks and facilities. In the following sections all the elements of the studied area, as well as the sources of hazard, are characterized in order to compile the fragmentary information from the literature and to identify the lack of information necessary to carry out an urban seismic risk analysis.

3.3 Seismic hazard

Chile represents one of the most seismically hazardous countries of the world, and constitutes a territory of special interest for the earthquake-engineering field. The high seismic activity is due to the action of the Nazca and South American plates, which formed a subduction zone under a large part of the country, as shown in Figure 3-10. Several seismic hazard studies have been developed for the Chilean territory and their specific cities along the time. One of the earliest study about the whole Chilean territory was carried out by Lomnitz (1969), with a probabilistic analysis and a seismic hazard map considering only the seismic events that exceeded a magnitude of 7.5 Ms. More recently, other authors have developed deterministic seismic hazard evaluations of the Chilean territory based on the past earthquakes data such as Barrientes (1988), Algermissen et al. (1992), F. Leyton et al. (2009) and Leyton, Ruiz, and Sepúlveda (2010).



Figure 3-10. Chilean subduction zone: Nazca and South American plates.

The seismic hazard of Valparaíso has been studied by different authors who developed seismic microzonation maps of the city. These studies commonly describe the dynamic characteristics of the soil, such as the ones carried out by Baquedano and Leyton (2012), Castañeda (2013), and the National Institute of Geology and Mining (SERNAGEOMIN 2018). The former used microvibration frequencies measured in strategical locations along the soil of the city (Figure 3-11a) to create a microzonation map. The hypothesis in this methodology states that the seismic response of the soil in high-intensity earthquake territories is not homogeneous. This phenomenon is called “site effect”, and it means that the seismic amplification strongly depends on the local configuration of the soil. The fundamental vibrations were obtained through the Nakamura method. The superficial geological characterization of Valparaíso (SERNAGEOMIN 1996) was used to determine the seismic microzonation map shown in Figure 3-11b. The lowest predominant frequencies, which ranged between 0.3 – 2.4 Hz (red and purple dots in Figure 3-11a), were recorded in the flat zones of Valparaíso, corresponding to the Port zone and the *Almendral* neighborhoods. Artificial and poorly compacted soil also characterize the flat areas constituted by coastal and current wind deposits (Qe class). The *Cerro Alegre* and *Cerro Concepción* zones were characterized by high predominant frequencies ranging between 4.0 - 6.5 Hz (green dots in Figure 3-11a), being areas with hard soils, classified as intrusive rocks of the Jurassic (JIV). In general, the frequencies increase progressively towards the highest zones of the city with rocky soils. The territory was divided into four seismic zones from I to IV, with IV being the most dangerous one (Figure 3-11b).

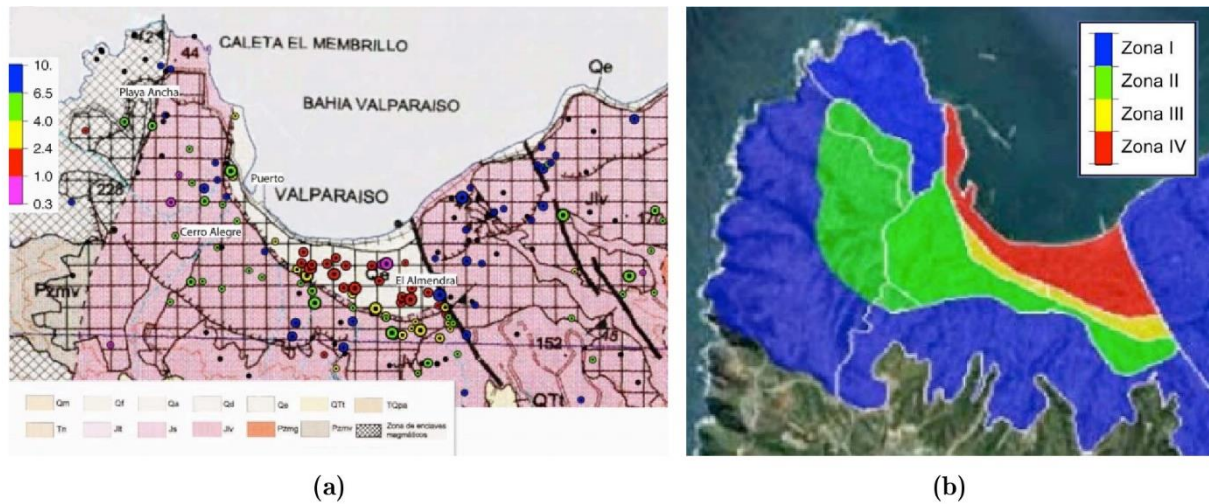


Figure 3-11. (a) Fundamental frequencies of the soil measured in different sites of Valparaíso (in Hz) used to define the (b) microzonation map (Baquedano and Leyton 2012).

SERNAGEOMIN (2018) has recently provided a complete web platform with the microzonation maps of the principal cities of the country. In the case of Valparaíso, the map divides the territory into 5 zones, ranging from A to E, with E being the most hazardous zone. Two parameters were analysed to configure the map. The first one is the average shear wave propagation of the soil, measured up to 30 meters' depth (V_{s30}), and the second one is the predominant period of the soil (T_0), associated to the application of the Nakamura technique which considers the maximum value of the HVSR curve (horizontal to vertical spectral ratios). Several measurements of both parameters were recorded in strategical locations of the city and classified as listed in Table 3-1. Additionally, three different seismic scenarios were simulated considering different Peak Ground Acceleration values (PGA), which correspond to different expected earthquakes of 8 Mw, 8.8 Mw and 9.2 Mw. Figure 3-13 shows the Scenario 3 where the PGA values range from 0.17g to 0.369g. According to the Instrumental Intensity Scale developed by the United State Geological Survey USGS, such PGA values corresponding to intensities of VI and VIII, respectively, in the MMI Scale, where light and moderate damage is expected.

The Chilean Seismic Code NCh 433 Of. 1996 (Instituto Nacional de Normalización 2009) divided the territory into three seismic zones (1, 2 and 3, being 3 the most hazardous one) based on the expected peak ground acceleration A_0 . The city of Valparaíso is classified in the Zone 3, as shown in Figure 3-14, with a maximum effective acceleration of the soil equal to 0.4g corresponding to an intensity of VIII in the MMI scale, where moderate to heavy damage is expected.

Table 3-1. Seismic classification of territory of the city of Valparaíso shown in Figure 3-12 according to SERNAGEOMIN (2018).

Category	1ST criterion Vs30 (m/s)	2nd criterion T0 (S)
A	≥ 900	< 0.15
B	≥ 500	< 0.30
C	≥ 350	< 0.4
D	≥ 180	< 1.0
E	< 180	-

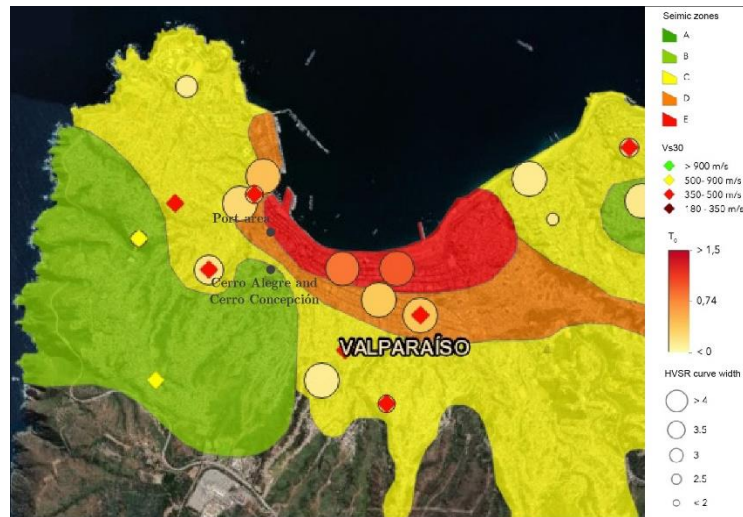


Figure 3-12. Seismic hazard map for the Scenario 3: PGA values ranging from 0.17g to 0.369g. SERNAGEOMIN (2019).

Based on the available studies on the seismic hazard of Valparaíso, it is noted that the Port area and the *Almendral* neighbourhood are the most seismic hazardous areas of the city (red and orange zones in Figure 3-12). This is due to the artificial and poorly compacted nature of the soil, which corresponds to the highest PGA values, and lowest fundamental frequencies and shear wave propagation values. The hills zones, including the *Cerro Alegre* and *Cerro Concepción*, are less seismically dangerous due to better conditions of the rocky soils, but they still present high values of PGA. The localized study of the geological and physical characteristics of the soil is very important in Valparaíso as these features play an important role in assessing the seismic risk of the urban buildings.

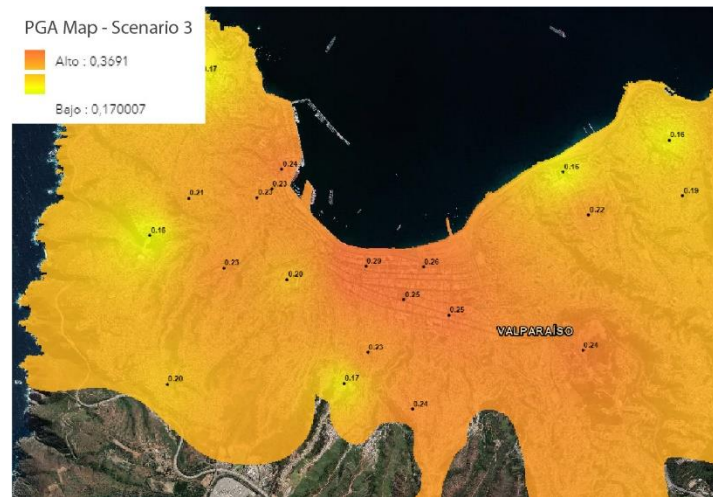


Figure 3-13. Seismic risk scenario of an expected earthquake of 9.2 Mw based on the local PGA values.

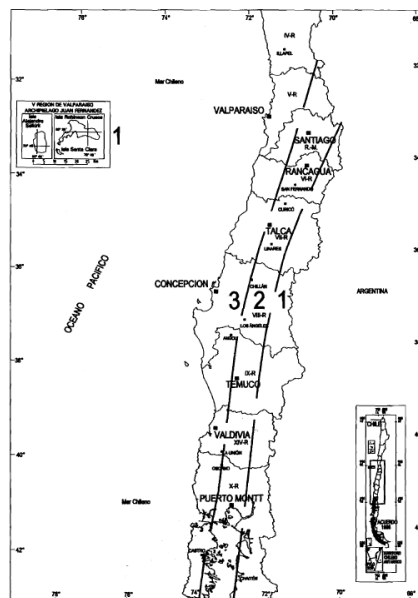


Figure 3-14. Seismic zonation of the central zone of Chile.

3.4 Emergency Limit Condition

Cities and urban settlements are not always well-prepared to suffer, manage and mitigate the effects of major natural disasters, such as high-intensity earthquakes. In these cases, such catastrophic events signify devastating consequences in terms of life, material and economical losses, as well as the partial or even total interruption of the vital functions of the city. The concept of resilience reflects the ability of a city exposed to hazard to resist, absorb, accommodate and recover from the effects of a disaster in a timely and efficient manner, including through the preservation and restoration of its essential basic structures and functions (UNISDR 2009). The resilience level of a settlement is tightly related to the existence of disaster risk reduction plans to mitigate the potential consequences of natural hazards. In this regard, a city has to be evaluated

as a complex system composed of strategic elements, which allow the minimum functionality of the basic and strictly necessary social, economic, political, cultural and environmental infrastructure after a major catastrophe. The acceptable risk and minimum functional urban structure of a settlement must be particularly determined based on the analysis of the exposed elements within the whole system.

In this thesis, the concept of Emergency Limit Condition (ELC) is adopted based on the initiative promoted by the Italian Civil Protection (Commissione tecnica per la microzonazione sismica 2014). This approach determines a set of integrated and coordinated mitigation strategies based on emergency management systems of the urban settlement. The analysis of the ELC is aimed to integrate particular interventions in the territory to mitigate the seismic risk at local scale, reassuring the emergency management systems (i.e. strategic buildings, emergency areas, routes, infrastructure of connection and accessibility). The main purpose of the analysis is that the urban settlement conserves the functionality of most of the strategic functions in case of an emergency, with connections and accessibility within the territorial context. Among the different limit conditions that could be defined for the urban settlements, the ELC corresponds to the conditions whereby, immediately after a seismic event, the urban settlements as a whole suffers physical and functional damage leading to the interruption of almost all the urban functions (Commissione tecnica per la microzonazione sismica 2014).

This study sets the ELC zone of the selected area within the historical centre of Valparaíso, including the neighbourhoods of the *Cerro Alegre*, *Cerro Concepción* and the Port downtown area. The ELC analysis is in line with the civil protection and emergency plans of the city (Comité Comunal de Protección Civil y Emergencia 2019; ONEMI 2016), which define the security zones and evacuation routes in case of tsunamis.

3.4.1 Civil protection and emergency plans

Valparaíso is not only a city prone to earthquakes but also to tsunamis, because of its coastal nature. This additional hazard encouraged the development of civil protection plans aimed to promote and coordinate seismic risk mitigations strategies. Evacuation plans are essential tools to systematize the emergency schemes through ad-hoc routes leading to safe areas.

The Civil Protection plan of Valparaíso proposes several evacuation routes to safe zones on the hills. According to MINVU (2017), the risky zones are those that can be potentially flooded by a tsunami, comprised between the coastline up to 30 meters above sea level zones, as shown in Figure 3-15. The plan also considers Meeting Points at the end of the evacuation routes. These designated places are meant to aid in the regrouping of people (minors, families, etc.) and facilitates any assistance that people may need. All of them must provide basic sanitary services, drinking water for the next 12 hours, as well as medical and psychological attention for possibly

injured people. Meeting points have commonly large dimensions and allow the access to emergency vehicles to a large number of people. The evacuation streets must have universal access with a minimum width of 11 meters, as well as public lighting and pavement in good condition. Pedestrians or vehicles normally use these routes with traffic towards the coast, in order to facilitate the flow of vehicles. The evacuation route must have ideally a slope lower than 12%, even though this rule is not always respected in Valparaíso. Figure 3-15 shows a part of the Tsunami Evacuation Plan of the city of Valparaíso developed by the Comité Comunal de Protección Civil y Emergencia (2019), which included the neighborhoods investigated in this doctoral thesis, i.e. the *Cerro Alegre* and *Cerro Concepción* as well as the Port downtown area. Figure 3-15 shows the unsafe zones which must be evacuated coloured red, while the evacuation routes are blue, and the safe lines and meeting points are green.

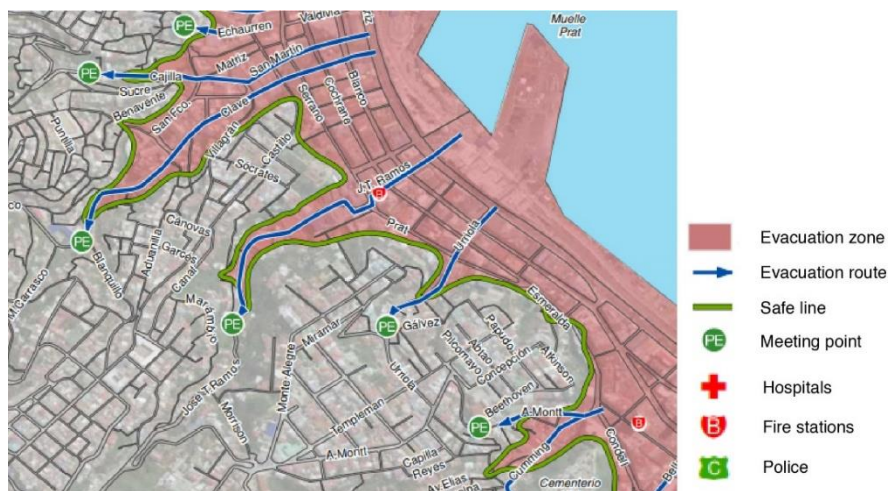


Figure 3-15. Tsunami Evacuation Plan for the city of Valparaíso. Neighbourhoods of *Cerro Alegre* and *Concepción* and Port downtown area (Comité Comunal de Protección Civil y Emergencia 2019).

Tsunami Inundation Maps are also used in Valparaíso to determine the potential impact of a flood in the city. These maps are developed based on recorded data of historical tsunamis combined with numerical simulation tools taking into account topographic, bathymetric and seismic data of the territory. Figure 3-16 depicts a Tsunami Inundation Map of the city of Valparaíso developed by the Hydrographic and Oceanographic Service of the Chilean Navy (SHOA 2012). The areas that could potentially flood in case of a major tsunami are delimited based on two sources of data: (i) the historical records of the 1730 earthquake, which provoked a subsequent tsunami, and (ii) a numerical simulation model. The numerical model was fed with topographic and bathymetric information, as well as with the urban plan of the city. The evidence of the flooded areas in the past tsunami was highlighted in the map to reference hazardous zones. The inundation map has a direct application in the civil protection plans executed by the local authorities, concerning the mitigation and prevention of tsunami impacts. Comparing both the Tsunami evacuation and the Tsunami inundation maps it is possible to recognize a good agreement between the unsafe zones and the potentially flood-prone areas.

The *Cerro Alegre* and *Cerro Concepción* neighborhoods are within the safe zones located at levels higher than 30 meters far away from areas of possible flooding, as shown in Figure 3-15 and Figure 3-16. Two evacuation routes connect the risky zones in the centre of the city with the safe zones in these neighborhoods, named the *Urriola* (Figure 3-17) and *Almirante Montt* streets. In the following section, the civil protection plan of the city of Valparaíso is used to delimit the area for the seismic risk assessment of this doctoral thesis. The study of this delimited zone of the city constitutes a first pilot case that may be extended in the future to other vital networks and elements of the city.



Figure 3-16. Tsunami Inundation Map of the city of Valparaíso developed by the Hydrographic and Oceanographic Service of the Chilean Navy (SHOA 2012).



Figure 3-17. Tsunami risk evacuation drill in (a) Urriola and (b) Alvaro Besa streets in the City of Valparaíso on September 5TH, 2018. (Photos by Adolfo Balboa Monroy - MINVU)

3.4.2 Mapping of the Emergency Limit Condition

Urban seismically hazardous zones need rigorous disaster mitigation plans to safeguard the population and also the vital functions of the city. Such strategies should guarantee both the civil protection and the structural integrity of the building stock after a major earthquake. The civil protection plans of Valparaíso regulate the evacuation of the population to avoid tsunami flooding catastrophes. However, such plans do not consider another crucial aspect, i.e. the assessment of the potential vulnerability of the buildings. In fact, the possible collapse of these structures, besides danger the lives of occupants might obstruct the usability of the emergency routes and safe areas in case of tsunami evacuation. The vulnerability assessment of the urban fabric requires a significant amount of resources and efforts to collect technical building data (if they are not publicly available) and to examine the buildings in-situ. Since this analysis is not always possible, or at least not for all the buildings of a determined area, the definition of an Emergency Limit Condition (ELC) represents an optimum criterion to bound the area for the analysis. This approach considers the analysis of strategic and potential interfering buildings that may block the emergency and safe areas defined by the civil protection plans. ELC includes emergency routes, strategic buildings for the emergency phase and potential interfering buildings. The interfering buildings are defined as those positioned along emergency areas (evacuation routes or safe areas) which might collapse, even partially, affecting the functionality of the necessary connections during the post-seism emergency.

The selected ELC system within the historical centre of Valparaíso comprises two emergency routes towards the *Cerro Alegre* and *Cerro Concepción*, both of them connecting two neuralgic locations in the downtown area with safe zones. The former –named Route A– is traced from the *Sotomayor* square, going through the *Prat* and *Urriola* streets up to the Meeting point located at 30 m height in the *Cerro Alegre*, as shown in Figure 3-18a. The second –named Route B– starts in the *Aníbal Pinto* square, going through the *Almirante Montt* street up the Meeting Point located at 30 m height in the *Cerro Concepción*, as shown in Figure 3-18b. There is only one strategic building within the route A, a fire station located in the *Sotomayor* square. The remaining buildings are evaluated as possibly interfering buildings, considering the criteria suggested by the Italian guidelines proposed by Commissione tecnica per la microzonazione sismica (2014).

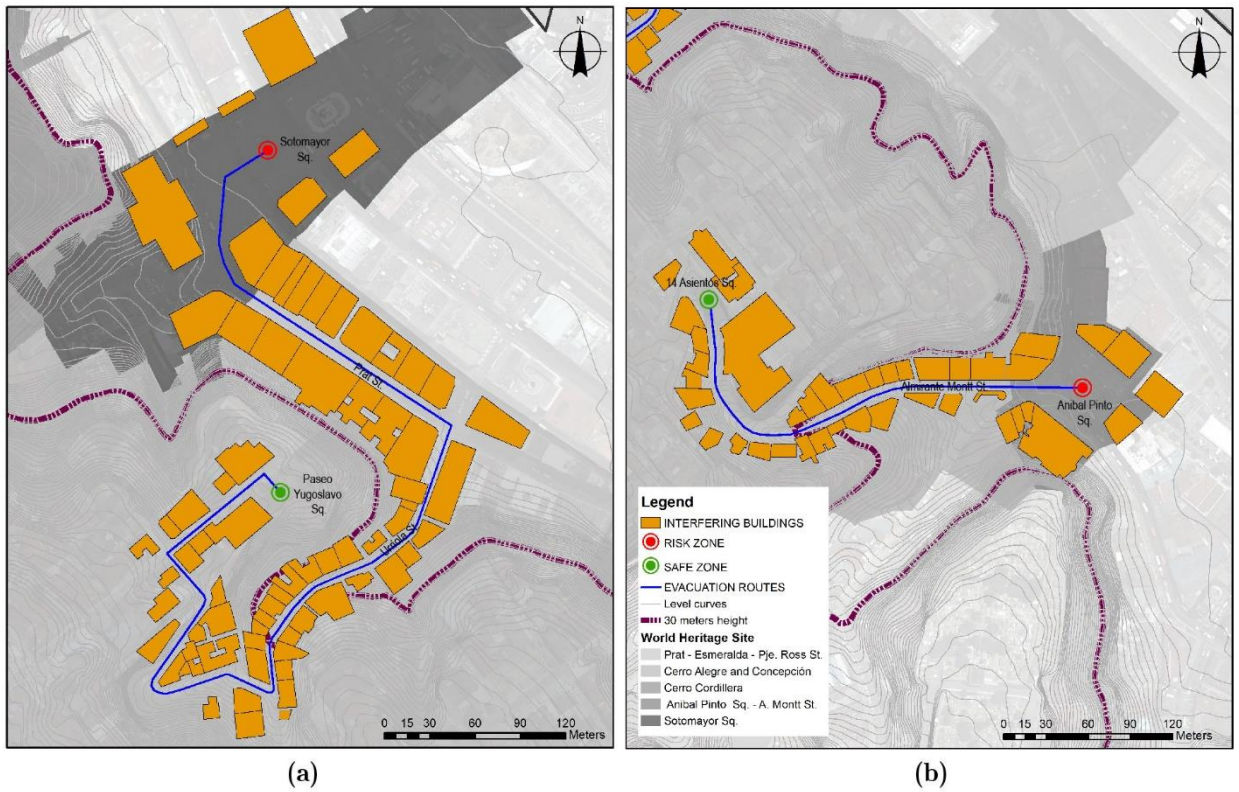


Figure 3-18. ELC system defined for the *Cerro Alegre, Cerro Concepción* and Port downtown area in Valparaíso: (a) Route A and (b) Route B for evacuation in case of emergency.

From a geometrical standpoint, the building must be considered as interfering if the height (H) of the building, measured up to the beginning of the roof, is higher than the distance (L) between the base of the building (B) and the opposite edge of the infrastructure of access or connection (emergency routes), as shown in Figure 3-19. This means that the debris resulted from the possible collapse of interfering building can hinder vehicles or people the access or transit along emergency evacuation routes.

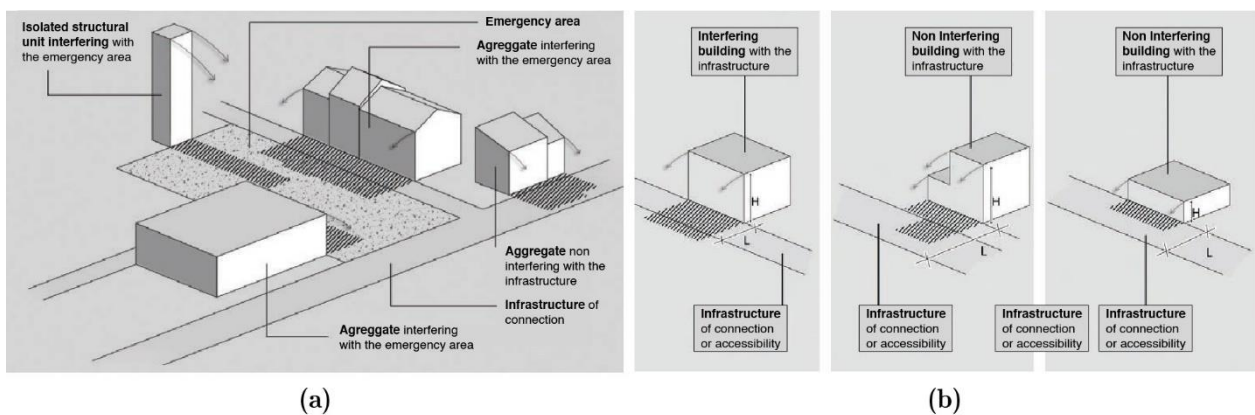


Figure 3-19. Interfering building on (a) safe zones and (b) evacuation infrastructure (Commissione tecnica per la microzonazione sismica 2014).

3.5 Building typologies

The defined Emergency Limit Condition (ELC) system is characterized by the predominant historical character of the urban fabric. The buildings constitute characteristic elements of some of the oldest neighbourhoods of the city. Most of the historical neighbourhoods of Valparaíso started growing in the zones closest to the coastal line, taking advantage of the flat zones and the proximity to the port, as is the case of the named Port downtown area. However, the flat zones were very scarce, and urbanization continued expanding towards highest zones on the hills. Within this process, the *Cerro Alegre* and *Cerro Concepción* neighbourhoods were ones of the first to be consolidated at the beginning of the eighteenth century, as detailed in Section 3.2. This growth pattern is a direct consequence of the spontaneous settlement characteristic of the inhabitants, who built their houses and neighbourhoods without any urban planning since the beginning.

The buildings located on the hills are characterized by a fearless adaptation the staggered hillsides, some of them with more than 40 degrees' slope (Figure 3-20a). A common adaptation strategy involved the use of stone or brick masonry basements (Figure 3-20b), as well as retaining walls to counteract the trusting effect of the soil. In the steepest hillsides, the buildings usually have staggered configurations in elevation, and combine the use of basement and retaining walls structures to create terraces and stabilize the terrain. Most of the buildings of the stock are enclosed in structural aggregates arranged in-row. This condition is sometimes interrupted by narrow passages existing between two buildings with public or private walkways or stairways (Figure 3-21a). Some wastelands are also present between buildings (Figure 3-21b).



Figure 3-20 (a) Buildings adapted to the stepped hillside in the Almirante Montt street, and (b) a mixed stone and masonry basement in the Urriola street.



Figure 3-21. (a) Narrow passage between two buildings in Urriola street, and (b) buildings next to a wasteland in Almirante Montt street.

The ELC zone is characterized by the structural heterogeneity of its urban fabric, mainly configured by timber frame, unreinforced masonry, reinforced concrete (RC), wrought iron and hybrid building typologies. It is certainly difficult to determine the main load-bearing systems of the buildings in a preliminary exterior inspection. However, an initial classification of the existent typologies can be made by judging the external aspects, scale and the construction culture of the city. Most of the buildings on the hills were conceived for residential use. This use is still predominant and currently extended to touristic and commercial facilities, e.g. hostels, restaurants, shops, etc. The residential architecture of the zone is characterized by a strong vernacular nature, where the oldest houses were built without any compliance with seismic codes. The neighbourhoods of *Cerro Alegre* and *Cerro Concepción* are considered excellent cases of study due to the pioneer character of the timber frame typology, with representative models of the residential architecture of the city. These objects represent an important part of the historical heritage of the city and are still well-preserved.

The timber frame buildings can be easily recognized by the typical use of corrugated iron planks covering the façade. Many of these buildings combine timber and masonry load-bearing systems, the last less notorious from exterior inspections. Masonry sidewalls are commonly present in structural aggregates, having both structural and firewall roles. In other cases, load-bearing masonry walls arrange the façades along the total or partial height of the building, with timber frame structures only for the internal partitions and stories. Masonry is commonly covered by lime plaster and painted, as shown in Figure 3-22a. Low-rise buildings (up to two stories) have usually timber frame for the main load-bearing structure, and masonry only for sidewalls. The high-rise buildings (up to five stories) usually combine timber and masonry load-bearing systems even in the façades, as shown in Figure 3-22. Most of the timber frame systems present regular façades, with bow windows or balconies, and few ornamentations. The in-plan layout of these

buildings often presents asymmetrical shape due to the irregular urban fabric and the distribution of the aggregate. However, the plan of the buildings is generally compact without significant appendixes or setbacks.



Figure 3-22. Hybrid timber-masonry building with masonry walls at the ground floor and timber frames at upper levels: (a) façade, and (b) internal view of the brick masonry wall.

According to Jiménez (2015), the timber structures usually follow the platform frame configuration where each story works as a platform to support the structures above. The walls are mainly configured by vertical posts, named studs, spaced $0.4 \div 0.6$ m each, and located between the top and bottom horizontal plates. The walls are braced by diagonal members usually crossing three studs, grouped according to “V” bracing systems. These diagonals are usually placed next to the openings, as shown in Figure 3-23a. The timber elements of the walls are connected using traditional carpentry joints, being the mortise-and-tenon and the notched the most frequent ones, as shown in Figure 3-24. These connections are usually reinforced using nails to fasten the pieces.



Figure 3-23. Timber frame load bearing systems: (a) bare frame wall built next to a masonry sidewall, and (b) platform frame configuration (Jiménez 2015).



Figure 3-24. Carpentry joints in timber frames: (a) tenon at the end of a stud, configuring the mortise-and-tenon joints, and (b) stud and diagonal connected by a notched joint (Jiménez 2015).

Adobe blocks constitute the common filling of the timber frames along the perimeter of the buildings, while the lath-and-plaster technique is used to cover the internal partitions, as shown in Figure 3-25. The cross-section of the elements of the façades vary from $0.15 \times 0.15 \text{ m}^2$ and $0.15 \times 0.10 \text{ m}^2$, while the internal elements have a smaller cross-section of $0.10 \times 0.10 \text{ m}^2$. The stories are composed of timber joists of $0.12 \times 0.05 \text{ m}^2$ cross-section and 0.4 m separation, as shown in Figure 3-23b. The roofs have usually pitched shape made of rudimentary timber trusses.



Figure 3-25. External wall filled with adobe blocks and (b) internal wall covered using the lath-and-plaster technique.

Most of the buildings located in the Port downtown house commercial, governmental, cultural and business activities, including banks, courts, private offices, and cultural institutions. Their use is propitiated by the monumental character and large dimensions of the buildings. Some of these constructions are the oldest of the stock, dating back to the late 19th and early 20th centuries, and present remarkable architectonic value. These buildings have neoclassical style, characterized by the use of symmetrical forms, decorative columns, triangular pediments, domed roofs, etc. Although they constitute a minority within the building stock, their remarkable historical value

makes them an important part of the present study (Figure 3-26). Unfortunately, original building information of these buildings is very scarce and few studies can reveal their structural configuration. An article of the time published in the *Concreto Revista de Ingeniería y Arquitectura* (1919) gives details of the structural configuration of one of this historical buildings: *La Bolsa de Valores de Vaparaíso*. The five-story building has 960 m² plan and 37.50 m height, and is located at the bottom of the *Cerro Alegre* in the intersection between the Urriola and Arturo Prat streets, in the corner of a structural aggregate in semi-staggered land, as shown in Figure 3-26a.

Important engineers or architects of this period, such as Carlos Claussen, Gustavo Jullian and the Italians Arnaldo Barison and Renato Schiavon, undertook the design of this Renaissance-style building, dating back to 1912. The building has a hybrid system made of wrought iron and RC structural members. The principal load-bearing system is made of laminated “C” profiles and complex trusses of wrought iron filled with plain concrete. The dimension of the profiles varies with the height of the buildings at each story. The first and second floors have the largest “C” section profiles with 0.25 m depth. The walls of the third and fourth floors have smaller “C” profiles with heights of 0.20 m and 0.15 m, respectively. The fifth story structure present double “T” profiles with 0.15 m height. The sidewalls of the building present wrought iron double “T” posts of 0.2 m height, spaced at 2.5 m and linked by at least two horizontal profiles. The thickness of the plain concrete fill of the frame is 0.25 m. The overall configuration of the interior walls is similar to that of the main façade, with iron profiles filled with plain concrete and thicknesses varying from 0.20 m to 0.4 m. Isolated continuous pillars support the upper stories and a dome structure in the central part of the building. The story systems are composed of double “T” beams, with varying section from 0.3 m to 0.2 m along the height of the building, according to the spans and load requirements. A set of secondary iron beams topped with concrete constitutes the slabs of the buildings. Tiles or wooden boards cover the floor, depending on the use of the rooms. The roof systems are composed of iron trusses covered by galvanizes iron sheets. Similar constructive solutions, stylistic patterns, materials and façade compositions are rather frequent in the neighbourhood, allowing the identification of analogous characteristics in contemporary buildings of the area.

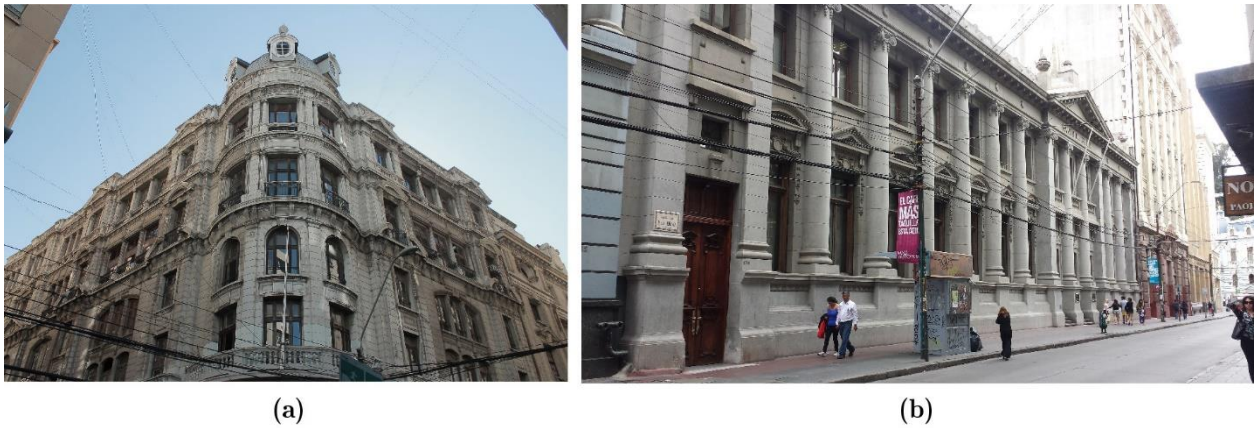


Figure 3-26. Hybrid wrought iron-RC buildings: (a) Ex Bolsa de Valores de Valparaíso and (b) Banco de Chile in Urriola street

The most recent buildings of the stock, located in the Port downtown area in the Anibal Pinto Square, were probably designed in compliance with the Chilean seismic standards NCh 433. Of 96 (Instituto Nacional de Normalización 2009) after their first release in 1960. Most of these buildings present more than seven stories, housing daily a large amount of people with consequent high exposure to seismic hazards. Most of these RC buildings present regular arrangements both plan and elevation. With exception of one isolated building, they are enclosed into structural aggregates.

Based on the existing building documentation, the external load-bearing systems of the buildings are entirely made of RC in line with the seismic code, while internal partitions can be made of brick masonry or light wrought iron profiles with thicknesses varying from 0.10 to 0.25 m. Brick masonry walls are composed of clay-fired bricks bonded with cement mortar. The roof structures, as well as the stories, are made of RC slabs supporting light steel trusses to achieve the minimum slope requirements. The foundations are commonly made of RC isolated or strip footings. Most of the RC buildings present very good conditions of conservation, given their newest character. However, subsequent addition of upper stories is a recurrent intervention within this type of building stock. In all these cases, the quality of the later intervention should be carefully evaluated in order to determine the influence of possible overloads on the global seismic response of the building.



Figure 3-27. Recent RC buildings built in the Port downtown: (a) Edificio del Consejo Nacional de la Cultura y las Artes in Sotomayor Square built in 1936-1942, and (b) Intendencia Regional de Valparaíso in Anibal Pinto square built in 1980.

3.6 Summary

This chapter presented a comprehensive characterization of three neighbourhoods of the historical centre of the city of Valparaíso, Chile: The Port downtown area, the *Cerro Alegre* and the *Cerro Concepción*. These neighbourhoods constitute the object of study of this doctoral thesis.

First, a historical overview of the social, cultural and urban development of the city was described to contextualize the genesis of the heterogeneous urban fabric, where timber frame, masonry, RC and wrought iron structures coexist.

Second, the available seismic hazard studies were presented with the aim to determine the on-site effects of the soil, which can negatively influence the behaviour of the buildings in case of seismic events. The local seismic hazard studies showed that the rocky areas on the hills present a lower seismic hazard, as they exhibited higher predominant frequencies of the soils than in other parts of the city. The flat areas of the downtown revealed to be the most seismically hazardous zones, characterized by a poorly compacted and artificial soil with the lowest predominant frequencies of the city. Therefore, the buildings on the Port downtown area should be carefully analysed taking into account the potential adverse effect of the soil in their seismic response.

The chapter presented the definition of an Emergency Limit Condition (ELC) in order to delimit the scope of the study by considering the vital functions of the urban stock and the exposed elements in the emergency areas. Two evacuation routes in case of tsunami were selected to determine the ELC, based on the Civil Protection Plan of the city. The streets include 111 potential interfering buildings which may interrupt the functionality of emergency areas and routes in case of their collapse.

The building typologies along the selected ELC were determined based on the available information from local archives and in-situ inspections. Most of the buildings present hybrid structural systems, being prevalent the combination of traditional timber frames with masonry walls. The historical monumental palaces are commonly hybrid structures made of wrought iron and RC. The most recent buildings of the Port downtown are made of RC and masonry load bearing structures

Chapter 4. Building survey forms for heterogeneous urban areas in seismically hazardous zones

4.1 Introduction

This chapter proposes a data-collection survey strategy for urban historical centres with heterogeneous structural typologies and lacking of consistent construction databases. The principal aim of the study is to define a methodology for typological building survey able to collect essential information for the subsequent seismic vulnerability assessment. The proposal considers relevant factors such as building morphology, structural configuration, damage conditions, and current condition of the building. The considered data provide the basic information to make a characterization of the existing typologies within the building stock relevant to seismic vulnerability. The methodology is based on the application of four typological survey forms historical centres with heterogeneous structural typologies, i.e. masonry, concrete, mixed steel/iron and timber frame structures. The proposals of ad-hoc survey forms for historical mixed steel/iron and timber frame structures constitute an important novelty of the present research. The forms were elaborated considering the influence of specific structural and non-structural parameters of the buildings that influence its seismic response. A guidance for the correct implementation of the forms is also presented considering pre-field survey activities, on-field survey applications, and management of the collected data.

The proposed methodology was applied to 111 buildings within the Emergency Limit Condition (ELC) zone of the historical centre of Valparaíso, Chile, defined in Chapter 3. The surveyed data allowed the statistical analysis of the building data, the characterization of the representative building typologies, as well as a preliminary detection of their most important vulnerabilities. The obtained results were implemented into a GIS platform to provide a suitable database for future seismic vulnerability analyses at the urban level.

The outline of the chapter is divided into three parts. Section 4.2 describes in detail the typological surveys (Section 4.2.1), considering all the sections in which is organized, and the parameters of evaluation. Section 4.3 gives a survey implementation plan divided into three stages: pre-field activities (4.3.1), on-field activities (4.3.2), and post-field activities (4.3.3). Section 4.3.4

presents a correlation among the three main activities. The proposed survey methodology was applied to three neighbourhoods of the historical centre of Valparaíso, Chile (Section 4.4). All the stages of this survey activity are detailed in Sections 4.4.1 and 4.4.2, while the results and statistical analysis are presented in Section 4.4.3. A summary of the methodology and its application is presented at the end of the chapter (Section 4.5).

4.2 Building survey methodology

This section presents a methodology to the survey of buildings in heterogeneous urban historical centres, focusing on the traditional structural typologies composed of masonry, reinforced concrete (RC), mixed steel/iron, and timber frame systems. The proposal includes survey strategies and calibrated tools to inspect each building in a reliable way. Four singular survey forms are set, each of them corresponding to a specific building typology, taking into account the structural parameters denoting the seismic vulnerability of the investigated building. The proposed survey forms constitute a tool for second level assessments of the seismic risk in existing buildings. Annex A reports all the survey forms developed in this research.

4.2.1 Typological survey forms

The proposed typological survey forms are divided into seven sections named: (1) General information; (2) Building typology; (3) Structural regularity; (4) Soil and foundation conditions; (5) Non-structural elements; (6) Damage conditions and; (7) Current conditions of conservations. The Section 2 “Building typology” is particularly calibrated for Reinforced Concrete (RC), Masonry, mixed iron/steel, and timber frame structures, as explained below.

The Section 1 “General Information” presents an overview of the building with the identifier number (ID) and the address. The use and number of occupants constitutes also a source of useful information to understand the role of the building within the urban asset, as suggested by Baggio et al. (2007) and FEMA (2015). Additionally, the user can insert some notes with a brief description of the physical appearance, and a possible graphical sketch, see Figure 4-1.

The Section 2 “Building Typology” (Figure 4-2) reports the main characteristics of the structural configuration. The number of stories and age of the buildings (Question 2.1 and 2.2) are preliminary data to determine the exposure in the study area, in accordance with FEMA (2015) and AeDES (Baggio et al. 2007) survey initiatives. The possible compliance with any local seismic design codes is also necessary to understand if the construction followed seismic criteria from past or present standards. The existence of later structural retrofits (e.g. insertion of tie rods, floor stiffening, etc.) or modifications that may have altered substantially the original structural system, (e.g. elevations, new floors or roofs, etc.), must be also reported in this section.

The identification of specific structural features, such as the nature of the load-bearing system and materials, are requested from Questions 2.3 (Figure 4-2) to 2.5 (Figure 4-3 to Figure 4-6). The structural system should be preliminary defined as hybrid or unique (Question 2.3). The forms allow the choice of a number of common hybrid typologies, as presented in the following.

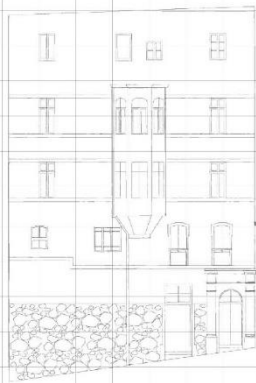
SECTION 1: GENERAL INFORMATION		S1
ID		3 0 0 6 - 5
NOTES		Five stories and yellow façade building
ADDRESS	STREET NAME	Urriola
	STREET NUMBER	4 8 5
	CITY	Valparaíso
USE	<input checked="" type="checkbox"/> RESIDENTIAL	<input type="checkbox"/> GOVERNMENTAL
	<input type="checkbox"/> COMMERCIAL	<input type="checkbox"/> TOURISTIC
	<input type="checkbox"/> INDUSTRIAL	<input type="checkbox"/> UNOCCUPIED
	<input type="checkbox"/> MEDICAL	<input type="checkbox"/> MIXED
	<input type="checkbox"/> EDUCATIONAL	
OCCUPANTS	<input type="checkbox"/> 0 - 10	
	<input checked="" type="checkbox"/> 10 - 100	
	<input type="checkbox"/> > 100	
		

Figure 4-1. Proposed survey form: Section 1 “General information”.

SECTION 2: BUILDING TYPOLOGY		S2
2.1 NUMBER OF STORIES		0 5
2.2 BUILDING AGE	2.2.1 YEAR OF CONSTRUCTION	1 9 0 0
	2.2.2 LATEST STRUCTURAL RETROFIT	2 0 1 4
	2.2.3 COMPLIANCE WITH SEISMIC CODES	<input checked="" type="checkbox"/> YES, YEAR 1 9 6 0 <input type="checkbox"/> No
2.3 STRUCTURAL SYSTEM		<input type="checkbox"/> UNIQUE <input checked="" type="checkbox"/> HYBRID
		2.4 STRUCTURAL MATERIALS
2.4.1 MAIN FAÇADE		<input checked="" type="checkbox"/> STONE MASONRY <input checked="" type="checkbox"/> BRICK MASONRY <input type="checkbox"/> RC <input checked="" type="checkbox"/> TIMBER <input type="checkbox"/> IRON / STEEL <input type="checkbox"/> ADOBE
2.4.2 SIDE WALLS		<input type="checkbox"/> STONE MASONRY <input checked="" type="checkbox"/> BRICK MASONRY <input type="checkbox"/> RC <input type="checkbox"/> TIMBER <input type="checkbox"/> IRON / STEEL <input type="checkbox"/> ADOBE
2.4.3 INTERNAL PARTITIONS		<input type="checkbox"/> STONE MASONRY <input type="checkbox"/> BRICK MASONRY <input type="checkbox"/> RC <input checked="" type="checkbox"/> TIMBER <input type="checkbox"/> IRON / STEEL <input type="checkbox"/> ADOBE
2.4.4 STORIES		<input type="checkbox"/> STONE MASONRY <input type="checkbox"/> BRICK MASONRY <input type="checkbox"/> RC <input checked="" type="checkbox"/> TIMBER <input type="checkbox"/> IRON / STEEL <input type="checkbox"/> ADOBE
2.4.5 ROOFS		<input type="checkbox"/> STONE MASONRY <input type="checkbox"/> BRICK MASONRY <input type="checkbox"/> RC <input checked="" type="checkbox"/> TIMBER <input type="checkbox"/> IRON / STEEL <input type="checkbox"/> ADOBE
2.4.1.1 RETROFITTED/ALTERED?		<input checked="" type="checkbox"/> No <input type="checkbox"/> Yes
2.4.2.1 RETROFITTED/ALTERED?		<input checked="" type="checkbox"/> No <input type="checkbox"/> Yes
2.4.3.1 RETROFITTED/ALTERED?		<input checked="" type="checkbox"/> No <input type="checkbox"/> Yes
2.4.4.1 RETROFITTED/ALTERED?		<input type="checkbox"/> No <input checked="" type="checkbox"/> Yes <i>Stiffening with wood planks</i>
2.4.5.1 RETROFITTED/ALTERED?		<input type="checkbox"/> No <input checked="" type="checkbox"/> Yes <i>Distributed tie rods</i>

Figure 4-2. Proposed survey form: Section 2 “Building Typology- Part I”.

Main lateral load resistant systems are identified according to the load-bearing systems and story structures. Each typological form identifies the most representative structural systems among those established by Eurocode 8 and Eurocode 5 (EN 1998-1 2004, CEN EC5 1.2 2004), the Italian standards of Construction (NTC 2008), the guidelines by the Italian National Group for Earthquakes Protection GNDT (2007), the SYNER-G project (Pitilakis et al. 2014), and the New Zealand technical guidelines for the Seismic Assessment of Existing Buildings (NZSEE 2016).

Vertical load-bearing systems are identified according to the type of material, the arrangement of resistant elements, and the quality of the whole system. According to the Seismic Design Handbook (Farzad 1989), the seismic behaviour and in-plane deformation of story systems are mostly influenced by the relative rigidity of the diaphragms compared to that of vertical resistant structures. The different typologies of stories are thus classified into rigid, semi-rigid, and flexible. The rigid stories are relatively stiffer than lateral force-resisting members and distribute the story shears to the supporting lateral members based on their relative rigidities. The flexible ones can experience flexural deformations in their own plane and thus they transmit the story shears to the lateral resisting members based on their tributary areas. Semi-rigid diaphragms basically represent a condition between rigid and flexible. The quality of the connections of the story with the vertical structures is also an important evaluation parameter. The survey forms are then particularized according to the construction material of the structural system, i.e. masonry, reinforced concrete, steel/iron and timber. All the different cases are carefully described in the following.

The first variant of the survey form applies to buildings with masonry load bearing system, see Figure 4-3. Masonry buildings represent one of the oldest and most widespread structural system around the world. The global dimension of the masonry heritage is reflected in the wide range of structural solutions, typologies, materials, in line with local available resources. The major concerns in the seismic assessment of historical masonry buildings are the unreinforced masonry structures lacking of engineering skills during their construction and adopting rudimentary materials and technologies. All these factors can constitute potential sources of high seismic vulnerability. In these cases, the masonry quality, as well as the actual effectiveness of past reinforcing interventions, must be carefully evaluated in order to identify correctly the seismic vulnerability. The proposed forms for masonry structures classify them into reinforced, confined, and unreinforced. Their seismic behaviour depends mainly on factors such as the type of materials, the regularity of the texture, and the quality of the connections.

The minimum requirements for wall thickness refers to the magnitudes reported in Eurocode 8, i.e. 0.35 m for unreinforced and 0.24 m for reinforced and confined masonry. Although such values actually refer to new construction and real thickness can largely vary from a masonry type to another, this tentative check can contribute to a quick preliminary assessment of the adequacy of the wall's geometry. The regularity in the geometrical organization of the blocks depends on their size homogeneity and the type of bond. Regular blocks arranged along regular layers are normally indicators of well-executed walls. Regarding the monolithic condition of the walls, it is important to evaluate the quality of both the existing mortar and the connections. Cementitious or hydraulic mortars commonly provide high resistances and are considered as the best quality ones. Inconsistent or floury mortars are defined as bad quality ones. Attributes contributing to the good seismic performance of the masonry structures by means of the so-called

“box behaviour” are well executed wall to wall interlocking, as well as uniformly distributed connection devices (e.g. tie rods, tie beams, anchors, and bracing systems). The identification of the load resistant system of masonry buildings is the purpose of Question 2.5. Specific categories are reported depending on the load-bearing and story systems (Figure 4-3). Existing masonry structural systems are complex and different combinations could be possible in real cases. Since trying to represent all the possible typologies would produce extremely complex forms, the proposed approach considers an approximation to nine classes, i.e. three possible classes for each masonry typology (reinforced, unreinforced stone and brick masonry). The first class includes buildings with no sources of vulnerability in the load-bearing resisting system (e.g. good thickness, regular texture and well executed connections), the second class presents some sources of vulnerability (e.g. insufficient thickness or irregular texture or bad connections), and the third class has numerous sources of vulnerability (e.g. insufficient thickness, irregular texture and bad connections). As for the description of the story typologies, it is based on relative stiffness and quality of the connection with the vertical elements. The *unknown* choice is also possible, since the inspection of floors is often challenging due to their difficult accessibility during the inspection activities. Lastly, the observation of the possible thrusting effect of the roof system is requested in the Question 2.6. The categories of non-thrusting, slightly thrusting, and thrusting roofs are defined according to relevant criteria formulated by GNDT (2007), Vicente (2008) and Pitilakis et al. (2014). According to these studies, non-thrusting roofs are horizontal or inclined with specific solutions to eliminate the thrust at the top of the supporting walls, e.g. metallic tie rods or timber truss systems. Slightly thrusting roofs are inclined with the roof ridge supported either by a load bearing wall or by a beam with a span to height ratio lower than 20. Thrusting roofs are all the other solutions not respecting the previous conditions.

2.5. MASONRY LATERAL LOAD RESISTANT SYSTEM		STORY SYSTEM	RIGID AND WELL CONNECTED			SEMI-RIGID AND CONNECTED			FLEXIBLE AND/OR BADLY CONNECTED		MULTI-RETROFITTED STORIES NOT CONNECTED TO WALLS	UNKNOWN
			CAST IN PLACE OR PRECAST RC SLAB WITH CONCRETE TOPPING	RC BEAMS WITH CONCRETE TOPPING/ FILL	METAL DECK WITH CONCRETE FILL	CAST IN PLACE OR PRECAST RC SLAB w/o CONCRETE TOPPING	TIMBER STORY WITH DOUBLE SHEATHING OF WOODEN BOARDS	TIMBER STORY WITH SINGLE SHEATHING OF WOODEN BOARDS AND STIFFENING ELEMENTS, OR CONCRETE TOPPING, WELL CONNECTED TO WALLS	TIMBER STORY WITH SINGLE SHEATHING OF WOODEN BOARDS	STEEL/ IRON BEAMS WITH BRICK/TILE CEILING (VAULTED OR NOT)		
			1	2	3	4	5	6	7	8		
LOAD BEARING SYSTEM												
REINFORCED OR CONFINED BRICK/CONCRETE MASONRY	GOOD QUALITY MORTAR AND CONNECTIONS AND THICKNESS HIGHER THAN 0.24 M	A	<input type="checkbox"/>	<input type="checkbox"/>	<input type="checkbox"/>	<input type="checkbox"/>	<input type="checkbox"/>	<input type="checkbox"/>	<input type="checkbox"/>	<input type="checkbox"/>	<input type="checkbox"/>	<input type="checkbox"/>
	POOR QUALITY MORTAR, OR POOR CONNECTIONS, OR THICKNESS LOWER THAN 0.24 M	B	<input type="checkbox"/>	<input type="checkbox"/>	<input type="checkbox"/>	<input type="checkbox"/>	<input type="checkbox"/>	<input type="checkbox"/>	<input type="checkbox"/>	<input type="checkbox"/>	<input type="checkbox"/>	<input type="checkbox"/>
	POOR QUALITY MORTAR AND CONNECTIONS, AND THICKNESS LOWER THAN 0.24 M	C	<input type="checkbox"/>	<input type="checkbox"/>	<input type="checkbox"/>	<input type="checkbox"/>	<input type="checkbox"/>	<input type="checkbox"/>	<input type="checkbox"/>	<input type="checkbox"/>	<input type="checkbox"/>	<input type="checkbox"/>
UNREINFORCED MASONRY	NATURAL STONE UNITS WITH GOOD TEXTURE AND CONNECTIONS, AND THICKNESS HIGHER THAN 0.35 M	D	<input type="checkbox"/>	<input type="checkbox"/>	<input type="checkbox"/>	<input type="checkbox"/>	<input type="checkbox"/>	<input type="checkbox"/>	<input type="checkbox"/>	<input type="checkbox"/>	<input type="checkbox"/>	<input type="checkbox"/>
	NATURAL STONE UNITS WITH IRREGULAR TEXTURE, OR BAD CONNECTIONS, OR THICKNESS LOWER THAN 0.35 M	E	<input type="checkbox"/>	<input type="checkbox"/>	<input type="checkbox"/>	<input type="checkbox"/>	<input type="checkbox"/>	<input type="checkbox"/>	<input type="checkbox"/>	<input type="checkbox"/>	<input type="checkbox"/>	<input type="checkbox"/>
	NATURAL STONE UNITS WITH IRREGULAR TEXTURE, BAD CONNECTIONS, AND THICKNESS LOWER THAN 0.35 M	F	<input type="checkbox"/>	<input type="checkbox"/>	<input type="checkbox"/>	<input type="checkbox"/>	<input type="checkbox"/>	<input type="checkbox"/>	<input type="checkbox"/>	<input type="checkbox"/>	<input type="checkbox"/>	<input type="checkbox"/>
	CLAY OR SAND-LIME BRICKS, GOOD QUALITY MORTAR AND CONNECTIONS, AND THICKNESS HIGHER THAN 0.24 M	G	<input type="checkbox"/>	<input type="checkbox"/>	<input type="checkbox"/>	<input type="checkbox"/>	<input type="checkbox"/>	<input checked="" type="checkbox"/>	<input type="checkbox"/>	<input type="checkbox"/>	<input type="checkbox"/>	<input type="checkbox"/>
	CLAY OR SAND-LIME BRICKS, BAD QUALITY MORTAR OR CONNECTIONS, OR THICKNESS LOWER THAN 0.24 M	H	<input type="checkbox"/>	<input type="checkbox"/>	<input type="checkbox"/>	<input type="checkbox"/>	<input type="checkbox"/>	<input type="checkbox"/>	<input type="checkbox"/>	<input type="checkbox"/>	<input type="checkbox"/>	<input type="checkbox"/>
CLAY OR SAND-LIME BRICKS, BAD QUALITY MORTAR AND CONNECTIONS, AND THICKNESS LOWER THAN 0.24 M	I	<input type="checkbox"/>	<input type="checkbox"/>	<input type="checkbox"/>	<input type="checkbox"/>	<input type="checkbox"/>	<input type="checkbox"/>	<input type="checkbox"/>	<input type="checkbox"/>	<input type="checkbox"/>	<input type="checkbox"/>	
2.6 ROOF SYSTEM			A <input type="checkbox"/> NON- THRUSTING			B <input type="checkbox"/> SLIGHTLY THRUSTING			C <input type="checkbox"/> THRUSTING			

Figure 4-3. Proposed survey form: Section 2 – part II for masonry lateral load systems.

The second variant of the survey form applies to buildings with reinforced concrete (RC) load bearing system, see Figure 4b. RC structural systems represent a widespread technique since XIX century. Although these typologies usually imply engineered design and construction, they might not respect the fundamental seismic criteria due to possible deficiencies referable to inaccurate project or execution stages. As well as for the survey masonry buildings, the compliance of RC buildings with the local seismic codes can help considerably to understand if they may present structural vulnerability to possible earthquakes. The proposed form for RC buildings classifies load bearing systems into moment resistant frames, shear walls, dual systems (resistant frames and structural walls), and mixed RC-masonry, see Question 2.5 of Figure 4b. Moment resistant frame systems resist vertical and lateral loads by spatial frames that can be filled or not with masonry structures. Shear wall systems resist vertical and lateral loads by vertical structural walls. Dual systems support vertical loads mainly by spatial frames, while walls and, to a lesser degree, frames provide resistance to lateral loads. Mixed RC-masonry systems include different varieties of typologies and arrangements inspired more by functional aspects than structural ones (Cattari and Lagomarsino, 2013), e.g. buildings characterized by perimeter masonry walls and internal RC frames, masonry buildings with enlargements or raising made of RC frames, and masonry buildings with RC walls enclosing staircases. Additionally, soft story building irregularities are reported in this section due to their remarkable source of seismic vulnerability (Guevara-Perez 2012). This structural weakness, also known as *open story*, is associated with a significant difference between the stiffness and resistance of one of the stories and the rest of them. The soft ground story is the most typical case of soft-story irregularity, i.e. in buildings with a large number of non-structural rigid components (such as masonry walls) connected to the columns in the upper stories, while the ground story presents high flexibility due to the null or reduced number of rigid elements. For the specific case of moment resistant frame systems, the description of the stiffening effect given by the possible presence of masonry infill is taken into account according to the simplified criteria reported in the GNDT manual for RC structures (GNDT 2007). The RC frames infill is considered of good quality and well-connected to the resisting frame if it is made of solid or half-hollowed bricks, the openings do not exceed the 30%, the height-thickness ratio is lower than 20%, and the gap with the frame is lower than 1 cm. Appropriate story systems in RC structures should have slab behaviour and high rigidity against in-plane deformations. These requirements can be reached thanks to a good quality of the connections and materials, as well as the presence of stiffening elements. Representative story system typologies commonly used in RC buildings are classified in the survey form as shown in Figure 4b. The categories for RC lateral load resistant system can vary from A1 to F7.

2.5. RC LATERAL LOAD RESISTANT SYSTEM		STORY SYSTEM	RIGID AND WELL CONNECTED			SEMI-RIGID AND CONNECTED		FLEXIBLE AND/OR BADLY CONNECTED	UNKNOWN	
			CAST IN PLACE OR PRECAST RC SLAB WITH CONCRETE TOPPING WELL CONNECTED TO VERTICAL RESISTANT ELEMENTS	RC BEAMS WITH CONCRETE TOPPING WELL CONNECTED TO VERTICAL RESISTANT ELEMENTS	METAL DECK WITH CONCRETE FILL	RIGID STORY POORLY CONNECTED TO VERTICAL RESISTANT ELEMENTS	CAST IN PLACE OR PRECAST RC SLAB W/O CONCRETE TOPPING	RC OR STEEL BEAMS W/O CONCRETE SLAB (LIGHTWEIGHT SHEATHING)		FLEXIBLE OR ANY NATURE STORY BADLY CONNECTED TO VERTICAL RESISTANT ELEMENTS
LOAD BEARING SYSTEM			1	2	3	4	5	6	7	8
MOMENT RESISTANT FRAME	WITH WELL CONNECTED AND GOOD QUALITY MASONRY INFILL. OPENINGS DO NOT EXCEED 30% OF WALL SURFACE. HEIGHT-THICKNESS RATIO LOWER THAN 20%	A	<input type="checkbox"/>	<input checked="" type="checkbox"/>	<input type="checkbox"/>	<input type="checkbox"/>	<input type="checkbox"/>	<input type="checkbox"/>	<input type="checkbox"/>	<input type="checkbox"/>
	WITH BADLY CONNECTED AND/OR POOR QUALITY MASONRY INFILL. OPENINGS EXCEED 30% OF WALL SURFACE. HEIGHT-THICKNESS RATIO HIGHER THAN 20%	B	<input type="checkbox"/>	<input type="checkbox"/>	<input type="checkbox"/>	<input type="checkbox"/>	<input type="checkbox"/>	<input type="checkbox"/>	<input type="checkbox"/>	<input type="checkbox"/>
	w/o INFILL	C	<input type="checkbox"/>	<input type="checkbox"/>	<input type="checkbox"/>	<input type="checkbox"/>	<input type="checkbox"/>	<input type="checkbox"/>	<input type="checkbox"/>	<input type="checkbox"/>
SHEAR WALL SYSTEM		D	<input type="checkbox"/>	<input type="checkbox"/>	<input type="checkbox"/>	<input type="checkbox"/>	<input type="checkbox"/>	<input type="checkbox"/>	<input type="checkbox"/>	<input type="checkbox"/>
DUAL SYSTEM: MOMENT RESISTANT FRAMES AND SHEAR WALLS		E	<input type="checkbox"/>	<input type="checkbox"/>	<input type="checkbox"/>	<input type="checkbox"/>	<input type="checkbox"/>	<input type="checkbox"/>	<input type="checkbox"/>	<input type="checkbox"/>
MIXED RC-MASONRY		F	<input type="checkbox"/>	<input type="checkbox"/>	<input type="checkbox"/>	<input type="checkbox"/>	<input type="checkbox"/>	<input type="checkbox"/>	<input type="checkbox"/>	<input type="checkbox"/>
SOFT-STORY BUILDINGS CAUSED BY UNFAVOURABLE DISCONTINUOUS COLUMNS (OPEN GROUND FLOOR) OR SIGNIFICANT STIFFNESS AND RESISTANCE DIFFERENCE BETWEEN THE GROUND AND UPPER LEVELS STRUCTURES		G	<input type="checkbox"/>	<input type="checkbox"/>	<input type="checkbox"/>	<input type="checkbox"/>	<input type="checkbox"/>	<input type="checkbox"/>	<input type="checkbox"/>	<input type="checkbox"/>

Figure 4-4. Proposed survey form: Section 2 – part II for reinforced concrete lateral load systems.

The third variant of the survey form applies to buildings with steel/iron mixed load bearing system, see Figure 5a. The possible presence of mixed typologies is frequent in historical centres with heterogeneous buildings. Mixed RC or masonry buildings can exhibit the presence of steel or iron resistant elements in their lateral load resistant system. The use of wrought iron/steel elements, in addition to RC or masonry members, was a common technique in old and large-scale buildings. Old steel/iron structures may be characterized by some uncertainties. In all these cases, it is very important to identify the contribution of resistant metal elements within the lateral load resistant system, in order to clarify the mixed character of the structure and to evaluate the established parameters for the survey form. Wrought iron frames systems, filled with concrete or masonry walls, are also rather typical in historical buildings, and the quality of the infill and connections are the most important parameters of evaluation. The form for mixed steel/iron structures classifies the vertical load-bearing systems into moment resistant frames, structural wall systems and dual systems. Each group defines the most representative systems, as shown in Figure 4-5. As the above typologies, story systems are defined by their relative rigidity and connection conditions. The categories for steel/iron lateral load resistant systems can vary from A1 to F7.

2.5. STEEL/IRON MIXED LATERAL LOAD RESISTANT SYSTEM		STOREY SYSTEM	RIGID AND WELL CONNECTED			SEMI-RIGID AND CONNECTED		FLEXIBLE AND/OR BADLY CONNECTED	UNKNOWN
			CAST IN PLACE OR PRECAST RC SLAB WITH CONCRETE TOPPING WELL CONNECTED TO VERTICAL RESISTANT ELEMENTS	RC OR STEEL BEAMS WITH CONCRETE TOPPING WELL CONNECTED TO VERTICAL RESISTANT ELEMENTS	METAL DECK WITH CONCRETE FILL	CAST IN PLACE OR PRECAST RC STORY W/O CONCRETE TOPPING	RC OR STEEL BEAMS W/O CONCRETE SLAB (LIGHTWEIGHT SHEATHING)	FLEXIBLE OR ANY NATURE STORY BADLY CONNECTED TO VERTICAL RESISTANT ELEMENTS	
			1	2	3	4	5	6	
LOAD BEARING SYSTEM									
MOMENT RESISTANT FRAME (MRF)	WITH WELL CONNECTED AND GOOD QUALITY MASONRY INFILL	A	<input type="checkbox"/>	<input type="checkbox"/>	<input type="checkbox"/>	<input type="checkbox"/>	<input checked="" type="checkbox"/>	<input type="checkbox"/>	<input type="checkbox"/>
	WITH CONCENTRIC OR ECCENTRIC BRACINGS	B	<input type="checkbox"/>	<input type="checkbox"/>	<input type="checkbox"/>	<input type="checkbox"/>	<input type="checkbox"/>	<input type="checkbox"/>	<input type="checkbox"/>
	W/O INFILL	C	<input type="checkbox"/>	<input type="checkbox"/>	<input type="checkbox"/>	<input type="checkbox"/>	<input type="checkbox"/>	<input type="checkbox"/>	<input type="checkbox"/>
DUAL SYSTEM: RESISTANT FRAMES AND STRUCTURAL WALLS	MRF WITH CONCRETE CORES	D	<input type="checkbox"/>	<input type="checkbox"/>	<input type="checkbox"/>	<input type="checkbox"/>	<input type="checkbox"/>	<input type="checkbox"/>	<input type="checkbox"/>
	MRF WITH CONCRETE WALLS	E	<input type="checkbox"/>	<input type="checkbox"/>	<input type="checkbox"/>	<input type="checkbox"/>	<input type="checkbox"/>	<input type="checkbox"/>	<input type="checkbox"/>
	MRF WITH MASONRY WALLS	F	<input type="checkbox"/>	<input type="checkbox"/>	<input type="checkbox"/>	<input type="checkbox"/>	<input type="checkbox"/>	<input type="checkbox"/>	<input type="checkbox"/>

Figure 4-5. Proposed survey form: Section 2 – part II for mixed steel/iron mixed lateral load systems.

The fourth variant of the survey form applies to buildings with timber frame load bearing system, see Figure 4-6. Timber dwellings represent an important part of the built heritage across the world. Historical timber structures are often associated with the concept of *vernacular architecture*, which refers to traditional structures made of local materials and following well-tried practice and configurations (Stevens Curls and Wilson 2015, Oliver 1997). For this reason, different structural solutions have been developed, among which original models can be clearly identified. The essential language governing the timber-framed heritage is the *Box Framing*. Box frame typologies are composed of a primary heavy frame bearing the loads, and a secondary structure of smaller dimension elements, setting the internal partitions of the structure and supporting the inner and outer coverings (Lewis 2009). *Braced, Stud, Balloon, and Platform* frames gradually replaced the earliest box frame archetype. Such generic typologies present slight changes in their configuration, such as smaller dimensions' pieces, use of bracing elements, different construction solutions (e.g. types of connections, frame arranged, joints, etc.) which simplify the frame configuration and the building process. It is important to note that timber structures can vary significantly depending on the local context, seismic demand, and available resources. Therefore, each specific solution must be carefully identified in studies related to the assessment of the seismic vulnerability of this type of structures. In general, low-rise timber buildings exhibit good structural performance and can ensure life safety for major earthquakes (NZSEE 2016). The good seismic behaviour is partly due to their lightness and ability to deform considerably without losing their load bearing capacity. The major sources of seismic vulnerability are given by elements increasing mass magnitude and introducing mass/stiffness irregular distribution, such as heavy wall partitions, weighty story systems, cantilevers, or asymmetrically distributed braced frames.

The load-bearing system of timber structures is typically composed of braces and diaphragm elements (shear walls and stories systems) that provide lateral stability to the building. The behaviour of these elements is strictly related to their physical properties, such as the type of wood, the cross-section, the thickness, the depth and slenderness ratio, and the connection details. In addition, the seismic performance of the timber shear walls is influenced by the stiffening elements, such as bracing systems and external sheathing.

2.5 TIMBER LATERAL LOAD RESISTANT SYSTEM		STORY SYSTEM	Rigid	SEMI-RIGID	FLEXIBLE	WEIGHTY RETROFITTED STORIES NOT CONNECTED TO WALLS	UNKNOWN
			JOISTS WITH DOUBLE LAYER OF WOODEN SHEATHING	JOISTS WITH SINGLE WOODEN SHEATHING AND BRACING ELEMENTS (DIAGONALS, BRACING GRID)	JOISTS WITH SINGLE WOODEN SHEATHING PERPENDICULAR TO THEM		
LOAD-BEARING SYSTEM			1	2	3	4	5
BRACED SYSTEMS (DIAGONALS, LET-IN BRACE, DOG-LEG, ETC.)	WITH NAILED OR CARPENTRY REINFORCED CONNECTIONS	A	<input type="checkbox"/>	<input checked="" type="checkbox"/>	<input type="checkbox"/>	<input type="checkbox"/>	<input type="checkbox"/>
	WITH CARPENTRY CONNECTIONS	B	<input type="checkbox"/>	<input type="checkbox"/>	<input type="checkbox"/>	<input type="checkbox"/>	<input type="checkbox"/>
	WITH BAD QUALITY CONNECTIONS	C	<input type="checkbox"/>	<input type="checkbox"/>	<input type="checkbox"/>	<input type="checkbox"/>	<input type="checkbox"/>
UNBRACED SYSTEMS	WITH NAILED OR CARPENTRY REINFORCED CONNECTIONS	D	<input type="checkbox"/>	<input type="checkbox"/>	<input type="checkbox"/>	<input type="checkbox"/>	<input type="checkbox"/>
	WITH CARPENTRY CONNECTIONS	E	<input type="checkbox"/>	<input type="checkbox"/>	<input type="checkbox"/>	<input type="checkbox"/>	<input type="checkbox"/>
	WITH BAD QUALITY CONNECTIONS	F	<input type="checkbox"/>	<input type="checkbox"/>	<input type="checkbox"/>	<input type="checkbox"/>	<input type="checkbox"/>

2.6 SECONDARY STIFFENING ELEMENTS	2.6.1 INFILL		2.6.2 EXTERNAL SHEATHING	
	<input type="checkbox"/> NO INFILL <input type="checkbox"/> BRICK OR STONE MASONRY <input checked="" type="checkbox"/> ADOBE	<input type="checkbox"/> QUINCHA <input type="checkbox"/> LATH AND PLASTER <input type="checkbox"/> OTHER	<input type="checkbox"/> NO SHEATHING <input type="checkbox"/> HORIZONTAL WOODEN BOARDS <input type="checkbox"/> HORIZONTALLY ORIENTED CORRUGATES STEEL SHEETS <input checked="" type="checkbox"/> VERTICALLY ORIENTED CORRUGATES STEEL SHEETS <input type="checkbox"/> OTHER	

2.7 ROOF SYSTEM	A <input checked="" type="checkbox"/> NON-THRUSTING	B <input type="checkbox"/> SLIGHTLY THRUSTING	C <input type="checkbox"/> THRUSTING

Figure 4-6. Proposed survey form: Section 2 – part II for timber lateral load systems.

Typical dispositions of the braces are shown in Figure 4-7a-c, i.e. let-in, diagonal, and dog leg. Adequate bracing and sheathing systems significantly improve the strength characteristics of a wall, e.g. double layer or diagonal boards, corrugated metal sheets, etc. Another important factor to consider in timber structures is the existence of infill within the main frame. Recent studies by Poletti and Vasconcelos (2015) and Duțu, Sakata, and Yamazaki (2015) have demonstrated that the presence of infill can significantly modify the whole seismic response due to the confining effect on the timber frame. The presence of the infill could increase considerably the stiffness, such as in the case of timber frames with masonry or stone infill, and thus a possible irregular distribution in plan of infilled frames may localize the damage on few shear walls of the structure in case of seismic actions. Weaker typologies are given by branches infill, adobe, *quincha* etc. (Ceccotti and Sandhaas 2015). The proposed survey form requires information about the type of infill in timber shear walls in Question 2.6.1 (Figure 4-6). The connections are critical for the deformation capacity of the timber structure. Nailed and well-reinforced carpentry connections are considered the most reliable types (CEN 2004). Unfavourable conditions are provided by carpentry joints with minor reinforcement (intended only to avoid disassembling), or by nail corrosion, mechanical damages, biotic attacks, etc. Question 2.5 of the proposed survey form for timber structures requests information about the vertical load-bearing condition, the existence of bracing systems and the condition of the connections. Additionally, Questions 2.6.1 and 2.6.2 request the presence of additional stiffening elements, such as infill and/or external sheathing. The behaviour of the diaphragm depends on the relative stiffness compared with the lateral stiffness of the connected vertical elements (NZSEE 2016). Sheathing elements or specific stiffening devices, such as cross ties, struts, etc., influence the rigid behaviour of the stories. According to Valluzzi et al. (2010), stories with double (or more) layer of timber board sheathing, or reinforced with wooden networks, are the most desirable typologies for the seismic case, followed by stories braced with wood or steel diagonals. Question 2.5 of the survey form defines the story typologies

according to their rigid, semi-rigid, and flexible behaviour, as shown in Figure 4-6. Weighty retrofitted stories non-connected to the walls are considered as unfavourable cases, such as stories with subsequent RC toppings, metal decks with RC topping, or any structure adding a significant mass without improving the connections with vertical elements. The categories for timber frame lateral load resistant systems can vary from A1 to F5, see Figure 4-6.

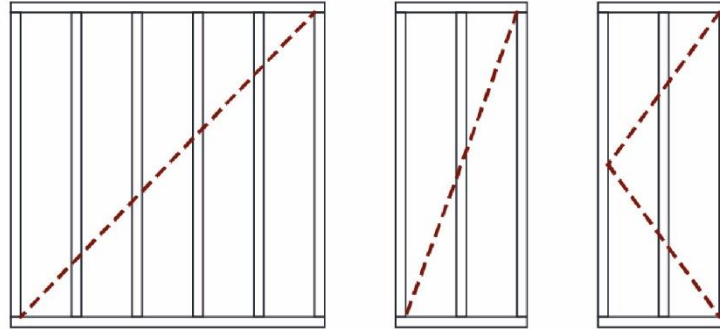


Figure 4-7. Timber main load-resistant systems: (a) Let-in brace, (b) Diagonal brace and (c) Dog leg brace.

The Section 3 of the proposed survey form is called “Structural Regularity” (Figure 4-8a) and assesses the morphology of the building in plan and in elevation. Main examination parameters are the overall dimensions of the building, the plan position (aggregate condition), the presence of irregularities (in plan and elevation), and the characteristics of the openings (alignment condition). The evaluation of all these parameters follows the procedures proposed by the GNDT II level manual (GNDT 2007) and the AeDES form (Baggio et al. 2007). The structural interaction with the adjacent buildings is evaluated by indicating the position of the building in the urban aggregate (Question 3.2, Figure 4-8a) since it can influence significantly the seismic performance (Formisano et al. 2015). Irregularities in plan are critical in seismic vulnerability evaluations, since asymmetrical shapes can induce dynamic torsional effects and thus severe damages to the structures. Buildings with elongated shapes or large protrusions are evaluated according to the criteria adopted from GNDT through ratios $\beta 1$ and $\beta 2$ (Equations (3) and (4)) where l is the longest side in plan, a is the shorter, and b the appendix dimension (Question 3.3, Figure 4-8a).

$$\beta 1 = a/l \times 100 \quad (3)$$

$$\beta 2 = b/l \times 100 \quad (4)$$

Irregularities in elevation are also critical and have to be identified (Question 3.5, Figure 4-8), especially in the cases of mass variation along the height, given by strong differences of plan, existence of setbacks, porches or tower shaped elements. The mass variation and setback conditions are both evaluated in percentage terms, being the former quantified by the ratio $\Delta A/A$ between the variation of area of the upper stories ΔA and the area of the ground floor A . The so-

called “tower condition” is evaluated by the ratio T/H where T and H are the tower and building heights, see Figure 4-8. The Section 3 of the survey form also takes into account the possible existence of misaligned openings, since they can considerably affect the seismic behaviour of the façades (R. Vicente et al. 2008).

SECTION 3: STRUCTURAL REGULARITY		IN ELEVATION	
3.1. DIMENSIONS	IN PLAN	3.4.1 HEIGHT	3.4.2 BASE
	AREA 0 1 5 0 m ²	0 1 2 m	0 0 8 m
3.2. POSITION	A <input type="checkbox"/> B <input type="checkbox"/> C <input checked="" type="checkbox"/> D <input type="checkbox"/> E <input type="checkbox"/>	3.4.3 AVERAGE STORY HEIGHT	0 4 m
	<p>A <input type="checkbox"/> $\beta 1 \geq 80$; $\beta 2 \leq 10$</p> <p>B <input checked="" type="checkbox"/> $60 \leq \beta 1 < 80$; $10 < \beta 2 \leq 20$</p> <p>C <input type="checkbox"/> $\beta 1 < 60$; $\beta 2 > 20$</p> <p>where:</p> <p>$\beta 1 = a/l \times 100$ $\beta 2 = b/l \times 100$</p>	3.5. IRRREGULARITY IN ELEVATION	
3.3. IRRREGULARITY IN PLAN		MASS VARIATION $\pm \Delta A/A$	SETBACK AND PORCHE EXISTENCES
		<p>A <input checked="" type="checkbox"/> $\Delta A/A \leq 10\%$;</p> <p>B <input type="checkbox"/> $10 < \Delta A/A \leq 20\%$;</p> <p>C <input type="checkbox"/> $\Delta A/A > 20\%$;</p>	<p>SETBACK $\leq 10\%$;</p> <p>$10 < \text{SETBACK} \leq 20\%$;</p> <p>SETBACK $> 20\%$;</p>
		TOWER CONDITION RATIO T/H	
		<p>A <input type="checkbox"/> REGULARLY DISTRIBUTED</p> <p>B <input checked="" type="checkbox"/> IRRREGULARLY DISTRIBUTED</p>	
	3.6 LAYOUT OF OPENINGS		

Figure 4-8. Proposed survey form: Section 3 “Structural regularity”.

Section 4 “Soil and foundations conditions” (Figure 4-9) examines the type of soil, the slope and the thrusting conditions of the terrain, as well as the existence and quality of the retaining walls and foundations according to GNDT (2007). Loose and thrusting soils in steeped terrains, or poor types of retaining walls and foundations, are unfavourable conditions that can seriously affect the seismic behaviour of the structures. RC cantilever or anchored retaining walls, as well as masonry or stone gravity walls, are considered as good typologies to reduce the thrusting effect of the soil. The presence of well-executed foundations clearly improves the seismic response of the buildings, especially for those settled in loose soils. The foundations shall be capable to transmit the loads received from the upper structures to the ground as uniformly as possible (CEN 2004). In this regard, well executed RC or masonry strips or isolated footings along all the structural elements are commonly considered as good solutions (Question 4.5, Figure 4-9). Significant differences in level foundation can also affect the seismic behaviour of the structure, and thus this possibility is considered explicitly in Question 4.6

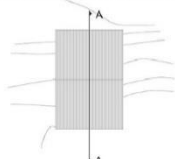
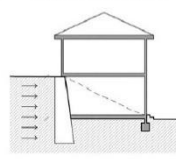
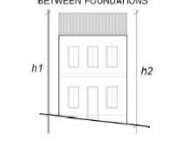
SECTION 4: SOIL AND FOUNDATIONS CONDITIONS				S4					
4.1 TYPE OF SOIL A <input checked="" type="checkbox"/> HARD ROCK B <input type="checkbox"/> LOOSE AND NON-THRUSTING C <input type="checkbox"/> LOOSE AND THRUSTING		4.2 TERRAIN SLOPE A <input type="checkbox"/> $\leq 10\%$ B <input type="checkbox"/> 11 - 20% C <input checked="" type="checkbox"/> 21 - 40 % D <input type="checkbox"/> 40% <		IN PLAN VIEW - CRITICAL TERRAIN SLOPE 		THRUSTING SOIL CONDITION 		LEVEL DIFFERENCES BETWEEN FOUNDATIONS 	
4.3 RETAINING WALLS CONDITION			4.4.1 TYPE OF FOUNDATIONS			4.4.2 MAXIMUM LEVEL DIFFERENCE BETWEEN FOUNDATIONS (Δh)			
4.3.1 TYPE A <input type="checkbox"/> CANTILEVER WALL B <input checked="" type="checkbox"/> GRAVITY WALL C <input type="checkbox"/> ANCHORED WALL D <input type="checkbox"/> NO WALL		4.3.2 MATERIAL A <input type="checkbox"/> RC B <input checked="" type="checkbox"/> STONE MASONRY C <input type="checkbox"/> BRICK MASONRY D <input type="checkbox"/> UNREINFORCED CONCRETE		A <input type="checkbox"/> RC STRIP OR ISOLATED FOOTING OR SLAB B <input checked="" type="checkbox"/> BRICK OR STONE MASONRY STRIP FOOTING C <input type="checkbox"/> STONE BASE D <input type="checkbox"/> OTHER			0 1 M		

Figure 4-9. Proposed survey form: Section 4 “Soil and foundations conditions”.

Section 5 “Non-structural elements” assesses the stability condition of accessory members that may fall down during the earthquake, such as balconies, chimneys, cornices, etc. (see Figure 4-10a). The potential hazard of these elements is evaluated in accordance with their dimensions and heaviness, and considering large/heavy elements badly connected to the main structure as the most unfavourable cases.

Section 6 “Damage condition” identifies the current grade of visible damage in the main structural elements, i.e. load-bearing systems, stories, roofs, and non-structural elements (Figure 4-10b). The observed damage level definition is based on the AeDES form (Baggio et al. 2007) that consider the European Macroseismic Scale EMS 98 and the GNDT guidelines. Damage grade D1 is slight and does not affect significantly the capacity of the building and the safety of its occupants, even against the falling of non-structural elements. Damage grade D2 is medium-severe and can partially affect the capacity of the structure but not bringing it to the collapse. Damage grade D3 is very heavy and could change the capacity of the structure significantly, bringing it to the collapse.

Finally, Section 7 “Current condition of conservation” evaluates the current state of the building as for the overall condition of the structural elements, see Figure 4-10c. The evaluation criteria consider factors such as the damage grade of the material (i.e. cracks, spalling, corrosion, decay, etc.), past maintenance interventions, hazardous structural additions, and presence of strengthening elements. The user must evaluated carefully later retrofit interventions since they might significantly jeopardize the capacity and global seismic behaviour of the building. Large structural additions, such as upper floors or badly connected enlargements, constitute unfavourable interventions. Three classes are established from A to C, where A is the most favourable condition.

SECTION 5: NON-STRUCTURAL ELEMENTS				S5
LARGE / HEAVY ELEMENTS	<input checked="" type="checkbox"/> PROJECTED WINDOWS	SMALL / LIGHT ELEMENTS	<input checked="" type="checkbox"/> CORNICES	<input type="checkbox"/> A
	<input type="checkbox"/> BALCONIES		<input checked="" type="checkbox"/> GUTTERS	<input checked="" type="checkbox"/> B
	<input type="checkbox"/> GALLERIES		<input type="checkbox"/> FAÇADE COVERING	
	<input type="checkbox"/> EXTERIOR STAIRS		<input type="checkbox"/> ORNAMENTS	
	<input type="checkbox"/> CHIMNEYS		<input checked="" type="checkbox"/> SIGNBOARDS	<input type="checkbox"/> C
				BUILDINGS WITHOUT PROJECTED ELEMENTS, OR WITH SMALL/LIGHT ELEMENTS WELL CONNECTED TO THE STRUCTURE. BALCONIES PART OF THE HORIZONTAL STRUCTURES. LIGHT AND WELL CONNECTED CHIMNEYS
				SMALL/LIGHT ELEMENTS BADLY CONNECTED TO THE STRUCTURE, OR LARGE/HEAVY ELEMENTS WELL CONNECTED
				LARGE/HEAVY ELEMENTS BADLY CONNECTED TO THE STRUCTURE, OR ELEMENTS ADDED LATER, BADLY EXECUTED OR CONNECTED TO THE STRUCTURE

(a)

SECTION 6: DAMAGE CONDITION					S6
	DAMAGE GRADE	NULL	D1 - SLIGHT	D2 - MEDIUM-SEVERE	D3 - VERY HEAVY
		1	2	3	4
6.1 LOAD-BEARING SYSTEM	A	<input checked="" type="checkbox"/>	<input type="checkbox"/>	<input type="checkbox"/>	<input type="checkbox"/>
6.2 STORIES	B	<input type="checkbox"/>	<input checked="" type="checkbox"/>	<input type="checkbox"/>	<input type="checkbox"/>
6.3 ROOFS	C	<input type="checkbox"/>	<input type="checkbox"/>	<input type="checkbox"/>	<input checked="" type="checkbox"/>
6.4 NON-STRUCTURAL ELEMENTS	D	<input type="checkbox"/>	<input type="checkbox"/>	<input checked="" type="checkbox"/>	<input type="checkbox"/>

(b)

SECTION 7: CURRENT CONDITION OF CONSERVATION			S7
A <input type="checkbox"/>	GOOD CONDITION OF RESISTANT ELEMENTS AND/OR MATERIALS. NO LATER STRUCTURAL ADDITIONS, OR SMALL AND WELL EXECUTED ONES	B <input checked="" type="checkbox"/>	SLIGHT TO MEDIUM DAMAGE GRADE OF RESISTANT ELEMENT AND/OR MATERIALS. SOME LATER STRUCTURAL ADDITIONS POORLY EXECUTED, OR LARGE ADDITIONS WELL EXECUTED
		C <input type="checkbox"/>	HEAVY DAMAGE GRADE OF RESISTANT ELEMENTS AND/OR MATERIALS. LARGE LATER STRUCTURAL ADDITIONS POORLY CONNECTED OR EXECUTED

(c)

Figure 4-10. Proposed survey form: (a) Section 5 “Non-structural elements”, (b) Section 6 Damage conditions and (c) Current condition of conservation.

4.3 Survey implementation plan

The application of the proposed survey methodology is intended for urban areas with residential or public buildings, housing blocks and traditional dwellings. Churches and masonry palaces constitute more peculiar construction systems deserving specific tools for survey and seismic assessment (Presidenza del Consiglio dei Ministri - Dipartimento della Protezione Civile, 2011a-b). The building survey implementation plan is divided into three stages: (1) pre-field activities, (2) on-field survey, (3) data management and outputs. Pre-field activities include essential works that must be developed prior to the on-field survey and the preparation of the survey forms. Lastly, proper management strategies are used to build suitable databases and outputs with GIS tools.

4.3.1 Pre-field activities

Pre-field activities are necessary to optimize the available resources and the operational efforts in terms of time and costs. The first stage of the pre-field activities is to determine the boundaries of the study area and the number of buildings to be investigated. After the recognition of the study area, all the elements must be labelled with an identifier number (ID) for the database. Local city administrations usually consider IDs to classify buildings in their databases, such as the land registry, and the IDs for the building survey should be the same of the local

existing ones. Local IDs are helpful to localize effectively the major technical information of the building in the archives or historical records.

The main pre-field activity is the collection of the existing information already gathered in local archives. This step is termed “desk survey” and it defines the remote data-collection procedures from local records, inventories or literature. The main aim is to collect the original documentation of the buildings from legitimate sources, such as drawings, plans, photos, technical specifications, etc. All this sources can provide remarkable historical and technical information about the building, see Figure 4-11. Backup and possible digitalization of the collected data, with a proper link to the buildings’ IDs, is also a very important step of the desk survey.

Another relevant step of pre-field activities is the use of taxonomy in defining the expected classes of buildings that characterize the area under investigation. The identification of the most representative structural typologies within the urban context will also allow to extrapolate meaningful data useful for buildings with missing information but similar characteristics. Good indicators of common features among the buildings could be the age, the construction materials, the stylistic resources, the façade configuration, the average height of the floors, etc. Typological surveys are frequently based on extrapolation strategies, like in the seismic vulnerability studies carried out by Taffarel et al. (2016) and Masi et al. (2014). Pre-field activities should also include a preliminary check of the completeness of the survey forms to be used during the following on-site survey. This control should be done with respect to the specific stock of buildings under investigation time by time. In fact, some specific integrations could be sometimes useful as a function of the specific structural typologies that characterize the region under investigation.

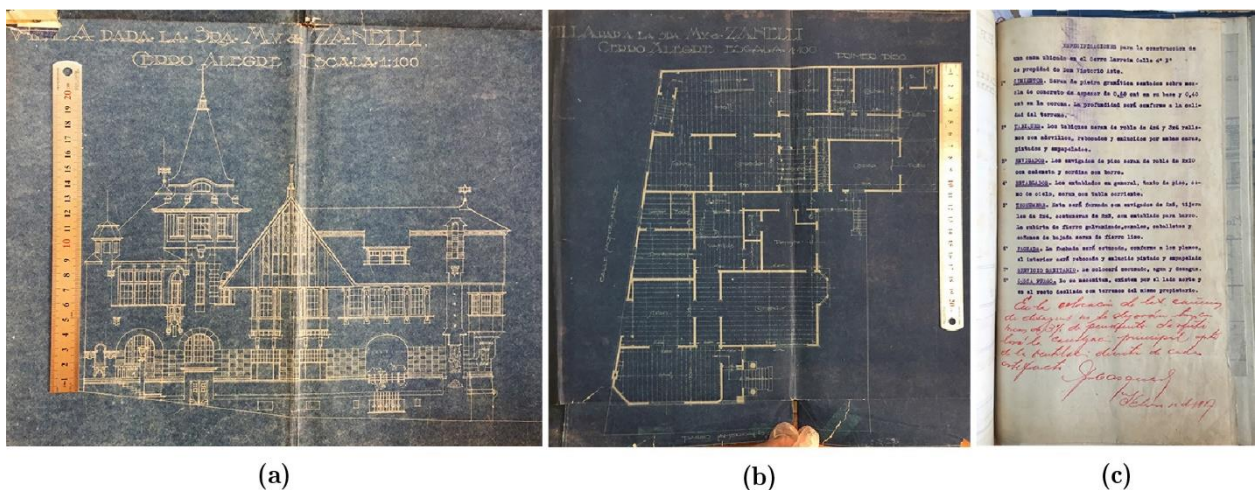


Figure 4-11. Example of pre-field desk survey: original technical documentation of the *Baburizza* building settled in Cerro Alegre in Valparaíso (Chile) constructed in 1917: (a) elevation drawing, (b) first-floor plan and (c) technical specification (source: Historical archive of Municipal Construction Management of Valparaíso, DOM).

The last pre-field stage is the preparation of a survey strategy, prior to on-field inspection, called survey path. This work implies the mapping of survey routes by taking into account the accessibility, the topographic conditions, the available resources, the time and number of examiners. Survey path strategies ensure a systematized survey and management of the resources.

4.3.2 On-field activities: use of the survey forms

Once the study area and the survey elements are defined in the pre-field activities, the buildings must be inspected on field, based on the survey requirements detailed in Section 4.2.1. In the pre-field activities, all the available desk information must be used to fill the surveys, and only the missing data should be gathered during the in-situ inspection. This strategy facilitates the optimization of the logistics of the survey, saving resources and time.

In building survey assessment, the ideal scenario would be the inspection of all the components of the stock. However, this is often an impracticable assumption in most of the cases due to many factors, e.g. limited survey resources (surveyors vs. time), buildings with restricted access, etc. In order to face these limitations, a typological survey must be carried out by inspecting a number of representative buildings of the existing stock. The selected cases should be characterized by favourable inspection conditions, which offer the possibility to inspect the structural system and the internal conditions properly. The best examples to be inspected are the buildings undergoing rehabilitation works, especially for masonry and timber frame buildings due to their structural systems usually hidden under the finishing elements (paint, sheathing, infill, etc.). In typological surveys, it is recommended the full inspection of more than one building per typology. This consideration facilitates the recognition of common attributes and possible differences within the building typology object of study.

In addition to the information required in the forms, the surveyed buildings must be extensively documented with photos, measurements, sketches, description, etc. Such information is helpful for the extrapolation of relevant data for the buildings with lacking information. Even though internal inspections cannot be carried out for all the cases of the stock, recording of data derived from external inspections is highly recommended for all the cases. These data could be helpful to compare and seek similarities with the surveyed representative cases, intended to get the best survey approximation for these buildings.

4.3.3 Post-field activities: data managements and outputs

All the data collected during the survey activities can be suitably compiled by using Geographical Information System (GIS) databases to evaluate the status of the study area. GIS is a methodical collection of computer software, geographic data, and designed tools to efficiently capture, store, update, analyse, and display all forms of geographically referenced information. These activities are essential in order to create reliable databases to understand the structural

characteristics of the different building typologies of the study area. Accurate databases with complete information contribute to improve the quality and reliability of the large-scale seismic vulnerability assessment.

The integration of GIS platforms is very common in the urban assessment due to their multiple possibilities of spatial analysis and statistical outcomes of large amount of georeferenced data. GIS environments allow creating unequivocal geometrical data with individual IDs, generated from digital maps or another graphical source, that are flagged with alphanumeric information. Digital data are organized in layers that are properly linked with the corresponding element's ID. This advantage allows feeding the database and analysing the information according to the user criteria, by information-crossing procedures and mapping. A major advantage of GIS platforms is their possible use as decision support systems (multicriteria decision analysis system) for environmental or large-scale resolutions (Malczewski 2006), such as in the case of seismic vulnerability applications. Identifying topologic relationships among the seismic hazardous buildings, strategic buildings (e.g. hospitals, governmental palaces, schools, etc.), and main evacuation routes, can be helpful to determine seismic risk scenarios, emergency limit conditions, risk mitigation plans, and prioritize future investments on the cities. Numerous researches such as RISK-UE (Mouroux et al. 2004), MARVASTO (Indirli 2009), as well as the works by Vicente et al. (2008) and Barbat et al. (2010), applied GIS tools to analyse the seismic vulnerability and to estimate the risk through different methods. Surveyed data by the form proposed in this research can be efficiently linked to GIS databases in order to get statistical results and plot useful maps for future seismic vulnerability analyses of the study areas.

4.3.4 Correlation among pre-field, on-field, and post-field survey activities

Figure 4-12 summarizes through a flow chart all the necessary working stages for the proposed methodology of building survey of historical buildings in urban centres. As discussed in the previous sections, the whole process consists in three main groups of activities, i.e. pre-field, on-field and post-field. These actions are all necessary to collect, gather and analyse the information about the buildings for the large-scale assessment of the seismic vulnerability.

Pre-field activities lead to gather all the original information of the building stock available from local archives. Mapping of survey area, selection of the buildings and labelling by IDs, are necessary to form the boundary of the urban survey. Subsequently, desk survey allows gathering original documental information from local archives, such as original plans, drawings and technical reports of the buildings (Output 1 in Figure 4-12). The collected data may be helpful to define a preliminary taxonomy of the representative typologies of the building stock. After having identified the representative building typologies of the study area, a typological on-field inspection of representative cases can be carried out. Survey path aids to plan logistically the on-site examinations and survey strategies.

On-field activities constitute the main core of the procedure and consist in on-site inspection of each building, and the identification of the representative and recurrent typologies. Photos, on-site measurements, drawings and morphological features of the building are expected to be collected by on-site inspections (Output 2 in Figure 4-12). All the gathered information allows also the completion of the building taxonomy for the investigated area. In the cases of buildings with restricted access or complex inspection conditions, data extrapolation from documental information of representative cases and the use of taxonomy can help to fill the gaps of information necessary for the survey forms. This procedure implies the use of the surveyed information derived from deeply inspected cases to feed the survey forms of similar buildings with lack of information. After on-site inspection and/or extrapolation processes, survey forms are completed (Figure 4-12 in Output 3). If some of the survey forms are still incomplete, deeper inspection to the buildings or representative typologies should be carried out, until obtaining all the necessary data for the seismic vulnerability assessment. Once all the buildings of the stock have been surveyed, post-field activities can be carried out. GIS database is built to store and analyse the surveyed data. Processing all the information allows to obtain the last outputs of the survey, i.e. maps, statistical results, and overall conclusions about the conditions of the urban building stock (Output 4). These final outputs are tools extremely necessary for the development of later policies of urban seismic risk assessment and mitigation.

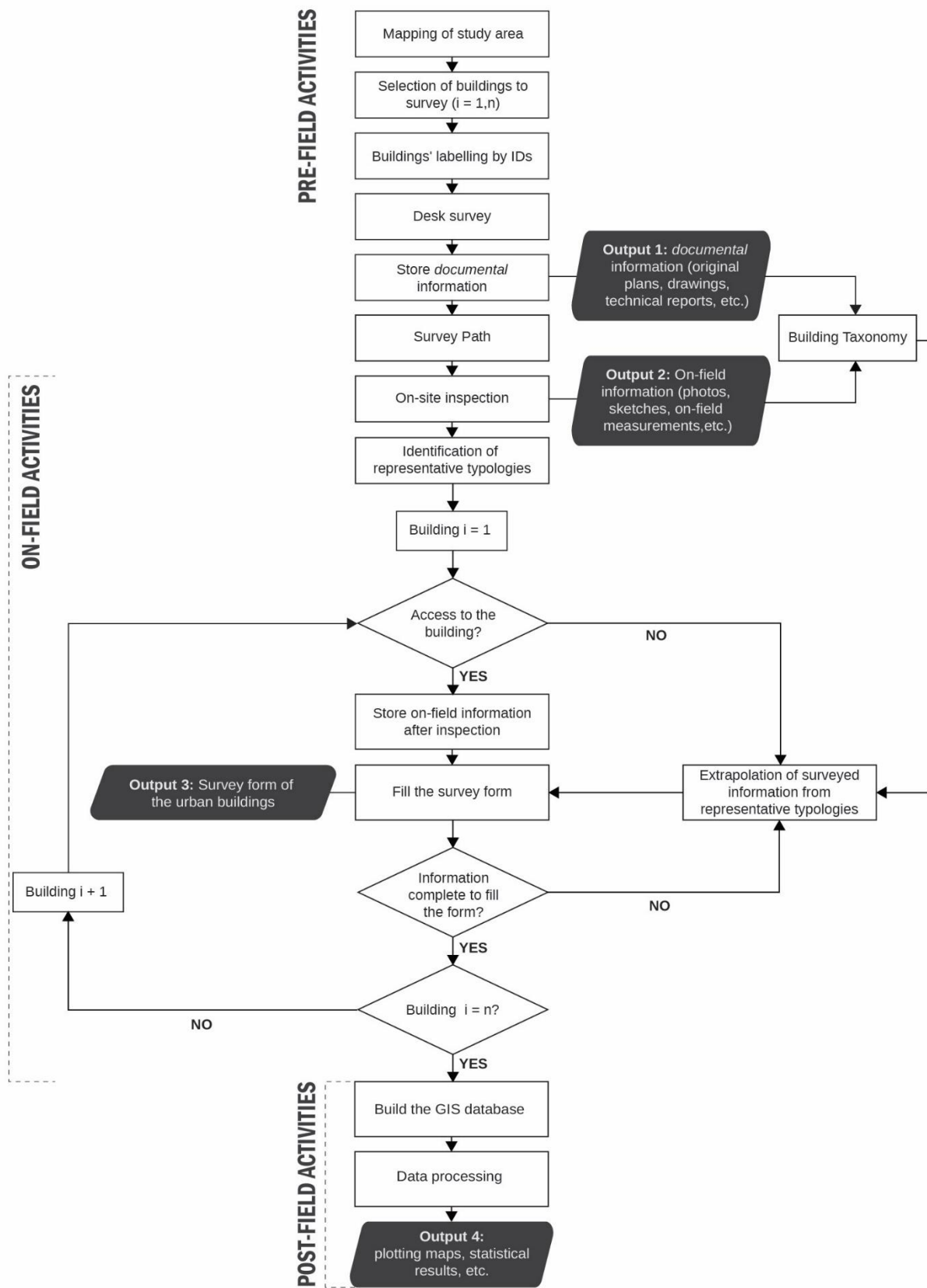


Figure 4-12. Flow chart of the building survey process.

4.4 Application to two neighbourhoods of the historical centre of Valparaíso, Chile

The city of Valparaíso (Chile) is an extremely high seismicity area. Historical earthquakes caused devastating consequences in the urban layout (8.2 Mw in 1906 and 8.0 Mw in 1985) and also the 2010 recent one produced visible damages on the built heritage. All these catastrophic events caused large economic and human losses to the city, due to the collapse of the buildings that had to be reconstructed in many occasions. In spite of the past consequences and constant exposure of the city, the available information about the post-earthquakes constructions conditions, such as technical reports or surveys, is very scarce. Valparaíso presents an exceptional geographic condition, configured by a bay, an artificial flat zone, and surrounding hills (the so-called “Cerros”) where most of the city developed. The urban configuration on the hills is rather complex due to the steeped and irregular territory, in contrast with the regular urban layout of the flat area (see Figure 4-13). The characteristic strategies of adaptation of the buildings to the slope, in addition to the valuable architectonic characters, is one of the most peculiar features of the built heritage of the city.

The building stock including in Emergency Limit Condition (ELC) zone, defined in Section 3.6 (Chapter 3), are surveyed by applying the described methodology in this section. Most of these buildings were built between the late 19th and early 20th century presenting valuable historical and heritage features. The ELC zone is part of the historic quarter of Valparaíso, which was declared World Heritage Site by UNESCO in 2003 after recognizing the outstanding value of its urban layout and architecture as perfectly adapted to exceptional geographic and topographic environmental conditions. 111 buildings including timber frame, masonry, RC, and mixed iron-RC buildings were surveyed in this stock, being the former the most common typology. Timber frame and masonry buildings commonly present a vernacular nature and residential use, while RC and mixed iron-RC buildings present large dimensions and house banks, offices other similar programs.

4.4.1 Pre-field survey

As already commented in Chapter 3, the surveyed study area was selected due to its historical condition and strategic position in the downtown area. This zone includes three portions of the World Heritage Site: (1) Cerro Alegre and Cerro Concepción; (2) Anibal Pinto square and Almirante Montt street, and (3) Bank area and Arturo Prat street. Cerro Alegre and Cerro Concepción are well-conserved historical and touristic neighbourhoods, while the others are centric zones on the flat downtown with primary commercial and bank activity. According to *The Regional Plan of Tsunami Evacuation of Valparaíso* (ONEMI 2016), downtown zones are tsunami risk areas and their evacuation routes are delimited in the Cerro Alegre and Cerro Concepción

towards safe-zones, as shown in Figure 4-13. Such evacuation routes are the same in case of the occurrence of an earthquake.

The building stock object of this study considers all the potential interfering buildings of the evacuation routes including in the Emergency Limit Condition (ELC) zone (Section 3.6 in Chapter 3). Buildings are considered interfering when their partial or total collapse can obstruct their evacuation routes and thus the functionality of the emergency networks at the ELC. A total number of 111 buildings are identified along the main evacuation routes of the study area, as shown in Figure 4-13c-d, as well as two empty lots. The building database was created with IDs assigned according to the local records by the Construction Management Department of Valparaíso (DOM). An important amount of original technical documentation such as plans, building specifications, drawings, and photos were collected from the DOM office archive. This source gathers original documents of the most important historical buildings of Valparaíso since 1900. Unfortunately, many of the oldest constructions do not have any available record, such as those built before the first proposal of the seismic design codes in 1960. Only 40% of the surveyed stock possessed projects documentation in the DOM archives. In addition, technical reports and published literature (Jorquera 2015; Hurtado, Santander, and Muñoz 2016; Sánchez and Jiménez 2011) could contribute to the pre-field survey activity about the representative buildings and architecture of the study area.

The historical centre of Valparaíso is characterized by the coexistence of different building typologies and materials. Suitable survey forms are necessary to gather knowledge on the seismic vulnerability of all the possible combinations of available structural systems. The large heterogeneity of the existing typologies of buildings is due to the multiple uses of the neighbourhoods. Cerro Alegre and Cerro Concepción have mostly residential buildings, where timber frames and masonry typologies are the most diffused structural solutions. Downtown areas surrounding Anibal Pinto and Sotomayor squares are mainly commercial and bank zones, composed of high-rise RC and mixed iron-RC exemplars. Most of the buildings of the surveyed stock were built between the last eighteenth and early nineteenth centuries and they present remarkable historical and architectonic values. Newer structures in RC were built under current seismic regulations but they are located outside the study area. Before on-site inspections, the study area was subdivided into five zones to perform a survey path and systematize the on-field survey inspection. This activity was carefully planned according to the morphological complexity of the buildings and their mutual proximity (Figure 4-13d).

4.4.2 On-field survey

The definition of the most representative features of each building typology is the result of the in-depth on-field inspection of archetypal buildings presenting favourable examination

condition. The gathered information allowed to characterize each typology and to define a building taxonomy for the investigated area of the historical centre of Valparaíso. The identification of common attributes in the buildings was essential to classify the different typologies and support data extrapolation procedures. All the buildings were inspected from the outside, but numerous buildings with full access were also inspected from the inside. The following sub-sections present a summary of the structural characterization of the 111 surveyed buildings according to the different material typologies of the study area.

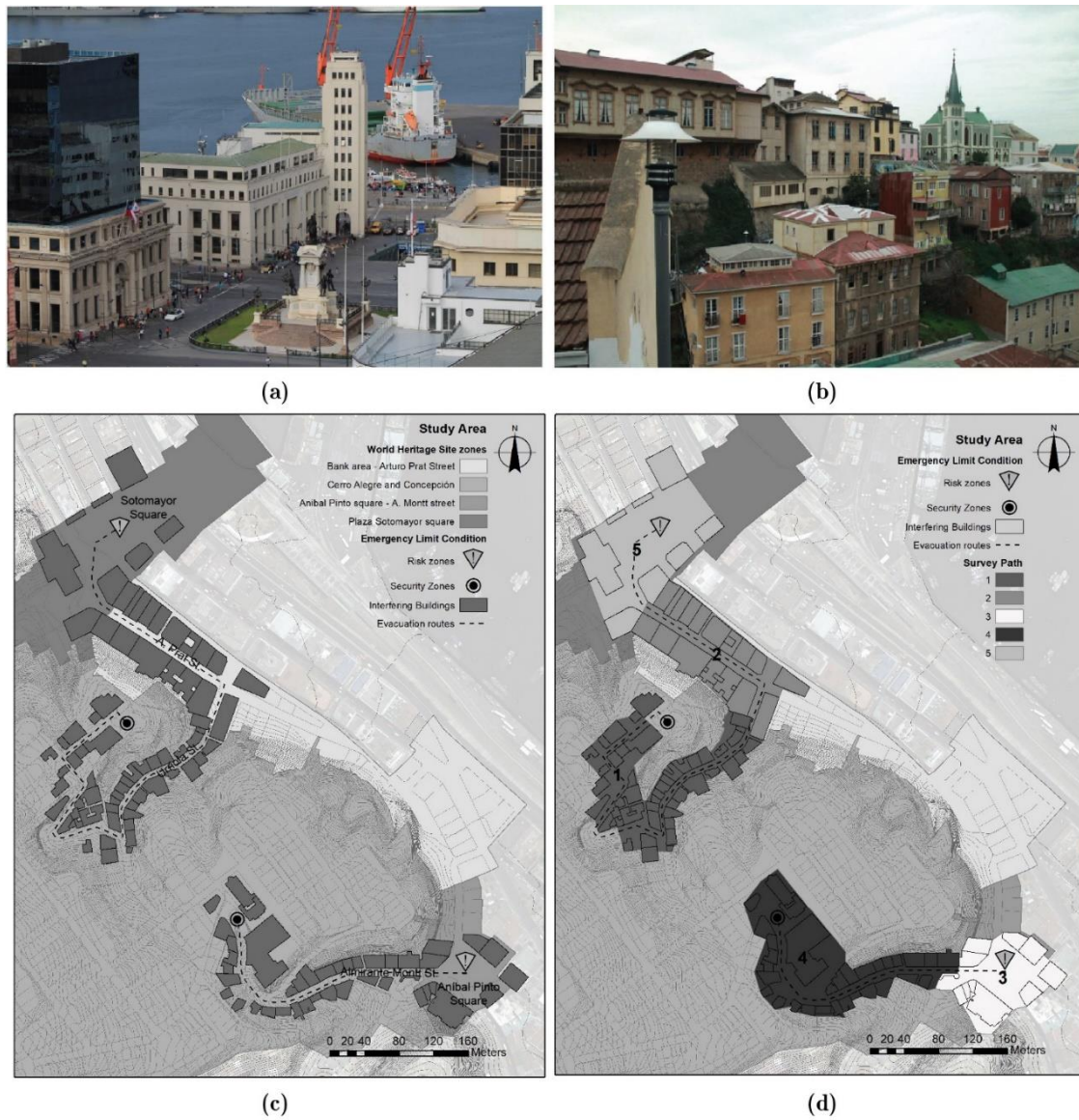


Figure 4-13. Pilot study-area of Valparaíso: (a) Sotomayor square, (b) Cerro Alegre and Cerro Concepción, (c) World Heritage Site zones with safety functions, possible interfering buildings and evacuation routes at the Emergency Limit Condition and (d) survey path.

Most of the masonry buildings of Cerro Alegre and Cerro Concepción present mixed use, combining residential, commercial and touristic activities. Ground levels are commonly for public use (restaurants, stores, etc.) while the upper floors consist of dwellings. The number of occupants varies between 10 to 100, which corresponds to a medium level of exposure. Particularly, masonry

buildings are mostly medium-rise having between 2 to 4 stories with an average height of 3.5 m each. Historical masonry constructions (see examples in Figure 4-14), built without anti-seismic design regulations in the early 20th century, were carefully inspected in this survey. Roofs and stories, as well as internal configurations, presented the most challenging inspection conditions due to restricted access. For such cases, data extrapolation and some hypotheses based on the literature were considered. Masonry walls are typically made of solid clay bricks with dimensions $0.41 \times 0.20 \times 0.06 \text{ m}^3$ bonded with good quality lime mortar (Hurtado, Santander, and Muñoz 2016), as shown in Figure 4-15. The thickness of the walls varies with the height of the buildings, presenting staggered shapes with changing dimensions at each story. This configuration facilitates the support of the story structures, as shown in Figure 4-14d (M. Salazar 2014). The thickness can vary from 0.25 m to 0.8 m along the height of the façades and it can be smaller in the sidewalls, e.g. 0.5 m to 0.25 m. The sidewalls also act as firewalls and are sometimes shared between two adjacent buildings. Several cases present iron tie rods connecting external walls to story structures. Internal load bearing walls typically consist of timber frame structures made of Oregon pine or Oakwood. Direct internal inspection is always a difficult activity, mainly because the walls are commonly covered by the plaster. Representative walls which presented good inspection conditions were evaluated in order to determine their typical configuration. The principal components of the timber frames are vertical elements, named studs or posts, spaced at $0.4 \div 0.6 \text{ m}$ from each other, and placed between horizontal elements called sills and plates. The posts are usually braced with diagonal elements, as shown in Figure 4-15a. This wall configuration is replicated along the height of the buildings and in-between the stories, according to the configuration called *platform frame*. The cross-section of the timber frame elements varies between $0.125 \times 0.125 \text{ m}^2$ to $0.10 \times 0.10 \text{ m}^2$ depending on the function of the frame, e.g. internal or external load-bearing wall. Generally, oak elements presented better state of conservation in terms of decay damage and biotic attack (termites), while pine ones showed more exposure to these damages, particularly in poorly insulated structures.

Stories were also difficult to inspect and representative cases allowed their characterization. These structures are commonly composed of timber joists spaced at $0.40 \div 0.45 \text{ m}$ along the direction perpendicular to the façade. Joist noggins maintain the distance between the joists and stiffen the structure. Wooden or metallic girders are commonly employed to reinforce the joist stories in critical areas, e.g. in the case of large spans, critical connections, etc. The stories are covered with a single layer of wooden boards perpendicularly oriented to the joist, see Figure 12c. A second layer of wooden boards at the intrados of the story provides additional stiffness to the structure. The general conditions to inspect roof structures revealed to be very unfavourable during the on-field survey in most of the investigated cases. Despite this limitation, previous studies could contribute to deepen the knowledge about these structures (Eujenio 2015). The typical roof configuration is made of rudimentary trusses presenting non-thrusting behaviour.

Exceptional cases are the “Anglican Church” and the “German School” at the end of Almirante Montt street, since they have very sophisticated roof structures.

With respect to the structural regularity, most of the masonry buildings presented regular shapes in plan and elevation and are enclosed in-row configurations. According to Formisano et al. (2011), the interaction of the buildings in aggregate affect meaningfully their seismic response. Buildings enclosed between lower constructions and placed at either the corner or the end of the aggregate were determined as the most vulnerable cases in this study. Most of the buildings of the study area have central positions in-row configuration and present similar heights in line, a condition which contributes to the good seismic behaviour of the buildings. According to Siano et al. (2017), irregular openings in a wall, e.g. with different horizontal dimensions or variable number, negatively affect the load path within the structure and the global seismic response. Even though most of the studied masonry buildings present regularly distributed openings, some critical cases presented irregularities such as offsets or openings with different dimensions, as shown in Figure 4-14b.

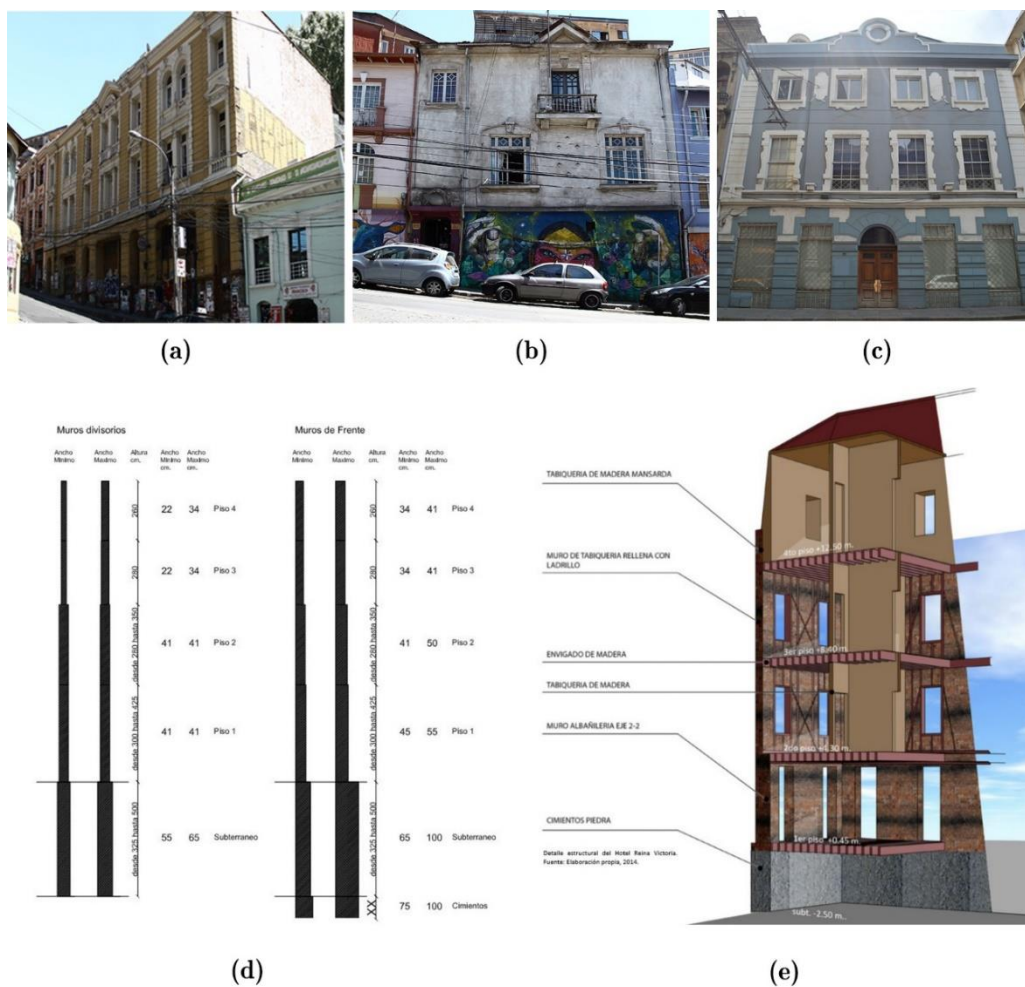


Figure 4-14. Typical features of masonry buildings in Valparaíso: (a-b) facades in Almirante Montt street, (c) facade in Arturo Prat street, (d) staggered masonry wall (images by Salazar (2014) and (e) main section of the *Hotel Reina Victoria* in Sotomayor square (by Salazar (2014)).

A large number of masonry buildings are located on Almirante Montt street, where the terrain is very steep (20 ÷ 40% slope). In these cases, the use of gravity retaining walls is recurrent to contain the surrounding thrusting soil. The thickness of a retaining wall is normally variable, and commonly vary between 2.0 m at the foundation to 0.5 m at the top. In some specific cases, these walls receive loads from the upper walls and story structures, as shown in Figure 4-16d. It should be noted that gravity walls are not present in hard rock soil zones, such as in the Almirante Montt and Urriola streets, as shown in Figure 4-16e. Gravity walls presented many difficulties of inspection due to their hidden condition. However, the representative ones investigated in the hills prove to be made of materials of suitable quality and derived from a good seismic design, given their satisfactory seismic performance during past-earthquakes. The typical foundation system is the brick or stone masonry strip footing. Raised buildings, commonly placed in significantly steep lots, make use of a platform made of quarry stone. These buildings sometimes present habitable basements built with stone or brick masonry gravity walls. Staggered buildings in steep terrains present commonly difference of levels in the foundations (1 ÷ 2 m average), a condition that negatively influences the seismic response of a structure according to GNDT (2007).



Figure 4-15. Typical features of masonry buildings in Valparaíso: (a) timber frame internal partition in Urriola street, (b) steel reinforcing structure, (c) timber story with reinforcing steel truss in Almirante Montt street.

Due to the historical and touristic character of the study area, a large number of buildings transformed their original residential use to new commercial or mixed uses. Largest buildings have apartments and hostels, with commercial activity at the ground floor. Most of the subsequent interventions were regulated by the current construction normative and proved to be well executed. Steel structures are typically used to create mezzanine stories or to reinforce the masonry walls and stories, as shown in Figures 12b-c. Internal timber frame partitions were commonly restored in the past by replacing the elements in bad state of conservation. Masonry buildings could resist several major earthquakes in the past, demonstrating their good seismic performance. However, the deterioration of the materials and the existence of some badly executed interventions constitutes major concern for future seismic vulnerability assessments.



Figure 4-16. Typical features of masonry buildings in Valparaíso: (d) gravity wall, (e) rock hillside visible from the interior of a building, and (f) side wall.

Most of the reinforced concrete (RC) buildings of the study area were built in compliance with the seismic design standards NCh 433.Of 96 (Instituto Nacional de Normalización 2009) after their first release in 1960. Chilean regulations for RC structures are very demanding due to the high seismicity of the territory. Minimum standards for material resistances and structural design are required in projects of RC structures and therefore they are generally reliable buildings if designed in compliance with construction standards. RC buildings are the largest ones of the surveyed stock in terms of area and height (see Figure 4-17). These characteristics are associated to their predominant commercial and governmental use, such as the banks and administrative buildings in Sotomayor and Anibal Pinto squares, as well as in Arturo Prat street. Most of these buildings house more than 100 occupants, reflecting their high exposure within the stock. According to FEMA (2015) vulnerability assessment, high-rise RC buildings should be penalized in order to increase the assessment of the potential hazard of these buildings, and thus to

encourage more in-depth analyses. RC surveyed buildings in the study area were identified as multi-story buildings (with more than 7 stories) and consequently must be carefully investigated.



Figure 4-17. Reinforced concrete buildings in Valparaíso: (a) Consejo de la Cultura y las Artes building (1918), (b) Compañía Chilena de Navegación Intraoceánica building (1955), (c) the Cooperativa Vitalicia building (1947), (d) the Bavestrello compound in Alvaro Besa street (1927), (e) corner building in Anibal Pinto square (1929) and (d) historical façade in Arturo Pratt Street.

Technical specifications of representative and contemporaneous RC buildings provided detailed information to characterize these building. The majority of these constructions present a unique structural system. The 63% of them were classified as A1 and A2, i.e. moment resistant frame structures filled with reinforced or unreinforced brick walls, and rigid and well connected stories, mostly cast in place RC beams with concrete topping slabs and dual systems respectively (see Figure 4-4). Internal partitions are commonly made of brick masonry or light wrought iron profiles with thicknesses varying from 0.10 to 0.25 m. Brick walls use clay-fired bricks bonded with mixed mortar of cement and sand. The good quality of the materials, as well as the rigorousness of the structural designs and execution of the project, lead to expect a good seismic behaviour of these buildings. Roof structures, as well as the stories, are made of RC slabs supporting light steel trusses to achieve the minimum slope requirements. However, roof and stories presented very challenging examination conditions due to sheathing and restricted access. Hence, their characterization was based on the existing technical reports of representative buildings, and the obtained information was then extrapolated to similar and contemporary constructions. RC structures have quite regular morphology. Few buildings present isolated plan position (Anibal Pinto and Sotomayor squares), while the remaining are enclosed in-row. Some of

the RC buildings present moderately decreasing mass from the ground level to the top, and the openings are regularly distributed in most of the cases. These configurations contribute to the good seismic response of the structures to past events. Most of the RC buildings are located in the flat zones (Sotomayor and Anibal Pinto squares), but a few of them are in direct contact with the hillsides, such as in the cases of buildings at Arturo Prat and Almirante Mont street. In these cases, retaining walls are made of RC to counteract the thrusting effect of the soil. The available technical specifications of the surveyed buildings indicated that the most typical foundations are RC isolated or strip footings. Most of the newer RC buildings present excellent conditions of conservation, given their anti-seismic solutions and newest character. Later addition of upper stories is a recurrent intervention in RC buildings. Even though some specific cases considered explicitly the possible later addition of stories and overloads in the original project, most of them did not. In these unfavourable cases, the quality of the later intervention must be carefully evaluated in order to determine its influence on the global seismic response of the building.

The oldest constructions of the study area are recognized as hybrid iron-RC structural typologies built between the late 19th and early 20th century. Even though they constitute a minority of the surveyed stock (only 5%), their remarkable architectonic and structural value position them as important targets of this study. Despite their historical character, there is a scarcity of technical information in DOM and very few past studies on their structural configuration. All the mixed iron-RC buildings are located in Arturo Prat street in the commercial zone of the downtown area. Originally, the largest buildings of the stock were conceived to house banks or governmental organizations. Similar constructive solutions, stylistic patterns, materials and façade compositions (Figure 4-14 and Figure 4-15) led to identifying them as analogous exemplars built with contemporary iron-RC techniques. Unfortunately, these buildings presented very unfavourable inspection conditions due to their large dimensions, complex configurations, and restricted access. To mitigate this difficulty, an in-depth inspection was carried out on a representative case of study in order to implement a reliable data extrapolation for the remaining analogous buildings. The similarities among the buildings were verified through available original information and overall field inspections in order to ensure the confidence of the extrapolation process.

The building of the *Bolsa de Valores de Valparaíso* was selected as case of study due to the excellent conditions of examination and the available technical reports which helped to make a consistent characterization of the hybrid structural typology. The structural and architectonic features of this buildings was widely described by *Concreto Revista de Ingeniería y Arquitectura* (1919) in Valparaíso. The construction of this Renaissance-style building, dating back to 1912 (Figure 4-18) was undertaken by important engineer-architects of this period such as Carlos Claussen, Gustavo Jullian and the Italians Arnaldo Barison and Renato Schiavon. The building is located at the bottom of the Cerro Alegre, in the intersection of the Urriola and Arturo Prat

streets, positioned in the corner of the row in a semi-staggered land. The construction covers an area of 960 m² and has 37.50 m height up to the dome. The main load-bearing system is made of laminated “C” profiles and complex truss systems of wrought iron, filled with plain concrete. The dimension of the profiles varies with the height of the buildings at each story. First and second floors have the largest section profiles, i.e. “C” profiles of 0.25 m depth. The walls of the third and fourth floors have smaller “C” profiles with heights of 0.20 m and 0.15 m, respectively. The fifth story structure present double “T” profiles with 0.15 m height. Sidewalls present wrought iron double “T” posts of 0.2 m height spaced at 2.5 m and linked by at least two horizontal profiles. The thickness of the plain concrete fill of the frame is 0.25 m. The overall configuration of interior walls is similar to that of the main façade, with iron profiles filled with plain concrete and thicknesses varying from 0.20 m to 0.4 m. Isolated continuous pillars support the upper stories and a dome structure in the central part of the building. The stories have double “T” beams, with varying section from 0.3 m to 0.2 m along the height of the building, according to the spans and load requirements. A set of secondary iron beams topped with concrete constitute the slabs of the buildings. Tiles or wooden boards cover the floor structure depending on the use of the rooms. Roofs are composed of iron trusses covered by galvanizes iron sheets. The last interventions date back to 1980 and 1981, and they did not bring significant changes to the primary structure.

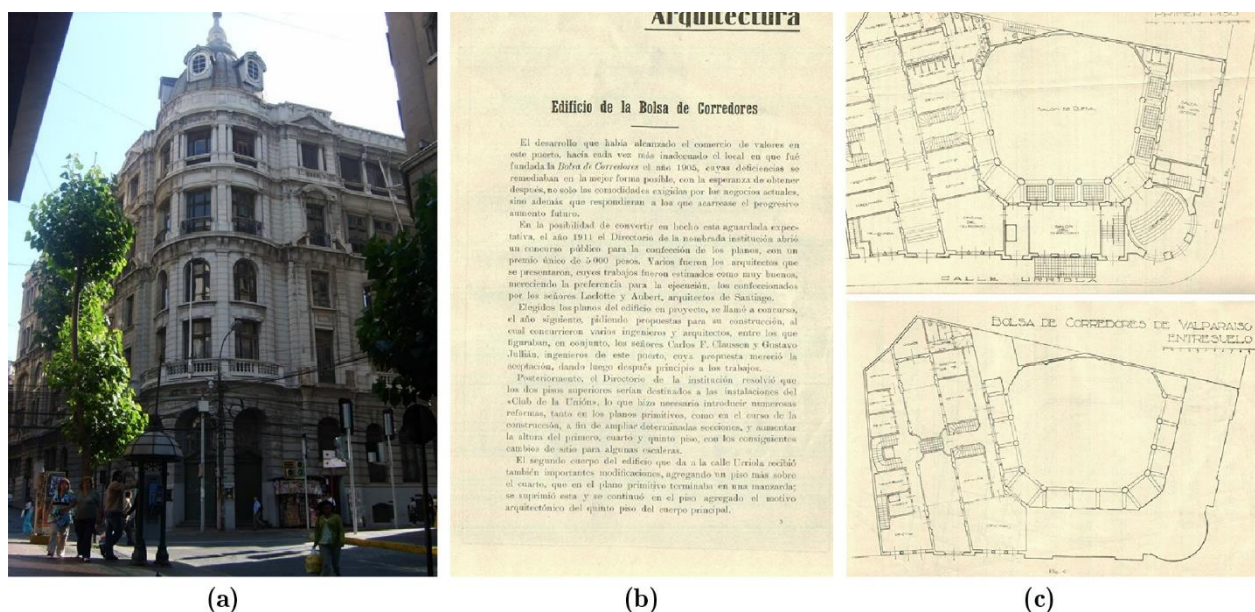


Figure 4-18. Typical mixed iron-reinforced concrete building (Bolsa de Valores de Valparaíso): (a) façade, (b-c) technical report and plan of the ground level.

On-site inspections allowed to determine the current condition of the structures, where the main issue was the bad condition of conservation of non-structural elements. The roof of the central foyer made of wood and plaster, surrounding the dome, made of wrought iron and glass, present medium-severe damage, as the detachment of a large amount of plaster and rainwater seepage see Figure 4-19a. The dome experiences corrosion of metal elements and deterioration of

the glass-metal joints, see Figure 14e. The visible remaining structures such as walls, columns, stairs, non-structural elements presented very good structural conditions (Figure 4-19).

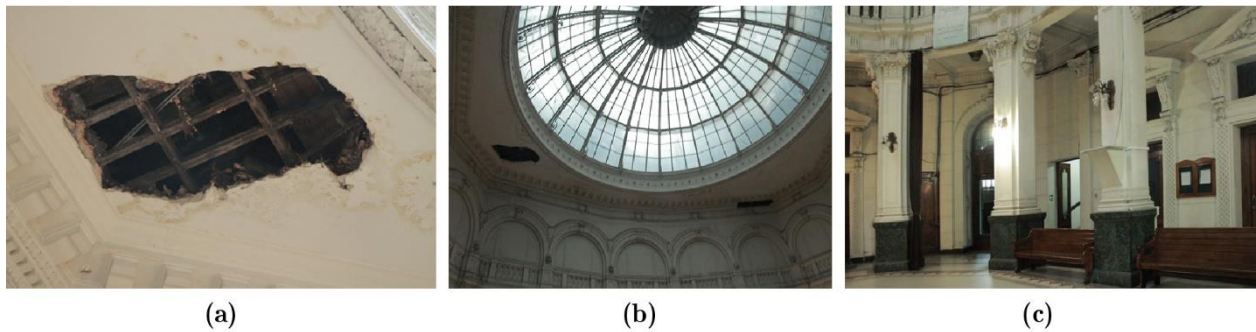


Figure 4-19 Typical mixed iron-reinforced concrete building (Bolsa de Valores de Valparaíso): (a-b) roof and dome damages and (c) interior columns

The remaining mixed iron-RC buildings of the stock presented very similar structural configurations due to their contemporary nature, proximity, and use of comparable elements, such as columns, domes, materials, etc. (Figure 4-20). Therefore, the data extrapolation results constituted a very reliable approximation. Despite this, future detailed examinations will be aimed at providing more accurate information about each one of these buildings. On the basis of the assumed extrapolation analysis, the main lateral load resistant systems of the mixed iron-RC buildings were classified as A5 (83%) and A1 (17%), i.e. moment resistant frame structures filled with unreinforced masonry (brick or RC blocks) and light steel stories or RC slabs.

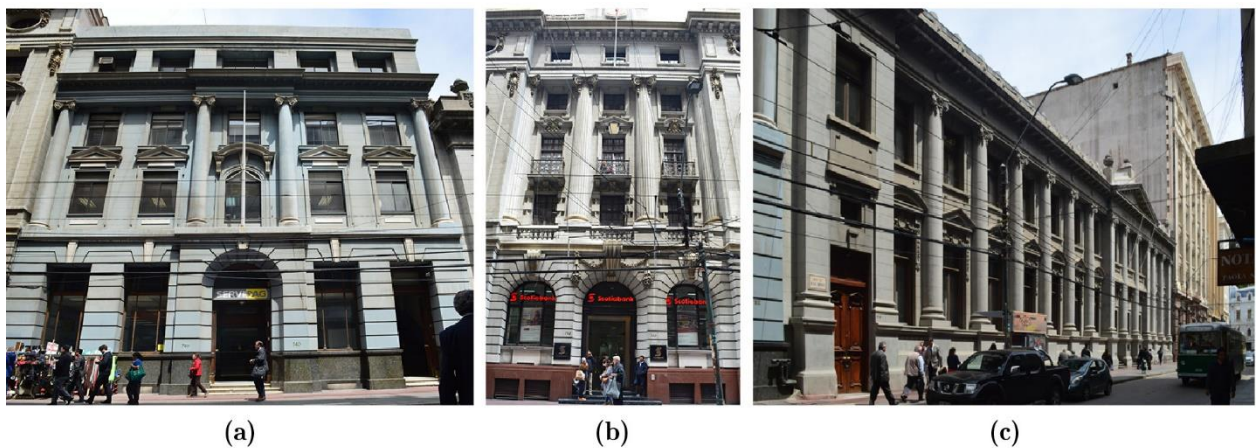


Figure 4-20. Typical mixed iron-RC buildings in Valparaíso: (a) Ex Banco de Chile dating back to 1919, (b) Ex Banco de Londres y Río de la Plata dating back to 1914, (c) Banco de Chile dating back to 1893.

Timber frame structures are the most diffused typologies in the historical centre of Valparaíso, and in the surveyed study area constitutes 40% of the building stock. The foreign influences of this type of buildings are clearly visible in the Cerro Alegre and Cerro Concepción. As stated in Jiménez (2015), similar timber frame typologies were frequently constructed in British and American territories. The foreign influence in architectural and technological solutions is evidenced by news advertisements of the time, which promoted pre-cast buildings from Europe

and imported material such as the Oregon Pine and Oakwood, as well as corrugated iron sheets. In addition, a noteworthy use of Victorian stylistic resources and architectural shapes can be found, such as sashes, bow windows and ornaments (Jiménez 2015). Local techniques and materials co-exist with foreign structural solutions in the timber dwellings of the historical centre of Valparaíso. The specific typologies of timber frame structures in Valparaíso became singular exemplars in Latin America due to their peculiar adaptation strategies to the complex topography of the territory. Most of the structures includes masonry elements such as foundations, sidewalls, retaining walls, and even present composite façades with lower stories built in masonry and upper ones in timber.

The main frames of timber structures are commonly hidden under the sheathing. This condition represented the principal obstacle to examine the configuration and conservation condition of the structure. Also, most of these buildings have residential use and consequently restricted access. These issues forced the use of data extrapolation techniques based on the study of different representative cases. The first step of this process was identifying the common features of these typologies i.e. materials, façade configuration, average height of the stories, stylistic resources, constructive solutions etc. to guarantee the confidence with the studied group (Figure 4-21). Buildings undergoing transformation or with a significant part of the structure uncovered or lightened were carefully examined to achieve the structural characterization.

Load-bearing systems are made of unique timber frames (Figure 4-21a) or mixed masonry-timber structures. In the second case, internal partitions are constituted by secondary timber frames in most of the cases. The frames are commonly made of heavy posts spaced at $0.4 \div 0.6$ m, braced with diagonal elements crossing the posts according to different configurations. Each diagonal crosses three posts, dividing the central one into two segments, and nailed at its ends to the internal faces of the external posts. The cross-sections of the elements revealed to be quite standard in all the surveyed buildings and could vary along the height of the building, as well as in the internal partitions, from 0.125×0.125 m² to 0.10×0.10 m². External walls are normally thicker than the internal ones due to the use of bigger timber elements. Reinforced carpentry joints connect most of the elements of the wall frames. The most common systems were the mortise-and-tenon, notching, and dovetail joints. Wrought iron and industrial nails of different dimensions are common as reinforcing elements for the connections. External walls are filled with adobe bricks, while internal ones with lath and plaster (see Figure 4-22a-b). Sidewalls are made of clay brick and lime mortar masonry, as described in the masonry building survey. The thickness of the walls usually decreases along the height of the buildings. This staggered condition allows supporting the stories that are usually made of timber joists with 0.05×0.15 m² cross section. These elements lean on the sidewalls and are connected by means of nails to the plates and sills of the lower and upper timber walls. Joists are spaced at 0.40 m each other and, as is the case of masonry buildings of Valparaíso, are covered by simple layers of wooden boards (Figure 4-22c).

The roofs are typically pitched and composed of rudimentary trusses. The 100% of the cases were classified in A1 (see Figure 4-6) in the survey form.

The most frequent typologies of wood adopted in the construction are Oak and the Oregon Pine. Oak pieces are used in the main structural elements, such as main beams and façade frames. Unfortunately, there is an important lack of information about the properties of the materials employed in these constructions. Future research is required to investigate the mechanical parameters of these recurrent qualities of wood, since they could be implemented in vulnerability studies of several timber structures of Valparaíso.

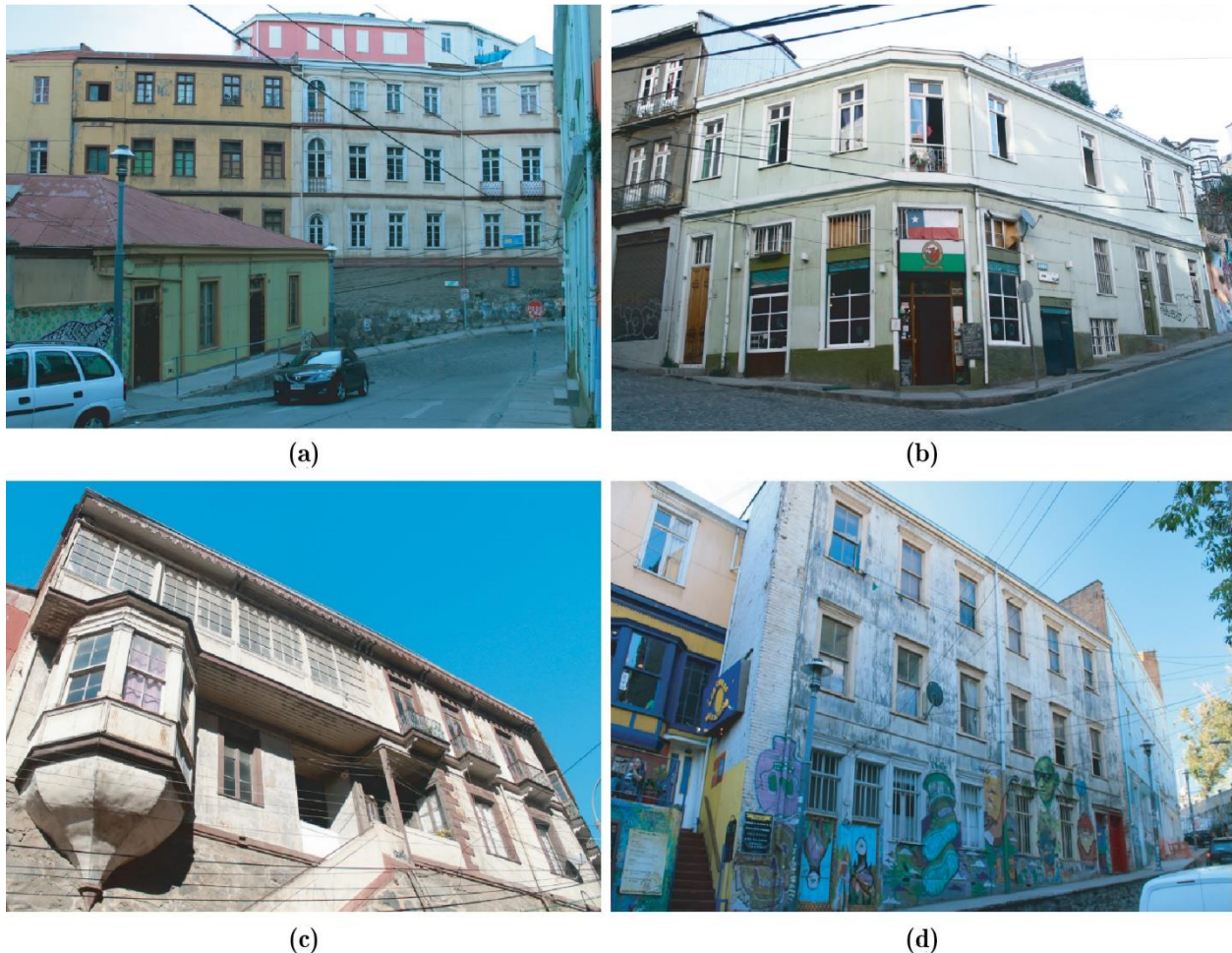


Figure 4-21. Typical timber frame buildings in Valparaíso: (a-b-c) located in Urriola and (d) Almirante Mont streets.

Most of the timber frame buildings present a regular shape in plan and elevation. As well as the aforementioned typologies, they are enclosed in-row configuration. A common pattern of timber frame structures is the configuration of the façade. The dimensions of openings are commonly regularly aligned and restricted by the internal disposition of the studs presenting very similar dimensions and appearances, see Figure 4-21. In addition, the use of the same windows typologies (sash and bow windows) and external sheathing (corrugated iron sheets) confirm the correspondence between these buildings.

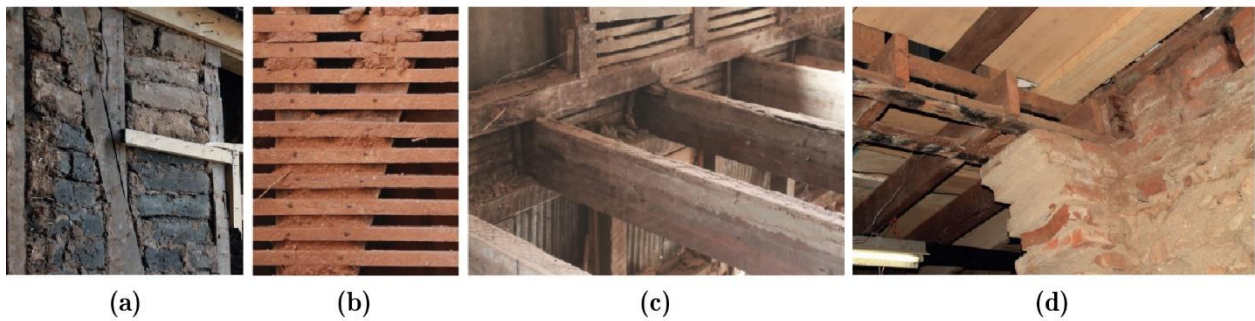


Figure 4-22. Typical timber structure configurations in Valparaíso: (a) external wall filled with adobe, (b) internal wall of lath and plaster, (c) connection of timber story to the walls and (d) connection of timber story to the brick strip footing foundation.

Timber frame is the most used structural system in the steep areas of Valparaíso. Their modularity and compatibility with other techniques, e.g. masonry, allowed the arrangement of well-adapted constructions. Also, the proved stability of the system against earthquakes, wind and thrusting soil effects positioned them as a very popular technique. Most of the buildings of the stock are placed in staggered lands, and had to make use of sophisticated construction solutions, see Figure 4-23. The high difference of levels among the foundations and the bad quality of the retaining walls are conditions that negatively affect the seismic performance of the buildings. The foundations are commonly brick or stone masonry strip footings Figure 4-22d. Brick masonry gravity walls are also employed to counteract the thrusting effect of the soil in staggered hillsides.

Buildings with large bow-windows, projecting stairs, gutters, ornaments or badly connected sheathing represent conditions of concern in case of earthquake. Non-structural elements do not present important damage conditions and were considered as null or slight in most of the cases. The damage recognition on the internal elements is always a challenging activity, thus external factors such as moisture detection and termites' residues on the surfaces are good indicators to identify damage conditions on structural elements. The degradation of the material by biotic attacks, decay, and mechanical damage, generates large concern in timber structures. Termite attacks are the main source of deterioration in Valparaíso, especially in elements made of pine. Medium to severe damage in structural elements can highly decrease their mechanical resistances and consequently jeopardize the global behaviour of the structure. A poor insulation of the structures interacting with the foundations and hillsides leads to accelerated decay of the wood due to the high moisture conditions. Depending on the level of damage, timber structures can be repaired by replacing the deteriorated pieces and this fact eases the maintenance of this type of buildings. Mechanical damages caused by major earthquakes or fires, such as partial detachment of portions of walls or structural elements, are the worst damage scenarios for these typologies.

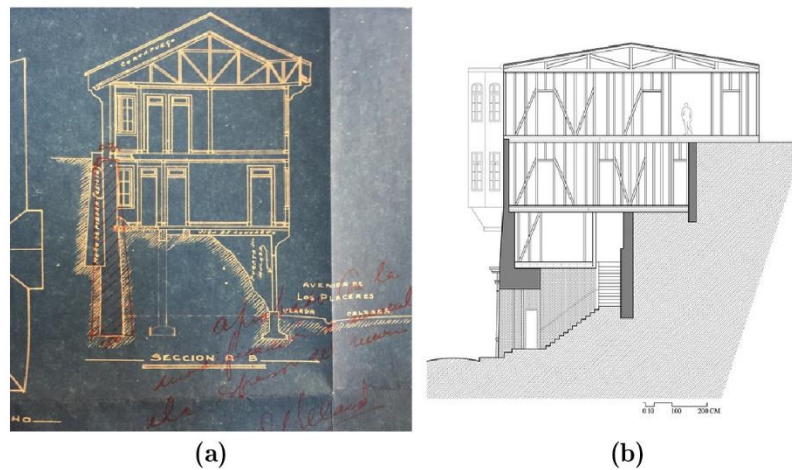


Figure 4-23. Typical slope adaptation strategies of historical buildings: (a) recurrent solution in Valparaíso dating back to 1932 and (b) house in Urriola street (1900s).

As well as masonry buildings, original timber dwellings were frequently transformed into touristic buildings, such as restaurants and hotels. Typical interventions are the addition of rooftop terraces and subdivision or rearrangement of the rooms by removal/addition of internal walls. The creation of “transparent walls” by removing the adobe infill is also a rather recurrent modification of the original system. Such later interventions were investigated carefully during the survey activities in order to detect possible sources of seismic vulnerability, such as addition of excessive massive elements or removal of stiffening components of the resisting system. However, later structural interventions or additions were executed in most cases by using wooden materials and light steel elements. These cases are categorized in the group A of the Section 7 of the form Figure 4-10c.

4.4.3 Survey results and statistical analysis

The survey forms presented in Section 4.2.1 were used to collect all the information about 111 buildings of the study area. This section summarizes the results to determine a preliminary register of the current state of the buildings and to develop suitable databases for future seismic vulnerability analysis. The use of GIS tools was essential to build explanatory maps of all the surveyed data, as well as to carry out data-crossing and topological analyses according to the territorial position of the urban buildings.

The Section 1 of the survey forms “General Information” identified 45% buildings with residential use and 27% as commercial establishments. The remaining 28% corresponded to touristic, governmental, educational, or mixed activities facilities. The 11% of the surveyed buildings currently hosts less than 10 occupants, the 63% between 10 and 100 occupants, and the 26% more than 100 occupants. The overall analysis of the results emerged from the first section of the survey forms could show the strategic character and high exposure of the study area.

The Section 2 of the survey forms “Building Typology” allowed to recognize most of the buildings as historical heritage, even though in some cases the exact date of constructions was unknown. The 76% of the buildings were not built in compliance with first releases of the Chilean Seismic Design code (since 1960), while the 34% were subjected to later retrofit according to current seismic standards. These results highlighted the vernacular character of the building stock, mainly based on local techniques and construction materials. This fact motivates a systematic survey to detect possible seismic vulnerabilities not conveniently handled before the introduction of the modern design concepts. A total of 93% of the buildings presented multi-story condition: 34% had 2 stories, 28% had 3 stories, and 38% had more than 4 stories. The highest buildings are on the flat area of the downtown, while the shorts constructions are on the hills. These data showed the remarkable heterogeneity of the aggregates and exhibited the potential interfering effect of the buildings in case of their collapse (Commissione tecnica per la microzonazione sismica 2014). These outcomes allowed the detection of the exposure of the buildings, thus the need to analyse in detail the most critical cases for future vulnerability analyses. Most buildings of the surveyed stock presented hybrid structural conditions (66%). The typical mixed typologies are timber frame-masonry and iron-RC. However, the hierarchy of each material in the structure can vary significantly, and this fact complicates the determination of the primary lateral load resistant system. The 41% of the buildings were identified as timber structure resisting systems, followed by masonry (31%), RC (24%), and mixed iron-RC structures (4%), as shown in Figure 4-24. These results were fundamental to understand the nature of the building stock, to determine the correct use of the forms and to examine the representative cases of each typology. These trends highlighted the intrinsic complexity of the surveyed area, due to the hybrid condition of the buildings and the overall heterogeneity of the stock.

Question 2.5 of Section 2 of the survey forms evaluates the structural configuration of the buildings. Materials and arrangements of the main lateral load resisting systems were identified in order to distinguish the possible weaknesses of the structures. Missing information about specific buildings led to the adoption of extrapolation data from representative cases-studies and, whenever necessary, to develop further field inspections.



Figure 4-24. GIS mapping of the structural typologies (a) and their statistical distribution (b). Representative timber frame dwelling (c), masonry building (d), mixed iron-RC building (e) and RC building (f).

The majority of masonry buildings are unreinforced with semi-rigid timber stories. The 64% of them were classified as G5, G6 and G7 since they present good quality structural configuration and conservation. The marginal compliance with seismic codes represented a major concern for these typologies. The remaining masonry buildings corresponded to reinforced and confined typologies with rigid and well connected stories, classified as A1, A2 and A6 and (18%). Such buildings were designed in compliance with the current seismic codes and thus lower vulnerability is expected.

The 81% of RC buildings were classified as A1, A2, D1, which correspond to good-quality load-bearing resistant systems, as shown in Figure 4-25. The remaining 19% corresponds to the

oldest and low-quality RC buildings, generally designed without compliance to modern seismic criteria and thus representing the most vulnerable types within the RC building stock.

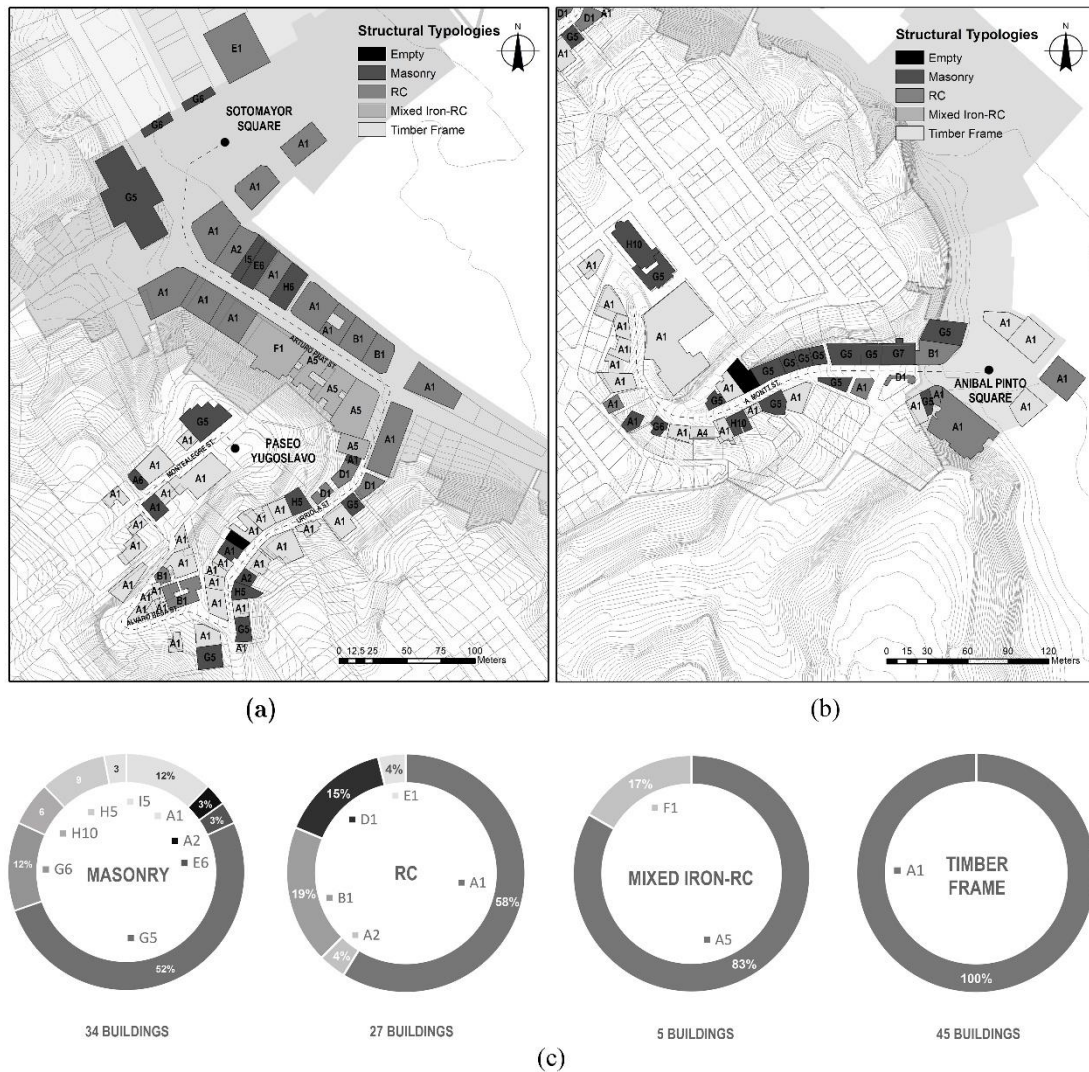


Figure 4-25. GIS mapping of lateral-load resisting systems of the buildings (a-b) and statistical distributions for each typology (c).

The large scale of the mixed iron-RC buildings and their restricted access hindered detailed on-site inspections. The great amount of similarities among these buildings allowed to extrapolate the documental information of the representative case of the building of the *Bolsa de Valores de Valparaíso*, whose structural features were described in Section 3.2.3. Although the mixed iron-RC buildings are minority into the stock, they presented high seismic exposure due to their large scale and amount of occupants. In addition, they are the oldest of the study area since they were built before 1900 without any compliance of seismic design codes. These conditions positioned them as potentially vulnerable building.

Timber frame structures presented a very regular structural pattern in all the surveyed cases and thus were classified as A1. The clear correspondance of all the inspected buildings of

the stock in terms of structural arrangement, materials, façade composition, non-structural elements, etc. fully justified the data extrapolation of representative cases to those with lack of information. The typical main load-bearing system correspond to stud frames braced with diagonals elements across the posts and rigid story systems, made of joist and sheathed with simple layer of wooden boards. This configuration is traditionally known as platform frame. Vertical load bearing systems are filled with adobe or coated by lath and plaster. Vertically oriented corrugated steel sheets cover the external walls. The reinforced carpentry joints, as well as the stiffening elements like diagonal braces and external sheathing, contribute to improve the behaviour of timber frame structures. Valparaíso's timber frame buildings are considered as reliable anti-seismic structures, as demonstrated by major past earthquakes. However, the current condition of the material and level of damage of the structural elements can might negatively affect the global behaviour of the structure. The material degradation of structural elements due to decay by humidity and termites' attacks increase the potential vulnerability of these buildings.

The Section 3 of the proposed survey forms “Structural Regularity” reported that only 16% of the buildings present unfavourable irregular shapes in plan (class C in the form). Most of the buildings presented regular plan without significantly protrusions or elongated shape which could affect the response of the structure. The enclosed conditions of the buildings in-row and aggregate configurations is a remarkable feature of the most of the buildings. The 60% of them has central position within the block, followed by the corner (30%), and isolated buildings (10%), as shown in Figure 4-26b. Adjacent buildings often share at least one perimeter wall. This interaction can highly influence the performance of the whole block/row configuration and should be considered in detail in further vulnerability analysis. Elevation configurations have also mostly regular arrangements, without important mass variation and setbacks. The openings on the façades are regularly distributed (92%) with absence of horizontal or vertical misalignments, as shown in Figure 4-26c. The prevalent regular morphology of the buildings is a good factor for the structural behaviour of the buildings under lateral seismic loads.

The foundation soil of the study area is mainly of good characteristics. According to the geological cartography records of Valparaíso (Gana et al. 1996), the 86% of the buildings are located in hills with hard rock soil. Only the 14% of the buildings are located in the flat area, which presents loose and non-thrusting soil conditions, classified as a poor category. Hillside's buildings present very extreme slope conditions, as shown in Figure 4-27. In these cases, retaining walls are usually employed to counteract the thrusting effect of the soil, especially when the buildings are directly interacting with the terrain. Masonry gravity walls are employed on the 63% of the cases, as shown in Figure 4-27b. The foundations typologies were identified based on the original documentation of the buildings and on-site inspections of few buildings undergoing restoration works. Brick strip footings are typically employed in masonry and timber frame structures (39% of the cases), while RC strip footings (36%) are used in RC and mixed iron-RC structures. The construction of flat terraces or quarry stone platforms is a common strategy in

staggered zones to level steeped terrains and reach stable foundation soils. All these evidences could show the general anti-seismic character of the structures as for the use of good quality foundations and retaining walls. Section 3 of the proposed survey form also helped to detect negative factors such as the extreme slope conditions leading to thrusting effects of the soil and level differences between foundations. According to GNDT (2007), this last factor can negatively affect the behaviour of the foundations, thus it needs to be specially considered in future vulnerability analyses.

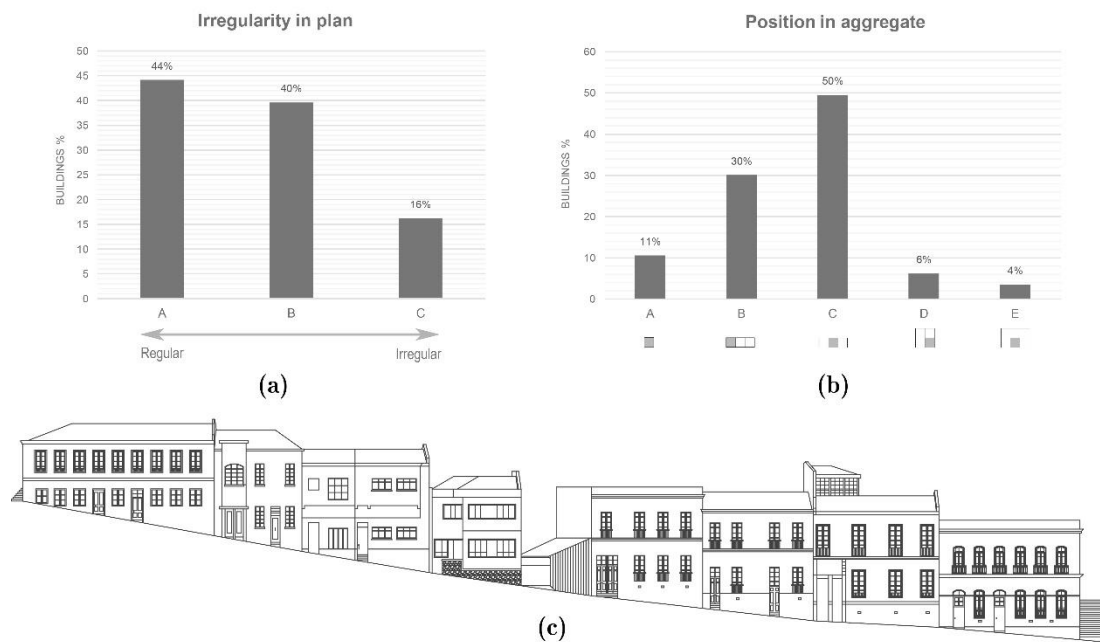


Figure 4-26. Buildings' irregularity (a), position in aggregate (b) and (c) façades of buildings along Urriola street.

The 77% of the buildings presented non-structural elements in good conditions, classified as A on the form (Section 6, Figure 4-10b). This group correspond to buildings without projected elements, or with small or light elements well connected to the main structure, i.e. with minor falling risks. The remaining 22% are classified as B and C, such as small/light elements badly connected to the main structure or large/heavy elements, which means high risk in case of falling such as projecting balconies, windows, stairs, galleries or large chimneys, ornaments, signboards, etc. Historical buildings on the downtown area exposed to major risk of falling due to their large and numerous projecting elements such as ornaments, windows and balconies. It should be noticed the pragmatic character of timber and masonry buildings constructions without critical presence of hazardous projected elements.

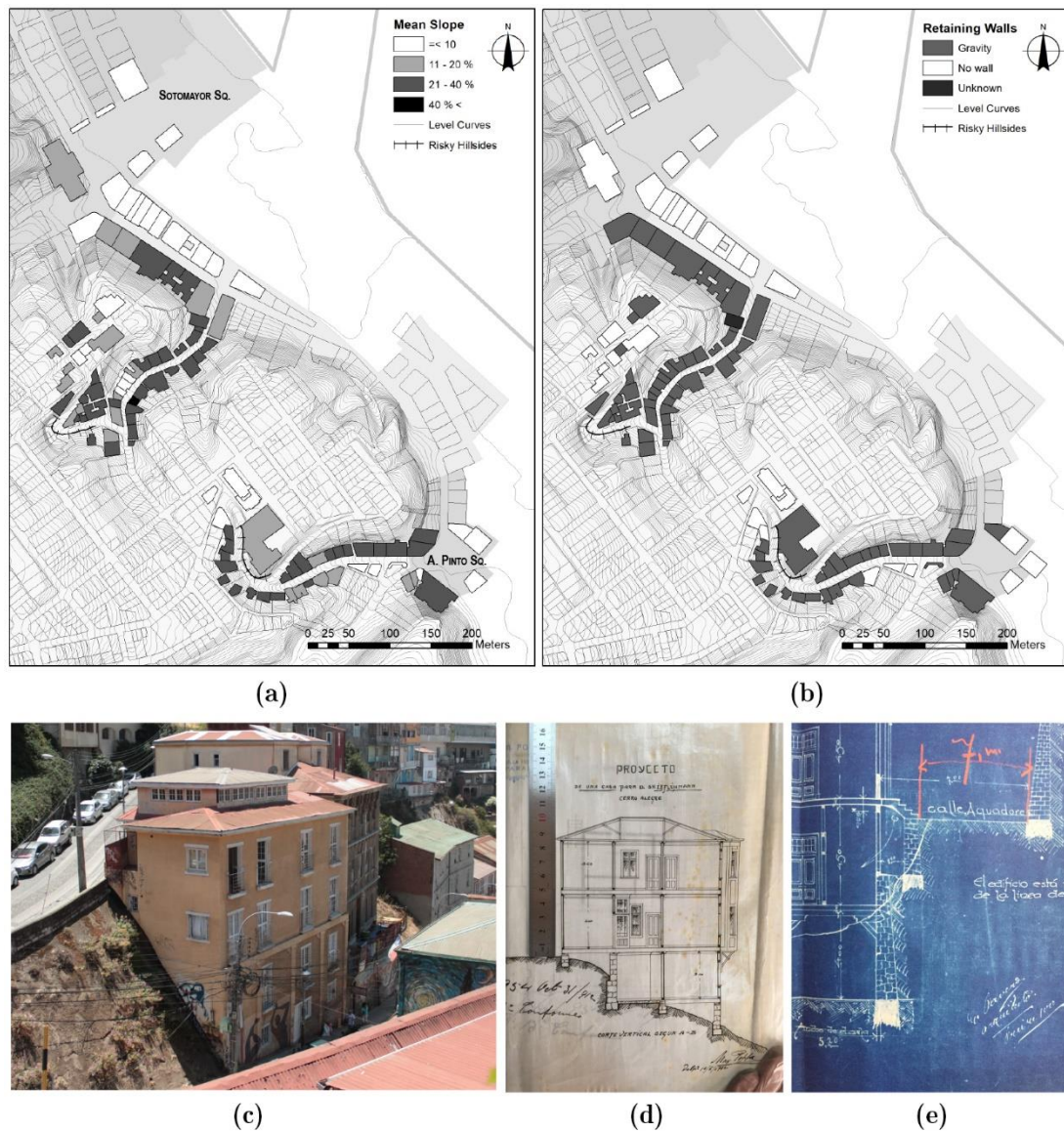


Figure 4-27. Slope and retaining walls configuration: a) GIS mapping of mean slope and (b) retaining wall typologies, (c) representative case in Almirante Montt street, (d-e) typical retaining walls and foundations.

The Section 7 of the proposed survey forms reported the damage condition of the buildings through the assessment of their principal structural and non-structural members. The damage grade assessment was one of the most difficult on-site activities due to the hidden condition of the structural elements. Several buildings allowed only limited inspection, especially for the interior structures, e.g. load-bearing systems, stories, and roofs. RC buildings presented the best condition of conservation, whereas iron-RC buildings exhibited damage in the external ornaments of the façade. Timber frame structures presented termites' attacks, especially in structural members made of pine. Moisture conditions showed to contribute to the decay of timber elements, especially in members in direct interaction with foundations or hillsides. Figure 4-28 shows some recurrent typologies of damage in the different surveyed typologies. In general, the current condition of conservation of the buildings is rather good. The 77% of the buildings is categorized

as class A in the survey form (Section 7 of Figure 4-10c and Figure 4-29), i.e. with null to slight damage level and/or buildings without later additions, as well as those with small enlargements well connected to the main structure. The good state of conservation of the buildings can be attributed to the heritage and protected character of the study area. The World Heritage Site title granted by UNESCO to the historical centre of Valparaíso forced buildings to fulfil intervention guides to maintain the original appearance into the protected zones. In addition, the touristic and economic activity of Cerro Alegre and Concepción neighbourhoods promoted the restoration of their historical buildings. However, in many cases, these improvements consisted only in external maintenance on the façade without significant structural interventions. These cases could not be considered as retrofitted buildings, and in-depth examinations are necessary to detect possible vulnerabilities at the main structural load bearing system. In addition, some structures presented inappropriate modifications, such as later executions of openings in the façade or alteration of load bearing elements (i.e. columns, shear walls, etc.), that were categorized as B and C, respectively. Non-regulated and/or bad executed interventions such as weighty story additions, open stories or projecting enlargements were carefully detected since they can negatively affect the global behaviour of the buildings.

The global analysis of the surveyed data in statistical terms provided an overview of the intrinsic vulnerability of the buildings to suffer damage in case of future seismic events. The evaluation of the relevant survey parameters brought to the identification of the structural arrangements, irregularities, environmental conditions, damage level and state of conservation of the main load bearing systems. The developed survey activity was very helpful to gain a preliminary understanding of the structural characteristics of the surveyed building stock. The use of GIS tools facilitated the analysis of the results and the detection of critical cases that need to be carefully inspected in further seismic vulnerability assessments. This research contributed to the creation of an extensive building database to support future seismic vulnerability analyses in Valparaíso.



Figure 4-28. Representative non-structural elements and damage conditions: (a) large dimension bow-window, (b) poorly connected balcony, (c) severe damage of RC cornice, (d) sheathing detachment, (e) empty timber frame wall and (f) timber joists attacked by termites.

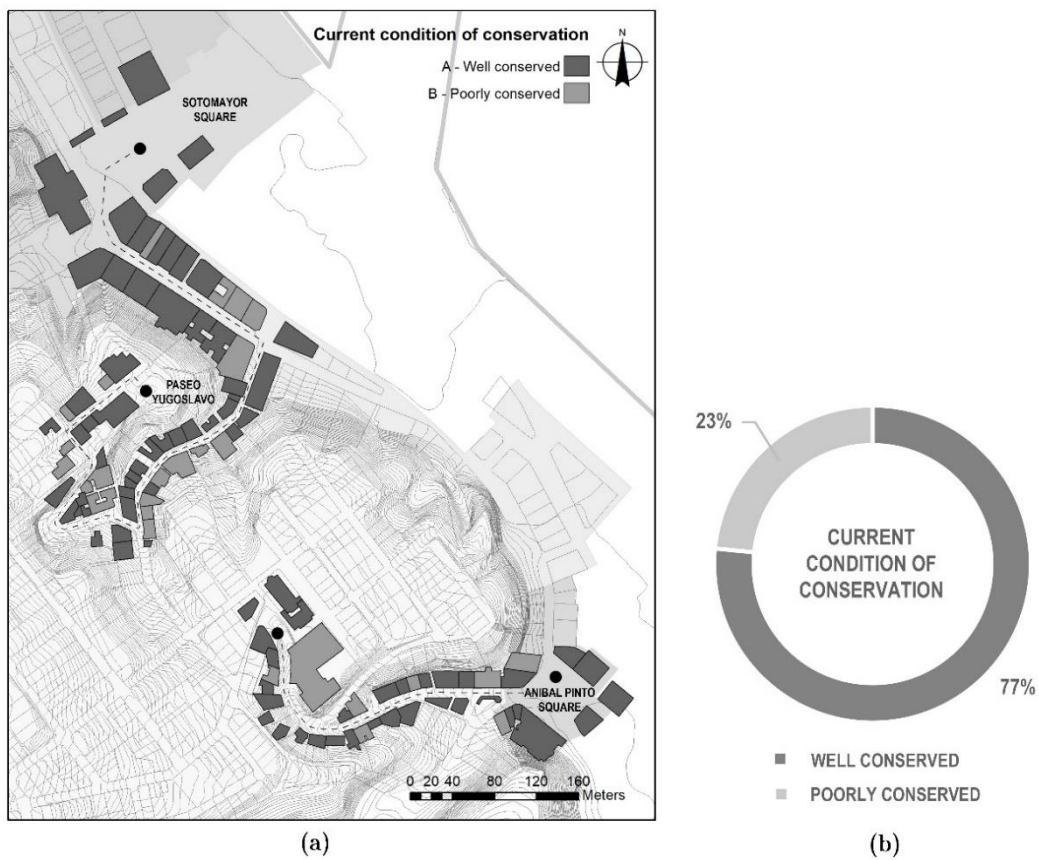


Figure 4-29. GIS mapping of current condition of conservation (a) and statistical results (b).

4.5 Summary

This chapter has presented a survey building methodology for data-collection procedures to feed large-scale seismic vulnerability assessment. The available strategies usually consider survey forms to gather information about the urban buildings. However, the application of these available survey forms poses important challenges for the case of the heterogeneous urban centres including different structural typologies. This work has proposed four specific survey forms for traditional structural typologies constructed with masonry, reinforced concrete, mixed steel-reinforced concrete, and timber. Such forms request essential information on the parameters necessary for seismic vulnerability assessment, by evaluating the lateral-load resisting system, regularity, condition of conservation, and existing damages. The evaluation parameters were defined based on the available strategies in literature and technical guidelines, as suggested by Eurocode 5 (EN 1998-1 2004, CEN EC5 1.2 2004), the Italian standards of Construction (NTC 2008), the guidelines by the Italian National Group for Earthquakes Protection GNDT (2007), the SYNER-G project (Pitilakis et al. 2014), and the New Zealand technical guidelines for the Seismic Assessment of Existing Buildings (NZSEE 2016). Additionally, a survey implementation plan was suggested including pre-field, on-field and post-field activities.

The survey forms were applied to the study of 111 buildings of the historical centre of Valparaíso, Chile. Typological full inspections were developed for a number of representative cases of each existent structural typology within the building stock. This information was useful to fill the surveys of buildings with lacking information but equivalent typology. The collected data allowed the definition of building taxonomies taking the structural configuration and current state of damage and conservation of the buildings into account, and the development of statistical analysis. The proposed methodology was complemented with the use of Geographic Information Systems to obtain a complete database with the structural characterization of the most representative typologies for future works of large-scale seismic vulnerability assessment.

Chapter 5. Calibration of simplified numerical models for timber frames and masonry walls

5.1 Introduction

Available modelling strategies usually deal with timber or masonry structures separately, as for the case of homogeneous building typologies. Few researchers could address the modelling of hybrid timber-masonry structures in the available literature (Ciocci, Sharma, and Lourenço 2018; Kouris and Kappos 2014). The lack of experimental data about this hybrid typology constitutes a major drawback in the calibration process of numerical models for the structural analysis of existing buildings, where timber frames are often constructed in combination with load-bearing masonry walls. Given this situation, the calibration of simplified numerical models for the analysis of hybrid timber-masonry buildings is addressed in this thesis. The study covers firstly the definition of proper methods for timber frames, and secondly the evaluation of reliable tools for masonry walls. Both stages of the calibration are based on a conventional approach in the scientific method, i.e. the comparison between the results derived from experiments available in the literature and the outcomes from the numerical simulations of the tests.

Three benchmark experimental programs on timber frame walls were selected to be simulated. The first one was carried out on the Pombalino typology existing in Portugal (Poletti 2013), and the other two on the *quincha* typology from Peru (Moore and D'Ayala (2011) and Torrealva, Vicente, and Michiels (2018)). Two experimental programs on masonry structures were considered for simulation, including both the in-plane and out-of-plane behaviour. The first one was carried out by Augenti et al. (2011), and the second one by Griffith and Vaculik (2007).

Timber and masonry structures were analysed by means of Lumped Plasticity Models (LPM) in beam Finite Element (FE) for timber frames, and continuum FE models for masonry structures. Nonlinear static analyses (NSA) were applied under displacement control to determine the capacity and global failures of the models built within the structural earthquake engineering software SAP2000 (CSI 2016b). The results were compared with the experiments in terms of load-deformation capacity curve and global failure modes.

The outline of the chapter is divided into four parts. Section 5.2 presents the benchmark experimental programs on the Portuguese “Pombalino” (Section 5.2) and the Peruvian “quincha” (Section 5.2.2) timber frames. Section 5.3 defines the calibration of the lumped plasticity models for timber frames, including the definition of the lumped plasticity FE model (Section 5.3) for the

numerical simulation of bare (Section 5.3.2) and infilled frames (Section 5.3.3). Section 5.4 presents the benchmark experimental programs selected for the calibration of masonry models, including in-plane and out-of-plane loaded masonry walls (Sections 5.4 and 5.4.2 respectively). The calibration of the continuum FE models for masonry is detailed in Section 5.5, including the definition of the constitutive model (Section 5.5) and the numerical simulation of the in-plane and out-of-plane loaded masonry frames (Sections 5.5.2 and 5.5.3 respectively).

5.2 Benchmark experimental programs for calibration of timber frames

5.2.1 Experimental tests on Portuguese “Pombalino” timber frames

An experimental campaign on the Pombalino timber frame typology, carried out by Poletti (2013) was selected as a suitable benchmark case to validate the numerical modelling strategy adopted for this research. Two experiments of this campaign were selected to be simulated, i.e. a bare frame and an infilled frame tested under lateral horizontal actions. The specimens were subjected to the same experimental conditions in order to study the influence of the infill on the lateral response.

The panel was constituted by a main frame of beams and posts braced with St. Andrew’s crosses, as shown in Figure 5-1a. The top and bottom beams had a $0.16 \times 0.12 \text{ m}^2$ cross-section, while the remaining elements had $0.08 \times 0.12 \text{ m}^2$. The connections between beams and posts, as well as those among intersecting diagonals, were made of half-lap carpentry joints, while the connections between the main frame and the diagonals were made by contact (Figure 5-1b). All the connections were fastened with a nail, as shown in Figure 5-1b. The infilled specimen presented the same configuration of the bare frame, as shown in Figure 5-1c.

The structural members of the frame were made of a Portuguese timber named *Pinus Pinaster*, while the masonry was composed of commercial bricks and lime mortar joints. The mechanical properties of the materials, summarized in Table 5-1 and Table 5-2, were experimentally evaluated in the same campaign (Poletti 2013). The timber walls were subjected to a vertical pre-compression of 25 kN applied downward at each post, and a horizontal displacement of 0.14 m applied at the top beam through a hydraulic servo-actuator. Quasi-static in-plane cyclic tests were performed until the maximum displacement capacity of the frames was reached.

Table 5-1. Mechanical properties of the Pombalino timber specimen: *Pinus pinaster* (Poletti 2013).

Young’s modulus E	1.1×10^7	kN/m ²
Density ρ	590	kg/m ³
Poisson’s ratio ν	0.3	-

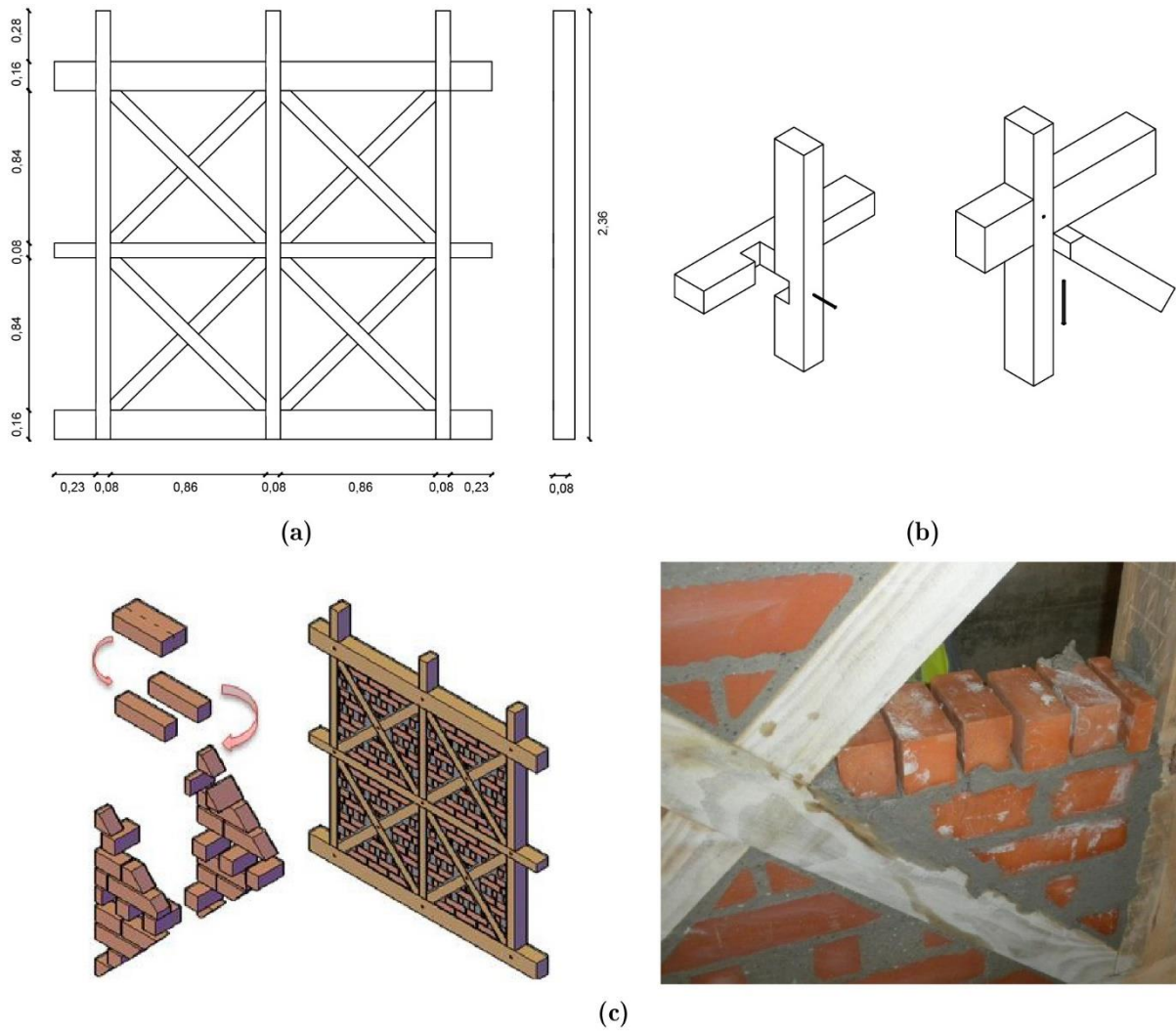


Figure 5-1. Pombalino wall specimens: (a) Bare frame (in m), (b) half-lap and connection by contact and (c) infilled frame (Poletti 2013).

Table 5-2. Mechanical properties of infill masonry in Pombalino frames (Poletti 2013)

Compression tests	Compressive strength σ_{\max}	7.53×10^3	kN/m ²
	Young's modulus E	6.744×10^6	kN/m ²
Shear tests	Shear strength τ_{\max}	200	kN/m ²
	Shear modulus G	1.064×10^6	kN/m ²

According to the observations documented by Poletti (2013), the bare frame specimen failed as soon as the central connection reached its maximum capacity. Since infill was not present in this test, the diagonals induced the failure of the central beam. After this drop of resistance, there was a gradual recovery of the load bearing capacity, as can be noted in in Figure 5-3. The wall reached a maximum capacity of 55.73 kN at 0.027 m displacement, and the global stiffness was 2.6×10^3 kN/m.

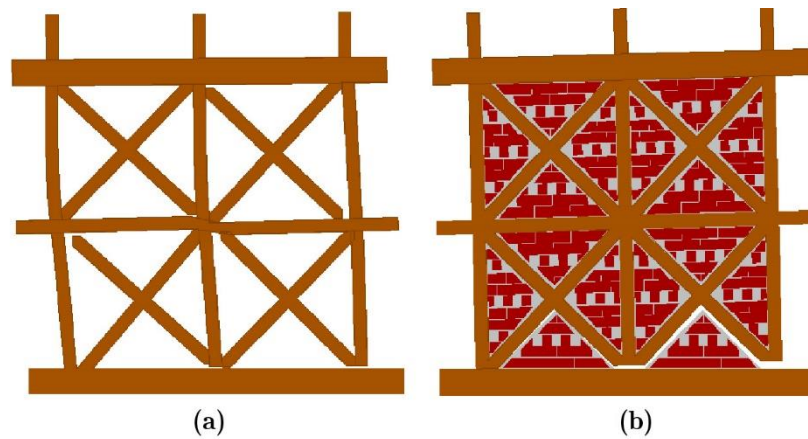


Figure 5-2. Deformation of the Pombalino specimens: (a) bare frame and (b) infilled frame (Poletti 2013).

The infilled specimen displayed a predominantly rocking behaviour with significant uplift of the posts. During the test, the diagonals transmitted important shear actions to the nailed half-lap connections (Poletti 2013). Once the diagonal connections reached excessive traction at the bottom of the frame, the specimen showed a slight decrease in terms of strength. At the end of the test, the nails placed at the bottom connections were severely deformed because of the pulling effect of the posts. According to Magenes and Calvi (1997) and Poletti (2013), this is a typical response of the rocking mechanisms for which high displacement can be reached with little reduction of strength. The infilled specimen experienced slightly higher strength and global stiffness than the bare frame, as shown in Figure 5-3. The frame reached a maximum capacity of 63.29 kN at 0.061 m displacement registering a global stiffness of 3.03×10^3 kN/m. Figure 5-2b shows the deformed shape of the frame.

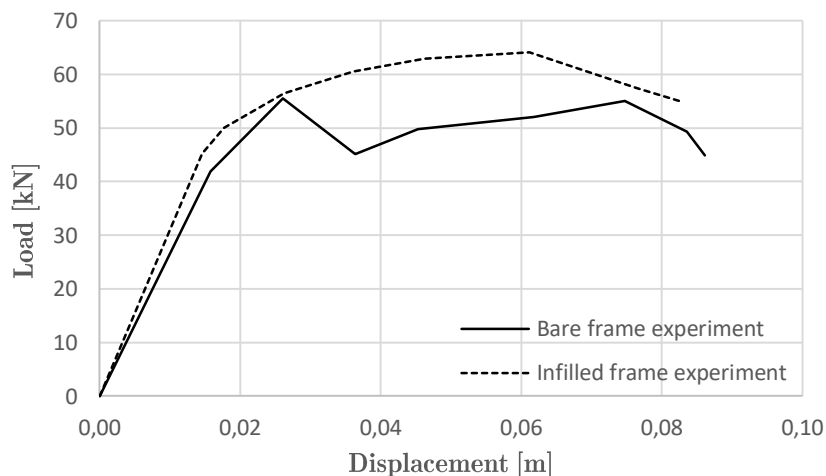


Figure 5-3. Experimental capacity curves of the bare frame and infilled Pombalino walls (Poletti 2013).

A representative sample of bottom half-lap connection of the frame was tested considering the same boundary and loading conditions of the campaign (Figure 5-4a). According to Poletti (2013), the connection experienced uplifting and rotation of the post that provoked a concentration of compressive stresses at the side opposite to the application of the lateral load.

This behaviour was very similar to the one observed in the timber wall at the compressed posts. The obtained load-displacement curve (Figure 5-4b) showed an initial linear response, followed by a nonlinear behaviour emerging close to the maximum capacity at 5.5 kN, and a sudden drop of resistance.

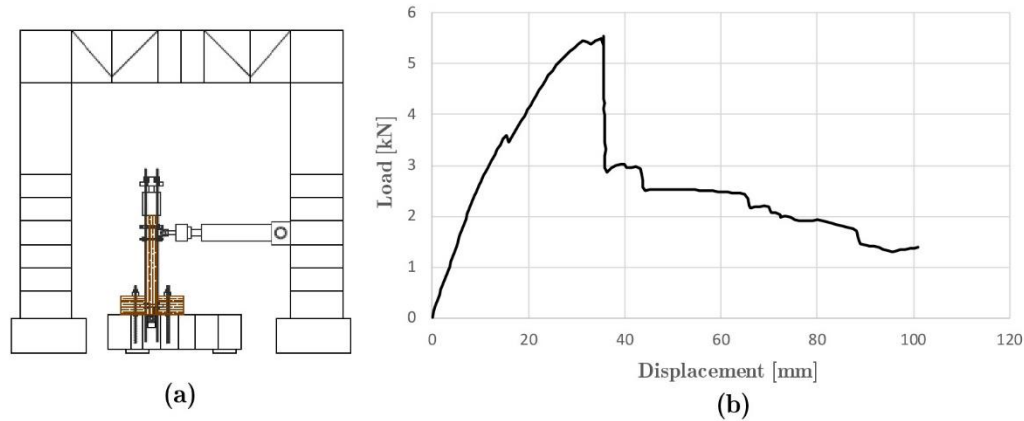


Figure 5-4. Experimental test on the half-lap connection of the Pombalino: (a) in-plane setup and (b) capacity curve (Poletti 2013).

5.2.2 Experimental tests on Peruvian “quincha” timber frames

The experimental campaign on Peruvian *quincha* typologies carried out by Moore and D’Ayala (2011) were also considered for further calibration of the numerical models for timber frames. A bare frame and an infilled frame, built in half-scale dimensions, were subjected to lateral loads. The geometry of the frames was based on surveys of traditional existing buildings in Peru, as reported in the studies of Quinn (2015, 2017).

The bare frame was made of four posts confined between two plates and braced with a tension diagonal, as shown in Figure 5-5. Posts and plates had $0.06 \times 0.08 \text{ m}^2$ cross-section, while the diagonal had $0.09 \times 0.03 \text{ m}^2$. Mortise-and-tenon traditional joints were used to connect the posts and plates, while the diagonal was fastened to the frame using nails, as shown in Figure 5-5. With respect to the materials, two different timber specimens were used to make the frame, i.e. *Sapelli* for the diagonal, and *Cypress* for the remaining elements. Table 5-3 summarizes the mechanical properties of the timber. The infilled specimen presented the same geometry of the bare frame. It was made of cane weaves covered with mud made of crushed cob blocks. The ratio among water and material components for mud was set according to the Peruvian standards (SENCICO 2017).

Table 5-3. Mechanical properties the half-scale *quincha* specimens: *Sapelli* and *Cypress* (Quinn 2015).

	Sapelli	Cypress	
Young’s modulus E	7.7×10^6	6.4×10^6	[kN/m ²]
Density ρ	400	390	[kg/m ³]
Poisson’s ratio ν	0.3	0.3	-

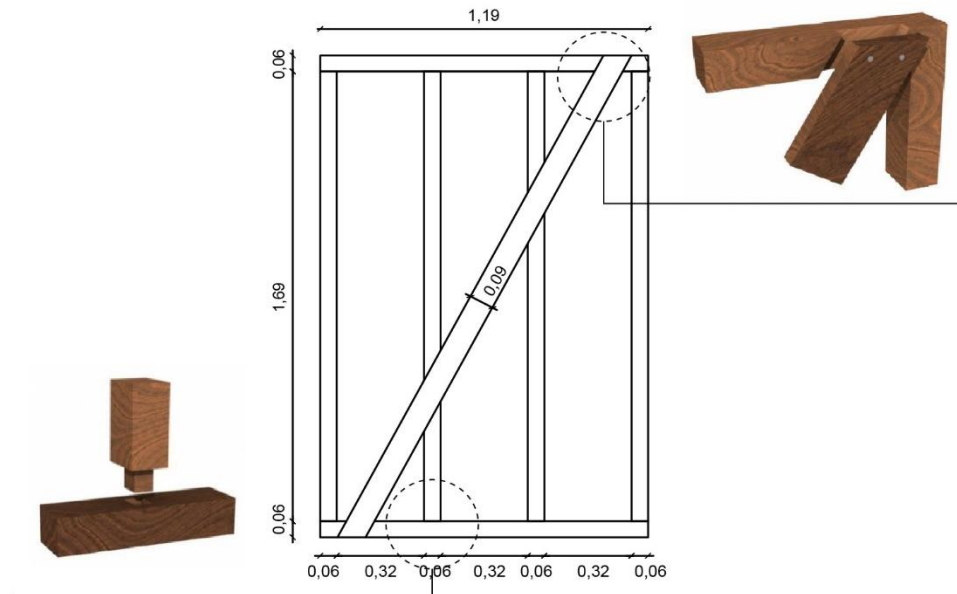


Figure 5-5. Half-scale quincha frame specimen: geometry and connections (in m).

The bases of the *quincha* specimens were fixed to the floor of the laboratory to prevent sliding effects during the experiments. Additionally, steel reinforcing bars were vertically disposed at each side of the frames to prevent out-of-plane movement. Both specimens were subjected to a vertical pre-compression of 4.4 kN/m applied at the top plate, and a horizontal displacement of 0.1 m was applied at the left corner of the top beam.

As reported by Quinn (2017), the bare frame deformation showed that the post closest to the applied load was deforming in a cantilevering shape, suffering relative rotation in the connections. The external post in the opposite side deformed in an S-shape, as can be noted in Figure 5-6a. The internal post-plate connections rotated more than the outer ones, due to the influence of the diagonal. The diagonal experienced also bending during the test, beside traction, due to the effect of the intermediate nailed connections. The ultimate failure of the frame occurred when the diagonal failed at an intermediate connection due to combined tension and bending (see Figure 5-6b). Before this failure, partial ones occurred at the top and bottom diagonal-plate connections. The load-displacement behaviour of the bare frame specimen, displayed in Figure 5-7, shows an initial linear branch up to a load of 1.6 kN, corresponding to the achievement of the maximum capacity of the diagonal. After this phase, the stiffness of the frame starts reducing gradually. The global stiffness of the wall was 180 kN/m.

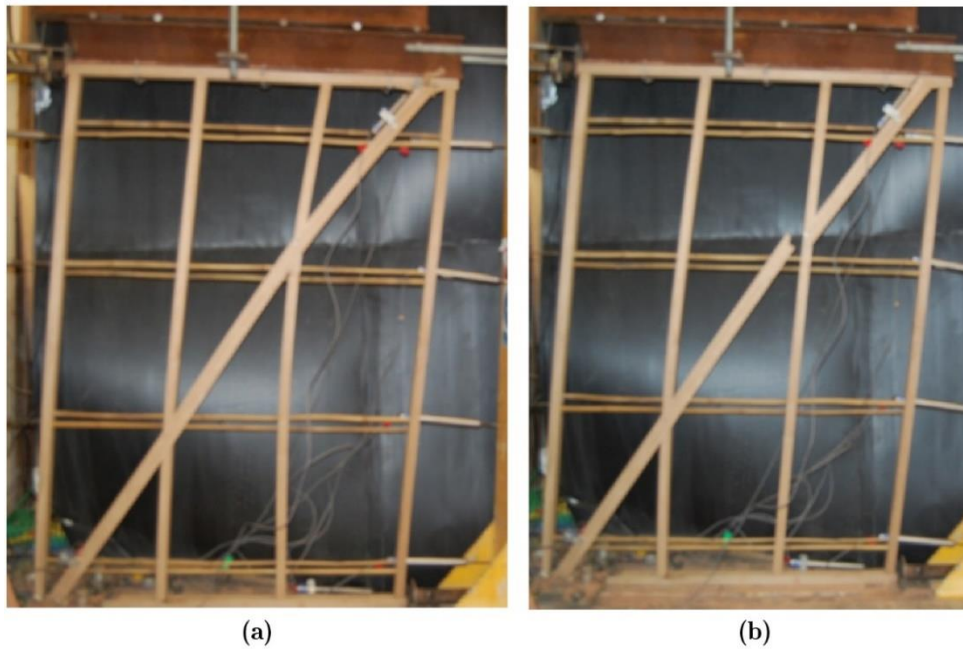


Figure 5-6. Deformation of the bare half-scale *quincha* specimen: (a) deflecting shape before and (b) after failure (Quinn 2015).

The infilled specimen started cracking at 0.017 m displacement and the first visible crack appeared in the bottom plate at 0.03 m displacement. After this phase, the wall experienced some out-of-plane movements, and a visible outward bowing of the right external post at 0.07 m displacement. Subsequently, the top plate-diagonal connection reached its ultimate capacity at a displacement of 0.08 m. At this stage, the diagonal moved 0.018 m downwards, as shown in Figure 5-8a, and the top plate bent due to this offset (Figure 5-8b). Figure 5-8c shows the deformed shape of the frame at a displacement of 0.085 m, just before the wall failed. Figure 5-7 displays the obtained load-displacement capacity curve. The wall reached a maximum capacity of 3.73 kN, and the global stiffness was 378 kN/m (Quinn 2015).

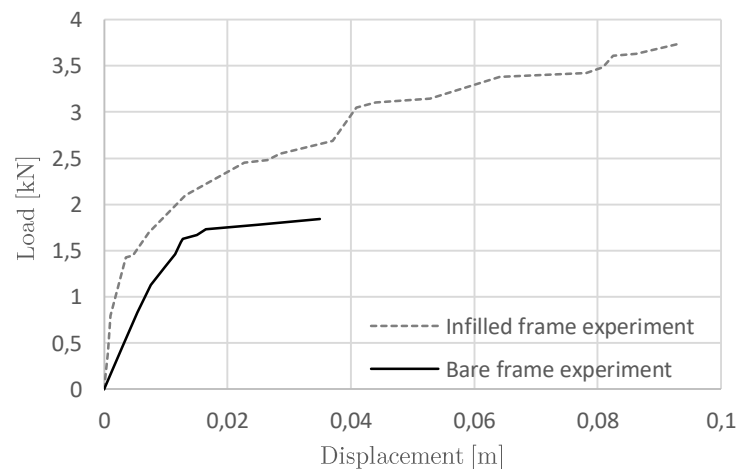


Figure 5-7 Experimental capacity curves of the bare and infilled half-scale *quincha* specimens.

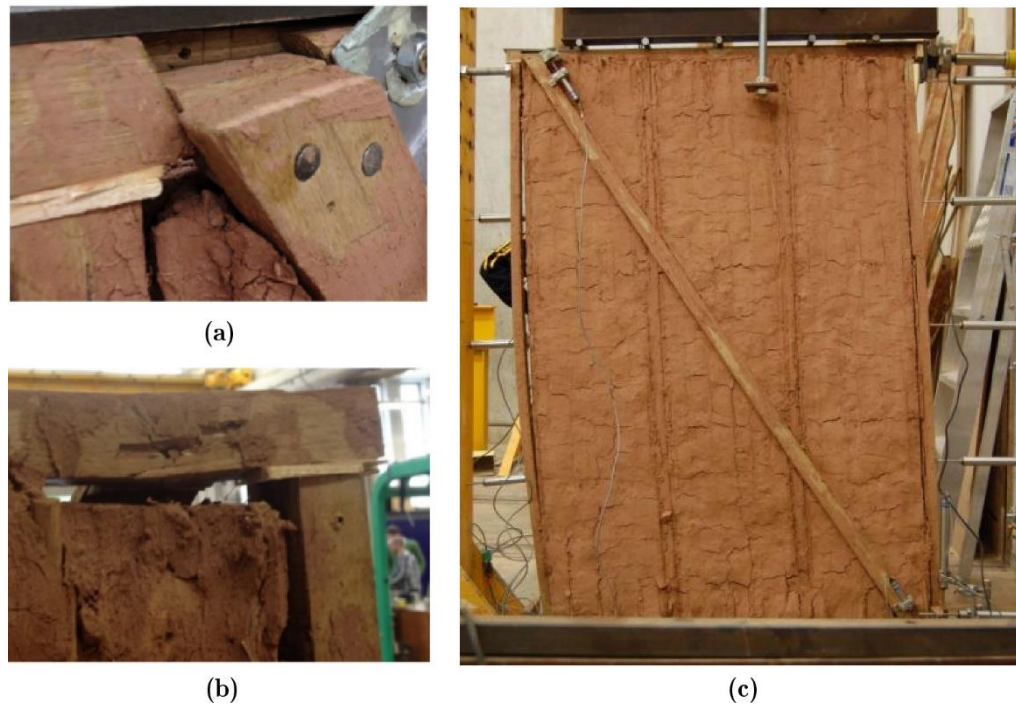


Figure 5-8. Deformation of the infilled half-scale *quincha* specimen: (a) movement of the diagonal, (b) bending of the top plate of the frame, and (c) deformation before failure (Quinn 2015).

Two isolated in-plane tests were performed on mortise-and-tenon connections in the same experimental campaign. The specimens had the same configuration as those of the frame test, as shown in Figure 5-9a. One specimen presented a very tight fit between the mortise and the tenon, and the other a loose fit between such parts. The posts presented the same cross-section as the wall, while the tenons had a 0.025 m^2 cross-section and 0.05 m height. During the tests, the posts were pushed horizontally inducing moment until failure (Quinn 2015). The obtained moment-rotation curves (Figure 5-9b) showed that the tight fit joint is stronger than the loose fit joint, reaching a maximum moment of 0.37 kNm , and a rotational stiffness of 8.1 kNm/rad , against 0.25 kNm and 2.6 kNm/rad respectively.

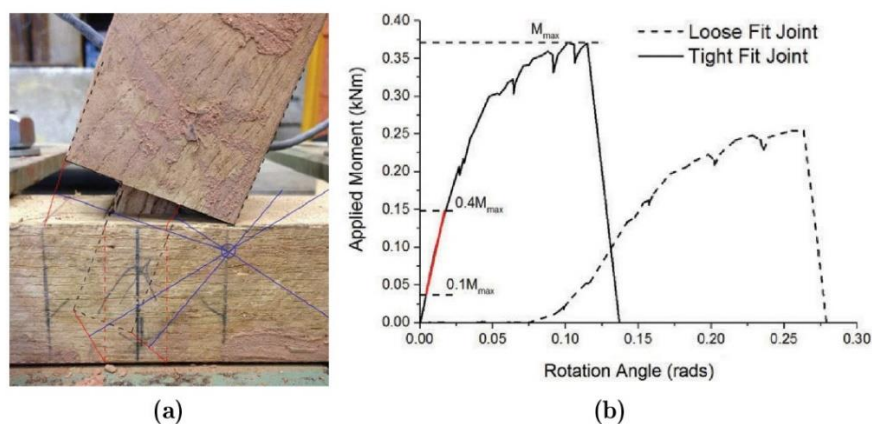


Figure 5-9. Experimental test on the mortise-and-tenon connection: (a) geometry and (b) obtained moment-rotation relationships (Quinn 2015).

The last experimental campaign used for calibration of the numerical models was that executed on a full-scale Peruvian *quincha* frame by Torrealva, Vicente, and Michiels (2018). The frame subjected to lateral loads was built in full-scale. The frame was configured by five posts spaced at 0.6 m to each other and confined between top and bottom plates. A diagonal in tension braced the panel, as shown in Figure 5-10a. Posts and plates had 0.08×0.06 m² cross-sections, while the diagonal had a 0.03×0.09 m² one. Mortise-and-tenon joints were employed to connect posts and beams, as shown in Figure 5-10b. The diagonal was fastened to the plates with four nails, and to the posts with three nails. The frame panel was filled with *quincha*, consisting of a woven cane network and mud mortar, coated with layers of mud plaster and finished with a fine gypsum layer. A timber specimen named *Moena Alcanfor* was used to make all the timber elements. The experimental tests and the obtained mechanical characterization of the materials are detailed in the work of Torrealva, Vicente, and Michiels (2018).

In order to prevent sliding movement during the experiment, the base of the panel was fixed by anchoring the bottom plate element to a RC beam, which in turn was anchored to a strong floor. A pre-compression load of 16 kN was applied at the top plate of the frame. Lateral cyclic loads were applied through a servo-hydraulic actuator with a maximum displacement capacity of 0.15 m at the left side of the top beam (Torrealva, Vicente, and Michiels 2018).

As stated by Torrealva, Vicente, and Michiels (2018), the wall started to crack after a displacement of 25 mm, with the damage progressively increasing up to the end of the test. Subsequently, the nails connecting the diagonal to the posts started to bend, and a crack appeared on the diagonal element. The tenons of the base lifted 10 mm from the mortises, and the diagonal cracked at the locations of the nails. This mechanism drove the intermediate connection to bend. After that, the plaster started to detach from the posts and the diagonal separated at both ends when the wall reached 140 mm of displacement. At this moment, the intermediate connection bent further, and the tenons of the base lifted 2.5 cm from the mortises. Despite the above deformations, the lateral load capacity remained stable and the wall did not suffer any additional structural damage. Torrealva, Vicente, and Michiels (2018) attributed this response to the flexibility of the *quincha* system given by the mortise-and-tenon connections, which worked as pins, allowing large deformations without causing failure. The panel reached a global stiffness of 800 kN/m and a maximum capacity of 13.06 kN, just before the diagonal-plate connection failed, reducing the stiffness of the frame progressively.

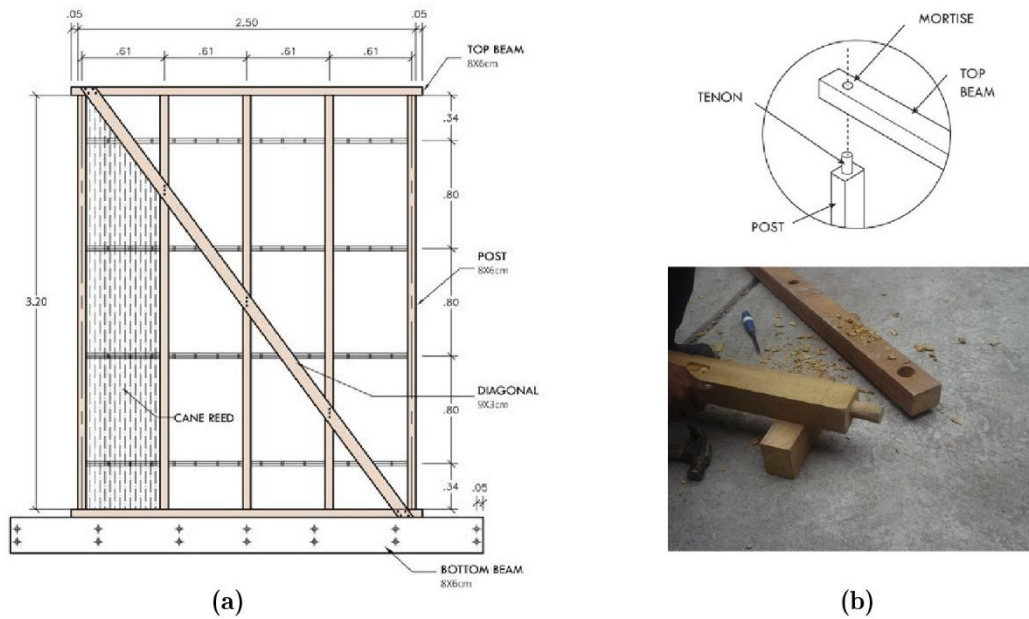


Figure 5-10. Full-scale *quincha* wall specimen: (a) geometry and (b) mortise-and-tenon connection (Torrealva, Vicente, and Michiels 2018)

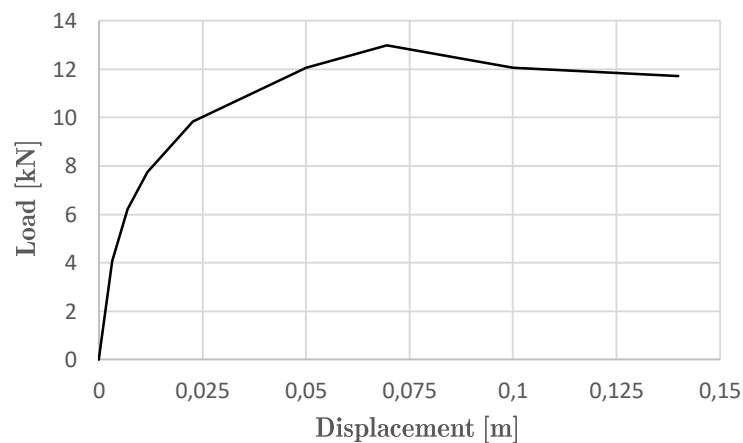


Figure 5-11. Experimental capacity curve of the full-scale *quincha* specimen.

5.3 Calibration of lumped plasticity models for timber frames

5.3.1 Lumped plasticity finite element model for timber frames

Different numerical modelling strategies can be adopted to represent the nonlinear behaviour of timber frame structures. The selection of a proper approach depends on several factors, including the expected accuracy of the results and the efficiency of the model, as well as the scale of the analysis, the available data, and the computational resources. Figure 5-12 shows the existing type of models usually adopted to represent the structural behaviour of frame elements (Astroza, Ebrahimian, and Conte 2015). On one hand, the distributed plasticity models (DPM), both in their *fibre-based* and *continuum* formats, require high computation costs and

constitute detailed strategies to represent the nonlinear behaviour of beam-like elements. On the other hand, lumped plasticity models (LPM) constitute simplified strategies based on linear elastic *frame* elements representing the timber members, while nonlinear *springs* and *hinges* introduce the nonlinearities at the nodes of the frames. The advantages of LPM lie in the simplicity of the parameters' definition, and in the lower computational costs than in DPM.

LPM is a suitable approach to simulate timber frame structures, after assuming that plasticisation of the structure commonly occurs in the connections at the frame members' ends, as shown in Figure 5-13. In these cases, the cross-section nonlinear behaviour at the connections has to be determined by experimental or analytical approaches. The definition of proper nonlinear moment-rotation or force-displacement relationships governing the behaviour of the rotational hinges or axial springs, as appropriate, is a crucial step to ensure reliable simulations of the local and global mechanisms expected in the model. The timber member is modelled using frame elements with linear elastic material properties where only elastic deformation is expected.

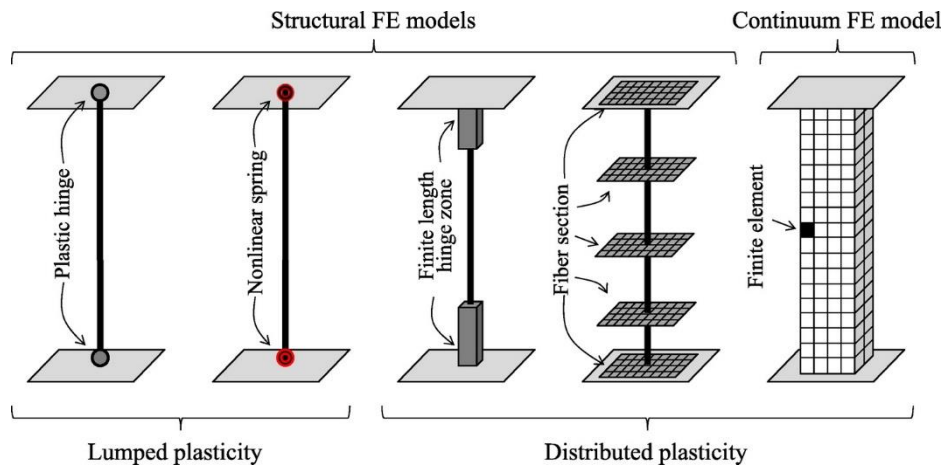


Figure 5-12. Types of nonlinear models for frame elements (Astroza, Ebrahimian, and Conte 2015)

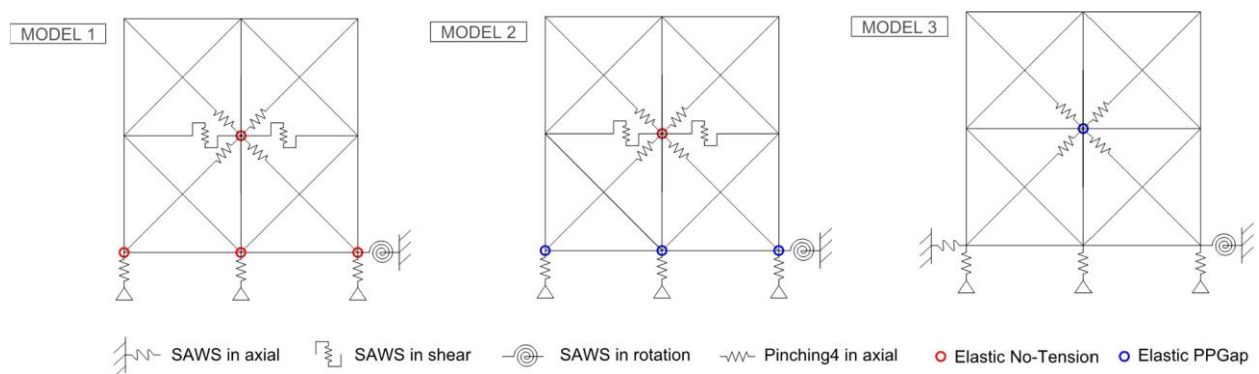


Figure 5-13. Lumped Plasticity Models of a Pombalino wall varying locations of nonlinearities (Lukic et al. 2018)

Considering the objectives of this research, a simplified lumped plasticity FE model was adopted to simulate the nonlinear behaviour of the timber frame structures. This solution enabled appropriate simulations with the minimum amount of time and computational resources, allowing

the assessment of entire buildings. Both linear elastic frame elements and nonlinear hinges are available in SAP2000 environment for the development of LPM. The definition of the models, including the nonlinear constitutive laws governing the behaviour of the connections, is determined for each particular benchmark experiment in the following sections.

5.3.2 Numerical simulation of experiments on bare timber frames

The LPM was adopted to simulate the experimental nonlinear response of the timber frames described in Section 5.2. The nonlinear load-deformation response of LPM models were calibrated according to the experimental evidence. Analytical calculations were executed in order to define the behaviour of the carpentry joint connections. The models were developed within the structural and earthquake engineering software SAP2000 (v20).

Firstly, the bare frame specimen of the Pombalino typology was modelled considering the same conditions of the experiment as for the geometry, the material properties, the loads, and the boundary conditions. The top and bottom plates of the frame had a $0.16 \times 0.12 \text{ m}^2$ cross-section, while the remaining elements had a $0.08 \times 0.12 \text{ m}^2$ cross-section, as shown in Figure 5-14a. The timber was modelled as a linear elastic isotropic homogeneous material, considering the mechanical properties listed in Table 5-4. A vertical load of 25 kN was applied at each post, and a lateral displacement of 0.1 m was applied at the top-left corner. The frame was pinned-supported at the base and restrained in the horizontal direction at the top-left node to allow the displacement application, in agreement with the experimental boundary conditions.

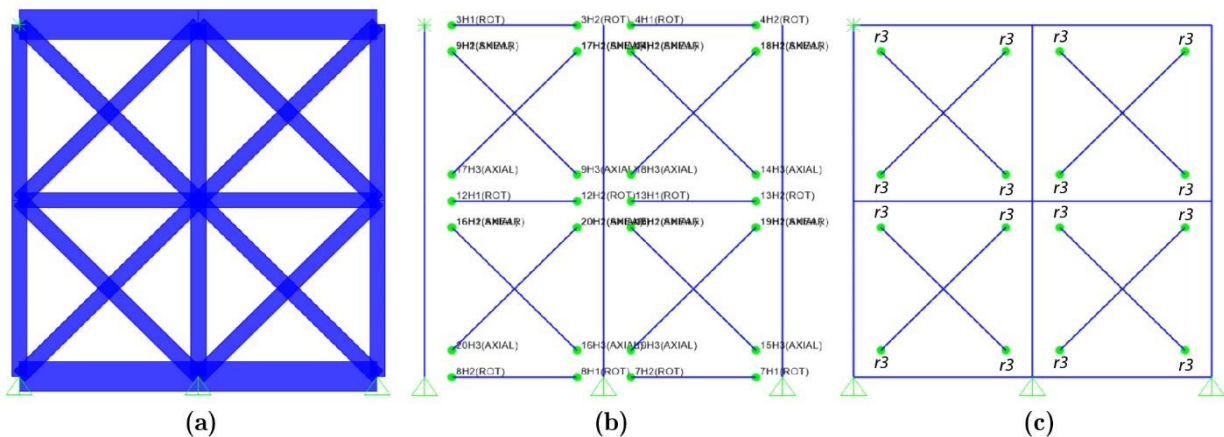


Figure 5-14. LPM of the Pombalino frame: (a) sections, (b) hinge/spring nonlinear elements and (c) moment releases.

Table 5-4. Mechanical properties of the Pombalino timber material: *Pinus pinaster*.

Young's modulus E	1×10^7	kN/m ²
Density ρ	0.3	-
Poisson's ratio ν	590	kg/m ³

The test on the half-lap connection specimen allowed determining the nonlinear behaviour of the carpentry joint that influences the whole frame response. As the connection experienced evident rotation during the test, a moment-rotation relationship was derived from the load-displacement experimental results, as depicted in Figure 5-15. According to Poletti, Lourenco, and Ciocci (2016), this curve can be idealized by considering a first linear branch up to the maximum capacity, followed by a plateau and a softening behaviour. The maximum moment of the connection was 4.4 kNm, reached at a rotation of 0.025 rad, while the initial and final rotational stiffness were estimated as 171 kNm/rad and 47 kNm/rad respectively. Nonlinear rotational hinges acting in the rotational deformational degree of freedom (DOF) were introduced into the model in the locations of the half-lap connections, as shown in Figure 5-14b.

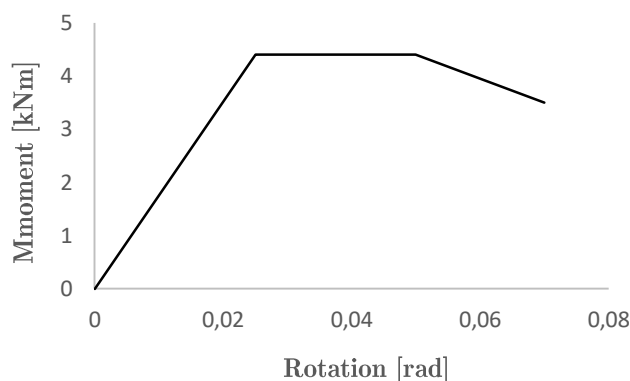


Figure 5-15. Moment-rotation relationship of half-lap connections of the Pombalino model.

Analytical studies were performed to calibrate the nonlinear behaviour of the connection by contact, due to the lack of specific experimental data. In this process, sensitivity analyses attempted to determine the stiffness and capacity of the connection within the whole frame model. In the first stage of the calibration, linear-elastic force-deformation relationships were assumed for all the connections of the frame. The rotational stiffness of the half-lap one was fixed, assuming the initial and final experimental stiffness values previously reported. Three different assumptions attempted to determine the best fit of the axial and shear stiffness of the connection by contact. The rotational DOF was assumed null to model this connection, as evidenced by the experiment. The axial and shear stiffnesses were decreased progressively until a good agreement was obtained between the global stiffness of the model and the experimental one, calculated as 2.60×10^3 kN/m. Linear spring elements were used to introduce the stiffness at the nodes where the connections are.

Table 5-5 summarizes the results of three linear model assumptions in agreement with the experimental result. The first model (M1) considered an axial stiffness equal to 5.20×10^3 kN/m, both in tension (k+) and compression (k-), and an infinite shear stiffness. According to Ciocci (2015), the axial stiffness in tension (k+) does not influence the global behaviour of the wall significantly, therefore the models M2 and M3 considered it to be equal to zero. The model M2 assumed an axial stiffness of 1.105×10^4 kN/m and a shear stiffness equal to zero. The last model

M3 examined the shear stiffness considering the same values of model M2 for both deformational degrees of freedom (DOFs). It is noticeable that shear stiffness does not seem to affect the results in the linear elastic analysis.

Table 5-5. Results of sensitivity analysis to estimate the linear stiffness of the connection by contact of the Pombalino model both for axial and shear behaviour.

			M1	M2	M3
Connection by contact	axial	k+ [kN/m]	5.20 ×	0	0
		k - [kN/m]	5.20 ×	1.105 × 10 ⁴	1.105 × 10 ⁴
	shear	k+ = k- [kN/m]	∞	∞	1.105 × 10 ⁴
	rotation	[kNm/rad]	0	0	0
Half-lap connection	axial	k+ = k- [kN/m]	∞	∞	∞
	shear	k+ = k- [kN/m]	∞	∞	∞
	rotation	kin + = kin -[kNm/rad]	171	171	171
		kfin + = kfin -[kNm/rad]	47	47	47
Global stiffness [kN/m]			2.60 ×	2.60 × 10 ³	2.60 × 10 ³

Based on the work of Ciocci (2015), nonlinearities were introduced into the model by estimating the capacity of the connection by contact and its nonlinear force-deformation control scheme. Figure 5-16a-b show the nonlinear laws of the connection both in terms of axial and shear deformational DOFs, wherein a softening behaviour was considered after the peak load (F_y) up to the ultimate displacement (d_u). F_y is calculated considering the compressive strength of the wood in the direction perpendicular to the grain f_{c90} , as well as the contact areas of the connection by applying Equation (5-1). Since the compressive strength was not derived from the experimental tests, different values of F_y , both in axial and shear DOFs, were considered until a good agreement was obtained between the model and the experimental results.

$$F_y = f_{c90} \times A \quad (5-1)$$

Equation (5-2) was used to determine the yield displacement value (d_y), where F_y is the capacity of the connection and k the initial stiffness.

$$d_y = \frac{F_y}{k} \quad (5-2)$$

According to Ciocci (2015), the ultimate displacement of the connection can be assumed as the same one reached by the half-lap connection ($d_u = 0.05$ m) since after the central connection

failed, the remaining connections no longer worked. The ultimate capacity of the connection was assumed zero when the ultimate displacement was reached (d_u).

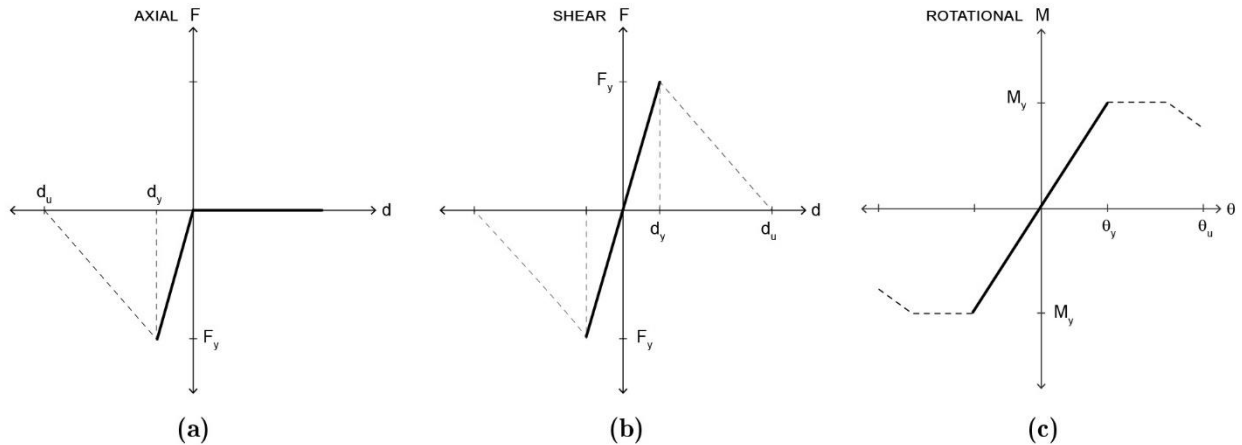


Figure 5-16. Nonlinear laws of the Pombalino model connections: (a) by contact axial behaviour, (b) by contact shear behaviour and (c) half-lap rotational behaviour.

Table 5-6 shows the assumptions having good agreement with the experimental results. For all of them, the initial stiffness was assumed to be equal to 9.050×10^3 kN/m, a value slightly lower than those obtained in the linear analysis. The capacity of the connection was set equal to 24 kN, both for the axial and shear deformational DOFs. The results were obtained applying NSA under displacement control. The numerical results were compared in terms of both global stiffness and capacity curves. As shown in Table 5-6, the Model C revealed the best fit with the experiment. In this assumption, F_y was estimated as 26 kN by considering a compressive strength f_{c90} of 4250 kN/m² for a contact area of 0.006 m². Due to the presence of empty spaces, only one of the two contact areas was considered for this calculation as recommended by Ciocci (2015).

Table 5-6. Parameter analysis on the connection by contact.

			Model A	Model B	Model C
Connection by contact	axial	F_y [kN]	24	25	26
		k_+ [Kn/m]	0	0	0
		k_- [Kn/m]	9050	9050	9050
	shear	F_y [kN]	24	25	26
		k_+ [Kn/m]	9050	9050	9050
		k_- [Kn/m]	9050	9050	9050
rotation	$k_+ = k_-$ [kNm/rad]	0	0	0	
Half-lap joint	axial	$k_+ = k_-$ [Kn/m]	∞	∞	∞
	shear	$k_+ = k_-$ [Kn/m]	∞	∞	∞
	rotation	k_{in} [kNm/rad]	171	171	171
		k_{fin} [kNm/rad]	47	47	47
Global Stiffness [kN/m]			2.604×10^3	2.595×10^3	2.603×10^3

Nonlinear axial and shear springs were used to introduce the nonlinearities into the model, as shown in Figure 5-14b. It is important to note that two different axial and shear springs were overlapped at the same node location to model the connection by contact. Moment releases were assigned at each diagonal node in order to avoid moment resistance (Figure 5-14c). The obtained load-displacement capacity curves of the three models are depicted in Figure 5-17.

The collapse mechanisms predicted by the model revealed a good agreement with the observed experimental response of the bare frame. Figure 5-17 highlights the instances A-E corresponding to the nonlinearities appeared during the simulations. Figure 5-18 and Figure 5-19 show the so-called “plastic state” of the hinges within the model, with dots of different colours according to the reached magnitude of plastic displacement/rotation. Nonlinearities started to appear at 0.017 m global displacement, when the axial springs of the compressed diagonals reached their maximum capacity. Subsequently, the rotational hinges located at the central and external post-beam connections plasticized, and the model failed when the central ones reached their ultimate capacity. As in the experiment, the shear effect provoked by the diagonal on the central node led to the failure of this connection. Once this happened, the diagonals no longer worked and the analysis stopped at a displacement of 0.088 m.

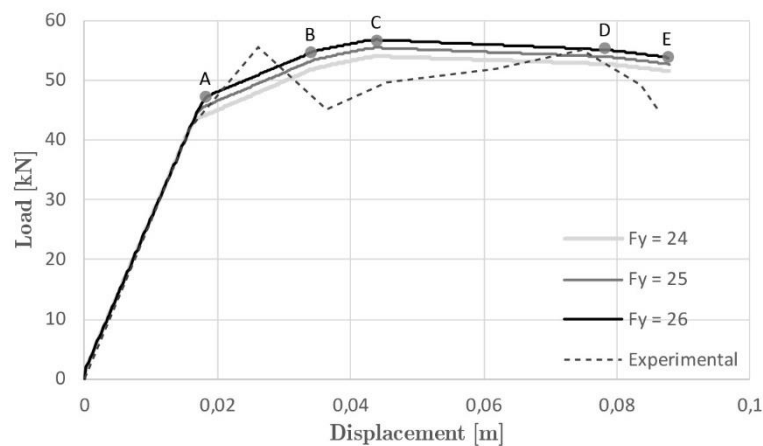


Figure 5-17. Parametric analysis of the capacity of the connection by contact. Grey dots indicates the achievement of the local mechanisms along the test.

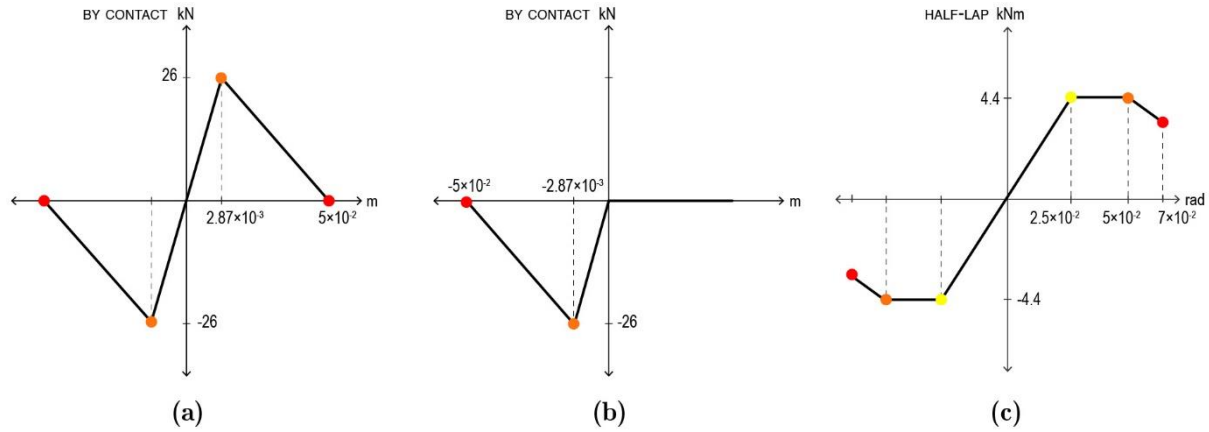


Figure 5-18. Nonlinear load-deformation relationships of the Pombalino model connections: (a) by contact axial behaviour, (b) by contact shear behaviour, and (c) half-lap rotational behaviour.

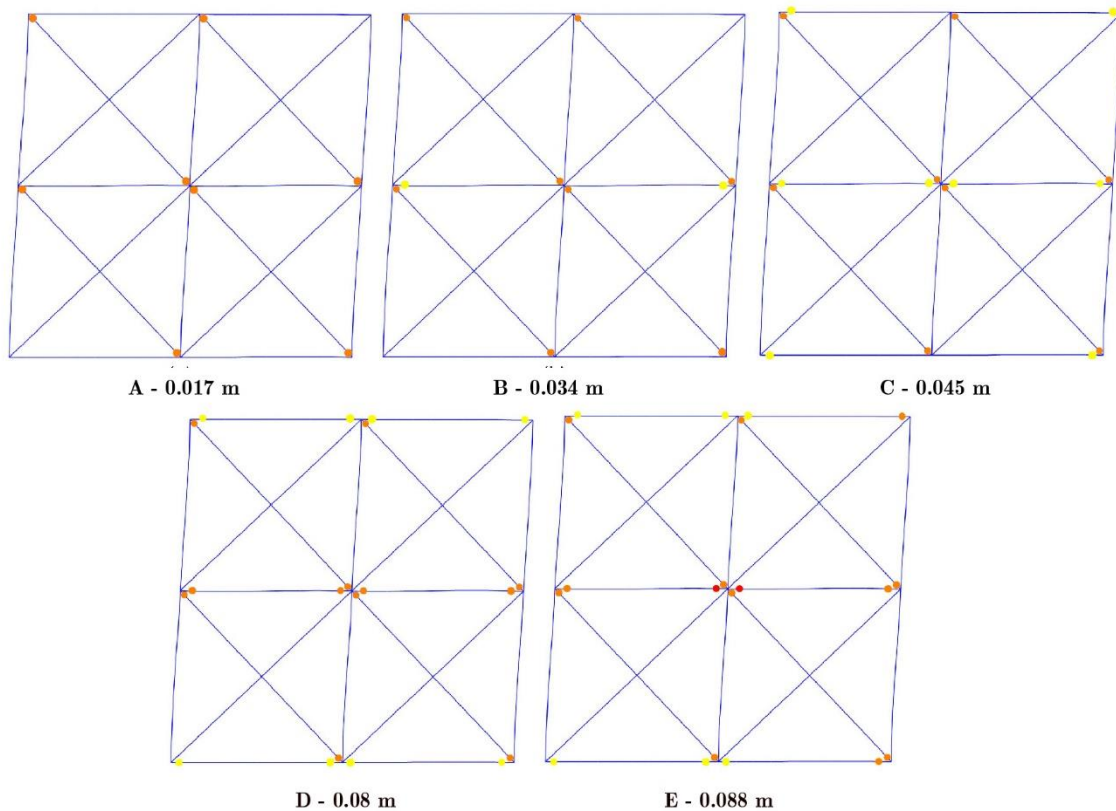


Figure 5-19. Collapse mechanisms predicting the response of the Pombalino wall at different phases of the analysis. Coloured dots indicate the plastic state of the connections according to Figure 5-16.

The numerical model of the *quincha* frame, tested in half-scale dimension by Moore and D'Ayala (2011), was calibrated by setting the nonlinear response of the connections. In this case, experimental data were only available for the mortise-and-tenon joints, which were used to connect the posts and beams elements. Therefore, analytical calculations were developed in order to predict the nonlinear behaviour of the nailed connections at the diagonals.

The post and plates elements of the model had $0.06 \times 0.08 \text{ m}^2$ cross-section, while the diagonal had $0.09 \times 0.03 \text{ m}^2$ cross-section, as shown in Figure 5-20a. Both *Cypress* and *Sapelli* timber

specimens were modelled using elastic isotropic materials properties listed in Table 5-3. A pre-compression load of 4.4 kN/m was applied through the top plate, followed by a horizontal displacement of 0.1 m in order to simulate the loading conditions of the experiment. To simulate the boundary conditions of the test, the nodes at the base were restrained in all the translational DOFs, while the top-left node was restrained in the horizontal translational direction allowing the application of lateral loads.

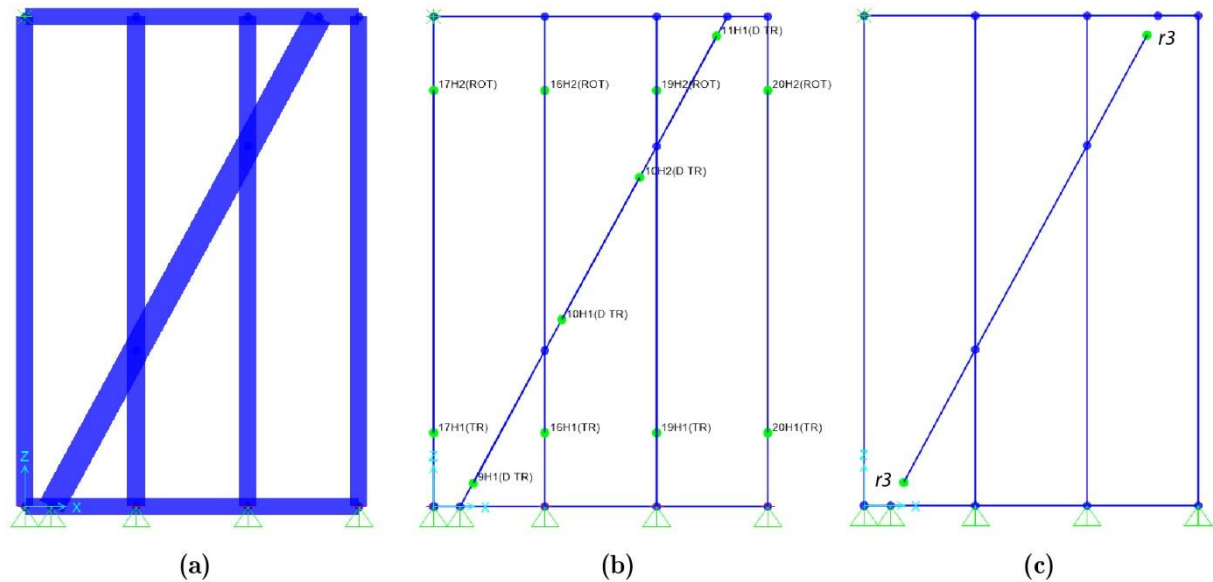


Figure 5-20. LPM of the half-scale *quincha* frame: (a) sections, (b) hinges and (c) moment releases.

The experimental moment-rotation response obtained from the loose fit mortise-and-tenon test (see Figure 5-9) was used to define the nonlinear relationship of this connection in the model. The experimental data was modified as a trilinear curve consisting of an initial linear behaviour, followed by a plateau and a brittle ultimate branch, as shown in Figure 5-21a. This connection had an initial rotational stiffness of 3.3 kNm/rad and a maximum moment of 0.25 kNm reached at rotation of 0.075 rad. Nonlinear rotational hinges acting on the moment deformational DOF were used to introduce the nonlinearities at the top post-beam nodes of the model, as shown in Figure 5-20b. According to Quinn (2017), the uplift experienced by the mortise-and-tenon joints at the bottom of the frame could be represented by defining the tensile elastic capacity of these connections. Figure 5-21b shows the stress-strain relationship defined by Quinn (2017) for these connections, based on the vertical uplift measurements on the tested frame. This relationship was used to model the axial stiffness of the springs attached at the bottom post-beam connections of the model, acting on the u1 deformational DOF, as shown in Figure 5-20b.

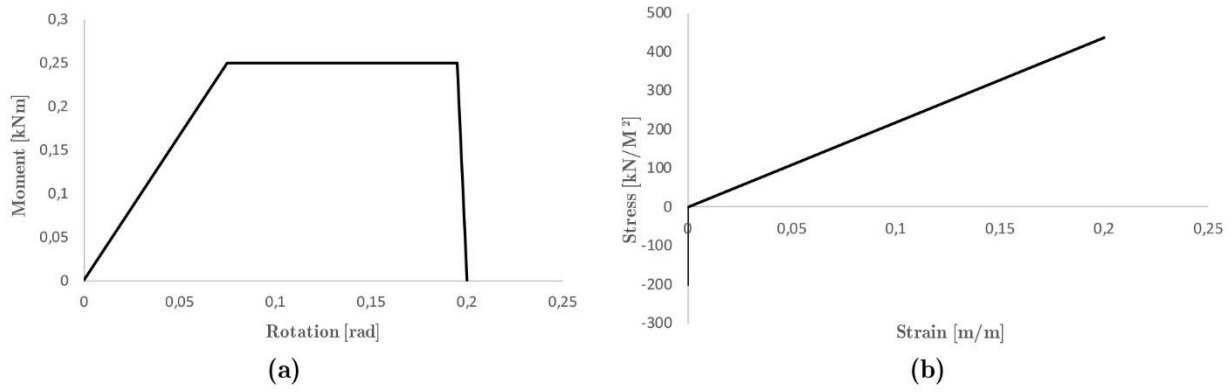


Figure 5-21. Nonlinear load-deformation relationships of the mortise-and-tenon connection for the half-scale *quincha* model: (a) rotational behaviour and (b) translational stress-stress relationship.

In the following cases, the capacity of the nailed connections $F_{v,Rk}$ is calculated by applying Equation (5-3) derived from the analytical methodology proposed by Eurocode 5 (CEN EC5 1.2 2004) for laterally loaded nails in single shear. This approach considers most of the essential parameters governing the response of nailed connections such as the mechanical properties of the materials, the grain direction, the geometry and number of the nails, and the type of loads.

$$F_{v,Rk} = 1,5 \sqrt{\frac{2\beta}{1+\beta}} \sqrt{2M_{y,Rk} f_{h,i,k} d + \frac{F_{ax,Rk}}{4}} \quad (5-3)$$

with,

$$\beta = \frac{f_{h,2,k}}{f_{h,1,k}} \quad (5-4)$$

Where, $F_{v,Rk}$ is the characteristic load-carrying capacity per shear plane fastener; $f_{h,i,k}$ is the characteristic embedment strength of the timber member; d is the fastener diameter; $M_{y,Rk}$ is the characteristic fastener yield moment; β is the ratio between the embedment strength of the timber members; and $F_{ax,Rk}$ is the characteristic axial withdrawal capacity of the fastener. For laterally loaded nails, the characteristic embedment strength and yield moment should be calculated according to Equations (5-5) and (5-6) or (5-7) respectively. For smooth nails made of wire, with a minimum tensile strength of 600 N/mm², the following characteristic values for yield moment should be considered:

$$M_{y,Rk} = \begin{cases} 0.3 f_u d^{2.6} & \text{for round nails} \\ 0.45 f_u d^{2.6} & \text{for square and groove nails} \end{cases} \quad (5-5)$$

Where, d is the nail diameter (in mm) and f_u is the tensile strength of the wire (in N/mm²). For nails with diameters up to 8 mm, the following characteristic embedment strength in timber apply:

$$\text{- without predrilled holes:} \quad F_{y,R,k} = 0.082 \rho_k d^{-0.3} \text{ N/mm}^2 \quad (5-6)$$

$$\text{- with predrilled holes:} \quad F_{y,R,k} = 0.082 (1 - 0.01d) \rho_k \text{ N/mm}^2 \quad (5-7)$$

Where, ρ_k is the characteristic timber density (in kg/m^3) and d is the nail diameter (in mm). Since the compressive strength value was not provided by the experimental tests, a sensitivity analysis was necessary.

Table 5-7 outlines the parameters involved in the calculation of the nailed connection capacity for the half-scale *quincha* frame. It is important to note that the tensile strength (f_u) value was not derived from experimental tests and can highly vary the response of the connections. The capacity of the nailed connections was assessed by means of a sensitivity analysis using different tensile strength (f_u) values in the model. According to Porteous and Kermani (2004), the most common type of nails are the smith steel wire nails, which commonly have a minimum tensile strength of 600 N/mm^2 . Furthermore, different reasonable tensile strength values of commercial nails (listed in Table 5-7) were considered to perform a sensitivity analysis of this parameter. By applying Expression (3) and assuming tensile strengths values of 500 N/mm^2 , 600 N/mm^2 , and 690 N/mm^2 , possible maximum capacity values of the connection were calculated as 1.535 N/mm^2 , 1.681 N/mm^2 , and 1.803 N/mm^2 respectively.

Table 5-7. Mechanical properties of the nails and timber of the half-scale *quincha* frame.

Length	76	[mm]
Diameter	3.2	[mm]
Head diameter	5	[mm]
Timber density	390	[kg/m ³]
t1	30	[mm]
t2	80	[mm]
	A	500
Tensile strength f_u	B	600 [N/mm ²]
	C	690
Number of nails	2	

The load-deformation relationship of the nailed connections was defined assuming a bilinear curve that considers an initial linear branch up to the maximum capacity of the connection, followed by a softening behaviour up to the ultimate capacity. The stiffness and yield displacement of the connection were determined through a sensitivity analysis until a good agreement between the model and the experiment was obtained. The results of the model were compared to those of the experiment with respect to the global capacity and the collapse mechanisms of the tested frame. The response of the model was in good agreement with the experiment, assuming a linear stiffness of 2130 kN/m and a maximum capacity of 1.8 N/mm^2 for the nailed connections, as shown in Figure 5-22a. The yield displacement d_y of the connection was

calculated as 8.45×10^{-4} m by applying Equation (5-2), while its ultimate displacement was defined as 5×10^{-3} m by applying a sensitivity analysis. Nonlinear axial springs were introduced at each node of the diagonal-frame connections, acting on the axial deformational DOF, as shown in Figure 5-20b. Furthermore, moment releases were specified at each external diagonal-beam node to avoid the moment resistance at these points, as shown in Figure 5-20c. NSA under displacement control was performed to obtain the results summarized in Figure 5-22b.

The collapse mechanisms predicted by the model were in good agreement with those observed during the experiment. Figure 5-22b displays the instances of local mechanisms during the simulation, while Figure 5-23 and Figure 5-24 show the so-called “plastic state” of the hinges within the model. Nonlinearities appeared at the bottom diagonal connection when the spring reached its maximum capacity at a displacement of 0.01 m. After this point, the remaining springs at the diagonal and some of the top hinges reached their maximum capacity. As in the experiment, the frame failed in shear when the top diagonal-beam connection failed reaching its ultimate capacity.

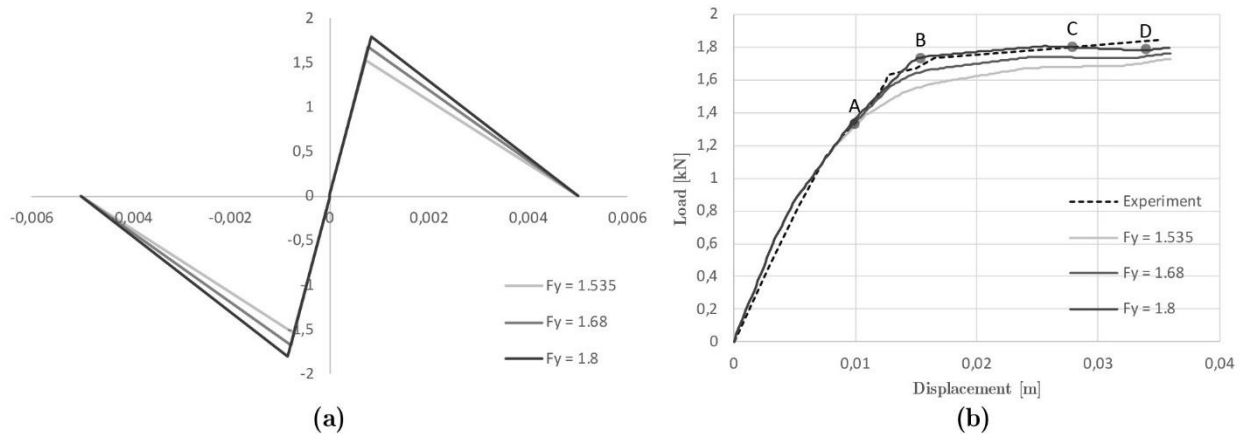


Figure 5-22. Sensitivity analysis for the *quincha* frame: (a) nonlinear load-deformation relationship for the nailed connection, and (b) obtained capacity curves of the bare frame model.

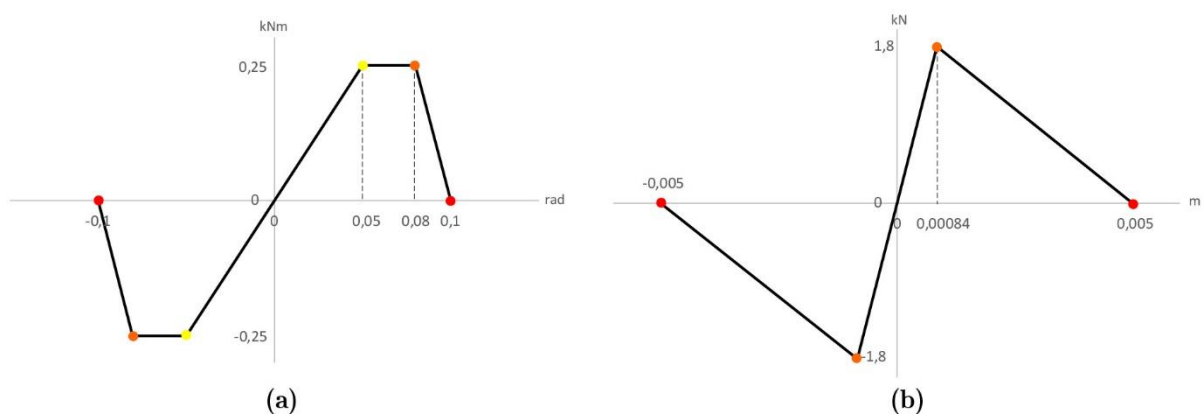


Figure 5-23. Nonlinear load-deformation relationships for the connections in LPM half-scale *quincha* model: (a) mortise-and-tenon behaviour, and (b) nailed connection behaviour.

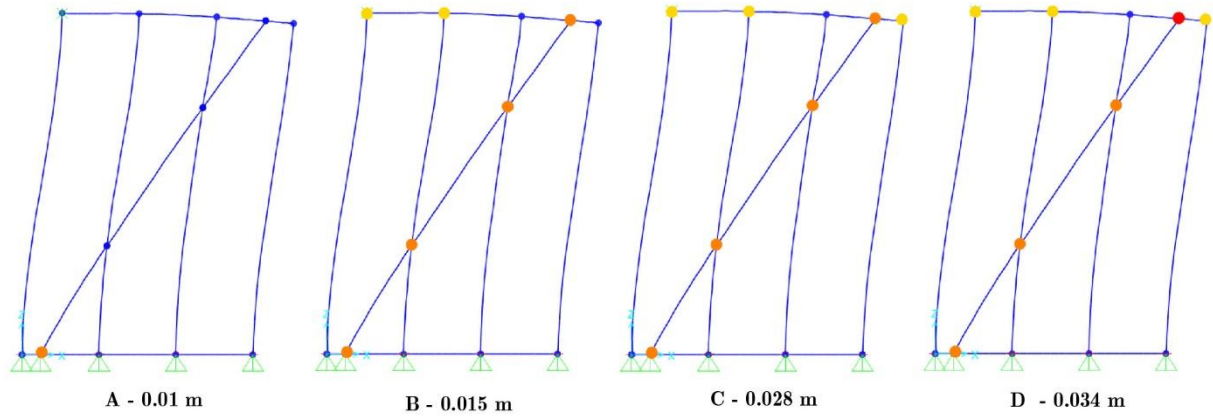


Figure 5-24. Collapse mechanisms predicting the response of bare frame half-scale *quincha* model at different phases of the analysis.

5.3.3 Numerical simulation of experiments on infilled timber frames

The modelling of the infill was addressed using the Equivalent Strut Method (ESM), originally introduced by Stafford-Smith (1963) and subsequently developed by Bertoldi, Decanini, and Gavarini (1993), to estimate its contribution within the bare frame models. The ESM is a simplified approach where the elastic in-plane stiffness of an uncracked solid masonry infill is represented with an equivalent strut of width ω given by Equation (5-8). Such a strut shall have the same thickness and modulus of elasticity of the infill panel that it represents. According to Stafford-Smith (1963), the equivalent width of the strut (ω) depends on a relative stiffness parameter λ_h given by Equation (5-9), and on the constants k_1 and k_2 also related to λ_h . The choice of what values to assign to these constants varies in the available scientific literature, based on different experimental studies. The values used in this research were introduced by Bertoldi, Decanini, and Gavarini (1993) and are shown in Table 5-8. The width of the equivalent strut can be calculated as follows:

$$\omega = \left(\frac{k_1}{\lambda_h} + k_2 \right) d \quad (5-8)$$

Where ω is the width of the frame, in m, d is the diagonal length of the infill panel, in m (Figure 5-25); λ_h is the relative stiffness coefficient, computed as follows:

$$\lambda_h = \sqrt[4]{\frac{E_m e \sin(2\theta)}{4E_c I_{col} h_m}} h \quad (5-9)$$

Where E_m is the elastic equivalent modulus corresponding to the complete cracking stage on the infill, in kN/m^2 ; e is the thickness of the infill panel, in m; θ is the angle whose tangent is the infill height-to-length aspect ratio, in rad; E_c is the expected modulus of elasticity of the infill material, in kN/m^2 ; I_{col} is the moment of inertia of the columns, in m^4 ; h_m is the height of the infill

panel, in m; and h is height of the column measured between centre lines of the beams, in m. (see Figure 5-25).

Table 5-8. Suggested values of k_1 and k_2 constants for the ESM according to Bertoldi, Decanini, and Gavarini (1993)

	k_1	k_2
$\lambda_h \leq 3.14$	1.3	0.178
$3.14 < \lambda_h < 7.85$	0.707	0.01
$7.85 \leq \lambda_h$	0.47	0.04

According to Decanini et al. (2004), the stiffness of the equivalent strut (kfm) corresponding to the complete cracking stage is given by Equation (5-10):

$$k_{fm} = \frac{E_m e \omega}{d} \quad (5-10)$$

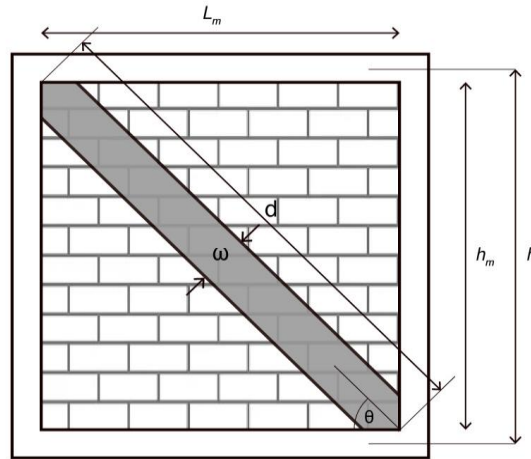


Figure 5-25. Geometric characteristics of the equivalent diagonal strut for the ESM application.

The resistance of the panel is simulated by an equivalent failure compressive strength (σ_{br}), which considers the different failure modes that could occur in both conventional tests and real structures subjected to seismic action. According to Decanini et al. (2004), four conventional failure modes have to be considered when computing the corresponding equivalent failure compressive stress: (a) diagonal tension, $\sigma_{br(1)}$, (b) bed-joint sliding, $\sigma_{br(2)}$, (c) crushing in the corners in contact with the frame, $\sigma_{br(3)}$, and (d) diagonal compression, $\sigma_{br(4)}$.

$$\sigma_{br(1)} = \frac{0.6 \tau_{m0} + 0.3 \sigma_o}{\omega/d} \quad (5-11)$$

$$\sigma_{br(2)} = \frac{(1.2 \sin \theta + 0.45 \cos \theta) f_{sr} + 0.3 \sigma_o}{\omega/d} \quad (5-12)$$

$$\sigma_{br(3)} = \frac{(1.2 \sin \theta + 0.45 \cos \theta) f_{sr} + 0.3 \sigma_0}{\omega/d} \quad (5-13)$$

$$\sigma_{br(4)} = \frac{1.16 \sigma_{m0} 0.3 \tau_{m0}}{k1 + k2 \lambda_h} \quad (5-14)$$

Where, σ_{m0} . is the vertical compression strength measured on masonry specimens, in kN/m^2 ; τ_{m0} is the shear strength measured with the diagonal compression test, in kN/m^2 ; f_{sr} is the slide resistance in the joints measured from the triplet test, in kN/m^2 ; and σ_0 is the vertical stress due to working loads, in kN/m^2 .

Once the equivalent failure compressive stress of the different failure modes have been determined, the minimum value $(\sigma_{br})_{\min}$, defines the most probable failure mode of the infill. The lateral strength of the equivalent strut is given eventually by Equation (5-15):

$$H_{\max} = (\sigma_{br})_{\min} e\omega \quad (5-15)$$

The nonlinear deformation acceptance criteria of the equivalent strut was determined according to Decanini et al. (2004) and Sassun et al. (2016). Figure 5-26 shows the proposed load-deformation law constituted by four branches. A first linear elastic one corresponds to the uncracked stage (H_{cr}), and it is followed by a post-cracking phase up to the maximum strength (H_{\max}), where F_m corresponds to the complete cracking stage of the infill panel. The third descending branch of the curve describes the post-peak strength deterioration of the infill until it reaches the residual strength H_{res} and displacement δ_{res} . According to Sassun et al. (2016), the drift ratios of the constitutive law can be assumed as $\delta_{cr} = 0.1\%$, $\delta_{\max} = 0.2\%$, $\delta_{res} = 0.8\%$ which correspond to the damage state of a slender infill panel based on experimental results.

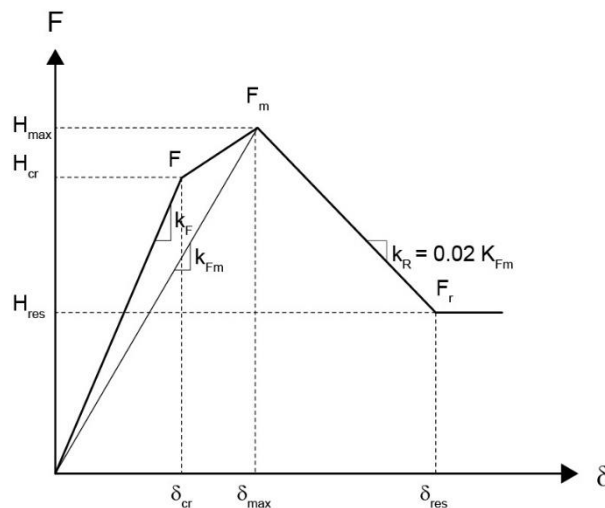


Figure 5-26. Nonlinear relationship definition for the strut in the ESM based on Decanini et al. (2004) and (Sassun et al. 2016).

The ESM models the strut by using linear elastic elements that are pin-connected to the surrounding frame. The nonlinear behaviour is introduced at the ends of the strut by using axial springs, containing the load-deformation laws of the panel shown in Figure 5-26. The Pombalino and *quincha* infilled models were calibrated following the described ESM approach. The first two cases incorporated the equivalent struts to the already calibrated bare frame models. NSA under displacement control was applied to obtain the lateral load-bearing response of the infilled models. The width of the equivalent strut of the Pombalino frame was calculated as 0.21 m after applying Equation (5-8), and considering the parameters listed in Table 5-9. Figure 5-27a shows the ESM configuration where the strut is highlighted in red and the axial springs in green. The stiffness coefficient λ_h was calculated as 12.325, considering coefficients $k_1 = 0.47$ and $k_2 = 0.04$, and the linear stiffness of the panel (k_{fm}) was calculated as 49740 kN/m by applying Equation (5-10).

Table 5-9. Parameters for the estimation of the equivalent strut of the Pombalino frame

h	1.9	[m]
h_m	1.74	[m]
E_c	10000000	[kN/m ²]
	5500000	
E_m	5500000	[kN/m ²]
e	0.12	[m]
I_{col}	0.00000512	[m ⁴]
d	2.52	[m]
ϑ	0.763	rad
λ_h	12.325	-

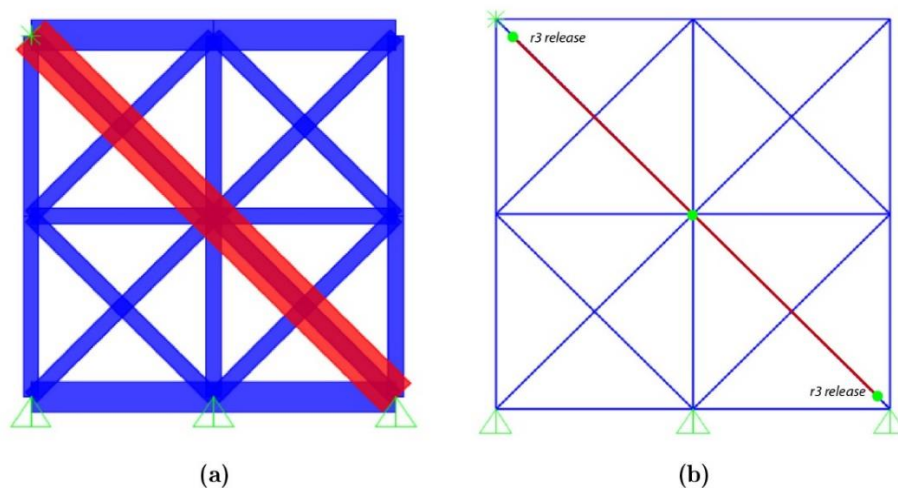


Figure 5-27. Model based on ESM of the Pombalino infilled frame: (a) geometry and (b) infill hinges locations and DOF releases.

The equivalent failure modes of the infill panel were calculated as follows: $\sigma_{br(1)} = 240.9$ kN/m²; $\sigma_{br(2)} = 13119$ kN/m²; $\sigma_{br(3)} = 5887.6$ kN/m²; and $\sigma_{br(4)} = 8622.9$ kN/m², using the mechanical

properties of masonry defined in Table 5-10. Given these results, a shear diagonal tension failure was predicted for the panel and the maximum lateral strength was calculated as 5.56 kN. Lastly, the deformation response of the strut displayed in Figure 5-29a was determined considering the following key values: $H_{\max} = 5.65$ kN; $H_{\text{cr}} = 4.53$ kN; $H_{\text{res}} = 1.98$ kN; $k_{\text{fc}} = 51293.25$ kN/m; $k_{\text{f}} = 205173$ kN/m; $k_{\text{r}} = -1025.87$ kN/m. The strain ratios δ_{cr} , δ_{\max} , and δ_{res} were calculated as 0.005 m, 0.01 m, 0.04 m respectively.

Table 5-10. Mechanical properties of the masonry infill panel for the calculation of the ESM.

Vertical compression strength σ_{m0}	7530	[kN/m ²]
Shear strength τ_{m0}	200	[kN/m ²]
Slide resistance in the joints f_{sr}	100	[kN/m ²]
Vertical stress σ_0	31.32	[kN/m ²]

Nonlinear axial springs were added at each node where the strut meets the frame, i.e. at the centre and the ends, as shown in Figure 5-27b. Table 5-11 summarized the masonry mechanical properties used to define the mechanical properties of the equivalent strut.

Table 5-11. Mechanical properties of the infill masonry of Pombalino (Poletti 2013).

Young's modulus E	5.5×10^6	kN/m ²
Density ρ	1800	Kg/m ³
Poisson's ratio ν	0.2	-

Figure 5-29b compares the numerical and experimental load-displacement capacity curves of the Pombalino infilled frame. A good agreement in terms of global stiffness is observed, and the maximum capacity is slightly underestimated by the model. Nonlinearities appeared at a global displacement of 0.015 m, when the axial springs of the struts reached their maximum capacity. After this phase, such springs were moving in the post-cracking branch, until one of them reached its ultimate capacity at a displacement of 0.073 m. The axial springs of the diagonals in compression reached their maximum capacity at the global displacement of 0.018 m, followed by a progressive failure of the rotational hinges of the main frame, as shown in Figure 5-28. This prediction is consistent with what occurred in the experiment. The diagonals separated from the main frame inducing the first loss of capacity followed by the collapse of the external half-lap connections. The analysis stopped when some of the rotational hinges reached their ultimate capacity and no longer worked.

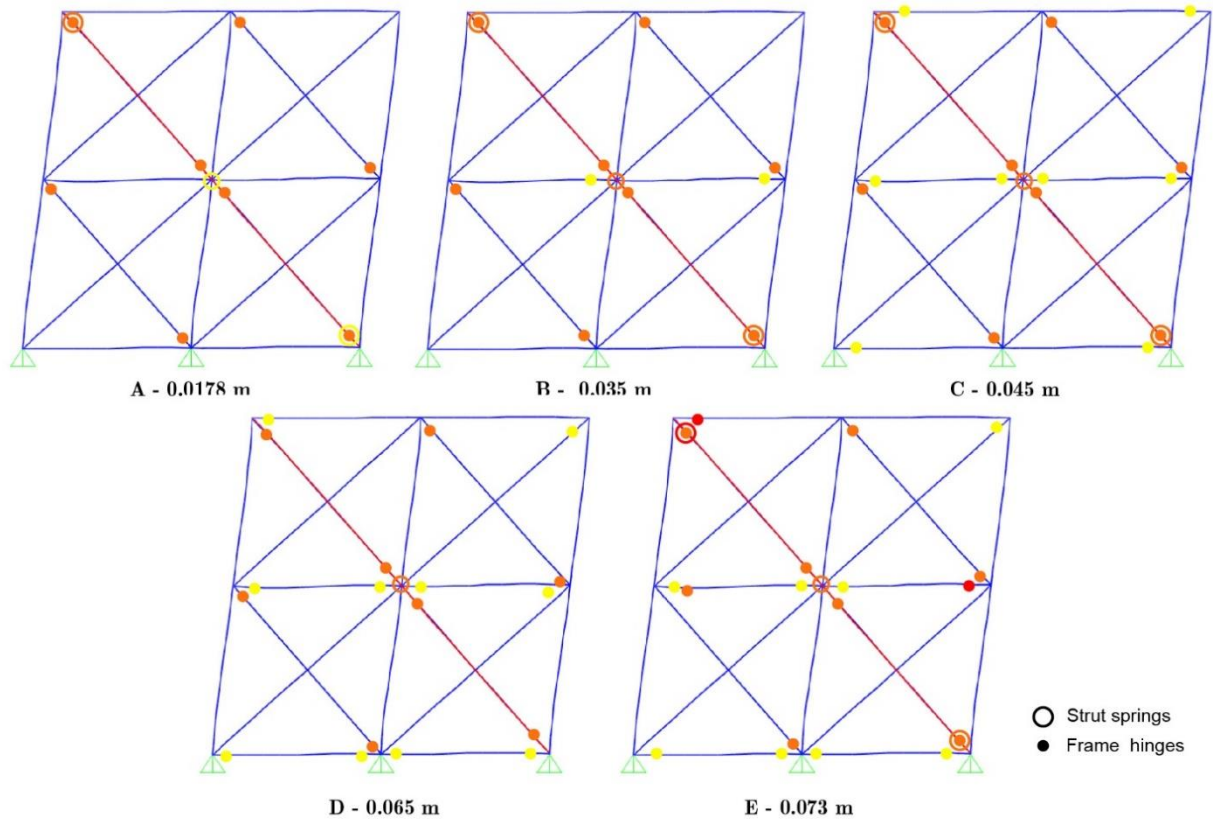


Figure 5-28. Model based on ESM of the Pombalino infilled frame: collapse mechanisms predicted different phases of the analysis.

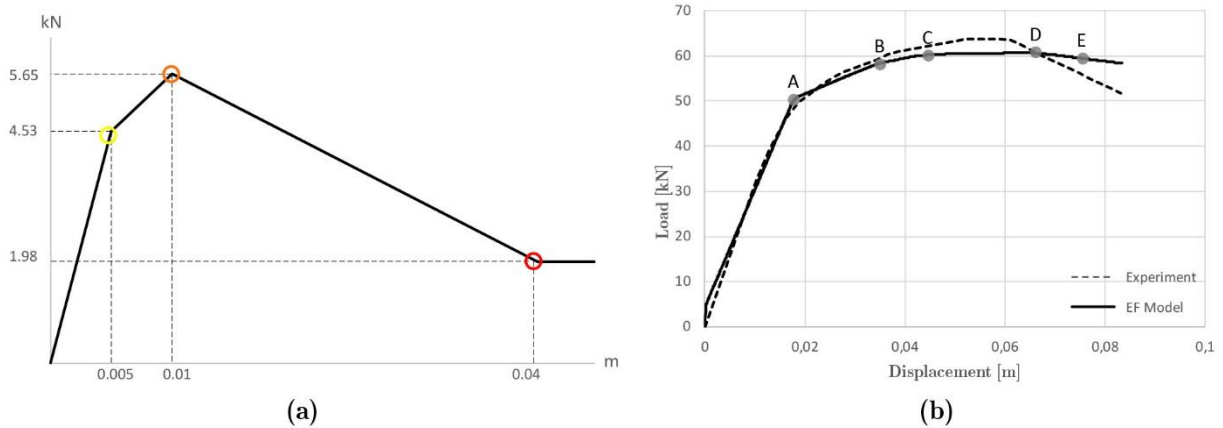


Figure 5-29. Model based on ESM of the Pombalino infilled frame: (a) nonlinear load-displacement relationship of the equivalent strut, and (b) numerical vs experimental capacity curves.

The equivalent strut of the infilled *quincha* frame tested by Moore and D’Ayala (2011), built in half-scale dimensions, was calculated as 0.228 m weight, by using the parameters listed in Table 5-12. The linear stiffness (kfc) of the strut was computed as 1798 kN/m by applying Equation (5-10). The mechanical properties of the adobe, summarized in Table 5-13, were used to determine the equivalent failure compressive modes of the panel $\sigma_{br(1)} = 77,37 \text{ kN/m}^2$, $\sigma_{br(2)} = 2140,9 \text{ kN/m}^2$, $\sigma_{br(3)} = 1391 \text{ kN/m}^2$, $\sigma_{br(4)} = 3821,1 \text{ kN/m}^2$. A shear diagonal tension $\sigma_{br(1)}$ failure

mode was predicted for the panel, while the maximum lateral strength H_{max} was calculated as 1.417 kN. Figure 5-31a displays the nonlinear load-displacement law controlling the strut, which considers the following key values: $H_{cr} = 1.135$ kN; $H_{max} = 1.417$ kN; $H_{res} = 0.496$ kN; $k_{fc} = 1789$ kN/m; $k_f = 7156$ kN/m; $k_r = -35,78$ kN/m; and δ_{cr} , δ_{max} , and δ_{res} strain ratios as 0.0055 m, 0.01 m, 0.04 m respectively.

Table 5-12. Parameters for the estimation of the equivalent strut of the half-scale infilled *quincha* frame.

h	1.76	[m]
h_m	1.64	[m]
E_c	6400000	[kN/m ²]
E_m	200000	[kN/m ²]
e	0.08	[m]
I_{col}	0.00000144	[m ⁴]
d	81.45	[m]
θ	0.96	rad
λ_h	6.94	-

Table 5-13. Mechanical properties of the adobe infill of the half-scale *quincha* model the calculation of the ESM.

Vertical compression strength σ_{m0}	1670	[kN/m ²]
Shear strength τ_{m0}	14	[kN/m ²]
Slide resistance in the joints f_{sr}	37.71	[kN/m ²]
Vertical stress σ_0	25.71	[kN/m ²]

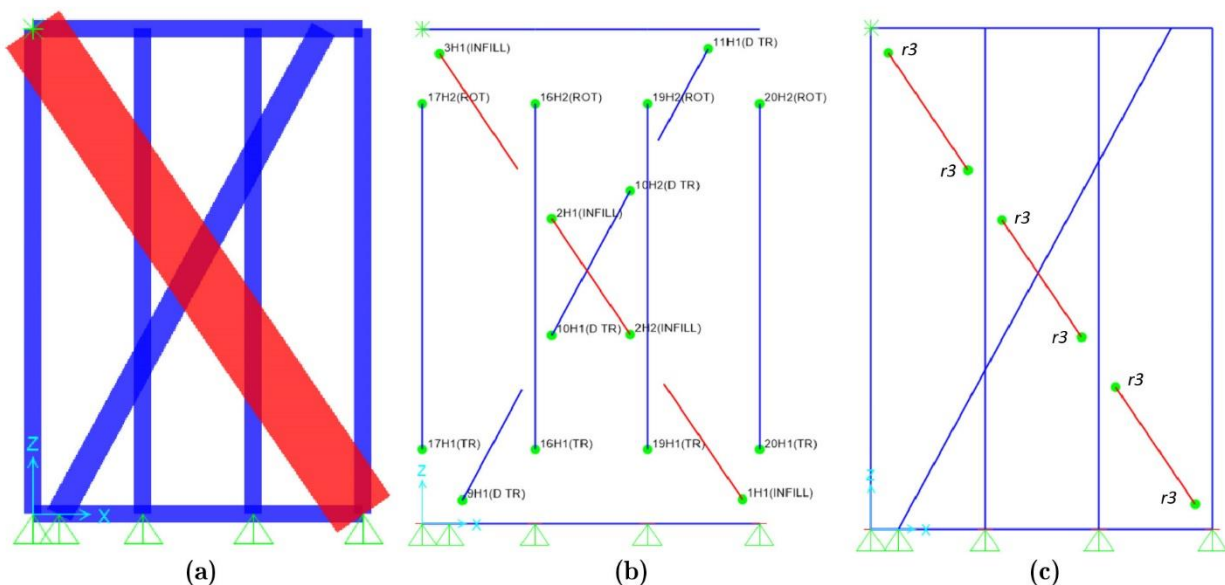


Figure 5-30. Model based on ESM of the half-scale infilled *quincha* frame: (a) geometry (b) strut hinges and (c) moment releases.

Table 5-14. Mechanical properties of adobe infill of the half-scale *quincha* frame.

Modulus of Elasticity E	[kN/m ²]	200000
Density ρ	[kg/m ³]	0.2213
Poisson's ratio ν	-	0.2

Comparisons between the model and the experiment showed a good agreement in terms of global stiffness and capacity, and the maximum strength was slightly overestimated by the model, as noted in Figure 5-31b. Figure 5-31b and Figure 5-32 display the capacity curve and the collapse mechanism predicted by the model. These results demonstrated to be consistent with what occurred in the experiment. Firstly, the springs of the strut reached their maximum capacity at a displacement of 0.002 m and 0.007 m (Instances A and B, Figure 5-32). After that, the axial springs of the diagonal and some rotational hinges at the top post-plate connection reached their maximum capacity (Instances B to E in Figure 5-32). The collapse of the frame occurred at a global displacement of 0.04 m, when the top spring of the diagonal reached its ultimate capacity. From this point on, the differences between the experimental and numerical behaviour can be attributed to the simplified modelling strategy used to represent the infill, which cannot represent critical local failures in detail.

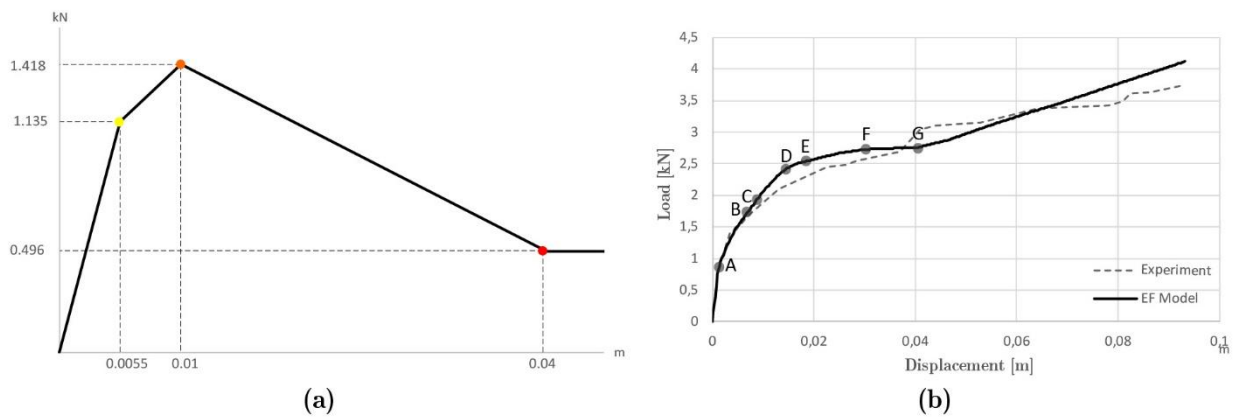


Figure 5-31. Model based on ESM of the half-scale infilled *quincha* frame: (a) nonlinear load-displacement relationship of the equivalent strut and (b) the numerical vs experimental capacity curves.

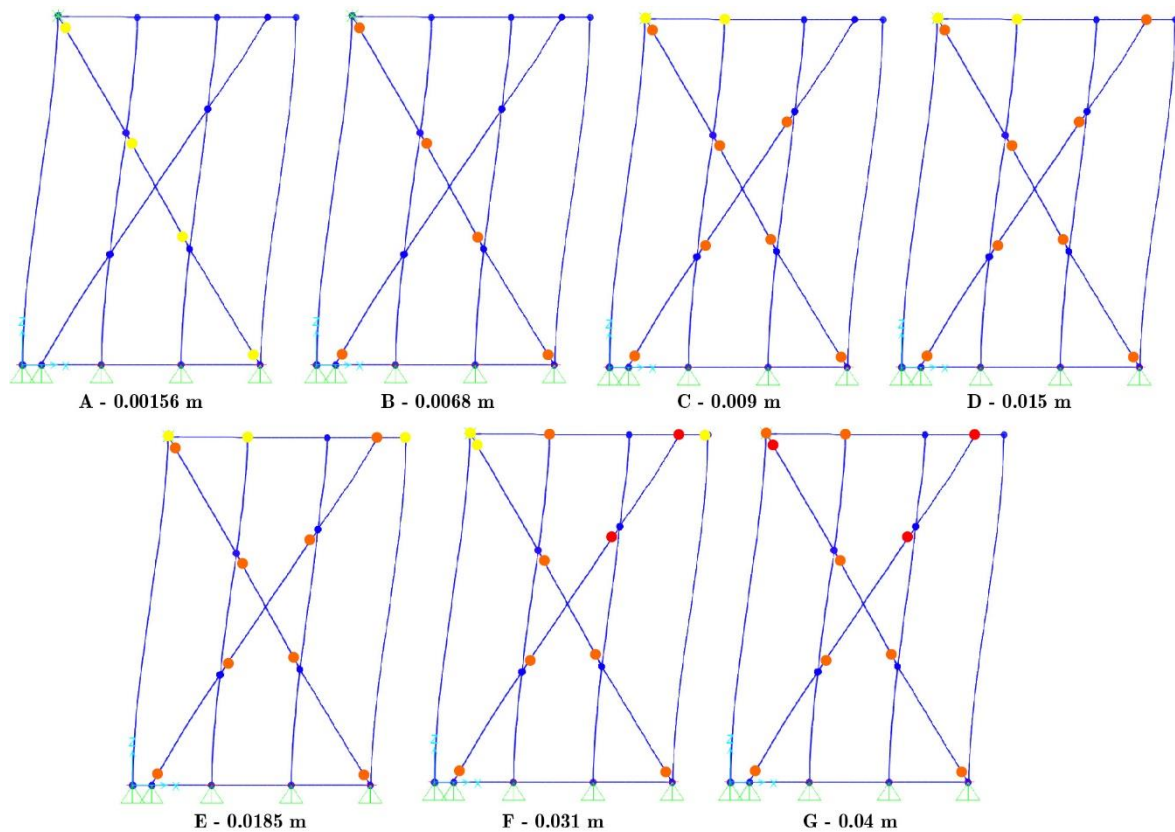


Figure 5-32. Model based on ESM of the half-scale infilled *quincha* frame: collapse mechanisms predicted at different phases of the analysis.

The numerical simulation of the full-scale *quincha* frame tested by Torrealva, Vicente, and Michiels (2018) is presented as the last example for the calibration of the LPM, with the infill represented by the ESM. As in the previous cases, the timber elements were modelled using frame elements with elastic parameters based on the mechanical properties of the *Moena Alcanfor* timber, summarized in Table 5-15. Post and plate elements had a cross-section of $0.08 \times 0.06 \text{ m}^2$, while the diagonal in tension had a cross-section of $0.03 \times 0.09 \text{ m}^2$, as shown in Figure 5-33a. The calibration of the mortise-and-tenon and nailed connections was executed considering both numerical results and analytical procedures.

Table 5-15. Mechanical properties of the *Moena Alcanfor* timber of the full-scale *quincha* frame (Perrone 2011).

Young's Modulus E	$1,18 \times 10^7$	kN/m ²
Density ρ	510	kg/m ³
Poisson's ratio ν	0.4	-

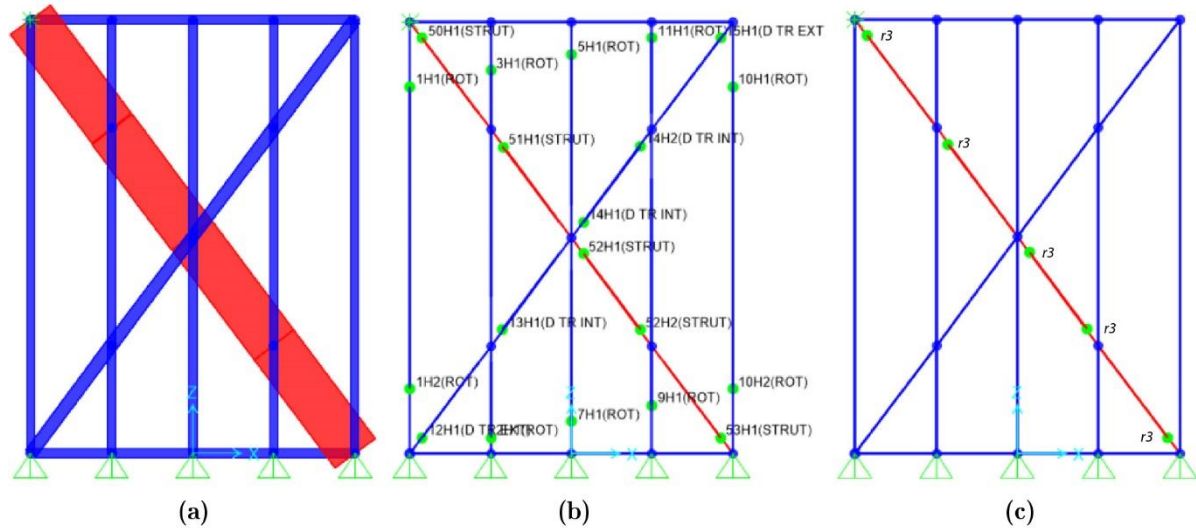


Figure 5-33. Model based on ESM of the full-scale infilled *quincha* frame: (a) geometry (b) strut hinges and (c) moment releases.

Perrone (2011) studied the nonlinear behaviour of the mortise-and-tenon connection of the full-scale *quincha* frame by developing the numerical micro model shown in Figure 5-34a. Figure 5-34b displays the moment-rotation response obtained from the model results, which was used to determine the nonlinear behaviour of this connection in the model. As in the previous cases, rotational hinges were introduced at each post-plate connections, as shown in Figure 5-33b.

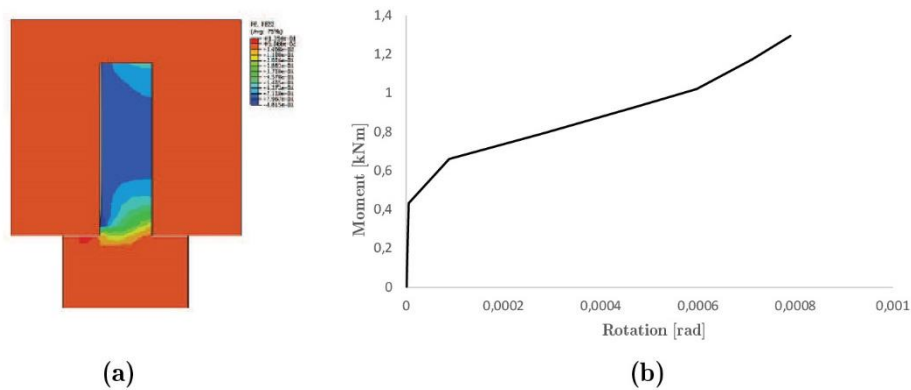


Figure 5-34. Micro model of mortise-and-tenon of the full-scale *quincha* frame: (a) plastic strain contour and (b) moment-rotation capacity (Perrone 2011).

The nailed connections were calibrated using the empirical model developed by Chui and Ni (1997) to estimate their load-embedment capacity, according to Equation (5-16). This model was based on the original proposal by Foschi (1974) but later modified to introduce the strength degradation effects on the calculation, as shown in Figure 5-35.

$$P = (P_0 + K_1|\delta|) \left(1 - e\left(-\frac{K_0|\delta|}{P_0}\right) \right) - (K_1 - K_2)(|\delta| - |\delta_p|)H(|\delta| - |\delta_p|) \quad (5-16)$$

Where P is the load per unit length at embedment deformation δ , in N; P_0 is the intercept of the first asymptote, in N/mm; K_0 is the initial stiffness, in N/mm²; K_1 is the slope of the first asymptote line, in N/mm²; K_2 is the slope of the second asymptote line, in N/mm²; δ_p is the deformation at ultimate strength, in mm (see Figure 5-35), and; $H(|\delta| - |\delta_p|)$ is the step function:

$$H(|\delta| - |\delta_p|) = \begin{cases} 1 & \text{for } |\delta| - |\delta_p| \geq 0 \\ 0 & \text{for } |\delta| - |\delta_p| < 0 \end{cases} \quad (5-17)$$

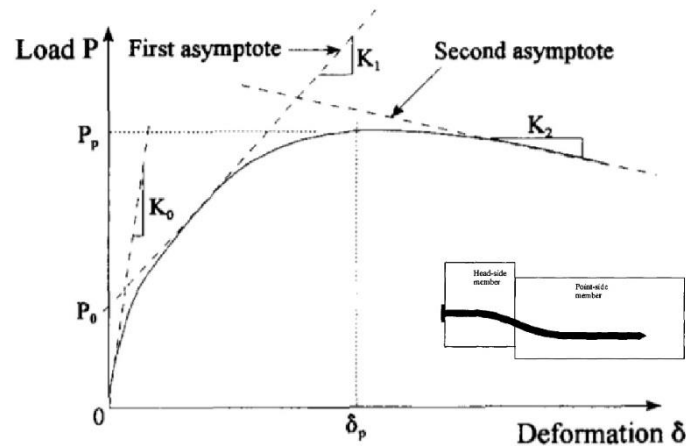


Figure 5-35. Load-embedment model for nailed connections proposed by Chui and Ni (1997).

The diagonal was connected to the plate with four nails, and to the post with three nails. Therefore, two particular models had to be defined for each connection. Due to the lack of experimental data on these specific connections, a benchmark experiment on a nailed connection subjected to shear loads (Xu 2006) was used to estimate the load-embedment capacity of the nails to be used within the model. The following initial parameters were extracted from the experiment to calculate the load-embedment relationship: $P_0 = 1.2$ kN/mm; $K_0 = 0.66$ kN/mm², $P_{\max} = 1.25$ kN; $\delta_0 = 0.53$ mm, $K_1 = 0.0059$ kN/mm²; $K_2 = 0.0013$ kN/mm² $\delta_p = 10$ mm. Sensitivity analyses were performed to adjust these values for the three and four nailed connections, by increasing P_0 until obtaining a good agreement between the model and the experiment. A higher load per unit length value (P) was assumed for the four nails connection respect to the three nails one in a ratio of 4:3. The initial stiffness (K_0) of each connection was calculated considering a displacement δ_0 of 3 mm. Figure 5-36 shows the obtained load-embedment curves of the connections constituted by the following parameters: for the four nails connections $P_0 = 21$ kN, $K_0 = 12.42$ kN/mm², $K_1 = 0.023$; $K_2 = -0.02$ kN/mm², and $\delta_p = 10.4$ mm; for the three nails connections $P_0 = 12,8$ kN; $K_0 = 7.57$ kN/mm², $K_1 = 0$; $K_2 = -0.072$ kN/mm², and $\delta_p = 10.4$ mm.

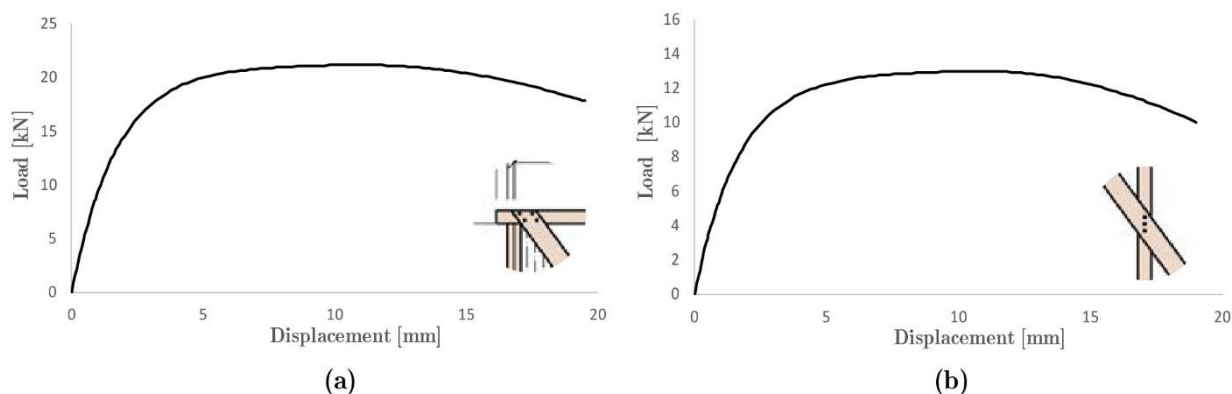


Figure 5-36. Load-embedment relationship of: (a) four nails diagonal-plate and (b) three nails diagonal-post connections of the full-scale *quincha* model.

The infill modelling is addressed again through the ESM. In this case, the equivalent width of the strut was 0.369 m, calculated by considering the parameters listed in **Error! Reference source not found.** The equivalent failure modes of the frame were estimated based on the mechanical properties of the adobe listed in Table 5-16 as: $\sigma_{br(1)} = 93.145 \text{ kN/m}^2$, $\sigma_{br(2)} = 2956.8 \text{ kN/m}^2$, $\sigma_{br(3)} = 1481.3 \text{ kN/m}^2$, $\sigma_{br(4)} = 31101 \text{ kN/m}^2$. Given these results, the most probable failure mode of the panel is the shear diagonal tension, $\sigma_{br(1)}$. The maximum strength of the panel was calculated as 2.75 kN by applying Equation (5-15). The above results were employed to define the load-displacement relationship controlling the deformation of the panel shown in Figure 5-37d, which was constituted by the following parameters: $H_{max} = 2.75 \text{ kN}$; $H_{cr} = 2.2 \text{ kN}$; $H_{res} = 0.96 \text{ kN}$; $k_{fc} = 1456 \text{ kN/m}$; $k_f = 5824.9 \text{ kN/m}$; $k_r = -29.12 \text{ kN/m}$; and $\delta_{cr} = 0.0045 \text{ m}$, $\delta_{max} = 0.0089 \text{ m}$, and $\delta_{res} = 0.036 \text{ m}$.

Table 5-16. Parameters for the estimation of the equivalent strut of the full-scale infilled *quincha* frame.

h	3.14	[m]
hm	3.08	[m]
Ec	12000000	[kN/m ²]
Em	200000	[kN/m ²]
e	0.08	[m]
Icol	0,0000014	[m ⁴]
d	4.06	[m]
ϑ	0.90885	rad
λh	9.21302	-

Table 5-17. Mechanical properties of the adobe infill of the full-scale *quincha* frame (E. Vicente and Torrealva 2014)

Vertical compression strength σ_{m0}	1670	[kN/m ²]
Shear strength τ_{m0}	14	[kN/m ²]
Slide resistance in the joints f_{sr}	37,71	[kN/m ²]
Vertical stress σ_0	25,71	[kN/m ²]

Figure 5-38 shows the comparison between the experimental and model load-displacement capacity curves. The results are in good agreement in terms of global stiffness, as well as maximum and ultimate capacity. The model reached a maximum load of 12.4 kN at a displacement of 0.092 m, presenting a slight error of 0.86%. On the other hand, the global stiffness of the model is 869 kN/m, 8% higher than that obtained in the experiment. The collapse mechanisms predicted by the model revealed that the axial springs of the strut and diagonal elements plasticized first, as shown in Figure 5-39 (Instances A-B). Subsequently, some of the springs of the diagonal reached their maximum capacity at a displacement of 0.0264 m (Instance B in Figure 5-39). Afterwards, some of the rotational hinges at the top and bottom connections of the frame entered in the plastic range (Instance C-D in Figure 5-39). The diagonal failed when one of the central springs reached its ultimate capacity (Instance E, Figure 5-39). After this stage, only the rotational hinges continued working in the model. This response was in good agreement with the experiment in terms of local and global mechanisms, since the stiffness of the experimental frame reduced after a central nailed connection failed, but it maintained its stability given the high flexibility of the mortise-and-tenon joints.

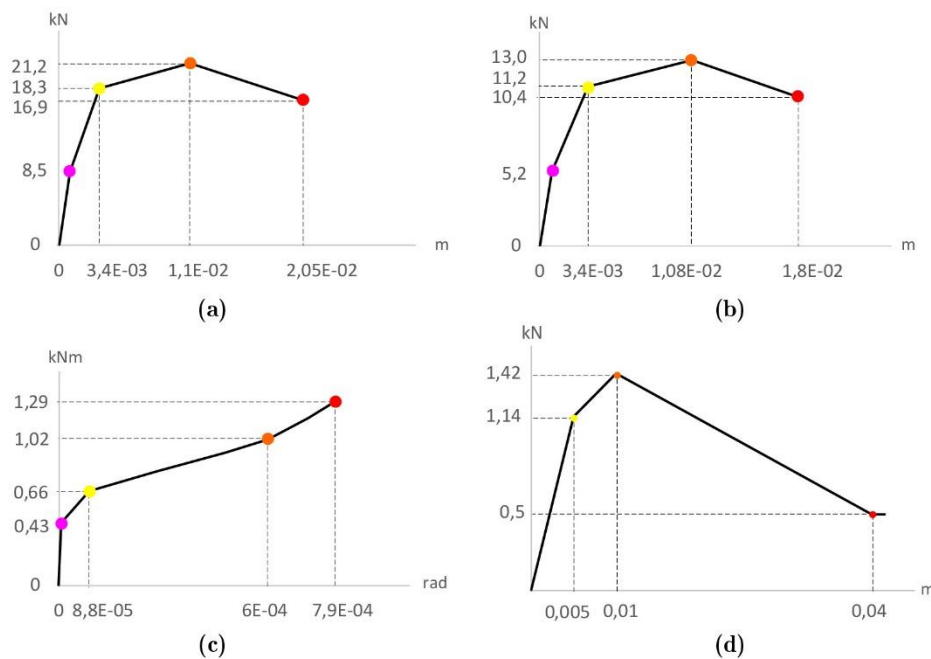


Figure 5-37. Model based on ESM of the full-scale infilled *quincha* frame: load-deformation relationships of (a) four and (b) three nails connections, (c) mortise-and-tenon connection, and (d) equivalent strut.

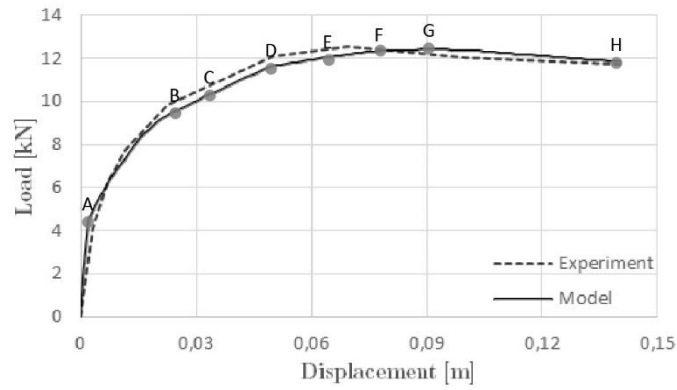


Figure 5-38. Model based on ESM of the full-scale infilled *quincha* frame: experimental vs numerical capacity curves.

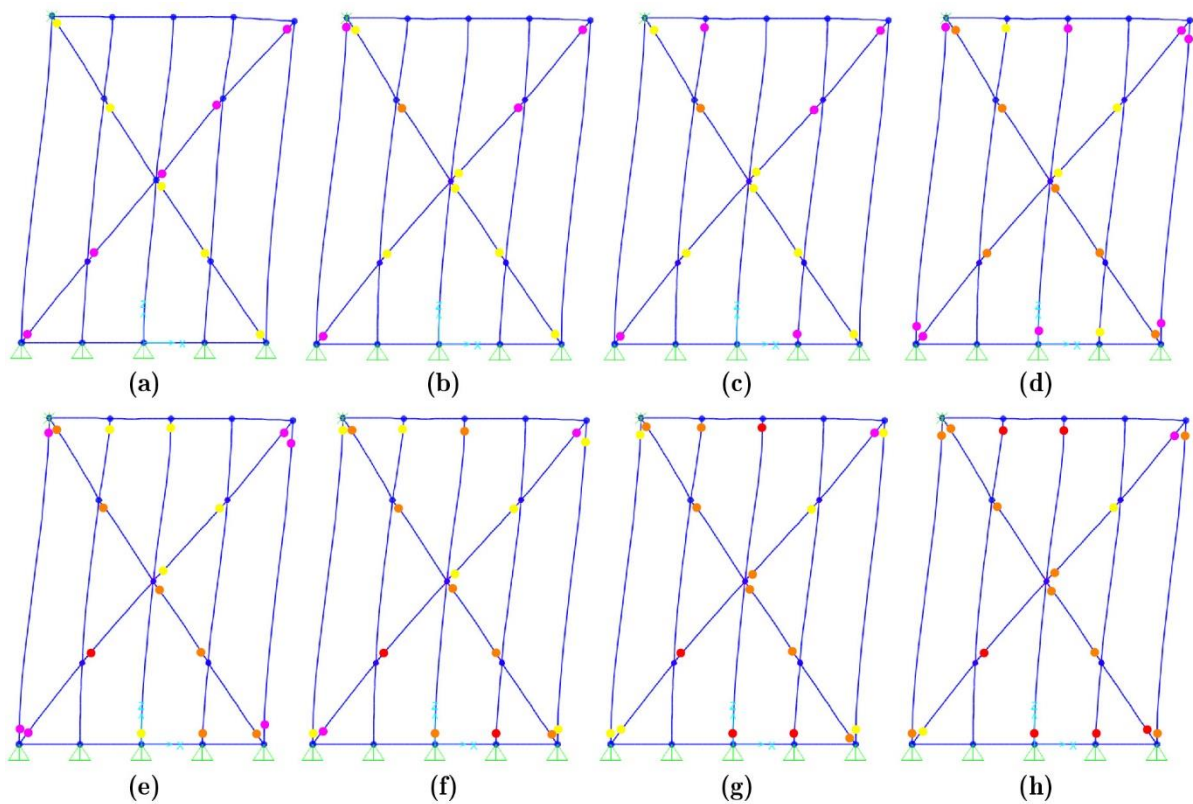


Figure 5-39. Model based on ESM of the full-scale infilled *quincha* frame: collapse mechanisms predicted at different phases of the analysis.

5.4 Benchmark experimental programs for calibration of masonry models

5.4.1 Experimental tests on in-plane loaded masonry walls

A full-scale unreinforced masonry (URM) wall with a central opening tested by Augenti et al. (2011) was selected as a benchmark case to calibrate the numerical model for masonry structures. The wall was subjected to monotonically increasing displacements until it experienced moderate damage. The specimen was built in single-leaf masonry by two URM piers connected

by a spandrel panel resting on a wood lintel, as shown in Figure 5-40. The wall was 5.10 m long, 3.62 m high and 0.31 m thick, whereas both the piers and the spandrel had a length of 1.70 m. As shown in Figure 5-40b, three masonry courses were built over the piers to apply the axial vertical forces and ensure structural continuity, thus simulating an ideal overlying storey. Lastly, the piers were rigidly connected to the strong floor of the laboratory by using RC beams. Potential out-of-plane mechanisms were avoided using three steel beams bolted to the columns of the transverse frames at both sides of the masonry wall.

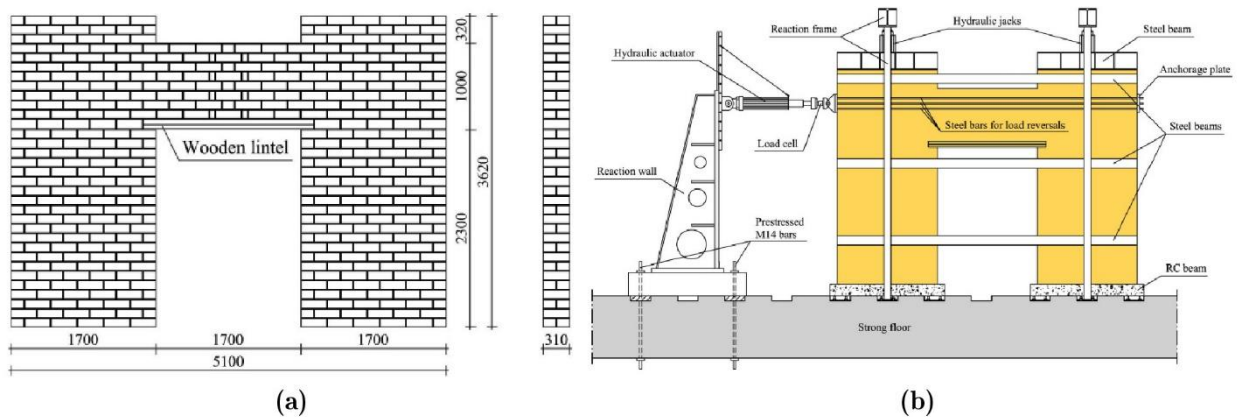


Figure 5-40 In-plane loaded URM specimen: (a) geometry and (b) test setup (in mm) (Augenti et al. 2011).

The brick units were made of tuff yellow stones joined with hydraulic mortar composed of natural sand and pozzolana-like reactive aggregates with a water-sand ratio by weight of 1:6:25. Preliminary laboratory tests were carried out by Augenti and Parisi (2010) aimed to evaluate the mechanical properties of both stones and mortar, following the European Standards (CEN 1999, 2005a, 2005b). The masonry properties, experimentally assessed through uniaxial compression and triplet tests by Augenti and Parisi (2010) and Parisi et al. (2011) are summarized in Table 5-18, Table 5-19 and Table 5-20.

Table 5-18. Mechanical properties of tuff brick units and mortar of the in-plane loaded masonry wall (Augenti et al. 2011).

Material	Tensile strength f_t (MPa)	Compressive strength f_c (MPa)	Young's modulus E (GPa)	Shear modulus G (GPa)
Yellow tuff units	0.23	4.13	1.54	0.44
Pozzolana-like mortar	1.43	2.50	1.52	0.66

Table 5-19. Mechanical properties of masonry obtained from compression tests for the in-plane loaded masonry specimen (Parisi et al. 2013).

Material	Compressive strength f_c (MPa)	Young's modulus E (GPa)	Shear modulus G (GPa)
Tuff masonry (compression \parallel to mortar bed joints)	3.85	2.07	0.86
Tuff masonry (compression \perp to mortar bed joints)	3.96	2.22	0.92

Table 5-20. Mechanical properties of tuff masonry of the in-plane loaded masonry wall (Parisi et al. 2011).

Tensile strength f_t (MPa)	Friction coefficient	Cohesion (MPa)
0.14	0.279	0.146

The wall was subjected to a vertical pre-compression load of 200 kN applied on each pier and maintained constant during the entire test. The lateral load was applied afterwards through a horizontal servo-controlled hydraulic actuator bolted to a non-prismatic reaction wall (Figure 5-40b). The test was performed under displacement control to obtain the strength degradation and cumulative damage in the softening range, until a displacement of 28 mm was reached, corresponding to an interstorey drift ratio of approximately 1% (Augenti et al. 2011).

At the end of the test, the piers cracked at the base, and vertical cracks owing to flexure occurred at the end and the middle sections of the spandrel, as shown in Figure 5-41. A rocking behaviour on the piers and diagonal shear cracking in the spandrel were more evident as the lateral displacement of the wall increased. According to Augenti et al. (2011), the lateral-load behaviour of the wall (Figure 5-42) was rather linear until the flexural cracking occurred at the piers. The lateral stiffness of the wall decreased significantly at a drift ratio of 0.06%, corresponding to a force of 99 kN when flexural cracks formed at the base of the piers due to the experienced rocking phenomenon. After this phase, the stiffness remained rather constant until the maximum resisting force was reached at a displacement of 19.74 mm (drift ratio of 0.65%). After this point, the occurrence of diagonal cracking in the spandrel panel induced an instantaneous resistance drop of approximately 15%. At larger displacements, the lateral resistance started to rise again until a force of 172 kN at a displacement of 27.18 mm (drift ratio equal to 0.89%). Figure 5-41 displays the crack pattern registered by the wall at the end of the test.

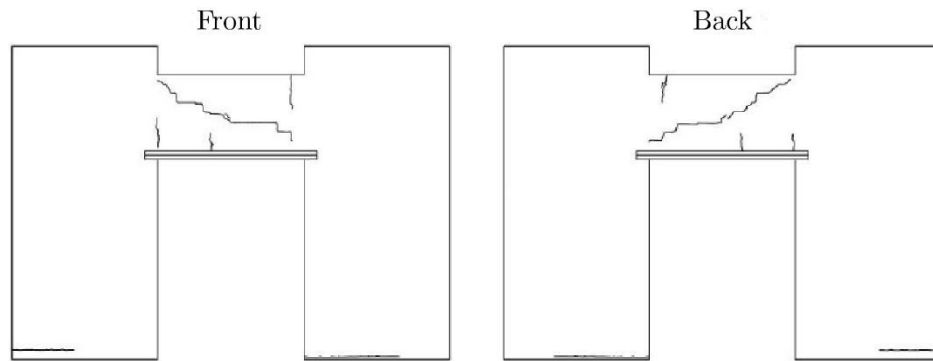


Figure 5-41. Experimental evidence of in-plane loaded masonry wall: damage patterns after the test (Augenti et al. 2011)

The obtained force-displacement capacity curve demonstrated that the global behaviour of the wall is mainly governed by the rocking motion of the piers. This phenomenon allowed large displacements of the panel until the diagonal shear failure in the spandrel panel affected the maximum resistance of the wall. The global stiffness of the wall was calculated to be 5.5×10^4 kN/m².

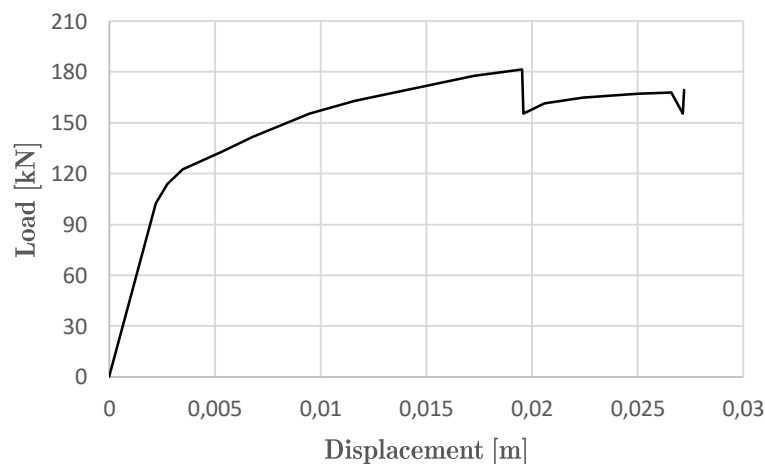


Figure 5-42. Experimental capacity curve of the in-plane loaded masonry wall (Augenti et al. 2011).

5.4.2 Experimental tests on out-of-plane loaded masonry walls

Experimental tests on an URM wall presented by Griffith and Vaculik (2007) was selected to calibrate the out-of-plane behaviour of the continuum model for masonry. A specimen corresponding to a solid wall (without openings) of 4 m width \times 2.5 m height \times 0.11 m thickness was studied in this research. In order to provide a realistic full moment contact along the vertical edge, return walls of 0.45 m length were built-in as part of the specimen, as shown in Figure 5-43b. The wall was subjected to an initial vertical pre-compression load of 100 kN/m² at the top, followed by a uniform pressure applied under displacement control at the centre of the front wall. Fixed support conditions were assumed at the left and right sides of the wall, while the top and bottom sides were simply supported. As part of the same campaign, experimental characterisation

tests on brick units, mortar, and masonry assemblages were performed to determine the mechanical behaviour of the materials. All the properties are summarized in Table 5-21 and Table 5-22.

Table 5-21. Brick unit mechanical properties of the out-of-plane loaded masonry wall.

Brick unit	Flexural strength (kN/m ²)	Young's modulus E (kN/m ²)
	3550	5.27×10^7

Table 5-22. Masonry mechanical properties of the out-of-plane loaded masonry wall.

Masonry	Flexural tensile strength f_t (kN/m ²)	Compressive strength f_c (kN/m ²)	Young's modulus E (kN/m ²)
	721	17600	3.188×10^6

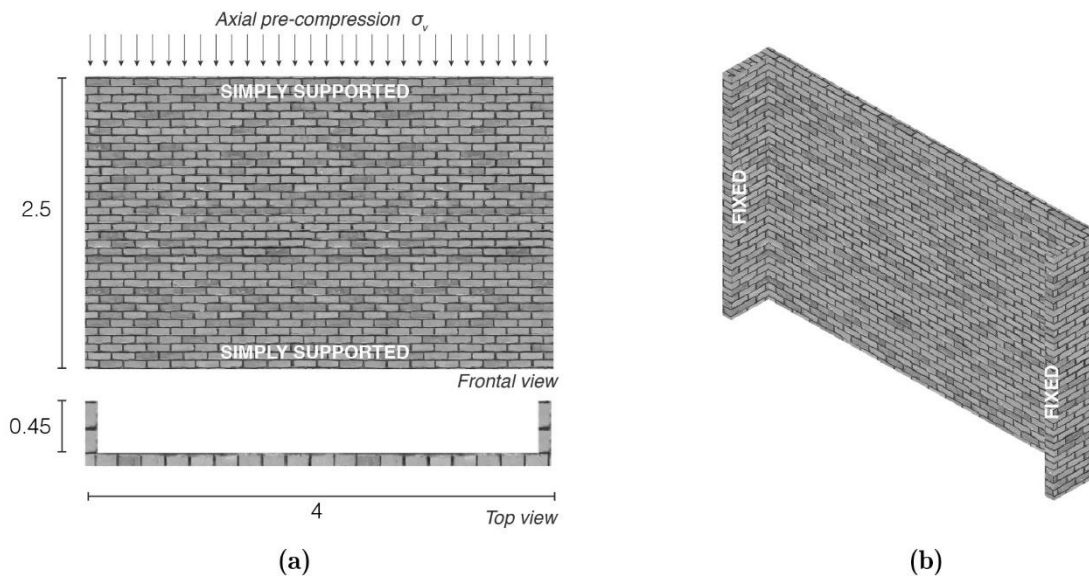


Figure 5-43. Out-of-plane loaded URM specimen: (a) frontal, top and (b) isometric views of the wall.

At the end of the test, the wall presented fully opened diagonal cracks in the surface, as well as partially developed cracks associated with the horizontal bending mechanisms at the vertical edge of the wall, as shown in Figure 5-44. According to Griffith and Vaculik (2007), this response demonstrated that once the wall reached the full static strength, the horizontal bending along the vertical edges gained an additional capacity to transfer the load of the diagonal mechanism. Figure 5-45 displays the obtained pressure-deflection capacity curve, which shows a constant post-peak strength plateau for displacements varying from 0.003 m to 0.025 m. Griffith and Vaculik (2007) argue that this apparent “plastic” behaviour can be attributed to the redistribution of diagonal bending moment resistance along the diagonal cracks to horizontal bending moment resistance along the vertical edges at the return walls.

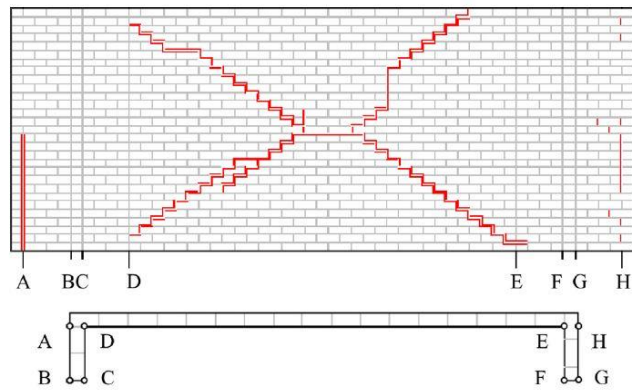


Figure 5-44. Damage pattern of the out-of-plane loaded masonry wall at the end of the test (Griffith and Vaculik 2007).

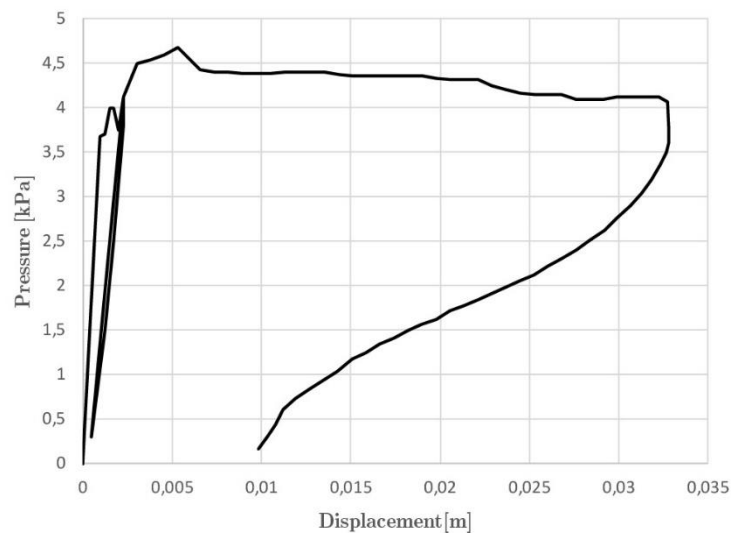


Figure 5-45. Experimental pressure-displacement capacity curve obtained for the out-of-plane loaded specimen (Griffith and Vaculik 2007).

5.5 Calibration of continuum models for masonry walls

5.5.1 Continuum finite element model for masonry structures

A FE continuum macro-mechanical modelling approach was adopted to analyse the structural behaviour of masonry subjected to in-plane and out-of-plane actions. Macro-models do not make any distinction between units and mortar, and masonry is simplified as a “continuous homogeneous material”, as explained in Roca et al. (2010).

The masonry FE models presented in the following sections were developed within the structural and earthquake engineering software SAP2000 (CSI 2016b). In this environment, shell elements are available to model the membrane and plate behaviour in planar or three-dimensional structures (CSI 2016a). The shell adopted in this thesis is a three or four-node formulation element (Figure 5-46a) which uses four-point numerical integration to compute the stiffness, and 2-by-2

Gauss integration points to evaluate the stresses, internal forces, and moments at the nodes. Figure 5-46b shows the positive internal stress definitions for a shell element.

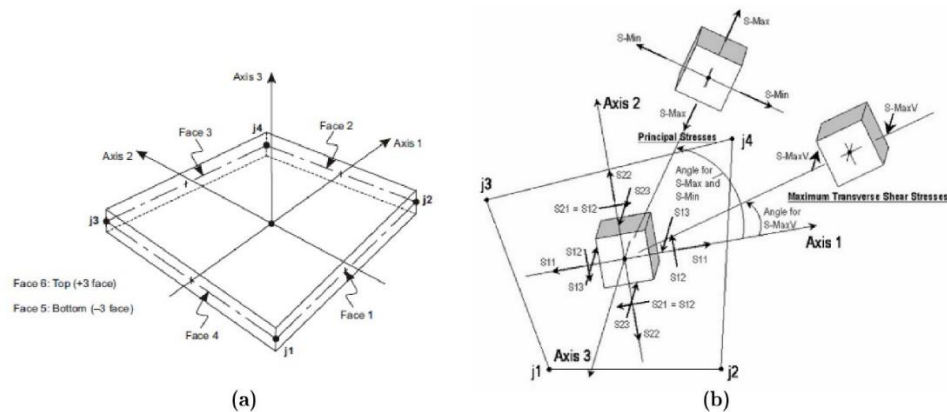


Figure 5-46 Shell definition in SAP2000: (a) four-node quadrilateral definition, and (b) positive direction of the internal stresses.

Shells can be homogeneous or layered elements, but nonlinear material properties can only be assigned to the latter in SAP 2000. Layered configurations allows any number of layers in the thickness direction of the element, where each of them must be defined considering an independent location, thickness, number of integration points, and material. Besides, the material behaviour must be determined for each of the three membrane stress components of a layer (σ_{11} , σ_{22} and, σ_{12} in Figure 5-46b), choosing between linear, nonlinear or inactive behaviour.

A two-dimensional nonlinear concrete material model is available for shell element applications in SAP2000. This model is based on the theories of Darwin-Pecknold (Darwin and Pecknold 1974, 1977) and Vecchio-Collins (Frank J. Vecchio and Collins 1986), which represent the concrete compression cracking and the shear behaviour under both monotonic and cyclic loading, considering a stress-strain constitutive model (CSI 2016a). Because the shear strength of a wall may depend substantially on the axial forces and bending moments, the Darwin-Pecknold model attempts to directly represent this coupling interaction. A co-axially rotating smeared crack model considers both cracking and crushing of the material. This model is considered appropriate for the applications to quasi-brittle materials like concrete and masonry.

The initial material axes are fixed relative to the wall element at the beginning of the analysis with nonlinear shell elements, as shown in Figure 5-47a. Figure 5-47b shows the normal and shear stresses components in the element, whereas Figure 5-47c shows the principal material axes that are parallel to the principal stress directions. The key assumption of the Darwin-Pecknold model is that uniaxial stress-strain relationships can be defined along each of the principal material axes. It is important to note that although the shear stress is zero in the principal material axes, the shear modulus is not zero. Therefore, when a strain increment is applied, the change in shear stress generally will not be zero. During the analysis, the principal stress directions, and hence the principal material axes, can rotate progressively. For this condition

of the model, the effective stress-strain relationships in the principal material axes are obtained by interpolating between the relationships in the axes of the previous step.

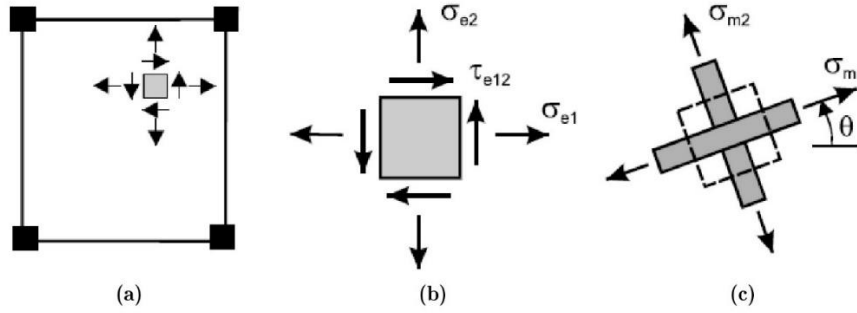


Figure 5-47. Initial and principle material axes of a shell element in SAP2000: (a) Finite Element with stress components at a point (b), and (c) material axes.

A stress-strain relationship of the material must be introduced to determine the nonlinear behaviour of shell elements. Annex B describes in detail the analytical formulation of the Darwin-Pecknold model defined in SAP2000, both considering the definition of the stress-strain curve and the theoretical base that explains how the material model works.

For isotropic materials, the stress-strain relationship represents the behaviour along each of the three axes, $\sigma_{11} - \varepsilon_{11}$, $\sigma_{22} - \varepsilon_{22}$, and, $\sigma_{33} - \varepsilon_{33}$. Both the tensile and compressive side of the stress-strain curve must be determined from each other following Equation (5-18):

$$\sigma_{ii}(\varepsilon_{ii}) = \begin{cases} \sigma_T(\varepsilon_{ii}), & \varepsilon_{ii} \geq 0 \\ \sigma_C(\varepsilon_{ii}), & \varepsilon_{ii} \leq 0 \end{cases} \quad (5-18)$$

Where $\sigma_T(\varepsilon)$ represents tensile behaviour, and $\sigma_C(\varepsilon)$ represents compressive behaviour subjected to the following restrictions:

$$\begin{aligned} \sigma_T(\varepsilon) &\geq 0, & \sigma_T(0) &= 0 \\ \sigma_C(\varepsilon) &\leq 0, & \sigma_C(0) &= 0 \end{aligned} \quad (5-19)$$

The shear stress-strain curve is computed internally from the direct axial stress-strain curve introduced by the user in SAP2000. The assumption is made that shearing behaviour can be computed from tensile and compressive responses acting at 45° to the material using Mohr's circle in the plane. For isotropic materials, the shear relationship is obtained from Equations (5-20) and (5-21).

$$\sigma_{ij}(\varepsilon_{ij}) = \begin{cases} \sigma_S(\varepsilon_{ij}), & \varepsilon_{ij} \geq 0 \\ -\sigma_S(\varepsilon_{ij}), & \varepsilon_{ij} \leq 0 \end{cases} \quad (5-20)$$

Where,

$$\sigma_S(\varepsilon_{ij}) = \frac{1}{4} (\sigma_T(\varepsilon_{ij}) - \sigma_C(-\varepsilon_{ij})), \quad \varepsilon_{ij} = \frac{1}{2} \gamma_{ij} \geq 0, \quad i \neq j \quad (5-21)$$

For frictional materials, friction and dilatational angles must be defined. The friction angle, ϕ , takes values $0 \leq \phi < 90^\circ$. For shear values different from zero, the stress is computed primarily using a directional model having linear stiffness up to a limiting stress given by:

$$|\sigma_{12}| \leq \tan \phi = \begin{cases} 0, & \sigma \geq 0 \\ -\sigma & \sigma < 0 \end{cases} \quad (5-22)$$

Where,

$$\sigma = \frac{1}{2} (\sigma_{11} + \sigma_{22}) \quad (5-23)$$

Compression values are necessary to derive the shear strength using Equation (5-23). Additionally, the cohesion is evaluated using Equation (5-21), but considering only the contribution to shear due to tension:

$$\sigma_s(\varepsilon_{12}) = \frac{1}{4} \sigma_T(\varepsilon_{12}), \quad \varepsilon_{12} = \frac{1}{2} \gamma_{12} \geq 0 \quad (5-24)$$

Where ε_{12} and γ_{12} are the direct and shear strains, respectively.

5.5.2 Numerical simulation of experiments on an in-plane loaded masonry frame

This section presents the numerical simulation of the URM wall tested under in-plane actions by Augenti et al. (2011) described in Section 5.4.1. The model attempted to reproduce the same geometry, boundary and loading conditions of the experiment, as shown in Figure 5-48. Modelling of the wooden lintel lying over the opening of the wall was neglected in this study. The wall was modelled using layered shell elements with a mesh composed of rectangular components of approximately $0.20 \times 0.28 \text{ m}^2$, with a total number of 258 finite elements, as shown in Figure 5-48. The section of the element was defined with only one layer of 0.31 m thickness, and four integration points along the thickness direction. The masonry material was defined as nonlinear for all its three membrane stress components, σ_{11} , σ_{22} and σ_{12} . The constitutive law considered an isotropic material with the linear elastic properties of masonry (summarized in Table 5-23), and the stress-strain nonlinear deformation relationship shown in Figure 5-49. The compressive part of the uniaxial stress-strain curve, represented by a parabolic law (Figure 5-49a), was determined considering the analytical model proposed by Turnšek and Sheppard (1998) and Kaushik, Rai, and Jain (2007) as described by Equation (5-25):

$$\frac{f_m}{f'_m} = A \frac{\varepsilon_m}{\varepsilon'_m} - B \left(\frac{\varepsilon_m}{\varepsilon'_m} \right)^C \quad (5-25)$$

Where f_m and ε_m are the compressive stress and strain in masonry respectively, and f'_m is the peak stress corresponding to the strain ε'_m . A, B, and C are coefficients describing the shape of

the curve. These coefficients have been experimentally calibrated by different authors. Kaushik, Rai, and Jain (2007) proposed to assume $A=2$, $B=1$ and $C=2$, while Turnšek and Sheppard (1998) proposed to consider $A=6.4$, $B=5.4$ and $C=1.17$.

As proposed by Kaushik, Rai, and Jain (2007), the ultimate displacement of the curve was determined considering it equal to $2.75 \varepsilon'_m$, for walls bonded with lime mortar. The tensile behaviour of masonry (Figure 5-49b) was defined considering a linear response until the peak tensile stress (f_t), which was estimated as 3.5% of the masonry compressive stress (0.135 MPa). The strain at the peak tensile stress (ε'_t) was assumed as 0.06‰, after executing sensitivity analyses.

Table 5-23. Mechanical properties of the masonry of the in-plane masonry model.

Material	Compressive strength f_c (Mpa)	Young's modulus E (GPa)	Shear modulus G (GPa)	Poisson's ratio ν
Tuff masonry	3.96	2.22	0.92	0.2

Shear strength of masonry is automatically computed from the axial stress-strain relationship in SAP2000 as explained in Section 5.5. Besides, the Coulomb friction model is considered as follows:

$$\tau = c + \sigma \tan \varphi \quad (5-26)$$

Where c is the cohesion, σ is the normal stress and $\tan \varphi$ is the friction coefficient. According to D'Ambra, Lignola, and Prota (2016), a friction angle equal to 23° was used to define the shear model, as also recommended by Eurocode 6 (CEN 2005b) for this masonry typology.

All the nodes at the base of the model were restrained in all the translational DOFs simulating the rigid support conditions of the experiment. An extra element was modelled at the left side of the wall to avoid unrealistic stress concentrations in this area due to the application of the lateral displacement on top, as shown in Figure 5-48. A vertical pre-compression of 200 kN was applied at each pier of the wall, followed by a lateral displacement of 0.03 m applied at a height of 3 m on the left side of the wall. NSA was performed considering two load patterns, both for vertical pre-compression and lateral displacement applications. The displacement was gradually applied in 6000 loads steps and monitored under prescribed displacement control.

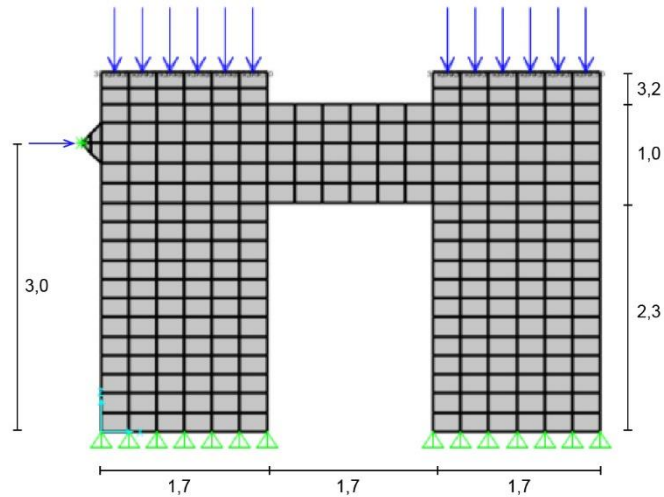


Figure 5-48. FE model of the in-plane loaded masonry wall tested by Augenti et al. (2011) (dimensions in m).

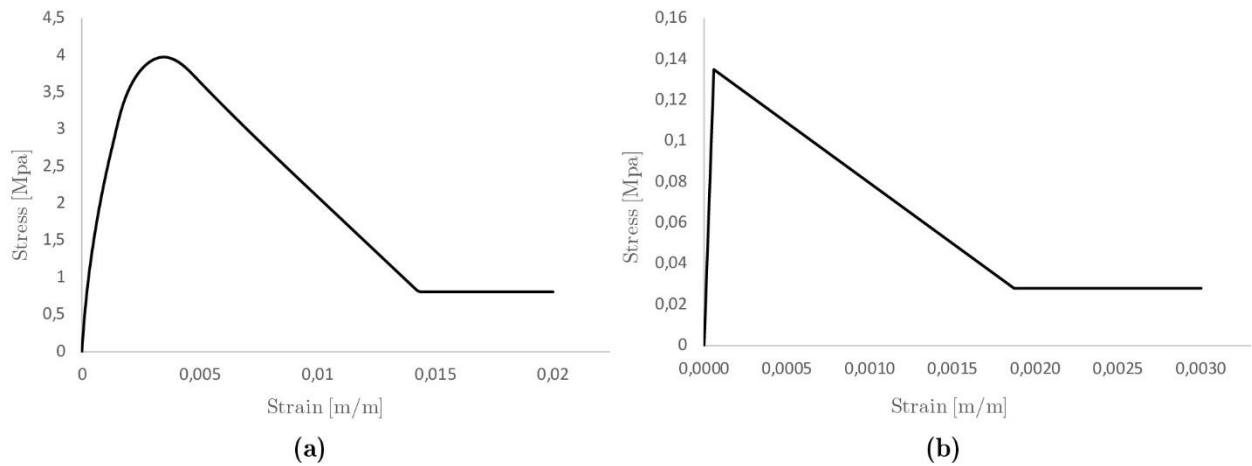


Figure 5-49. Stress-strain uniaxial relationships for masonry: (a) compressive and (b) tensile behaviours.

The capacity curve of the model depicted in Figure 5-50 shows that the initial stiffness of the wall was well predicted by the model. However, the maximum capacity and ultimate displacement were highly underestimated. The same result was obtained by D'Ambra, Lignola, and Prota (2016), who said that this difference is mainly due to the rocking phenomenon exhibited for the wall, which is not correctly captured by the material model. The masonry stress-strain relationship of Figure 5-49 can only simulate the initial stage of the analysis, including the elastic part and the first damage propagation after the formation of cracks at the piers, and the analysis cannot capture the subsequent development of the failure mechanism occurred in the experiment. A higher strain deformation capacity is required to achieve greater deformations of the model without increasing the strength capacity. According to D'Ambra, Lignola, and Prota (2016), this behaviour can be obtained by incrementing artificially the peak strain value, as shown in Figure 5-51. This simplification allowed the model to reproduce correctly the rocking behaviour due to

the base rotation of the piers in the experiment. An alternative approach to reproduce correctly the test results by advanced numerical simulation is addressed in-depth in Saloustros et al. (2017).

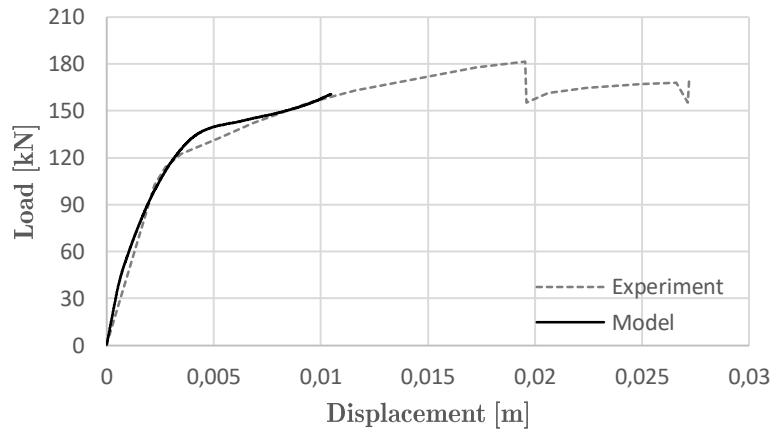


Figure 5-50. Experimental vs. numerical capacity curves of the in-plane loaded masonry wall using the material nonlinear relationship defined in Figure 5-49.

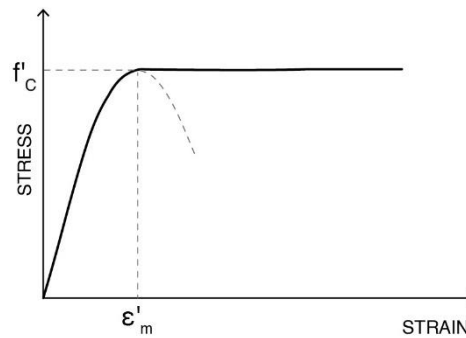


Figure 5-51. Simplified compressive stress-strain relationship for the masonry material of the in-plane loaded masonry wall as proposed by D'Ambra, Lignola, and Prota (2016)

Figure 5-52 displays the load-displacement capacity curve obtained using the simplified material model. In the curve, the local failure mechanisms occurring during the analysis are highlighted with the instances A to D. The results revealed a good match compared to the experiment in terms of global stiffness, maximum and ultimate capacity of the wall, which reached a maximum capacity of 180.8 kN, presenting a slight error of 0.4%. The initial stiffness was estimated as 4.35×10^4 kN/m having a difference of 5.9% with the experiment.

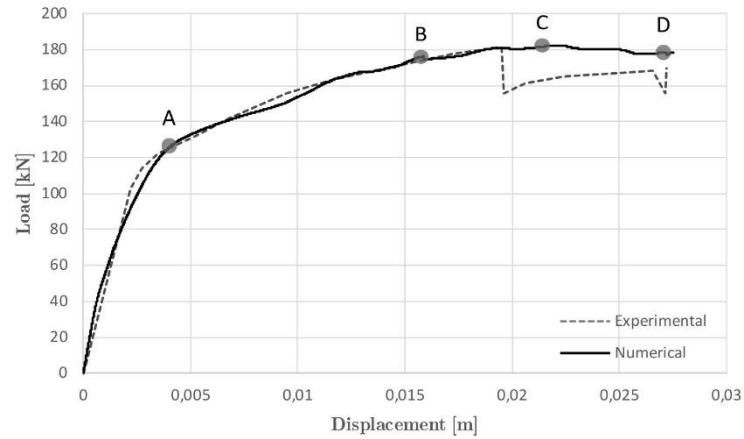


Figure 5-52. Experimental vs numerical capacity curves of the in-plane loaded masonry wall using the material nonlinear relationship defined in Figure 5-51.

Figure 5-53 shows the principal compressive stress contours corresponding to the instances highlighted in Figure 5-52Figure 5-50, suggesting the formation of the resistant mechanism characterized by diagonal struts at the piers and the central spandrel, whereas significant compressive stress is registered at the base of the pier. Figure 5-54 shows the principal tensile strain contours indicating the development of the cracking damage throughout the instances A-D of Figure 5-52. Cracking at the centre of the spandrel and at the base of the piers appear at Instance A, followed by diagonal cracking development in both spandrel and piers in instances B and C. This mechanism also occurred in the experiment at a displacement of 0.019 m. After the wall reached its maximum strength at instance C, the stiffness of the frame slightly decreased, and the model could not capture the resistance drop of 15% observed in the experiment.

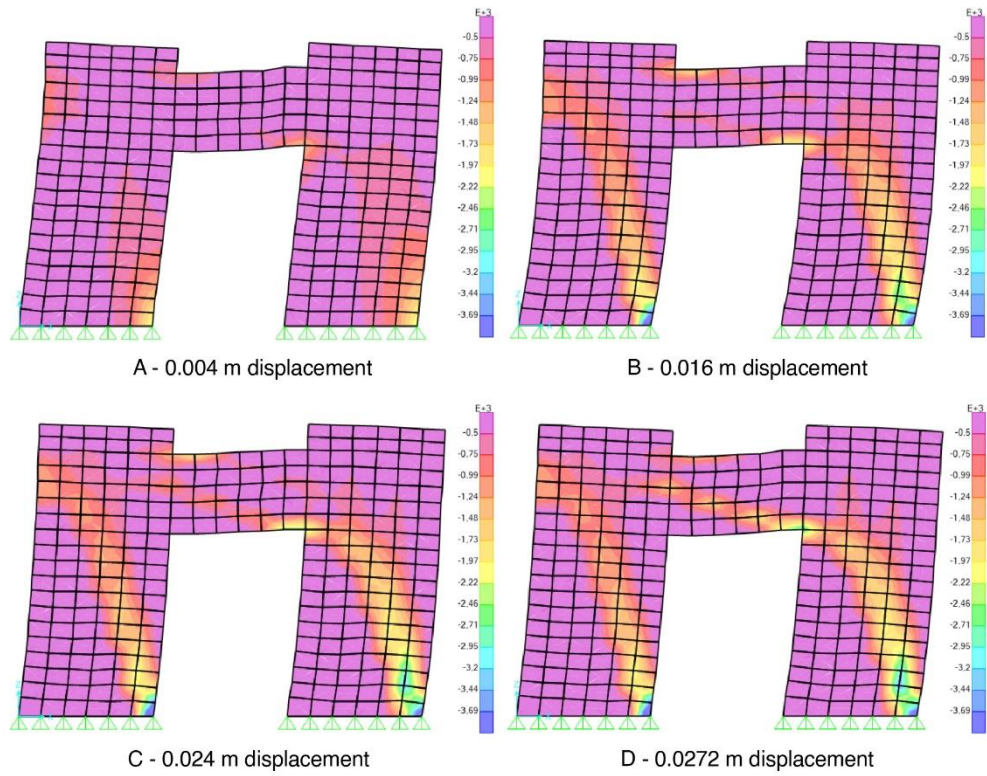


Figure 5-53. FE results of the in-plane loaded masonry: principal compressive stress contour at the stages of the analysis highlighted in Figure 5-52.

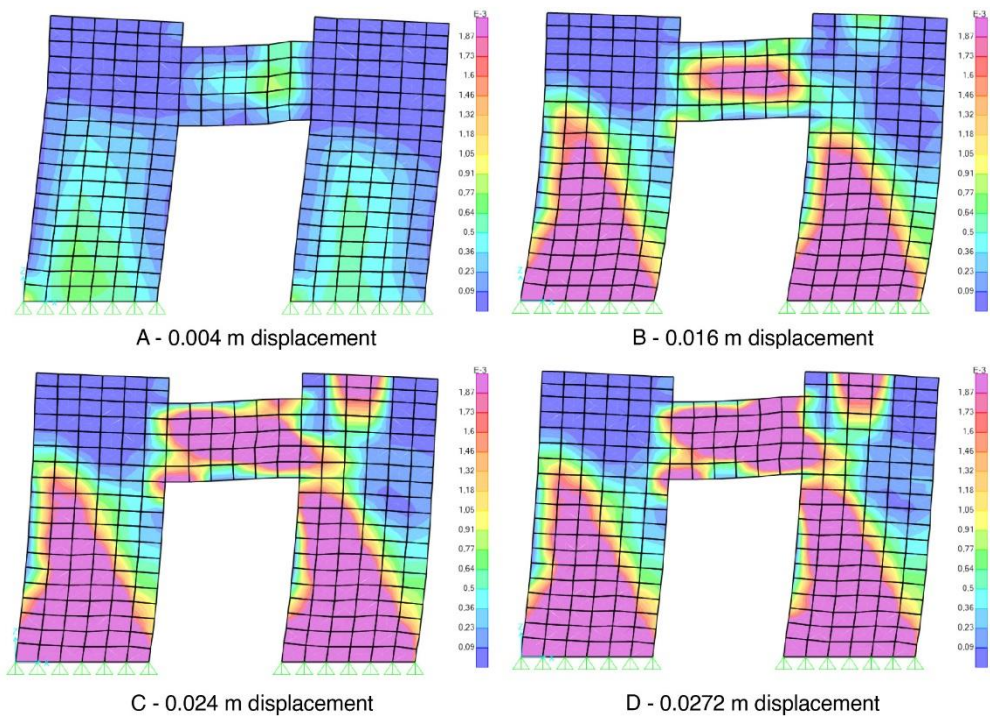


Figure 5-54. FE results of the in-plane loaded masonry: principal tensile strain contour at the stage of the analysis highlighted in Figure 5-52.

5.5.3 Numerical simulation of experiments on out-of-plane loaded masonry walls

The nonlinear analysis of the out-of-plane behaviour of masonry using FEM needs an accurate definition of the elements, as well as of the modelling parameters. Due to this, preliminary tests were developed to calibrate the model in the software SAP2000. The parameters of study were the number of shell elements (mesh refinement), and the number of integration points (IP) along the element's thickness direction. Such parameters control the precision of the results, but also determine the computational costs of the analysis. Therefore, preliminary linear static analyses (LSA) of URM walls aimed to determine the convergence to the "exact" results derived from analytical solutions. Then, nonlinear static analyses (NSA) were executed. Once an optimal model calibration was reached, it was used to develop the numerical simulation of the wall tested under out-of-plane actions by Griffith and Vaculik (2007).

The parametric analyses started with the model of a wall subjected to a uniformly distributed load of 3 kPa on its surface, as shown in Figure 5-55a. This model can be simplified by modelling only a transversal slice of the wall. Figure 5-55b shows the boundary conditions of the wall, which was simply supported at the top (vertical roller), fixed at the base, and free at the two lateral sides. First, the mesh refinement was studied by increasing the number of elements from 10 to 60. These elements had square areas, making the width of the element variable from $0.20 \times 0.20 \text{ cm}^2$ to $0.03 \times 0.03 \text{ m}^2$, i.e. turning the wall narrower as the number of elements increases. The thickness of the wall was 0.4 m. Table 5-24 presents the material properties assumed for the wall. The Poisson's ratio was considered zero in order to avoid strains in the in-plane direction of the wall. The compressive stress-strain material model was assumed to be linear elastic, and the self-weight of the wall was not considered. A friction angle ϕ equal to 23° was used to define the shear model, as recommended by Eurocode 6 (CEN 2005b) for this masonry typology.

Five LSA were executed on different models having 10, 20, 30, 40 and 60 elements. The analytical solution of each case was derived from the well-known Timoshenko Beam Theory. The maximum displacement and the minimum stress captured by the model were measured at the maximum deflection point, at $3/5$ of the span of the wall, while the maximum stress was controlled at the base of the model. Figure 5-56 shows the maximum displacement reached by the models compared to the analytical solution. The results demonstrated that the models configured with less than 30 elements were not able to capture the actual behaviour of the wall, either in terms of maximum displacements or in terms of stresses (Figure 5-57).

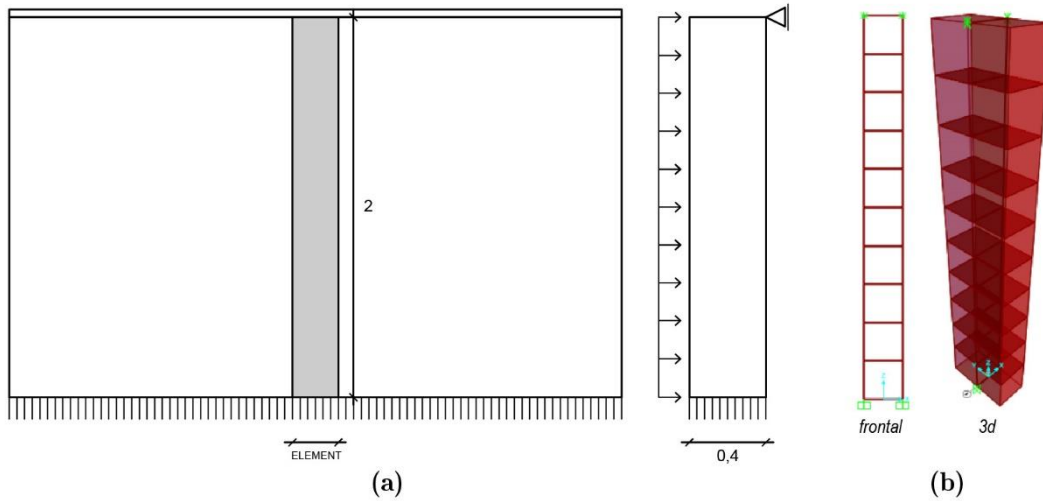


Figure 5-55. Out-of-plane loaded masonry wall: (a) geometry (modelled part in grey) and (b) shell FE model configuration.

Table 5-24. Material properties of the FE model of the out-of-plane loaded wall.

Young's Modulus E	5	GPa
Poisson's ratio ν	0	
Density ρ	1800	kg/m ³
Tensile strength f_t	0,50	MPa
Fracture energy G_f	200	Nm/m ²

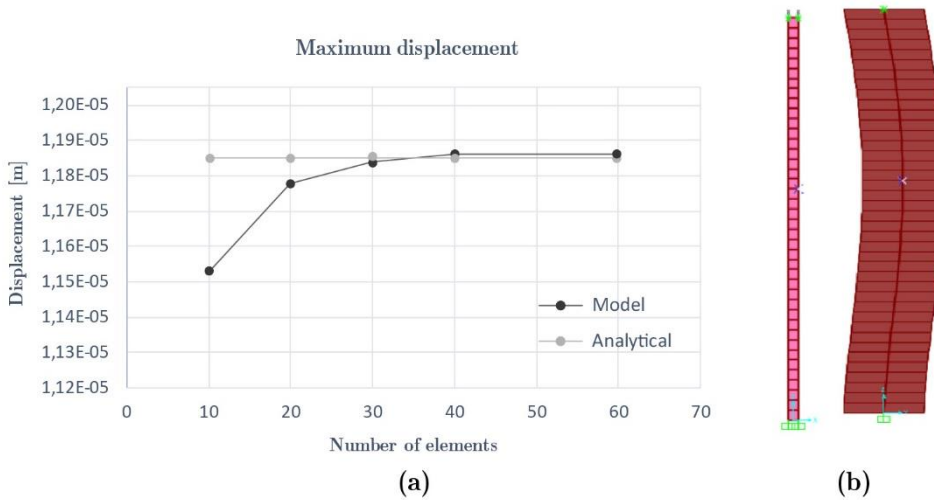


Figure 5-56. Results of the out-of-plane loaded wall: (a) convergence of the maximum FE displacement and (b) deformation of the forty element FE model.

The number of IPs along the thickness direction of the shell elements was examined by running nonlinear analyses. Four different models constituted by 10, 20, 40, and 60 elements were studied by considering 4, 9, 18 and 32 IPs. Each layer of the layered section properties admits only 5 IPs in SAP2000, thus the number of layers should increase to evaluate higher IP into the model. The obtained results confirmed that the models with less than 30 elements were not able to reproduce

the nonlinear response properly, as can be noted in Figure 5-58a. The number of IPs contributed only to smooth the curves and did not influence the global capacity of the wall, as can be noted in Figure 5-58b. The results evidenced that the number of elements configuring the mesh governed the accuracy of the out-of-plane results, while the number of IPs along the thickness direction plays a secondary role. Consequently, the mesh refinement in a FE of a wall must be carefully determined to balance both the number of elements and their size.

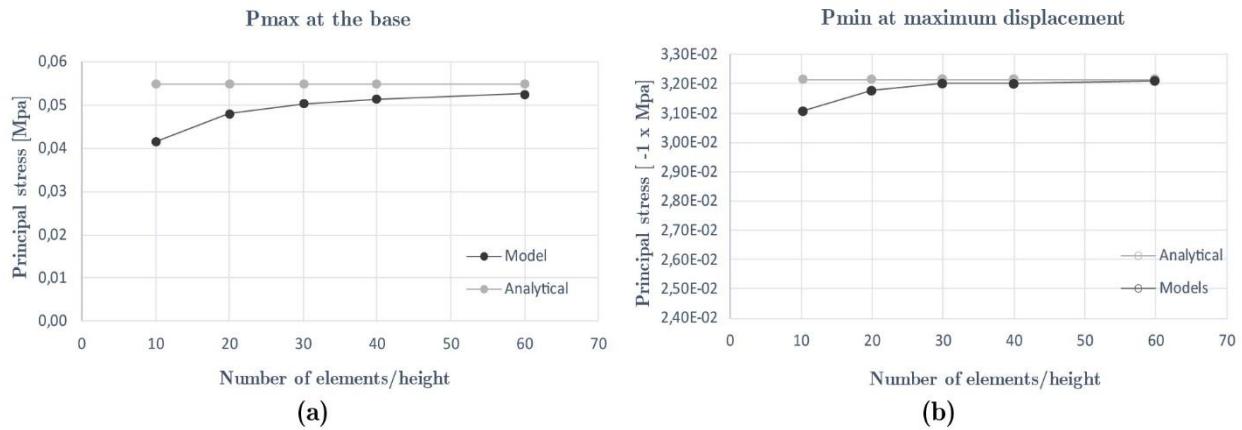


Figure 5-57. FE results of the out-of-plane loaded wall: convergence of the principal stress of the models measured at (a) the base of the model and (b) the maximum displacement point.

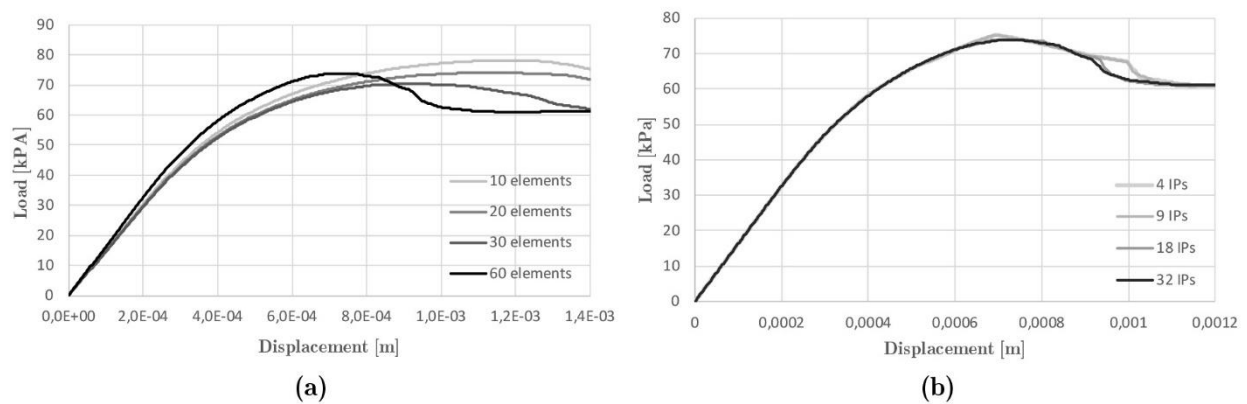


Figure 5-58. FE results of the out-of-plane loaded wall: (a) with 32 IPs and different number of elements and (b) 60 elements and different number of IPs.

A similar parametric analysis was performed considering a masonry panel based on the experimental campaign carried out by Gazzola (1985), and analysed also by Lourenço (2000) and Zalat (2015). Since this wall had a symmetrical configuration, only half of the panel was modelled by assuming appropriate symmetric boundary conditions, as shown in Figure 5-9. The base, top and right edges of the wall were simply supported by restraining the out-of-plane node translation. The left edge had symmetrical supports, where the in-plane horizontal translation and the out-of-plane rotations were fixed. The material of the wall was modelled assuming the same properties of the previous case (see Table 5-24), except for the fracture energy equal to 400 Nm/m². A

friction angle ϕ equal to 23° was considered to determine the shear model. The mesh refinement was studied considering four element sizes (h) corresponding to sections $775 \times 10^{-4} \text{ m}^2$, $180 \times 10^{-4} \text{ m}^2$, $140 \times 10^{-4} \text{ m}^2$, and $72 \times 10^{-4} \text{ m}^2$. The influence of the IPs along the thickness direction of the wall was examined considering 4, 9, and 18 IPs for each mesh size. LSA was carried out to study the displacement and stress convergence of the model. Figure 5-60 compares the results of the maximum displacement and stress reached by the model, measured at the centre of the panel. The results shown minimal differences between the fine and coarse mesh both in maximum displacement and stress, which is lower than 4.3%.

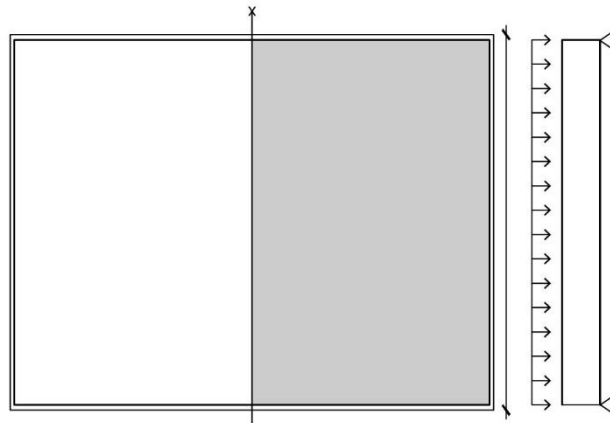


Figure 5-59. Geometry of the wall tested by Gazzola (1985) with the modelled part in grey.

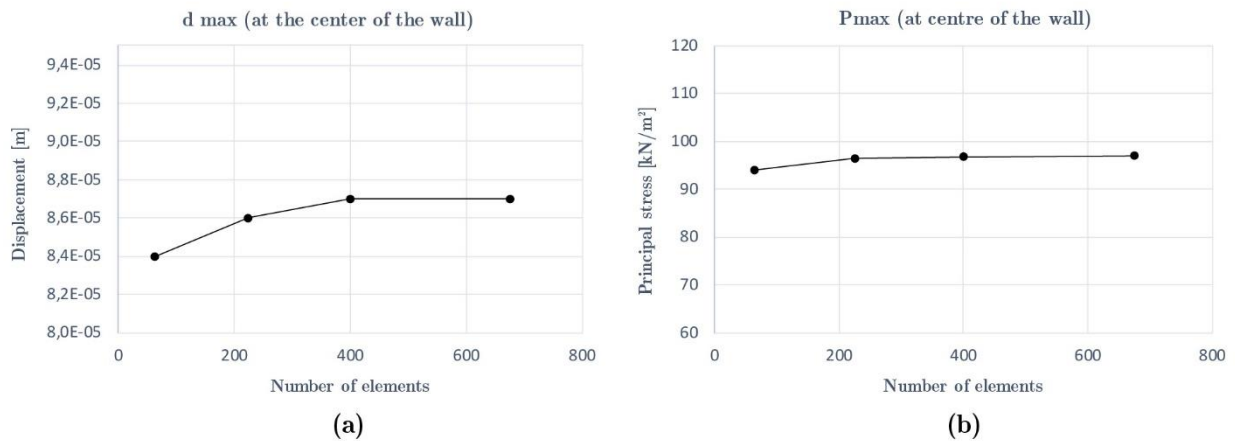


Figure 5-60. Linear elastic results of wall model.

NSA under displacement control was performed to study the influence of the mesh refinement and of the through-thickness IPs on the nonlinear response of the model. The results in Figure 5-61a show that the models with less than 64 elements were not able to capture accurately the nonlinearities. However, very small differences in terms of initial stiffness and peak load is recorded by using different mesh sizes. As can be seen from Figure 5-61b, there was a slight difference in terms of capacity between the 4 to 9 IPs models, whereas the increment from 9 to 18 IPs does not have a major influence on the out-of-plane response of the wall. The model

showed the typical response of walls subjected to out-of-plane loads, where cracking started to appear at the mid-height of the bottom face of the panel, as shown in Figure 5-62a. According to Lourenço (2000), predominant cracking occurred in the shorter span direction of the panel up to the peak load, which corresponds to higher bending moments and lower tensile strengths. After the peak load, the typical yield-line type of collapse appears with marked softening lines. The results obtained are consistent with those shown in Figure 5-62c that were obtained by Lourenço (2000) at the ultimate pressure.

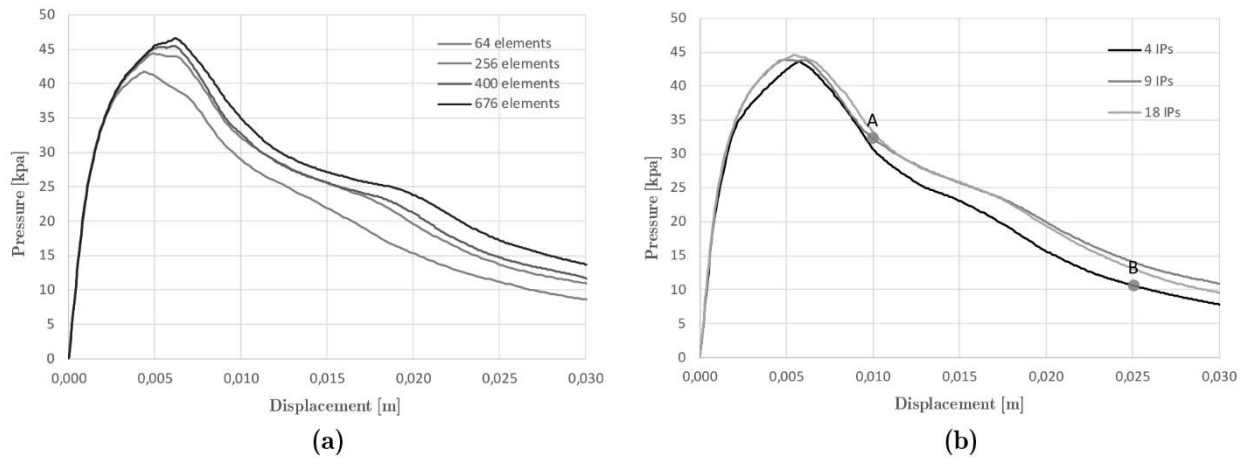


Figure 5-61. Results of the sensitivity analyses of Wall 2 FEM model considering: (a) a mesh refinement in the model with 9 IPs and (b) different IPs in the model of 676 elements.

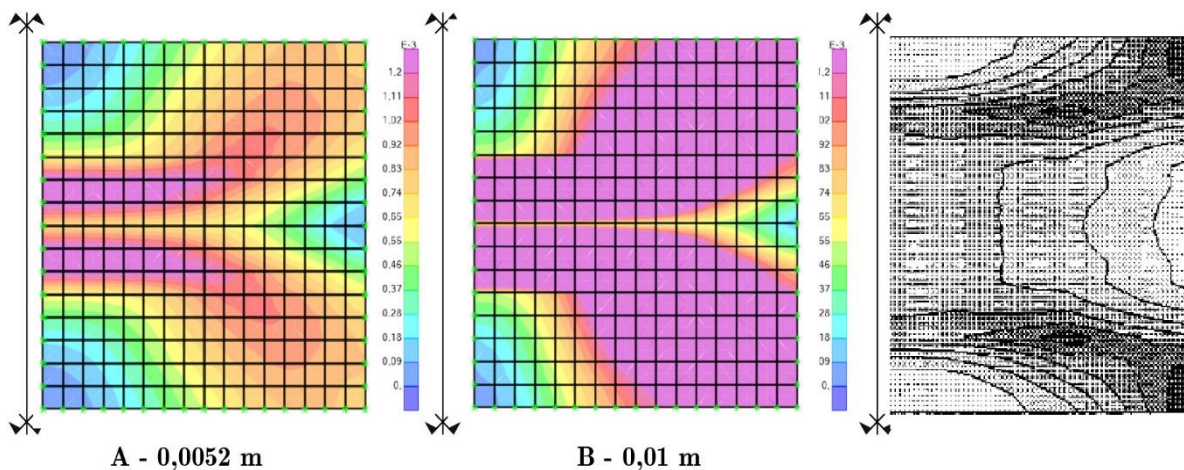


Figure 5-62. FE results of the wall: principal strain contours in the bottom face at the (a) peak load, and (b) post peak, referring to the instances shown in Figure 5-61b. (b) Plastic strain at the ultimate pressure obtained by Lourenço (2000).

The last numerical simulation is the URM wall tested under out-of-plane actions by Griffith and Vaculik (2007). Petracca et al. (2017) provided an in-depth analysis of this complex experiment, by developing sophisticated computations based on micro-modelling and multi-scale modelling. This thesis adopts a simplified modelling instead, and explores the capability of the

selected continuum FE macromodel to reproduce the experimental test. The calibration results from the previous parametric study were taken into account. The numerical model attempted to reproduce the experimental behaviour of the wall by replicating its boundary and loading conditions, as shown in Figure 5-63. Given the symmetrical layout of the wall, only the left part of the panel was modelled considering appropriate symmetrical boundary conditions. The base and top edges of the panel were simply supported by fixing the out-of-plane DOFs. The vertical edge of the return wall was fixed in all the DOFs, and a symmetry axis along the right edge considered fixed horizontal translation, as well as the out-of-plane rotations.

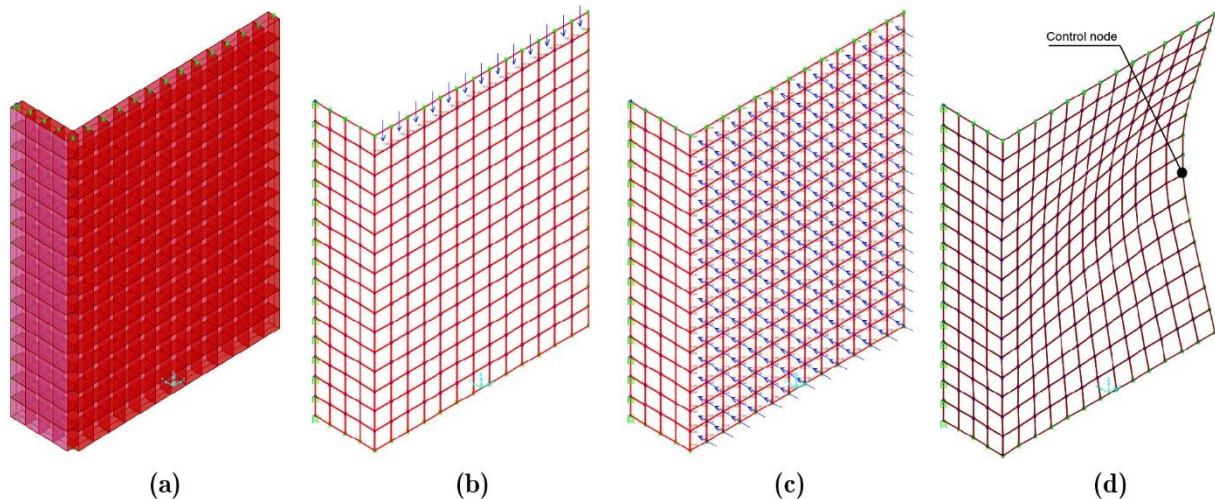


Figure 5-63. FE results of out-of-plane loaded masonry wall tested by Griffith and Vaculik (2007): (a) geometry, (b) surface pressure, (c) vertical pre-compression and (d) deformation.

The section of the wall is 0.11 m, set with two shell layers of 0.055 m thickness and a total of 10 IPs along the thickness direction. The masonry material was defined as nonlinear for all of the three membrane stress components of the layer, σ_{11} , σ_{22} and σ_{12} . A friction angle ϕ equal to 23° was considered to describe the shear model. The model is composed of 300 elements of $0.15 \times 0.15 \text{ m}^2$ size.

Due to the nonlinear nature of the problem, a plastic stress-strain constitutive law defined the behaviour of the material model, based on the mechanical properties summarized in Table 5-25. The compressive behaviour of masonry was described by means of the analytical model of Equation (5-25), proposed by Kaushik, Rai, and Jain (2007), that is shown in Figure 5-64a. The tensile behaviour was represented by the bilinear stress-strain relationship shown in Figure 5-64b. The curve is composed by an elastic branch up to the maximum tensile strength f_t , defined as the 2% of f_c . The tensile fracture energy of the model G_f was set equal to 0.04 kN/m based on sensitivity analysis in order to find an agreement with experimental results. The residual tensile strength was set equal to 50% of f_t . Such rather high value was derived from a careful sensitivity analysis, as lower values for this parameter were not able to represent correctly the post-peak experimental behaviour. According to Griffith and Vaculik (2007), the definition of a proper post-peak strength plateau is meaningful for the case of simply supported out-of-plane loaded walls.

Petracca et al. (2017) also highlighted an “apparent” plastic behaviour of the wall tested by Griffith and Vaculik (2007), with an almost constant post-peak strength plateau, as will be discussed in the following. Therefore, the assumed rather high value of the residual strength is motivated by the need of ensuring the correct redistribution of stresses after the peak load and the development of the mechanism with yield-line type of failure.

Table 5-25. Masonry material properties of the model.

Tensile strength f_t	352	[kN/m ²]
Compressive strength f_c	17600	[kN/m ²]
Young’s modulus E	5.27×10^7	[kN/m ²]
Fracture Energy G_f	0.04	[kN/m]
Poisson’s ratio	0.2	-

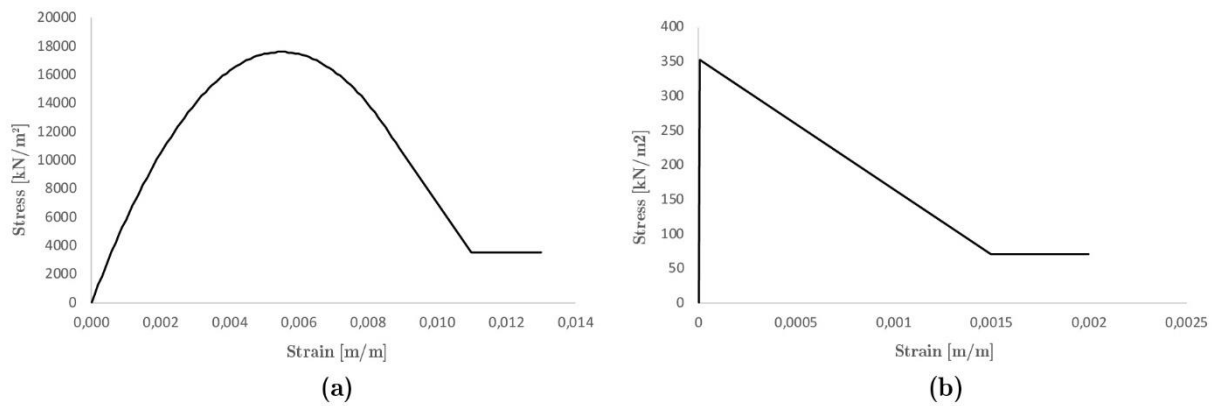


Figure 5-64. (a) Compressive and (b) tensile stress-strain relationship of masonry material for the out-of-plane loaded wall tested by Griffith and Vaculik (2007).

The analysis was developed in two steps. First, a vertical pre-compression of 100 kPa was applied at the top of the wall, followed by an out-of-plane pressure imposed to the outer surface of the main wall under displacement control. The deflection of the wall was measured at the centre of the wall, where the maximum displacement was expected, as shown in Figure 5-63d. Figure 5-5-65. shows the comparison between the experimental and the numerically calibrated pressure-deflection curve, evidencing a very good agreement.

Figure 5-66. shows the evolution of the principal tensile strains during different stages of the analysis. At the peak capacity (Instance A in Figure 5-5-65.), the model displays diagonal cracking developed an extensive damaged zone, together with a horizontal crack in the centre of the wall, in agreement with the experimental evidence (see Figure 5-44). Vertical cracking occurs also at the intersections of the return walls with the front one. As discussed by Griffith and Vaculik (2007), and highlighted also by Petracca et al. (2017), the apparent post-peak plastic behaviour shown in Figure 5-5-65. may be attributed to a full redistribution of bending moment along the diagonal cracks to horizontal bending along the vertical edges of the wall. The bending restraints

exerted by the return walls provided additional capacity against the transfer of load from the diagonal bending mechanism.

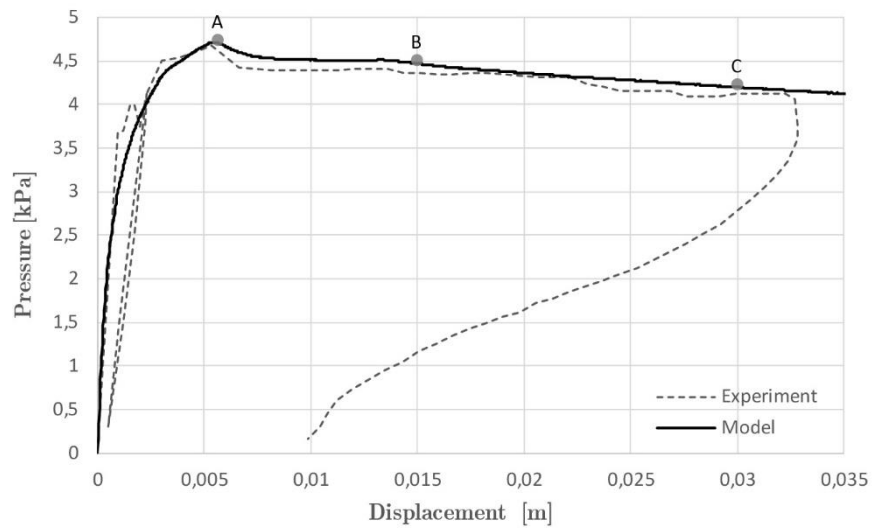


Figure 5-5-65. Experimental vs. numerical pressure-deflection curves of the out-of-plane loaded wall tested by Griffith and Vaculik (2007).

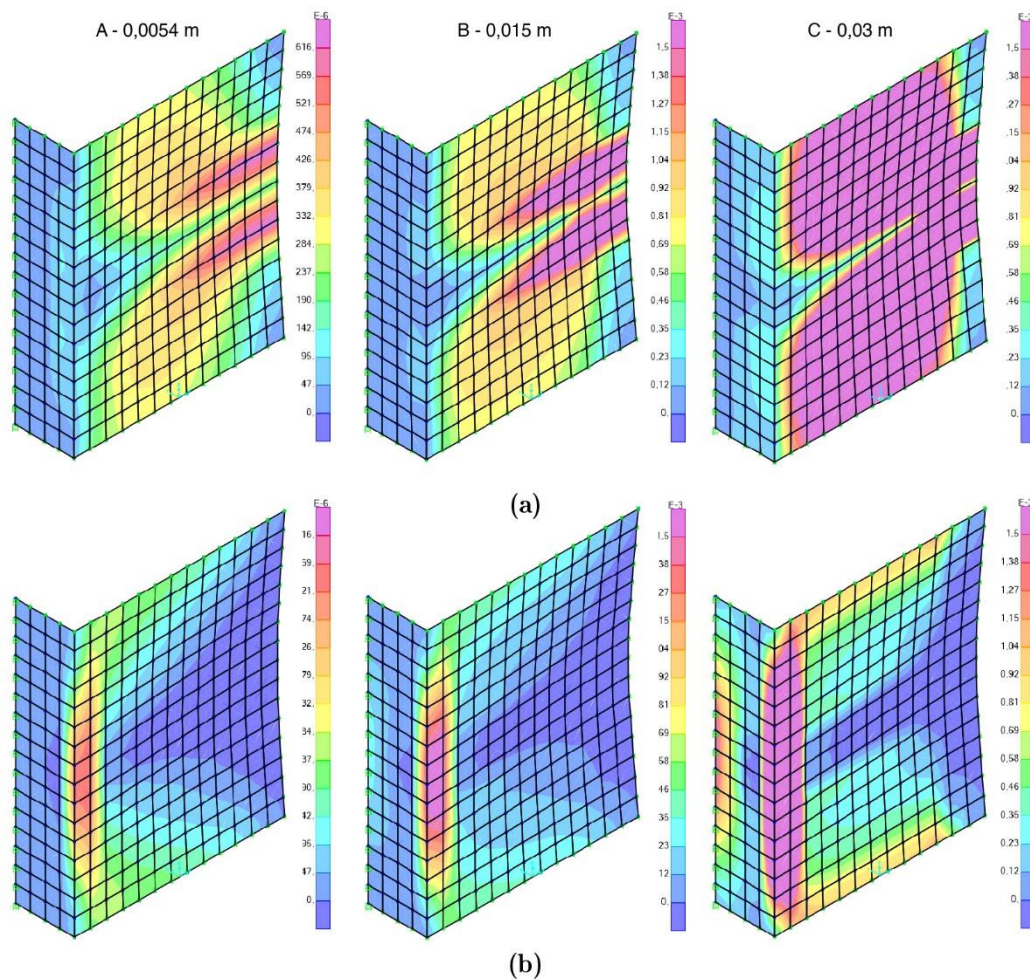


Figure 5-66. FE results of the out-of-plane loaded wall tested by Griffith and Vaculik (2007): principal tensile strain in the (a) bottom and (b) top faces measured at different instances A, B and C as shown in Figure 5-5-65.

It is worth noticing that more sophisticated computational strategies, like those adopted by Petracca et al. (2017), are certainly able to reproduce more accurately the experiments, thanks to their capability of modelling the complex behaviour of masonry even at the level of the interaction among the constituents (bricks and joints). However, the adopted continuum FE model shows to be able to represent correctly the development of the failure mechanisms and the load-displacement response. For this reason, it can be concluded the considered simplified approach can provide results that are worthy of consideration for large-scale analyses of masonry structures.

5.6 Summary

This chapter presented the calibration of simple lumped plasticity and continuum finite element (FE) models to represent the behaviour of timber and masonry structures. The proposed calibration methodology was based on the comparison between the numerical results and the evidence of benchmark experimental tests.

The lumped plasticity model (LPM) was used for the calibration of two timber frame typologies tested under lateral loads, i.e. the Portuguese “Pombalino” frames (Poletti 2013b; Poletti and Vasconcelos 2015) and the Peruvian “*quincha*” frames (Moore and D’Ayala 2011; Torrealva, Vicente, and Michiels 2018). The LPM calibrations considered two main parameters of study, i.e. the nonlinear behaviour of the connections, and the presence of infill. The former aspect was addressed through the definition of hinge and spring elements within the FE model, with proper moment-curvature or force-displacement nonlinear behaviours. The latter effect was simulated by applying the Equivalent Strut Method (ESM). Nonlinear static analysis (NSA) was applied to attain the results in terms of capacity curves and damage patterns. All the numerical simulations showed satisfactory results compared with the experimental evidence. The timber frame LPM represented accurately the local collapse of the connections occurred in the experiment, which allowed a good understanding of the global collapse and damage patterns of the investigated structures. The contribution of the infill was properly simulated by the ESM in a phenomenological and simplified manner, providing good agreement with the experiments in terms of global stiffness and capacity.

Two benchmark experiments were considered to calibrate the continuum macro-mechanical FE models of masonry, taking into account their in-plane (Augenti et al. 2011) and out-of-plane (Griffith and Vaculik 2007) nonlinear behaviours. Masonry was considered as a homogeneous material with average properties, defined by the constitutive model based on the theories of Darwin-Pecknold (Darwin and Pecknold 1974, 1977) and Vecchio-Collins (Frank J. Vecchio and Collins 1986). The masonry models were capable to reproduce correctly the results of the experiments in terms of maximum capacity and collapse mechanisms, both for the in-plane and out-plane loaded walls. The used smeared crack model allowed the correct identification of the overall damage mechanisms occurred in the tested walls.

Based on the good results derived from the simplified numerical approaches that have been explored in this chapter, it is possible to conclude that these calibrated tools can be applied to the analysis of timber and masonry buildings.

Chapter 6. Numerical modelling of hybrid timber-masonry building typologies of Valparaíso

6.1 Introduction

This chapter presents different applications of simple numerical modelling strategies capable of simulating the seismic behaviour of hybrid timber-masonry structures. The overall objective of this study is the definition of a simple but reliable structural analysis model for the study of the complex historical buildings located in the city of Valparaíso, Chile.

After the calibration of the Lumped Plasticity Models (LPM) for timber frames, and the continuum finite element (FE) models for unreinforced masonry (URM) walls, both presented in the Chapter 5, the study evaluates the compatibility of the two models working together. Two hybrid timber-masonry buildings existing in the city of Valparaíso (Chile) were modelled. The two selected cases of study are representative of the historical housing architecture of the city, and were previously characterized by Jimenez (2015). The mechanical properties of the materials were defined based on the available data for this specific typology. The behaviour of the connections was modelled based on the benchmark experiments analysed in Chapter 5, as they presented important similarities with those of Valparaíso.

Nonlinear static analysis (NSA) was applied under displacement control to determine the capacity and global failures of the models, built within the structural earthquake engineering software SAP2000 (CSI 2016b). Mass-proportional horizontal force distributions were applied in the two main directions of the buildings to simulate the effect of the earthquake actions. The results were plotted in terms of load-displacement capacity curves, showing the corresponding global failure mechanisms.

Section 6.2 presents the description and characterization of the buildings including both geometrical and structural features. Section 6.3 explains the main characteristics of the masonry and timber frame models. Section 6.4 presents the seismic analysis of the buildings, and Section 6.5 reports the evaluation of their seismic performance according to the seismic hazard of Valparaíso.

6.2 Description and characterisation of the buildings

The two selected cases of study were constructed between late 19th and early 20th century in the Cerro Alegre neighbourhood, within historical zone of the city of Valparaíso, Chile. Both buildings were designed and constructed using the same structural arrangement, as reported by Jiménez (2015), i.e. timber *platform frame* system combined with URM walls. The disposition of the structural elements, as well as the type of materials, connections, infill systems, and finishing are very similar in both cases. The main differences lie in the design and scale of the buildings.

Building 1 corresponds to a three-storey building dating back to 1909. It was designed by the architect *Juan Blezard*, as revealed in the original drawings shown in Figure 6-1. The building is located in the number 558 of the *Lautaro Rosas* street, with a central position in a building aggregate, as shown in Figure 6-2 and Figure 6-6a. The first and second levels of the building are 87.39 m², while the third level has the half of the built area and an exterior terrace (Figure 6-3). The structural system is composed of two main bays along the longest direction of the building, which are divided by perpendicular internal partitions distributing the rooms.

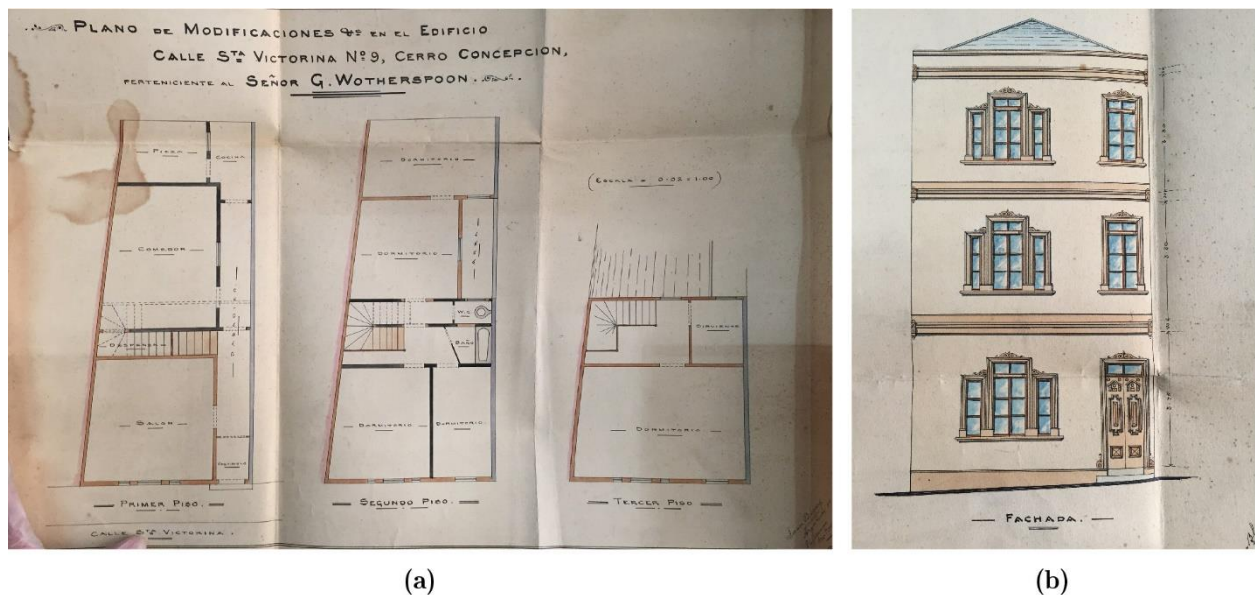


Figure 6-1. Original drawings of Building 1 located in the number 558 of the Lautaro Rosas street in the Cerro Alegre, (a) plans and (b) elevation. Source: *Registro Patrimonial de la Dirección de Obras Municipales de Valparaíso (DOM)*.



Figure 6-2. Building 1: north elevation (Jiménez 2015).

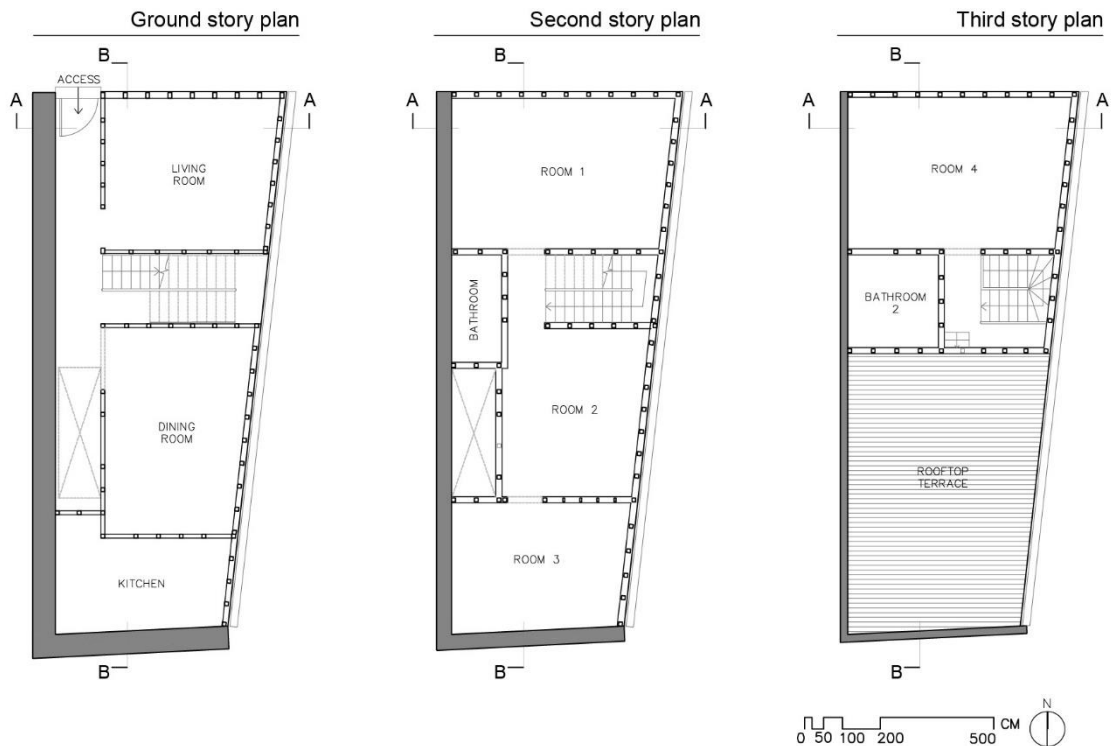


Figure 6-3. Building 1: plans (Jiménez 2015).

Building 2, shown in Figure 6-6b, is a two-storey building originally projected as a house but currently reformed for commercial use. The available data about the building were gathered when it was under restoration. This fact permitted a complete and detailed on-site inspection of the constructive system. The building is located in the number 167 of the *Paseo Dimalow* street, having a central position in an in-row aggregate of four buildings, as displayed in Figure 6-4. The date of construction is unknown, but it was possible to recognize the building in cartographic

drawings since 1879. The building presented regular shape both in plan and elevation, as can be observed in Figure 6-4 and Figure 6-5. The structural system has three bays, where the main one corresponds to a central corridor in-between the different rooms of the building.



Figure 6-4. Building 2: north elevation.

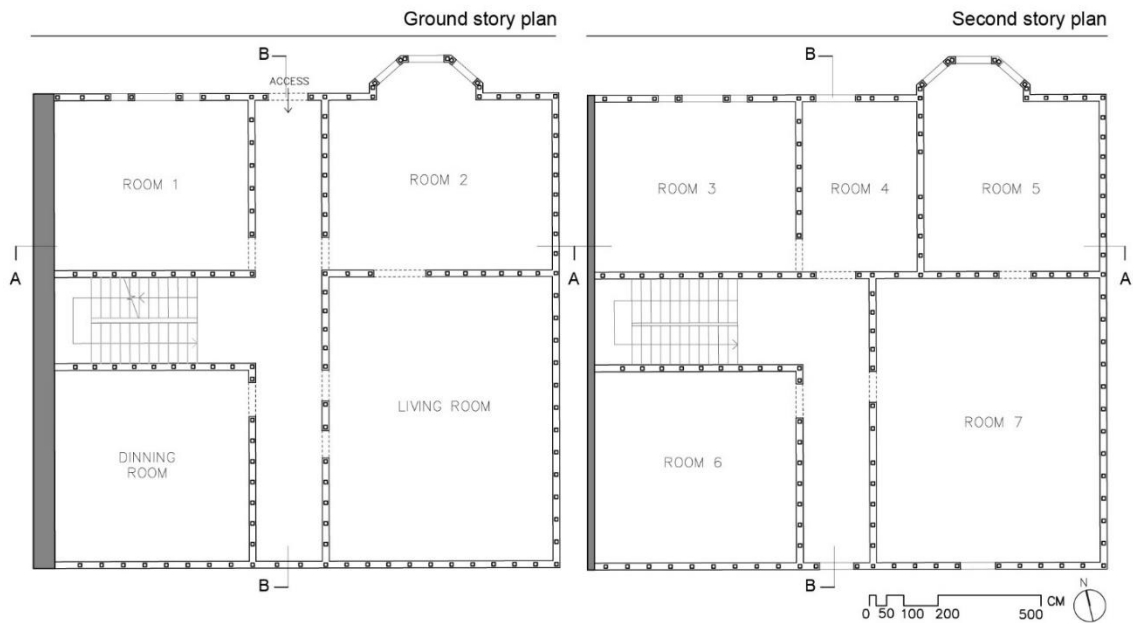


Figure 6-5. Building 2: plans

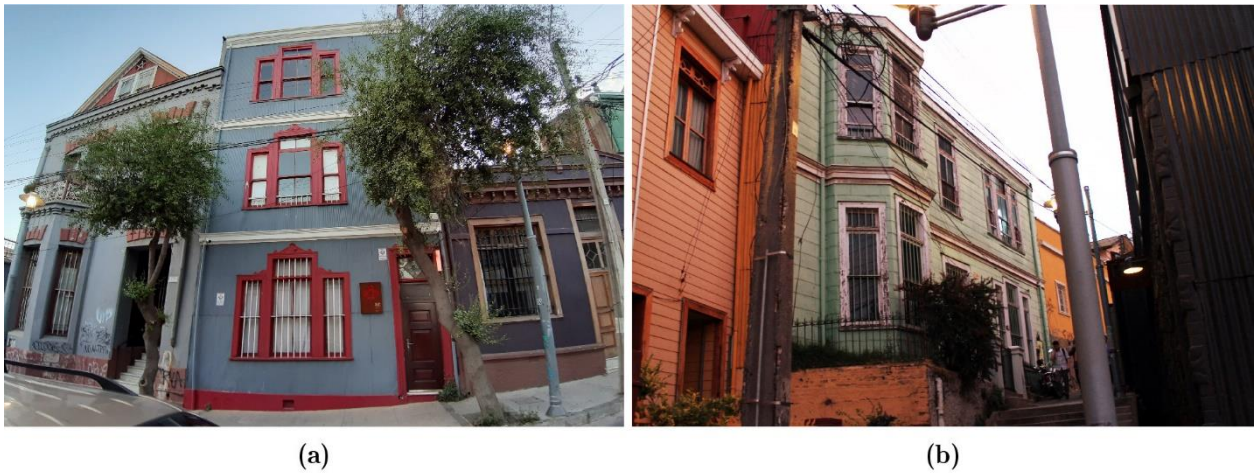


Figure 6-6. Cases of study in the Cerro Alegre neighbourhood: (a) Building 1, located at 558 *Lautaro Rosas* street, and (b) Building 2, located at 167 *Paseo Dimalow* street, Valparaíso, Chile.

Both cases are hybrid typologies composed of timber frames and URM walls. The timber frames are organised following the traditional *platform frame* configuration. This typology is composed of a light timber frame in which a storey platform is constructed at each floor. The studs for the next floor are usually erected on this platform with an intervening soleplate, as shown in Figure 6-7 and Figure 6-8.

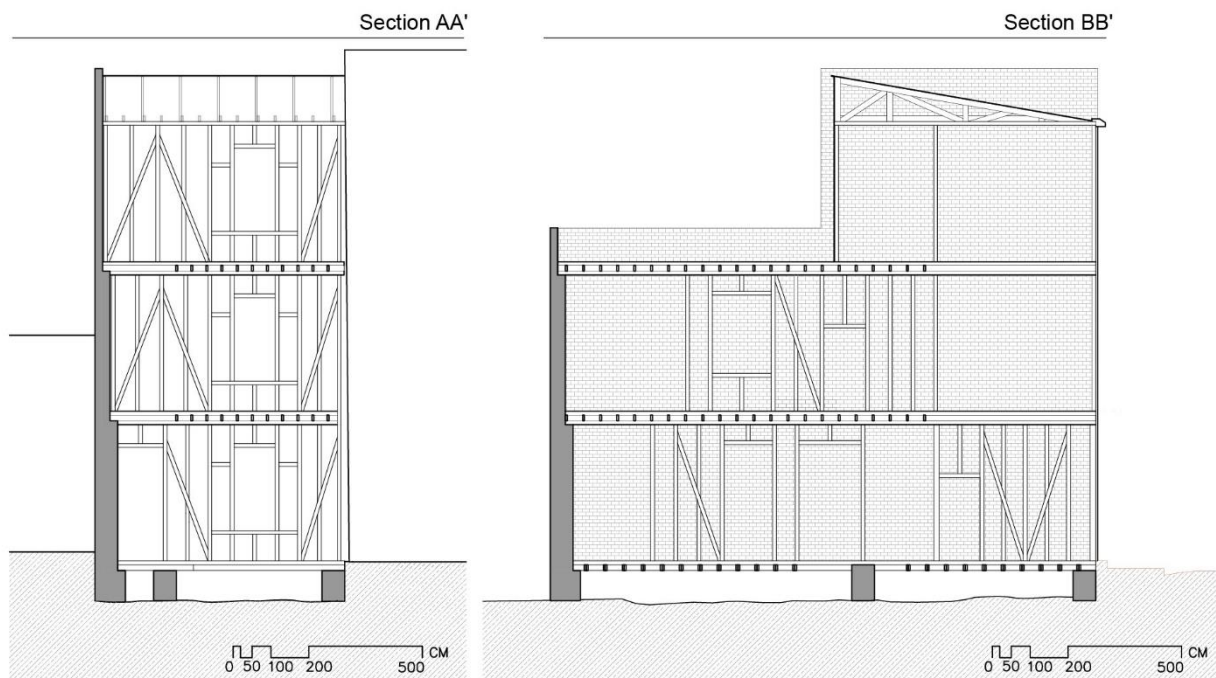


Figure 6-7. Sections AA and BB of Building 1, as reported in the drawings of Figure 6-3.

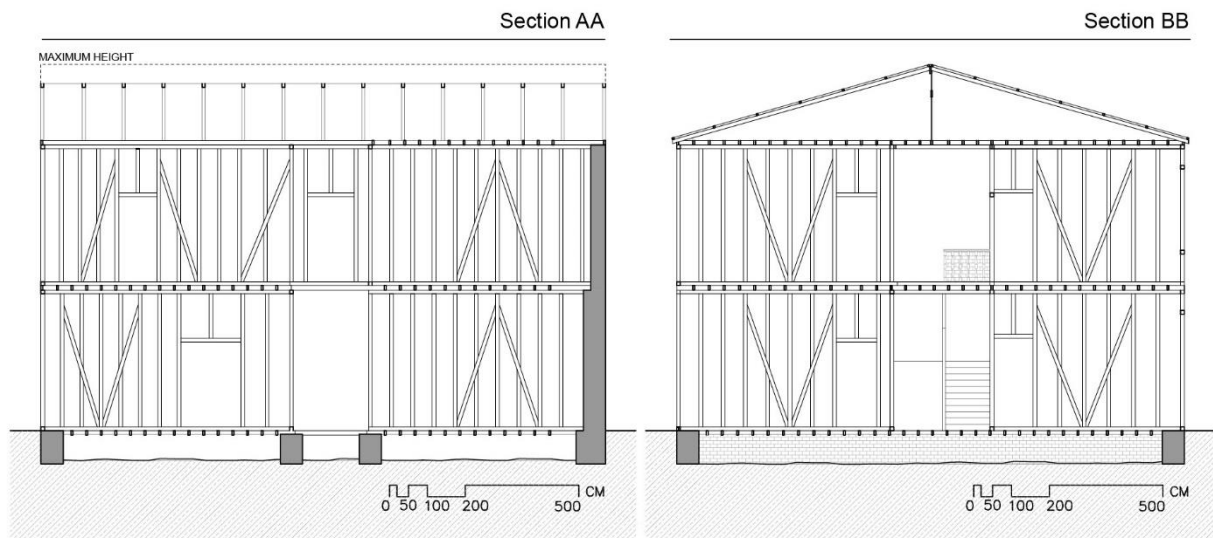


Figure 6-8. Sections AA and BB of Building 2, as reported in the drawings of Figure 6-5.

Figure 6-9 shows the representative arrangement of the timber frame system in the buildings. The walls are configured by stud elements, spaced $0.4 \div 0.6$ m each, and distributed between the top and bottom plates. Diagonal braces are usually introduced every two studs, and they are located next to the openings, as shown in Figure 6-9. Most of the elements configuring the wall have a rectangular cross-section of $0.10 \text{ m} \times 0.10 \text{ m}^2$. Traditional carpentry joints reinforced with nails are used to connect the timber elements, being mortise-and-tenon and notched connections the predominant ones (Figure 6-9a-d). Mortise-and-tenon joints are used to connect post and plates elements, including the sills of the openings, while notched joints connect the diagonals with the main frame, as shown in Figure 6-9. Adobe blocks of $0.50 \times 0.10 \times 0.08 \text{ m}^3$ fill the external walls of the façade, while lath-and-plaster are used for the internal partitions. Externally, corrugated iron planks cover the walls. The joists of the storeys have $0.125 \times 0.05 \text{ m}^2$ cross-section, and are separated every 0.4 m. The joists are nailed over the sills of the frame and embedded into the masonry, as shown in Figure 6-10. Wooden boards of 0.10 m width and 0.01 m thickness, nailed at the top and bottom of the joists, constitute the floors and ceilings. Rudimentary trusses are supported by the walls and form the roof, with inclined rafters shaping pitched roofs, with around 10% slope. Wooden ribbons over the trusses support the corrugated iron planks covering the roof structure.

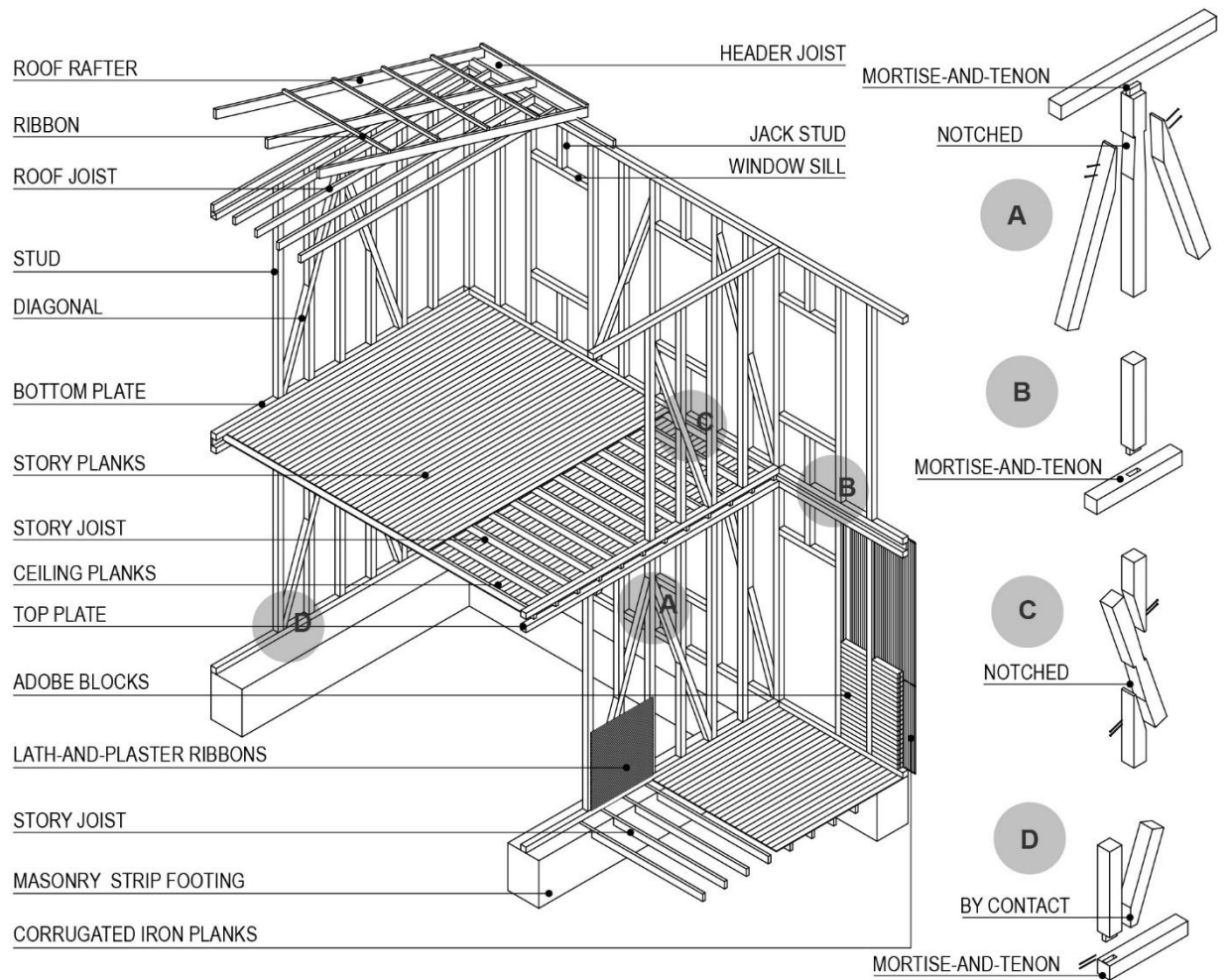


Figure 6-9. Isometric view of a representative timber *platform frame* system of Valparaíso.

As reported by Jiménez (2015), most of the timber elements are made of Oakwood and Oregon Pine wood. However, different timber species might configure some other parts of the frame system. In both the selected structures, URM load-bearing sidewalls are connected to the timber frames at the storey levels. The walls are made of fired clay bricks of $0.38 \times 0.195 \times 0.06$ m³ and lime mortar, arranged in English bond. The sidewalls have variable thickness along the height, varying at each storey, as shown in Figure 6-11 and Figure 6-12. Building 1 has back and side walls with a thickness varying from 0.6 m to 0.2 m from the bottom to the top levels. Building 2 has walls with thickness varying from 0.6 m to 0.4 m along the elevation. The storeys are supported by joists commonly embedded or simply supported over the bricks, as shown in Figure 6-10b. The sidewalls are not shared with the load bearing system of the adjacent buildings, and they are placed only next to each other with the function of firewalls. The foundations under the load-bearing walls and timber frames are strip footings made of brick masonry, built on rocky soil, with 0.6 m thickness and 0.80 m height.



Figure 6-10. Storey system configurations: (a) joists between top and bottom sills of the walls and, (b) joists embedded into the masonry strip footings.

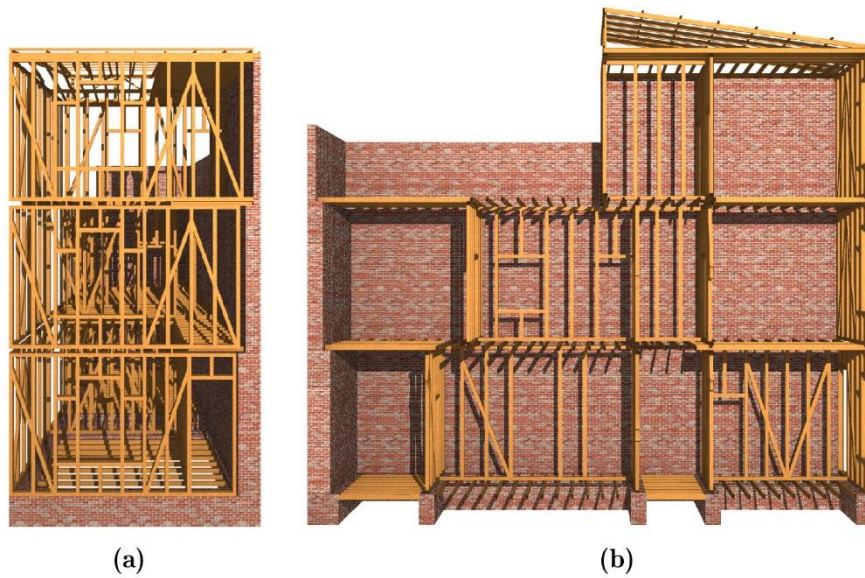


Figure 6-11. Structural configuration of Building 1: (a) frontal and (b) transversal section views.



Figure 6-12. Structural configuration of Building 2: (a) frontal and (b) transversal section views.

6.3 Numerical models of the hybrid timber-masonry structures

LPM and continuum FE models were used to simulate the nonlinear behaviour of the two hybrid timber-masonry buildings. Both models were calibrated individually based on benchmark experiments, as presented in Section 5. Analytical calculations were executed to describe the behaviour of the carpentry joints, due to the lack of experimental data for the specific typologies of Valparaíso. These hypotheses and assumptions were considered a reasonable approximation due to the structural similarities between the selected benchmark experiments and the examined cases of study.

The behaviour of the timber frame structures is governed by the nonlinear behaviour of the connections, named mortise-and-tenon (stud-plate link) and connection by contact (diagonal-stud link). The rotational behaviour of mortise-and-tenon joints was investigated in previous studies (Chun, Yue, and Pan 2011; Xie et al. 2018; Chen, Qiu, and Lu 2016; Ogawa, Sasaki, and Yamasaki 2016). Analytical calculations were made in order to obtain the moment-rotation relationship of mortise-and-tenon joints, based on the simplified calculation procedure proposed by Chen, Qiu, and Lu (2016). The peak bending moment was calculated as 3.6 kNm considering the geometrical properties of the tenon, a friction coefficient of 0.25 and the mechanical properties of the Oak timber listed in Table 6-1. Nonlinear hinges were added at each mortise-and-tenon connection to model its rotational behaviour, as depicted in Figure 6-13, defined with the moment-rotation relationship shown in Figure 6-14a.

Table 6-1. Mechanical properties of the Oak timber (Perez 1990).

Tangential compression strength $f_{c,t}$	46.65	MPa
Tangential Young's modulus in compression $E_{c,t}$	12798	MPa
Friction coefficient μ	0.25	-

An axial nonlinear behaviour with zero rotation was considered for the connections by contact, assuming the same constitutive law used in to model of the diagonal connection of the Pombalino frame (see Section 5.3.2.). The above assumption is justified by the very similar geometrical configuration and cross-section of the elements in the connections. Nonlinear axial springs acting on the horizontal translational DOF were introduced at each node where the diagonals meet the frame, as shown in Figure 6-13. Figure 6-14b shows the axial load-displacement relationship of the connection, with dots of different colours indicating the so-called “plastic state” of the hinges/springs within the model, according to the reached magnitude of plastic displacement/rotation. The timber material was modelled using isotropic linear elastic properties, according to the parameters of the Oak timber defined by Perez (1990), and listed in Table 6-2.

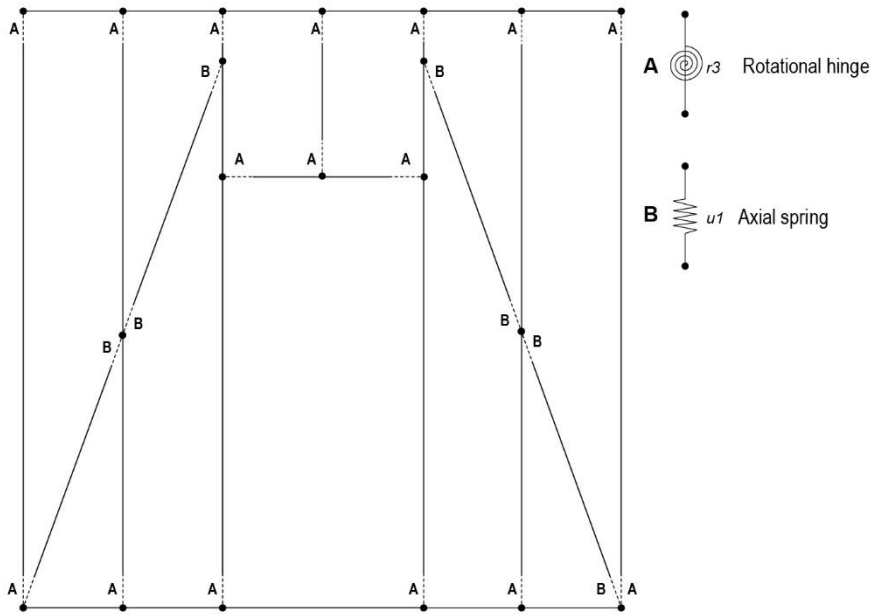


Figure 6-13. Location of the hinges and springs within the frame elements of the lumped plasticity models of Building 1 and Building 2.

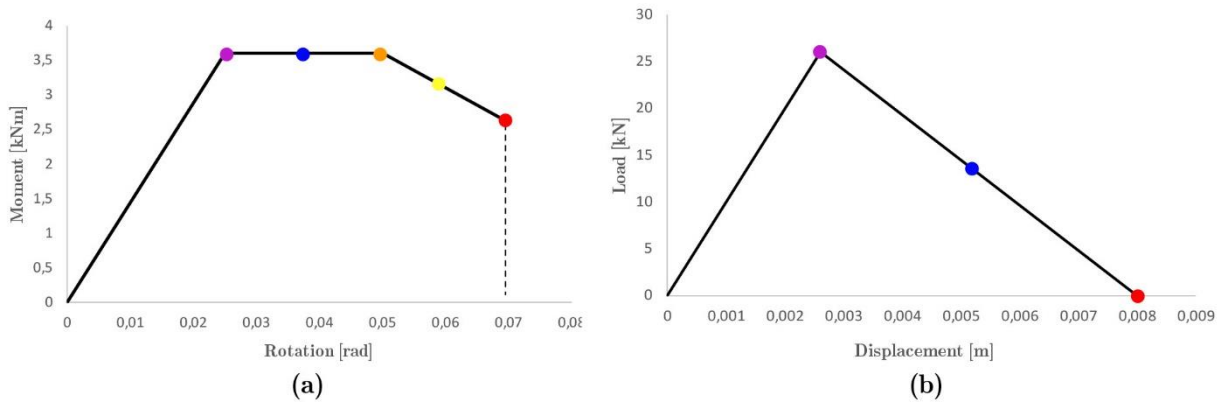


Figure 6-14. Constitutive laws for the carpentry joints in the lumped plasticity model of timber frames: (a) rotational behaviour of the mortise-and-tenon joints, and (b) axial behaviour of the connections by contact.

Table 6-2. Mechanical properties of the Oak timber used in the Building 1 and 2 models(Perez 1990).

Young's Modulus E	$1,212 \times 10^7$	[kN/m ²]
Density ρ	6,24	[kN/m ³]
Poisson's ratio ν	0.3	-

The URM walls were modelled following the continuum FE approach described in Section 5.5. The uniaxial nonlinear stress-strain relationship of the material was defined considering the model proposed by Kaushik, Rai, and Jain (2007) (see Equation 25 in Section 5.5.2). The required mechanical properties of the material were defined based on the average characteristic values proposed by the Italian standards (Italian Ministry of Infrastructure and Transport 2018; NTC-

Circolare 2018) for existing URM in solid brick and lime mortar, listed in Table 6-3. Reductions factor of 0.7 and 0.8 were applied respectively to compressive strength and Young's modulus values to account for thickness of mortar joints higher than 13 mm, as recommended by the Italian standards. Figure 6-16 displays the constitutive law of the material assuming a compressive strength f_c of 2415 kN/m², and a tensile strength f_t corresponding to 5% f_c . Based on the experimental studies of Kaushik, Rai, and Jain (2007) on masonry walls, the peak compressive strain capacity ε'_m was considered as 0.00325 m/m, while the ultimate compressive strain was estimated as 2.75 ε'_m . Equations (6-1) and (6-2) define the fracture energy-based approach with softening behaviour (Figure 6-15), according to the Total Strain Crack model proposed by Vecchio and Collins (1993), and the studies of Reinhardt (1984) and Hordijk (1991). Both theories relate to a characteristic crack bandwidth for smeared crack models, as reported in the following expressions:

$$\frac{G_f}{h} = \frac{f_t \cdot \varepsilon_{cr}}{2} \quad (6-1)$$

$$h = \sqrt{a} \quad (6-2)$$

Where G_f is the fracture energy, h is the crack bandwidth of the finite element for quadratic shell elements, f_t is the tensile strength of masonry, ε_{cr} is the ultimate cracked tensile strain, and a is the area of the finite element.

Table 6-3. Mechanical properties of solid brick and lime mortar masonry according to the Italian standards NTC-Circolare (2018), for the constitutive law of masonry for the Buildings 1 and 2.

Young's Modulus E	1.2×10^6	[kN/m ²]
Compressive strength f_c	2415	[kN/m ²]
Density ρ	18	[kN/m ³]
Poisson's ratio ν	0,2	-

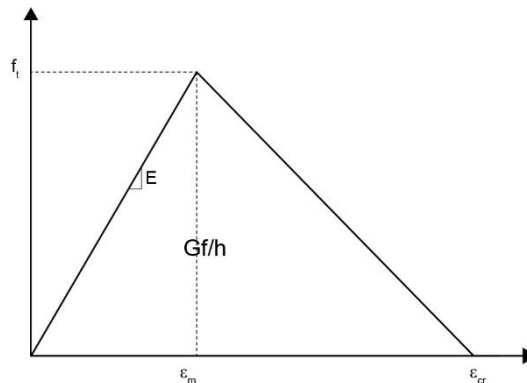


Figure 6-15. Fracture energy-based relationship used to define the tensile constitutive law of masonry for the Buildings 1 and 2.

The fracture energy G_f of masonry was assumed as 0.05 kN/m, based on past studies on URM by Petracca et al. (2017), Lourenço (2000) and Bocca, Carpinteri, and Valente (1989). The maximum elastic strain ε_m was calculated as 1×10^{-4} m/m and the ultimate cracked strain ε_{cr} as 2.8×10^{-3} m/m. Figure 6-16 shows the stress-strain constitutive law, which controls the nonlinear and cracking behaviour of the investigated masonry structures. The masonry material was defined using linear elastic isotropic properties considering the mechanical parameters listed in Table 6-3 and the nonlinear stress-strain relationship shown in Figure 6-16. A friction angle of 23° was assumed to define the shear model, based on the Eurocode 6 (CEN 2005b) recommendations.

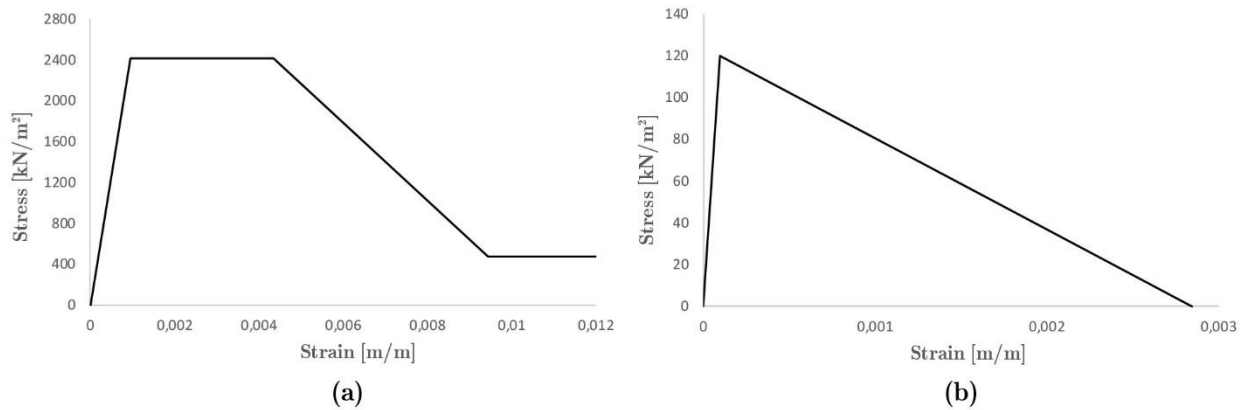


Figure 6-16. Uniaxial constitutive laws defining the behaviour of the masonry material for the Buildings 1 and 2: (a) compression and (b) tension stress-strain relationships.

6.4 Seismic analysis of two hybrid timber-masonry buildings of Valparaíso

Numerical models including the LPM of timber frames and continuum FE model of masonry walls were used to simulate the behaviour of the two cases of study, as shown in Figure 6-17. In both cases, the frame elements configuring the load-bearing systems had 0.10×0.10 m² cross-section, except for the joists, which had 0.125×0.05 m² cross-section. Rigid connections were assumed to connect the joist with the frame and the masonry walls, since they are usually embedded into the bricks, or nailed between the top and bottom plates of the timber frames supporting the weight of the upper walls. All the frame elements were divided at any intermediate joints along their length, as well as in any other intersection with other frames or members. The infill in the façade frames was simulated by applying the Equivalent Strut Method (ESM) considering the mechanical properties of the adobe (MINVU 2013). The internal partitions of the buildings were modelled as bare frames since they are normally covered using other techniques such as the lath-and-plaster system. Furthermore, a very typical practice in this type of buildings is the removal of all the infill or covering of some internal partitions to create open spaces at the interior of the buildings, as discovered after on-site inspections.

Masonry walls were modelled using nonlinear layered shell elements as defined in Section 5.5 and 5.5.3. Two layers with four integration points each configure the section of the shell

elements. The walls were meshed considering rectangular elements of $0.4 \times 0.2 \text{ m}^2$ size. The variable thickness of the walls along the elevation was defined for each particular case. The walls of Building 1 had variable thicknesses from 0.6 m to 0.2 m from the bottom to the top levels, while the walls of Building 2 had variable thicknesses from 0.6 m and 0.4 m. The roofs systems were not modelled in order to simplify the analysis. This decision was made after a sensitivity analysis, which demonstrated a negligible contribution of the roof structure on the overall response of the building. Fixed and pinned supports restrained the base of masonry walls and timber frame elements respectively, as shown in Figure 6-17. Both support conditions restrain all the translational displacements, while the fixed support restraints also the rotations. These boundary conditions simulated the existence of good quality foundations.

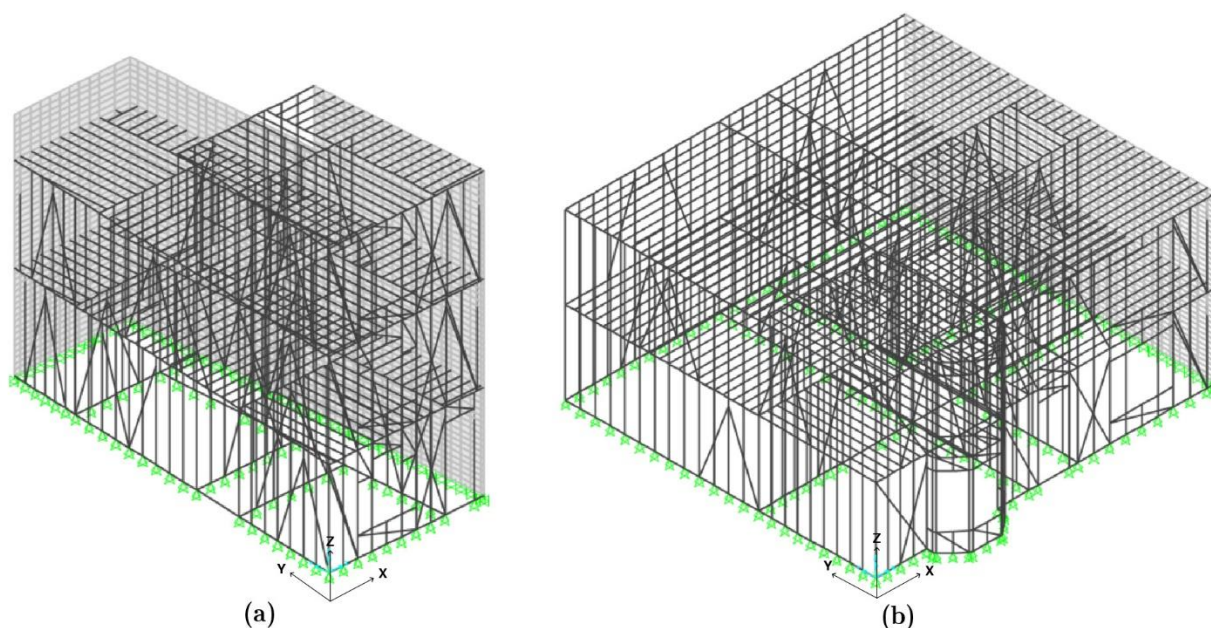


Figure 6-17. Numerical models of (a) Building 1 and (b) Building 2.

NSA was performed along the two main directions of the models (X and Y) by applying separately horizontal forces proportional to the mass distribution of the buildings. The magnitude of the loading was increased incrementally up to the ultimate capacity of the model. The analyses were monitored in displacement control considering strategic nodes at the highest level of the structure to describe the response of the structures. All the analyses were set using an iteration convergence tolerance of 1×10^{-4} as recommended by SAP2000 (CSI 2016b). The results of the analyses were presented in terms of acceleration-displacement capacity curves. The obtained damage patterns of the buildings were analysed in order to determine the occurred local and global collapse mechanisms.

Figure 6-18a-b displays the capacity curves obtained for the Building 1 in the X and Y directions respectively. The stiffening effect of the infill in the façade was examined by removing the equivalent struts but maintaining the inertial mass of the infill in a second model, named

Model B. The results revealed that the building presented a higher capacity in the Y direction, as expected, being the longest one. The presence of equivalent struts (Model A) increased the capacity of the building analysed in the X direction in 15%, while the initial stiffness slightly incremented, as shown in Figure 6-18a. The model presented convergence problems for the case B analysed in the Y direction. Despite this, no significant differences were detected between the Model A and B analysed in this direction, as displayed in Figure 6-18b. A summary of the results obtained only for the Model A analysed in both directions are presented below.

In the X direction, the model reached the maximum capacity at the acceleration of 0.26 g (394.2 kN base shear) and displacement of 0.034 m, whereas the ultimate displacement was recorded at 0.05 m with a slight reduction of 1.4% of shear capacity. The initial stiffness of the model was 2.58×10^4 kN/m. The building entered in the nonlinear range once a tensile crack appeared at the base of the overturning masonry wall perpendicular to the applied load (Point 1 in Figure 6-18a). Figure 6-19a displays the localization of principal tensile strains at the base the wall at the same point. The overturning mechanism around the base of the wall was activated and progressively developed (Figure 6-19b) until reaching the ultimate strain value of 0.0028 m/m (Figure 6-19b-c). The overturning mechanism of the wall interested also the connection with the perpendicular one in the final stage, with a partial formation of a vertical crack at the corner (Figure 6-19c). After the development of the overturning mechanism in the wall (between Points B and C in Figure 6-18a), some joints plasticized in the timber frames parallel to the applied load until reaching their ultimate capacity at the end of the analysis, as shown in Figure 6-19d. Most of the damaged connections were the ones located at the diagonals in tension. The overall collapse of the building is governed by the overturning of the masonry wall, which triggered the collapse of some axial springs at the diagonal elements of the frames. The redistribution of the lateral forces to the timber frame system after the failure of masonry could explain the apparent overall ductile behaviour of the structure, as shown by the capacity curve Figure 6-18a.

The NSA of the Building 1 in the Y direction presented the double of the capacity of that in the X direction, reaching 0.53 g (824 kN base shear) at a displacement of 0.0032 m. As in the X direction, the masonry walls demonstrated to play a central role in the structural response of the building. The characteristic global collapse is governed by the shear sliding at the base of the masonry wall parallel to the applied load, as shown in Figure 6-20. The joints of the timber frames remained elastic up to the end of the analysis. This result evidenced that the masonry wall parallel to the direction of horizontal loading could resist the whole seismic action, due to its higher rigidity. The ultimate capacity of the building is considered as the 80% of the maximum shear base load (F_{\max}), based on the Limit State definition for URM structures given by the Italian standards (NTC-Circolare 2018), being 653 kN and 0.42 g at a displacement of 0.0044 m. The initial stiffness of the model was 5.82×10^5 kN/m. Table 6-4 summarizes the main results of the Model A analysed in the X and Y directions.

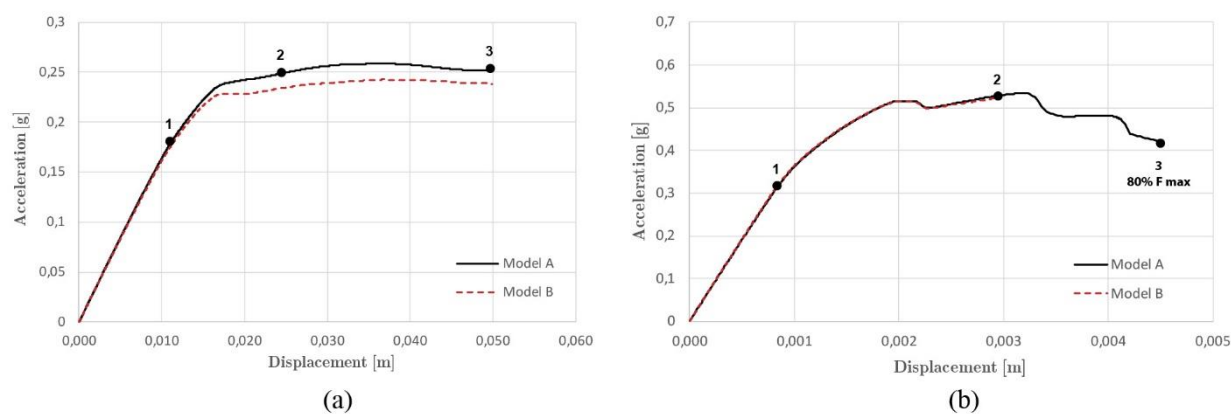


Figure 6-18. Capacity curves obtained for Building 1 in the (a) X and (b) Y analysis directions.

Table 6-4. Summary of the results obtained for the Building 1 simulated in the X and Y directions.

Building	Initial stiffness [kN/m]	Maximum capacity			Ultimate capacity		
		Load [kN]	Acceleration [g]	displacement [m]	Load [kN]	Acceleration [g]	displacement [m]
X	2.58×10^4	398.54	0.26	0.037	388.7	0.25	0.050
Y	5.82×10^5	824	0.53	0.0032	653	0.42	0.0044

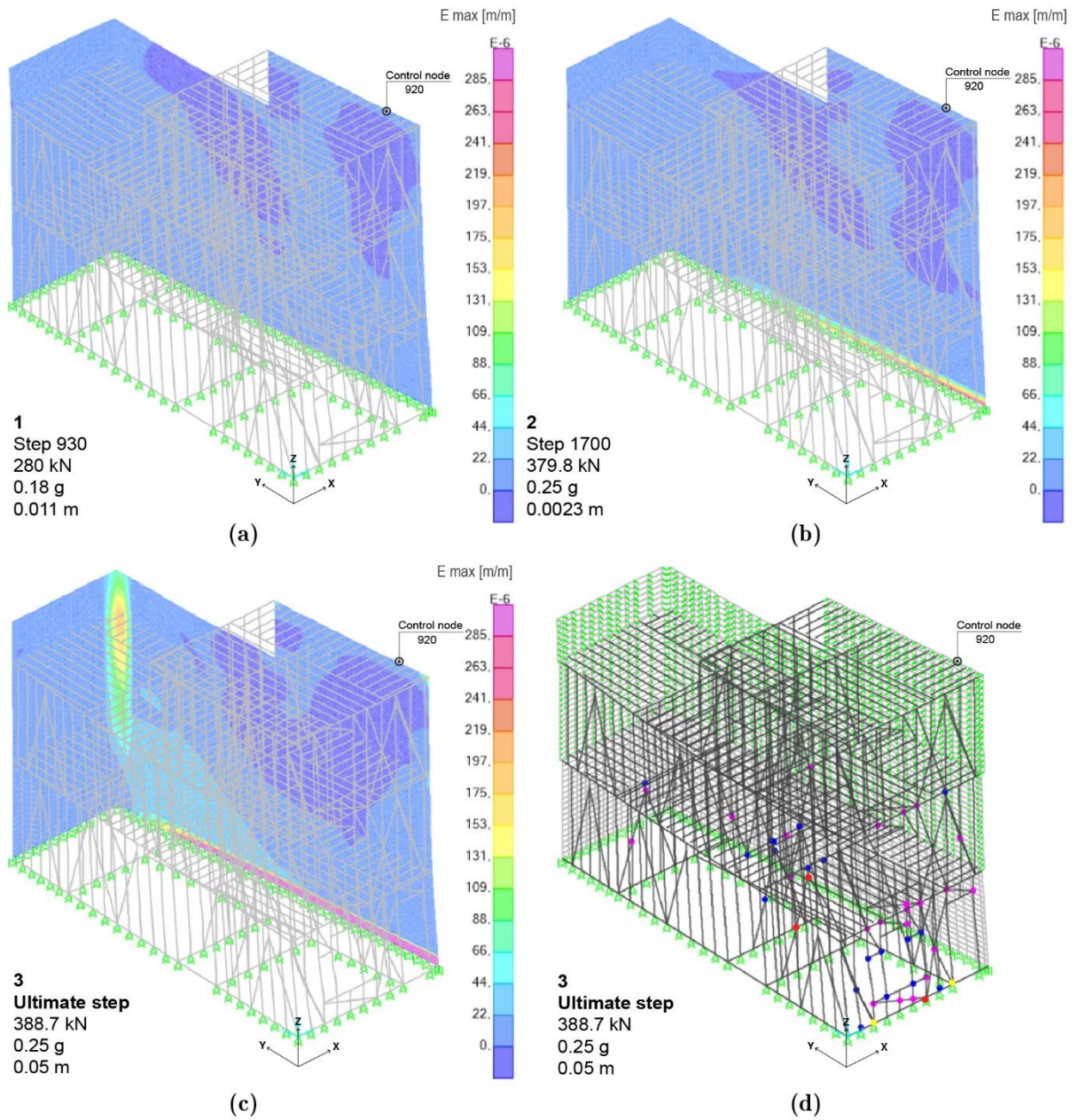


Figure 6-19. Seismic analysis of Building 1 in the X direction. Principal tensile strain contours (a) at a displacement of 0.011 m (Point 1 in Figure 6-18a), (b) at a displacement of 0.0023 m (Point 2 in Figure 6-18a), and at a displacement of 0.05 m (Point 3 in Figure 6-18a). (d) Hinges/springs plasticized at the ultimate step of the analysis in the timber frames (Figure 6-18a).

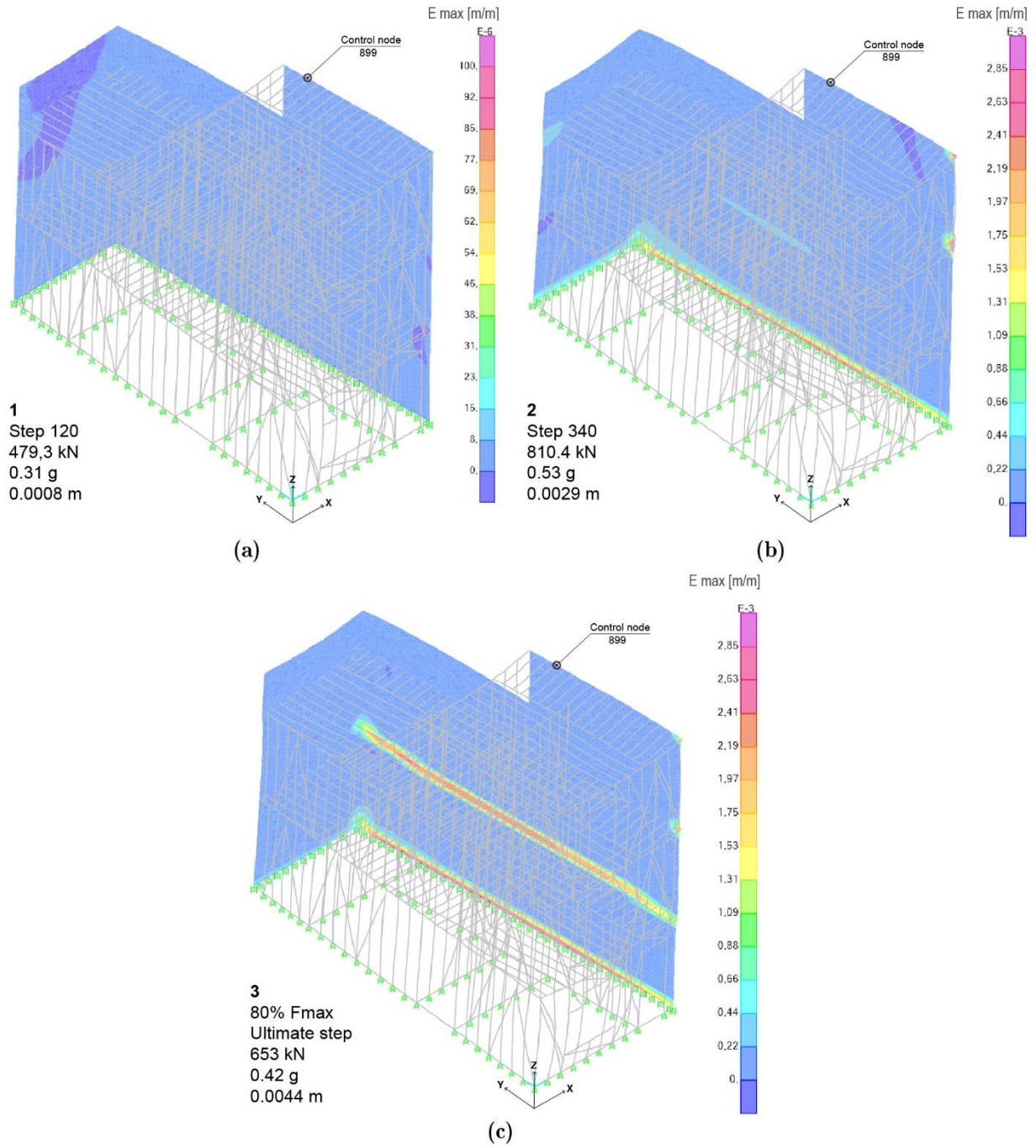


Figure 6-20. Seismic analysis of Building 1 in the Y direction. Principal tensile strain contours (a) at a displacement of 0.0008 m (Point 1 in Figure 6-18b), (b) at a displacement of 0.0029 m (Point 2 in Figure 6-18b), and at a displacement of 0.0044 m (Point 3 in Figure 6-18b).

Figure 6-21a-b displays the capacity curves obtained from the analyses of Building 2 in the X and Y directions respectively. The results demonstrated that the building presents a higher capacity in the Y direction, as was expected, being the one with the larger masonry resistant area. The model presented convergence problems for the case A analysed in the Y direction. Despite this, the stiffening effect of the equivalent struts was more evident in the Y direction analysis (Model A), as shown in Figure 6-21b. In this case, the maximum capacity and initial stiffness of the building increased in 19% and 18 %, respectively. On the other hand, there were no significant difference between Model A and B analysed in the X direction, as noted in Figure 6-21a. Table 6-5 presents a summary of the results obtained from the Model A of Building 2 for both analysis directions.

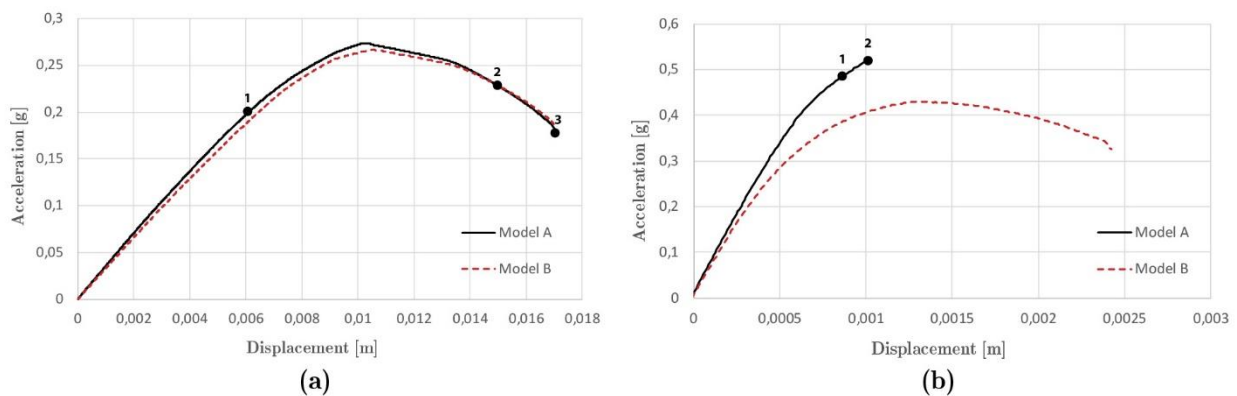


Figure 6-21. Capacity curves obtained for the Building 2 in the (a) X and (b) Y direction analyses.

Table 6-5. Summary of the results obtained for the Building 2 simulated in the X and Y directions.

Building	Initial stiffness	Maximum capacity			Ultimate capacity		
		Load	Acceleration	displacement	Load	Acceleration	displacement
2	[kN/m]	[kN]	[g]	[m]	[kN]	[g]	[m]
X	3.7×10^4	303.1	0.27	0.01	194.4	0.18	0.017
Y	7.4×10^5	564.8	0.52	0.001	564.8	0.52	0.001

In the X direction, the Model A reached a maximum acceleration capacity of 0.27 g (303.1 kN base shear) at a displacement of 0.0093 m, whereas the ultimate displacement was recorded at 0.017, with a significant reduction of 40% of the shear capacity. The initial stiffness of the model was 3.7×10^4 kN/m. The building entered in the nonlinear range once a horizontal crack started to appear at the base of the masonry wall once it reached the maximum tensile capacity of 0.0001 m/m. This damage is attributed to the overturning mechanism governing the failure mode of the wall. After this phase, some of the springs located in the timber frames parallel to the applied load reached their maximum capacity and plasticized progressively up to the end of the analysis. Figure 6-22d displayed the hinges formed at the ultimate step of the analysis. The cracking at the base of the wall progressively developed towards the total damage at the end of the analysis, as shown in Figure 6-22b-c. The characteristic global collapse of the building is partially governed by the overturning mechanism of the masonry wall and the collapse of some

axial springs in the diagonal elements. The results reveal a kind of collaborative behaviour in the hybrid structural system, where seismic forces are transmitted to the timber frame elements after the failure of the wall. This response propitiates a nonlinear response of the building with a limited amount of ductility.

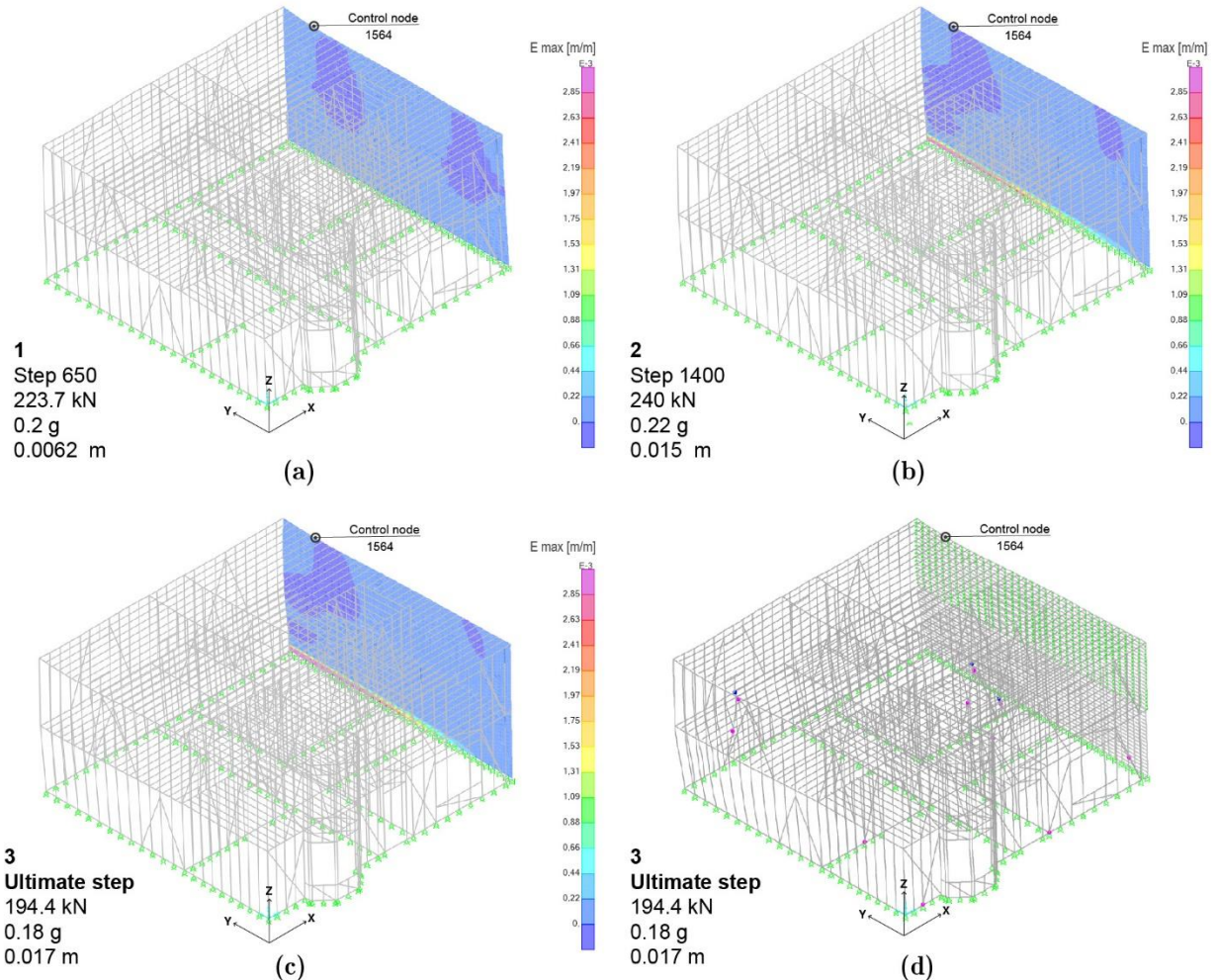


Figure 6-22. Seismic analysis of Building 2 in the X direction. Principal tensile strain contours (a) at a displacement of 0.0062 m (Point 1, Figure 6-21a), (b) at a displacement of 0.015 m (Point 2, Figure 6-21a), and at a displacement of 0.017 m (Point 3 in Figure 6-21a). (d) Hinges/springs plasticized at the ultimate step of the analysis in the timber frames (Point 3 in Figure 6-21a).

The NSA of the Building 2 in the Y direction presented the double of the capacity of that in the X direction, reaching 0.54 g (590 kN base shear) at a displacement of 0.00011 m (Model A). The building entered in the plastic range once a horizontal cracking appeared at the base of the wall once the maximum tensile strain of 0.0001 m/m was reached, as shown in Figure 6-23a. A shear sliding mechanism is activated because of the in-plane loading conditions of the wall. After this point, the cracking pattern developed a narrow damage zone until the analysis stopped due to convergence problems. The joints of the timber frames remained elastic until the analysis stopped. The convergence problems can be attributed to the quasi-brittle behaviour of the masonry, which experienced a quick drop of resistance. The analysis of the Model B considering

only the mass of the infill, reached a maximum capacity of 0.43 g (466.4 kN base shear) at a displacement of 0.0013 m, whereas the ultimate displacement was recorded at 0.0024 m with a reduction of 28% of shear capacity, as shown in Figure 6-21b.

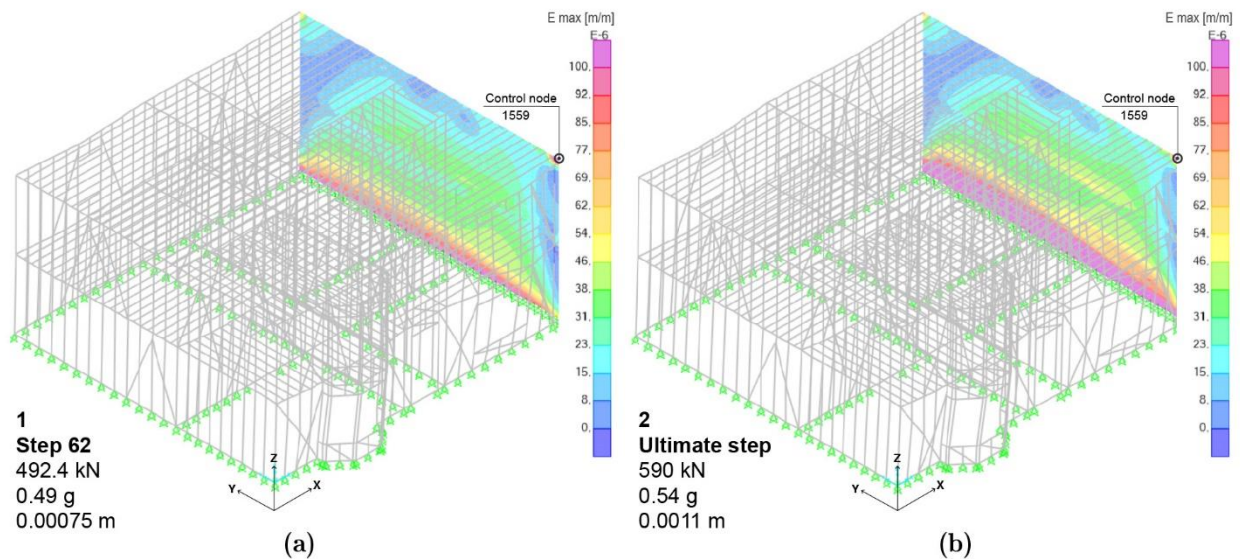


Figure 6-23. Seismic analysis of Building 2 in the Y direction. Principal tensile strain contours (a) at a displacement of 0.00075 m (Point 1 in Figure 6-21b), (b) at a displacement of 0.0011 m (Point 2 in Figure 6-21b).

6.5 Seismic performance of the buildings for the seismic hazard in Valparaíso

The seismic performance of the Buildings 1 and 2 was evaluated by considering the seismic hazard of the city of Valparaíso and applying the N2 Method (N2M) (P. Fajfar and Eeri 2000) as considered in the Italian standards (NTC-Circolare 2018). This analysis was necessary in order to verify that structural members were not damaged beyond threshold limits of forces and displacement implied by the seismic demand. The N2M aims at determining a target displacement (also known as “performance point”) of the structure as the intersection between the capacity (pushover) curve and the inelastic demand spectrum. The target displacement determines the estimated base shear and displacement undergone by the structure when subjected to the earthquake whose demand is represented by the demand curve. The N2M derives results for the Multi Degree Of Freedom (MDOF) system after simplifying it to an equivalent Single Degree Of Freedom (SDOF) system.

According to the Italian standards, the capacity curve of the MDOF system, which represents the relationship between the base shear force and control node displacement, can be transformed into that of an equivalent SDOF system, as shown in Figure 6-24.

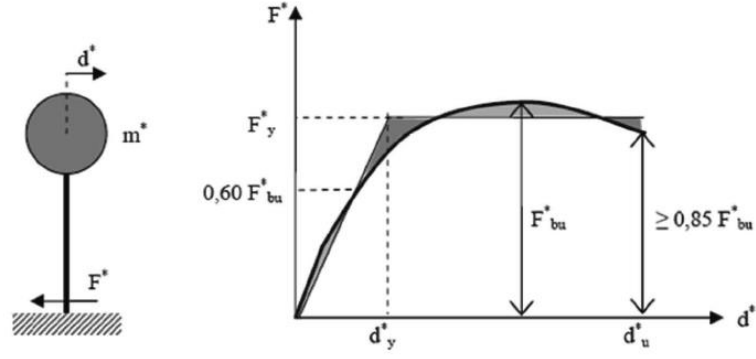


Figure 6-24. Equivalent SDOF system and bilinear idealization of the capacity curve (NTC-Circolare 2018).

The force F^* and displacement d^* of the equivalent SDOF system are computed according to Equations (6-3) and (6-4) respectively:

$$F^* = \frac{F_b}{\Gamma} \quad (6-3)$$

$$d^* = \frac{d_c}{\Gamma} \quad (6-4)$$

Where F_b and d_c are, respectively, the base shear force and the control node displacement of the Multi Degree of Freedom System MDOF, and Γ is the transformation factor given by Equation (6-5):

$$\Gamma = \frac{\varphi^T M \delta}{\varphi^T M \varphi} \quad (6-5)$$

Where δ is a vector denoting the direction of the earthquake, φ is the fundamental vibration shape of the MDOF system normalized so that the value of the top displacement is equal to 1, and M is the mass matrix of the MDOF system.

The equivalent SDOF capacity curve is simplified to a bilinear system by considering a first elastic range followed by a perfectly-plastic branch, as shown in Figure 6-24. F_{bu} represents the maximum capacity of the MDOF system, and $F_{bu}^* = F_{bu}/\Gamma$ of the equivalent SDOF system. The elastic branch of the bilinear idealization is commonly identified by tracing a tangent line from the origin through the $0.6 F_{bu}^*$ point of the capacity curve. The yield force F_y^* is determined by equating the areas under the actual capacity curve and the bilinear idealization, for a ultimate displacement d_u^* corresponding to a drop of the peak resistance less than or equal to $0.15 F_{bu}^*$.

The elastic period of the idealized bilinear system is calculated as follows:

$$T^* = 2\pi \sqrt{\frac{m^*}{k^*}} \quad (6-6)$$

Where $m^* = \varphi^T M \delta$ and k^* is the stiffness.

In the case than $T^* \geq T_c$ (Figure 6-25a), where T_c is the characteristic period of the ground motion, the target displacement of the SDOF inelastic system is assumed to be equal to that of an elastic system of the same period:

$$d^*_{\max} = d^*_{e,\max} = S_{De}(T^*) \quad (6-7)$$

In the case than $T^* < T_c$ (Figure 6-25b), the target displacement for the inelastic SDOF system is higher that the elastic one, and is determined as shown in Figure 6-25b using the following expression:

$$d^*_{\max} = \frac{d^*_{e,\max}}{q^*} \left[1 + (q^* - 1) \frac{T_c}{T^*} \right] \geq d^*_{e,\max} \quad (6-8)$$

Where q^* is the ratio between the accelerations corresponding to the elastic and inelastic systems:

$$q^* = \frac{S_e(T^*)m^*}{F_y^*} \quad (6-9)$$

If $q^* \leq 1$ then $d^*_{\max} = d^*_{e,\max} = S_{De}(T^*)$.

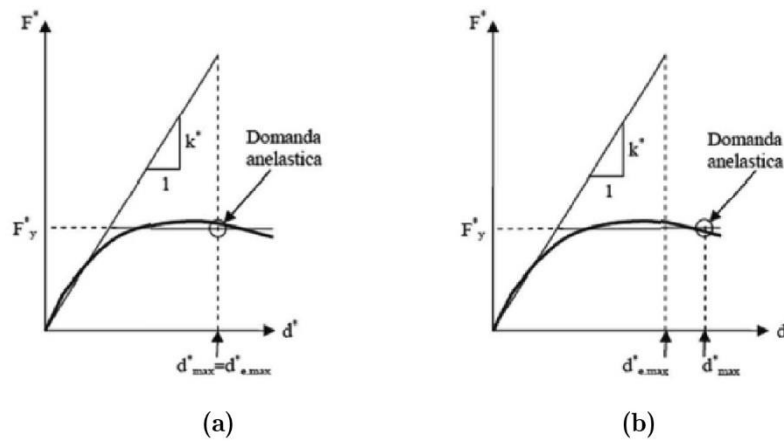


Figure 6-25. Target displacement in the N2 method for: (a) $T \geq T_c$ and (b) $T < T_c$ (NTC-Circolare 2018).

The target displacement d_{\max} of the MDOF system is given eventually by Equation (6-10):

$$D_{\max} = \Gamma d^*_{\max} \quad (6-10)$$

The seismic demand of the Buildings 1 and 2 (see Section 6.4) is defined by considering two different spectra, shown in Figure 6-26 and Figure 6-27. The former is calculated following the Chilean standards NCh433 Of.96 (Instituto Nacional de Normalización 2009) for a building with

a soil type II and maximum ground acceleration $A_0=0.4$ (Zone 3). The latter corresponds to the elastic spectra of the 2010 earthquake recorded for the city of Valparaíso (Boroschek, Soto, and León 2010). Figure 6-27 displays different acceleration records using critical damping ratios of 0.00, 0.02, 0.05, 0.1 and 0.2 for different components: N-S (COMP 1-L), vertical (COMP 2-V), and E-W (COMP 3-L). The acceleration demand considering a damping ratio of 0.05 was selected for the following analyses, as highlighted in Figure 6-27.

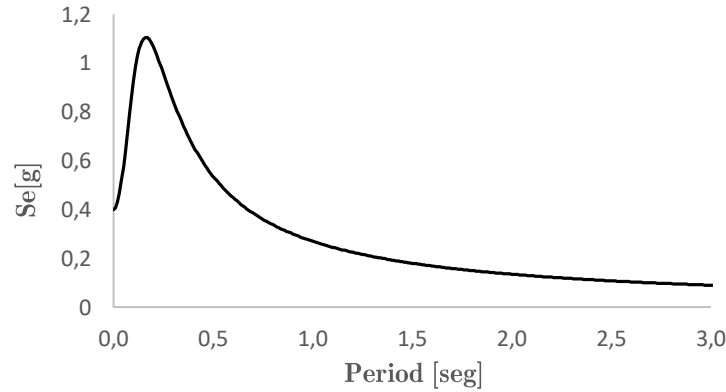


Figure 6-26. Seismic demand of Valparaíso NCh433 Of. 96: Building Category II, Seismic Zone 3 (0.4g) and Type of Soil 2.

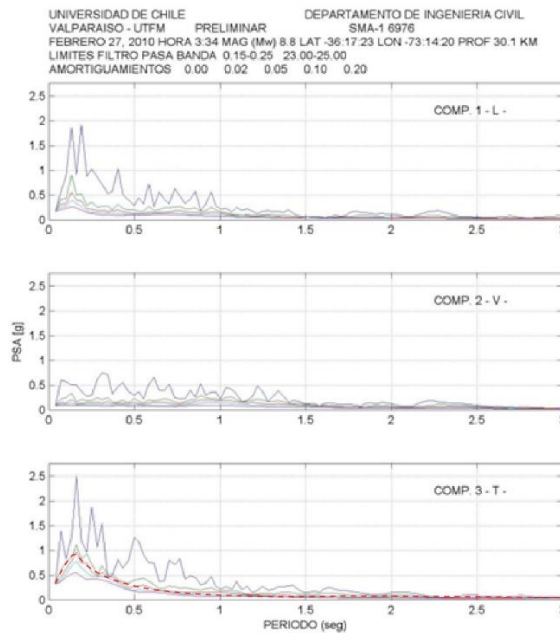


Figure 6-27. Demand spectra of the 2010 Earthquake recorded in the city of Valparaíso. (Boroschek, Soto, and León 2010)

Figure 6-28 and Figure 6-29 show the application of the N2M to Buildings 1 and 2 in the X and Y directions. Table 6-6 summarizes the characteristics of the equivalent SDOF systems of the two buildings that were used to evaluate the seismic performance of the buildings by means of the N2M.

Table 6-6. Characteristics of the equivalent SDOF systems of building 1 and 2.

	Building 1		Building 2	
	X	Y	X	Y
Γ	2.03	3.94	3.57	2.67
m^* [kN-s ² /m]	30.3	14.3	18.8	5.58
F_y^* [kN]	188	190	80	200
d_y [m]	0.0074	0.00032	0.0022	0.00026
T^* [s]	0.22	0.03	0.14	0.017

The target displacement of Building 1 for the X direction-analysis is in the plastic range for the demand spectra of the Chilean seismic code, and in the elastic range, close to the yield displacement for the 2010 earthquake, see Figure 6-28. This means that although the 2010 earthquake did not induce damage to the building, for the seismic hazard foreseen by the Chilean standards the building may undergo some moderate damage. In fact, the numerical analysis in this second case shows that the masonry walls are affected by some damage, as well as some axial springs of the diagonal elements. The target displacement for the Y direction analysis remains in the elastic stage for both the demand spectra of the Chilean seismic code and the 2010 Earthquake.

Table 6-7. Building 1 seismic assessment results: target displacements.

	NCh433 Chilean code		2010 Earthquake spectrum	
	X	Y	X	Y
d_{\max}^* [m] (SDOF)	0.012	0.00011	0.0074	0.00013
D_{\max} [m] (MDOF)	0.025	0.00043	0.015	0.00053

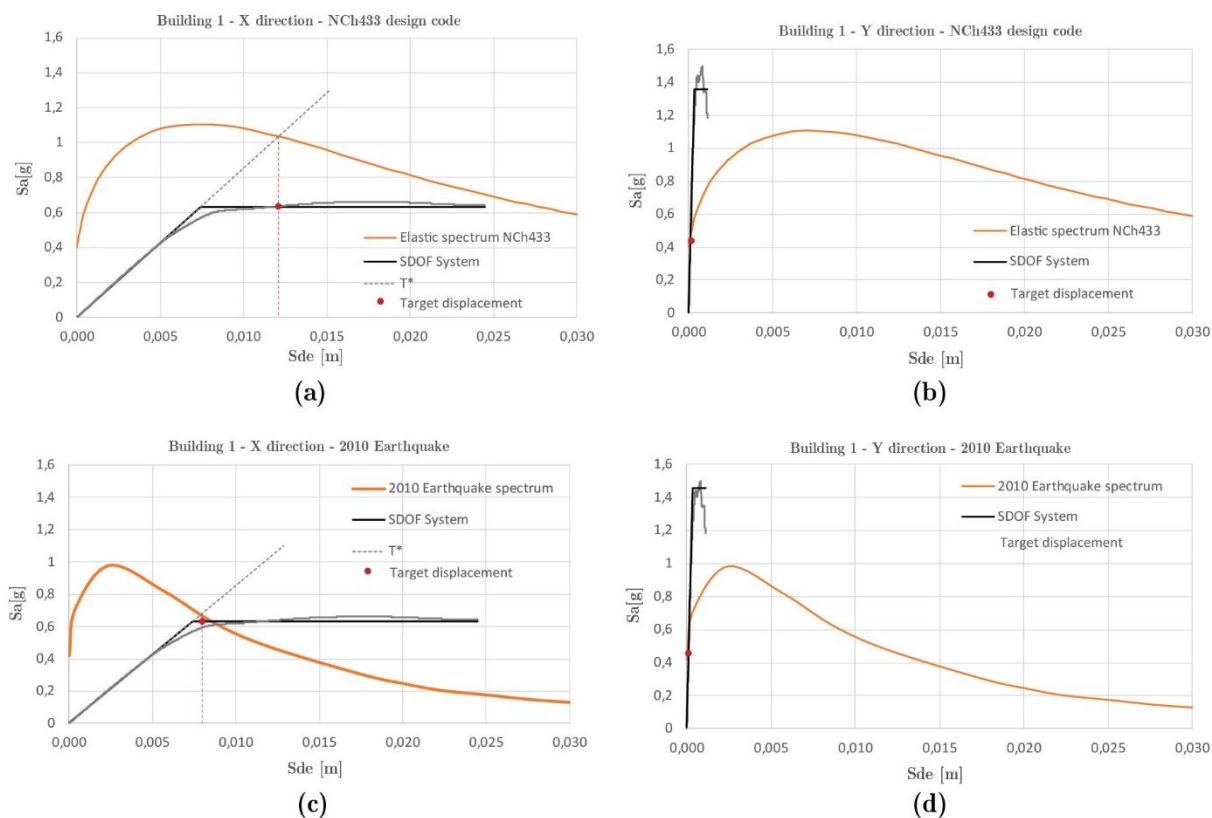


Figure 6-28. Application of the N2 method to Building 1 in the X and Y directions, according to the demand spectra of (a-b) the Chilean seismic code NCh433, and (c-d) of the 2010 Earthquake.

Building 2 exhibits a very good seismic performance when analysed in the Y direction, as the target displacement remains in the elastic stage for both demand spectra, as shown in Figure 6-28b-d. However, the analysis in the X direction shows a target displacement rather close to the ultimate displacement for the case of the demand spectrum of the 2010 Earthquake, and target displacement higher than the ultimate one for the case of the demand spectra of the Chilean seismic code. Both results seem rather conservative if compared with the limited evidence of structural damage after the 2010 Earthquake. However, there are no data from detailed damage survey of the building after that seismic event, and the damage may have been hidden under the structure covering or by subsequent repairs. An in-situ inspection of the building executed in 2015 showed that several timber elements were recently replaced due to their bad state of conservation. In addition, it is worth noticing that the numerical analyses do not consider the actual aggregate configuration of the buildings, which would contribute to increase the structural capacity and stiffness of the system. To conclude, it is also worth highlighting that the directionality of the earthquake is also a very important and influent parameter, as the building presents very different capacities in the X and Y direction.

Table 6-8. Building 2 seismic assessment results: target displacements.

	Design seismic demand		2010 Earthquake spectrum	
	X	Y	X	Y
d_{\max}^* [m] (SDOF)	0.0056	0.00003	0.006	0.00013
D_{\max} [m] (MDOF)	0.012	0.00008	0.021	0.00036

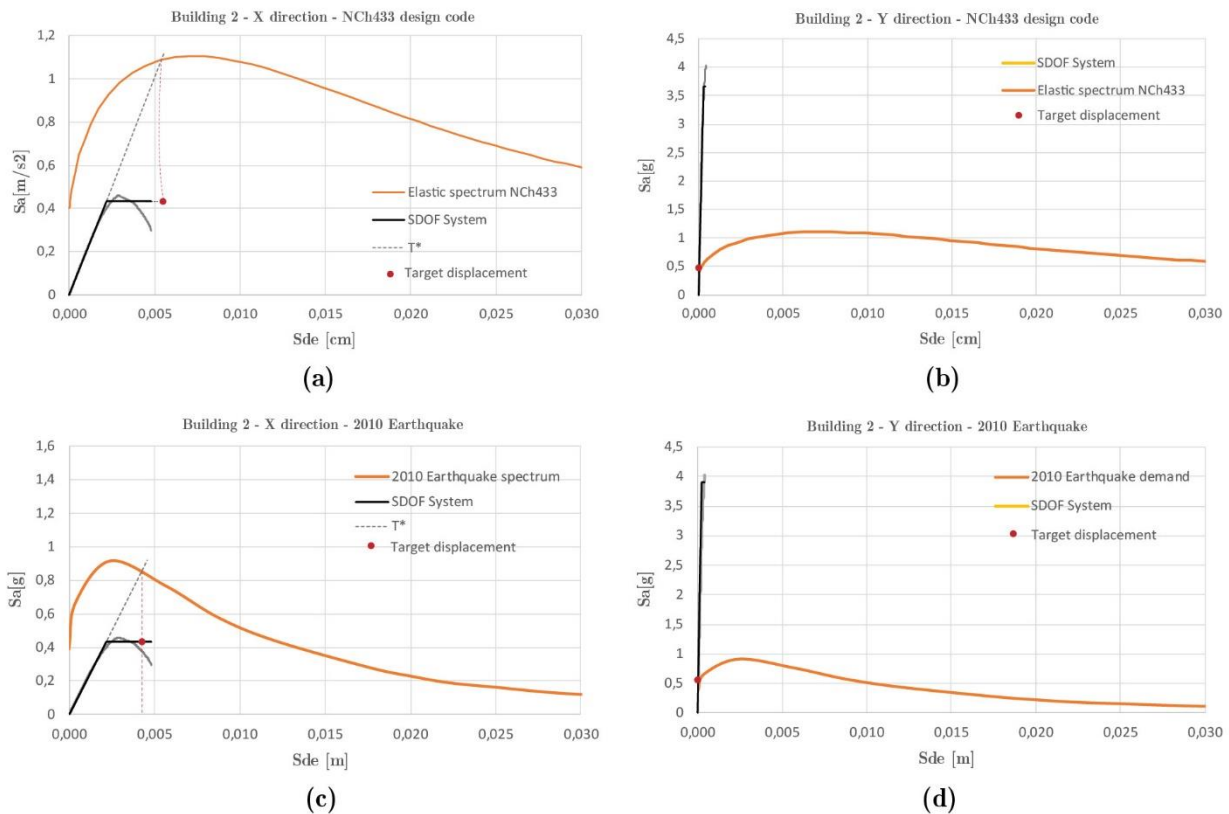


Figure 6-29. Application of the N2 method to Building 2 in the X and Y directions, according to the demand spectra of (a-b) the Chilean seismic code NCh433, and (c-d) of the 2010 Earthquake.

6.6 Summary

A Lumped Plasticity Model (LPM) and a continuum Finite Element (FE) approach were adopted to analyse the seismic response of two hybrid timber-masonry buildings existent in the historical centre of Valparaíso, Chile. The numerical models were defined based on the calibration methodology set in Chapter 5, which referred to benchmark experimental cases with numerous similarities with the structural typologies in Valparaíso. The LPM of the timber frame structures were built after a proper setting of the nonlinear rotational and translational behaviours of two timber connections, i.e. the mortise-and-tenon and the connection by contact. The nonlinear constitutive law for the mortise-and-tenon was estimated analytically based on the model proposed by Chen, Qiu, and Lu (2016), while the law of the connection by contact was calibrated for the Pombalino frame model and extrapolated to set the behaviour of the diagonal connections of the

cases of study. The continuum model defining the response of masonry was defined by using the characteristic properties of existing URM and lime mortar as defined by the Italian standards (NTC-Circolare 2018).

Nonlinear Static Analysis (NSA) was performed in the two main directions of the models (X and Y) by applying a horizontal loading pattern with forces proportional to the mass distribution of the buildings. The results demonstrated that masonry walls have a central role in the lateral response of the buildings since they contribute to resist a major part of the applied loads, especially in the Y direction. In both analysis directions, the masonry walls are the first elements that reach their maximum capacity. In the Y direction, only the masonry walls reach their ultimate capacity, while the internal timber frames resist the applied actions without undergoing any damage. In this direction, the collapse of the masonry walls is given by a base shear mechanism provoked by a sliding failure at the base of the wall. In the X direction, the forces are redistributed to the timber frames after a nonlinear response of the masonry walls is triggered, and subsequently some of the springs reach their ultimate capacity. The collapse condition is given by the overturning mechanism around the base of the masonry walls, as well as the failure of the internal springs located at the diagonal connections. Both the buildings a good seismic capacity in the Y direction.

The seismic performance of the buildings was assessed by applying the N2 Method (N2M) for two different seismic demand spectra, i.e. the earthquake design spectrum of Valparaíso bases on the NCh433 Of. 96 standards (Instituto Nacional de Normalización 2009), and the spectrum of the 2010 Earthquake occurred in the city.

Building 1 demonstrated a very good seismic performance in the Y direction, where the target displacement remained in the elastic range for both seismic demands. In the X direction, the target displacement resulted slightly higher than the yield displacement for the 2010 earthquake spectrum, and in the nonlinear range for the Chilean standards demand spectrum. Almost null and moderate damage is expected respectively on the structural system for these two seismic demand levels.

Building 2 presented also a very good seismic performance in the Y direction for both demand spectra. In the X direction, the target displacement is very close to the ultimate displacement for the 2010 earthquake spectrum, and beyond it for the Chilean standards demand spectrum. These results would suggest important damage both in the masonry walls and timber frame connections. However, these outcomes of the numerical analyses seem very conservative, as after the 2010 earthquake no severe damage was reported. This difference may be associated with other factors that could influence to a certain extent the seismic performance of the buildings, such as the structural aggregate condition and the actual directionality of the 2010 earthquake.

Chapter 7. Seismic vulnerability assessment of heterogeneous urban neighbourhoods. Application to Valparaíso, Chile.

7.1 Introduction

This chapter proposes a prospective study of the seismic vulnerability of the buildings included in the Emergency Limit Condition (ELC) system presented in Chapter 3. A hybrid methodology is developed for the extension of the Vulnerability Index Method (VIM) for the evaluation of the hybrid timber–masonry buildings studied in the previous chapters. The proposal considers the calibration of a new vulnerability form based on a sensitivity analysis derived from numerical simulations, and expert judgement. The new form attempts to be equivalent to the ones proposed by Formisano et al. (2015) and GNDT-II (GNDT-SSN 1994) for masonry and reinforced concrete (RC) buildings, respectively, with the aim to evaluate the seismic vulnerability of urban areas with heterogeneous building stock by using the three forms simultaneously.

The central part of this chapter is focused on the development of a numerical study to determine the seismic response and expected damage of some representative structural typologies within the ELC system. Several models are studied in order to represent the boundary conditions of the parameters under study. The numerical modelling strategy is based on that proposed in Chapter 6 for the buildings of Valparaíso. The methodology adopted to calibrate the new form includes the nonlinear static analysis of the models to investigate the effect of each parameter, and the evaluation of the seismic performance by applying the N2 method (N2M). The obtained results are compared in terms of a Mechanical Vulnerability Index (I_M) in order to assign specific scores and classes related with each new parameter of the vulnerability form. The VIM is implemented to evaluate 111 buildings within the ELC system by applying the new form for timber–masonry buildings, as well as the already available forms for RC and masonry buildings. The results are used to elaborate a vulnerability map in the GIS environment in order to have an overall understanding of the vulnerability of the buildings in the territory. This analysis aids to detect the most vulnerable areas on which future investigations should be focused.

This chapter is divided into two main parts. Section 7.2 describes the proposal of the new form for the application of the VIM to hybrid timber–masonry building typologies. Section **Error! Reference source not found.** details the proposed methodology to calibrate the new vulnerability form. Section 7.2.2 explains the calibration of the new parameters based on numerical simulations, and Section 7.2.3 summarizes the layout of the new form including the classes, scores and weights. Section 7.3 presents the seismic vulnerability analysis of the ELC system of the neighbourhoods of *Cerro Alegre*, *Cerro Concepción* and the Port in Valparaíso, Chile.

7.2 Proposal of a building form for the application of the vulnerability index method to hybrid timber-masonry structures

7.2.1 Calibration of the seismic vulnerability form

The VIM, originally introduced by Benedetti and Petrini (1984), and further developed in other works (GNDT-SSN 1994; R. Vicente et al. 2008; Formisano et al. 2015; Basaglia et al. 2018; Cara et al. 2018; Ferreira, Rodrigues, and Vicente 2020)

is an indirect or empirical vulnerability method based on the assessment of typological indicators, which examine the seismic vulnerability of the buildings. This method uses standard typological forms to evaluate the structural and non-structural features of the buildings, based on the study of different structural and non-structural parameters. Each parameter represents one of the main features that may influence the seismic response of a certain building typology. The parameters are distributed into classes of increasing vulnerability from A to D, which have an assigned score. A weight is assigned to each parameter, which denotes the level of influence on the overall seismic vulnerability of the building. The classes are assigned to each parameter based on external inspection of the buildings to compute a vulnerability index, which is defined as the weighted sum of the scores associated with the selected vulnerability class of each evaluation parameter.

This section proposes the calibration of a new vulnerability form for hybrid timber–masonry structural typologies in compliance with the VIM to estimate properly the influence of some particular features of the seismic behaviour of the buildings of Valparaíso. The new form includes some of the original parameters for masonry structures (Benedetti and Petrini 1984; GNDT-SSN 1994) and those proposed by Formisano et al. (2015) to account the influence of aggregate structural conditions on the seismic vulnerability of the buildings. The latter was included considering that most of the buildings including in the ELC system are within in-row aggregates. However, the new form is based on the re-examination of the 15 parameters listed in Table 7-1. Each parameter was previously studied in order to determine a suitable calibration strategy. Due to the different nature and requirements of each parameter, three different sets are adopted to formulate the form. The first set considers the group of parameters that can be properly evaluated

using the classes, scores and weights proposed by Formisano et al. (2015) for masonry buildings. This group includes the parameters P4, P5, P8, P9 and all those evaluating the structural aggregate conditions of the buildings (P11 to P14). The second set considers the parameters that requires a redefinition of the classes, weights and scores based on qualitative analyses and expert judgement. This group includes the parameters P1 and P2, which apprise the organization, quality and nature of the load-bearing systems. Such parameters are calibrated taking into account the building taxonomies proposed in Chapter 4 (Jiménez 2015), and the published literature around the seismic structural behaviour of timber and masonry structures. The third set considers the analytical analysis of the parameters by performing numerical simulations to determine the seismic behaviour of the buildings. For this case, physical numerical models representing existing vulnerability cases of each parameter were determined to assign the classes and scores of the parameters. Nonlinear Static Analysis (NSA) and the N2M are employed to analyse the seismic vulnerability of the cases of study following the results presented in Chapter 6. This group considers the parameters P3, P6, P7 and P10.

Table 7-1. Parameters of evaluation for the new Vulnerability Index form for hybrid timber–masonry buildings (bold character denotes the parameters based on sensitivity analysis by numerical modelling)

N ^o	Parameter
P1	Organization of vertical structures
P2	Nature of the load-bearing systems
P3	Distribution of the resisting elements
P4	Location of the building and type of foundation
P5	Plan regularity
P6	Vertical regularity
P7	Type of storey system
P8	Roofing system
P9	Non-structural elements
P10	State of conservation
P11	Presence of adjacent buildings with different heights
P12	Position of the building in the aggregate
P13	Number of staggered storeys
P14	Structural typological heterogeneity among adjacent structural units
P15	Structural typological heterogeneity among adjacent buildings

7.2.2 Calibration of the new parameters for hybrid timber-masonry buildings based on numerical simulations

A numerical investigation of the structural characteristics of some representative building typologies within the ELC system is developed to determine how these variations influence their global seismic behaviour. This methodology is applied to determine the cases representing the existing vulnerability scenarios within the ELC system for each parameter. Several models are simulated considering both hybrid timber–masonry and homogeneous timber frame structural systems to assign the classes and punctuation of the parameters P3, P6, P7 and P10 in the form. A representative timber frame structural unit of the city of Valparaíso was selected to be modelled as a reference case. The examined two-storeys building (Figure 7-1) has a vertical load-bearing system made of timber elements of $0.1 \times 0.1 \text{ m}^2$ cross-section. The walls of the façade are filled with adobe blocks, whereas the internal frame walls are empty. The story system is made of timber joists of $0.125 \times 0.05 \text{ m}^2$ spaced 0.4 m each, as shown in Figure 7-1. The building has a surface area of 70 m^2 per storey and a total height of 7.2 m. This reference case is configured based on the typical structural arrangement of the buildings of Valparaíso.

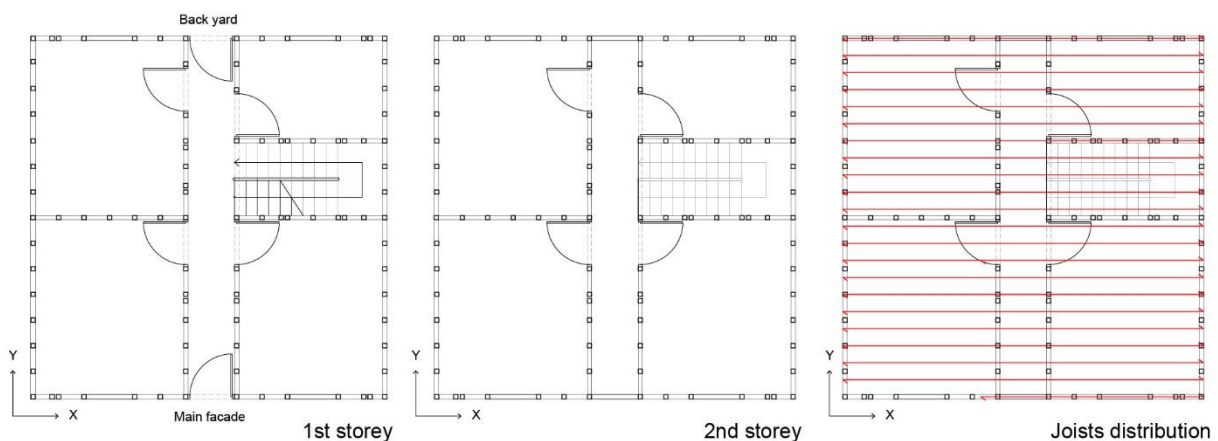


Figure 7-1. Typical structural unit of Valparaíso: plan layouts at different storeys.

The modelling strategy used to represent the reference case is the same of the one used in the Chapter 6 for the simulation of two existing buildings of Valparaíso. Timber frame and masonry structures are modelled using Lumped Plasticity (LPM) (Figure 7-2) and Continuum Finite Element (FE) approaches, respectively, considering the same procedure, material properties, load conditions and nonlinear constitutive laws described in Section 6.3. Nonlinear Static Analysis (NSA) is applied to determine the seismic capacity of the models by applying separately a uniform horizontal acceleration, i.e. horizontal forces proportional to the mass distribution of the buildings.

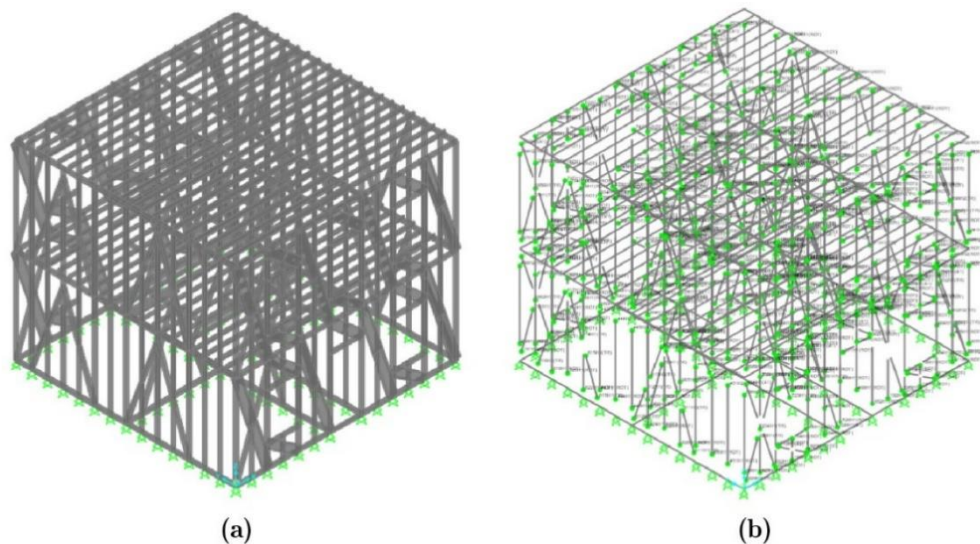


Figure 7-2. Typical structural unit of Valparaíso composed of timber frames: FE model based on Lumped Plasticity Method.

Different structural variations are then introduced into this reference model in order to identify the influence of some specific structural arrangements on the seismic behaviour of the buildings. These variations for the sensitivity analysis include the presence of unreinforced masonry walls in the load bearing system (Parameter P3), the existence of vertical irregularities (Parameter P6), the type of story systems (parameter P7) and the state of conservation of the structural elements (parameter P10). The Parameter 3 studies the influence of irregularities in the load-bearing system due to the existence of URM sidewalls connected to timber frame walls, based on the variations inspected in Chapter 4. In this case, only the most important typical irregularities of the buildings under analysis are investigated. The Parameter 6 considers the existence of vertical irregularities in the form of open galleries and cantilevers since they are the most typical variations within the buildings of the ELC system. The Parameter 7 considers the existence of storey systems with different stiffness, ranging from the flexible original typology to the retrofitted configurations added in recent times in the existing buildings. Lastly, the Parameter 10 investigates the influence of the damage at the connections and in timber elements on the seismic vulnerability of the buildings.

The N2M (Fajfar and Eeri 2000) is applied to determine the seismic performance of the buildings as considered in the Italian standards (NTC-Circolare 2018), following the same procedure explained in Section 6.5. This study expresses the seismic demand by means of the response spectrum included in the Chilean seismic design standards NCh433 Of.96 (Instituto Nacional de Normalización 2009) for a building of category II and a maximum ground acceleration $A_0=0.4g$ (see Figure 6.26). The building's behaviour is assessed by computing a Mechanical Vulnerability Index (I_M), which allows to evaluate the structural vulnerability as proposed by Formisano et al. (2015):

$$I_M = \frac{D_{\max}}{D_u} \quad (7-1)$$

where D_{\max} is the maximum horizontal displacement (target displacement) required by the seismic demand, and D_u is the ultimate displacement as obtained by the NSA. The latter quantity is evaluated as the displacement related to a 20% drop of the capacity after reaching its maximum value. In the cases with a very high vulnerability, the maximum horizontal displacement can overcome the ultimate displacement. The I_M values range from 0 to 1, where 1 indicates that the building has reached its ultimate displacement capacity. Therefore, the I_M associated with each case is used to categorize the buildings into vulnerability classes according to the range of obtained values. The buildings with highest I_M correspond the most vulnerable class. The parameters are catalogued into four classes of increasing vulnerability from A to D, which are associated with a score varying from 0 to 45, following the standard format of the VIM. The case with higher I_M value represents the most vulnerable class (Class D) of each parameter, with the highest associated score equal to 45, whereas the remaining scores and classes are proportionally computed considering the differences between the I_M values obtained from the analysis of each case. The following subsections discuss the calibration of the parameters P3, P6, P7 and P10 using the explained analytical procedure.

(P3) Distribution of the resisting elements

The ELC system of Valparaíso is characterized by the predominant vernacular nature of the buildings which is reflected in the singular organization of their structural systems. Most of the buildings of the stock are arranged in-row structural aggregates (Figure 7-3) separated by URM firewalls. These walls have often a structural role in only one of the structural units they are separating, inducing irregularities in the resisting structural system. This study assesses the influence of the irregular organization of the resisting system due to the presences of URM and the influence of different number of storeys. The sensitivity study of this parameter includes some of the most common building typologies identified within the ELC stock (see Section 4.4). Figure 7-4 and Figure 7-5 show the studied variation among the models by considering (i) the number of storeys (from 2 to 4), and (ii) the existence and position of external URM walls. The influence of the variation of numbers of stories is evaluated considering only the model of a homogeneous building made of timber frame walls filled with adobe blocks. The effect of irregularities on the resisting system due to the presence of URM sidewalls is studied considering three different arrangements. The first building (HOM-3) refers to a homogeneous three-storey building (HOM-3). The second building typology (HET-I-3) refers to a heterogeneous building typology with a URM masonry wall along one of its lateral sides connected to timber frame walls. The third building typology (HET-II-3) refers to a heterogeneous building typology with two URM perpendicular walls along its lateral and back sides. Typologies HET-I and HET-II, with one and two masonry walls respectively, correspond to those of two real buildings of Valparaíso analysed

in Chapter 6. Considering the beneficial effect of an adjacent structure when loading towards the X direction, it is possible to assume that the analyses performed in the Y direction represents better the seismic vulnerability of the investigated buildings. NSA was applied in the Y direction of the buildings in order to determine their seismic response. The seismic vulnerability of the buildings is afterwards assessed by employing the N2M.



Figure 7-3. In-row aggregate conditions of the buildings of the Almirante Montt street belonging to the ELC System of Valparaíso.

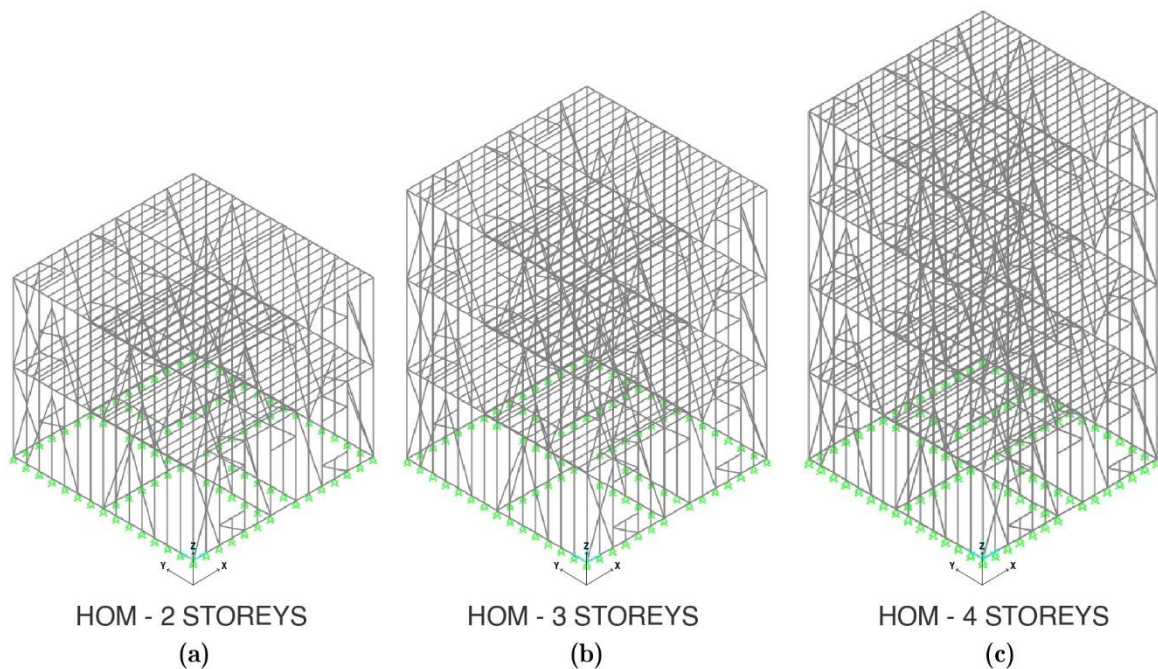


Figure 7-4. Parameter 3 “Distribution of the resisting elements”: numerical models for the analysis of the influence of the variation of the number of storeys on seismic vulnerability.

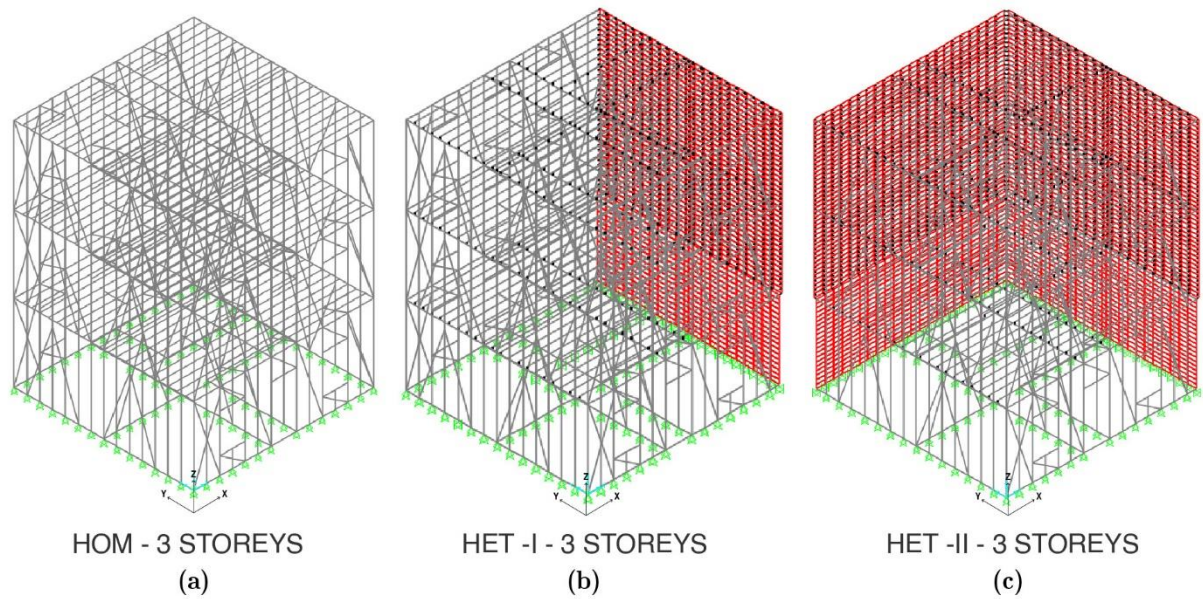


Figure 7-5. Parameter 3 “Distribution of the resisting elements”: numerical models for the analysis of the influence of the hybrid timber-masonry structural system on seismic vulnerability.

Figure 7-6 shows the capacity curves obtained from models analysed in the Y direction. It is important to highlight that these results need to be interpreted with caution, focusing on the relative difference between the different structural typologies, neglecting the effect of the adjacent buildings. The latter effect will be considered afterwards in the evaluation of the Parameters 11 to 14. The dots on the curves highlight the target displacement of the structures derived from the application of the N2M for the seismic demand in the city of Valparaíso. The triangular marker represents the case in which the target displacement overcomes the ultimate displacement, i.e. the most vulnerable case of the group (HET-II-3).

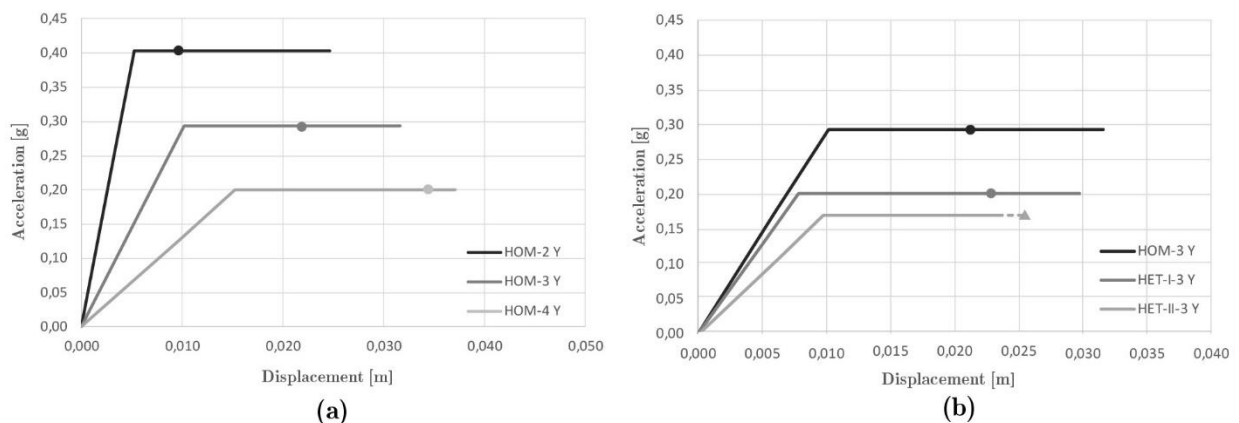


Figure 7-6 Parameter 3 “Distribution of resisting elements”. Capacity curves and target displacements from the models in the Y analysis direction: (a) variation of number of storeys in the homogeneous cases (HOM 2 to 4), and (b) influence of the hybrid timber-masonry resisting system (HOM-3, HET-I-3 and HET-II-3).

Figure 7-7 shows the I_M values obtained for each model analysing the variation of the number of storeys by applying Equation (7-1). As noted from these results, the vulnerability increases with the number of storeys. This effect can be due to the added masses in elevation, as well as to the higher flexibility associated with the increase of slenderness of the buildings. The taller the building is the more flexible it is, as noted in Figure 7-6a. The failures in the homogeneous timber buildings are in the diagonal connections of the frame walls parallel to the applied load at the upper stories, as shown in Figure 7-8.

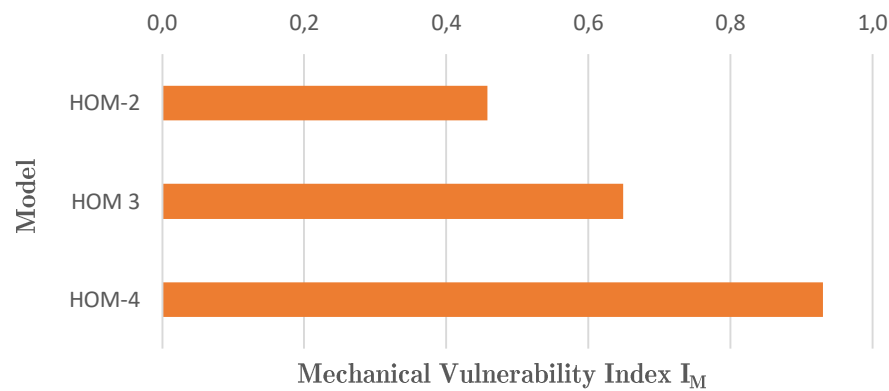


Figure 7-7 Parameter 3 “Distribution of plan resisting elements”: variation of the number of storeys. Mechanical Vulnerability Indexes I_M from the analysis in the Y direction.

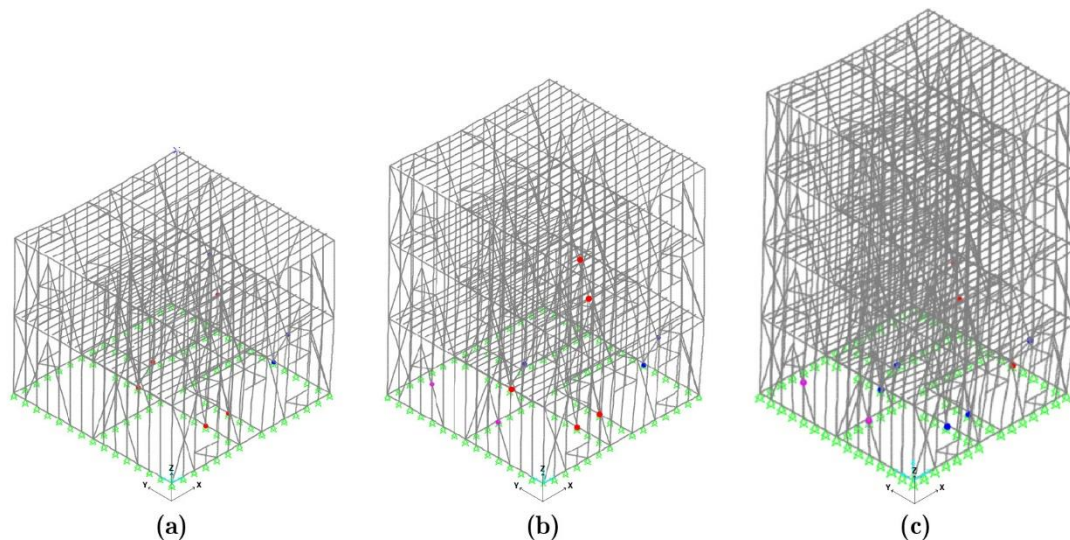


Figure 7-8. Parameter 3 “Distribution of plan resisting elements”: seismic analysis in the Y direction of the models showing the global collapse mechanisms of the buildings due to the hinges formation (red dots refer to their ultimate state) at the ultimate displacement.

The study of the irregularities of the resisting system revealed that the addition of URM walls increases the vulnerability of the buildings, as noted in Figure 7-9. The cases with one (HET-I-3) and two (HET-II-3) walls increase their vulnerability of 16% and 35% compared with the homogeneous case. This effect can be associated with both the increase of inertial forces given by the added mass of the URM walls, which reduces the capacity of the buildings compared with the

HOM case, and with the introduced irregularity, which introduces torsional effects and makes the global behaviour remarkably affected by the brittleness of the individual URM walls.

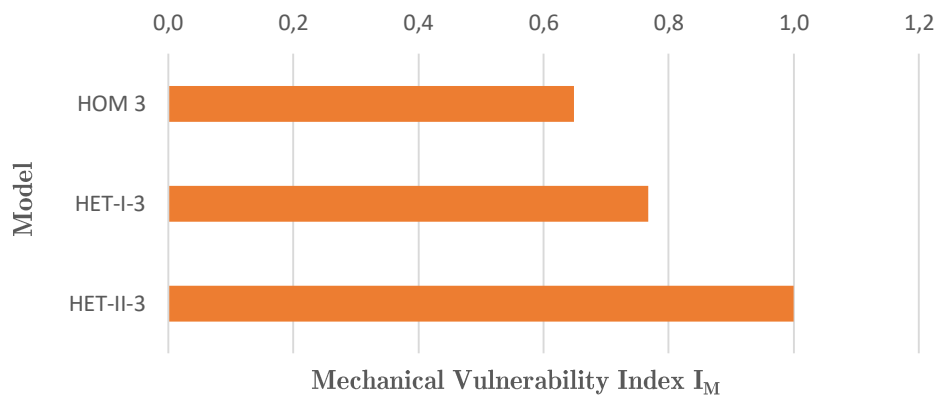


Figure 7-9. Parameter 3 “Distribution of plan resisting elements”: influence of the hybrid timber-masonry resisting system. Mechanical Vulnerability Indexes I_M from the analysis in the Y direction.

The global mechanisms of the homogeneous case (HOM-3) is governed by the failure of some of the diagonal connections of the frame walls parallel to the applied load at the lower storeys, as shown in Figure 7-10a. Similarly, the case with one wall (HET-I-3) fails along with the most of the diagonal connections of frame walls located parallel to the applied load, and especially those located at the wall opposite to the URM wall at the lower storeys of the building, as shown in Figure 7-10b. In this case, the URM wall does not suffer critical structural damage. This response is associated with an important torsional effect due to the high difference in stiffness between the masonry wall and timber frames. The building with two perpendicular URM walls (HET-II-3) reveals a different global mechanism mainly governed by the overturning mechanism at the base of the URM wall perpendicular to the applied load, as shown in Figure 7-10c. In this case, the ductility of the system is strongly affected by the brittleness of the out-of-plane mechanism of a masonry wall.

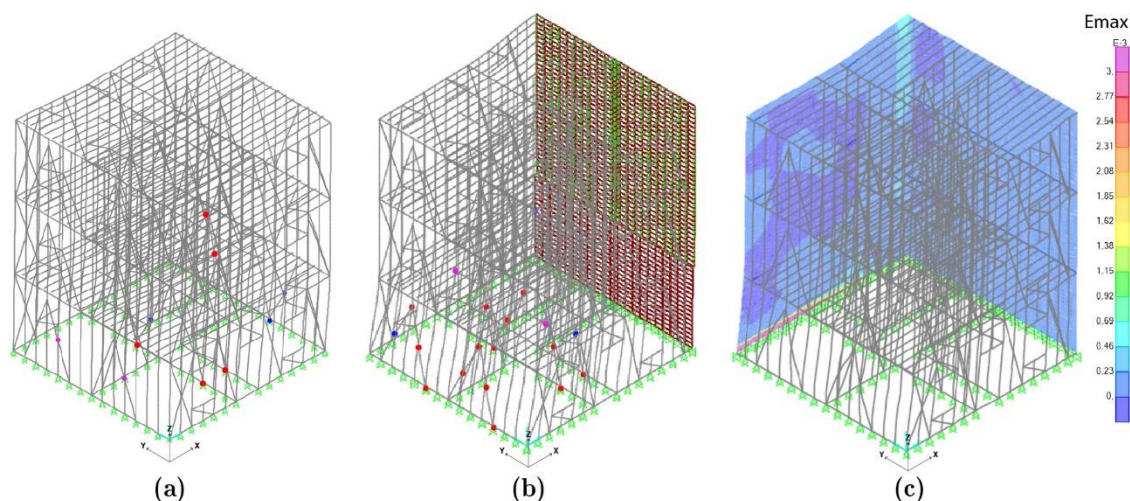


Figure 7-10. Parameter 3 “Distribution of plan resisting elements”: seismic analysis in the Y direction showing the global collapse mechanisms due to the hinges formation (red dots refer to their ultimate state in models HOM and HET-I), and the principal tensile strains contour (from 0 up to the ultimate strain equal to 0.0028 in HET-II) at the ultimate displacement.

The evaluation of classes and scores of the Parameter 3 for the VIM form is based first on the comparison of the IM indicator among the analyses studying the variation of the number of stories for the HOM typology, see Table 7-2. The cases HOM-2, HOM-3 and HOM-4 are assigned to classes A, B, and C, respectively, see Table 7-4. As the hybrid timber-masonry resistant systems HET-I and HET-II (Table 7-3) introduce further degree of seismic vulnerability compared with HOM typology, as described above, these cases correspond to one class worse than the HOM cases with the same number of storeys. This means that if the building with four storeys and homogeneous structural system (HOM-4) corresponds to Class C and score 30, the cases with four storeys but heterogeneous structural systems (HET-I-4 and HET-II-4, grouped as HET-4 in Table 7-4) are class D with score 45. The building with three storeys and homogeneous structural system (HOM-3) corresponds to Class B and score 10, whereas the cases with three storeys but heterogeneous structural systems (HET-I-3 and HET-II-3, grouped as HET-3 in Table 7-4) are class C with score 30. Finally, the building with two storeys and homogeneous structural system (HOM-2) corresponds to Class A and score null, whereas the cases with two storeys but heterogeneous structural systems (HET-I-2 and HET-II-2, grouped as HET-2 in Table 7-4) are class B with score 10. Table 7-4 summarizes the scores and classes assigned to each case.

Table 7-2. Parameter 3 “Distribution of the resisting elements”: Mechanical vulnerability index of the analysis of the variation of the number of storeys on seismic vulnerability.

MODELS	d_{MAX} [m]	d_u [m]	I_M	ΔI_M
HOM-2	0,0109	0,024	0,458	0,000
HOM-3	0,021	0,032	0,649	-0,191
HOM-4	0,034	0,037	0,931	-0,473

Table 7-3. “Distribution of the resisting elements”: Mechanical vulnerability index of the analysis of of the influence of the hybrid timber-masonry structural system on seismic vulnerability

MODELS	d_{MAX} [m]	d_u [m]	I_M	ΔI_M
HOM 3	0,021	0,032	0,65	-0,191
HET-I-3	0,023	0,030	0,77	-0,309
HET-III-3	0,026	0,023	1,00	-0,542

Table 7-4. Parameter 3 “Distribution of the resisting elements”: Scores and classes assignment.

MODELS	Score	Class
HOM-2	0	A
HOM-3, HET-2	10	B
HOM-4, HET-3	30	C
HET-4	45	D

(P6) Vertical regularity

Irregularities in the vertical load-bearing system can be important sources of vulnerability since they could provoke significant stiffness changes negatively affecting their seismic behaviour. The typical variations are due to the existence of open galleries (porches) in Valparaíso at the bottom storeys and small cantilevers in the main façades. These variations have commonly conservative dimensions and regular shape, as shown in Figure 7-11. This study evaluates the influence of open galleries and cantilevers at the lower and upper storeys, respectively.

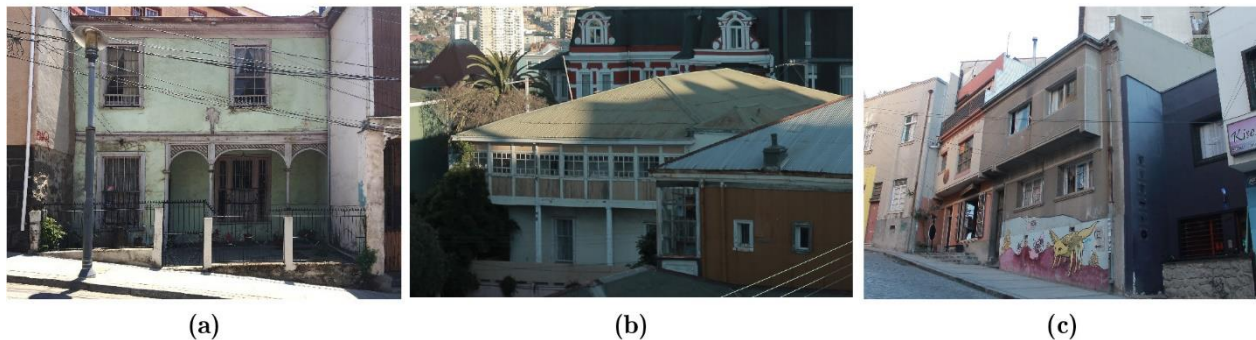


Figure 7-11. Vertical irregularities of the buildings of Valparaíso.

Figure 7-12 shows the models defined to study the influence of the vertical irregularities on the buildings of Valparaíso. For this parameter, only the homogeneous structural case is selected. The reference case (Figure 7-12a) is modified in order to represent the buildings with a gallery and a cantilever in the bottom and upper storeys, respectively. The second case has a setback of 1.2 m in the main façade at the ground level, and eight posts support the upper storey, as shown in Figure 7-12b. The case with a cantilever is represented by extending 1.2 m the upper story of the main façade, as shown in Figure 7-12c. NSA and the N2M were applied in the Y direction of the buildings to determine their seismic vulnerability orthogonal to the façade. The effect of the

vertical irregularities in the load-bearing is expected to be rather similar in the heterogeneous cases composed of masonry and timber frame walls.

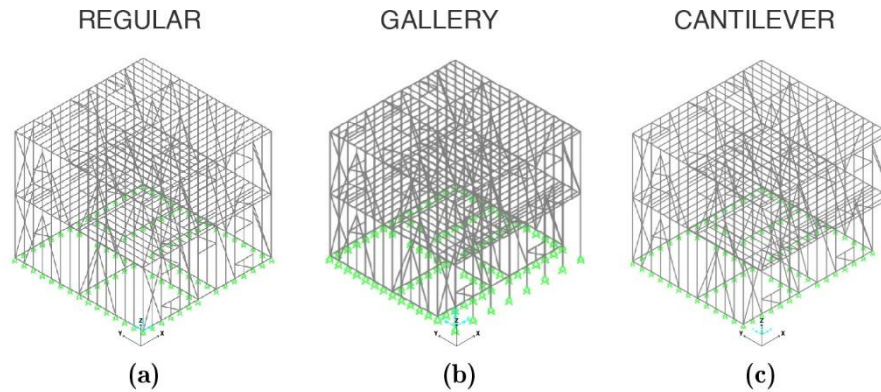


Figure 7-12. Parameter 6 “Vertical regularity”: numerical models.

Figure 7-13 shows the obtained capacity curves from the analyses in the Y direction. The results obtained from the simulations reveal that the variations in the vertical configuration have slight influence on the seismic behaviour of the buildings. The collapse mechanism of the buildings is governed by the failure of some of the diagonal connections of the timber frame walls located parallel to the applied load, similar to that occurred in the homogeneous cases analysed in the Parameter 3. Figure 7-14 compares the IM obtained for all the cases under study by applying the Equation (7-1). In this case, there is almost no difference between the buildings with gallery and cantilever variations in terms of IM. Besides, the differences among these cases and the regular one is limited, increasing the vulnerability by only 13%. Therefore, only two vulnerability classes are defined for this parameter. Buildings with regular vertical configurations represent the Class A scored with 0, and buildings with presence of cantilevers or galleries represent the Class B scored with 5 in the form. Table 7-5 summarized the I_M , scores and classes assigned to each case.

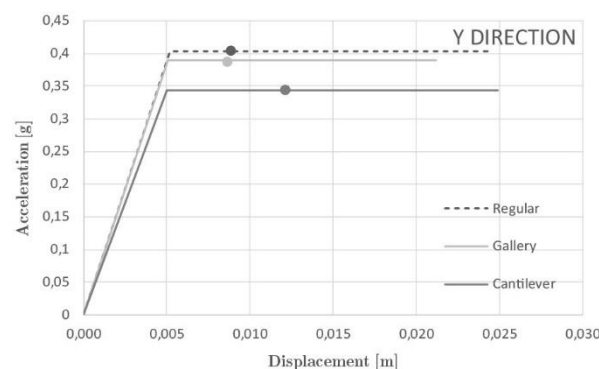


Figure 7-13. Parameter 6 “Vertical regularity”: Capacity curves and target displacement from the analysis in the Y direction.

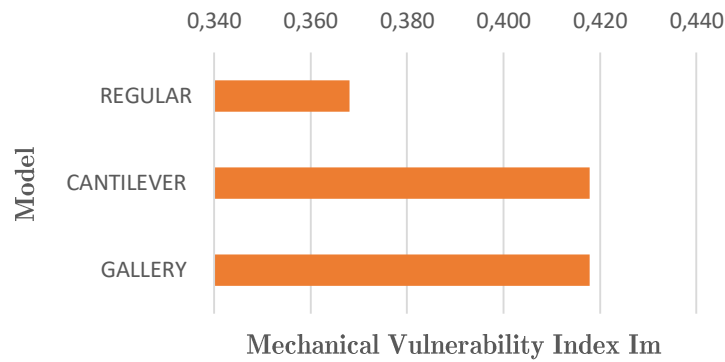


Figure 7-14. Parameter 6 “Vertical Regularity”: Mechanical Vulnerability Index I_M from the analysis in the Y direction.

Table 7-5. Parameter 6 “Vertical Regularity”: Scores and classes assignment.

MODELS	d_{MAX} [m]	d_u [cm]	I_M	Score	Class
REGULAR	0,00877	0,02383	0,368	0	A
CANTILEVER	0,01041	0,02492	0,418	5	B
GALLERY	0,00886	0,02119	0,418	5	B

(P7) Type of storey system

This parameter accounts for the in-plane stiffness of the storey systems based on their characteristic configurations. The relative stiffness of the horizontal diaphragm with respect to the stiffness of the vertical load-bearing systems determines how the shear forces and torsional moments transfer to the vertical members. Three types of storey systems are considered to investigate the influence of this parameter in the vulnerability of the structure: (i) flexible, (ii) light retrofitted (denoted as “LR”), and (iii) weighty retrofitted (denoted as “WR”). The flexible case is represented by considering a storey system made of timber joists. The LR and WR storeys are represented by using diaphragm constraints and creating links among the joints located within a storey plane such that they move together as a planar diaphragm, rigid against in-plane deformation but susceptible to out-of-plane deformations and associated effects. The difference between LR and WR storeys lies in the increment of mass to represent the presence of heavy stiffening interventions. The LR case has the same mass of the flexible case, and reproduce a condition in which the storey is stiffened by light steel or timber added members. The WR case reproduces the addition of a reinforced concrete topping of 0.05 m on the timber joists. Perfect connections are assumed among the frame and shell elements in all the cases. The influence of the type of storey is analysed by considering homogenous timber frame load-bearing systems. The relevant effect of this parameter can also be extrapolated to hybrid timber–masonry structures as

a simplification. NSA and the N2M were applied in the Y direction of the models to determine their seismic vulnerability orthogonal to the façade.

Figure 7-15 shows the obtained capacity curves of the models analysed in the Y direction. The results demonstrate that the type of storey has significant influence on the seismic capacity of the buildings. The presence of a light retrofitted storey increases the stiffness of the building in 37% with respect to the flexible case, as noted in Figure 7-15a. On the other hand, the case with weighty retrofitted storeys experience a significant decrease of 80% of acceleration capacity with respect to remaining cases. This effect is associated with the significant mass increment given by a weighty retrofitted intervention. The evidence from these results confirm the hypothesis that light retrofitted storeys substantially improve the seismic capacity of the buildings, whereas weighty retrofitted storeys increase their vulnerability. The characteristic collapse mechanism of the models is governed by the failure of some of the diagonal connections of the diagonal elements of the walls parallel to the applied load, similarly to the homogeneous cases analysed in the Parameter 3.

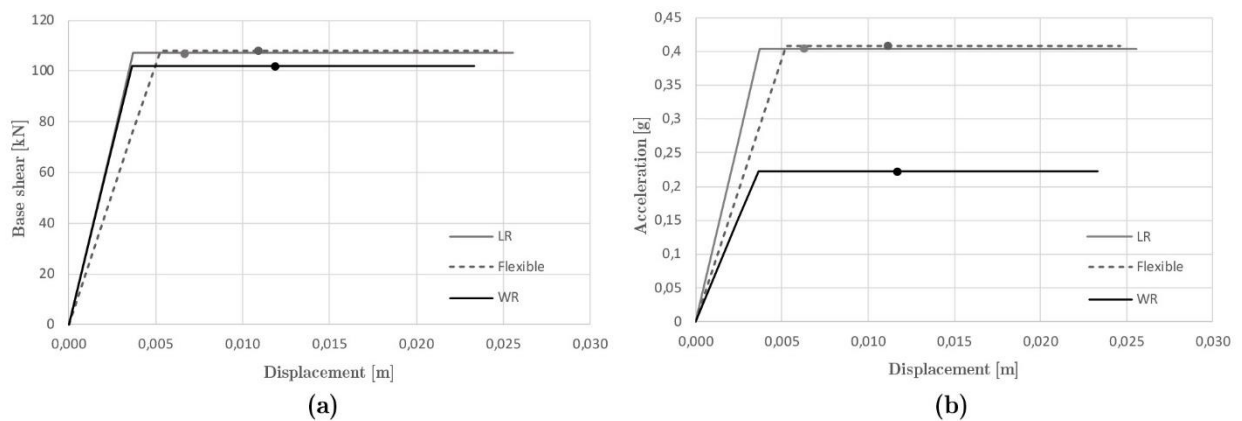


Figure 7-15 Parameter 7 “Type of storey system”: Capacity curves and target displacement from the analysis in the Y direction in terms of (a) base-shear-displacement and (b) acceleration-displacement.

Figure 7-16 compares the I_M obtained for all the cases by applying the Equation (7-1). The scores and classes were determined by evaluating the proportional differences of I_M (ΔI_M) among the cases with respect to the most vulnerable case, corresponding to the building with WR storey representing the Class D punted with 45 in the form. The cases with a light retrofitting (LR) represent the Class A scores with 0, whereas the flexible cases represent the Classes B-C and C, scores with 35. Table 7-6 summarizes the calibrated scores and classes of each case.

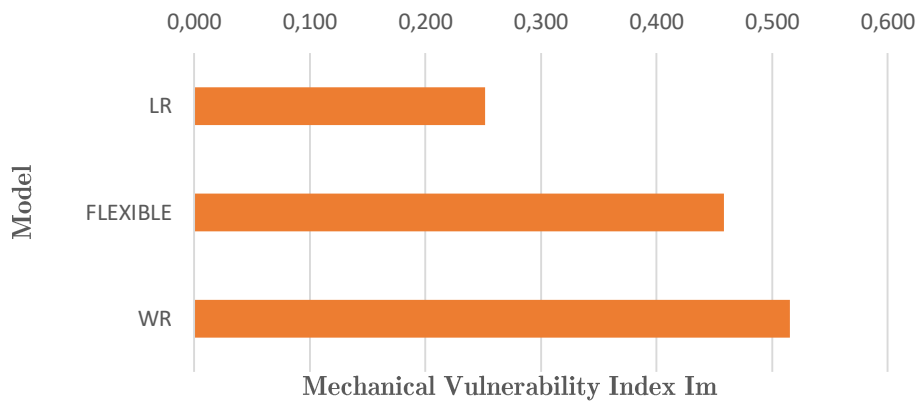


Figure 7-16. Parameter 7 “Type of storey system”: Mechanical Vulnerability Index I_M from the analysis in the Y direction.

Table 7-6. Parameter 7 “Type of storey system”: Scores and classes assignment.

MODELS	d_{MAX} [m]	d_u [m]	I_M	ΔI_M	Score rel.	Score	Class
LR	0,0064	0,0256	0,25	0,000	0	0	A
FLEXIBLE	0,0109	0,0238	0,46	-0,204	35	35	B-C
WR	0,0120	0,0233	0,52	-0,263	45	45	D

(P10) State of conservation

The state of conservation of the hybrid timber–masonry building of Valparaíso is mainly affected by the deterioration and damage of the timber frame elements and the joints. This is explained by the fact that timber frame walls are more exposed to decay than the masonry ones, which have mainly firewall roles and are commonly protected by the adjacent buildings. Common causes of wooden element degradation are termites’ attacks, faulty ventilation, exposure to moisture and the contact of these with the ground or masonry foundations, as shown in Figure 7-17.

Determining the influence of these factors in seismic vulnerability of the structural system is not simple in practice. On the one hand, the initial data regarding the mechanical properties of old materials is commonly unknown, so it is difficult to compare with the current properties of the materials. Also, the inherent natural wood variability can highly affect the ageing effect on different species. Cavalli et al. (2016) discussed the relevant literature around the mechanical properties of structural timber elements affected by ageing effects, demonstrating that the modulus of elasticity (MOE) is one of the most critical parameters involved in the loss of resistance of the timber elements. Several experimental data obtained from bending tests of old and new timber specimens revealed that MOE decreased between 15 to 42% for old timber elements (Cavalli et al. 2016). On the other hand, the mechanical damage on the timber connections can significantly affect the transfer of loads and reduce the capacity of the building. The type of connection and its specific mechanical properties also plays an important role in determining the

type and degree of damage. For instance, the looseness of the pieces of the mortise-and-tenon and dovetail joints decreases the capacity of the connections. Xue et al. (2019) tested mortise-and-tenon and dovetail joints with different degrees of looseness where the strength and stiffness reduced up to three times for the more loose samples. Quinn (2015) also compared the experimental results of two mortise-and-tenon joints specimens with loose and tight fit, where the tight connection was three times stiffer and 40% stronger than the loose one.

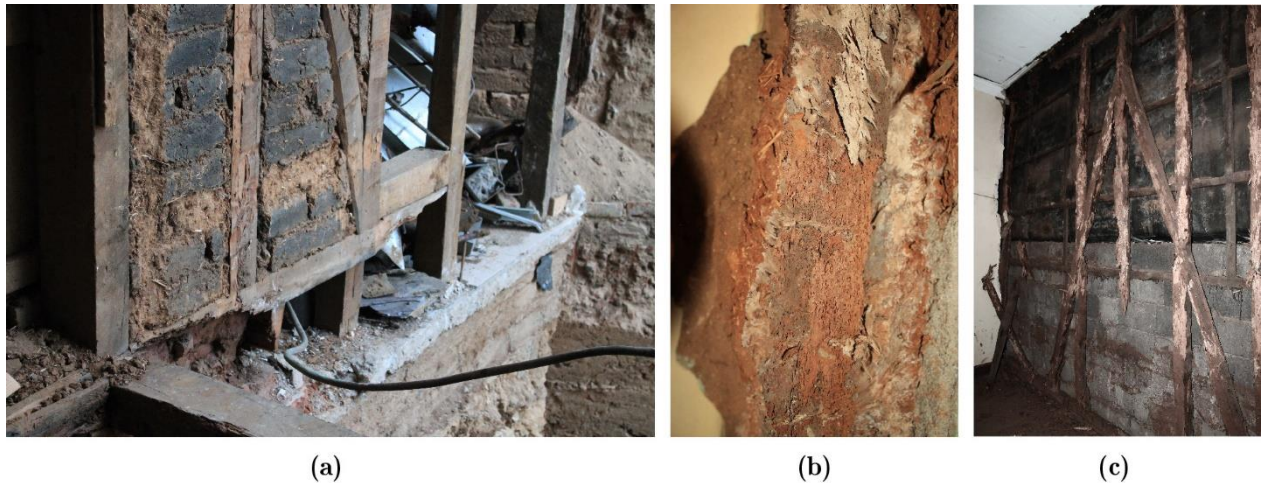


Figure 7-17. Deterioration of timber elements of different buildings in Valparaíso due to: (a) exposure to moisture, (b) termites' infestation, and (c) faulty ventilation and moisture.

Based on the above criteria, Parameter 10 investigates the influence of existing damage in the wooden elements and the joints in the seismic vulnerability of the structures. Four different models of homogeneous timber frame structural systems were set to evaluate the influence of these variations on the reference buildings. The first case (denoted as “Regular” in the following) assumes well-conserved conditions of both timber elements and joints. The second case (denoted as “MOE”) simulates deteriorated timber elements by reducing the elastic modulus of the material by 25%. The third case (denoted as “CONN”) assumed well-conserved timber elements but damaged connections by reducing their stiffness and strength capacity 30%. The last case (denoted as “MOE+CONN”) combines both timber deterioration and damage on the connections as defined in the previous cases. NSA and the N2M were applied in the Y direction of the buildings to determine their seismic vulnerability orthogonal to the façade.

Figure 7-18 displays the obtained capacity curves of the models analysed in the Y direction. The comparison of the results demonstrates that the case simulating the damage on the timber elements (MOE) denotes an important stiffness variation of 29% respect to the case without any type of damage (REGULAR), but a very slight reduction in terms of capacity. The case simulating the damage on the connections (CONN) presents a reduction of 34% in terms of capacity with respect to the regular case. As expected, the most critical case corresponds to the one simulated damage on both timber elements and connections, which reveals a reduction of 29% and 36% in terms of stiffness and capacity, respectively. These results demonstrate that global stiffness of the

buildings is mainly affected by the generalized damage on the timber elements, whereas the damage on the connection has a major influence in the reduction of the capacity of the buildings. The latter can be associated with the fact that the reduction of stiffness in the connections is very slight and the damage on them is much localized focused only in few of them located in the diagonals of the walls parallel to the applied load. The global collapse mechanism of the models is governed by the failure of the diagonal connections of the walls parallel to the applied load.

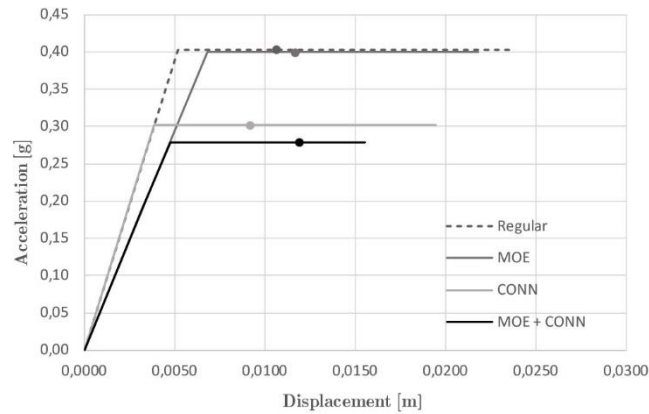


Figure 7-18. Parameter 10 “Physical conditions”: Capacity curves and target displacement.

Figure 7-19 compares the mechanical vulnerability index I_M obtained for the different cases by applying the Equation (7-1). The MOE+CONN represents the Class D punted with 45 in the form. The remaining classes and scores are assigned by establishing a proportional correlation between the I_M values with respect to the most vulnerable class. The case without damage (REGULAR) represents the Class A punted with 0, whereas the cases with damage on the connection (CONN) and the timber elements (MOE) represent the Class B and C, scored with 5 and 14 in the form, respectively. Table 7-6 summarizes the calibrated scores and classes of each case.

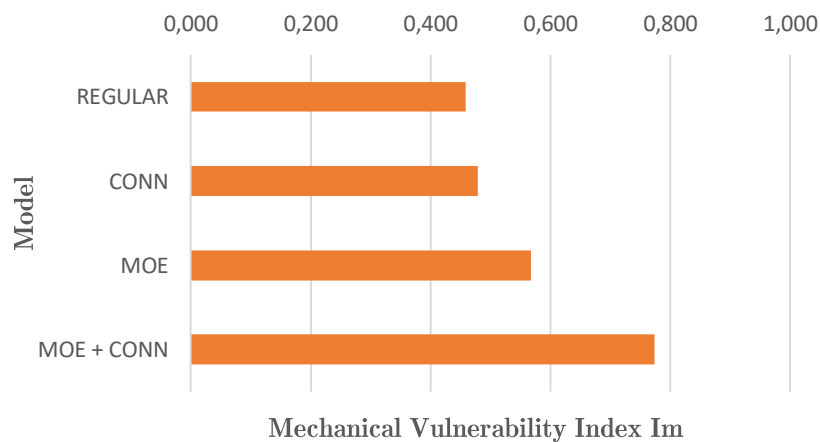


Figure 7-19. Parameter 10 “State of conservation”: Mechanical Vulnerability Index I_M from the analysis in the Y direction.

Table 7-7 Parameter 10 “Physical conditions”: Scores and classes assignment.

MODELS	d_{MAX} [m]	d_u[m]	I_M	ΔI_M	Score rel.	Score	Class
REGULAR	0,0109	0,0238	0,456	0,462	0	0	A
CONN	0,0093	0,0195	0,478	0,654	3	5	B
MOE	0,0120	0,0211	0,568	0,713	16	15	C
MOE + CONN	0,0121	0,0156	0,773	1,000	45	45	D

7.2.3 Proposed seismic vulnerability form

Table 7-8 displays the calibrated form for timber–masonry building typologies of the city of Valparaíso. The scores and classes of the calibrated parameters are based on the results presented in 7.2.2. and the remaining ones on those proposed by (Formisano et al. 2015). As in the original form developed by Benedetti and Petrini (1984), the weights of the parameters reflect the relative importance of each element in the seismic behaviour of the structure. Benedetti and Petrini (1984) defined three different importance groups: (i) primary importance elements, (ii) important elements, (iii) and secondary elements. These groups are expressed in quantitative terms attributing weights, ranging between 0.25 to 1.5 based on the importance of the parameter in quantifying the building vulnerability. Specifically, they are defined as follows: primary importance elements equal to 1.5; important elements between 0.5 to 1: and secondary elements lower than 0.5. A detailed guideline for the systematic evaluation of each parameter and application of the form is explained in Annex D.

Table 7-8. Vulnerability Index form for timber–masonry buildings.

N ^o	Parameters	Classes C _{v,i}				Weight
		A	B	C	D	p _i
1	Organization of vertical structures	0	5	20	45	1
2	Nature of the load-bearing system	0	5	25	45	0.25
3	Distribution of the resisting elements	0	10	30	45	1.5
4	Location of the building and type of foundation	0	5	25	45	0.75
5	Plan regularity	0	5	25	45	0.5
6	Vertical regularity	0	5	-	-	0.25
7	Type of storey system	0	35	35	45	1
8	Roofing system	0	15	25	45	0.75
9	Non-structural elements	0	0	25	45	0.25
10	State of conservation	0	5	15	45	1
11	Presence of adjacent buildings with different heights	-20	0	15	45	1
12	Position of the building in the aggregate	-45	-25	-15	0	1.5
13	Number of staggered storeys	0	15	25	45	0.5
14	Structural typological heterogeneity among adjacent structural units	-15	-10	0	45	1.2
15	Percentage differences of opening areas among adjacent buildings	-20	0	25	45	1

7.3 Seismic vulnerability at the Emergency Limit Condition of the neighbourhoods of Cerro Alegre, Cerro Concepción and the Port in Valparaíso, Chile.

7.3.1 Evaluation of the seismic vulnerability

The VIM is adopted to study the seismic vulnerability of the buildings within the ELC system of Valparaíso. This stock is characterized by its heterogeneous nature composed by hybrid timber–masonry, masonry and RC structural typologies, as mapped in Figure 7-20. The 68% of the building belong to the hybrid timber–frame and masonry classes, whereas the remaining 32% correspond to RC structural typologies. Considering this, specific vulnerability forms were implemented to evaluate each particular case. The hybrid timber–masonry buildings were evaluated by using the proposed vulnerability form detailed in Table 7-8, following the guideline attached in Annex D. The masonry buildings were assessed with the VIM form proposed by Formisano et al. (2015), displayed in Table 7-9, and the RC buildings using the VIM form proposed by GNDT-II (GNDT-SSN 1994), shown Table 7-10.

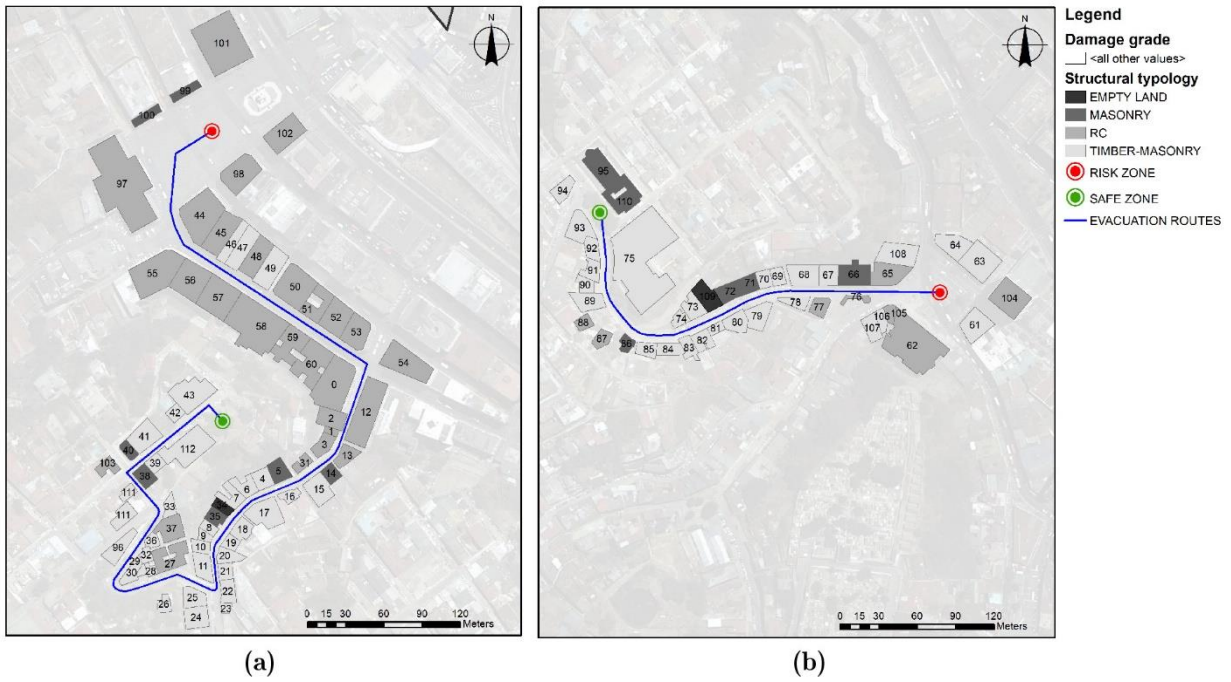


Figure 7-20. Structural typologies and FID labels of (a) Route A and (b) Route B.

The classes and corresponding scores of each parameter in the forms are assigned by inspecting both geometrical, morphological and structural features of the buildings. The computation of the vulnerability index considers the sum of all the weighted scores of each parameter by applying Equation (7-2), for masonry and timber–masonry buildings.

$$I_V = \sum_{i=1}^{15} C_{v,i} \cdot p_i \quad (7-2)$$

The vulnerability index of RC buildings is computed by considering only the sum of the scores, which is normalized using the correlations expressed in Table 7-10, as proposed by (GNDDT-SSN 1994). The obtained I_V values are normalized from 0 to 100 for a better understanding of the results for all the cases.

Table 7-9. Masonry Vulnerability Index form (Formisano et al. 2015).

Parameters	Class $C_{v,i}$				Weight
	A	B	C	D	p_i
P1 Organization of vertical structures	0	5	25	45	1,00
P2 Nature of the load-bearing system	0	5	25	45	0,25
P3 Distribution of the resistant elements	0	5	25	45	1,50
P4 Location of the building and type of foundation	0	5	25	45	0,75
P5 Plan regularity	0	5	25	45	0,50
P6 Vertical regularity	0	5	25	45	1,00
P7 Type of story system	0	5	15	45	0,75
P8 Roofing	0	15	25	45	0,75
P9 Details	0	0	25	45	0,25
P10 Physical conditions	0	5	25	45	1,00
P11 Presence of adjacent buildings with different heights	-20	0	15	45	1,00
P12 Position of the building in the aggregate	-45	-25	-15	0	1,50
P13 Number of staggered stories	0	15	25	45	0,50
P14 Structural typological heterogeneity among adjacent structural units	-15	-10	0	45	1,20
P15 Percentage differences of opening areas among adjacent buildings	-20	0	25	45	1,00

Table 7-10. RC Vulnerability Index form proposed by GNDT-II

Parameters	Class $C_{v,i}$				Vulnerability Index
	A	B	C	D	
P1 Type and organization of resisting system	0	-1,0	-2,0		$I_v^* = \sum_{i=1}^{11} C_{vi}$ Normalization: a) If $I_v^* > -6.5$, $I_v = -10.07 \cdot I_v^* + 2.5175$ b) If $I_v^* < -6.5$, $I_v = -1.731 \cdot I_v^* + 56.72$
P2 Quality of resisting system	0	-0.25	-0.5		
P3 Conventional strength	0.25	0	-0.25		
P4 Building position and foundations	0	-0.25	-0.5		
P5 Horizontal diaphragms	0	-0.25	-0.5		
P6 Plan configuration	0	-0.25	-0.5		
P7 In height configuration	0	-0.25	-1.5		
P8 Connection and critical elements	0	-0.25	-0.5		
P9 Low ductility elements	0	-0.25	-0.5		
P10 Non-structural elements	0	-0.25	-0.5		
P11 General maintenance conditions	0	-0.5	-1,0	-2.45	

Figure 7-21 depicted the normalized vulnerability indexes of the buildings within the ELC system by applying the VIM. The results of this prospective study show that the 50% of the buildings have an index between 0 to 20, which is considered as low to medium vulnerability, the 35% are between 20 to 30 and only the 15% exceed the 40, corresponding to medium-high and high levels of vulnerability respectively. The predominant low vulnerability of the buildings can be associated with several factors. First of all, the strong “seismic culture” of the city of Valparaíso

is reflected in the use of appropriate seismic resistant structures, even in vernacular or ancient structures built without compliance with seismic codes.

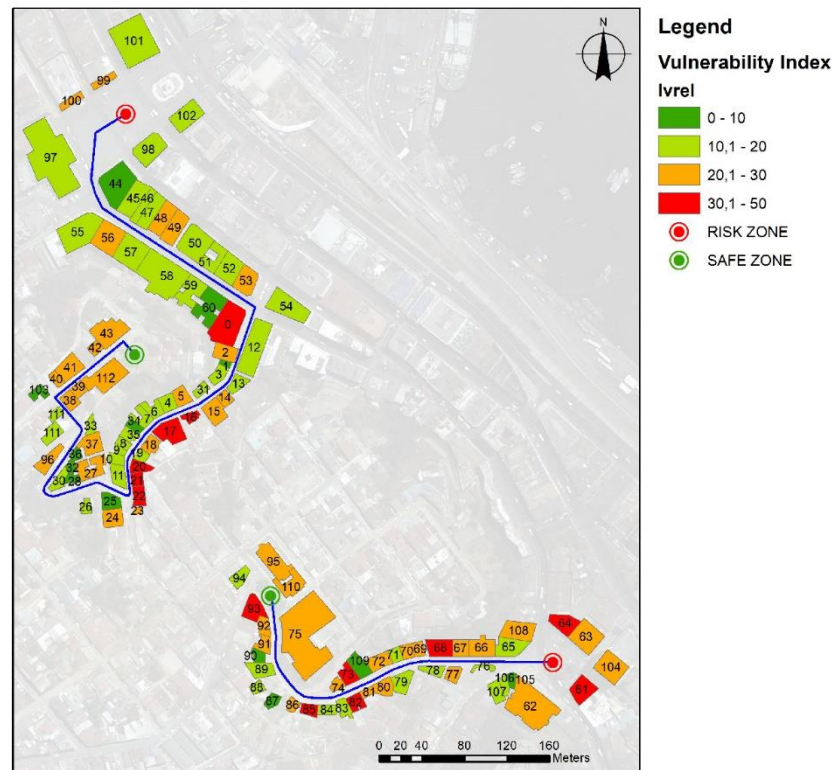


Figure 7-21. Normalized vulnerability indexes of the ELC system of Valparaíso.

The buildings made of hybrid timber–masonry structures have an average normalized vulnerability index of 21, which demonstrates a generalized low-medium vulnerability of the buildings. This trend can be associated with several factors. Firstly, most of the buildings present good quality load-bearing systems given by the use of proper bracing systems in the frame walls made of hardwood elements (Oak or Oregon Pine), which are well connected to the URM sidewalls (Figure 7-22) through semi-rigid storey systems, therefore are classified as A or B in the Parameters 1 and 2. Besides, most of the buildings have two and three storeys and are configured by hybrid structural systems made of timber frame and at least one URM sidewall. This effect is appraised in the P3, where most of the buildings are categorised in the Class B. In addition, most of the buildings have regular configuration both in plan and elevation (P5 and P6) and non-thrusting roof systems (P8). As noted in Figure 7-21, most of the buildings are enclosed in row structural aggregates, which highly contribute to decrease the vulnerability of the buildings, as evaluated from Parameters 11 to 15. Generally, the buildings are enclosed between buildings of the same typology, or between those with more rigid resisting systems (RC) that contribute to this favourable evaluation (Parameter 14). Some sources of vulnerability come from the slopped conditions of the terrain, especially in the buildings located in the Urriola and Almirante Montt streets (P4), and from the poor state of conservation of the buildings (P10). Fifteen buildings of this group present the highest normalized vulnerability between 30 and 50. In these cases, the

vulnerability is associated with different factors. As remarked in the vulnerability map (Figure 7-21), six buildings of the Urriola St. (labelled as 15,16,17, 20, 21 and 22) show vulnerable conditions. These cases are the tallest of the street (4 storeys), made of hybrid timber and URM walls, therefore categorized as D in the Parameter 3. Besides, all they are historical buildings with very poor state of conservation (P10). The same occurred with some buildings of the Urriola St. (68 and 85 in the map). On the other hand, eight buildings of this vulnerability group present header positions in the structural aggregates (15, 16, 17, 93, 85, 68, 41 and 94), which certainly increase their vulnerability with respect to the enclosed ones (Figure 7-23b, building 93).



Figure 7-22. Timber-masonry buildings: (a) masonry and timber frame interaction and (b) joist-masonry wall connection.



Figure 7-23. Timber-masonry buildings: located in (a) Almirante Montt street (labelled with 92 and 93 in Figure 7-21, respectively) and (b) Urriola street (21 and 22 in Figure 7-21).

The average normalized vulnerability index of the masonry structures is equal to 25, which expresses a medium-high level of vulnerability. Most of the buildings of this group were built before the release of the first seismic Chilean code (1960), however they present a good quality masonry made of clay brick and lime mortar in regular brickwork. (Class A and B in the 232

Parameters 1 and 2, respectively). These buildings are commonly well-connected to the story systems, with the use of metallic ties as inspected on-field. The assessment of the conventional strength of the buildings demonstrated that the 77% of the buildings have a favourable distribution of their resisting elements in plan (Classes A and B). Only two buildings of the stock located in the Sotomayor square (99 and 100) are categorized in Class C. This condition is attributed with the slender shape of the buildings in plan (Figure 7-24a), which is also penalized in the Parameter 5 “Plan regularity”. Furthermore, both these buildings have header positions in the structural aggregate, which contribute to increase their vulnerability. The building labelled as 95, 110 and 40 also present higher vulnerabilities mainly attributed to their isolated condition and visible damage on existing masonry (Figure 7-24b).



Figure 7-24. Masonry buildings (a) Historical constructions in Sotomayor square (label 99 and 100 in Figure 7-21), and (b) reinforced masonry building with visible damage in masonry (label 40).

Lastly, the RC buildings of the stock present an average of normalized vulnerability index of 18, which positions them as the less vulnerable of the stock. These results are associated with the newest nature of the RC buildings, most of them built in compliance with the Chilean seismic codes. These buildings present well-executed earthquake resistant systems, without existences of low-ductility elements and made of good quality materials. Furthermore, they present the better state of conservation of the stock, since most of them are located in the downtown area housing most of the commercial activity of the city. However, particular attention must be given to the taller and oldest buildings of the stock (Figure 7-25), which exceed the 25 points on the evaluation (buildings 0, 77, 104, 27, 37 and 62 in Figure 7-21).

It is important to highlight that there are some complex buildings within the analysed stock i.e. historical palaces and churches (*Palacio Baburizza*, *Palacio Bavestrello*, *Iglesia Anglicana* and *Edificio de la Armada de Chile*) that would need more in-depth vulnerability studies given they very particular structural arrangement. Therefore, the results presented in this Chapter must

be interpreted with caution as a preliminary analysis of a prospective study, since more investigation would be necessary for some specific structural typologies.

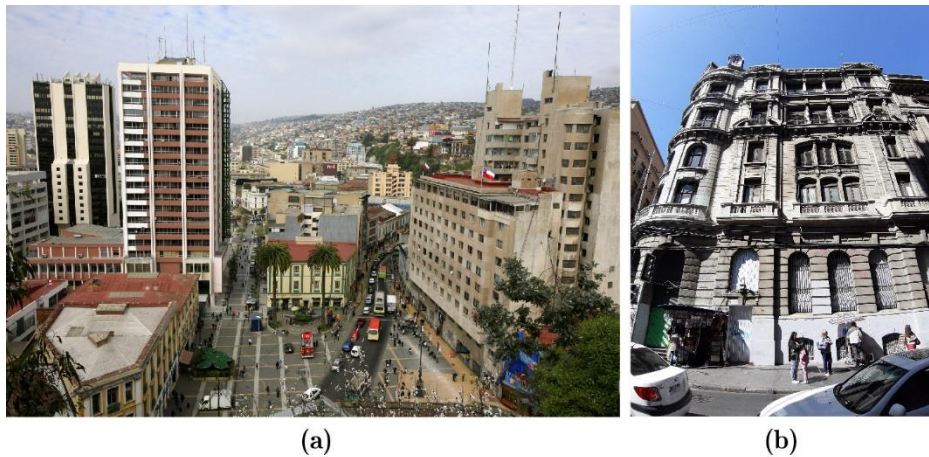


Figure 7-25. Reinforced concrete buildings (a) Tallest buildings in Almirante Montt square (label 61 and 62 in Figure 7-21) and (b) reinforced masonry building with critical damage in the masonry (label 0).

7.3.2 Final remarks

The vulnerability study of the buildings of the ELC systems allowed to recognise the critical points of the evacuation routes that could be potentially affected by the partial or total collapse of the building in case of an earthquake. One of the most critical zones is located in Urriola Street where six buildings of more than 3 storeys present high vulnerability indexes, as shown in X. A very concerning case is the corner building at the intersection of the Urriola and Arturo Prat streets (see Figure 7-25b). This correspond to a six-storey buildings made of traditional RC and iron structural system dating from 1915. Given by the large dimensions of the building, a partial or total collapse of the building could completely block the street, and prevent the access of the people to the evacuation route. Besides, the building presents numerous and large non-structural elements which could fall and injured people during the evacuation. A similar effect is expected if some of the buildings located in the upper part of the route collapsed, given by the narrow character of the street (see Figure 7-23b). Further mitigation strategies should be addressed to improve the state of conservation of these buildings, as well as plan strengthening interventions to safeguard the function of the evacuation route.

Another critical zone is located on the Anibal Pinto Square and Almirante Montt street. The former is characterized by the presence of high-rise RC buildings of more than 14 storeys which could potentially affect the access to the evacuation route towards security zone in the Almirante Montt Street in case of collapse. The Almirante Montt street present localized critical points given by the vulnerability of five buildings located at different height of the street. All these cases have more than three storeys and their collapse could trigger the partial block of the street which have also a narrow character.

7.4 Summary

This Chapter has presented a preliminary calibration of a new form for the evaluation of traditional timber–masonry buildings in compliance with the Vulnerability Index Method (VIM). This study has considered the re-examination of the original parameters, vulnerability classes and the associated scores included in the original form proposed by Benedetti and Petrini (1984), as well as those included by Formisano et al. (2015) for the evaluation of masonry structures in structural aggregates.

Three different sets of parameters were adopted by considering their particular nature and requirements. Some parameters were directly adopted from the aforementioned studies by judging their suitable applicableness to the timber–masonry buildings. These parameters are the ones related to the position of the building and foundations, in plan regularity, roof system, non-structural elements, and structural aggregate conditions. The classes of the parameters that involve the evaluation of the quality and nature of the structural systems were redefined based on the building taxonomies proposed in Chapter 4 and the scientific knowledge around the seismic performance of timber and masonry structures.

A numerical study was performed to reassign the classes and scores of the parameters that take into account the influence of irregularities on the structural system, type of storey systems, and the state of conservation of the structures. A sensitivity analysis was developed by applying nonlinear static analysis to determine the seismic capacity of several representative models of each parameter. The seismic performance of the buildings was analysed by applying the well-known N2 Method (N2M) considering the seismic demand of the city of Valparaíso. A mechanical vulnerability index was computed for each representative case to determine the seismic vulnerability and reassign the scores and classes.

The last part of the Chapter has presented the seismic vulnerability of 111 buildings in Valparaíso by applying the VIM. The analysis involved the application of the new VIM form for timber-masonry buildings, together with those existent in literature for masonry and reinforced concrete buildings. The computation of the vulnerability index for each building allows to determine the seismic vulnerability and the associated impact of their potential collapse on the evacuation routes inserted in the Emergency Limit Condition System of the study zone.

Chapter 8. Conclusions

8.1 Summary

The potential devastating consequences of major earthquakes in inhabited territories due to the collapse of the urban buildings has generated growing concern in the local community and engineering field. This concern has led to a great innovation in the development of seismic vulnerability assessment strategies. The seismic vulnerability of a building is defined as its proneness to experience damage in the case of occurrence of a seismic event, and its evaluation is not straightforward especially in structures located in historical urban centres.

Further contributions are still necessary in this important field of research, especially with regard to the vulnerability assessment of existing buildings. Among them, it is worth mentioning the development of robust databases with detailed information about the typologies and characteristics of the urban buildings, which are essential to provide the input data for the subsequent stage of evaluation of their seismic response. Another open field of research is that focused on the development of reliable methods for the assessment of the seismic vulnerability of existing buildings at a large scale. As many different typologies of buildings are available in the historical centres of the cities worldwide, the proposed methodologies have to be adapted to the different constructions, materials, and structural systems. Among the least investigated ones up to the date, it is worth mentioning the buildings composed of timber frames and masonry walls.

Chapter 2 of this thesis has offered a review of the available strategies for the large-scale assessment of the seismic risk. The analysis of the state of the art has focused especially on the seismic vulnerability approaches since they represent a central stage of risk assessment studies. A discussion around the suitability of the existing methodologies for different scenarios has been presented by explaining their requirements and scopes. Among the different available approaches in the literature, the easiest are the empirical or indirect methods. These procedures are expeditious, and based on simple vulnerability functions derived from post-earthquake surveys of damaged buildings. The current state of practice shows the difficulties related to the formulation of indirect methods in historical centres where there are no post-earthquake damage data available, and with unique traditional structural typologies. The most sophisticated procedures are the analytical or direct methods, based on the use of advanced numerical simulations to determine the seismic performance of the building. The accurate assessment of the seismic capacity of the existing buildings by nonlinear structural analyses, e.g. by using the Finite Element Method, makes the direct methods too expensive for large-scale urban assessments, due to the large computation costs and need for large amount of input data. The chapter has also analysed in

depth the available numerical modelling methods for the simulation of the seismic behaviour of the buildings, and the building survey strategies given their fundamental role in the seismic vulnerability assessments.

Chapter 3 has presented a brief overview of the case study of this doctoral thesis, consisting of three historical neighbourhoods of the city of Valparaíso, Chile, named *Cerro Alegre*, *Cerro Concepción* and the Port downtown area. This urban area has been selected, besides its important cultural value as heritage UNESCO World Heritage Site, due to its heterogeneous composition with different structural typologies, where hybrid timber–masonry buildings predominate. The city is characterized by a high exposition to seismic hazard, and to tsunamis. The case study of Valparaíso is challenging as its traditional buildings are unique and there are no detailed records about their performance after past major earthquakes. In addition, the local archives present fragmentary information about the characteristics of the existing buildings. The application of conventional seismic vulnerability methods is not feasible in Valparaíso, and this fact has motivated the research developed in this thesis, aimed at developing a reliable vulnerability assessment method at the urban level based on numerical simulations executed on representative typologies, i.e. the timber frame and masonry wall structures. The first part of Chapter 3 has explained the seismic hazard of the territory based on collected historical and technical data from the published literature and local archives. The second part of the chapter has established the object of the study by defining the Emergency Limit Condition (ELC) system within the selected three neighborhoods. This approach considers the analysis of strategic and potential interfering buildings that may block the emergency and safe areas defined by the civil protection plans, and especially the evacuation routes in the case of a tsunami. The analysis of this delimited system aims to conserve the functionality of the strategic urban functions in case of an emergency, with connections and accessibility within the territorial context. The identification of the ELC system has constituted a first pilot case that may be extended in the future to other vital networks and exposed elements in the city. The last part of Chapter 3 has introduced a brief characterization of some of the most representative structural systems existing in the ELC system. This characterization has revealed the important lack of technical building data, especially of ancient buildings, which constitutes a drawback for the development of the necessary studies on seismic vulnerability.

Chapter 4 has proposed a building survey strategy for heterogeneous urban areas in seismically hazardous zones, which lack consistent construction databases, such as the identified ELC system in the historical centre of Valparaíso. Four different typological survey forms have been proposed for masonry, reinforced concrete (RC), timber frame, and steel/iron structural systems. These forms gather information about the structural and non-structural features of the buildings that could influence their seismic response. The objective of the procedure has been the creation of a building taxonomy characterising the stock under analysis to determine the main sources of vulnerability in existing structures. A guidance for the systematic implementation of the forms is offered including the essential stages as the pre-field survey activities, on-field applications, and

post-field management of the collected data. The forms have been used to characterize the buildings existing in the ELC system of Valparaíso.

Chapter 5 has addressed the calibration of simplified and practice-oriented numerical models to simulate the seismic behaviour of timber frame and masonry structures. This study has dealt with the definition of proper modelling methods for timber frames and masonry walls. Different benchmark experimental programs on timber frame and masonry walls have been selected for simulation. The calibration of the models has been executed based on the comparisons between the results derived from experiments available in literature and the results from the numerical simulations of the tests. Four experiments on bare frame and infilled specimens of the Pombalino typology and “Quincha” walls have been selected to calibrate the timber frame models, whereas two experimental programs on masonry structures have been considered for simulation, including both the in-plane and out-of-plane behaviour of walls. Lumped Plasticity Models (LPM) and continuum Finite Element (FE) models have been adopted for timber frames and masonry walls, respectively. Nonlinear Static Analysis (NSA) has been performed to determine the capacity and failure mechanisms of the models. The proposed models have shown their capability to represent correctly the development of the failure mechanisms and the load-displacement response in all the simulations.

Chapter 6 has presented the application of the calibrated models to simulate the seismic behaviour of two representative timber–masonry buildings existing in the city of Valparaíso. The two models have combined LMP in beam FE elements with a continuum FE model for masonry walls. The mechanical properties of the materials have been defined based on the available data for this specific typology. The behaviour of the connections has been modelled based on the benchmark experiments analysed in Chapter 5, as they present important similarities with those of Valparaíso. Mass-proportional horizontal force distributions have been applied in the two main directions of the modelled buildings to simulate the effect of the earthquake actions through NSA. The models have shown to be capable of predicting the behaviour of the buildings by considering the interaction between timber frames and masonry structures. The N2 method (N2M) has allowed the evaluation of the performance of the buildings for two different seismic demands, corresponding to the spectra related to seismic design standards NCh433 Of. 96 (Instituto Nacional de Normalización 2009) for the city of Valparaíso, and to the 2010 Earthquake in Valparaíso. This application of the N2M has allowed the determination of the displacement demands of the buildings for the two different seismic scenarios.

Chapter 7 has proposed an extension of the well-known Vulnerability Index Method (VIM) to the hybrid timber–masonry building typologies. A new VIM form has been calibrated, in compliance with the existing ones for other structural typologies, and taking into account new criteria for the evaluation of some specific parameters. Some parameters have required a new definition of classes, weights and scores based on the results derived from numerical analyses. This approach has taken into account the building taxonomy proposed in Chapter 4, as well as the published literature around the seismic structural behaviour of timber and timber-masonry

structures. A sensitivity analysis by means of numerical simulations on some representative structural typologies has determined the influence of different structural parameters on the seismic response. Several physical models have been analysed to determine the quantitative influence of morphological and structural variations on the seismic behaviour of the buildings. The outcomes of the analyses have led to the evaluation of the classes, scores and weights. The NSA and the N2M have been employed to determine the seismic capacity and performance of each case. The seismic performance of each model has been quantified in terms of a Mechanical Vulnerability Index (I_M) (Formisano et al. 2015) which is the ratio between the horizontal displacement required by the seismic demand and the ultimate displacement. Scores and classes have been determined by evaluating the ranges of variation of the results. Finally, the weights of the new calibrated parameters have been formulated based on their importance within the global seismic behaviour of the structure, as established by Benedetti and Petrini (1984).

The seismic vulnerability assessment of the ELC zone, which is characterised by a heterogeneous building stock, has required the application not only of the novel VIM form for timber-masonry buildings, but also of the VIM forms already available for masonry and RC structural systems. The obtained vulnerability indexes for each building have been mapped by using a Geographic Information System (GIS) to display a territorial overview of the seismic vulnerabilities of the buildings in the urban tissue. These results constitute the point of departure for future seismic risk management and mitigation strategies with the aim to keep strategic routes and emergency zones safe in case of an earthquake. Knowing the seismic vulnerability of the buildings in inhabited zones, especially in those involved in emergency plans, contributes to raise the awareness of the seismic risk in both the citizens' community and civil protection organizations, and gives preliminary information to develop mitigation plans and seismic protection policies.

8.2 Conclusions

The conclusions of this thesis can be summarized as following:

- Seismic risk management at large-scale requires a comprehensive understanding of the urban territories, hazards and vulnerability of the exposed elements in case of an earthquake. To reach these goals, systematized work stages need to be preliminarily established, considering the scope of the study, the available technical data and the resources. Successful seismic risk assessment studies include the following essential activities:
 - (i) The implementation of building survey strategies to compile technical data and create building taxonomies characterizing the structural systems and their main sources of vulnerability, especially in cities lacking consistent building databases.
 - (ii) The selection of a suitable seismic vulnerability assessment method that allows the evaluation of the specific structural typologies existing in the territory under analysis.

- Hybrid seismic vulnerability approaches provide a suitable theoretical frame to address the assessment of urban areas lacking of consistent databases about post-earthquakes building damages. In this framework, numerical methods are helpful to predict the seismic nonlinear behaviour of specific structural systems, and they allow the calibration of simpler empirical (indirect) methods for large-scale applications.
- The use of macro modelling approaches to simulate the seismic behaviour of timber frame and masonry structures is an appropriate strategy to develop efficient and practice-oriented models. The numerical models proposed in this thesis, based on Lumped Plasticity and Continuum Finite Element models, can predict correctly the seismic capacity and collapse mechanisms of timber frame and masonry wall structures. These features have been demonstrated by means of the simulation of different benchmark experiments on timber frames tested by Poletti et al. (2015), Moore and D'Ayala (2011), Torrealva and Vicente (2012), and masonry walls tested by Augenti et al. (2011) and Griffith and Vaculik (2007)
- The proposed numerical models based on LPM and Continuum FEM have simulated the seismic response of two representative hybrid timber–masonry buildings of the city of Valparaíso. This application allows the identification of the local failures of the structural members of the buildings, leading to their global collapse. The results of this study have enhanced the understanding of the roles of timber and masonry structures in hybrid buildings, where seismic forces are transmitted to the timber frame elements after the failure of the wall. This response propitiates the nonlinear response of the buildings with a limited amount of ductility.
- Parametric analyses based on numerical simulations permit to identify the sources of vulnerability within the representative buildings of Valparaíso and reassign classes, scores and weights of the new parameters of the VIM form.
- The calibration of a new VIM form for hybrid timber–masonry buildings, based on numerical simulations of different typological structures and consistent sensitivity analysis of relevant parameters, has allowed the execution of the assessment of a heterogeneous urban area, comprising also heritage RC and masonry construction typologies.
- The use of a GIS framework has allowed the visualization at a large scale of the seismic vulnerability of buildings along strategic pathways of a city, and especially for the ELC after an earthquake. The use of GIS allows the identification of buildings requiring mitigation measures in the future in order to ensure the functionality of the evacuation routes during an earthquake.

8.3 Main contributions

This research has provided the following original contributions:

- The definition of a novel building survey strategy for heterogeneous urban areas in seismically hazardous zones. Specific typological survey forms have been proposed for masonry, timber

frame, RC, and mixed steel/iron structural buildings to collect essential information required for the seismic vulnerability assessment. The proposals of ad-hoc survey forms for historical mixed steel/iron and timber frame structures constitute an important novelty of this research. This study has contributed to the creation of a support tool for building taxonomies useful for studies oriented to the assessment of seismic vulnerability in cities lacking consistent building databases.

- The application of the proposed building survey forms to 111 buildings existing in the historical centre of the city of Valparaíso. This activity has permitted a preliminary overview of the vulnerability state of the existing buildings. Furthermore, it has contributed to fill the gap of technical knowledge around these structural typologies. Typological building taxonomy has characterized the structural attributes affecting the seismic performance and exposition of the buildings, i.e. the type of use, occupancy, date of construction, structural configuration, type of soil, and current conditions of conservation.
- The formulation and calibration, based on rigorous comparisons with available experimental tests, of simplified numerical models to simulate the seismic behaviour of hybrid timber–masonry buildings, by using LPM for frames and continuum FEM for walls. The adoption of macro-modelling approaches has allowed the derivation of practice-oriented numerical simulations characterised by simplicity in model preparation and low computational cost in the analysis, offering a good balance between efficiency and accuracy. The comprehensive numerical study has addressed in depth the following aspects:
 - (i) The calibration of the models based on the comparison between the results derived from experiments available in the literature and the outcomes from the numerical simulations of the tests.
 - (ii) The derivation of phenomenological constitutive laws to determine the nonlinear behaviour of traditional timber frame joints connecting the main timber frame structural elements, namely mortise-and-tenon and connections by contact. For timber frame modelling, nonlinear hinges and spring elements concentrate the nonlinearities at the end nodes of elastic frame elements, representing the nonlinear behaviour of the connections.
 - (iii) Modelling the influence of the masonry infill within the timber frame panels by using the simplified Equivalent Strut Method (ESM).
 - (iv) The derivation of a simplified constitutive model to represent the nonlinear behaviour of unreinforced masonry (URM) walls, for both tensile and compression responses. For masonry modelling, the smeared crack approach represents the damage propagation in the structures during the nonlinear analysis.
 - (v) The proper representation of the interaction between timber and masonry structural elements.
- The numerical application of the calibrated FE models to simulate the nonlinear seismic behaviour of two traditional hybrid timber–masonry buildings of the city of Valparaíso. The simulations have offered a good understanding of the interaction between timber frame and

masonry structures in hybrid typologies by predicting the sequence of local mechanisms occurring in the structures up to their ultimate capacity and collapse of the building. This contribution opens a research line in the field of numerical modelling of historical buildings of the city of Valparaíso, and even of other similar timber–masonry typologies in Latin America.

- The extension of the applicability of the VIM to the evaluation of hybrid timber–masonry buildings. The calibration of a new VIM form for this typology has allowed the implementation of the method in a built-up area with heterogeneous structural typologies, such as the case of the three selected neighbourhoods of Valparaíso.
- The seismic vulnerability assessment at the urban scale of an identified ELC system in Valparaíso by applying the VIM. This study has contributed to the increase of the knowledge around the main sources of vulnerability of the buildings belonging to two of the main evacuation routes of the city of Valparaíso in the case of an earthquake. The results of this study have provided a preliminary knowledge to detect the buildings that might threaten the evacuation routes in case they experienced a partial or total collapse. This understanding may permit to carry out mitigation measures to ensure the minimum functionality of the ELC system in case of future seismic events. These results can be useful to upgrade civil protection plans, in agreement with conservation initiatives of the built cultural heritage.

8.4 Suggestions for future work

This thesis closes with the following suggestions for future research work:

Numerical modelling

- The improvement of the numerical modelling strategies for simulating the seismic behaviour of timber frame and masonry structures. This thesis has adopted, as a preliminary contribution to the topic, the commercial software SAP2000 (CSI 2016b). The available constitutive models for the LPM and continuum FEM in SAP2000 were originally developed for RC frame and wall structures, and thus they have required several adjustments prior to their execution in this thesis. Instead of using a general-purpose program, a specific numerical tool could be formulated for the structural analysis of timber frame structures, including also suitable moduli for the modelling of masonry walls.
- The increase of the level of detail in the modelling representation for specific case studies. This research has considered, as a first approach, a very simple numerical model, made of 1D FE elements for timber frames and 2D continuous FE for masonry walls, with simplified constitutive models, as the objective was the calibration of a practice-oriented numerical tools suitable for large-scale assessments, and thus with limited computation cost. A more detailed representation of the materials may be explored by using enhanced material models to improve the representation of the damage and collapse mechanisms

for the most complex types of timber-masonry structures. For instance, the use of more sophisticated models would be recommended for a more accurate representation of damage propagation in masonry (P. Lourenço et al. 2018) and timber structures (Lukic et al. 2018). These improved models may include important aspects that have been neglected for the sake of preserving the simplicity of the numerical approach in this thesis, such as the representation of the anisotropic behaviour of both timber and masonry materials, as well as the description of their nonlinear dynamic behaviour. It is important to highlight, however, that the more complex and sophisticated the model, the higher the computational cost. Therefore, a good balance between accuracy and calculation effort should be always maintained for practice oriented large-scale simulations, while keeping enhanced models for specific analyses of complex problems deserving in-depth investigations.

- The improvement of the description of the mechanical laws for timber connections. This thesis has considered simple empirical laws derived from available experiments, and modelled by means of spring-like elements. More detailed models could be formulated including frictional effects as well as a more precise description of the interaction among all the members involved in the connection, e.g. steel nails and cut pieces of timber.
- The execution of additional experimental tests to assess the structural behaviour of timber-masonry structures. An important drawback encountered during the calibration of the numerical models has been the lack of experimental data on the structural systems representative of the traditional architecture of the city of Valparaíso. This lacking has made the calibration of the numerical models rather difficult, leading to the consideration of the only experiments available for similar structural systems in other countries, e.g. Portugal and Perú, as well as of typical mechanical properties of the materials reported in literature. The development of new experimental data on these structural typologies would be very useful to improve the accuracy of the simulations in future research. Such experimental campaigns should include a comprehensive study of the material properties (timber, masonry and adobe), as well as tests on the masonry and timber frame walls, and traditional joints under lateral loading (e.g. Poletti et al. 2015; Torrealva and Vicente 2012; Moore and D’Ayala 2011).
- The comprehensive numerical study of the influence of the aggregate configuration on timber-masonry buildings. This thesis has not addressed the simulation of groups of buildings according to urban block configurations, but only of individual units. It is well-known that the aggregate configuration enhances remarkably the seismic response of the buildings, as demonstrated in Formisano and Massimilla (2018), Formisano et al. (2015) and Ramos and Lourenço (2004). As a preliminary attempt, this thesis has considered as a reference the results found by Formisano et al. (2015) for masonry buildings. Future numerical simulations may consider the detailed modelling of the buildings of Valparaíso grouped according to the existing aggregate configurations.

- The evaluation of the effect of the direction of the horizontal forces on the seismic response of the buildings. This study has considered as a first approach the X and Y “principal” directions of the buildings in the NSA. Recent studies (Kalkbrenner, Pelà, and Sandoval 2019) have shown that multi-directional pushover analyses can lead to improved results on the seismic vulnerability of existing buildings, especially when the structure is irregular and local failure mechanisms predominate.
- The formulation of numerical models for other hybrid typologies recurrent in historical centres, e.g. steel/iron-RC and steel/iron-masonry structures. These buildings are rather frequent in historical urban centres, and their hybrid character often implies a high degree of irregularity. For this reason, detailed numerical studies on these types of structural typologies may contribute to a better knowledge of their seismic behaviour.

Seismic risk and vulnerability assessment

- The extension of the vulnerability assessment to other structural typologies existing in heterogeneous urban centres prone to earthquakes. As shown in this thesis, the seismic vulnerability assessment of the buildings requires a comprehensive evaluation of the singular structural parameters influencing their seismic response. The calibration of proper vulnerability forms for other building typologies, i.e. steel, hybrid RC-steel/iron, hybrid/iron-masonry is recommended to extend the scope of this thesis (Sangiorgio et al. 2019; Omar and Mahmoud 2017; Salazar and Ferreira 2020; Taffarel et al. 2014).
- The enlargement of the seismic vulnerability assessment to other neighbourhoods of the city of Valparaíso. This task represents a very interesting challenge given the predominant vernacular nature of the residential buildings of the city, comprising a wide variety of existing construction and structural systems, added to the uncertainties associated to the lack of building technical data, and the lack of compliance with current seismic codes. Inherent work-stages linked to the extension of the seismic vulnerability assessment are the data-collection strategies to create robust building databases by applying the proposed survey methodology developed in Chapter 4. This activity would contribute to build a whole building taxonomy of the city to identify the sources of seismic vulnerability in different structural typologies. As data collection is a rather time-demanding process, a possible recommendation is the implementation of systematized and massive survey strategies, guided by large scope projects, governmental or civil protection initiatives.
- The enhancement of the seismic vulnerability assessment by considering uncertainties associated with the change of the earthquake direction. Substantial work on this field was reported in previous studies (Basaglia et al. 2018, and Cara et al. 2018), which evaluated the effect of the earthquake direction through an “elliptical” vulnerability concept. This effect can be accounted by modifying the Parameter 3 “Distribution of resisting elements” also known as “Conventional Strength” in the VIM to consider the effect of different possible earthquakes directions.

- Further analytical investigations to determine the seismic vulnerability and damage grade of the buildings given different levels earthquake intensity, after the application of the VIM to the historical centre of Valparaíso. The Macroseismic Method (Giovinazzi and Lagomarsino 2004) represents a suitable approach for this type of studies. This method derived analytical correlations between the vulnerability index and the Macroseismic Scale by employing Damage Probability Matrices and vulnerability functions consistent with damage surveys after major earthquakes. Several authors employed the theoretical framework of the method to calibrate proper correlations for different building typologies, i.e. Giovinazzi and Lagomarsino (2004) and Ferreira, Rodrigues, and Vicente (2020), Vicente et al. (2008), Basaglia et al. (2018). Extended applications of the VIM are required to obtain enough amount of data towards the construction of damage probability matrices and correlate the vulnerability index results with a macroseismic scale.
- The study of the socio-economic impacts in case of a major earthquake due to the partial or total collapse of the buildings. The implementation of socio-economic loss estimation models is recommended to quantify the short-term and long-term impacts, such as the effect on people and communities, casualties, damage to buildings and residences, disruption of vital networks of the cities as well as the estimation of repair costs (i.e. (Ferreira, Rodrigues, and Vicente 2020; FEMA 2003; HAZUS 1999; Basaglia et al. 2020)). These studies would also enable the cost-benefit analysis of the localized strengthening solutions in the most vulnerable buildings and optimize the risk management and mitigation strategies.
- The evaluation of seismic strengthening solutions towards the reduction of the seismic vulnerability of existing timber–masonry buildings. Once the main vulnerabilities of the buildings have been detected, seismic retrofitting techniques compliant with building conservation principles could be managed in order to get cost-efficient mitigation strategies. The impact of such strategies on the territory may be evaluated by updating the vulnerability indicators on existing buildings, leading to the evaluation of the expected damage grade in the urban system for different levels of seismic hazard. The use of GIS maps may help to support this activity and to optimize the allocation of resources on the territory to mitigate the vulnerability of the urban asset.
- The extension of the proposed vulnerability procedures to account for other types of hazards, beside the seismic one. In the specific case of the city of Valparaíso, it would be very interesting a study addressing the combined risk due to earthquakes, fires and tsunamis.

References

- Algermissen, S.T., E. Kausel, S. Hanson, and P.C. Thenhaus. 1992. "Earthquake Hazard in Chile." *Revista Geofísica* 37: 195–218.
- American Society of Civil Engineers (ASCE). 2014. *Seismic Evaluation and Retrofit of Existing Buildings. Standard ASCE/SEI 41-17*. Edited by ASCE. <https://doi.org/10.1016/j.aqpro.2013.07.003>.
- Astroza, Rodrigo, Hamed Ebrahimian, and Joel P. Conte. 2015. "Material Parameter Identification in Distributed Plasticity FE Models of Frame-Type Structures Using Nonlinear Stochastic Filtering." *Journal of Engineering Mechanics* 141 (5): 04014149. [https://doi.org/10.1061/\(ASCE\)EM.1943-7889.0000851](https://doi.org/10.1061/(ASCE)EM.1943-7889.0000851).
- ATC. 1985. "Earthquake Damage Evaluation Data for California (ATC-13)." *Applied Technology Council*. <http://nisee.berkeley.edu/elibrary/Text/S22323>.
- . 1996. "ATC40, Seismic Evaluation and Retrofit of Concrete Buildings." *Applied Technology Council* 1: 334. <https://doi.org/10.1193/1.1586093>.
- Augenti, N, F Parisi, A Prota, and G Manfredi. 2011. "In-Plane Lateral Response of a Full-Scale Masonry Subassemblage with and without an Inorganic Matrix-Grid Strengthening System." *Journal of Composites for Construction* 15 (4): 578–90. [https://doi.org/10.1061/\(ASCE\)CC.1943-5614.0000193](https://doi.org/10.1061/(ASCE)CC.1943-5614.0000193).
- Augenti, N, and Fulvio Parisi. 2010. *Constitutive Models for Tuff Masonry under Uniaxial Compression. Journal of Materials in Civil Engineering - J MATER CIVIL ENG*. Vol. 22. [https://doi.org/10.1061/\(ASCE\)MT.1943-5533.0000119](https://doi.org/10.1061/(ASCE)MT.1943-5533.0000119).
- Baggio, C., A. Bernardini, R. Colozza, L. Corazza, M. Bella, G. Pasquale, M. Dolce, et al. 2007. "Field Manual for Post-Earthquake Damage and Safety Assessment and Short Term Countermeasures (AeDES)." *JRC Scientific and Technical Reports*.
- Baquedano, F., and F. Leyton. 2012. "Frecuencia Predominante de Los Suelos de Valparaíso-Viña Del Mar y Propuest de Microzonificación Preliminar." In *VII Congreso Chileno de Geotécnia*. Santiago (Chile).
- Barbat, A. H., M. L. Carreño, L. G. Pujades, N. Lantada, O. Cardona, and M.C. Marulanda. 2010. "Seismic Vulnerability and Risk Evaluation Methods for Urban Areas. A Review with Application to a Pilot Area." *Structure and Infrastructure Engineering* 6 (4): 499–499. <https://doi.org/10.1080/15732479.2010.481841>.
- Barrientes, S. 1988. "Slip Distribution of the 1985 Central Chile Earthquake." *Tectonophysics* 145: 225–24.
- Basaglia, Alberto, Alessandr Aprile, Enrico Spacone, and Francesco Pilla. 2018. "Performance-Based Seismic Risk Assessment of Urban Systems." *International Journal of Architectural Heritage* 12 (7–8): 1131–49.
- Basaglia, Alberto, Alessandra Aprile, Enrico Spacone, and Luca Pelà. 2020. "Assessing Community Resilience, Housing Recovery and Impact of Mitigation Strategies at the Urban Scale: A Case Study after the 2012 Northern Italy Earthquake." *Bulletin of Earthquake Engineering* 18 (13): 6039–74. <https://doi.org/10.1007/s10518-020-00919-8>.
- Belmouden, Y., and P. Lestuzzi. 2009. "An Equivalent Frame Model for Seismic Analysis of

- Masonry and Reinforced Concrete Buildings.” *Construction and Building Materials* 23 (1): 40–53. <https://doi.org/10.1016/j.conbuildmat.2007.10.023>.
- Benedetti, D., and M.A. Parisi. 1988. “Seismic Vulnerability and Risk Evaluation for Old Urban Nuclei.” *Earthquake Engineering and Structural Dynamics* 16: 183–201.
- Benedetti, D., and V. Petrini. 1984. “Sulla Vulnerabilità Sismica Di Edifici in Muratura i Proposte Di Un Metodo Di Valutazione.” *L’industria Delle Costruzioni* Vol. 18: pp.66-74.
- Bertoldi, S.H., L.D. Decanini, and C. Gavarini. 1993. “Telai Tamponati Soggetti Ad Azioni Sismiche Un Modello Semplificato Confronto Sperimentale e Numerico.” In *6th Convegno Nazionale L’Ingegneria Sismica in Italia*, 815–24. Perugia.
- Bilgin, H., and O. Korini. 2014. “A New Modeling Approach in the Pushover Analysis of Masonry Structures.” *International Students’ Conference of Civil Engineering, ISCCE, 10-11 May 2012, Epoka University, Tirana, Albania*, no. May: 10–11.
- Bocca, Pietro, Alberto Carpinteri, and Silvio Valente. 1989. “Fracture Mechanics of Brick Masonry: Size Effects and Snap-Back Analysis.” *Materials and Structures* 22: 364–73. http://staff.polito.it/alberto.carpinteri/papers/CARPINTERI_1989_N.72_MS.pdf.
- Boroschek, R., P. Soto, and R. León. 2010. “Registros Del Terremoto 27 de Febrero de 2010.” Santiago (Chile).
- Brzev, B, C. Scawthorn, A.W. Charleson, L. Allen, M Greene, K Jaiswal, and V. Silva. 2013. “GEM Building Taxonomy Version 2.0.”
- Calvi, G. M., R. Pinho, G. Magenes, J. J. Bommer, L. F. Restrepo-Vélez, and H. Crowley. 2006. “Development of Seismic Vulnerability Assessment Methodologies over the Past 30 Years.” *ISET Journal of Earthquake Technology* 43 (472): 75–104.
- Cara, Selma, Alessandra Aprile, Luca Pelà, and Pere Roca. 2018. “Seismic Risk Assessment and Mitigation at Emergency Limit Condition of Historical Buildings along Strategic Urban Roadways. Application to the ‘Antiga Esquerra de L’Eixample’ Neighborhood of Barcelona.” *International Journal of Architectural Heritage* 12 (7–8): 1055–75. <https://doi.org/10.1080/15583058.2018.1503376>.
- Cardona, O.D., and L.E. Yamin. 1997. “Seismic Microzonation and Estimation of Earthquake Loss Scenarios: Integrated Risk Mitigation Project of Bogota, Colombia.” *Earthquake Spectra* 13 (4): 795–814.
- Castañeda, R. 2013. “Actualización de La Microzonificación Sísmica de La Ciudad de Valparaíso.” Universidad Técnica Federico Santa María. <https://repositorio.usm.cl/handle/11673/2984>.
- Cavalli, Alberto, Daniele Cibecchini, Marco Togni, and Hélder S. Sousa. 2016. “A Review on the Mechanical Properties of Aged Wood and Salvaged Timber.” *Construction and Building Materials*. Elsevier Ltd. <https://doi.org/10.1016/j.conbuildmat.2016.04.001>.
- Ceccotti, A., and C. Sandhaas. 2015. “A Proposal for a Procedure to Evaluate the Seismic Vulnerability of Historic Timber Frame Buildings.” In *Historical Earthquake-Resistant Timber Frames in the Mediterranean Area*, edited by Ruggieri Nicola, Gennaro Tampone, and Raffaele Zinno, 1st ed., 105–18. Switzerland: Springer International Publishing. <https://doi.org/10.1007/978-3-319-16187-7>.
- CEN. 1999. “EN 1926. Natural Stone Test Methods—Determination of Compressive Strength.”
- . 2004. “Eurocode 8: Design of Structures for Earthquake Resistance. Part 1: General Rules, Seismic Actions and Rules for Buildings. EN 1998-1:2004.” Vol. 3. Brussels.
- . 2005a. “EN 14580. Natural Stone Test Methods Determination of Static Elastic Modulus Active, Most Current Details History References Organization: CEN Publication Date: 1

-
- April 2005 Status: Active Page Count: 18 ICS Code (Mineral Materials and Products): 91.100.1.”
- . 2005b. “EN 1996-1-1: Eurocode 6: Design of Masonry Structures - Part 1-1: General Rules for Reinforced and Unreinforced Masonry Structures.” <https://www.phd.eng.br/wp-content/uploads/2015/02/en.1996.1.1.2005.pdf>.
- CEN EC5 1.2. 2004. “Eurocode 5 – Design of Timber Structures Part 1-2: General – Structural Fire Design.” *Eurocode 5 – Design of Timber Structures* 2004: 1–69. <https://doi.org/10.1680/cien.2001.144.6.39>.
- Chen, Chunchao, Hongxing Qiu, and Yong Lu. 2016. “Flexural Behaviour of Timber Dovetail Mortise-Tenon Joints.” *Construction and Building Materials* 112 (June): 366–77. <https://doi.org/10.1016/j.conbuildmat.2016.02.074>.
- Chui, Y. H., and C. Ni. 1997. “Load-Embedment Response of Timber to Reverse Cyclic Load.” *Wood and Fiber Sci.* 29 (2): 148–60.
- Chun, Qing, Zhi Yue, and JianWu Pan. 2011. “Experimental Study on Seismic Characteristics of Typical Mortise-Tenon Joints of Chinese Southern Traditional Timber Frame Buildings.” *SCIENCE CHINA Technological Sciences* 54 (9): 2404–11. <https://doi.org/10.1007/s11431-011-4448-3>.
- Ciucci, M. P. 2015. “Structural Analysis of the Timber Structure of Ica Cathedral, Peru.”
- Ciucci, M.P., S. Sharma, and P. B. Lourenço. 2018. “Engineering Simulations of a Super-Complex Cultural Heritage Building: Ica Cathedral in Peru.” *Meccanica* 53 (7): 1931–58. <https://doi.org/10.1007/s11012-017-0720-3>.
- Coburn, A.W., and R. Spence. 2002. *Earthquake Protection*. Edited by John Wiley & Sons Ltd. Chichester, England.
- Comité Comunal de Protección Civil y Emergencia. 2019. “Plano de Evacuación Ante Tsunami. Región de Valparaíso. Comuna de Valparaíso - Sector Barrio Puerto.” ONEMI. 2019. <https://www.onemi.gov.cl/wp-content/uploads/2019/07/Valparaíso-puerto.pdf>.
- Commissione tecnica per la microzonazione sismica. 2014. *Manuale per l'analisi Della Condizione Limite per l'Emergenza (CLE) Dell'insediamento Urbano. Versione 1.0*. 1.0. Roma: Dipartimento della Protezione Civile. <http://www.protezionecivile.gov.it/resources/cms/documents/CLE2.pdf>.
- Concreto Revista de Ingeniería y Arquitectura. 1919. “Edificio de La Bolsa de Corredores.” *Concreto Revista de Ingeniería y Arquitectura*, 1919.
- CSI. 2016a. “CSI Analysis Reference Manual.”
- . 2016b. “Technical Notes Manual For SAP2000.” www.csiamerica.com.
- Curls, J.S, and S. Wilson. 2015. *The Oxford Dictionary of Architecture*. 3th ed. Oxford: Oxford University Press. <https://doi.org/10.1093/acref/9780199674985.001.0001>.
- D’Ambra, C., G.P. Lignola, and A. Prota. 2016. “Multi-Scale Analysis of In-Plane Behaviour of Tuff Masonry.” *The Open Construction and Building Technology Journal* 10 (1): 312–28. <https://doi.org/10.2174/1874836801610010312>.
- D’Ayala, D., A. Meslem, D. Vamvatsikos, K. Porter, T. Rossetto, H. Crowley, and V. Silva. 2013. “Guidelines for Analytical Vulnerability Assessment - Low/Mid-Rise.” *GEM Technical Report* 08: 162. <https://doi.org/10.13117/GEM.VULN-MOD.TR2014.12>.
- Darwin, D, and D.A.W. Pecknold. 1974. “Inelastic Model for Cyclic Biaxial Load-Ing of Reinforced Concrete.” URBANA, ILLINOIS.
- . 1977. “Nonlinear Biaxial Stress-Strain Law for Concrete.” *Journal of the Engineering*

- Mechanics Division* 103 (2): 231–41.
- Decanini, Luis, Fabrizio Mollaioli, Andrea Mura, and Rodolfo Saragoni. 2004. “Seismic Performance of Masonry Infilled R/C Frames.” In *13th World Conference on Earthquake Engineering*.
<http://citeseerx.ist.psu.edu/viewdoc/download?doi=10.1.1.471.603&rep=rep1&type=pdf>.
- Dumova-Jovanoska, E. 2000. “Fragility Curves for Reinforced Concrete Structures in Skopje (Macedonia) Region.” *Soil Dynamics and Earthquake Engineering* 19 (6): 455–66.
[https://doi.org/10.1016/S0267-7261\(00\)00017-8](https://doi.org/10.1016/S0267-7261(00)00017-8).
- Duğu, A., H. Sakata, and Y. Yamazaki. 2015. “Experimental Study on Timber-Framed Masonry Structures.” In *Historical Earthquake-Resistant Timber Frames in the Mediterranean Area*, edited by Nicola Ruggieri, Gennaro Tampone, and Raffaele Zinno, 171. Springer, Cham.
- Endo, Yohei, Luca Pelà, Pere Roca, Francesca da Porto, and Claudio Modena. 2015. “Comparison of Seismic Analysis Methods Applied to a Historical Church Struck by 2009 L’Aquila Earthquake.” *Bulletin of Earthquake Engineering* 13 (12): 3749–78.
<https://doi.org/10.1007/s10518-015-9796-0>.
- Eujenio, N. 2015. “Sistema Constructivo de Madera En Armaduras de Techumbre.” Tesis de licenciatura, Universidad Técnica Federico Santa María.
- Fah, D., F. Kind, K. Lang, and D. Giardini. 2001. “Earthquake Scenarios for the City of Basel.” *Soil Dynamics and Earthquake Engineering* 21 (5): 405–13.
- Fajfar, P., and M. Eeri. 2000. “A Nonlinear Analysis Method for Performance Based Seismic Design.” *Earthquake Spectra*. Vol. 16.
- Fajfar, P., and P. Gaspersic. 1996. “The N2 Method for the Seismic Damage Analysis of RC Buildings.” *Earthquake Engineering & Structural Dynamics* 25 (1): 31–46.
[https://doi.org/10.1002/\(SICI\)1096-9845\(199601\)](https://doi.org/10.1002/(SICI)1096-9845(199601)).
- Fajfar, Peter. 1999.
- Farzad, N. 1989. *The Seismic Design Handbook. Structural Engineering Series, Van Nostrand Reinhold, New York*. 2^o. Springer Science+Business Media, LLC.
<https://doi.org/10.1007/978-1-4615-1693-4>.
- FEMA. 2003. “HAZUS MH MR4 - Multi-Hazard Loss Estimation Methodology.” Washington D.C. www.fema.gov/plan/prevent/hazus.
- . 2015. “Rapid Visual Screening of Buildings for Potential Seismic Hazards: A Handbook (FEMA P-154).” *Federal Emergency Management Agency*, no. January: 388.
<https://doi.org/10.4231/D3M90238V>.
- Ferreira, Tiago Miguel, Hugo Rodrigues, and Romeu Vicente. 2020. “Seismic Vulnerability Assessment of Existing Reinforced Concrete Buildings in Urban Centers.” *Sustainability (Switzerland)* 12 (5): 1–20. <https://doi.org/10.3390/su12051996>.
- Formisano, A., G. Florio, R. Landolfo, and F. M. Mazzolani. 2015. “Numerical Calibration of an Easy Method for Seismic Behaviour Assessment on Large Scale of Masonry Building Aggregates.” *Advances in Engineering Software* 80 (C): 116–38.
<https://doi.org/10.1016/j.advengsoft.2014.09.013>.
- Formisano, A., R. Landolfo, and F. M. Mazzolani. 2015. “Numerical Calibration of an Easy Method for Seismic Behaviour Assessment on Large Scale of Masonry Building Aggregates.” *Advances in Engineering Software* 80 (C): 116–38.
<https://doi.org/10.1016/j.advengsoft.2014.09.013>.
- Formisano, A., and A. Massimilla. 2018. “A Novel Procedure for Simplified Nonlinear Numerical

-
- Modeling of Structural Units in Masonry Aggregates.” *International Journal of Architectural Heritage* 12 (7–8): 1162–70. <https://doi.org/10.1080/15583058.2018.1503365>.
- Formisano, A, G Florio, R Landolfo, and M Mazzolani, F. 2011. “Un Metodo per La Valutazione Su Larga Scala Della Vulnerabilità Sismica Degli Aggregati Storici.” *XV Covegno ANDIS - L’Ingegneria Sismica in Italia*.
- Foschi, R.O. 1974. “Load-Slip Characteristics of Nails.” *Wood Science* 7 (1): 69–74.
- Fraume, Mabel-Cristina Marulanda, Omar-Darío Cardona, Paula Marulanda Fraume, Martha-Liliana Carreño, and Alex H Barbat. 2020. “Evaluating Risk from a Holistic Perspective to Improve Resilience: The United Nations Evaluation at Global Level.” <https://doi.org/10.1016/j.ssci.2020.104739>.
- Freeman, S.A. 1998. “Development and Use of Capacity Spectrum Method.” In *Proc. 6th ;.S. National Conf. Earthquake Engng*. Seattle.
- Freeman, S.A., J.P. Nicoletti, and J.V Tyrell. 1975. “Evaluations of Existing Buildings for Seismic Risk -A. Case Study of Puget Sound Naval Shipyard, Bremerton, Washington.” In *Proceeding of the U.S. National Conference on Earthquake Engineers, EERI.*, 113–22. Berkeley.
- Gazzola, E.A. 1985. “Bending of Concrete Masonry Walls at Different Angles to the Bed Joints.” In *3rd North American Masonry Conference*.
- Giovinazzi, Sonia, and Sergio Lagomarsino. 2004. “A Macroseismic Method for the Vulnerability Assessment of Buildings.” *13th World Conference on Earthquake Engineering*, no. 896: 1–6.
- GNDT-SSN. 1994. “Scheda Di Esposizione e Vulnerabilità e Di Rilevamento Danni Di Primo Livello e Secondo Livello (Muratura e Cemento Armato).” Roma.
- GNDT. 2007a. “Manuale per Il Rilevamento Della Vulnerabilità Sismica Degli Edifici. Istruzione per La Compilazione Della Scheda Di 2° Livello.” Abruzzo.
- . 2007b. “Manuale Per Il Rilevamento Della Vulnerabilità Sismica Degli Edifici.” Abruzzo.
- Griffith, M.C, and J. Vaculik. 2007. “Out-of-Plane Flexural Strength of Unreinforced Clay Brick Masonry Walls.” *TMS Journal*, 53–68.
- Grünthal, G. 1998. “European Macroseismic Scale 1998.” Vol. 15. Luxembourg: Centre Européen de Géodynamique et de Séismologie.
- Guevara-Perez, L. T. 2012. “Soft Story and Weak Story in Earthquake Resistant Design: A Multidisciplinary Approach.” In *In Proceedings of the 15th World Conference on Earthquake Engineering - WCEE*, 518–19. Lisboa.
- Gupta, I D. 2002. “The State of the Art in Seismic Hazard Analysis.” *ISET Journal of Earthquake Technology, Paper No. 428*. Vol. 39. <http://home.iitk.ac.in/~vinaykg/Iset428.pdf>.
- Hancilar, Ufuk, Fabio Taucer, and Christina Corbane. 2013. “Empirical Fragility Functions Based on Remote Sensing and Field Data after the 12 January 2010 Haiti Earthquake.” *Earthquake Spectra* 29 (4): 1275–1310. <https://doi.org/10.1193/121711EQS308M>.
- Harris, Gilberto. 1996. *Emigración y Políticas Gubernamentales En Chile Durante El Siglo Diecinueve*. Edited by Ediciones Universitarias de Valparaíso de la Universidad Católica de Valparaíso. Valparaíso.
- HAZUS. 1999. “HAZUS - Multi-Hazard Loss Estimation Methodology.” National Institute of Building Sciences.
- Hordijk, D.A. 1991. “Local Approach to Fatigue of Concrete.” Delft University of Technology. <https://repository.tudelft.nl/islandora/object/uuid%3Afa87147b-8201-47ed-83d7-b812b09c5fbb>.

- Hurtado, M., M Santander, and G. Muñoz. 2016. “Construction Features of the Historical Architecture in Valparaiso Harbor: The Brick Masonry Buildings of the Architect EOF Harrington.” *Journal of Construction* 15 (3): 67–76.
- Indirli, M. 2009. “Organization of a Geographic Information System (GIS) Database on Natural Hazards and Structural Vulnerability for the Historic Center of San Giuliano Di Puglia (Italy) and the City of Valparaiso (Chile).” *International Journal of Architectural Heritage* 3 (4): 276–315. <https://doi.org/10.1080/15583050902803780>.
- Instituto Nacional de Normalización. 2009. “NCh433.Of1996 Modificada En 2009 - Earthquake Resistant Design of Buildings,” 1–43. <http://ecommerce.inn.cl/index.php>.
- Italian Ministry of Infrastructure and Transport. 2018. “NTC 2018 - D.M. 17.01.18: Aggiornamento Delle ‘Norme Tecniche per Le Costruzioni,’” 1–198.
- Jiménez, B. 2015. “Los Entramados Tradicionales de Madera En Los Cerros Alegre y Concepción. Caracterización Histórica y Técnica de Las Viviendas de Finales Del Siglo XIX y Comienzos Del XX.” Tesis de licenciatura, Universidad Técnica Federico Santa María.
- Jorquera, N. 2015. “Culturas Sísmicas: Estrategias Vernaculares de Sismorresistencia Del Patrimonio Arquitectónico Chileno.” *Arquitecturas Del Sur* 32 (46): 18–29.
- Kalkbrenner, Philip, Luca Pelà, and Cristián Sandoval. 2019. “Multi Directional Pushover Analysis of Irregular Masonry Buildings without Box Behavior.” *Engineering Structures* 201 (December): 109534. <https://doi.org/10.1016/j.engstruct.2019.109534>.
- Kappos, Andreas J. 2016. “An Overview of the Development of the Hybrid Method for Seismic Vulnerability Assessment of Buildings.” *Structure and Infrastructure Engineering* 12 (12): 1573–84. <https://doi.org/10.1080/15732479.2016.1151448>.
- Kappos, Andreas J., Georgios Panagopoulos, Christos Panagiotopoulos, and Gregorios Penelis. 2006. “A Hybrid Method for the Vulnerability Assessment of R/C and URM Buildings.” *Bulletin of Earthquake Engineering* 4 (4): 391–413. <https://doi.org/10.1007/s10518-006-9023-0>.
- Kassem, Moustafa Moufid, Fadzli Mohamed Nazri, and Ehsan Noroozinejad Farsangi. 2020. “The Seismic Vulnerability Assessment Methodologies: A State-of-the-Art Review.” *Ain Shams Engineering Journal*. Ain Shams University. <https://doi.org/10.1016/j.asej.2020.04.001>.
- Kaushik, Hemant B., Durgesh C. Rai, and Sudhir K. Jain. 2007. “Stress-Strain Characteristics of Clay Brick Masonry under Uniaxial Compression.” *Journal of Materials in Civil Engineering* 19 (9): 728–39. [https://doi.org/10.1061/\(ASCE\)0899-1561\(2007\)19:9\(728\)](https://doi.org/10.1061/(ASCE)0899-1561(2007)19:9(728)).
- Khazai, Bijan., Fouad. Bendimerad, Omar D. Cardona, Martha-Liliana Carreño, Alex H. Barbat, and Christopher G. Burton. 2015. “Guide to Measuring Urban Resilience: Principles, Tools and Practice of Urban Indicators.” Quezon City. https://www.researchgate.net/publication/275637093_A_Guide_to_Measuring_Urban_Resilience_Principles_Tools_and_Practice_of_Urban_Indicators.
- Kouris, L.A.S., and A.J. Kappos. 2012. “Detailed and Simplified Non-Linear Models for Timber-Framed Masonry Structures.” *Journal of Cultural Heritage* 13 (1): 47–58. <https://doi.org/10.1016/j.culher.2011.05.009>.
- . 2014. “A Practice-Oriented Model for Pushover Analysis of a Class of Timber-Framed Masonry Buildings.” *Engineering Structures* 75: 489–506. <https://doi.org/10.1016/j.engstruct.2014.06.012>.
- Kunnumkal, S.M., D Veneciano, S. Joseph, and U. Gupta. 2002. “Earthquake Loss Under Limited Transportation Capacity: Assessment, Sensitivity and Mitigation.” In *7th USNCEE*

Conference. Boston, USA.

- Lantada, M^a Nieves. 2007. "Evaluación Del Riesgo Sismico Mediante Métodos Avanzados y Tecnicas GIS. Aplicación a La Ciudad de Barcelona." Universidad Politécnica de Cataluña.
- Lantada, N., J. Irizarry, A. H. Barbat, X. Goula, A. Roca, T. Susagna, and L. G. Pujades. 2010. "Seismic Hazard and Risk Scenarios for Barcelona, Spain, Using the Risk-UE Vulnerability Index Method." *Bulletin of Earthquake Engineering* 8 (2): 201–29.
<https://doi.org/10.1007/s10518-009-9148-z>.
- Lewis, M. B. 2009. "Stud and Balloon Frames." In *The Pacific Connection*, edited by M.B. Lewis, 48–73. Melburne: Association for Preservation Technology International.
- Leyton, F., S. Ruiz, and S. Sepúlveda. 2010. "Andean Geology." *Andean Geology* 37 (2): 455–72.
https://scielo.conicyt.cl/scielo.php?script=sci_arttext&pid=S0718-71062010000200011.
- Leyton, F., S. Ruiz, S. A. Sepúlveda, and S. Sepúlveda. 2009. "Preliminary Re-Evaluation of Probabilistic Seismic Hazard Assessment in Chile: From Arica to Taitao Peninsula." *Adv. Geosci.* Vol. 22. www.adv-geosci.net/22/147/2009/.
- Lin, Yu-Yuan, Kuo-Chun Chang, and Yuan-Li Wang. 2004. "Comparison of Displacement Coefficient Method and Capacity Spectrum Method with Experimental Results of RC Columns." *Earthquake Engineering & Structural Dynamics* 33 (1): 35–48.
<https://doi.org/10.1002/eqe.336>.
- Lomnitz, C. 1969. "An Earthquake Risk Map of Chile." In *Proceedings of the Fourth World Conference on Earthquake Engineering 1*, 161–71.
- Lourenço, P., J. Pereira, F. Greco, and C. Cancino. 2018. "Seismic Retrofitting Project Recommendations for Advanced Modeling of Historic Earthen Sites Research Report." Guimaraes. www.getty.edu/conservation.
- Lourenço, Paulo B. 2000. "Anisotropic Softening Model for Masonry Plates and Shells." *Journal of Structural Engineering* 126 (9): 1008–16. [https://doi.org/10.1061/\(ASCE\)0733-9445\(2000\)126:9\(1008\)](https://doi.org/10.1061/(ASCE)0733-9445(2000)126:9(1008)).
- Lukic, R., E. Poletti, H. Rodrigues, and G. Vasconcelos. 2018. "Numerical Modelling of the Cyclic Behavior of Timber-Framed Structures." *Engineering Structures* 165 (March): 210–21.
<https://doi.org/10.1016/j.engstruct.2018.03.039>.
- Magenes, G, and G.M. Calvi. 1997. "In-Plane Seismic Response of Brick Masonry Walls." *Earthquake Engineering and Structural Dynamics* 26: 1091-1112.
- Magenes, Guido. 2000. "A Method for Pushover Analysis in Seismic Assessment of Masonry Buildings." *12th World Conference on Earthquake Engineering (WCEE)*, no. January 2000: 1–8.
- Malczewski, J. 2006. "GIS-Based Multicriteria Decision Analysis: A Survey of the Literature." *International Journal of Geographical Information Science* 20 (7): 703–26.
<https://doi.org/10.1080/13658810600661508>.
- Masi, A., L. Chiauzzi, C. Samela, L. Tosco, and M. Vona. 2014. "Survey of Dwellings Buildings for Seismic Loss Assessment at Urban Scale: The Case Study of 18 Villages in Val D ' Agri , Italy" 13 (2): 471–86.
- Masi, Angelo. 2003. "Seismic Vulnerability Assessment of Gravity Load Designed R/C Frames." *Bulletin of Earthquake Engineering* 1 (3): 371–95.
<https://doi.org/10.1023/B:BEEE.0000021426.31223.60>.
- Masi, Angelo, Leonardo Chiauzzi, Carmelinda Samela, Luigi Tosco, and Marco Vona. 2014. "Survey of Dwelling Buildings for Seismic Loss Assessment at Urban Scale: The Case Study

- of 18 Villages in Val d'Agri, Italy." *Environmental Engineering and Management Journal* 13 (2): 471–86. <https://doi.org/10.30638/eemj.2014.051>.
- MINVU. 2013. "NTM 002 Proyecto de Intervención Estructural de Construcciones de Tierra."
- . 2017. "Guía de Referencia Para Sistemas de Evacuación Comunales Por Tsunami. Manual Práctico de Planificación e Implementación." Vol. 6. Santiago (Chile).
- Monteiro, R., P. Ceresa, V. Cerchiello, J. Dabeeq, A. Di Meo, and B. Borzi. 2016. "Towards Integrated Seismic Risk Assessment in Palestine. Application to the City of Nablus." In *VII European Congress on Computational Methods in Applied Sciences and Engineering.*, edited by M. Papadrakakis, V. Papadopoulos, G. Stefanou, and V. Pleveris. Crete Island, Greece. <https://doi.org/10.7712/100016.2235.12031>.
- Moore, D, and D. D'Ayala. 2011. "Racking Behaviour of Traditional Peruvian Shear Walls." University of Bath.
- Mouroux, P., E. Bertrand, M. Bour, B. L. Brun, S. Depinois, and P. Masure. 2004. "The European RISK-UE Project: An Advanced Approach To Earthquake Risk Scenarios." *Proc: 13h World Conference on Earthquake Engineering*, no. 3329.
- Najam, Fawad Ahmed. 2018. "Nonlinear Static Analysis Procedures for Seismic Performance Evaluation of Existing Buildings – Evolution and Issues." In , 180–98. Springer, Cham. https://doi.org/10.1007/978-3-319-61914-9_15.
- NTC-Circolare. 2018. "Circolare 21 Gennaio 2019 n. 7 C.S.LL.PP. Istruzioni per l'applicazione Dell'aggiornamento Delle 'Norme Tecniche per Le Costruzioni' Di Cui Al D.M. 17/01/2018." *Consiglio Superiore Dei Lavori Pubblici*.
- NTC. 2008. "Technical Norms for Construction (in Italian)." Rome, Italy. www.cslp.it.
- NZSEE. 2016. *The Seismic Assessment of Existing Buildings Technical Guidelines for Engineering - Section C9 - Timber Buildings*. Edited by A. Cunninghame and Sandy Cole.
- Ogawa, Keita, Yasutoshi Sasaki, and Mariko Yamasaki. 2016. "Theoretical Estimation of the Mechanical Performance of Traditional Mortise–Tenon Joint Involving a Gap." *Journal of Wood Science* 62 (3): 242–50. <https://doi.org/10.1007/s10086-016-1544-9>.
- Oliveira, V. 2016. *Urban Morphology. An Introduction to the Study of the Physical Form of Cities*. Edited by Springer International Publishing. 1st ed. Switzerland: Springer International Publishing. <https://doi.org/10.1007/978-3-319-32083-0>.
- Oliver, P. 1997. *The Encyclopaedia of Vernacular Architecture of the World*. New York: Cambridge University Press.
- Omar, Amellal, and Bensaibi Mahmoud. 2017. "Calculation of Seismic Vulnerability Index for Steel Structures." In *Energy Procedia*, 139:558–64. Elsevier Ltd. <https://doi.org/10.1016/j.egypro.2017.11.253>.
- ONEMI. 2016. "Plan de Protección Civil Municipal - Valparaíso." Chile Preparado. 2016. <http://www.onemi.cl/wp-content/uploads/2017/09/Valparaíso-Laguna-Verde.pdf>.
- ONEMI - División de Protección Civil. 2009. "Informe Consolidado N° 1 Sismo Destructivo Del 03 Marzo 1985." <http://repositoriodigitalonemi.cl/web/bitstream/handle/2012/1094/SismoDestructivoMarzo1985.pdf?sequence=1&isAllowed=y>.
- Palacios, Alfredo. 2015. *Entre Ruinas y Escombros. Los Terremotos En Chile Durante Los Siglos XVI Al XIX*. Edited by Ediciones Universitarias de Valparaíso PUCV. Valparaíso.
- Panagiotis, A., and P. Vagelis. 2015. *Handbook of Research on Seismic Assessment and Rehabilitation of Historic Structures*. Hershey PA: IGI Global. <https://doi.org/10.4018/978->

- Pantò, B., L. Silva, G. Vasconcelos, and P. B. Lourenço. 2019. “Macro-Modelling Approach for Assessment of out-of-Plane Behavior of Brick Masonry Infill Walls.” *Engineering Structures* 181 (August 2018): 529–49. <https://doi.org/10.1016/j.engstruct.2018.12.019>.
- Parisi, F., G. P. Lignola, N. Augenti, A. Prota, and G. Manfredi. 2011. “Nonlinear Behavior of a Masonry Subassemblage Before and After Strengthening with Inorganic Matrix-Grid Composites.” *Journal of Composites for Construction* 15 (5): 821–32. [https://doi.org/10.1061/\(ASCE\)CC.1943-5614.0000203](https://doi.org/10.1061/(ASCE)CC.1943-5614.0000203).
- Parisi, Fulvio, Ivano Iovinella, Alberto Balsamo, Nicola Augenti, and Andrea Prota. 2013. “In-Plane Behaviour of Tuff Masonry Strengthened with Inorganic Matrix-Grid Composites.” *Composites Part B: Engineering* 45 (1): 1657–66. <https://doi.org/10.1016/j.compositesb.2012.09.068>.
- Pasticier, L., A. Claudio, and M. Fragiaco. 2007. “Non-Linear Seismic Analysis and Vulnerability Evaluation of a Masonry Building by Means of the SAP2000 V.10,” no. November 2007: 467–85. <https://doi.org/10.1002/eqe>.
- Pelà, Luca. 2018. “New Trends and Challenges in Large-Scale and Urban Assessment of Seismic Risk in Historical Centres.” *International Journal of Architectural Heritage*. Taylor and Francis Inc. <https://doi.org/10.1080/15583058.2018.1520858>.
- Perez, Vicente. 1990. “Manual de Cálculo de Construcciones En Madera.” Santiago (Chile).
- Perrone, Monia. 2011. “Study of El Comercio Hotel, Lima (Peru). Numerical Modelling of a Historic Earthen Building Made of Non-Conventional Materials and Located in Seismic Zones.” Università degli Studi “G. d’Annunzio” Chieti - Pescara.
- Petracca, Massimo, Luca Pelà, Riccardo Rossi, Sergio Oller, Guido Camata, and Enrico Spacone. 2017. “Multiscale Computational First Order Homogenization of Thick Shells for the Analysis of Out-of-Plane Loaded Masonry Walls.” *Computer Methods in Applied Mechanics and Engineering* 315: 273–301. <https://doi.org/10.1016/j.cma.2016.10.046>.
- Petrovčić, Simon, and Vojko Kilar. 2013. “Seismic Failure Mode Interaction for the Equivalent Frame Modeling of Unreinforced Masonry Structures.” *Engineering Structures* 54: 9–22. <https://doi.org/10.1016/j.engstruct.2013.03.050>.
- Pitilakis, K., P. Franchin, B. Khazai, and H. Wenzel. 2014. “SYNER-G: Systemic Seismic Vulnerability and Risk Assessment of Complex Urban, Utility, Lifeline Systems and Critical Facilities: Methodology and Applications.” *Geotechnical, Geological and Earthquake Engineering* 31. <https://doi.org/10.1007/978-94-017-8835-9>.
- Poletti, E. 2013a. “Characterization of the Seismic Behaviour of Traditional Timber Frame Walls.”
- . 2013b. “Characterization of the Seismic Behaviour of Traditional Timber Frame Walls.” Universidade do Minho.
- Poletti, E., P.B. Lourenco, and M. P. Ciocci. 2016. “Numerical Approaches for the Analysis of Timber Frame Walls Numerical Analysis.” In *Historical Earthquake-Resistant Timber Framing in the Mediterranean Area. HEaRT 2015.*, edited by Helena Cruz and et al., 183–92. Springer Nature. <https://doi.org/10.1007/978-3-319-39492-3>.
- Poletti, E., and G. Vasconcelos. 2015. “Seismic Performance of Traditional Half-Timbered Walls: Experimental Results.” In *Historical Earthquake-Resistant Timber Frames in the Mediterranean Area*, edited by Nicola Ruggieri, Gennaro Tampone, and Raffaele Zinno, 171. Switzerland: Springer, Cham.

- Poletti, E., G. Vasconcelos, J. M. Branco, and A. M. Koukouviki. 2015. “Mechanical Characterization of Traditional Timber Connections: Experimental Results.” *Mecânica Experimental* 25: 43–54. http://www-ext.lnec.pt/APAET/pdf/Rev_25_A5.pdf.
- Porteous, J., and A. Kermani. 2004. *Structural Timber Design to Eurocode 5*. 2nd ed. Vol. 2004. Oxford: Blackwell Science Ltd. <https://doi.org/10.1680/cien.2001.144.6.39>.
- Quinn, Natalie. 2015. “Structural Characterization and Numerical Modeling of Historic Quincha Walls Structural Characterization and Numerical Modeling of Historic Quincha Walls.” *International Journal of Architectural Heritage*, no. December. <https://doi.org/10.1080/15583058.2015.1113337>.
- . 2017. “A Seismic Assessment Procedure for Historic Structures.”
- Ramos, Luis F., and Paulo B. Lourenço. 2004. “Modeling and Vulnerability of Historical City Centers in Seismic Areas: A Case Study in Lisbon.” *Engineering Structures* 26 (9): 1295–1310. <https://doi.org/10.1016/j.engstruct.2004.04.008>.
- Reinhardt, Hans Walter. 1984. “Fracture Mechanics of an Elastic Softening Material like Concrete.” <https://www.semanticscholar.org/paper/Fracture-Mechanics-of-an-Elastic-Softening-Material-Reinhardt/78a8ccfe2f84bf4bc0646d5dde0fd2c7182d11fe>.
- Reinhorn, A. M. 1997. “Inelastic Analysis Techniques in Seismic Evaluations.” In *Eismic Design Methodologies for the Next Generation of Codes*, edited by H. Krawinkler and Peter Fajfar, 277–87. Balkema, Rotterdam. <https://doi.org/10.1201/9780203740019-25>.
- Roca, Pere, Miguel Cervera, Giuseppe Gariup, and Luca Pela’. 2010. “Structural Analysis of Masonry Historical Constructions. Classical and Advanced Approaches.” *Archives of Computational Methods in Engineering* 17 (3): 299–325. <https://doi.org/10.1007/s11831-010-9046-1>.
- Rossetto, T., D. D’Ayala, I. Ioannou, and A. Meslem. 2014. “Evaluation of Existing Fragility Curves.” *Geotechnical, Geological and Earthquake Engineering* 27: 47–93. https://doi.org/10.1007/978-94-007-7872-6_3.
- Rossetto, T., and A. Elnashai. 2005. “A New Analytical Procedure for the Derivation of Displacement-Based Vulnerability Curves for Populations of RC Structures.” *Engineering Structures* 27 (3): 397–409. <https://doi.org/10.1016/j.engstruct.2004.11.002>.
- Salazar, L. Gerardo F., and Tiago Miguel Ferreira. 2020. “Seismic Vulnerability Assessment of Historic Constructions in the Downtown of Mexico City.” *Sustainability (Switzerland)* 12 (3). <https://doi.org/10.3390/su12031276>.
- Salazar, M. 2014. “El Carácter Técnico/Constructivo En La Obra de E.O.F. Harrington.” Tesis de Licenciatura, Universidad Técnica Federico Santa María.
- Saloustros, Savvas, Miguel Cervera, and Luca Pelà. 2019. “Challenges, Tools and Applications of Tracking Algorithms in the Numerical Modelling of Cracks in Concrete and Masonry Structures.” *Archives of Computational Methods in Engineering* 26 (4): 961–1005. <https://doi.org/10.1007/s11831-018-9274-3>.
- Saloustros, Savvas, Luca Pelà, Miguel Cervera, and Pere Roca. 2017. “Finite Element Modelling of Internal and Multiple Localized Cracks.” *Computational Mechanics* 59 (2): 299–316. <https://doi.org/10.1007/s00466-016-1351-6>.
- . 2019. “Tracking of Localized Cracks in the Finite Element Analysis of Masonry Walls.” In *RILEM Bookseries*, 18:919–28. Springer Netherlands. https://doi.org/10.1007/978-3-319-99441-3_99.
- Sánchez, A., and C. Jiménez. 2011. “Valparaíso: La Ciudad-Puerto Más Importante de Chile y

-
- La Vulnerabilidad de Su Patrimonio Arquitectónico a Los Riesgos Sísmicos.” *Estudios Geográficos* 72 (271): 559–89. <https://doi.org/10.3989/estgeogr.201122>.
- Sangiorgio, V., G. Uva, S. Ruggieri, and J.M. Adam. 2019. “Calibration of Seismic Vulnerability Index for Masonry Churches Based on AHP Including Architectural and Artistic Assets.” In *3rd International Conference on International Conference on Recent Advances in Nonlinear Design, Resilience and Rehabilitation of Structures CoRASS*, edited by H. Barros, J. Ferreira, J. Addam, and N. Delatte. Coimbra.
- Sassun, Kathy, Timothy J Sullivan, Paolo Morandi, and Donatello Cardone. 2016. “Characterising the In-Plane Seismic Performance of Infill Masonry.” *Bulletin of the New Zealand Society for Earthquake Engineering* Vol 49 (No. 1): 100–117.
- SENCICO. 2017. “Norma E.080 Diseño Y Construcción Con Tierra Reforzada.” *Reglamento Nacional de Edificaciones*. http://procurement-notices.undp.org/view_file.cfm?doc_id=109376.
- SERNAGEOMIN. 1996. “Mapa Geológico Del Área de Valparaíso-Curacaví.”
- . 2018. “Sistema de Información Georreferenciada de Amenaza Sísmica.” 2018. <https://sernageomin.maps.arcgis.com/apps/webappviewer/index.html?id=ca94a78f9b1e4ca1898b3e67bc5b7090>.
- SHOA. 2012. “Valparaíso-Viña Del Mar. Carta de Inundación Por Tsunami (CITSU) Referida Al Evento Del Año 1730.” Valparaíso.
- Siano, R., V. Sepe, G. Camata, E. Spacone, P. Roca, and L. Pelà. 2017. “Analysis of the Performance in the Linear Field of Equivalent-Frame Models for Regular and Irregular Masonry Walls.” *Engineering Structures* 145 (May): 190–210. <https://doi.org/10.1016/j.engstruct.2017.05.017>.
- Siano, Rossella, Pere Roca, Guido Camata, Luca Pelà, Vincenzo Sepe, Enrico Spacone, and Massimo Petracca. 2018. “Numerical Investigation of Non-Linear Equivalent-Frame Models for Regular Masonry Walls.” *Engineering Structures* 173 (October): 512–29. <https://doi.org/10.1016/j.engstruct.2018.07.006>.
- Siano, Rossella, Vincenzo Sepe, Guido Camata, Enrico Spacone, Pere Roca, and Luca Pelà. 2017. “Analysis of the Performance in the Linear Field of Equivalent-Frame Models for Regular and Irregular Masonry Walls.” *Engineering Structures* 145 (August): 190–210. <https://doi.org/10.1016/j.engstruct.2017.05.017>.
- Singhal, Ajay, and Anne S. Kiremidjian. 1996. “Method for Probabilistic Evaluation of Seismic Structural Damage.” *Journal of Structural Engineering* 122 (12): 1459–67.
- Sonekar, Kamal, and S V Bakre. 2015. “Pushover Analysis of Masonry Buildings.” *Journal of Civil Engineering and Environmental Technology* 2 (11): 18–22.
- Spyrakos, C., and A Francioso. 2012. “Shaking Table Test and Pushover Analysis on a Scaled Masonry Building.” *15th World Conference on Earthquake Engineering*.
- Stafford-Smith, B. 1963. “Lateral Stiffness of Infilled Frames.” *Journal of Structural Division, ASCE* Vol.88 (No. ST 6): pp 183-199.
- Staniscia, S., E. Spacone, and V. Fabietti. 2017. “Performance-Based Urban Planning: Framework and L’Aquila Historic City Center Case Study.” *International Journal of Architectural Heritage* 11 (5): 1–28. <https://doi.org/10.1080/15583058.2017.1287977>.
- Taffarel, S., C. Marson, G. Bettiol, F. Da Porto, and C. Modena. 2014. “Seismic Vulnerability Assessment of Israeli Historical Cetres.” In *9th International Conference on Structural Analysis of Historical Constructions*, 14–17. Mexico City.

- Taffarel, S, C Marson, C Valotto, M Roverato, M Munari, F Porto, and C Modena. 2016. “Seismic Vulnerability Maps of Timisoara Historical Center Based on Fragility Curves.” In *10th International Conference on Structural Analysis of Historical Constructions*, 1605–12. Leuven.
- Torrealva, Daniel, and Erika Vicente. 2012. “Experimental Evaluation of Seismic Behavior of Quincha Walls from the Historical Centre of Lima–Peru.” *Proceedings of the 15th World Conference in Earthquake Engineering*.
http://www.iitk.ac.in/nicee/wcee/article/WCEE2012_3170.pdf.
- Torrealva, Daniel, Erika Vicente, and Tim Michiels. 2018. “Testing of Materials and Building Components of Historic Adobe Buildings in Peru.” Los Angeles.
- Turnšek, V, and P Sheppard. 1998. “The Shear and Flexural Resistance of Masonry Walls.” In *International Research Conference on Earthquake Engineering*, 517–73.
- UNDRO. 1979. “Natural Disasters and Vulnerability Analysis.” Geneva.
- UNISDR. 1999. “Risk Assessment Tools for Diagnosis of Urban Areas Against Seismic Disasters (RADIUS).” <http://www.geohaz.org/risk-assessment-tools-for-diagnosis-of-u>.
- . 2009. “Terminology on Disaster Risk Reduction.” *International Strategy for Disaster Reduction (ISDR)* 1st: 35. <https://doi.org/978-600-6937-11-3>.
- Urbina, M. X. 2002. *Los Conventillos de Valparaíso, 1880-1920: Fisonomía y Percepción de Una Vivienda Popular Urbana*. Ediciones Universitarias de Valparaíso.
- Valluzzi, M. R., E. Garbin, and M. D. Benetta. 2010. “In-Plane Strengthening of Timber Floors for the Seismic Improvement of Masonry Buildings.” *WCTE 2010. 11th World Conference on Timber Engineering*, no. June 2016: 2–8.
- Vásquez, Nelson, Ricardo Iglesias, and Mauricio Molina. 1999. *Cartografía Histórica de Valparaíso*. Edited by Ediciones Universitarias. Valparaíso.
- Vecchio, F. J., and M. P. Collins. 1993. “Compression Response of Cracked Reinforced Concrete.” *Journal of Structural Engineering* 119 (12): 3590–3610.
[https://doi.org/10.1061/\(ASCE\)0733-9445\(1993\)119:12\(3590\)](https://doi.org/10.1061/(ASCE)0733-9445(1993)119:12(3590)).
- Vecchio, Frank J., and Michael P. Collins. 1986. “The Modified Compression-Field Theory for Reinforced Concrete Elements Subjected to Shear.” *ACI Journal Proceedings* 83 (2): 219–31. <https://doi.org/10.14359/10416>.
- Vicente, Erika, and Daniel Torrealva. 2014. “Mechanical Properties of Historical Adobe in Perú.” In *9th International Conference on Structural Analysis of Historical Constructions*, edited by F Peña and M Chávez. Mexico City. https://f-origin.hypotheses.org/wp-content/blogs.dir/1981/files/2018/05/TERRA-2016_Th-4_Art-216_Vicente.pdf.
- Vicente, R. 2008. “Estratégias e Metodologias Para Intervenções de Reabilitação Urbana. Avaliação Da Vulnerabilidade e Do Risco Sísmico Do Edificado Da Baixa de Coimbra.” PhD diss, Aveiro University.
- Vicente, R., S. Parodi, S. Lagomarsino, H. Varum, and J. A. R. Mendes da Silva. 2008. “Seismic Vulnerability Assessment Damage Scenarios and Loss Estimation. Case Study of the Old City Centre of Coimbra, Portugal.” In *The 14th World Conference on Earthquake Engineering*. Beijing.
- Whitman, Robert V., John W. Reed, and Sheu-Tien Hong. 1974. “Earthquake Damage Probability Matrices.” *Proceedings of the Fifth World Conference on Earthquake Engineering, Rome, Italy*. [https://doi.org/Vol. 2, pp. 2531-2540](https://doi.org/Vol.2,pp.2531-2540).
- Xie, Qifang, Long Wang, Peijun Zheng, Lipeng Zhang, and Weibing Hu. 2018. “Rotational

-
- Behavior of Degraded Traditional Mortise-Tenon Joints: Experimental Tests and Hysteretic Model.” *International Journal of Architectural Heritage* 12 (1): 125–36. <https://doi.org/10.1080/15583058.2017.1390629>.
- Xu, Jian. 2006. “Development of a General Dynamic Hysteretic Light-Frame Structure Model and Study on the Torsional Behavior of Openfront Light-Frame Structures.” Washington State University.
- Xue, Jianyang, Rui Guo, Liangjie Qi, and Dan Xu. 2019. “Experimental Study on the Seismic Performance of Traditional Timber Mortise-Tenon Joints with Different Looseness under Low-Cyclic Reversed Loading.” *Advances in Structural Engineering* 22 (6): 1312–28. <https://doi.org/10.1177/1369433218814167>.
- Zalat, Zsofia. 2015. “Numerical Modelling of Out-of-Plane Behavior of Masonry Structural Members.” Universitat Politècnica de Catalunya.

Annex A. Building survey forms for heterogeneous urban areas in seismically hazardous zones

This Annex presents the proposed survey forms to gather building data for future seismic vulnerability assessment, as presented in Chapter 4 and already published in Jiménez et. al (2018). Figure A-1 to Figure A-4 show the specific parts of the forms (Section 1 and 2) for masonry, reinforced concrete, mixed iron-RC and timber frame buildings, Figure A-5 presents the common sections for all the above typologies (Section 3 to 7).

SURVEY FORM FOR EXISTING BUILDINGS IN SEISMICALLY HAZARDOUS URBAN AREAS												
FORM A - MASONRY STRUCTURES												
										DATE <input type="text"/> <input type="text"/> <input type="text"/> <input type="text"/> <input type="text"/> <input type="text"/>		
SECTION 1: GENERAL INFORMATION S1												
ID <input type="text"/> <input type="text"/> <input type="text"/> <input type="text"/> <input type="text"/> <input type="text"/>		NOTES <div style="border: 1px solid black; height: 100px;"></div>										
ADDRESS	STREET NAME											
	STREET NUMBER <input type="text"/> <input type="text"/> <input type="text"/> <input type="text"/>											
	CITY											
USE	<input type="checkbox"/> RESIDENTIAL		<input type="checkbox"/> GOVERNMENTAL									
	<input type="checkbox"/> COMMERCIAL		<input type="checkbox"/> TOURISTIC									
	<input type="checkbox"/> INDUSTRIAL		<input type="checkbox"/> UNOCCUPIED									
	<input type="checkbox"/> MEDICAL		<input type="checkbox"/> MIXED									
	<input type="checkbox"/> EDUCATIONAL											
OCCUPANTS	<input type="checkbox"/> 0 - 10											
	<input type="checkbox"/> 10- 100											
	<input type="checkbox"/> > 100											
SECTION 2: BUILDING TYPOLOGY - MASONRY STRUCTURES S2												
2.1 NUMBER OF STORIES <input type="text"/> <input type="text"/>		2.4 STRUCTURAL MATERIALS										
2.2 BUILDING AGE	2.2.1 YEAR OF CONSTRUCTION <input type="text"/> <input type="text"/> <input type="text"/> <input type="text"/>		2.4.1 MAIN FAÇADE		2.4.2 SIDE WALLS		2.4.3 INTERNAL PARTITIONS		2.4.4 STORIES		2.4.5 ROOFS	
	2.2.2 LATEST STRUCTURAL RETROFIT <input type="text"/> <input type="text"/> <input type="text"/> <input type="text"/>		<input type="checkbox"/> STONE MASONRY		<input type="checkbox"/> STONE MASONRY		<input type="checkbox"/> STONE MASONRY		<input type="checkbox"/> STONE MASONRY		<input type="checkbox"/> STONE MASONRY	
	2.2.3 COMPLIANCE WITH SEISMIC CODES		<input type="checkbox"/> BRICK MASONRY		<input type="checkbox"/> BRICK MASONRY		<input type="checkbox"/> BRICK MASONRY		<input type="checkbox"/> BRICK MASONRY		<input type="checkbox"/> BRICK MASONRY	
	<input type="checkbox"/> YES, YEAR <input type="text"/> <input type="text"/> <input type="text"/> <input type="text"/> <input type="checkbox"/> No		<input type="checkbox"/> RC		<input type="checkbox"/> RC		<input type="checkbox"/> RC		<input type="checkbox"/> RC		<input type="checkbox"/> RC	
		<input type="checkbox"/> TIMBER		<input type="checkbox"/> TIMBER		<input type="checkbox"/> TIMBER		<input type="checkbox"/> TIMBER		<input type="checkbox"/> TIMBER		
		<input type="checkbox"/> IRON / STEEL		<input type="checkbox"/> IRON / STEEL		<input type="checkbox"/> IRON / STEEL		<input type="checkbox"/> IRON / STEEL		<input type="checkbox"/> IRON / STEEL		
		<input type="checkbox"/> ADOBE		<input type="checkbox"/> ADOBE		<input type="checkbox"/> ADOBE		<input type="checkbox"/> ADOBE		<input type="checkbox"/> ADOBE		
2.3. STRUCTURAL SYSTEM		<input type="checkbox"/> UNIQUE		2.4.1.1 RETROFITTED/ ALTERED?		2.4.2.1 RETROFITTED/ ALTERED?		2.4.3.1 RETROFITTED/ ALTERED?		2.4.4.1 RETROFITTED/ ALTERED?		
		<input type="checkbox"/> HYBRID		<input type="checkbox"/> No		<input type="checkbox"/> No		<input type="checkbox"/> No		<input type="checkbox"/> No		
				<input type="checkbox"/> Yes		<input type="checkbox"/> Yes		<input type="checkbox"/> Yes		<input type="checkbox"/> Yes		
2.5. MASONRY LATERAL LOAD RESISTANT SYSTEM			RIGID AND WELL CONNECTED			SEMI-RIGID AND CONNECTED			FLEXIBLE AND/OR BADLY CONNECTED			
			STORY SYSTEM	CAST IN PLACE OR PRECAST RC SLAB WITH CONCRETE TOPPING	RC BEAMS WITH CONCRETE TOPPING/ FILL	METAL DECK WITH CONCRETE FILL	CAST IN PLACE OR PRECAST RC SLAB W/O CONCRETE TOPPING	TIMBER STORY WITH DOUBLE SHEATHING OF WOODEN BOARDS	TIMBER STORY WITH SINGLE SHEATHING OF WOODEN BOARDS AND STIFFENING ELEMENTS, OR CONCRETE TOPPING, WELL CONNECTED TO WALLS	TIMBER STORY WITH SINGLE SHEATHING OF WOODEN BOARDS	STEEL/IRON BEAMS WITH BRICK/TILE CEILING (VAULTED OR NOT)	WEIGHTY RETROFITTED STORIES NOT CONNECTED TO WALLS
LOAD BEARING SYSTEM			1	2	3	4	5	6	7	8	9	10
REINFORCED OR CONFINED BRICK/CONCRETE MASONRY	GOOD QUALITY MORTAR AND CONNECTIONS AND THICKNESS HIGHER THAN 0.24 M		A	<input type="checkbox"/>	<input type="checkbox"/>	<input type="checkbox"/>	<input type="checkbox"/>	<input type="checkbox"/>	<input type="checkbox"/>	<input type="checkbox"/>	<input type="checkbox"/>	<input type="checkbox"/>
	POOR QUALITY MORTAR, OR POOR CONNECTIONS, AND THICKNESS LOWER THAN 0.24 M		B	<input type="checkbox"/>	<input type="checkbox"/>	<input type="checkbox"/>	<input type="checkbox"/>	<input type="checkbox"/>	<input type="checkbox"/>	<input type="checkbox"/>	<input type="checkbox"/>	<input type="checkbox"/>
	POOR QUALITY MORTAR AND CONNECTIONS, AND THICKNESS LOWER THAN 0.24 M		C	<input type="checkbox"/>	<input type="checkbox"/>	<input type="checkbox"/>	<input type="checkbox"/>	<input type="checkbox"/>	<input type="checkbox"/>	<input type="checkbox"/>	<input type="checkbox"/>	<input type="checkbox"/>
UNREINFORCED MASONRY	NATURAL STONE UNITS WITH GOOD TEXTURE AND CONNECTIONS, AND THICKNESS HIGHER THAN 0.35 M		D	<input type="checkbox"/>	<input type="checkbox"/>	<input type="checkbox"/>	<input type="checkbox"/>	<input type="checkbox"/>	<input type="checkbox"/>	<input type="checkbox"/>	<input type="checkbox"/>	<input type="checkbox"/>
	NATURAL STONE UNITS WITH IRREGULAR TEXTURE, OR BAD CONNECTIONS, OR THICKNESS LOWER THAN 0.35 M		E	<input type="checkbox"/>	<input type="checkbox"/>	<input type="checkbox"/>	<input type="checkbox"/>	<input type="checkbox"/>	<input type="checkbox"/>	<input type="checkbox"/>	<input type="checkbox"/>	<input type="checkbox"/>
	NATURAL STONE UNITS WITH IRREGULAR TEXTURE, BAD CONNECTIONS, AND THICKNESS LOWER THAN 0.35 M		F	<input type="checkbox"/>	<input type="checkbox"/>	<input type="checkbox"/>	<input type="checkbox"/>	<input type="checkbox"/>	<input type="checkbox"/>	<input type="checkbox"/>	<input type="checkbox"/>	<input type="checkbox"/>
	CLAY OR SAND-LIME BRICKS, GOOD QUALITY MORTAR AND CONNECTIONS, AND THICKNESS HIGHER THAN 0.24 M		G	<input type="checkbox"/>	<input type="checkbox"/>	<input type="checkbox"/>	<input type="checkbox"/>	<input type="checkbox"/>	<input type="checkbox"/>	<input type="checkbox"/>	<input type="checkbox"/>	<input type="checkbox"/>
	CLAY OR SAND-LIME BRICKS, BAD QUALITY MORTAR OR CONNECTIONS, OR THICKNESS LOWER THAN 0.24 M		H	<input type="checkbox"/>	<input type="checkbox"/>	<input type="checkbox"/>	<input type="checkbox"/>	<input type="checkbox"/>	<input type="checkbox"/>	<input type="checkbox"/>	<input type="checkbox"/>	<input type="checkbox"/>
CLAY OR SAND-LIME BRICKS, BAD QUALITY MORTAR AND CONNECTIONS, AND THICKNESS LOWER THAN 0.24 M		I	<input type="checkbox"/>	<input type="checkbox"/>	<input type="checkbox"/>	<input type="checkbox"/>	<input type="checkbox"/>	<input type="checkbox"/>	<input type="checkbox"/>	<input type="checkbox"/>	<input type="checkbox"/>	
2.6 ROOF SYSTEM			A <input type="checkbox"/> NON-THRUSTING			B <input type="checkbox"/> SLIGHTLY THRUSTING			C <input type="checkbox"/> THRUSTING			

Figure A-1. Survey form for masonry buildings (Section 1 and 2).

SURVEY FORM FOR EXISTING BUILDINGS IN SEISMICALLY HAZARDOUS URBAN AREAS
FORM B - REINFORCED CONCRETE STRUCTURES

DATE

SECTION 1: GENERAL INFORMATION **S1**

ID **NOTES**

ADDRESS
STREET NAME _____
STREET NUMBER
CITY _____

USE
 RESIDENTIAL GOVERNMENTAL
 COMMERCIAL TOURISTIC
 INDUSTRIAL UNOCCUPIED
 MEDICAL MIXED
 EDUCATIONAL

OCCUPANTS
 0 - 10
 10- 100
 > 100

SECTION 2: BUILDING TYPOLOGY - REINFORCED CONCRETE STRUCTURES **S2**

2.1 NUMBER OF STORIES <input type="text"/> <input type="text"/>		2.4 STRUCTURAL MATERIALS				
2.2 BUILDING AGE	2.2.1 YEAR OF CONSTRUCTION <input type="text"/> <input type="text"/> <input type="text"/> <input type="text"/>	<input type="checkbox"/> STONE MASONRY	<input type="checkbox"/> STONE MASONRY	<input type="checkbox"/> STONE MASONRY	<input type="checkbox"/> BRICK MASONRY	<input type="checkbox"/> RC
	2.2.2 LATEST STRUCTURAL RETROFIT <input type="text"/> <input type="text"/> <input type="text"/> <input type="text"/>	<input type="checkbox"/> BRICK MASONRY	<input type="checkbox"/> BRICK MASONRY	<input type="checkbox"/> BRICK MASONRY	<input type="checkbox"/> RC	<input type="checkbox"/> TIMBER
	2.2.3 COMPLIANCE WITH SEISMIC CODES <input type="checkbox"/> YES, YEAR <input type="text"/> <input type="text"/> <input type="text"/> <input type="text"/> <input type="checkbox"/> No	<input type="checkbox"/> RC	<input type="checkbox"/> RC	<input type="checkbox"/> RC	<input type="checkbox"/> IRON / STEEL	<input type="checkbox"/> IRON / STEEL
2.3. STRUCTURAL SYSTEM <input type="checkbox"/> UNIQUE <input type="checkbox"/> HYBRID		2.4.1.1 RETROFITTED/ ALTERED? <input type="checkbox"/> No <input type="checkbox"/> Yes	2.4.2.1 RETROFITTED/ ALTERED? <input type="checkbox"/> No <input type="checkbox"/> Yes	2.4.3.1 RETROFITTED/ ALTERED? <input type="checkbox"/> No <input type="checkbox"/> Yes	2.4.4.1 RETROFITTED/ ALTERED? <input type="checkbox"/> No <input type="checkbox"/> Yes	2.4.5.1 RETROFITTED/ ALTERED? <input type="checkbox"/> No <input type="checkbox"/> Yes

		RIGID AND WELL CONNECTED			SEMI-RIGID AND CONNECTED			FLEXIBLE AND/OR BADLY CONNECTED	UNKNOWN	
		1	2	3	4	5	6	7		
2.5. RC LATERAL LOAD RESISTANT SYSTEM	STOREY SYSTEM	CAST IN PLACE OR PRECAST RC SLAB WITH CONCRETE TOPPING WELL CONNECTED TO VERTICAL RESISTANT ELEMENTS	RC BEAMS WITH CONCRETE TOPPING WELL CONNECTED TO VERTICAL RESISTANT ELEMENTS	METAL DECK WITH CONCRETE FILL	RIGID STORY POORLY CONNECTED TO VERTICAL RESISTANT ELEMENTS	CAST IN PLACE OR PRECAST RC SLAB w/o CONCRETE TOPPING	RC OR STEEL BEAMS w/o CONCRETE SLAB (LIGHTWEIGHT SHEATHING)	FLEXIBLE OR ANY NATURE STORY BADLY CONNECTED TO VERTICAL RESISTANT ELEMENTS		
	LOAD BEARING SYSTEM									
	MOMENT RESISTANT FRAME	WITH WELL CONNECTED AND GOOD QUALITY MASONRY INFILL. OPENINGS DO NOT EXCEED 30% OF WALL SURFACE. HEIGHT-THICKNESS RATIO LOWER THAN 20%	A	<input type="checkbox"/>	<input type="checkbox"/>	<input type="checkbox"/>	<input type="checkbox"/>	<input type="checkbox"/>	<input type="checkbox"/>	<input type="checkbox"/>
		WITH BADLY CONNECTED AND/OR POOR QUALITY MASONRY INFILL. OPENINGS EXCEED 30% OF WALL SURFACE. HEIGHT-THICKNESS RATIO HIGHER THAN 20%	B	<input type="checkbox"/>	<input type="checkbox"/>	<input type="checkbox"/>	<input type="checkbox"/>	<input type="checkbox"/>	<input type="checkbox"/>	<input type="checkbox"/>
	w/o INFILL	C	<input type="checkbox"/>	<input type="checkbox"/>	<input type="checkbox"/>	<input type="checkbox"/>	<input type="checkbox"/>	<input type="checkbox"/>	<input type="checkbox"/>	
	SHEAR WALL SYSTEM	D	<input type="checkbox"/>	<input type="checkbox"/>	<input type="checkbox"/>	<input type="checkbox"/>	<input type="checkbox"/>	<input type="checkbox"/>	<input type="checkbox"/>	
	DUAL SYSTEM: MOMENT RESISTANT FRAMES AND SHEAR WALLS	E	<input type="checkbox"/>	<input type="checkbox"/>	<input type="checkbox"/>	<input type="checkbox"/>	<input type="checkbox"/>	<input type="checkbox"/>	<input type="checkbox"/>	
	Mixed RC-Masonry	F	<input type="checkbox"/>	<input type="checkbox"/>	<input type="checkbox"/>	<input type="checkbox"/>	<input type="checkbox"/>	<input type="checkbox"/>	<input type="checkbox"/>	
	SOFT-STOREY BUILDINGS CAUSED BY UNFAVOURABLE DISCONTINUOUS COLUMNS (OPEN GROUND FLOOR) OR SIGNIFICANT STIFFNESS AND RESISTANCE DIFFERENCE BETWEEN THE GROUND AND UPPER LEVELS STRUCTURES	G	<input type="checkbox"/>	<input type="checkbox"/>	<input type="checkbox"/>	<input type="checkbox"/>	<input type="checkbox"/>	<input type="checkbox"/>	<input type="checkbox"/>	

Figure A-2. Survey form for RC buildings (Section 1 and 2).

SURVEY FORM FOR EXISTING BUILDINGS IN SEISMICALLY HAZARDOUS URBAN AREAS
FORM C - STEEL/IRON MIXED STRUCTURES

DATE

SECTION 1: GENERAL INFORMATION **S1**

ID

NOTES

ADDRESS

STREET NAME _____

STREET NUMBER

CITY _____

USE

RESIDENTIAL GOVERNMENTAL

COMMERCIAL TOURISTIC

INDUSTRIAL UNOCCUPIED

MEDICAL MIXED

EDUCATIONAL

OCCUPANTS

0 - 10

10- 100

> 100

SECTION 2: BUILDING TYPOLOGY - STEEL/IRON MIXED STRUCTURES **S2**

2.1 NUMBER OF STORIES <input type="text"/> <input type="text"/>		2.4 STRUCTURAL MATERIALS				
2.2 BUILDING AGE	2.2.1 YEAR OF CONSTRUCTION <input type="text"/> <input type="text"/> <input type="text"/> <input type="text"/>	<input type="checkbox"/> STONE MASONRY	<input type="checkbox"/> STONE MASONRY	<input type="checkbox"/> STONE MASONRY	<input type="checkbox"/> BRICK MASONRY	<input type="checkbox"/> RC
	2.2.2 LATEST STRUCTURAL RETROFIT <input type="text"/> <input type="text"/> <input type="text"/> <input type="text"/>	<input type="checkbox"/> BRICK MASONRY	<input type="checkbox"/> BRICK MASONRY	<input type="checkbox"/> BRICK MASONRY	<input type="checkbox"/> RC	<input type="checkbox"/> TIMBER
	2.2.3 COMPLIANCE WITH SEISMIC CODES <input type="checkbox"/> YES, YEAR <input type="text"/> <input type="text"/> <input type="text"/> <input type="text"/> <input type="checkbox"/> No	<input type="checkbox"/> RC	<input type="checkbox"/> RC	<input type="checkbox"/> RC	<input type="checkbox"/> IRON / STEEL	<input type="checkbox"/> IRON / STEEL
2.3. STRUCTURAL SYSTEM <input type="checkbox"/> UNIQUE <input type="checkbox"/> HYBRID		2.4.1.1 RETROFITTED/ ALTERED? <input type="checkbox"/> No <input type="checkbox"/> Yes	2.4.2.1 RETROFITTED/ ALTERED? <input type="checkbox"/> No <input type="checkbox"/> Yes	2.4.3.1 RETROFITTED/ ALTERED? <input type="checkbox"/> No <input type="checkbox"/> Yes	2.4.4.1 RETROFITTED/ ALTERED? <input type="checkbox"/> No <input type="checkbox"/> Yes	2.4.5.1 RETROFITTED/ ALTERED? <input type="checkbox"/> No <input type="checkbox"/> Yes

2.5. STEEL/IRON MIXED LATERAL LOAD RESISTANT SYSTEM	LOAD BEARING SYSTEM	STORY SYSTEM	RIGID AND WELL CONNECTED			SEMI-RIGID AND CONNECTED			FLEXIBLE AND/OR BADLY CONNECTED	UNKNOWN
			1	2	3	4	5	6	7	
			CAST IN PLACE OR PRECAST RC SLAB WITH CONCRETE TOPPING WELL CONNECTED TO VERTICAL RESISTANT ELEMENTS	RC BEAMS WITH CONCRETE TOPPING WELL CONNECTED TO VERTICAL RESISTANT ELEMENTS	METAL DECK WITH CONCRETE FILL	RIGID STORY POORLY CONNECTED TO VERTICAL RESISTANT ELEMENTS	CAST IN PLACE OR PRECAST RC STORY W/O CONCRETE TOPPING	RC OR STEEL BEAMS W/O CONCRETE SLAB (LIGHTWEIGHT SHEATHING)	FLEXIBLE OR ANY NATURE STORY BADLY CONNECTED TO VERTICAL RESISTANT ELEMENTS	
MOMENT RESISTANT FRAME (MRF)	With WELL CONNECTED AND GOOD QUALITY MASONRY INFILL	A	<input type="checkbox"/>	<input type="checkbox"/>	<input type="checkbox"/>	<input type="checkbox"/>	<input type="checkbox"/>	<input type="checkbox"/>	<input type="checkbox"/>	<input type="checkbox"/>
	With CONCENTRIC OR ECCENTRIC BRACINGS	B	<input type="checkbox"/>	<input type="checkbox"/>	<input type="checkbox"/>	<input type="checkbox"/>	<input type="checkbox"/>	<input type="checkbox"/>	<input type="checkbox"/>	<input type="checkbox"/>
	W/O INFILL	C	<input type="checkbox"/>	<input type="checkbox"/>	<input type="checkbox"/>	<input type="checkbox"/>	<input type="checkbox"/>	<input type="checkbox"/>	<input type="checkbox"/>	<input type="checkbox"/>
DUAL SYSTEM: RESISTANT FRAMES AND STRUCTURAL WALLS	MRF WITH CONCRETE CORES	D	<input type="checkbox"/>	<input type="checkbox"/>	<input type="checkbox"/>	<input type="checkbox"/>	<input type="checkbox"/>	<input type="checkbox"/>	<input type="checkbox"/>	<input type="checkbox"/>
	MRF WITH CONCRETE WALLS	E	<input type="checkbox"/>	<input type="checkbox"/>	<input type="checkbox"/>	<input type="checkbox"/>	<input type="checkbox"/>	<input type="checkbox"/>	<input type="checkbox"/>	<input type="checkbox"/>
	MRF WITH MASONRY WALLS	F	<input type="checkbox"/>	<input type="checkbox"/>	<input type="checkbox"/>	<input type="checkbox"/>	<input type="checkbox"/>	<input type="checkbox"/>	<input type="checkbox"/>	<input type="checkbox"/>

Figure A-3. Survey form for steel/iron mixed buildings (Section 1 and 2).

SURVEY FORM FOR EXISTING BUILDINGS IN SEISMICALLY HAZARDOUS URBAN AREAS								
FORM D - TIMBER STRUCTURES								
						DATE <input type="text"/> <input type="text"/> <input type="text"/> <input type="text"/> <input type="text"/> <input type="text"/> <input type="text"/> <input type="text"/>		
SECTION 1: GENERAL INFORMATION S1								
ID	<input type="text"/> <input type="text"/> <input type="text"/> <input type="text"/> <input type="text"/> <input type="text"/>		NOTES					
ADDRESS	STREET NAME							
	STREET NUMBER							
	CITY							
USE	<input type="checkbox"/> RESIDENTIAL	<input type="checkbox"/> GOVERNMENTAL						
	<input type="checkbox"/> COMMERCIAL	<input type="checkbox"/> TOURISTIC						
	<input type="checkbox"/> INDUSTRIAL	<input type="checkbox"/> UNOCCUPIED						
	<input type="checkbox"/> MEDICAL	<input type="checkbox"/> MIXED						
	<input type="checkbox"/> EDUCATIONAL							
OCCUPANTS	<input type="checkbox"/> 0 - 10							
	<input type="checkbox"/> 10- 100							
	<input type="checkbox"/> > 100							
SECTION 2: BUILDING TYPOLOGY - TIMBER FRAME STRUCTURES S2								
2.1 NUMBER OF STORIES		2.4 STRUCTURAL MATERIALS						
2.2 BUILDING AGE	2.2.1 YEAR OF CONSTRUCTION		2.4.1 MAIN FAÇADE	2.4.2 SIDE WALLS	2.4.3 INTERNAL PARTITIONS	2.4.4 STORIES	2.4.5 ROOFS	
	2.2.2 LATEST STRUCTURAL RETROFIT		<input type="checkbox"/> STONE MASONRY	<input type="checkbox"/> STONE MASONRY	<input type="checkbox"/> STONE MASONRY	<input type="checkbox"/> STONE MASONRY	<input type="checkbox"/> STONE MASONRY	
	2.2.3 COMPLIANCE WITH SEISMIC CODES		<input type="checkbox"/> BRICK MASONRY	<input type="checkbox"/> BRICK MASONRY	<input type="checkbox"/> BRICK MASONRY	<input type="checkbox"/> BRICK MASONRY	<input type="checkbox"/> BRICK MASONRY	
<input type="checkbox"/> YES, YEAR <input type="text"/> <input type="text"/> <input type="text"/> <input type="text"/> <input type="checkbox"/> No		<input type="checkbox"/> RC	<input type="checkbox"/> RC	<input type="checkbox"/> RC	<input type="checkbox"/> RC	<input type="checkbox"/> RC		
2.3. STRUCTURAL SYSTEM		<input type="checkbox"/> TIMBER	<input type="checkbox"/> TIMBER	<input type="checkbox"/> TIMBER	<input type="checkbox"/> TIMBER	<input type="checkbox"/> TIMBER		
<input type="checkbox"/> UNIQUE		<input type="checkbox"/> IRON / STEEL	<input type="checkbox"/> IRON / STEEL	<input type="checkbox"/> IRON / STEEL	<input type="checkbox"/> IRON / STEEL	<input type="checkbox"/> IRON / STEEL		
<input type="checkbox"/> HYBRID		<input type="checkbox"/> ADOBE	<input type="checkbox"/> ADOBE	<input type="checkbox"/> ADOBE	<input type="checkbox"/> ADOBE	<input type="checkbox"/> ADOBE		
		2.4.1.1 RETROFITTED/ ALTERED?	2.4.2.1 RETROFITTED/ ALTERED?	2.4.3.1 RETROFITTED/ ALTERED?	2.4.4.1 RETROFITTED/ ALTERED?	2.4.5.1 RETROFITTED/ ALTERED?		
		<input type="checkbox"/> No	<input type="checkbox"/> No	<input type="checkbox"/> No	<input type="checkbox"/> No	<input type="checkbox"/> No		
		<input type="checkbox"/> Yes	<input type="checkbox"/> Yes	<input type="checkbox"/> Yes	<input type="checkbox"/> Yes	<input type="checkbox"/> Yes		
2.5 TIMBER LATERAL LOAD RESISTANT SYSTEM		STORY SYSTEM	RIGID	SEMI-RIGID	FLEXIBLE	WEIGHTY RETROFITTED STORIES NOT CONNECTED TO WALLS	UNKNOWN	
LOAD-BEARING SYSTEM			JOISTS WITH DOUBLE LAYER OF WOODEN SHEATHING	JOISTS WITH SINGLE WOODEN SHEATHING AND BRACING ELEMENTS (DIAGONALS, BRACING GRID)	JOISTS WITH SINGLE WOOD-EN SHEATHING PERPENDICULAR TO THEM			
			1	2	3	4	5	
BRACED SYSTEMS (DIAGONALS, LET-IN BRACE, DOG-LEG, ETC.)	WITH NAILED OR CARPENTRY REINFORCED CONNECTIONS		A	<input type="checkbox"/>	<input type="checkbox"/>	<input type="checkbox"/>	<input type="checkbox"/>	<input type="checkbox"/>
	WITH CARPENTRY CONNECTIONS		B	<input type="checkbox"/>	<input type="checkbox"/>	<input type="checkbox"/>	<input type="checkbox"/>	<input type="checkbox"/>
	WITH BAD QUALITY CONNECTIONS		C	<input type="checkbox"/>	<input type="checkbox"/>	<input type="checkbox"/>	<input type="checkbox"/>	<input type="checkbox"/>
UNBRACED SYSTEMS	WITH NAILED OR CARPENTRY REINFORCED CONNECTIONS	D	<input type="checkbox"/>	<input type="checkbox"/>	<input type="checkbox"/>	<input type="checkbox"/>	<input type="checkbox"/>	
	WITH CARPENTRY CONNECTIONS	E	<input type="checkbox"/>	<input type="checkbox"/>	<input type="checkbox"/>	<input type="checkbox"/>	<input type="checkbox"/>	
	WITH BAD QUALITY CONNECTIONS	F	<input type="checkbox"/>	<input type="checkbox"/>	<input type="checkbox"/>	<input type="checkbox"/>	<input type="checkbox"/>	
2.6 SECONDARY STIFFENING ELEMENTS	2.6.1 INFILL		2.6.2 EXTERNAL SHEATHING					
	<input type="checkbox"/> NO INFILL	<input type="checkbox"/> QUINCHA	<input type="checkbox"/> NO SHEATHING <input type="checkbox"/> HORIZONTAL WOODEN BOARDS <input type="checkbox"/> HORIZONTALLY ORIENTED CORRUGATES STEEL SHEETS <input type="checkbox"/> VERTICALLY ORIENTED CORRUGATES STEEL SHEETS <input type="checkbox"/> OTHER					
	<input type="checkbox"/> BRICK OR STONE MASONRY	<input type="checkbox"/> LATH AND PLASTER						
<input type="checkbox"/> ADOBE	<input type="checkbox"/> OTHER							
2.7 ROOF SYSTEM		A <input type="checkbox"/> NON- THRUSTING		B <input type="checkbox"/> SLIGHTLY THRUSTING		C <input type="checkbox"/> THRUSTING		

Figure A-4. Survey form for timber frame buildings (Section 1 and 2).

SECTION 3: BUILDING DESCRIPTION S3						
6. DIMENSIONS	PLAN		ELEVATION			
	AREA <input type="text"/> <input type="text"/> <input type="text"/> <input type="text"/> M ²		9.1 HEIGHT <input type="text"/> <input type="text"/> <input type="text"/> M	9.2 BASE <input type="text"/> <input type="text"/> <input type="text"/> M	9.3 AVERAGE FLOOR HEIGHT <input type="text"/> <input type="text"/> <input type="text"/> M	
7. POSITION	<input type="checkbox"/> A <input type="checkbox"/> B <input type="checkbox"/> C <input type="checkbox"/> D <input type="checkbox"/> E		<input type="checkbox"/> A <input type="checkbox"/> B		<input type="checkbox"/> A <input type="checkbox"/> B <input type="checkbox"/> C	
8. IRREGULARITY	A <input type="checkbox"/> $\beta_1 \geq 70$; $\beta_2 \leq 10$ B <input type="checkbox"/> $40 \leq \beta_1 < 70$; $10 < \beta_2 \leq 30$ C <input type="checkbox"/> $\beta_1 < 40$; $\beta_2 > 30$		10. POSITION IN ROW		11. IRREGULARITY	
	<p>Ratio β_1 and β_2 where: $\beta_1 = a/l \times 100$ $\beta_2 = b/l \times 100$</p>		<input type="checkbox"/> A <input type="checkbox"/> B <input type="checkbox"/> C <input type="checkbox"/> D		A <input type="checkbox"/> REGULAR B <input type="checkbox"/> FAIR REGULAR C <input type="checkbox"/> IRREGULAR	
			12. OPENINGS			
			12.1 SHAPES REGULARITY AND CONTINUITY IN THE FAÇADE A <input type="checkbox"/> REGULAR B <input type="checkbox"/> FAIR REGULAR C <input type="checkbox"/> IRREGULAR			
			12.2 ALIGNMENT OF OPENINGS AMONG ADJACENT A <input type="checkbox"/> ALIGNED B <input type="checkbox"/> FAIR ALIGNED C <input type="checkbox"/> MISALIGNED			
			12.3 OPENING RATIO (Op_r) A <input type="checkbox"/> $Op_r \leq 0.3$ B <input type="checkbox"/> $0.3 < Op_r \leq 0.6$ C <input type="checkbox"/> $0.6 < Op_r$		where: $Op_r = \frac{\text{opening areas}}{\text{façade area}}$	
SECTION 4: SOIL CONDITIONS AND FOUNDATIONS S4						
13. TYPE OF SOIL	14. SLOPE CONDITION	15. THRUSTING SOIL RATIO (TS_r):		Diagram A - In plan view	Diagram B - Section AA	Diagram C - Elevation
A <input type="checkbox"/> HARD ROCK B <input type="checkbox"/> LOOSE AND NON-THRUSTING C <input type="checkbox"/> LOOSE AND THRUSTING	A <input type="checkbox"/> 0 - 20% B <input type="checkbox"/> 20 - 40 % C <input type="checkbox"/> 40% <	A <input type="checkbox"/> $0 < d/h < 0.3$ B <input type="checkbox"/> $0.3 < d/h < 0.6$ C <input type="checkbox"/> $d/h > 0.6$				
16. MAXIMUM QUOTA DIFFERENCE (Δh)						
<input type="text"/> <input type="text"/> <input type="text"/> M						
17. RETAINING WALLS CONDITIONS			18. FOUNDATION CONDITIONS			
17.1 TYPE	17.2 MATERIAL	17.3 QUALITY		18.1 TYPE	18.2 QUALITY	
A <input type="checkbox"/> CANTILEVER WALL B <input type="checkbox"/> GRAVITY WALL C <input type="checkbox"/> ANCHORED D <input type="checkbox"/> PLINT WALL E <input type="checkbox"/> NON-EXISTENT	A <input type="checkbox"/> RC B <input type="checkbox"/> BRICK OR STONE MASONRY C <input type="checkbox"/> POURED CONCRETE	A <input type="checkbox"/> GOOD B <input type="checkbox"/> FAIR C <input type="checkbox"/> POOR D <input type="checkbox"/> UNKNOWN		A <input type="checkbox"/> RC STRIP OR ISOLATED FOOTING OR SLABS B <input type="checkbox"/> BASEMENT C <input type="checkbox"/> BRICK OR STONE MASONRY STRIP FOOTING D <input type="checkbox"/> CRAWL SPACE	A <input type="checkbox"/> GOOD B <input type="checkbox"/> FAIR C <input type="checkbox"/> POOR D <input type="checkbox"/> UNKNOWN	
SECTION 5: NON-STRUCTURAL ELEMENTS S5						
GROUP 1	GROUP 2		19. NON-STRUCTURAL ELEMENTS	<input type="checkbox"/> A	<input type="checkbox"/> B	<input type="checkbox"/> C
<input type="checkbox"/> PROJECTED WINDOWS <input type="checkbox"/> OPENING FRAMES <input type="checkbox"/> BALCONIES <input type="checkbox"/> GALLERIES <input type="checkbox"/> EXTERIOR STAIRS <input type="checkbox"/> CORNICES <input type="checkbox"/> CHIMNEYS	<input type="checkbox"/> GUTTERS <input type="checkbox"/> FAÇADE COVERING <input type="checkbox"/> ORNAMENTS <input type="checkbox"/> SIGNBOARDS		<input type="checkbox"/> - GROUP 1 AND 2: ELEMENTS OF ANY DIMENSION WELL CONNECTED TO THE MAIN STRUCTURE <input type="checkbox"/> - GROUP 1: SMALL OR MEDIUM DIMENSIONS WELL CONNECTED <input type="checkbox"/> - GROUP 2: SMALL ELEMENTS FAIR OR POORLY CONNECTED	<input type="checkbox"/> - GROUP 1: MEDIUM ELEMENTS FAIR OR POORLY CONNECTED <input type="checkbox"/> - GROUP 2: WELL CONNECTED <input type="checkbox"/> - GROUP 1: LARGE ELEMENTS WELL CONNECTED <input type="checkbox"/> - GROUP 2: MEDIUM ELEMENTS POORLY OR BAD CONNECTED	<input type="checkbox"/> - GROUP 1: LARGE OR MEDIUM DIMENSIONS BAD CONNECTED <input type="checkbox"/> - GROUP 2: WELL OR POOR CONNECTED	
SECTION 6: DAMAGE CONDITIONS S6						
STRUCTURAL SYSTEM	DAMAGE GRADE		NULL	D1 SLIGHT	D2 MEDIUM	D3 VERY HEAVY
			1	2	3	4
	20.1 WALLS	A	<input type="checkbox"/>	<input type="checkbox"/>	<input type="checkbox"/>	<input type="checkbox"/>
	20.2 FLOORS	B	<input type="checkbox"/>	<input type="checkbox"/>	<input type="checkbox"/>	<input type="checkbox"/>
	20.3 ROOFS	C	<input type="checkbox"/>	<input type="checkbox"/>	<input type="checkbox"/>	<input type="checkbox"/>
	20.4 NON STRUCTURAL ELEMENTS	D	<input type="checkbox"/>	<input type="checkbox"/>	<input type="checkbox"/>	<input type="checkbox"/>
SECTION 7: CURRENT STATE AND CONSERVATION S7						
A	B		C			
<input type="checkbox"/> - SUBSEQUENT STRUCTURAL INTERVENTIONS WELL EXECUTED <input type="checkbox"/> - WELL CONSERVED OR WITHOUT SUBSEQUENT INTERVENTIONS BUILDINGS <input type="checkbox"/> - WELL STRENGTHENED STRUCTURES <input type="checkbox"/> - SMALL INTERVENTIONS REGULARLY EXECUTED	<input type="checkbox"/> - LARGE SUBSEQUENT STRUCTURAL INTERVENTIONS POORLY EXECUTED <input type="checkbox"/> - ONLY EXTERNAL MAINTENANCE <input type="checkbox"/> - POOR STRENGTHENED STRUCTURES <input type="checkbox"/> - MEDIUM OR SMALL INTERVENTIONS BAD EXECUTED		<input type="checkbox"/> - LARGE OR MEDIUM SUBSEQUENT STRUCTURAL INTERVENTIONS BAD EXECUTED <input type="checkbox"/> - BAD CONSERVED BUILDINGS WITHOUT MAINTENANCE <input type="checkbox"/> - BAD STATE OF CONSERVATION OR PERFORMING STRENGTHENING ELEMENTS			

Figure A-5. Survey form for all the building typologies (Section 3 to 7).

Annex B. Darwing-Pecknold material

Figure B-1a shows the uniaxial stress-strain behaviour based on the Darwin-Pecknold model material. As can be noted in this diagram, the compressive response increases monotonically from point O to U, and has a constant trend between points U and L. This behaviour can be defined by a trilinear or elastic-perfectly-plastic curve, where the loss of strength from point L to R is optional. The constant stress between R and X (Figure B-1b) represents the residual strength of the material. A tri-linear approximation of a use-defined curve can also be computed, as shown in Figure B-1b. In this figure, f'_c corresponds to the peak compression stress and ϵ'_c to the corresponding peak strain. The initial stiffness (E_0) of the simplified curve is equal to the slope between the origin and closest material stress-strain point in compression. Point Y is determined so that the area under the trilinear stress-strain curve up to the point of maximum compression stress f'_c is identical to that of the user-defined stress-strain curve. The point of maximum compression stress closest to the origin is Point U. The point of maximum compression stress furthest from the origin is Point L. If U and L points coincide (Figure B-1b), the U point is placed at the strain value corresponding to $0.98 f'_c$ on the defined stress-strain curve. The point L is placed at the greatest of two strain values: (a) the strain corresponding to the maximum compression stress, or (b) 1.05 times the strain at point U. If the defined material model has strength loss after the point of maximum compression stress, point R must be included (CSI 2016a).

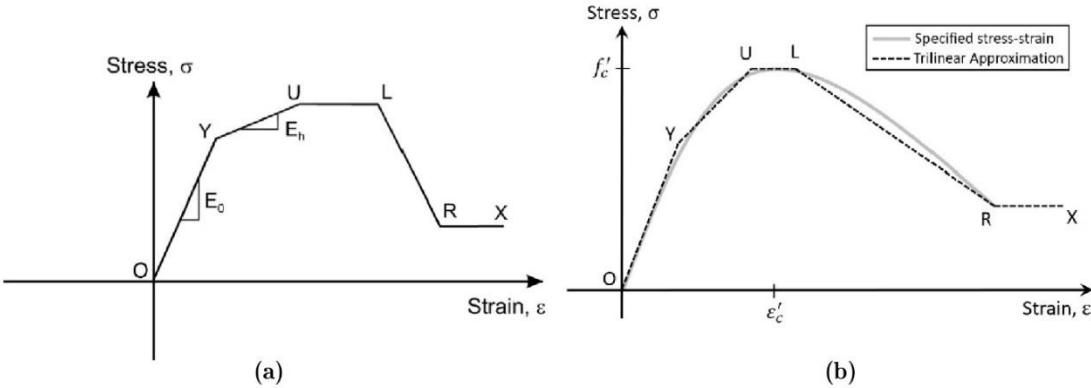


Figure B-1. Uniaxial relationship and (b) tri-linear approximation of the material stress-strain curve (CSI 2016b)

The material model behaviour presents an initial linear elastic behaviour up to reach the yielded or cracked stage during the analysis (still between the O and Y points in Figure B-1a). The initial value of Young's modulus is E_0 , and Poisson's ratio is ν as defined in the Expression (B-1).

$$\begin{Bmatrix} d\sigma_1 \\ d\sigma_2 \\ d\sigma_3 \end{Bmatrix} = \frac{1}{1-v^2} \begin{bmatrix} E_0 & vE_0 & 0 \\ vE_0 & E_0 & 0 \\ 0 & 0 & E_0 \frac{1-v}{2} \end{bmatrix} \begin{Bmatrix} d\varepsilon_1 \\ d\varepsilon_2 \\ d\tau_{12} \end{Bmatrix} \quad (\text{B-1})$$

Expression (B-1) is independent of the stress and strain directions, and therefore it applies in both the initial and principal material axes. The material model employs a rectangular interaction surface with no explicit stress interaction in the two directions. The effect of biaxial compression stress on the compression strength of the material is not taken into account. After the material reaches its yielding point, the material elastic modulus changes and the Poisson's ratio is neglected. Generally, the stresses, strains and moduli will be different along the two principal directions. The Expression (B-1) is modified for the material nonlinearities as follow:

$$\begin{Bmatrix} d\sigma_{m1} \\ d\sigma_{m2} \\ d\tau_{m12} \end{Bmatrix} = [D_{emp}] \begin{Bmatrix} d\varepsilon_{m1} \\ d\varepsilon_{m2} \\ d\tau_{m12} \end{Bmatrix} \quad (\text{B-2})$$

or

$$d\sigma_m = D_{emp} d\varepsilon_m \quad (\text{B-3})$$

where D_{emp} is the elastic-plastic constitutive matrix in principal material axes, given by:

$$D_{emp} = \frac{1}{1-v^2} \begin{bmatrix} E_1 & v\sqrt{E_1E_2} & 0 \\ v\sqrt{E_1E_2} & E_2 & 0 \\ 0 & 0 & G_m \end{bmatrix} \quad (\text{B-4})$$

The shear modulus in the main material axes G_m is specified to maintain coaxiality between the principal stresses and strains. The corresponding relationship in the initial material axes is obtained by applying the rotation between the initial and principal material axes.

When fragile materials are subjected to shear stress, they often cracks in one direction and are subjected to compression in the other direction. Failure in shear may occur when the material crushes in compression. Vecchio and Collins (1986) demonstrated that the compression strength of concrete depends on the magnitude of the tensile strain in the perpendicular direction. Figure B-2a shows the relationship between the compression strength and perpendicular tensile strain developed in Vecchio and Collins (1986), as implemented in the material model of SAP2000 (CSI 2016a).

Equation (5), formulated by Vecchio and Collins (1986), is used to compute the compression strength reduction factor, r :

$$r = \frac{1}{0.8 - 0.34 \frac{\varepsilon_m}{\varepsilon_c'}} \leq 1 \quad (\text{B-5})$$

where ε_m is the instantaneous tension strain in the perpendicular direction and ε_c' is the specified uniaxial crushing strain in compression. If the material has compression strain along one material axis and tensile strain along the other, the compression strength reduction factor is calculated using Equation (5). The minimum compression strength reduction factor used is based on magnitude of compressive stress σ as follows:

$$r_{min} = \begin{cases} 1.0 & \sigma < 0.2f_c' \\ 0.25 & \sigma < 0.5f_c' \end{cases} \quad (\text{B-6})$$

Linearly interpolated for $0.2f_c' < \sigma < 0.5f_c'$

More than one strength reduction can occur during the analysis. If the new reduction factor is smaller than the old one, the new factor is ignored. If the new factor is updated, the stress-strain relationship is modified as indicated in Figure B-2b, and the elastic modulus does not change.

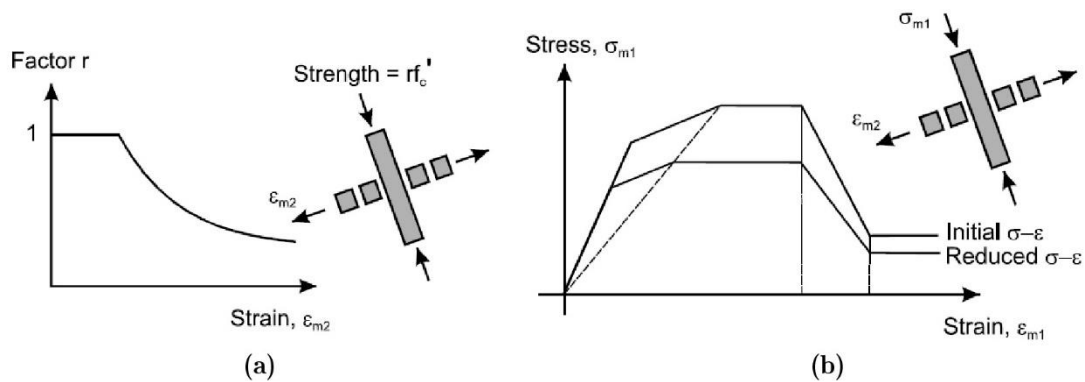


Figure B-2. (a) Reduction in compression strength due to tensile strength in the perpendicular direction and (b) change in strain-stress curve.

Annex C. Guideline for the application of the VIM for timber-masonry buildings

A guideline for the application of the vulnerability form for timber-masonry buildings proposed in Chapter 7 is detailed below.

Parameter 1 – Organization of vertical structures

This parameter identifies the main features of the structural system, defined as the system withstanding more than 70% of the seismic forces (Formisano et al. 2015). The competence of the structural system must be evaluated by assessing the efficiency of the connections between the vertical and horizontal load-bearing systems. For the assessment timber-masonry buildings the following features must be inspected:

- (i) The main load-bearing systems, including walls and storeys systems;
- (ii) The grade of rigidity of the structural system based on the presence of stiffening elements (bracing systems, covering planks or wooden boards, infill, etc.);
- (iii) The deformation capacity of the storey systems and;
- (iv) The quality of the connection between the vertical and horizontal load-bearing systems.

Bases on these features, the classes are defined as following:

Class A

- Rigid-resistant timber frame structures given by the presence of proper bracing system in the frame load-bearing walls (diagonals, dog-leg, let in brace, Saint Andres crosses, etc.) properly connected to rigid or semi-rigid storeys allowing a good transmission of the loads across the structure to the foundations.
- Presence of additional stiffening elements such as metal/wooden planks or wooden boards covering the load-bearing walls.
- and presence of good quality masonry walls (reinforced, confined, or well organized URM) well-connected to the storey systems through ties, metal planks, etc.

Class B

- Rigid-resistant timber frame structures due to the presence of proper bracing system in the vertical load-bearing walls (diagonals, dog-leg, let in brace, Saint Andres crosses, etc.) which are poorly connected to rigid or semi-rigid storey systems, hindering the transmission of the loads across the structure.
- Deformable-weak timber frame structures configured by poorly braced vertical load-bearing systems lacking stiffening elements but properly connected to rigid or semi-rigid storey

systems. Presence of covering stiffening elements such as metal/wooden planks or wooden boards on the walls.

- and presence of good quality masonry walls (reinforced, confined, or well organized URM) well-connected to the storey systems through ties, metal planks, etc.

-

Class C

- Rigid-resistant timber frame systems due to the presence of bracing system in the vertical load-bearing walls (diagonals, dog-leg, let in brace, Saint Andres crosses, etc.) which are badly connected to semi-rigid or flexible storey systems, hindering the transmission of the loads across the structure. Lacking additional stiffening elements such as metal or wooden planks or boards covering the structure.

- Deformable-weak timber frame systems without bracing systems but properly connected to semi-rigid or flexible storey systems. Presence of covering stiffening elements such as metal/wooden planks or wooden boards on the walls.

- and presence good quality masonry walls (reinforced, confined, or well organized URM) poorly-connected to the storey systems i.e. lacking of ties, metal planks, etc.

-

Class D

- Deformable-weak timber frame systems lacking of bracing systems badly connected to semi-rigid or flexible storey systems. Poor presence of covering stiffening elements such as metal/wooden planks or wooden boards on the walls.

- Presence of unreinforced masonry load-bearing systems badly connected to the storey systems in absence of ties, metal planks, etc.

- Presence weighty retrofitted storey systems.

- and presence bad quality masonry walls (clay or sand-lime bricks with bad quality mortar and thickness lower than 0.24 m) well-connected to the storey systems i.e. lacking of ties, metal planks, etc.

Parameter 2 – Nature of the load bearing system

This parameter appraises the quality of the structural system based on different criteria such as the type of construction materials, workmanship features and execution efficacy. According to Eurocode 5 (CEN EC5 1.2 2004), the structural elements made of hardwood present better resistant capacity as well as durability than the ones made of softwoods. The quality of the load-bearing system made of timber frame elements can also be evaluating according the dimension and distribution of the vertical resisting elements. A good quality wall is commonly configured by elements with large cross-sections (10 x 10 cm²) distributed each 0.4-0.6 m. The execution and maintenance of the connections are very important factors in determine the quality of timber frame systems since determines the correct transmission of the seismic loads along the structure.

For hybrid timber-masonry structural systems the brickwork type and quality of the material, including bricks and mortar, may be assessed. The criteria of evaluation are summarized as follow:

- (i) Type of wood (hardwood/softwood)
- (ii) Cross sections of the structural elements of the vertical load-bearing system
- (iii) Quality of the connections among the structural elements (carpentry joints execution, state of conservation, existent biotic damage, deformations)
- (iv) Quality of the masonry in case of mixed structural systems

Based on these criteria, the classes are defined as following:

Class A

- Timber frame systems principally made of hardwood elements (most of 70% of the structural elements) of large cross-sections (posts bigger than $10 \times 10 \text{ cm}^2$). Well executed and/or conserved carpentry connections (well designed, no biotic or mechanical damage, properly reinforced, etc.).
- Timber frame systems principally made of hardwood elements (most of 70% of the structural system) of small cross-sections (lower than $10 \times 10 \text{ cm}^2$) but properly distributed along the walls (studs spaced at maximum 0.7 m each other). Well executed and/or conserved carpentry connections (well designed, no biotic or mechanical damage, properly reinforced, etc.).
- Good quality masonry walls i.e. reinforced, confined, or well organized URM made of clay or sand-lime blocks with good quality mortar, connections and thickness higher than 0.24 m.
-

Class B

- Timber frame systems principally made of hardwood elements (most of 70% of the structural elements) of large cross-sections (bigger than $10 \times 10 \text{ cm}^2$) but poorly executed and/or conserved carpentry connections (badly designed, presenting biotic or mechanical damage, without reinforcement systems, etc.).
- Timber frame systems principally made of softwood elements (most of 70% of the structural elements) of small cross-sections (lower than $10 \times 10 \text{ cm}^2$) but properly distributed along the walls (studs separated more than 70 cm between them). Well executed and/or conserved carpentry connections (well designed, no biotic or mechanical damage, properly reinforced, etc.).
- Good quality masonry walls i.e. reinforced, confined, or well organized URM made of clay or sand-lime blocks with good quality mortar, connections and thickness higher than 0.24 m.
-

Class C

- Timber frame systems principally made of hardwood elements (most of 70% of the structural elements) of large cross-sections (bigger than $10 \times 10 \text{ cm}^2$) but poorly executed and/or conserved carpentry connections (badly designed, presenting biotic or mechanical damage, without reinforcement systems, etc.).

- Timber frame systems principally made of softwood elements (most of 70% of the structural elements) of small cross-sections (lower than $10 \times 10 \text{ cm}^2$) but properly distributed along the walls (studs separated more than 70 cm between them). Well executed and/or conserved carpentry connections (well designed, no biotic or mechanical damage, properly reinforced, etc.).
- Regular quality masonry walls i.e. reinforced, confined, or well organized URM made of clay or sand-lime blocks with good quality mortar, connections and thickness lower than 0.24 m.
-
-

Class D

- Timber frame systems principally made of hardwood elements (most of 70% of the structural elements) of large cross-sections (bigger than $10 \times 10 \text{ cm}^2$) but sparsely distributed along the wall (studs separated more than 70 cm between them). Poor executed carpentry connections (bad designed, presenting biotic or mechanical damage, without reinforcement systems, etc.).
- Timber frame systems principally made of softwood elements (most of 70% of the structural system) of small cross-sections (lower than $10 \times 10 \text{ cm}^2$) but sparsely distributed along the wall (studs separated more than 70 cm between them). Bad executed carpentry and/or conserved carpentry connections (bad designed, presenting biotic or mechanical damage, without reinforcement systems, etc.).
- Poor quality unreinforced masonry walls made of clay or sand-lime blocks with bad quality mortar, connections and thickness lower than 0.24 m.

Parameter 3 – Distribution of the resisting elements

This parameter evaluates the seismic performance of different timber frame and timber-masonry building typologies based on the configuration of the vertical resistant elements. The results of numerical simulations performed in Section 7.2.1 were used to classify the vulnerability of the studied typologies as defined below:

Class A

- Buildings with homogeneous timber-frame structural systems and two storeys.

Class B

- Buildings with homogeneous timber-frame structural systems up to three storeys.
- Buildings with heterogeneous timber-masonry structural systems up to two storeys.

Class C

- Buildings with homogeneous timber-frame structural systems up to four storeys.
- Buildings with heterogeneous timber-masonry structural systems up to three storeys.

Class D

- Buildings with heterogeneous timber-masonry structural systems four or more storeys.

Parameter 4 – Location of the buildings and foundations

The Parameter 4 “Location of the buildings and foundations” evaluates the influence of both consistency and slope of soil category and height differences between the foundations by evaluating the following parameters:

- (i) Percentage slope of the terrain p , evaluated perpendicular to the contour level lines
- (ii) Artificial terracing and equilibrium of the embankments
- (iii) Consistency of the terrain (rocky or loose soils)
- (iv) Existence of foundations
- (v) Possible height differences between the foundations of the building (Δh)

Based on these criteria the classes are defined as following:

Class A

- Building seated on rocky soils with a slope p lower than 10%
- Building seated on loose and non-thrusting soil with slope p equal to or lower than 10%. Foundations at the same height ($\Delta h=0$).

Class B

- Building seated on rocky soils with a slope p between 10% and 30% ($10\% < p \leq 30\%$) and foundations disposed at any level ($\Delta h = \text{any}$)
- Building seated on loose soil with difference level among the foundation of maximum 1 m ($\Delta h < 1$ m) in absence of unbalanced soils due to embankments. The above should also satisfy the following conditions:
- The slope of the terrain p should be lower than 10% ($10\% < p$) and the difference level among the foundations is different from zero.

Class C

- Building seated on rocky soils with a slope p between 30% and 50% ($30\% < p \leq 50\%$) and foundations at any level ($\Delta h = \text{any}$).
- Building seated on loose soil with difference level among the foundation of maximum 1 m ($\Delta h < 1$ m). The above should also satisfy the following conditions:
- Absence of unbalanced soils due to embankments and slope of the terrain p between 30% and 50% ($30\% < p \leq 50\%$) due to the existence of good executed retaining walls.
- Absence of unbalanced soils due to embankments, building with foundations and slope of the terrain p lower than 50% ($50\% < p$).

Class D

- Buildings without foundations seated on any type of terrain with a slope higher than 30% ($p > 30\%$) and unstable terrain due to the existence of embankments and/or Lacking of well executed retaining walls.
- Buildings seated on rocky soils with slope p lower than 50% ($p > 50\%$) and unstable terrain due to the existence of embankments. Lacking well-executed retaining walls.
- Building seated on loose soil with difference level among the foundation lower than 1 m ($\Delta h < 1$ m).

Parameter 5 – Plan regularity

This parameter appraises the shape of the building in plan. In the case of a building with rectangular shape, the ratio $\beta_1 = a/l \times 100$ between the dimension of the shorter and longest side is significant. In the case of buildings of irregular shapes or with existences of appendices, it will be necessary to evaluate the extent of the deviation. This can be done using the ratio $\beta_2 = b/l \times 100$ (Figure C-1).

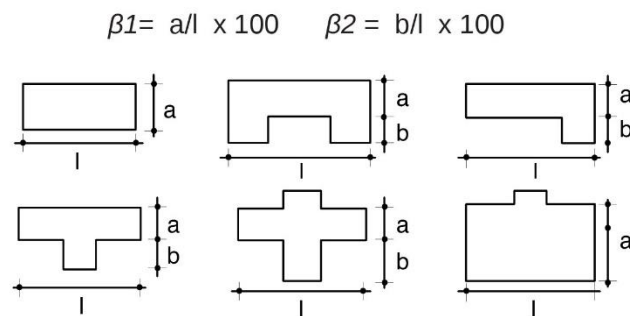


Figure C-1. Parameter 5 “Plan regularity”.

Class A

- $\beta_1 \geq 80$; $\beta_2 \geq 10$

Class B

- $60 \leq \beta_1 \leq 80$; $10 \leq \beta_2 \leq 20$

Class C

- $40 \leq \beta_1 \leq 60$; $20 \leq \beta_2 \leq 30$

Class D

- $\beta_1 < 40$

Parameter 6 – Vertical regularity

This parameter evaluates the existence of irregularities in the vertical load-bearing system due to the presence of galleries and cantilevers and the bottom and upper storeys respectively. The vulnerability classes of this parameter were defined based on the seismic performance analyses developed in Section 7.2.1. According to these results, the classes are defined as follow:

Class A

- Buildings with regular configuration along their height.

Class B

- Buildings with presence of open galleries or cantilevers at the bottom and upper storeys respectively.

Parameter 7 – Storey systems

This parameter evaluates the degree of rigidness and deformation capacity of the storey systems. The vulnerability classes are defined based on the numerical investigation developed in Section 7.2.1 for buildings with flexible, light retrofitted and weighty retrofitted storeys.

Based on the numerical results the classes are classified as follow:

Class A

Buildings with light retrofitted storey system:

- Timber joist storeys with double (or more) layer of timber board sheathing disposed in different directions, or reinforced with wooden boards or FRP technology.
- Timber joist storeys properly braced with wood or steel diagonals (Saint Andres's crosses, wooden cross or solid bringing).

Class B

- Buildings with flexible storey systems:
Joist storeys with single wooden sheathing disposed perpendicular to the joist direction.

Class C

Buildings with weighty retrofitted storey systems:

- Joist storeys retrofitted with RC toppings, metal decks with RC toppings or any structure adding significant mass without improving the connection with the vertical resistant elements (non-connected).

Parameter 8 – Roofing

This parameter analyses the roof typology and the possible thrusting actions applied to the vertical load-resisting system. There are two main characteristics that determines the influence of the roof on the seismic behaviour of the buildings: its type and weight. The former takes into account the determination of four classes (Figure C-2), while the second affects the determination of the weight attributed to this parameter. The necessary elements of evaluation are:

- a) The worst type of roof system configuring the building: thrusting, slightly thrusting, non-thrusting.
- b) The weight of the roof based on its materiality

Thrusting roofs are those that transfer the load directly to the walls (Figure C-2a) inducing the outward collapse of the walls. The thrusting effects of a roof structure are commonly mitigated using horizontal tying elements such as the case of trusses or ties (Figure C-2b). In these cases, the mass of the roof compresses the vertical resistant elements supporting it and the thrust acts in tension counteracting the outward effect. Inclined roofs, or those supported by internal load bearing walls (Figure C-2) are classified as slightly thrusting. Weighty retrofitted roofs or those filled or covered with heavy materials (adobe, bricks, tiles, etc.) are classified as heavy roofs.

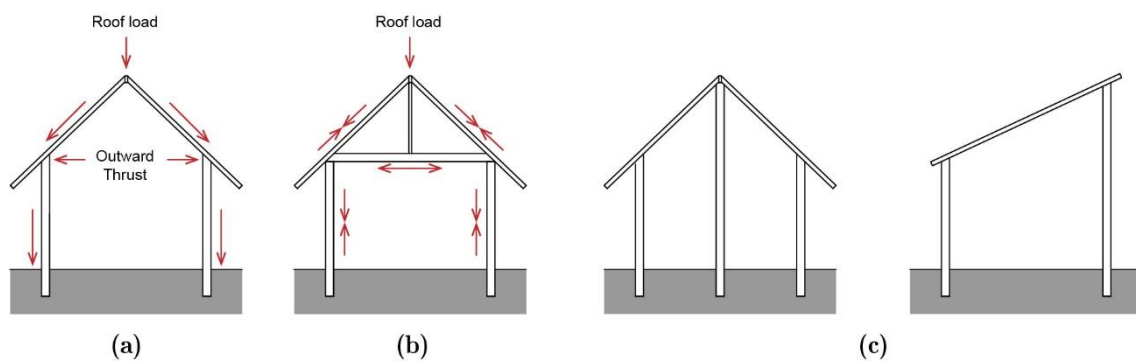


Figure C-2. Parameter 8 “Roofing”. Type of roofs: (a) thrusting, (b) non-thrusting, and (c) slightly thrusting.

Class A

- Non-thrusting and light roofs

Class B

- Non-thrusting and heavy roofs
- Slightly thrusting and light roofs

Class C

- Slightly thrusting and heavy roofs

Class D

- Thrusting and heavy roofs

Parameter 9 – Details

The parameter 9 “Details” classifies non-structural external elements that may partially or totally collapse and cause damage to people or elemental infrastructure in case of fall. The potential hazard of the elements is assessed in accordance with their dimensions and heaviness as well as and the quality of its connections to the resistant system. Large or/and heavy elements badly connected to the structure are the most unfavourable cases. The following elements can be considered as large/heavy elements: projected window; opening frames; balconies; galleries; exterior stairs; cornices; chimneys; or any other element of considerable dimension or weight. Smaller or lighter elements such as gutters, façade covering, ornaments, signboards, or any elements of small or light characteristics must be also evaluated even though they do not signify major hazard. All the above are secondary elements in the vulnerability assessment for which it makes no sense to make distinctions between the first two classes. The classes are defined as following:

Class A-B

- Buildings without external and internal accessory elements, or with only small or light ones which are well-connected to the structural elements.
- Buildings with exterior large/heavy elements well-connected to the resistant systems, and well-connected internal false ceilings.

Class C

- Buildings with large/heavy elements poorly connected to structural elements due to bad execution or deterioration of the connections.
- Buildings with external accessory elements of small/light conditions bad connected to the structural elements

Class D

- Buildings with exterior large/heavy elements poorly or badly connected to the structural elements.
- Buildings with projected elements subsequently added to the main structural system.

Parameter 10 – State of conservation

The parameter 10 “State of conservation” the influence of existing damage in the wooden elements and the joints in the seismic vulnerability of the structures. The mechanical and biotic damage on the structural elements are ones of the main hazards that could decrease the resistant capacity of the load-bearing systems. The above is especially dangerous when the damage is spread in the connections since they are in charge of transmitting and distributing the seismic loads through the structure. The classes are defined considering the following criteria:

- (a) Biotic or mechanical damage on the structural timber elements and/or carpentry connections. Several structural deteriorations due to termites or fungi attack, partial or total lacking of structural pieces, several deformations due to high stresses on the connections or must be penalized.
- (b) Bad executed interventions which are poorly connected to the main structural system, oversized or bad maintained must be appraised.

Based on the above criteria the classes are defines as follow:

Class A

- Buildings without damaged on the timber elements nor connections

Class B

- Buildings with localized damage on their timber connections.

Class C

- Buildings with extended damage on their timber elements.

Class D

- Buildings with damage on both timber elements and connections.

Parameter 11 – Presence of adjacent buildings with different height

This parameter evaluates the influence of adjacent buildings with different heights on the structural vulnerability of the building of study. According to Formisano et al. (2015), the most dangerous cases are when the building is within two shorter constructions since the constraining action of adjacent buildings is partially provided only, the central building is free to deform laterally at the last levels. The classes are defined as following (Figure C-3):

Class A

- Building enclosed between buildings of the same height

Class B

- Building with the same height and a tallest one
- Building enclosed between two tallest adjacent buildings

Class C

- Building enclosed between one building of the same height and a shorter one.
- Building enclosed between a tallest and a shorter building

Class D

- Building enclosed between two shorter buildings

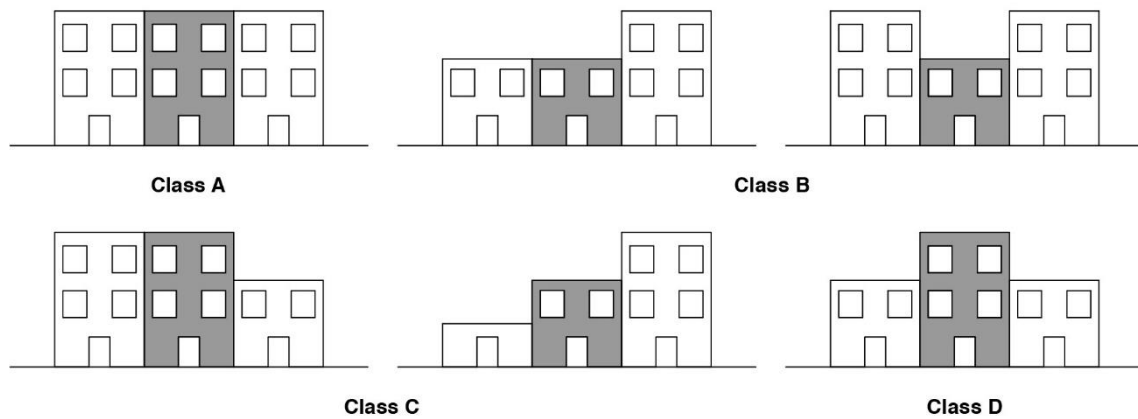


Figure C-3. Parameter 11 “In-elevation interaction” Vulnerability classes.

Parameter 12 – Position of the buildings in the aggregate

This parameter assesses the in-plan influence of the position of the buildings within a structural aggregate. Formisano et al. (2015) considered the evaluation of four different positions of the building named (a) isolated, (b) within other buildings, (c) in the aggregate, and (d) in a leading position of an in-row aggregate. Isolated buildings are always more vulnerable than a building within any type of structural aggregate, while the cases within two buildings present the lower vulnerability of the four cases (Figure C-4).

Class A

- Buildings within a structural aggregate

Class B

- Buildings between two buildings enclosed in row

Class C

- Buildings in a corner position within a structural aggregate

Class D

- Buildings in a leading position within an in-row structural aggregate
- Isolated buildings

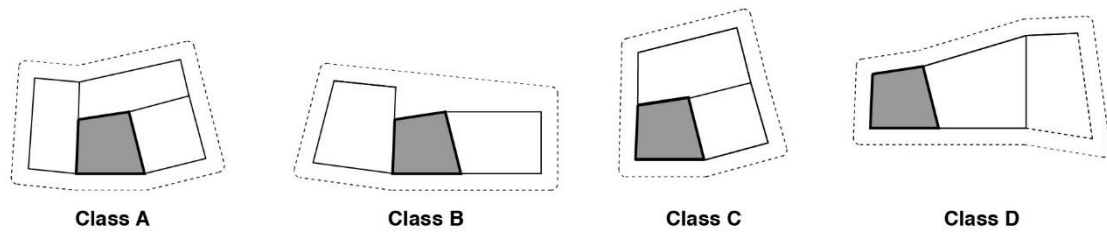


Figure C-4- Parameter 12 “Plan interaction”: Vulnerability classes.

Parameter 13 – Number of staggered storeys

This parameter studies the influence of staggered storeys among aggregate buildings. Formisano et al. (2015) analysed five different cases of staggered floors named (a) total absence of staggered floors; (b) presence of one staggered storey (c) presence of two staggered storeys at the same level; (d) presence of two staggered storeys at different levels; and (e) presence of four staggered storeys (Figure C-5). Based on the numerical study carried out by Formisano et al. (2015), it is known that this parameter has a slight influence on the whole vulnerability of the building. However, if the number of staggered storeys increases, the vulnerability of the building augments.

Class A

- No staggered storeys

Class B

- Presence of two staggered storeys

Class C

- Presence of four staggered storeys

Class D

- Presence of more than four staggered storeys

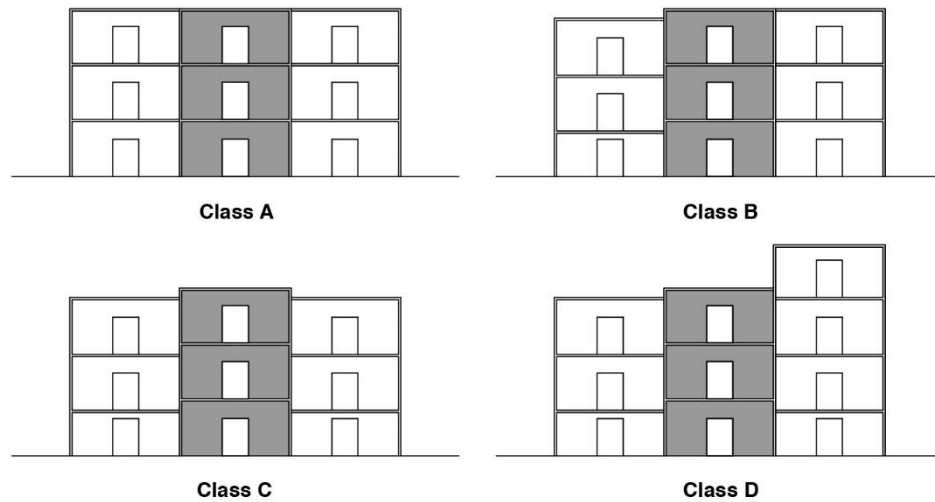


Figure C-5. Parameter 13 “Number of staggered storeys”: Vulnerability classes.

Parameter 14 – Structural typological heterogeneity among adjacent structural units

This parameter evaluates the structural or typological heterogeneity among adjacent structural units. Formisano et al. (2015) studied four possible cases named (a) aggregate buildings are homogeneous from typological and structural standpoint, (b) the building is adjacent to buildings made of the same material but erected with a construction technique worse than the examined one, (c) the building is enclosed by buildings made of the same material but erected with a construction technique better than the examined one, and (d) the building has a structural typology very different from that of adjacent buildings. The worst condition is when the base structural unit is next to units made of materials having greater strength. On the contrary, the most favourable condition is achieved when the study building is adjacent to a RC building (Figure C-6).

Class A

- Adjacent RC building

Class B

- Structural aggregate with homogeneous structural typologies

Class C

- The studied building has a better quality of the materials than the adjacent building

Class D

- The studied structural unit is next to units made of materials having greater strength

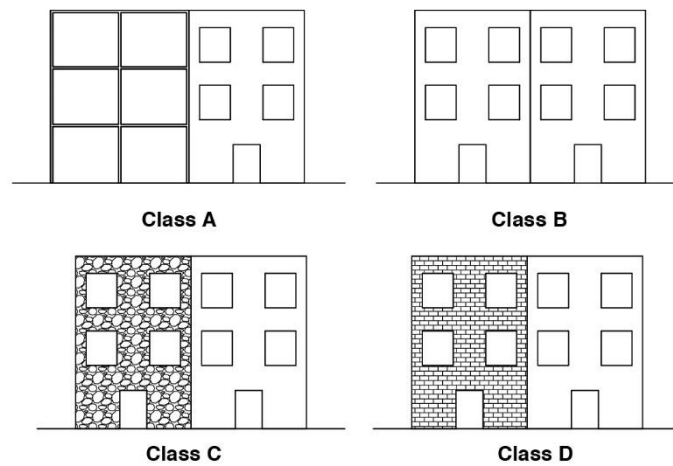


Figure C-6. Parameter 14 “Structural heterogeneity”: Vulnerability classes.

Parameter 15 – Percentage differences of opening areas among adjacent buildings

This parameter evaluates the percentage difference of opening areas among adjacent structural units. Formisano et al. (2015) numerically appraised five possible configurations named (a) no difference among adjacent facades; (b) difference more than 50%; (c) difference more than 25% (both sides); (d) difference less than 25%, and (e) difference more than 25% (from one side only). The results demonstrated that the worst condition is achieved when the opening area of the study units is less than 25% the adjacent units one (Figure C-7).

Class A

- Equal opening percentage between the studied structural unit and the adjacent buildings

Class B

- Less than 25% of opening differences between the studied structural unit and the adjacent buildings

Class C

- More than 25% of opening differences between the studied structural unit and the adjacent buildings

Class D

- More than 50% of opening differences between the studied structural unit and the adjacent buildings

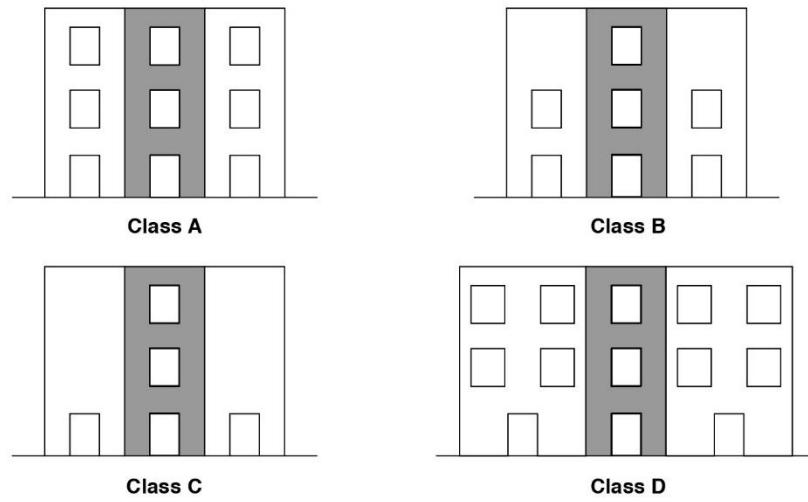


Figure C-7. Parameter 15 “Percentage difference between the structural unit and the adjacent building”: Vulnerability classes.

Annex D. Vulnerability index results of the ELC

FID	ADDRESS	Date of construction or last retrofitting	Structural typology	Iv	Iv,norm
0	Prat 790	1905	RC	-2,75	30,21
1	Urriola 358	1963	RC	-0,50	7,55
2	Urriola 332-342	1994	RC	-1,75	20,14
3	Urriola 378-396	1963	RC	-0,75	10,07
4	Urriola 426-428	2004	TIMBER-MASONRY	-35,75	14,26
5	Urriola 404-410	Unknown	MASONRY	60	28,95
6	Urriola 434-438	Unknown	TIMBER-MASONRY	-12	18,03
7	Urriola 434-438	Unknown	TIMBER-MASONRY	-12	18,03
8	Urriola 472	1978	TIMBER-MASONRY	-12	18,03
9	Urriola 476	2010	TIMBER-MASONRY	-15,75	17,43
10	Urriola 484-488	Unknown	TIMBER-MASONRY	-7	18,82
11	Urriola 498	Unknown	TIMBER-MASONRY	-10,5	18,27
12	A. Pratt 804-814	1981	RC	-1,00	12,59
13	Urriola 365	1950	RC	-1,50	17,62
14	Urriola 379	2011	MASONRY	24,5	23,41
15	Urriola 383	2016	TIMBER-MASONRY	30,75	24,82
16	Urriola 407-415	Unknown	TIMBER-MASONRY	70	31,06
17	Urriola 427-451	Unknown	TIMBER-MASONRY	69,25	30,94
18	Urriola 451	Unknown	TIMBER-MASONRY	56,75	28,95
19	Urriola 469	Unknown	TIMBER-MASONRY	-5,75	19,02
20	Urriola 471	2015	TIMBER-MASONRY	108	37,09
21	Urriola 491 - 495	Unknown	TIMBER-MASONRY	100,5	35,90
22	Urriola 507 565	Unknown	TIMBER-MASONRY	83	33,12
23	Urriola 565	2004	TIMBER-MASONRY	20	23,11
24	Urriola 530-542	Unknown	TIMBER-MASONRY	34,25	25,38
25	Urriola 516-526	Unknown	TIMBER-MASONRY	-90,75	5,52
26	Urriola 539	Unknown	TIMBER-MASONRY	-28,25	15,45
27	Alvaro Besa 520-534, 630-634	1927	RC	-2,50	27,69
28	Alvaro Besa 542	1985	TIMBER-MASONRY	-96,75	4,57
29	Alvaro Besa 552-592	1986	TIMBER-MASONRY	-92	5,32
30	Alvaro Besa 566	Unknown	TIMBER-MASONRY	0	19,94
31	Urriola 378-396	1963	RC	0,00	10,07
32	Alvaro Besa 610	1927	TIMBER-MASONRY	-72	8,50
33	Miramar 224	1954	TIMBER-MASONRY	-28	15,49
34	Urriola 452	-	EMPTY LAND		0,00
35	Urriola 464	1950	MASONRY	-12,5	17,64
36	Alvaro Besa 520-534 and 630-634	1927	TIMBER-MASONRY	-90,5	5,56
37	Alvaro Besa 520-534 and 630-634	Unknown	RC	-2,50	27,69
38	Montealegre 181	2010	MASONRY	45	26,61
39	Montealegre 149 - 173	2010	TIMBER-MASONRY	16,25	22,52

FID	ADDRESS	Date of construction or last retrofitting	Structural typology	Iv	Iv,rel
40	Montealegre 162	Unknown	MASONRY	43,75	26,41
41	Montealegre 132-138	Unknown	TIMBER-MASONRY	16,75	22,60
42	Paseo Yugoslavo 176	2008	TIMBER-MASONRY	18,25	22,84
43	Pza. Sotomayor 233	1936	TIMBER-MASONRY	45	22,52
44	Arturo Prat 647	1981	RC	-0,25	5,04
45	Arturo Prat 653	1980	RC	-1,00	12,59
46	Arturo Prat 655	Unknown	TIMBER-MASONRY	-21,75	16,48
47	Arturo Prat 667	1993	TIMBER-MASONRY	-21,75	16,48
48	Arturo Prat 677	Unknown	RC	-1,75	20,14
49	Arturo Prat 725	1967	TIMBER-MASONRY	34,5	25,42
50	Arturo Prat 733	1970	RC	-1,00	12,59
51	Arturo Prat 757-773	1998	RC	-1,00	12,59
52	Arturo Pratt 765	Unknown	RC	-1,25	15,11
53	Arturo Pratt 778	Unknown	RC	-1,75	20,14
54	Arturo Prat 1201-1207	1980	RC	-1,5	17,62
55	Arturo Prat 630-632	Unknown	RC	-1,50	17,62
56	Arturo Prat 668	1914	RC	-1,75	20,14
57	Arturo Prat 612	1970	RC	-1,25	15,11
58	Arturo Prat 732	1926	RC	-1,50	17,62
59	Arturo Prat 740	1960	RC	-1,50	17,62
60	Arturo Prat 762 -772	1975	RC	0,00	2,52
61	Pza. Anibal Pinto 339-341	1858	TIMBER-MASONRY	168,25	46,66
62	Plaza Anibal Pinto 1184	1947	RC	-2,50	27,69
63	Cumming 45-59	1861	TIMBER-MASONRY	49,25	27,76
64	Pza. Anibal Pinto 1175	1857	TIMBER-MASONRY	71,75	31,33
65	Almirante Montt 14-38	2009	RC	-1,50	17,62
66	Almirante Montt 42	Unknown	MASONRY	10,75	21,26
67	Almirante Montt 48	Unknown	TIMBER-MASONRY	33	25,18
68	Almirante Montt 60	2011	TIMBER-MASONRY	91,75	34,51
69	Almirante Montt 70	Unknown	TIMBER-MASONRY	30,5	24,78
70	Almirante Montt 96	Unknown	TIMBER-MASONRY	21,75	23,39
71	Almirante Montt 108-128	Unknown	MASONRY	-9,5	18,10
72	Beethoven 126 142-154	2014	MASONRY	27,50	23,88
73	Almirante Montt 142-154	2014	TIMBER-MASONRY	140,5	42,26
74	Almirante Montt 168	2004	TIMBER-MASONRY	41,75	26,57
75	Pilcomayo 591	1870	TIMBER-MASONRY	16,75	22,60
76	Almirante Montt 2	1990	RC	-1,25	15,11
77	Almirante Montt 51	1990	RC	-2,25	25,18
78	Almirante Montt 97, 107-109	Unknown	TIMBER-MASONRY	-9,25	18,47
79	Almirante Montt 107-109	2015	TIMBER-MASONRY	-12	18,03
80	Almirante Montt 137	Unknown	TIMBER-MASONRY	35,5	25,58
81	Almirante Montt 217	Unknown	TIMBER-MASONRY	0,5	20,02
82	Almirante Montt 167-169	Unknown	TIMBER-MASONRY	83	33,12
83	Almirante Montt 175	Unknown	TIMBER-MASONRY	-28,25	15,45
84	Almirante Montt	Unknown	TIMBER-MASONRY	-60,75	10,29

FID	ADDRESS	Date of construction or last retrofitting	Structural typology	Iv	Iv,rel
85	Almirante Montt 175	Unknown	TIMBER-MASONRY	88	33,92
86	Almirante Montt 213	Unknown	MASONRY	27,5	23,88
87	Almirante Montt 227-231	2009	RC	0,25	0,00
88	Almirante Montt 235	1996	RC	-2,25	17,62
89	Almirante Montt 235	2016	TIMBER-MASONRY	-25,75	15,85
90	Almirante Montt 249	Unknown	TIMBER-MASONRY	-64,5	9,69
91	Almirante Montt 251-253	Unknown	TIMBER-MASONRY	23	23,59
92	Almirante Montt 269	Unknown	TIMBER-MASONRY	43	26,77
93	Almirante Montt 269	Unknown	TIMBER-MASONRY	74,25	31,73
94	Almirante Mont 316	Unknown	TIMBER-MASONRY	-21,25	16,56
95	Pilcomayo 566	1858	MASONRY	45,5	26,69
96	Alvaro Besa 385	2004	TIMBER-MASONRY	58	29,15
97	Pza. Sotomayor 594	1908	RC	-1,25	15,11
98	Pza. Sotomayor 147	1955	RC	-1,50	17,62
99	Pza. Sotomayor 160	1902	MASONRY	60,5	29,03
100	Pza. Sotomayor 250	Unknown	MASONRY	60,5	29,03
101	Pza. Sotomayor 50	1990	RC	-1,25	15,11
102	Pza. Sotomayor 77	1999	RC	-0,75	10,07
103	Montealegre 244	1963	RC	-0,50	7,55
104	Melgarejo 669	2003	RC	-2,25	25,18
105	Pza. Anibal Pinto 1154	Unknown	RC	-0,50	7,55
106	Cumming 3	Unknown	TIMBER-MASONRY	-38	13,90
107	Cumming 5	Unknown	TIMBER-MASONRY	-14,5	17,63
108	Pza. Anibal Pinto 1178	Unknown	TIMBER-MASONRY	27	24,23
109	Almirante Montt 142-154	-	EMPTY LAND		0,00
110	Pilcomayo 566	1950	MASONRY	21,75	22,98
111	Pasaje Leighton 229	2010	TIMBER-MASONRY	-9,5	18,43
112	Paseo Yugoslavo 243	Unknown	TIMBER-MASONRY	16,25	22,52